TESIS DE LA UNIVERSIDAD DE ZARAGOZA

2015

24

Noemí Gil Lalaguna

# Estudio de la gasificación de lodos de EDAR en lecho fluidizado: efecto de la atmósfera reactiva, evaluación energética y limpieza del gas producto

Departamento

Ingeniería Química y Tecnologías del Medio Ambiente

Director/es

Sánchez Cebrián, José Luis

Murillo Esteban, María Benita



ISSN 2254-7606

Prensas de la Universidad Universidad Zaragoza

Universidad Zaragoza
1542

Tesis Doctoral

# ESTUDIO DE LA GASIFICACIÓN DE LODOS DE EDAR EN LECHO FLUIDIZADO: EFECTO DE LA ATMÓSFERA REACTIVA, EVALUACIÓN ENERGÉTICA Y LIMPIEZA DEL GAS PRODUCTO


Autor

Noemí Gil Lalaguna

Director/es

Sánchez Cebrián, José Luis
Murillo ESteban, María Benita

**UNIVERSIDAD DE ZARAGOZA**

Ingeniería Química y Tecnologías del Medio Ambiente

Departamento de Ingeniería Química y Tecnologías del Medio Ambiente
Universidad Zaragoza

instituto de investigación en ingeniería de Aragón
Universidad de Zaragoza

# ESTUDIO DE LA GASIFICACIÓN DE LODOS DE EDAR EN LECHO FLUIDIZADO. EFECTO DE LA ATMÓSFERA REACTIVA, EVALUACIÓN ENERGÉTICA Y LIMPIEZA DEL GAS PRODUCTO

**TESIS DOCTORAL**

presentada por

**NOEMÍ GIL LALAGUNA**

Noviembre de 2014, Zaragoza

*A mi familia, especialmente para él*

La presente Tesis Doctoral, que lleva por título "*Estudio de la gasificación de lodos de EDAR en lecho fluidizado. Efecto de la atmósfera reactiva, evaluación energética y limpieza del gas producto"*, realizada por Dña. Noemí Gil Lalaguna y dirigida por los doctores D. José Luis Sánchez Cebrián y Dña. María Benita Murillo Esteban se presenta como compendio de las siguientes publicaciones:

i. N. Gil-Lalaguna, J.L. Sánchez, M.B. Murillo, E. Rodríguez, G. Gea. (2014) "*Air steam gasification of sewage sludge in a fluidized bed. Influence of some operating conditions*". **Chemical Engineering Journal** 248, 373-382.

ii. N. Gil-Lalaguna, J.L. Sánchez, M.B. Murillo, V. Ruiz, G. Gea. (2014) "*Air steam gasification of char derived from sewage sludge pyrolysis. Comparison with the gasification of sewage* sludge". **Fuel** 129, 147-155.

iii. N. Gil-Lalaguna, J.L. Sánchez, M.B. Murillo, M. Atienza-Martínez, G. Gea. (2014) "*Energetic assessment of air-steam gasification of sewage sludge and of the integration of sewage sludge pyrolysis and air-steam gasification of char*". **Energy** 76, 652-662.

iv. N. Gil-Lalaguna, J.L. Sánchez, M.B. Murillo, G. Gea. (2015) "*Use of sewage sludge combustion ash and gasification ash for high-temperature desulphurization of different gas streams*". **Fuel** 141, 99-108.

Lo que se hace constar en cumplimiento del Reglamento sobre Tesis Doctorales de la Universidad de Zaragoza (artículos 19 y 20), aprobado según el Acuerdo de 20/12/2013 del Consejo de Gobierno de la Universidad de Zaragoza.

**D. José Luis Sánchez Cebrián** y **Dña. María Benita Murillo Esteban**,

ambos Profesores Titulares de Universidad en el Departamento de Ingeniería Química y Tecnologías del Medio Ambiente de la Universidad de Zaragoza, y miembros del Grupo de Procesos Termoquímicos del Instituto Universitario de Investigación en Ingeniería de Aragón (I3A)

**INFORMAN** que:

La presente memoria titulada

***"Estudio de la gasificación de lodos de EDAR en lecho fluidizado. Efecto de la atmósfera reactiva, evaluación energética y limpieza del gas producto"***

ha sido realizada por Dña. Noemí Gil Lalaguna bajo nuestra dirección en el Departamento de Ingeniería Química y Tecnologías del Medio Ambiente, y

**AUTORIZAN** su presentación como compendio de publicaciones.

Y para que así conste, firmamos este informe en Zaragoza, a 24 de Noviembre de 2014.

Fdo. Prof. Dr. José Luis Sánchez Cebrián

Fdo. Prof. Dra. María Benita Murillo Esteban

## AGRADECIMIENTOS

El trabajo reflejado en esta Tesis Doctoral ha sido realizado en el Grupo de Procesos Termoquímicos (GPT) del Instituto de Investigación en Ingeniería de Aragón (I3A), gracias a una beca predoctoral que me concedió el Ministerio de Educación entre los años 2010 y 2014 (ayuda de posgrado para la formación de profesorado universitario). Por lo tanto, el primer agradecimiento debe ser para ambas instituciones, por el apoyo técnico y económico prestado. De forma particular, me gustaría agradecer también al director del GPT, Rafael Bilbao, por la oportunidad que me brindó en el inicio de esta etapa.

Si hoy estoy escribiendo estas líneas de agradecimientos es, en buena parte, gracias a mis directores, la Dra. María Benita Murillo y el Dr. José Luis Sánchez. Gracias Mari Beni por animarme a unirme al grupo, hace ya más de 5 años, para hacer el Proyecto Fin de Carrera con vosotros. Allí empezó todo esto. Gracias José Luis por "animarme" a terminar con esto. Gracias a los dos por vuestros consejos, orientación y apoyo en muchos momentos duros, no sólo relacionados con la investigación.

Gracias a mis compañeros del GPT, tanto a los que seguís por aquí, como a los que estáis fuera. Gloria, gracias por tus consejos y por estar siempre disponible. Isabel, Javi, Fernando, Alberto, Ester y Gorka, gracias por enseñarnos y aconsejarnos a los que llegamos por aquí un poco después que vosotros. Ana, Javi, María, Lorena, Lucía, Manu, María y Violeta, gracias por las risas y los buenos momentos en la nave, en el despacho, en el café, en la comida… ¡Que hubiese sido de mí algunos días sin ellos! Olga, Guille y Beatriz, gracias por vuestra ayuda siempre que os la he pedido. Gracias a Eva, Victor, Ana y David, por vuestro trabajo y buena disposición en el laboratorio.

De puertas para afuera de la universidad también tengo mucho que agradecer. En primer lugar a mi padre, porque se lo debo todo. A mi madre y a mi hermana, por su paciencia y por estar siempre allí, en lo bueno y en lo malo. A mis amigas, siempre con palabras de ánimo para todo. Y como no, a Óscar, por ser cómo es y por haber aguantado todo lo que, al final, supone hacer una Tesis.

# ÍNDICE

# 1. INTRODUCCIÓN GENERAL Y OBJETIVOS

La presente Tesis Doctoral ha sido desarrollada en el Grupo de Procesos Termoquímicos (GPT), perteneciente al Instituto de Investigación en Ingeniería de Aragón (I3A) de la Universidad de Zaragoza. Entre las principales líneas de investigación desarrolladas por el GPT se puede destacar el tratamiento termoquímico de biomasa y residuos orgánicos mediante procesos de gasificación y pirólisis, la producción de biodiesel y mejora de sus propiedades, la eliminación de contaminantes de gases de combustión ($NO_x$ y hollín) y la producción de hidrógeno a partir del reformado catalítico de corrientes acuosas.

El presente trabajo se engloba dentro del campo de la valorización energética de residuos y, más concretamente, el proceso estudiado es la gasificación de lodos de estaciones depuradoras de aguas residuales urbanas (EDAR). Los lodos de EDAR son el subproducto generado en el proceso de depuración de las aguas residuales provenientes de zonas urbanas. La cantidad generada de este residuo ha aumentado mucho en los últimos años como consecuencia de la implementación de la legislación europea referente al tratamiento de aguas residuales urbanas (Directiva 91/271/CEE). En la Unión Europea se están produciendo anualmente más de 10 millones de toneladas de lodo seco (Kelessidis y Stasinakis, 2012). Por esta razón, la correcta gestión de los lodos de forma económica y sin poner en riesgo la salud pública y el medio ambiente se ha convertido en un reto importante en el ámbito del tratamiento de las aguas residuales.

Dado el contenido en materia orgánica de los lodos, uno de los procesos que puede plantearse para su aprovechamiento energético es la gasificación, proceso que centra el estudio desarrollado en esta Tesis. La gasificación puede definirse como la conversión térmica de un material carbonoso en una atmósfera netamente reductora, generando un gas combustible y un residuo sólido. El producto de interés de la gasificación es el gas, compuesto principalmente de CO, $CO_2$, $H_2$, vapor de agua, $CH_4$ y otros hidrocarburos ligeros y $N_2$ (en el caso de gasificar con aire). La proporción de estos gases varía en función de la composición de la materia prima y las condiciones del proceso. El gas producto de la gasificación ofrece varias opciones para su aprovechamiento, desde su uso como combustible en motores de combustión interna o en turbinas de gas para la generación de electricidad en ciclos combinados, hasta su uso como materia prima en la obtención de productos químicos como metanol, amoníaco, o líquidos Fischer-Tropsch (Wender, 1996). Además del producto gaseoso y del residuo sólido, durante la gasificación se genera también una mezcla de vapores orgánicos fácilmente condensables, denominada alquitrán, que abandona el gasificador junto

con el gas. La formación de alquitrán es una de las principales limitaciones para la implantación de los procesos de gasificación, ya que su presencia en el gas conlleva problemas operacionales debido a su facilidad para condensar, formar aerosoles y polimerizar, dando lugar a estructuras más complejas y provocando problemas de ensuciamiento y taponamiento en tuberías y equipos para el aprovechamiento del gas, como motores y turbinas.

Los inicios de la investigación relacionada con la gasificación de lodos de EDAR en el Grupo de Procesos Termoquímicos se remontan a la década de los años 90, cuando se realizaron las primeras pruebas a escala de laboratorio en colaboración con la empresa Cadagua S.A. En base a los resultados experimentales obtenidos, durante los años 2001-2003 el GPT trabajó junto con el departamento de I+D de Cadagua S.A. en el diseño y puesta a punto de una planta piloto de lecho fluidizado de 100 $kg \cdot h^{-1}$ para la gasificación de lodos de EDAR. En el año 2003 se comenzó con la experimentación en dicha planta, pero los problemas asociados con el trabajo a gran escala pronto plantearon la necesidad de trasladar de nuevo el estudio del proceso a escala de laboratorio para conocer mejor la influencia de las condiciones de operación. Desde entonces, la gasificación y pirólisis de lodos de EDAR ha sido una importante línea de trabajo en el GPT, contando con el apoyo financiero de los Ministerios de Educación y Ciencia, de Ciencia e Innovación, y de Economía y Competitividad en sucesivas convocatorias de proyectos (CT2004-05528, CT2007-66885, CT2010-20137 y CT2013-47260).

De forma más concreta, el desarrollo de esta Tesis ha contado con el apoyo financiero del Ministerio de Economía y Competitividad gracias al proyecto *"Valorización de lodos de EDAR mediante un proceso de pirólisis: estudio y mejora de la aplicabilidad de sus productos (CTQ2010-20137)"*, así como del Ministerio de Educación a través de una ayuda de posgrado para la formación de profesorado universitario *(beca FPU, referencia AP2009-3446)* concedida a la doctoranda durante los cuatro últimos años para la realización de la Tesis Doctoral.

La mayoría de los estudios que se encuentran en la bibliografía sobre gasificación de lodos de EDAR (Adegoroye y cols., 2004; Dogru y cols., 2002; Midilli y cols., 2001; Petersen y Werther, 2005; Tae-Young y cols., 2009), incluyendo el trabajo previo desarrollado en el GPT (Aznar y cols., 2007; Aznar y cols., 2008; Manyà y cols., 2005; Manyà y cols., 2006), utilizan aire para gasificar lodo seco. Sin embargo, teniendo en cuenta que el contenido de humedad del lodo antes del secado térmico puede superar el 70% tras su estabilización y deshidratación mecánica mediante filtros prensa y centrifugación (Manara y Zabaniotou, 2012), la gasificación del lodo húmedo podría ser una opción interesante para su aprovechamiento. Los estudios publicados acerca de la gasificación de lodo húmedo (o gasificación de lodo seco con vapor para simular el proceso) no son muy numerosos (Domínguez y cols., 2006; Nipattummakul y

cols., 2010; Xie y cols., 2010; Zhang y cols., 2011). El principal inconveniente de la gasificación con vapor de agua es que es un proceso endotérmico, por lo que requiere un aporte continuo de energía. Esta energía puede obtenerse mediante la adición de aire u oxígeno al medio de gasificación gracias a la combustión parcial de parte de la materia orgánica. La escasez de trabajos publicados acerca de la gasificación de lodos con mezclas de vapor de agua y aire como agente gasificante motivó el estudio realizado en la primera parte de la Tesis. Este estudio pretende profundizar en el conocimiento del efecto de la atmósfera reactiva en la distribución de productos y en la calidad del gas. Puesto que la materia prima disponible era un lodo digerido anaeróbicamente y secado térmicamente, la adición de vapor de agua al medio de reacción permitió simular el proceso de gasificación de un lodo húmedo. Los resultados de este estudio se recogen en el primer artículo del compendio de publicaciones que componen la Tesis:

i. N. Gil-Lalaguna, J.L. Sánchez, M.B. Murillo, E. Rodríguez, G. Gea. (2014) *"Air steam gasification of sewage sludge in a fluidized bed. Influence of some operating conditions"*. Chemical Engineering Journal 248, 373-382.

Como ya se ha comentado anteriormente, la presencia de alquitrán en el gas de gasificación supone un importante inconveniente para el aprovechamiento del gas. En comparación con la biomasa original, y desde el punto de vista de la formación de alquitrán, el sólido resultante del proceso de pirólisis de la misma (*char*) puede ser una materia prima preferible para la gasificación, ya que gran parte de la materia volátil responsable de la formación del alquitrán se elimina durante el tratamiento de pirólisis. La pirólisis (o descomposición térmica en atmósfera inerte) de lodos de EDAR ha sido ampliamente estuadiada en el GPT durante los últimos años (Fonts y cols., 2008; Fonts y cols., 2009; Gil-Lalaguna y cols., 2010). Aunque la pirólisis rápida está orientada a maximizar la producción de líquido, la fracción mayoritaria en la pirólisis de lodo es el sólido (en torno a un 50% en masa). La fracción orgánica de este *char* le confiere cierto valor energético que puede ser aprovechado mediante procesos de combustión o gasificación. Esta idea es la base de otro de los estudios desarrollados en la Tesis, consistente en la gasificación del *char* obtenido en la pirólisis de lodos de EDAR. Los resultados de este estudio y su comparación con los datos obtenidos en la gasificación directa del lodo se detallan en el segundo artículo del compendio de publicaciones de la Tesis:

ii. N. Gil-Lalaguna, J.L. Sánchez, M.B. Murillo, V. Ruiz, G. Gea. (2014) *"Air steam gasification of char derived from sewage sludge pyrolysis. Comparison with the gasification of sewage sludge"*. Fuel 129, 147-155.

Además de la viabilidad operacional de los procesos termoquímicos, el estudio de los mismos desde un punto de vista energético es un aspecto clave de cara a su posible desarrollo industrial. Por lo tanto, dado el carácter endotérmico de las reacciones de gasificación con vapor de agua, se consideró interesante realizar una evaluación energética para determinar si la energía disponible en los productos de ambos procesos (gasificación directa del lodo y combinación de la pirólisis de lodo y gasificación del *char*) es suficiente para cubrir el coste energético de dichos procesos, así como del secado térmico del lodo. La etapa de secado térmico permite reducir el volumen de residuo, facilitando su manipulación antes del tratamiento termoquímico. Sin embargo, el secado del lodo conlleva un gran consumo energético que encarece la gestión del residuo. El aporte de esta energía mediante los propios productos de la gasificación y pirólisis del lodo sería la opción más económica. Los resultados de este estudio energético se han publicado en otro de los artículos que forma parte del compendio de publicaciones de la Tesis:

iii. N. Gil-Lalaguna, J.L. Sánchez, M.B. Murillo, M. Atienza-Martínez, G. Gea. (2014) *"Energetic assessment of air-steam gasification of sewage sludge and of the integration of sewage sludge pyrolysis and air-steam gasification of char"*. Energy 76, 652-662.

Los siguientes estudios desarrollados en la Tesis se centran en la limpieza del gas producto de la gasificación de lodo. Además de alquitrán, este gas contiene otras impurezas que tienen su origen en la propia composición del lodo. Es el caso del sulfuro de hidrógeno ($H_2S$), formado durante la gasificación del lodo como consecuencia de la presencia de compuestos con azufre. La presencia de $H_2S$ en el gas de gasificación conlleva problemas ambientales y operacionales, causando la corrosión de tuberías, motores y turbinas, así como el envenenamiento de los catalizadores más comúnmente utilizados para el craqueo de los alquitranes, por lo general basados en níquel (Hepola y Simell, 1997a). Existen diferentes procesos para la eliminación de $H_2S$ de corrientes gaseosas, tanto a baja como a alta temperatura. Los procesos de desulfuración a alta temperatura se basan en la reacción química de óxidos metálicos con el $H_2S$ para formar sulfuros metálicos que quedan retenidos en forma sólida. Las cenizas resultantes del tratamiento termoquímico de la biomasa o de residuos orgánicos están compuestas por diversos metales y óxidos metálicos, por lo que su uso para la desulfuración de gases puede ser una opción interesante debido a su bajo coste. Es el caso de las cenizas

obtenidas en el tratamiento termoquímico del lodo, cuya aplicación para la eliminación del $H_2S$ generado en el propio proceso supondría una ventaja desde el punto de vista del aprovechamiento integral de los subproductos. Por lo tanto, el siguiente estudio de la Tesis se centró en evaluar la capacidad de retención de azufre de las cenizas obtenidas tanto en la gasificación como en la combustión del lodo de EDAR, utilizando para ello diversos gases sintéticos con el fin de evaluar el efecto de la atmósfera reactiva. Este estudio se encuentra publicado en otro de los artículos de la Tesis:

iv. N. Gil-Lalaguna, J.L. Sánchez, M.B. Murillo, G. Gea. (2015) "*Use of sewage sludge combustion ash and gasification ash for high-temperature desulphurization of different gas stream*s". Fuel 141, 99-108.

La eliminación del alquitrán presente en el gas de gasificación sigue centrando muchos estudios en el campo de la gasificación de biomasa ya que, hasta la fecha, este problema no ha sido resuelto de forma satisfactoria a escala industrial. El reformado catalítico de los alquitranes con catalizadores de níquel parece ser una de las vías más eficaces (Anis y Zainal, 2011; De Lasa y cols., 2011). Sin embargo, la operación de estos catalizadores durante largos períodos de tiempo conlleva ciertos problemas de pérdida de actividad por fenómenos de sinterización, formación de carbono sobre los centros activos o envenenamiento con azufre. Por lo tanto, el diseño de catalizadores de níquel resistentes a estos fenómenos de desactivación representa todavía un gran desafío. En este contexto se desarrolló el último estudio de la Tesis, llevado a cabo durante una estancia de investigación en el *VTT Technical Research Centre of Finland*. Dado que el gas obtenido en la gasificación de lodos de EDAR presenta un importante contenido de $H_2S$, el objetivo de este estudio fue la evaluación de la actividad y estabilidad de diversos catalizadores de níquel preparados y modificados con varios promotores. El artículo correspondiente a este estudio se encuentra en fase de revisión para su publicación en la revista Fuel: "*Catalytic activity of nickel-alumina catalysts modified with iron, manganese, calcium and copper for tar reforming under a $H_2S$-containing atmosphere*".

En resumen, los artículos que componen la presente Tesis Doctoral presentan una clara unidad temática: el estudio de la gasificación de lodos de EDAR y de diversos procesos para la limpieza y mejora de la calidad del gas producto.

## Objetivos

El objetivo principal de la Tesis es profundizar en el estudio de la gasificación de lodos de EDAR para mejorar las propiedades del gas producto mediante la optimización de las condiciones de operación y la aplicación de distintos tratamientos secundarios de limpieza del gas. La consecución de este objetivo global ha conllevado la realización de diversas tareas:

- Revisión y actualización de la bibliografía en el campo del aprovechamiento energético de lodos de EDAR, la gasificación de biomasa y la limpieza del gas producto.
- Estudio experimental de la influencia de algunas condiciones de operación en la distribución de productos y calidad del gas obtenido en la gasificación de lodos de EDAR con mezclas de aire y vapor de agua.
- Estudio experimental de la gasificación del *char* obtenido en la pirólisis del lodo como alternativa para reducir la presencia de alquitrán en el gas. Comparación con los resultados obtenidos en la gasificación directa del lodo.
- Evaluación energética de las etapas de gasificación de lodo y de *char*, incluyendo también el análisis del proceso de pirólisis en el que se genera el *char* gasificado y de la etapa previa de secado térmico del lodo.
- Estudio experimental de la eliminación de $H_2S$ de diferentes gases sintéticos utilizando las propias cenizas obtenidas en la combustión y gasificación de lodos de EDAR.
- Estudio experimental de la actividad y estabilidad de varios catalizadores de níquel modificados con distintos promotores para el reformado de compuestos modelo de alquitrán en presencia de $H_2S$.

# 2. ANTECEDENTES

## 2.1. Lodos de EDAR. Problemática y vías de gestión

Los lodos de Estaciones Depuradoras de Aguas Residuales (EDAR) son el subproducto derivado del proceso de depuración de las aguas residuales provenientes de zonas urbanas o de vertidos industriales de composición similar a las de éstas. Estos lodos son el resultado de la acumulación tanto de microorganismos derivados del tratamiento biológico de las aguas como de la materia orgánica y mineral que se encontraba disuelta o suspendida en el agua y que no ha sido degradada durante el proceso. Los lodos de EDAR son considerados como un residuo no peligroso en el Catálogo Europeo de Residuos (Decisión 2001/118/CE).

En la Figura 2.1 se muestra un diagrama de las etapas que habitualmente forman parte del proceso de depuración de aguas residuales.

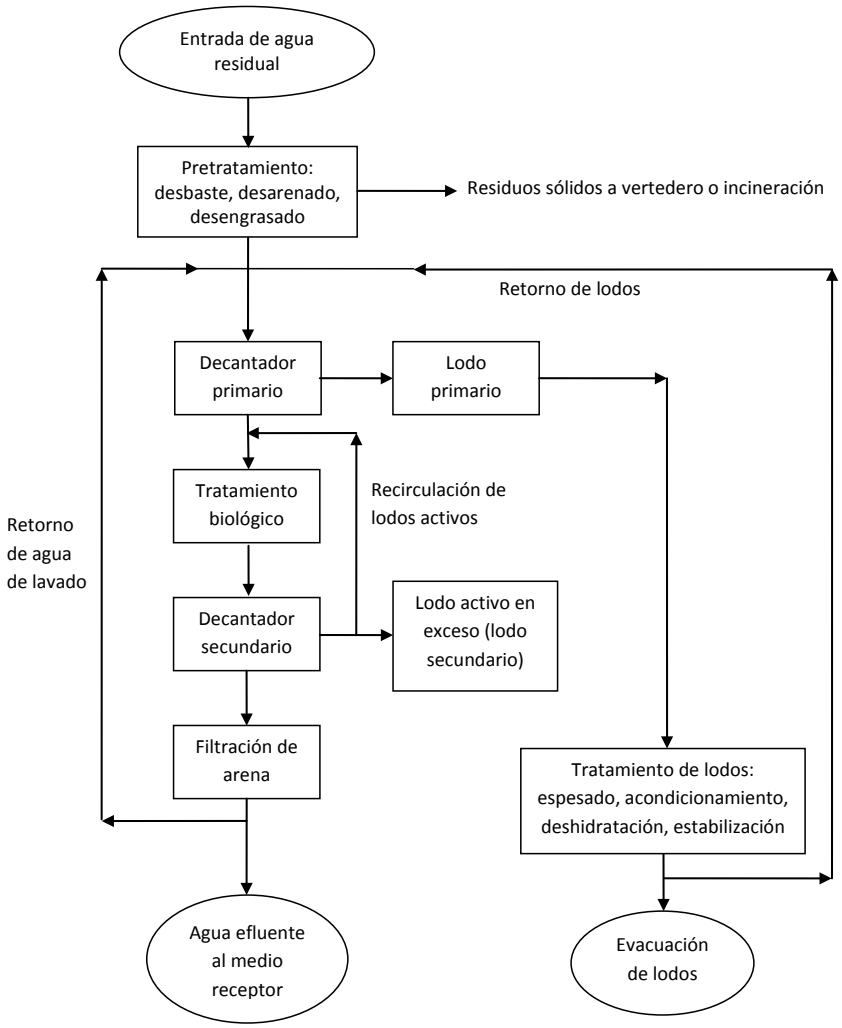


Figura 2.1. Diagrama del proceso de depuración de aguas residuales (Kiely, 1999).

Tras las etapas de desbaste, desarenado y desengrasado, en la decantación primaria se consigue una separación de los sólidos más finos suspendidos en el agua como consecuencia de la diferencia de densidades. Después, en el tratamiento secundario o tratamiento biológico, la materia orgánica biodegradable del agua es metabolizada mediante diversos tipos de microorganismos. Este proceso se suele llevar a cabo en un tanque aireado donde las aguas residuales y los microorganismos permanecen en contacto (lodo activo) y, después, los coágulos microbianos sedimentan en el tanque de decantación secundaria.

El lodo resultante de las etapas de decantación primaria y secundaria es un residuo líquido biodegradable cuyo contenido de agua puede alcanzar el 95%, ocupando por tanto un gran volumen. Por lo tanto, antes de su evacuación y disposición final, este residuo debe someterse a ciertos tratamientos para facilitar su manejo y evitar problemas sanitarios y medioambientales. Con el espesado (por gravedad o flotación) y deshidratación mecánica del lodo (centrífugas, filtros prensa, filtros banda) se consigue reducir el volumen de residuo mediante la eliminación parcial del agua hasta aproximadamente un contenido de humedad del 70% (Manara y Zabaniotou, 2012). Por otro lado, los tratamientos de estabilización del fango permiten reducir la presencia de agentes patógenos, así como la capacidad de putrefacción del lodo y los desagradables olores asociados a ella. La digestión anaerobia es uno de los métodos de estabilización más extendidos en las plantas de tratamiento de gran capacidad, pero existen otras opciones como la digestión aerobia, el compostaje o la estabilización química mediante la adición de cal. Por último, el secado térmico del lodo como etapa final del tratamiento da lugar a un residuo sólido con un contenido de humedad inferior al 10%. A pesar del coste adicional que conlleva, la implantación de plantas para el secado térmico de los lodos como etapa previa a la incineración de los mismos ha cobrado especial importancia en los últimos años (Kelessidis y Stasinakis, 2012).

La composición del lodo generado en las estaciones depuradoras está fuertemente condicionada por la carga contaminante del agua residual y por el tipo de tratamiento aplicado en el proceso. En términos generales, estos lodos están formados por: (i) agua, que puede suponer desde un pequeño porcentaje hasta un 95% del lodo; (ii) materia orgánica no tóxica (aproximadamente un 60% en base seca), en la que se incluyen constituyentes biológicos como ácidos nucleicos, proteínas, carbohidratos y lípidos, y materia orgánica no digerida en el proceso, como celulosa; (iii) materia inorgánica: silicatos, aluminatos, compuestos de calcio y de magnesio, etc.; (iv) elementos nutrientes: nitrógeno, fósforo y potasio; (v) pequeñas concentraciones de elementos contaminantes como metales pesados (zinc, cromo, plomo, cobre, níquel, mercurio, etc.), compuestos orgánicos persistentes (pesticidas, disolventes

industriales, colorantes, plastificantes, agentes tensoactivos, etc.) y agentes patógenos, que suponen un riesgo medioambiental y sanitario en el caso de una mala gestión de los lodos (Manara y Zabaniotou, 2012; Rulkens, 2008).

En cumplimiento con la legislación europea, los estados miembro de la Unión Europea están obligados a recoger y tratar las aguas residuales provenientes de núcleos urbanos con una población superior a 2000 habitantes equivalentes. Así lo especifica la Directiva 91/271/CEE sobre el tratamiento de las aguas residuales urbanas. Como resultado del cumplimiento de esta normativa, la producción de lodos de EDAR ha aumentado considerablemente en las dos últimas décadas debido a la implantación de nuevas estaciones depuradoras y al desarrollo de tecnologías de depuración más eficaces. La producción anual de lodos en la Unión Europea prácticamente se duplicó en el período de tiempo de 1992 a 2005, pasando de 6,5 a 10,9 millones de toneladas anuales de materia seca. Las predicciones apuntan a que en el año 2020 se superarán las 13 millones de toneladas anuales. En el caso particular de España, los últimos datos disponibles del Registro Nacional de Lodos del Ministerio de Agricultura, Alimentación y Medio Ambiente (año 2009) lo sitúan entre los cinco países europeos con mayor producción de lodos, generando alrededor de 1,2 millones de toneladas anuales de materia seca. Desde el año 2000, la producción de lodos en España se ha incrementado en un 41%, siguiendo la misma tendencia que los datos europeos.

Aunque el residuo final representa sólo un pequeño porcentaje del volumen total de agua tratado en una estación depuradora, su acondicionamiento y tratamiento supone más del 50% de los costes de operación de la planta (Spinosa y cols., 2011). Esto, unido al fuerte incremento de su producción, hace que la gestión y eliminación de los lodos de forma económica y segura para la salud pública y el medio ambiente sea un reto importante en la actualidad.

La política en materia de gestión de lodos de EDAR está condicionada en gran medida por factores geográficos, culturales, económicos, etc., y la flexibilidad entre las distintas vías de gestión varía de un país a otro. Sin embargo, de forma general, dado que los lodos de EDAR son considerados como un residuo no peligroso (código CER 190805), les es de aplicación el principio de jerarquía establecido en la normativa vigente de gestión de residuos (Directiva 2008/98/CE). La prevención, reutilización, reciclado y otras formas de valorización (incluyendo la recuperación energética) son, por este orden, prioritarios frente a la eliminación del residuo en vertedero.

Actualmente, las opciones más comunes para la gestión de lodos de EDAR en la Unión Europea incluyen su reutilización en la agricultura y en la restauración de terrenos, la

incineración y el depósito en vertedero (Kelessidis y Stasinakis, 2012; Manara y Zabaniotou, 2012). Dado su contenido en materia orgánica y nutrientes (nitrógeno y fósforo), la aplicación de los lodos en suelos agrícolas, ya sea de forma directa o tras una etapa de compostaje, es la opción más utilizada a nivel europeo (53% del lodo producido según datos del año 2005), seguida de la incineración (19%) y el depósito en vertedero (17%). El porcentaje restante incluye métodos como el almacenamiento temporal o la recuperación de terrenos (Kelessidis y Stasinakis, 2012).

Aunque los lodos de EDAR representan una fuente natural de nutrientes y materia orgánica para su aplicación en suelos agrícolas, la presencia de sustancias nocivas (metales pesados, toxinas y agentes patógenos) ha suscitado cierta controversia sobre la reutilización agrícola del lodo debido a los posibles efectos adversos de estos contaminantes en la cadena alimentaria. La Directiva 86/278/CEE relativa a la protección del medio ambiente en la utilización de los lodos con fines agrícolas regula esta práctica, haciendo indispensable el control de las dosis de aplicación del lodo en función de sus características y las del suelo donde va a ser aplicado, y estableciendo valores límite para la concentración de metales pesados tanto en el lodo como en el suelo. Algunos países europeos han adoptado límites mucho más restrictivos que los establecidos en la citada directiva europea, así como valores límite para lo concentración de contaminantes orgánicos y agentes patógenos (Kelessidis y Stasinakis, 2012). El depósito en vertedero ha sido otra de las vías habituales para la eliminación de los lodos de depuradora. Sin embargo, debido a la prohibición del vertido de desechos líquidos orgánicos, así como a las restricciones establecidas para el depósito de residuos sólidos biodegradables (Directiva 1999/31/CEE), la eliminación de los lodos en vertederos mostró un continuo y significativo retroceso entre 1992 y 2005, disminuyendo del 33% al 17% de los lodos producidos en la Unión Europea. Por otro lado, el porcentaje de lodos incinerados se duplicó en dicho período, pasando del 11 al 21% (Kelessidis y Stasinakis, 2012). La incineración de los lodos, como la de cualquier residuo, también se encuentra sometida a la legislación europea (Directiva 2010/75/UE).

En España, el Plan Nacional Integrado de Residuos (PNIR 2008-2015) establece las medidas a tomar de cara a la gestión de los lodos de EDAR. Entre estas medidas se incluye la reducción de la cantidad de fangos destinada a vertedero (12% como máximo en 2015) y se promueve la reutilización del lodo mediante su aplicación en suelos agrícolas, fijando un objetivo mínimo del 67% de los lodos para el año 2015. Según los datos del Registro Nacional de Lodos, estos objetivos han sido claramente sobrepasados en los últimos años, destinando

en torno a un 83% de los lodos a fines agrícolas, un 8% a vertedero y un 5% a incineración (datos del año 2009).

Dado que el uso agrícola del lodo parece estar cada vez más cuestionado, su valorización energética mediante procesos termoquímicos (combustión, pirólisis y gasificación) ofrece una alternativa interesante para su gestión, convirtiendo la parte orgánica del residuo en energía útil y/o productos de valor añadido, y quedando sólo la fracción mineral para su disposición final. Desde el punto de vista del contenido energético, el poder calorífico del lodo seco (12-20 $MJ \cdot kg^{-1}$) es comparable, por ejemplo, al del lignito (15-27 $MJ \cdot kg^{-1}$) (Manara y Zabaniotou, 2012). La gasificación de lodos de depuradora es el proceso en el que se centra la presente Tesis Doctoral.

## 2.2. Aspectos generales de la gasificación

La gasificación es un proceso termoquímico en el que un sustrato carbonoso se transforma en un gas combustible en presencia de un agente gasificante (aire, oxígeno, vapor de agua o dióxido de carbono), en una atmósfera de reacción netamente reductora. El producto de interés de la gasificación es el gas, compuesto principalmente de CO, $CO_2$, $H_2$, vapor de agua, $CH_4$ y otros hidrocarburos ligeros y $N_2$ (en el caso de gasificar con aire). La proporción de estos gases varía en función de la composición de la materia prima y las condiciones del proceso. El gas producto de la gasificación ofrece varias opciones para su aprovechamiento, desde su uso como combustible en motores de combustión interna o en turbinas de gas para la generación de electricidad, hasta su uso como materia prima en la obtención de productos químicos como metanol, amoníaco o líquidos Fischer-Tropsch (Wender, 1996). Además del gas, en el proceso de gasificación se obtiene también un residuo sólido con cierto contenido en carbono debido a la incompleta conversión de la materia orgánica inicial, y una mezcla de vapores orgánicos aromáticos y poliarómaticos denominada alquitrán.

El proceso de gasificación transcurre a través de varias etapas (Antal y cols., 1979). En primer lugar se produce el secado del sólido y el desprendimiento de la materia volátil (pirólisis). El sólido resultante, rico en carbono fijo, se gasifica mediante su reacción con $O_2$, $CO_2$, $H_2$ o $H_2O$. A la vez se producen también otras reacciones secundarias entre los gases y los productos volátiles generados, dando lugar al producto final. Las reacciones de gasificación del sólido son lentas en comparación con la liberación de la materia volátil y las reacciones en fase gas, por lo que estas reacciones son habitualmente la etapa limitante del proceso. La secuencia y duración de las etapas varía con el tipo de reactor utilizado.

La química del proceso de gasificación es muy compleja pero, en general, las principales reacciones gas-sólido y gas-gas que tienen lugar en el gasificador son las siguientes (Mondal y cols., 2011):

| | | | |
|---|---|---|---|
| Combustión parcial: | $C + ½\ O_2 \longrightarrow CO$ | $\Delta H_{298K} = -110\ kJ \cdot mol^{-1}$ | (ec. 2.1) |
| Combustión completa: | $C + O_2 \longrightarrow CO_2$ | $\Delta H_{298K} = -393\ kJ \cdot mol^{-1}$ | (ec. 2.2) |
| *Water-gas:* | $C + H_2O \leftrightarrow CO + H_2$ | $\Delta H_{298K} = 131\ kJ \cdot mol^{-1}$ | (ec. 2.3) |
| Boudouard: | $C + CO_2 \leftrightarrow 2CO$ | $\Delta H_{298K} = 172\ kJ \cdot mol^{-1}$ | (ec. 2.4) |
| Metanación: | $C + 2H_2 \leftrightarrow CH_4$ | $\Delta H_{298K} = -75\ kJ \cdot mol^{-1}$ | (ec. 2.5) |
| *Water-gas shift*: | $CO + H_2O \leftrightarrow CO_2 + H_2$ | $\Delta H_{298K} = -41\ kJ \cdot mol^{-1}$ | (ec. 2.6) |
| Reformado con vapor: | $CH_4 + H_2O \leftrightarrow CO + 3H_2$ | $\Delta H_{298K} = 205\ kJ \cdot mol^{-1}$ | (ec. 2.7) |
| Reformado en seco: | $CH_4 + CO_2 \leftrightarrow 2CO + 2H_2$ | $\Delta H_{298K} = 247\ kJ \cdot mol^{-1}$ | (ec. 2.8) |

La gasificación se presenta como una de las tecnologías más prometedoras para la obtención de energía. El gas producto de la gasificación puede ser utilizado de varias formas para la producción de electricidad o calor. Los motores de combustión interna en conexión con gasificadores de lecho fijo o lecho fluidizado a presión atmosférica ofrecen una interesante alternativa para potencias eléctricas moderadas (entre 50 $kW_e$ y 10 $MW_e$). Para una mayor generación eléctrica (> 5 $MW_e$), las turbinas de gas son la mejor tecnología, siendo los gasificadores de lecho fluidizado el tipo de reactor más adecuado (Spliethoff, 2001). En términos generales, los motores o turbinas de gas permiten alcanzar eficiencias eléctricas de hasta el 30% (sin incluir la recuperación del calor residual). En el caso de las turbinas de gas de alta potencia eléctrica (> 25 $MW_e$), la eficiencia eléctrica puede superar el 40% en los ciclos combinados, en los que además de la turbina de gas se incorpora una turbina de vapor y una caldera para la recuperación del calor residual. Así, la integración de la gasificación en ciclos combinados (GICC) se presenta como una alternativa viable económicamente, de mayor eficiencia que otras tecnologías convencionales y de menor impacto ambiental, ya que permite la eliminación de los contaminantes del gas de gasificación antes de su combustión. Esta etapa de limpieza del gas resulta fundamental para evitar dificultades técnicas en el aprovechamiento energético del mismo (Martínez y cols., 2012).

En la actualidad existen alrededor de 117 plantas de gasificación operando alrededor de todo el mundo, de las que un 39% generan combustible, 19% generan electricidad y 42% productos químicos. El 49% de las 117 plantas usan carbón y un 36% usan coque de petróleo. La capacidad instalada total de las plantas de gasificación suma 24000 $MW_e$, con un crecimiento anual de alrededor del 10% (Concha y cols., 2009). Algunas de las plantas de GICC

más importantes son la de Puertollano en España (*Elcogas S.A,* 335 $MW_e$), la de Buggenum en Holanda (*Willem-Alexander Power Plant*, 253 $MW_e$), la de Tampa en Florida, EEUU (*Tampa Electric's Polk Power Station*, 260 $MW_e$) y la de West Terre Haute en Indiana, EEUU (*Wabash River Generating Station,* 262 $MW_e$).

En el caso de la gasificación de biomasa, su explotación comercial presenta una serie de desafíos tecnológicos y logísticos, relacionados principalmente con la cadena de suministro y el pretratamiento de la biomasa (Asadullah, 2014). A pesar de ello, varias plantas de GICC se han desarrollado a escala de demostración y a nivel comercial en todo el mundo como alternativa al uso de combustibles fósiles para la producción de electricidad (Kinoshita y cols., 1997). La primera y más destacable se construyó en Värnamo (Suecia) utilizando astillas de madera para producir 6 MW eléctricos y 9 MW térmicos (Ståhl y Neergaard, 1998). Esta instalación funcionó entre 1993 y 1999, pero tuvo que ser cerrada por motivos económicos. Las casi 3600 h de funcionamiento como planta integrada demostraron la posibilidad de utilizar el gas de gasificación obtenido en una turbina de gas en condiciones estables, con un poder calorífico de tan solo 3,8 $MJ \cdot kg^{-1}$. Desde la década de los años 90, otros proyectos de gasificación de biomasa a escala de demostración o semi-comercial se han desarrollado en todo el mundo, utilizando diferentes tecnologías, entre las que se pueden citar *Lurgi Technology, Termiska Processor Sweden AB., Renugas Process*, etc. (Spliethoff, 2001).

Una de las principales limitaciones para una mayor implantación de la gasificación a nivel comercial es la presencia de alquitrán en el gas producto. En el contexto de la gasificación, la definición más ampliamente aceptada es la que define los alquitranes como el grupo de compuestos orgánicos más pesados que el benceno, sin tener en cuenta el *soot* (hollín) ni el *char* (residuo sólido carbonoso) (Neeft y cols., 2002). El tolueno y el naftaleno son algunos de los compuestos mayoritarios en el alquitrán, junto con el fenol cuando la temperatura de operación es baja (< 800 ºC) (Spliethoff, 2001). La presencia de alquitrán en el gas de gasificación conlleva problemas operacionales debido a su facilidad para condensar (< 450 ºC), formar aerosoles, y polimerizar dando lugar a estructuras más complejas, lo cual provoca problemas de ensuciamiento y taponamientos en tuberías y equipos donde vaya a ser utilizado el gas, como motores y turbinas (McKendry, 2002b). Además, los compuestos presentes en el alquitrán constituyen un serio problema medioambiental por su carácter persistente y tóxico (Nisbet y Lagoy, 1992).

El valor límite de concentración de alquitrán en el gas de gasificación depende del uso final del mismo. Como valor de referencia suele fijarse una concentración máxima de 100 $mg \cdot m^{-3}N$ para el uso del gas en motores de combustión interna y de 5 $mg \cdot m^{-3}N$ para su uso en

turbinas (Spliethoff, 2001). Los gasificadores disponibles hoy en día en el mercado superan con creces estos valores límite, variando entre 0,5 y 100 $g \cdot m^{-3}N$ en función de la materia prima, las condiciones de operación y, fundamentalmente, el tipo de reactor (Devi y cols., 2003). El proceso de gasificación puede tener lugar en diversos tipos de reactores, siendo los gasificadores de lecho fijo (*updraft* o *downdraft*), de lecho fluidizado o de flujo arrastrado los más utilizados (Mondal y cols., 2011). Los gasificadores de lecho fijo son adecuados para plantas de baja capacidad, mientras que los gasificadores de lecho fluidizado son más habituales en instalaciones de mayor tamaño (> 5 $MW_t$) (Spliethoff, 2001). Con la configuración de lecho fluidizado (que es la tecnología utilizada en el presente trabajo) se consigue una mayor tasa de conversión del sólido en comparación con los gasificadores de lecho fijo debido a que el movimiento del lecho favorece el buen contacto sólido-gas y mejora la transferencia de masa y calor. El contenido de partículas y de alquitrán en el gas procedente de los gasificadores de lecho fluidizado es habitualmente superior al de los reactores de lecho fijo *downdraft* (corriente descendente) e inferior al de los gasificadores *updraft* (contracorriente) (Han y Kim, 2008). Los valores habituales de contenido de alquitrán en la gasificación de biomasa en lecho fluidizado oscilan entre 8 y 15 $g \cdot m^{-3}N$ (Corella y cols., 2006). Dado que estos valores son muy superiores a los límites establecidos, la reducción del contenido de alquitrán en el gas de gasificación es un aspecto clave para su aprovechamiento. Como se detalla más adelante, las tecnologías de eliminación de alquitrán se dividen en dos grandes grupos: métodos primarios, que incluyen todas las medidas adoptadas dentro del propio gasificador para producir un gas lo más limpio posible, y métodos secundarios o de limpieza del gas aguas abajo del gasificador.

## 2.3. Influencia de las condiciones de operación en el proceso de gasificación

Tanto la formación de alquitrán como la calidad del gas producto de la gasificación se ven fuertemente influenciadas por las condiciones de operación. Por lo tanto, una adecuada selección de los parámetros de operación es, por sí misma, un método primario para reducir la formación de alquitrán.

La temperatura es uno de los parámetros más influyentes en el proceso de gasificación de biomasa, afectando tanto a la cinética como a la termodinámica de las reacciones y, por tanto, a la composición del gas y a su concentración de alquitrán. Dada la complejidad y simultaneidad de las reacciones durante el proceso de gasificación, la evolución de los distintos compuestos gaseosos ($H_2$, CO, $CO_2$, $CH_4$,...) con la temperatura presenta variaciones en función del intervalo de temperatura y del predominio de unas u otras reacciones. En

general, bajas temperaturas de gasificación conllevan un alto contenido de alquitrán y un bajo contenido de CO y $H_2$ en el gas producto (Asadullah, 2014). El aumento de la temperatura conduce a un mayor rendimiento a gas en detrimento de la concentración de alquitrán, que puede reaccionar a través de diferentes mecanismos (Li y Suzuki, 2009a). El reformado con vapor (ec. 2.9) y el reformado en seco (ec. 2.10) son algunas de las reacciones de eliminación de alquitrán más importantes.

Reformado con vapor: $C_nH_m + n\ H_2O \leftrightarrow n\ CO + (n + m/2)\ H_2$ $\Delta H > 0$ (ec. 2.9)

Reformado en seco: $C_nH_m + n\ CO_2 \leftrightarrow 2n\ CO + (m/2)\ H_2$ $\Delta H > 0$ (ec. 2.10)

El intervalo de temperatura más habitual para la gasificación de biomasa es 750-900 ºC. Por lo general, se requieren temperaturas de operación por encima de 800 ºC para lograr una alta conversión del carbono sólido y un bajo contenido de alquitrán en el gas producto (Devi y cols., 2003). Reducciones en el contenido de alquitrán de hasta un 75-95% fueron observadas por diversos autores al aumentar la temperatura de gasificación desde 700 hasta 800-820 ºC (Li y Suzuki, 2009a; Narváez y cols., 1996). Sin embargo, aunque desde el punto de vista de la eliminación del alquitrán interesa aumentar la temperatura de operación, otros factores limitan dicha temperatura, como puede ser el riesgo de fusión y aglomeración de las cenizas o la necesidad de materiales y especificaciones más exigentes para la construcción y mantenimiento del gasificador (Asadullah, 2014).

Las reacciones químicas envueltas en el proceso de gasificación no sólo se ven afectadas por la temperatura, sino también por la presión parcial de los distintos reactivos en el medio de reacción. Por lo tanto, el tipo de agente gasificante es un factor clave en la composición y aplicabilidad del gas producto. El aire es el agente gasificante más habitual debido a su bajo coste, pero el nitrógeno introducido con el aire diluye la mezcla gaseosa (en torno a un 50% vol. de $N_2$), dando como resultado un gas con un bajo poder calorífico (PCI = 4-6 $MJ \cdot m^{-3}N$). Este contenido energético puede ser suficiente para el uso del gas en calderas, motores o turbinas, pero no para el transporte del gas a través de tuberías debido a su baja densidad energética (Bridgwater, 1995). La gasificación con oxígeno puro evita la dilución del gas, aumentando su poder calorífico hasta 10-14 $MJ \cdot m^{-3}N$, pero el coste del proceso aumenta considerablemente debido a la necesidad de una unidad de separación de aire para la obtención del oxígeno. Además del aire u oxígeno, el vapor de agua puede ser también utilizado como medio de gasificación. La presencia de vapor de agua favorece el desplazamiento de las reacciones *water-gas* (ec. 2.3), *water-gas shift* (ec. 2.6) o el reformado de hidrocarburos con vapor (ec. 2.7) hacia la producción de $H_2$. La obtención de productos químicos y combustibles sintéticos a partir del gas de gasificación requiere un gas de síntesis de alta calidad, formado

mayoritariamente por $H_2$ y CO en una proporción adecuada ($H_2$/CO = 2-3 mol·mol$^{-1}$). En la literatura se pueden encontrar valores de concentración de $H_2$ de hasta un 60% en el gas producto de la gasificación de biomasa con vapor (Herguido y cols., 1992). La composición del alquitrán también parece verse afectada por el medio de reacción. El alquitrán formado durante la gasificación con vapor de agua es más reactivo y fácil de destruir con catalizadores que el formado en la gasificación con aire (Gil y cols., 1999a; McKendry, 2002b). Asimismo, Gil y cols. (1999a) encontraron mayores contenidos de alquitrán en la gasificación con vapor (30-80 g·m$^{-3}$N) que en la gasificación con aire (2-20 g·m$^{-3}$N), aunque esto podría tener su origen en la menor temperatura de operación alcanzada en el primer caso.

La relación entre el flujo de agente gasificante alimentado por unidad de masa de biomasa es también un importante factor de operación en la gasificación (Devi y cols., 2003). En el caso de gasificar con aire u oxígeno, esta ratio viene dada por la relación equivalente (RE), que es el cociente entre la cantidad de oxígeno alimentado por gramo de biomasa y la cantidad estequiométrica de oxígeno necesaria para la combustión completa de un gramo de biomasa. En la gasificación con aire, RE habitualmente oscila entre 0,2 y 0,4 (Narváez y cols., 1996). Un aumento de RE supone una mayor disponibilidad de oxígeno en el medio de reacción, lo que facilita la combustión de la materia volátil y la disminución del contenido de alquitrán en el gas, mejorando la producción de gas y la conversión del sólido (Kinosita y cols., 1994; Narváez y cols., 1996). Sin embargo, la composición del gas se ve negativamente afectada por el excesivo aumento de RE, debido al incremento de las fracciones de $CO_2$ y $N_2$ (al gasificar con aire), lo que conlleva una disminución del poder calorífico del gas. La influencia de RE en la concentración de $H_2$, CO o $CH_4$ puede mostrar diversas tendencias en función de otros factores como el tipo de biomasa, el intervalo de temperatura o la presencia de vapor de agua en el medio (Kumar y cols., 2009). En el caso de la gasificación con vapor de agua, el parámetro habitualmente utilizado es la relación másica entre la cantidad de vapor de agua y la cantidad de biomasa alimentados (*S/B* del inglés *steam to biomass ratio*). El aumento de la relación *S/B* favorece la conversión del sólido y disminuye la concentración de alquitrán en el gas, lo que puede atribuirse a una mayor extensión de la reacciones de reformado con vapor (ec. 2.9). Sin embargo, el aumento de la relación *S/B* por encima de cierto límite puede repercutir de forma negativa en la distribución de productos como consecuencia de la disminución de la temperatura de reacción.

A diferencia de la gasificación con aire u oxígeno, que conlleva la combustión parcial de la biomasa en condiciones subestequiométricas, la gasificación del carbono con vapor de agua es una reacción endotérmica y requiere un aporte continuo de energía. Dado que la transferencia

de calor a elevadas temperaturas presenta serias dificultades, la operación del gasificador en régimen autotérmico es la opción más interesante. Para ello, la adición de cierta cantidad de oxígeno junto con el vapor de agua puede proporcionar la energía necesaria en el medio de reacción gracias a la combustión parcial de la materia prima. Los estudios relacionados con el uso de mezclas de aire (u oxígeno) y vapor de agua como agente gasificante en la gasificación de biomasa no son muy numerosos (Campoy y cols., 2009; Gil y cols., 1997; Lv y cols., 2004; Pinto y cols., 2003), por lo que se requieren más estudios para profundizar tanto en los aspectos operacionales como energéticos del proceso.

Gasificación de lodos de EDAR

En el caso concreto de la gasificación de lodos de EDAR (proceso en el que se centra esta Tesis), los primeros estudios publicados se remontan a mediados de los años 90 (Bacaicoa y cols., 1995). Desde entonces, la gasificación de lodos de EDAR ha sido estudiada como una posible alternativa para su conversión en energía útil, con el objetivo de reducir a la vez el volumen de residuo y el impacto medioambiental que puede ocasionar su mala gestión. Los trabajos publicados tanto a escala de laboratorio (Adegoroye y cols., 2004; Aznar y cols., 2008; Manyà y cols., 2005; Tae-Young y cols., 2009) como en planta piloto (Campoy y cols., 2014; Dogru y cols., 2002; Midilli y cols., 2001; Petersen y Werther, 2005; Van der Drift y cols., 2001) confirman la posibilidad de obtener un gas combustible a partir del lodo. Por ejemplo, Midilli y cols. (2001) realizaron experimentos de gasificación de lodo con aire en un reactor *downdraft* (10 $kW_e$), obteniendo un gas combustible con un PCI de aproximadamente 3,8 $MJ \cdot m^{-3}N$. Hasta la fecha no se conocen proyectos de gasificación de lodo a nivel comercial, pero sí que se han desarrollado algunos proyectos a escala de demostración directamente en estaciones depuradoras, utilizando el gas producto para la producción de electricidad en un ciclo combinado (75 $kW_e$ en la planta de Balingen, en Alemania) o para el secado del lodo (1,5 $MW_t$ en la planta de Mannheim, en Alemania) (Judex y cols., 2012).

La mayoría de los estudios de gasificación de lodo que se encuentran en la bibliografía se centran en el uso de aire para gasificar lodo seco, siendo la relación equivalente (RE) y la temperatura las variables más estudiadas. Sin embargo, teniendo en cuenta que el contenido de humedad en el lodo tras la deshidratación mecánica y antes del secado térmico puede alcanzar el 70% (Manara y Zabaniotou, 2012), la gasificación del residuo húmedo puede ser una alternativa interesante. Los estudios de gasificación de lodo húmedo que se encuentran en la literatura no son muy numerosos (Domínguez y cols., 2006; Xie y cols., 2010; Zhang y cols., 2011), pero todos ellos muestran una mejora de la producción de $H_2$ como consecuencia de la gasificación de la materia orgánica del lodo con su propio contenido de humedad. Como

simulación al proceso de gasificación de lodo húmedo, Nipattummakul y cols. (2010) observaron una producción de $H_2$ de hasta tres veces mayor al usar vapor de agua en lugar de aire para gasificar lodo seco. La escasez de estudios acerca del efecto de la atmósfera reactiva en la calidad del gas producto de la gasificación de lodos motivó parte del estudio desarrollado en esta Tesis.

Gasificación de *char* de pirólisis

Además de las condiciones de operación, la composición de la biomasa (contenido en cenizas, materia volátil, carbono fijo, humedad,…) condiciona la distribución de productos en la gasificación. Desde el punto de vista de la reducción de alquitrán, el producto sólido resultante de la pirólisis de biomasa (*char* de pirólisis) puede ser una materia prima más adecuada para la gasificación que la propia biomasa original. Además de ser una de las primeras etapas en los procesos de gasificación y combustión de la biomasa, la pirólisis es, en sí misma, un proceso termoquímico que consiste en la descomposición térmica de un sustrato carbonoso en atmósfera inerte. Durante la pirólisis de biomasa se produce la liberación de gran parte de su contenido volátil que, tras condensar, da lugar al líquido de pirólisis o *bio-oil*. La fracción líquida es el producto de interés de la pirólisis rápida (Bridgwater y Peacocke, 2000), aunque en ella se genera también una importante fracción de producto sólido. La estructura y composición de este sólido son bastante diferentes a las de la biomasa original, con una mayor estructura porosa y un mayor contenido de carbono fijo. Dicha estructura porosa ha dado lugar al uso de estos materiales en la preparación de carbones activos (González y cols., 2009) y su aplicación como adsorbentes para la eliminación de contaminantes (metales pesados, colorantes, fenoles, $NO_x$…) (Raveendran y Ganesh, 1998). Por otro lado, el contenido de carbono remanente en el *char* puede ser aprovechado energéticamente mediante procesos de combustión o gasificación (Di Blasi, 2009). El estudio de la gasificación de *char* de diferente origen lignocelulósico ha cobrado especial interés en los últimos años, pero los estudios publicados hasta la fecha son todavía escasos. Algunos de estos trabajos se centran en el estudio de la reactividad y modelado cinético del proceso (Haykiri-Acma y cols., 2006; Márquez-Montesinos y cols., 2002; Nilsson y cols., 2014), y otros muestran la posibilidad de obtener un gas de buena calidad, con una fracción molar de $CO+H_2$ que puede alcanzar el 88% del gas (Chaudhari y cols., 2003), un contenido en $H_2$ superior al 50% en la gasificación con vapor (Yan y cols., 2010) y al 25% en la gasificación con aire (Salleh y cols., 2010), y un poder calorífico superior a 4 $MJ \cdot m^{-3}N$ (He y cols., 2012).

En el caso particular de la pirólisis rápida de lodo de EDAR, el *char* puede llegar a ser el producto mayoritario, a pesar de no ser el producto de interés (rendimiento del 35-55%)

(Fonts y cols., 2008; Fonts y cols., 2012; Inguanzo y cols., 2002; Pokorna y cols., 2009; Shen y Zhang, 2003). Su reutilización como material adsorbente ha sido investigado por algunos autores, aunque los resultados han mostrado una baja superficie específica (50-150 $m^2 \cdot g^{-1}$) en comparación con la de los carbones activos comerciales (> 500 $m^2 \cdot g^{-1}$) debido a su alto contenido inorgánico (Smith y cols., 2009). El aprovechamiento energético de este tipo de *char* apenas ha sido estudiado y los trabajos que se encuentran en la bibliografía son estudios cinéticos y de reactividad que apenas hacen hincapié en las propiedades del gas producto (Nilsson y cols., 2012; Nowicki y cols, 2011; Scott y cols., 2005), por lo que la gasificación del *char* resultante de la pirólisis de lodos de EDAR ha sido objeto de otro de los estudios desarrollados en la Tesis.

## 2.4. Limpieza del gas producto de la gasificación

Como se ha comentado anteriormente, las tecnologías de eliminación de alquitrán pueden clasificarse en métodos primarios y secundarios. Además de una apropiada selección de las condiciones de operación, la adición de catalizadores en el propio gasificador es otro de los tratamientos primarios que puede ayudar a reducir la formación de alquitrán. El uso de minerales naturales, como la dolomita o la olivina, o de catalizadores metálicos basados en hierro o níquel ha sido ampliamente estudiado, obteniéndose reducciones del contenido de alquitrán en el gas superiores al 50%, y llegando a niveles de hasta 1-2 $g \cdot m^{-3}N$ en algunos casos (De Andrés y cols., 2011; Gil y cols., 1999b; Miccio y cols., 2009; Olivares y cols., 1997; Rapagnà y cols., 2000). Sin embargo, los problemas de desactivación por deposición de carbono y de erosión y arrastre de las partículas en el caso del uso de materiales naturales en lechos fluidizados impide la operación durante largos períodos de tiempo (De Andrés y cols., 2011).

Los exigentes requisitos de calidad fijados para la mayoría de las aplicaciones del gas hacen necesaria una limpieza adicional del gas aguas abajo del gasificador. Los tratamientos secundarios de eliminación de alquitrán se clasifican en métodos físicos, craqueo térmico o craqueo catalítico. Entre los sistemas de limpieza físicos se incluye el uso de ciclones, precipitadores electrostáticos, filtros (filtros de tela, filtros de cerámica...), torres lavadoras o *scrubbers* y adsorción en carbón activo (Abu El-Rub y cols., 2004; Anis y Zainal, 2011). La mayoría de estos métodos requieren del enfriamiento del gas para la separación del alquitrán condensado en pequeñas gotas o aerosoles, lo que conlleva una disminución de la eficiencia energética del proceso. Las partículas sólidas arrastradas por el gas también quedan retenidas en este tipo de dispositivos junto con los aerosoles de alquitrán. La eficiencia en la eliminación de alquitrán se sitúa, por ejemplo, en torno a un 40% con el uso de precipitadores

electrostáticos y en un 70% con filtros de tela, mientras que las torres lavadoras de gases de tipo *venturi* pueden alcanzar eficiencias de hasta el 90% (Anis y Zainal, 2011; Han y Kim, 2008). Además del enfriamiento del gas, la gestión del residuo generado al separar el alquitrán del gas, sin ser destruido, es otro de los inconvenientes en este tipo de tratamientos de limpieza.

Mediante la conversión del alquitrán en moléculas más ligeras como $H_2$, CO y $CH_4$ se evitan los problemas de gestión, a la vez que se incrementa la producción final de gas. Dado el control cinético en estas reacciones (Abu El-Rub y cols., 2004; Anis y Zainal, 2011), la descomposición del alquitrán requiere temperaturas extremadamente altas (craqueo térmico) o, bien, el uso de catalizadores (craqueo o reformado catalítico). El alquitrán derivado de la biomasa es muy refractario y difícil de craquear sólo por efecto térmico, necesitando temperaturas por encima de los 1000 ºC para la ruptura de sus enlaces, con los problemas técnicos y energéticos que esto conlleva (Brandt y Henriksen, 2000; Bridgwater, 1995). El uso de catalizadores permite disminuir la temperatura de craqueo, pudiendo operar incluso a la temperatura del gas a su salida del gasificador, lo que supone un óptimo dese el punto de vista energético. Todas estas ventajas han hecho que el craqueo catalítico de los alquitranes haya centrado muchos estudios desde la década de los 80.

El craqueo o reformado catalítico del alquitrán implica la adsorción disociativa de los hidrocarburos en los centros activos del catalizador (fase metálica), donde se produce la deshidrogenación y, posteriormente, la reacción con vapor de agua (ec. 2.9) o con $CO_2$ (ec. 2.10) (Han y Kim, 2008). Entre los sólidos más estudiados para el reformado del alquitrán se pueden destacar algunos minerales y rocas naturales como la olivina, la dolomita o la calcita, y catalizadores preparados a base de metales alcalinos y metales de transición (Abu El-Rub y cols., 2004; Anis y Zainal, 2011; De Lasa y cols., 2011; Sutton y cols., 2001a). La dolomita calcinada ha sido uno de los minerales más estudiados, mostrando conversiones de alquitrán superiores al 95% en determinadas condiciones (Delgado y cols., 1997). Para mayores niveles de pureza, los catalizadores basados en metales de transición, y especialmente los catalizadores de níquel, ofrecen una buena alternativa. A temperaturas superiores a 740 ºC, los catalizadores de níquel no sólo favorecen la eliminación del alquitrán, sino también el reformado del metano con vapor (ec. 2.7) y el ajuste de la relación $H_2$/CO a través de la reacción *water-gas shift* (ec. 2.6) (Sutton y cols., 2001a). Conversiones de alquitrán del 98-99% han sido obtenidas con catalizadores de níquel utilizados comercialmente para otros procesos de reformado con vapor (Aznar y cols., 1998; Zhang y cols., 2004). Sin embargo, la desactivación de este tipo de catalizadores es uno de los principales inconvenientes para su aplicación en la gasificación a gran escala. Los fenómenos de desactivación más habituales en

este tipo de catalizadores son: (i) la sinterización, que se produce en condiciones severas de temperatura e implica la migración de pequeñas partículas de níquel dispersas sobre la superficie del catalizador para formar partículas más grandes, disminuyendo así la presencia de centros activos; (ii) la deposición de carbono sobre los centros activos, que cobra especial importancia cuando el contenido de alquitrán en el gas es alto; algunos estudios apuntan a un valor límite de 2 $g \cdot m^{-3}N$ para evitar en gran medida este fenómeno (Aznar y cols., 1998); y (iii) el envenenamiento de los centros activos debido a la presencia de impurezas en el gas de gasificación, como cloro o azufre (Abu El-Rub y cols., 2004; Anis y Zainal, 2011; De Lasa y cols., 2011; Sutton y cols., 2001a).

Buena parte de la literatura existente acerca del craqueo catalítico de alquitrán se centra en la preparación y modificación de catalizadores de níquel con diferentes soportes y promotores para mejorar su actividad y estabilidad. El soporte del catalizador juega un papel clave en la dispersión de la fase activa. Diferentes óxidos metálicos ($Al_2O_3$, MgO, $ZrO_2$, $TiO_2$, $SiO_2$ o $CeO_2$) y materiales naturales (dolomita, olivina o carbón activo) han sido utilizados como soporte en la preparación de catalizadores de níquel (Courson y cols., 2000; Kimura y cols, 2006; Li y cols., 2009b; Miyazawa y cols., 2006; Park y cols., 2010; Sato y Fujimoto, 2007; Srinakruang y cols., 2006; Wang y cols., 2005). Algunos estudios apuntan al conjunto níquel-alúmina ($Al_2O_3$) como uno de los catalizadores más eficaces para la eliminación de alquitrán (Sutton y cols., 2001b), aunque sin estar exento de desactivación (Swierczynski y cols., 2007). La incorporación de metales alcalinos (Na, K) o de elementos de transición (Ru, Rh, Mn, Mo, W, Zr, Mn) en catalizadores de níquel ha sido también objeto de muchos estudios, obteniendo en algunos casos resultados positivos en cuanto a la actividad, reducibilidad, regenerabilidad, propiedades mecánicas y resistencia frente a los fenómenos de desactivación, especialmente la debida a la deposición de carbono (Bona y cols., 2008; Dou y cols., 2003; Nishikawa y cols., 2008; Richardson y Grey, 1997; Seok y cols., 2002; Yung y cols., 2009; Zhang y cols., 2007).

Además de alquitrán, el gas procedente de la gasificación de biomasa o de residuos orgánicos puede contener otras impurezas como consecuencia de la propia composición de la materia prima. Es el caso del $H_2S$, que se forma durante la gasificación de materiales que contienen azufre (Meng y cols., 2010), como es el caso de los lodos de EDAR. La presencia de $H_2S$ en el gas de gasificación conlleva tanto problemas ambientales, relacionados con las emisiones de $SO_2$ en la combustión del gas, contribuyendo así a la lluvia ácida, como operacionales, relacionados con la corrosión de tuberías, motores y turbinas, y con la desactivación de los catalizadores de níquel utilizados para el craqueo del alquitrán. La presencia de $H_2S$ en los gases de gasificación ha dado lugar a diversos estudios para

profundizar en el fenómeno de envenenamiento de los catalizadores de níquel con azufre (Engelen y cols., 2003; Hepola y Simell, 1997a; Hepola y Simell, 1997b; Struis y cols., 2009). El azufre queda adsorbido en los catalizadores de níquel en diferentes estados químicos en función de las condiciones de operación. Aunque parte del azufre queda químicamente adsorbido de forma irreversible, otra parte puede desorberse a alta temperatura (900 ºC), lo que hace que el catalizador pueda recuperar parte de su actividad inicial cuando el $H_2S$ es eliminado de la corriente gaseosa (Hepola y Simell, 1997b). El envenenamiento de los catalizadores de níquel con $H_2S$ puede evitarse mediante el acondicionamiento previo del gas de gasificación, pero la incorporación de promotores que puedan mejorar su estabilidad en presencia de $H_2S$ resulta también un factor interesante. Ambos aspectos han sido abordados en esta Tesis.

Existen diversos tratamientos para la eliminación del $H_2S$ de corrientes gaseosas, tanto a baja como a alta temperatura. El lavado de los gases con disolventes básicos es uno de los procesos más utilizados en la industria química (Yildirim y cols., 2012). También el uso de carbones activos y del *char* procedente de procesos de pirólisis (incluyendo la pirólisis de lodos de EDAR) para la adsorción física de $H_2S$ ha sido ampliamente estudiado (Bagreev y Bandosz, 2005; Bandosz, 2002; Gutiérrez-Ortiz y cols., 2014; Primavera y cols., 1998; Ros y cols., 2006; Yuan y Bandosz, 2007). Ambos procesos requieren el enfriamiento del gas para la retención del $H_2S$, lo que resulta desfavorable desde el punto de vista energético. En cambio, con los procesos de desulfuración a alta temperatura se evita el enfriamiento del gas sólo para su limpieza, evitando también la condensación del alquitrán en el caso del gas de gasificación. Los procesos de desulfuración a alta temperatura se basan en la reacción química del $H_2S$ con determinados óxidos metálicos, de forma que el azufre queda retenido en forma de sulfuros metálicos. Los óxidos de zinc, manganeso, cobre, hierro y calcio son algunos de los óxidos con mayor capacidad para retener $H_2S$ (Álvarez-Rodríguez y Clemente-Jul, 2008; Cheah y cols., 2009; Elseviers y Verelst, 1999; Meng y cols., 2010; Park y cols., 2005; Tamhankar y cols., 1981; Westmoreland y Harrison, 1976), aunque todos ellos presentan límites de operación relacionados principalmente con el tipo de atmósfera reactiva y con la temperatura.

Dado el contenido metálico de la fracción inorgánica de la biomasa, el uso de las cenizas resultantes de los tratamientos termoquímicos para la desulfuración de gases a alta temperatura podría ser una opción interesante debido a su bajo coste. En el caso de los lodos de EDAR, en los que su fracción inorgánica se sitúa en torno al 40% con importantes contenidos de calcio y hierro (Manara y Zabaniotou, 2012), la reutilización de sus cenizas para la eliminación del $H_2S$ generado en el propio proceso supondría una ventaja desde el punto de

vista del aprovechamiento integral de los subproductos. En este contexto se desarrolló el último de los estudios que componen esta Tesis, en el que se utilizaron cenizas de combustión y de gasificación de lodo para la eliminación de $H_2S$ bajo distintas atmósferas gaseosas, continuando así con un trabajo previo desarrollado en el GPT (García y cols., 2011).

# 3. MATERIALES Y MÉTODOS

## 3.1. Materiales

### *3.1.1. Materia prima para la gasificación: lodos de EDAR y char de pirólisis del lodo*

Los residuos utilizados como materia prima para los experimentos de gasificación fueron el lodo procedente de la estación depuradora de aguas residuales de Butarque, en Madrid, y el *char* resultante de su proceso de pirólisis. En esta depuradora, las aguas son sometidas a un tratamiento de depuración mediante lodos activos y, posteriormente, los lodos se estabilizan mediante digestión anaerobia y son secados térmicamente. La muestra de lodo, recibida en forma granulométrica, se sometió a un proceso de molienda y tamizado hasta alcanzar un tamaño de partícula de 250-500 μm.

En la Tabla 3.1 se presenta una breve caracterización de ambos materiales. El análisis inmediato se realizó de acuerdo a las especificaciones de normas estándar (ISO-589-1981 para la humedad, ISO-1171-1976 para las cenizas, ISO-5623-1974 para la materia volátil). El análisis elemental (C, H, N, S) fue realizado en el *Servicio de Análisis del Instituto de Carboquímica (Zaragoza)*, utilizando un analizador elemental Carlo Erba EA1108. El poder calorífico superior de los sólidos (PCS) se midió en el laboratorio con un calorímetro IKA C-2000 y su capacidad calorífica específica (Cp) se determinó por calorimetría diferencial de barrido con un equipo Netzsch DSC 200 Maia (atmósfera inerte, 40 mL $N_2 \cdot min^{-1}$).

Tabla 3.1. Caracterización del lodo y del *char.*

| | Lodo | Char |
|---|---|---|
| Análisis inmediato (% másico, base húmeda) | | |
| Humedad | 6,48 | 1,70 |
| Cenizas | 39,04 | 74,20 |
| Volátiles | 50,09 | 15,02 |
| Carbono fijo (por diferencia) | 4,39 | 9,08 |
| Análisis elemental (% másico, base húmeda) | | |
| C | 29,50 | 15,49 |
| H | 4,67 | 0,97 |
| N | 5,27 | 1,85 |
| S | 1,31 | 0,35 |
| PCS ($MJ \cdot kg^{-1}$) | 12,8 | 5,2 |
| PCI ($MJ \cdot kg^{-1}$) | 11,8 | 5,0 |
| $Cp_{25ºC}$ ($kJ \cdot kg^{-1} \cdot K^{-1}$) | 1,15 | 0,82 |

El porcentaje másico de carbono fijo en el *char* (9,08%) se duplicó con respecto al valor inicial del lodo (4,39%) como consecuencia del tratamiento térmico de carbonización que, en mayor o menor medida, tiene lugar durante un proceso de pirólisis. Sólo el 15 % del carbono contenido en el lodo está en forma de carbono fijo, mientras que este valor alcanza el 59% en el *char*.

### *3.1.2. Cenizas de combustión y gasificación de lodos de EDAR*

Las cenizas resultantes de los procesos de gasificación y combustión del lodo anteriormente descrito han sido utilizadas para la retención de $H_2S$ bajo diferentes atmósferas gaseosas.

Para la obtención de las cenizas, la combustión del lodo se llevó a cabo en una mufla en atmósfera de aire, manteniendo una temperatura de 900 ºC durante dos horas (20 $ºC \cdot min^{-1}$). Por otro lado, las cenizas de gasificación utilizadas son el residuo sólido obtenido en uno de los experimentos de gasificación de lodo (experimento 5 en la Tabla 3.6). Ambas muestras de ceniza fueron caracterizadas mediante diversas técnicas. Los posibles restos de C, H, S y N se midieron con un analizador elemental Leco TruSpec Micro. Sus propiedades texturales (superficie específica, volumen de poro y tamaño medio de los poros) se determinaron a partir de isotermas de adsorción de $N_2$, utilizando un equipo Micromeritics TriStar II 3000 (métodos BET y BJH). Las muestras fueron previamente desgasificadas a 200 ºC durante 8 h bajo un flujo de $N_2$, y después las isotermas de adsorción-desorción se obtuvieron a -196 ºC y a temperatura ambiente, respectivamente. El contenido de metales en las muestras de ceniza fue determinado por el *Servicio de Análisis Químico de la Universidad de Zaragoza*, mediante espectroscopía de emisión atómica con plasma de acoplamiento inductivo (ICP-OES), utilizando un espectrómetro Thermo Elemental IRIS Intrepid. Las muestras fueron disueltas mediante digestión ácida en un sistema de reacción de microondas (CEM MARS). La Tabla 3.2 recoge los resultados de todos estos análisis.

Tabla 3.2. Caracterización de las cenizas de combustión y gasificación de lodos de EDAR.

| | Ceniza de combustión | Ceniza de gasificación |
|---|---|---|
| Análisis elemental (% másico, base húmeda) | | |
| C | 0,15 | 3,14 |
| H | n.d. | n.d. |
| N | 0,28 | 0,77 |
| S | 0,46 | 0,41 |
| Superficie específica ($m^2 \cdot g^{-1}$) | 6,5 | 6,7 |
| Volumen de poro ($cm^3 \cdot g^{-1}$) | 0,02 | 0,02 |
| Tamaño medio de poro (nm) | 12,0 | 10,9 |
| Contenido en metales ($mg \cdot g^{-1}_{ceniza}$) | | |
| Al | 52 | 61 |
| Ca | 65 | 84 |
| Fe | 192 | 116 |
| K | 14 | n.a. |
| P | 63 | 51 |
| Mg | 17 | n.a. |
| Na | 4 | n.a. |
| Si | 122 | n.a. |
| Ti | 4 | n.a. |

n.d.: no detectado; n.a.: no analizado.

Como se observa en la Tabla 3.2, el análisis elemental de la ceniza de gasificación muestra un mayor contenido de carbono como consecuencia de la incompleta conversión del contenido orgánico del lodo durante el proceso de gasificación. Ambas cenizas presentan además una pequeña fracción de azufre antes de su uso como material desulfurante (en torno a 0,4%). Las propiedades texturales de ambos sólidos son muy pobres, pero su potencial como material desulfurante radica en su contenido metálico. Entre los metales analizados por ICP-OES, los elementos mayoritarios fueron Fe, Si, Al y Ca. Entre ellos, la reacción de los óxidos de hierro y calcio con $H_2S$ está termodinámicamente favorecida en determinadas condiciones de operación (Westmoreland y Harrison, 1976). Por otro lado, las diferencias observadas en el contenido metálico de ambos sólidos ponen de manifiesto que la fracción inorgánica del lodo no permanece completamente inerte durante los procesos de combustión y gasificación. Especialmente notable es la diferencia observada en el contenido de hierro, que podría explicarse teniendo en cuenta que parte del contenido inicial de hierro en el lodo puede estar en forma de cloruro de hierro ($FeCl_3$) como consecuencia de la utilización de este compuesto como agente coagulante en el tratamiento de las aguas residuales. Durante la combustión, el exceso de oxígeno favorece la retención del hierro en el sólido en forma de óxidos. Sin embargo, durante el proceso de gasificación, la escasa presencia de oxígeno limita la conversión total del $FeCl_3$ a óxidos de hierro. Esto puede provocar que, dado que el punto de

ebullición del $FeCl_3$ se sitúa en torno a 315 ºC, parte del contenido inicial del hierro en el sólido abandone el reactor junto con el gas.

Otro de los análisis realizados a las cenizas de lodo antes de su uso en las pruebas de desulfuración fue la determinación de su estructura cristalina mediante difracción de rayos X (XRD). Este análisis fue realizado por el *Servicio de Difracción de Rayos X y Análisis por Fluorescencia de la Universidad de Zaragoza*, utilizando un difractómetro Rigaku D-Max, equipado con un ánodo de cobre (tensión de 40 kV y corriente de 80 mA). Las mediciones se realizaron en el intervalo de 5º a 95º del ángulo de Bragg (2Θ), con una velocidad de barrido de $0.03^{o}\cdot s^{-1}$. La detección de las fases cristalinas se realizó de acuerdo con la base de datos del *Centro Internacional de Datos de Difracción (JCPDS, 2000).* En la Figura 3.1 se muestran los dos difractogramas XRD obtenidos para ambas muestras de ceniza. Especies como el cuarzo, la calcita, óxidos de hierro y diferentes fosfatos de calcio y hierro han sido detectadas mediante esta técnica. El estado de oxidación del hierro es una de las principales diferencias en la estructura cristalina de ambos sólidos. El hierro aparece en forma de hematita ($Fe_2O_3$) en la ceniza de combustión y en forma de magnetita ($Fe_3O_4$) en la ceniza de gasificación, debido a la menor disponibilidad de oxígeno en este segundo caso. Coherentemente, el color rojizo característico de la hematita sólo se observó en las cenizas de combustión.

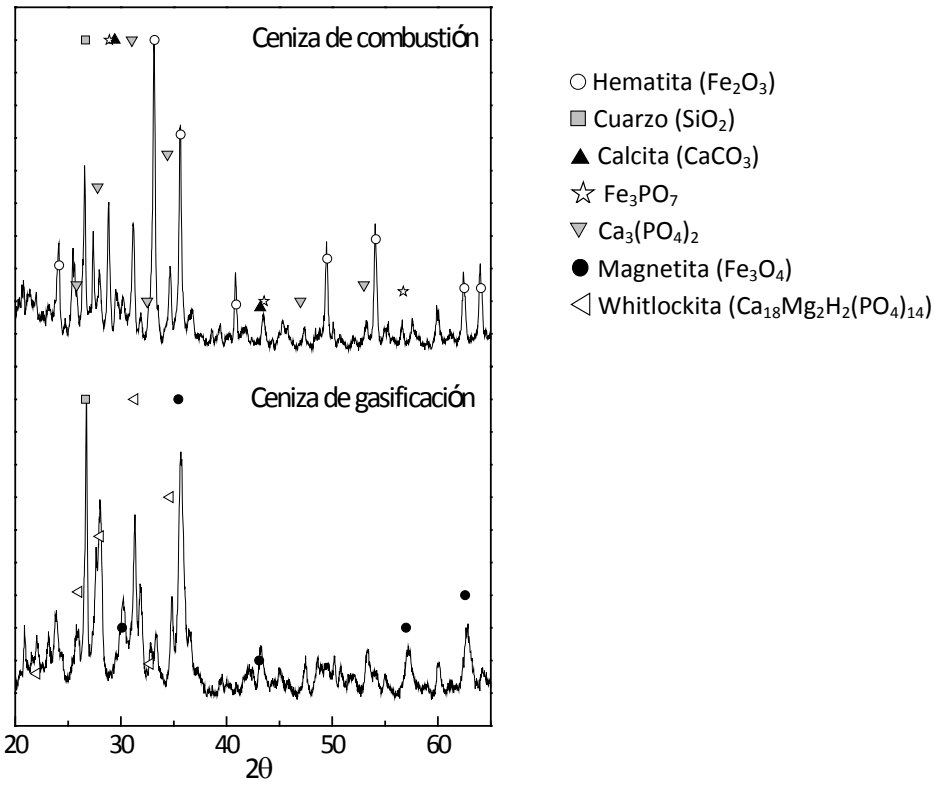


Figura 3.1. Difractogramas XRD de las cenizas de combustión y gasificación de lodo.

### *3.1.3. Catalizadores de níquel*

Se prepararon diferentes catalizadores de níquel soportados sobre alúmina ($Ni/Al_2O_3$) mediante la incorporación de Fe, Ca, Mn o Cu con el fin de evaluar el efecto de estos promotores en la estabilidad y actividad del catalizador para el reformado de alquitrán en presencia de $H_2S$. La elección de estos metales se basó en la capacidad de sus óxidos para reaccionar con $H_2S$ (Westmoreland y Harrison, 1976). En el caso de que la reacción del $H_2S$ con el promotor se viera favorecida frente a su reacción con los centros activos de níquel cabría esperar una disminución, o al menos un retardo, en la desactivación del catalizador.

Los catalizadores fueron preparados en el laboratorio por el método de impregnación por humedad incipiente de $\gamma$-$Al_2O_3$ (250-315 μm) con las disoluciones acuosas de los correspondientes nitratos de los metales de interés: $Ni(NO_3)_2{\cdot}6H_2O$, $Ca(NO_3)_2{\cdot}4H_2O$, $Fe(NO_3)_3{\cdot}9H_2O$, $Cu(NO_3)_2{\cdot}3H_2O$ y $Mn(NO_3)_2{\cdot}4H_2O$. Tanto el nitrato de níquel como el nitrato de cada promotor se disolvieron en una única disolución y se impregnaron sobre la $Al_2O_3$ en un solo paso. Después de la impregnación, el sólido se secó en una estufa a 110 ºC durante 24 h y, después, se calcinó en una mufla, en atmósfera de aire, de acuerdo con la siguiente rampa de temperatura: 120 ºC durante 20 min, 200 ºC durante 30 min, 320 ºC durante 90 min y, por último, 700 ºC o 900 ºC durante 120 minutos. La temperatura final de calcinación se varió entre 700 y 900 ºC para evaluar su influencia sobre la actividad y estabilidad del catalizador. La fracción másica de cada metal en los catalizadores fue de un 8% (tanto de níquel como de cada promotor). Las propiedades texturales y los difractogramas XRD de los sólidos calcinados se obtuvieron de forma análoga a la descrita en la sección 3.1.2 para las cenizas de lodo. Los resultados obtenidos se muestran en la Tabla 3.3 y en la Figura 3.2, respectivamente.

Tabla 3.3. Propiedades texturales de los catalizadores calcinados.

| | Tª final de calcinación | $Ni/Al_2O_3$ | $Ni/Ca/Al_2O_3$ | $Ni/Fe/Al_2O_3$ | $Ni/Cu/Al_2O_3$ | $Ni/Mn/Al_2O_3$ |
|---|---|---|---|---|---|---|
| Superficie específica ($m^2{\cdot}g^{-1}$) | 700 ºC | 120,5 | 61,7 | 108,1 | 105,1 | 96,6 |
| | 900 ºC | 96,4 | 52,7 | 72,6 | 62,4 | 71,2 |
| Volumen de poro ($cm^3{\cdot}g^{-1}$) | 700 ºC | 0,35 | 0,24 | 0,31 | 0,32 | 0,28 |
| | 900 ºC | 0,33 | 0,22 | 0,25 | 0,25 | 0,25 |
| Tamaño medio de poro (nm) | 700 ºC | 11,1 | 15,1 | 11,0 | 11,8 | 11,3 |
| | 900 ºC | 13,2 | 16,3 | 13,5 | 15,7 | 13,7 |

La adición de los promotores supuso una importante reducción de la superficie específica del catalizador, así como una disminución en el volumen de poro. Esto parece indicar un exceso de carga metálica en los catalizadores modificados. La adición de calcio ($Ni/Ca/Al_2O_3$) dio lugar a la mayor pérdida de superficie específica (reducción del 50%), al mayor tamaño

medio de poro y al menor volumen de poro. Las propiedades texturales también se vieron afectadas por la temperatura final de calcinación. La superficie específica se redujo y el tamaño medio de poro aumentó al aumentar la temperatura de 700 a 900 ºC debido, probablemente, a la sinterización de las partículas metálicas.

A modo de ejemplo, la Figura 3.2 muestra los difractogramas XRD de dos de los catalizadores calcinados a 700 y 900 ºC ($Ni/Mn/Al_2O_3$ y $Ni/Cu/Al_2O_3$). Las muestras son poco cristalinas y apenas se observan diferencias en los difractogramas de los catalizadores preparados a la misma temperatura final de calcinación, independientemente del metal añadido como promotor. La fase mayoritaria en las muestras calcinadas a 700 ºC fue la $\gamma$-$Al_2O_3$. La anchura de los picos correspondientes a esta fase dificulta la detección de otros óxidos metálicos que cabría esperar encontrar en las muestras, como el NiO. Como excepción, la muestra de $Ni/Cu/Al_2O_3$ calcinada a 700 ºC mostró dos picos de difracción a 35,6º y 38,8º, que se corresponden con el CuO. El aumento de la temperatura de calcinación hasta 900 ºC supuso una mayor cristalinidad de los sólidos (picos un poco más estrechos y definidos). El $NiAl_2O_4$ aparece como la fase mayoritaria en todas estas muestras. La identificación de otros posibles aluminatos presentes en las muestras es difícil, ya que todos ellos son fases de tipo espinela y presentan patrones XRD muy similares entre sí y al de la alúmina.

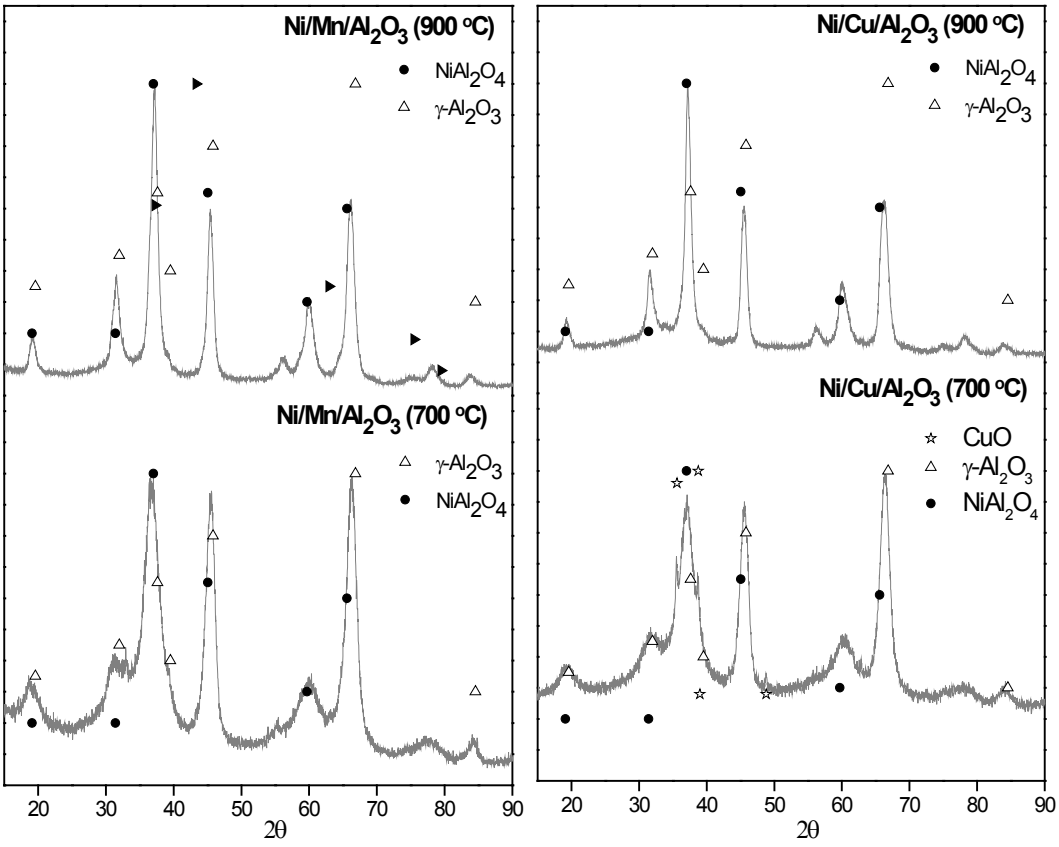


Figura 3.2. Difractogramas XRD de los catalizadores $Ni/Mn/Al_2O_3$ y $Ni/Cu/Al_2O_3$ calcinados a 900 y 700 ºC.

## 3.2. Instalaciones y procedimiento experimental

### *3.2.1. Sistema experimental para la gasificación*

Los experimentos de gasificación de lodo de EDAR y de su *char* de pirólisis se llevaron a cabo en un reactor de lecho fluidizado a escala de laboratorio (< 1 kg·h$^{-1}$), operando a presión atmosférica. La Figura 3.3 muestra un esquema de la configuración experimental utilizada.

La pirólisis del lodo, en la que se obtuvo el *char* posteriormente gasificado, se llevó a cabo en una instalación similar a la que se muestra en la Figura 3.3. Se utilizó $N_2$ como agente fluidizante (velocidad de fluidización unas 8 veces mayor que la velocidad de mínima fluidización) y la temperatura de pirólisis fue de 530 ºC. El tiempo medio de residencia del sólido en el reactor fue de unos 8 min y el de los gases y vapores producidos de 1 s.

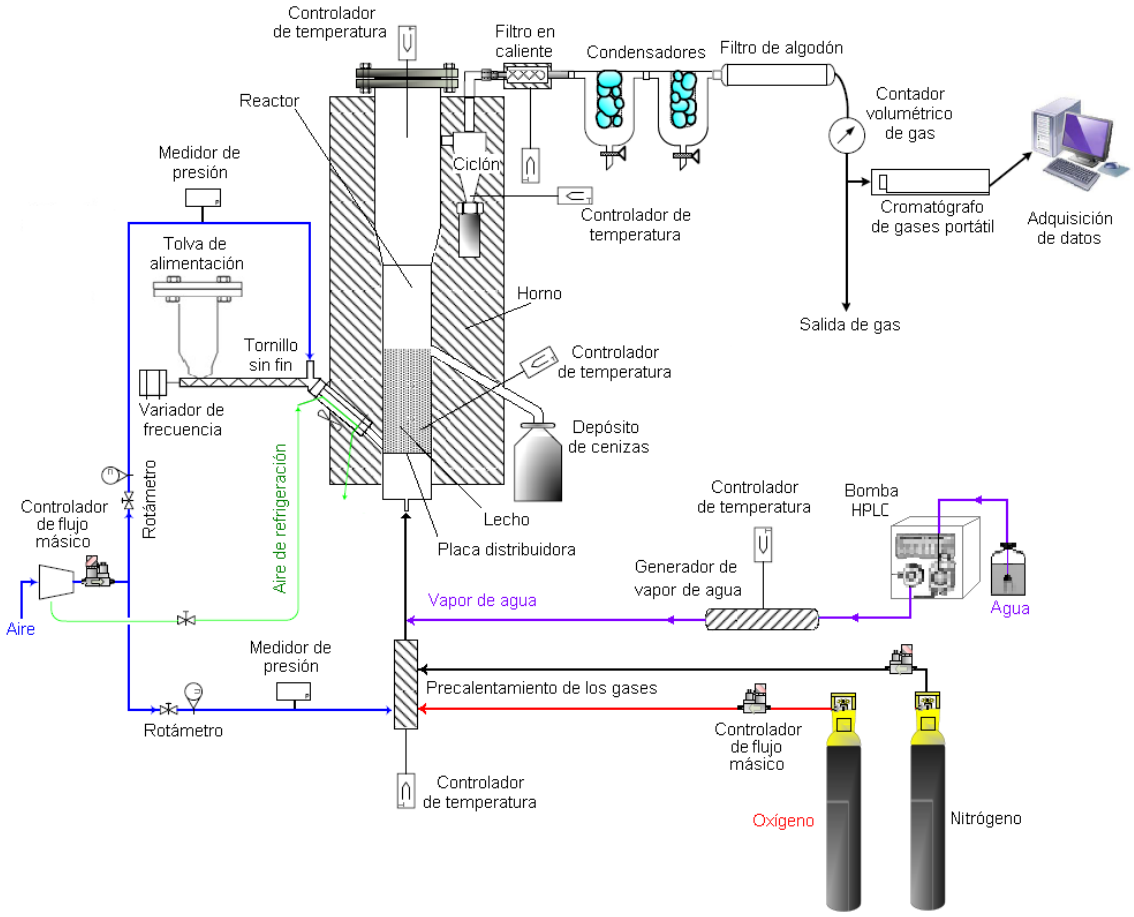


Figura 3.3. Instalación experimental de gasificación.

El gasificador es un reactor tubular construido en acero refractario AISI-310. El cuerpo del reactor mide unos 127 cm y su sección varía a lo largo del mismo dividiendo el reactor en dos zonas: una zona para el lecho (4 cm de diámetro interno) y una zona *"freeboard"* (7 cm de diámetro interno). El reactor se calienta mediante un horno eléctrico, que cuenta con tres

zonas de calentamiento independientes (lecho, *freeboard* y ciclón), midiendo la temperatura en cada una de ellas con termopares tipo K y utilizando controladores PID para su control.

La materia prima sólida se encuentra almacenada en una tolva. El giro del tornillo sinfín de la tolva, que se acciona mediante un motor controlado con un variador de frecuencia, permite la alimentación del sólido en continuo. La alimentación procedente de la tolva entra a la parte inferior del lecho a través de una tubería inclinada unos 45º. Para evitar la descomposición del sólido antes de su llegada al lecho, dicha conducción se refrigera mediante la circulación de aire a través de una camisa externa al tubo. El caudal de alimentación de sólido se fijó en torno a 2,1 $g \cdot min^{-1}$ en todos los experimentos de gasificación (mínimo valor conseguido con el sistema de alimentación).

Como lecho inicial para empezar cada experimento se utilizó ceniza de lodo obtenida en experimentos anteriores (alrededor de 120 g). Gracias a una tubería lateral, situada unos 30 cm por encima de la placa distribuidora, las cenizas acumuladas en el lecho durante el experimento pueden abandonar el reactor por efecto rebosadero.

El efecto de la atmósfera reactiva en el proceso de gasificación se evaluó utilizando diferentes mezclas de vapor de agua y aire como agente gasificante/fluidizante. En los casos con mayor necesidad de oxígeno, la corriente de aire se enriqueció con oxígeno puro para mantener una velocidad de fluidización similar en todos los experimentos realizados con el mismo material. Esta velocidad de fluidización fue 5-7 veces mayor que la velocidad de mínima fluidización durante la gasificación de lodo y 2-3 veces mayor durante la gasificación de *char*. El menor contenido orgánico en el *char* justifica la menor necesidad de agente gasificante y, por tanto, esta diferencia en la velocidad de fluidización.

Los caudales de gas (aire y oxígeno) se ajustan mediante controladores de flujo másico, mientras que el caudal de agua se regula mediante una bomba HPLC, y se evapora antes de su entrada al reactor. La mayor parte del agente gasificante se alimenta a través de la placa distribuidora situada en la parte inferior del reactor, pero una parte del aire (en torno a un tercio del caudal requerido) se desvía hacia el sistema de alimentación de sólido para facilitar su movimiento a través de la tubería. Las dos entradas de aire cuentan con manómetros que permiten observar posibles aumentos de presión producidos por obstrucciones o taponamiento en el sistema.

El tiempo de residencia de los vapores y gases en el reactor fue de alrededor de 7-8 s durante la gasificación de lodo, y de 17-18 s durante la gasificación de *char*, debido al menor caudal de gas utilizado. A su salida del reactor, la corriente de gas pasa a través de un ciclón y

de un filtro caliente (ambos a 450 ºC para evitar la condensación de los alquitranes), en los que se recogen las partículas sólidas arrastradas por el gas. A continuación, los gases y vapores pasan a través de dos condensadores enfriados con un baño de hielo, donde condensan el agua y el alquitrán. Para evitar daños en los siguientes dispositivos, un filtro de algodón situado detrás de los condensadores retiene los posibles aerosoles arrastrados por la corriente de gas. Después, el volumen de gas seco y libre de partículas y alquitranes se mide con un contador volumétrico (G4 Gallus 2000) y su composición se analiza en línea utilizando un cromatógrafo de gases portátil (Agilent 3000-A, con una columna tipo Plot U y otra de tamiz molecular), calibrado para determinar los porcentajes volumétricos de $H_2$, CO, $CO_2$, $CH_4$, $C_2H_4$, $C_2H_6$, $C_2H_2$, $N_2$ y $H_2S$. Los experimentos tuvieron una duración de 90 min en el caso de la gasificación de lodo y de 60 min en la gasificación de *char* (menor disponibilidad de material). Una vez finalizado cada experimento, el rendimiento a los productos sólido y líquido se determinó por diferencia de pesada de los dispositivos de recogida antes y después del experimento. Ambos productos fueron caracterizados por diferentes técnicas.

La fracción líquida se recuperó de los condensadores utilizando metanol como disolvente para su lavado. Su contenido de agua se determinó mediante valoración Karl Fischer (equipo Mettler Toledo V20), de modo que la cantidad de alquitrán presente en la muestra podía determinarse por diferencia, descontando también la cantidad de metanol añadido para el lavado de los condensadores. Además, la cantidad de carbono orgánico presente en las muestras líquidas se midió con un analizador de carbono orgánico total (analizador TOC-L CSH/CSN Shimadzu), obteniendo así otra idea aproximada del contenido de alquitrán. Por último, la composición del alquitrán (sólo del producido en la gasificación del lodo) se analizó de forma cualitativa mediante un sistema de cromatografía de gases que combina un espectrómetro de masas y un detector de ionización de llama (cromatógrafo Agilent 5975C GC/MSD combinado con Agilent 7890A GC).

Respecto al producto sólido, su composición elemental (C, H, N, S) se determinó con un analizador elemental Leco TruSpec Micro y su contenido en ceniza se determinó de acuerdo con una norma estándar (ISO 1171-1976).

### *3.2.2. Sistema experimental para los ensayos de retención de $H_2S$*

Las pruebas de desulfuración se realizaron en una instalación experimental más pequeña que la anterior, utilizando un reactor tubular de cuarzo (40 cm de longitud y 1 cm de diámetro interno) y operando a presión atmosférica y en configuración de lecho fijo. La Figura 3.4 muestra un esquema de la instalación utilizada.

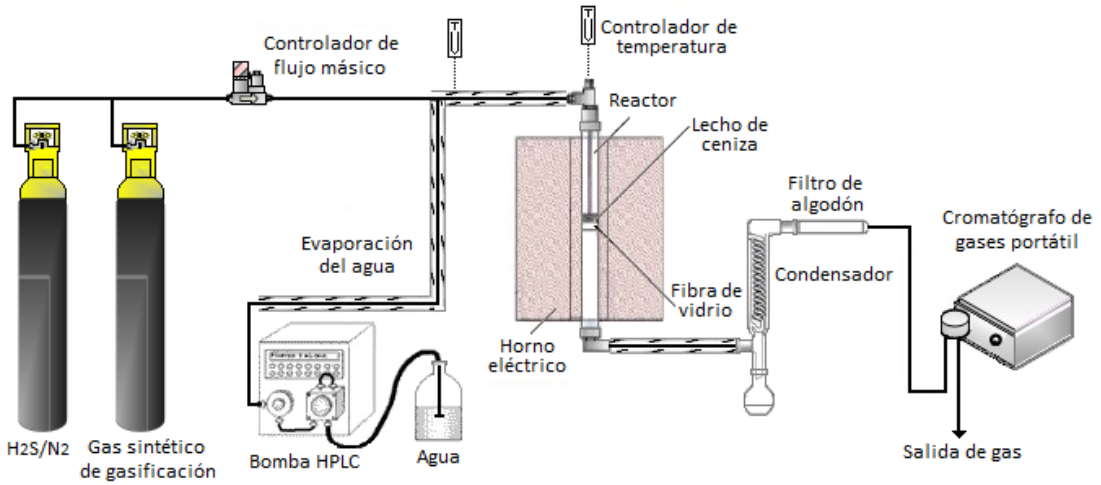


Figura 3.4. Instalación experimental para las pruebas de desulfuración.

En cada experimento se utilizó 1 g de sólido desulfurante (ceniza de combustión o de gasificación de lodo). El sólido se introduce en el reactor apoyado sobre un poco de lana de vidrio a una distancia de unos 18 cm desde la parte superior del reactor (donde no hay gradientes importantes de temperatura). El reactor se coloca en el interior de un horno cilíndrico. La temperatura del sólido se mide con un termopar tipo K (1/16“ de diámetro) cuyo extremo se sitúa en el interior del lecho, y se controla con un sistema de control PID.

El gas se alimenta por la parte superior del reactor y sale por la parte inferior de éste. El caudal de gas se ajusta con un controlador de flujo másico. Dicho caudal fue de 50 mLN·min$^{-1}$ en todos los experimentos. Se utilizaron dos gases diferentes con el fin de evaluar el efecto de la atmósfera reactiva en el proceso de desulfuración. Uno de ellos era una mezcla que contenía sólo $H_2S$ y $N_2$ (5000 ppm $H_2S$), lo que permitía estudiar el proceso sin la interferencia de ningún otro gas. La otra mezcla gaseosa utilizada fue un gas sintético de composición similar a la de un gas de gasificación, con 5000 ppm de $H_2S$, lo que permitía simular condiciones más reales para la eliminación de $H_2S$. La composición de ambos gases se muestra en la Tabla 3.4.

Tabla 3.4. Composición de los gases utilizados en las pruebas de desulfuración (% vol., base seca).

| | Mezcla $H_2S/N_2$ | Gas sintético de gasificación |
|---|---|---|
| CO | -- | 10,0 |
| $CO_2$ | -- | 15,0 |
| $H_2$ | -- | 10,0 |
| $CH_4$ | -- | 4,0 |
| $C_2H_6$ | -- | 0,2 |
| $C_2H_4$ | -- | 1,5 |
| $C_2H_2$ | -- | 0,2 |
| $H_2S$ | 0,5 | 0,5 |
| $N_2$ | 99,5 | 58,6 |

Dado que los gases de gasificación presentan cierto contenido en humedad, en algunos experimentos se añadió vapor de agua junto con el gas para analizar su impacto en la capacidad desulfurante de las cenizas. El caudal de agua líquida (0-1 $g \cdot h^{-1}$) se reguló con una bomba HPLC y se evaporó antes de su entrada al reactor. El tiempo de contacto gas-sólido se eligió en base a experimentos anteriores (García y cols., 2011) y una vez que se hubo comprobado que no existía control difusional externo en el proceso (se obtuvieron resultados muy similares para distintos caudales de gas). La velocidad espacial del gas varió entre 3,7 y 4,7 $h^{-1}$ (en términos de volumen) según el caudal de vapor de agua alimentado.

A la salida del reactor se colocaron en serie un pequeño condensador y un filtro de algodón para retener la humedad del gas, evitando así que pudiese dañar el cromatógrafo de gases (Agilent 3000-A) utilizado para analizar la composición del gas de salida. El análisis en modo casi continuo de la concentración del gas permite obtener las llamadas "*curvas de ruptura*" para el $H_2S$, en las que se representa la evolución de su caudal (o concentración) con el tiempo. El caudal de $H_2S$ que abandona el reactor puede calcularse a partir de los datos de composición, utilizando el nitrógeno de los gases como estándar interno debido a su carácter inerte en el proceso. El tiempo de reacción establecido inicialmente fue de 120 min, pero en algunos casos el experimento se alargó más de 300 min hasta detectar el punto de ruptura de las curvas (momento en el que la presencia de $H_2S$ en el gas comienza a ser significativa). Como referencia para el punto de ruptura se eligió una concentración de $H_2S$ de 100 ppm, valor intermedio entre los límites fijados habitualmente en la literatura para, por ejemplo, la aplicación del gas de gasificación en turbinas de gas (20-750 ppm) (Meng y cols., 2010).

Tras los experimentos, la cantidad de azufre retenido en las muestras de ceniza se determinó con un analizador elemental Leco TruSpec Micro. Además, a modo de ejemplo, una de las muestras fue caracterizada morfológica- y químicamente mediante otras técnicas: (i) microscopía electrónica de barrido combinada con espectroscopía de energía dispersiva de rayos X (SEM/EDX), y (ii) espectroscopía fotoelectrónica de rayos X (XPS). Ambos análisis fueron realizados por el *Laboratorio de Microscopía Avanzada del Instituto de Nanociencia de Aragón*. El análisis SEM/EDX fue realizado con un microscopio FEI Inspeccione F50, sin aplicar revestimiento metálico externo a la muestra sólida. Para el análisis EDX se utilizó el modo de imagen de electrones retrodispersados. Por otro lado, el análisis XPS se realizó con un espectrómetro Kratos AXIS Ultra DLD, utilizando una fuente de rayos X monocromática Al Kα (1486,6 eV) y una presión en la cámara de medida de $3 \cdot 10^{-8}$ Pa.

### *3.2.3. Sistema experimental para los ensayos de actividad de los catalizadores*

Esta parte del trabajo experimental fue desarrollada durante una estancia de investigación en el *VTT-Technical Research Centre of Finland*. El objetivo del estudio fue la evaluación de la actividad y estabilidad de varios catalizadores de níquel soportados sobre alúmina y modificados con diferentes promotores para el reformado de compuestos modelo de alquitrán en presencia de $H_2S$. Estos ensayos de actividad se realizaron en un reactor de cuarzo de lecho fijo a escala de laboratorio (1 cm de diámetro interno), operando a presión atmosférica y en un intervalo de temperatura de 700-900 ºC. La Figura 3.5 muestra un esquema de la instalación experimental.

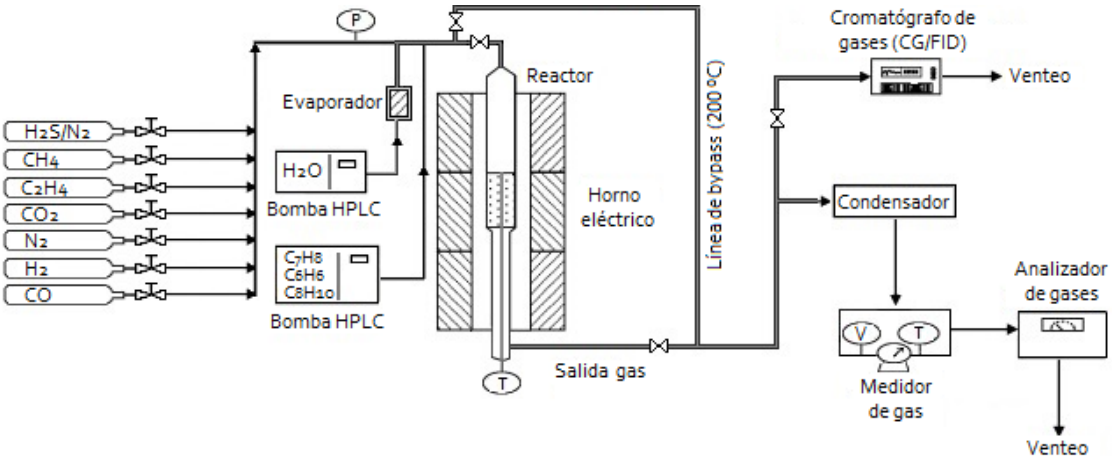


Figura 3.5. Instalación experimental para los ensayos de actividad de los catalizadores para el reformado de compuestos modelo de alquitrán.

El reactor de cuarzo cuenta con una placa fritada en su interior para soportar el lecho de sólido. En cada experimento se utilizaron 2 g de catalizador. El reactor se calienta dentro de un horno eléctrico cilíndrico y la temperatura del lecho se controla gracias a un termopar tipo K introducido en su interior. Además, para evitar condensaciones en las líneas de la instalación, la temperatura de las mismas se mantenía siempre a 200 ºC.

Para simular el gas obtenido en el proceso de gasificación de lodos de EDAR se utilizó una mezcla de gases (CO, $CO_2$, $H_2$, $N_2$, $CH_4$ y $C_2H_4$), vapor de agua y compuestos modelo de alquitrán habitualmente presentes en los gases de gasificación (tolueno, benceno y naftaleno), con una concentración de 15 $g \cdot m^{-3}N$. La composición de la mezcla utilizada se detalla en la Tabla 3.5. El caudal de los distintos gases se ajustó mediante controladores de flujo másico, mientras que el caudal de los líquidos (agua y mezcla de alquitrán) se reguló mediante sendas bombas HPLC. El caudal total alimentado fue de 1 $LN \cdot min^{-1}$, lo que dio lugar a una elevada velocidad espacial del

gas (25000 $h^{-1}$ en condiciones normales de presión y temperatura) con el objetivo de fomentar la desactivación del catalizador para profundizar en su estudio.

Tabla 3.5. Composición de la mezcla sintética de gases y vapores utilizada en los ensayos de actividad.

| | % vol. |
|---|---|
| $H_2O$ | 30,0 |
| CO | 6,6 |
| $CO_2$ | 12,5 |
| $H_2$ | 13,6 |
| $CH_4$ | 2,2 |
| $C_2H_4$ | 1,1 |
| $H_2S$ | 0,3 |
| $N_2$ | 33,4 |
| Contenido de alquitrán en el gas | 15 $g \cdot m^{-3}N$ |
| Composición del alquitrán | tolueno/naftaleno/benceno 80/10/10 (% másico) |

La corriente de gases y vapores que sale del reactor se analiza en línea con un cromatógrafo de gases equipado con un detector de ionización de llama (Agilent 7980A), calibrado para la cuantificación del benceno, tolueno, naftaleno, metano y etileno. La duración de cada análisis era de unos 33 min. A continuación, los compuestos condensables se retienen en un sistema de condensación formado por dos frascos lavadores con isopropanol y agua, respectivamente, colocados en serie y refrigerados en un baño de hielo. Tras secar el gas, se mide su caudal y su correspondiente temperatura, y se dirige a un analizador de gases (Sick Maihak S710), que mide de forma continua la fracción volumétrica de CO, $CO_2$ e $H_2$.

Antes de comenzar cada experimento, se determinó también la composición exacta del gas que iba a ser alimentado al reactor para comprobar que era la correcta.

Las muestras usadas de catalizador fueron caracterizadas mediante difracción de rayos X y análisis de su composición elemental, utilizando los mismos equipos que para la caracterización de las cenizas de lodo (sección 3.1.2).

## 3.3. Condiciones de operación y diseño de experimentos

### *3.3.1. Experimentos de gasificación*

El estudio de la influencia de algunos factores de operación en la distribución de productos y calidad del gas producto obtenido tanto en la gasificación de lodo como en la gasificación de *char* se realizó planteando un diseño de experimentos factorial $2^k$, siendo 2 el número de niveles (o valores) de cada factor y k el número de factores. Este diseño experimental permite evaluar no sólo el impacto de los factores de operación, sino también la posible existencia de interacciones entre ellos, lo que significa que el efecto de un factor sobre

una variable respuesta está condicionado por el valor de otro factor. El error experimental se evaluó mediante tres réplicas realizadas en el punto central del diseño (valor medio de todos los factores), lo que también permite evaluar la linealidad o la curvatura en la respuesta de las variables analizadas.

Los tres factores de operación modificados durante los experimentos de gasificación fueron, en ambos casos, los siguientes: (i) temperatura de gasificación (770-850 ºC); (ii) relación gasificante (RG), que es la cantidad de agente gasificante ($H_2O+O_2$) alimentado por unidad de masa de lodo o *char* en base seca y libre de cenizas (0,8-1,1 $g \cdot g^{-1}_{org}$); y (iii) la composición del medio de gasificación, representada por la relación $H_2O/O_2$ (1-3 $mol \cdot mol^{-1}$). Estos tres factores y sus respectivos intervalos de estudio se eligieron en base a otros trabajos publicados en la bibliografía sobre gasificación de biomasa con mezclas de aire y vapor de agua en lecho fluidizado (Campoy y cols., 2009; Gil y cols., 1997; Lv y cols., 2004; Pinto y cols., 2003), y teniendo en cuenta también los resultados de estudios previos realizados en el GPT, el régimen de fluidización en el que se desea trabajar y los límites operacionales de la planta experimental. Las condiciones de operación en los experimentos de gasificación se resumen en la Tabla 3.6.

Tabla 3.6. Condiciones de operación en los experimentos de gasificación de lodo y de *char*.

| **Gasificación de lodo de EDAR** | | | | | | | |
|---|---|---|---|---|---|---|---|
| Núm. exp. | (T, RG, $H_2O/O_2$) valores codificados | T (ºC) | RG ($g \cdot g^{-1}_{org}$) | $H_2O/O_2$ | RE (%) | S/B ($g_{H2O} \cdot g^{-1}_{org}$) | % vol. $O_2$ en el aire/ aire enriquecido |
| 1 | 1,1,1 | 850 | 1,1 | 3 | 17 | 0,71 | 21 |
| 2 | -1,1,1 | 770 | 1,1 | 3 | 17 | 0,71 | 21 |
| 3 | 1,-1,1 | 850 | 0,8 | 3 | 12 | 0,52 | 21 |
| 4 | -1,-1,1 | 770 | 0,8 | 3 | 12 | 0,52 | 21 |
| 5 | 1,1,-1 | 850 | 1,1 | 1 | 32 | 0,39 | 33 |
| 6 | -1,1,-1 | 770 | 1,1 | 1 | 32 | 0,39 | 33 |
| 7 | 1,-1,-1 | 850 | 0,8 | 1 | 23 | 0,27 | 27 |
| 8 | -1,-1,-1 | 770 | 0,8 | 1 | 23 | 0,27 | 27 |
| 9,10,11 | 0,0,0 | 810 | 0,95 | 2 | 19 | 0,52 | 23 |
| **Gasificación de *char* de pirólisis de lodo** | | | | | | | |
| Núm. exp. | (T, RG, $H_2O/O_2$) valores codificados | T (ºC) | RG ($g \cdot g^{-1}_{org}$) | $H_2O/O_2$ | RE (%) | S/B ($g_{H2O} \cdot g^{-1}_{org}$) | % vol. $O_2$ en el aire/ aire enriquecido |
| 12 | 1,1,1 | 850 | 1,1 | 3 | 17 | 0,71 | 27 |
| 13 | -1,1,1 | 770 | 1,1 | 3 | 17 | 0,71 | 27 |
| 14 | 1,-1,1 | 850 | 0,8 | 3 | 12 | 0,52 | 21 |
| 15 | -1,-1,1 | 770 | 0,8 | 3 | 12 | 0,52 | 21 |
| 16 | 1,1,-1 | 850 | 1,1 | 1 | 32 | 0,39 | 40 |
| 17 | -1,1,-1 | 770 | 1,1 | 1 | 32 | 0,39 | 40 |
| 18 | 1,-1,-1 | 850 | 0,8 | 1 | 23 | 0,27 | 33 |
| 19 | -1,-1,-1 | 770 | 0.,8 | 1 | 23 | 0,27 | 33 |
| 20,21,22 | 0,0,0 | 810 | 0,95 | 2 | 19 | 0,52 | 29 |

*RE (relación equivalente): porcentaje del aire estequiométrico alimentado realmente*

*S/B: cantidad de vapor de agua alimentado por unidad de masa de lodo o char seco y libre de cenizas.*

La segunda columna de la Tabla 3.6 muestra el valor de los factores en términos codificados, siendo -1 el límite inferior y 1 el límite superior del intervalo de estudio de cada factor (y 0 el punto central). Esta es la forma habitual de expresar el valor de los factores en el diseño de experimentos factorial $2^k$, ya que permite una rápida identificación del factor con mayor influencia sobre cada variable respuesta.

Los resultados experimentales obtenidos para cada variable respuesta han sido analizados estadísticamente mediante análisis de varianza (ANOVA). Este análisis se basa en la comparación de la varianza asociada al error experimental con la varianza ocasionada por la modificación de los factores. La comparación se realiza mediante el test F de Fischer y permite discriminar si el efecto observado es estadísticamente significativo frente al error experimental con un inivel de confianza predeterminado (95% en este estudio). El análisis ANOVA se realizó con el software Design-Expert 7.1.

La evolución de las variables respuesta con los factores de operación puede modelarse empíricamente teniendo en cuenta los efectos significativos mostrados por el análisis ANOVA:

$$V = \alpha+\beta_1 \cdot F_1+\beta_2 \cdot F_2+\beta_3 \cdot F_3+\beta_{12} \cdot F_1 \cdot F_2+\beta_{13} \cdot F_1 \cdot F_3+\beta_{23} \cdot F_2 \cdot F_3+\beta_{123} \cdot F_1 \cdot F_2 \cdot F_3 \qquad \text{(ec. 3.1)}$$

donde V representa cualquier valor de una variable respuesta, $\alpha$ es el valor promedio de todo el conjunto de resultados experimentales obtenidos para dicha variable, $F_i$ es el valor codificado del factor "i", $\beta_i$ es el coeficiente asociado al factor "i", $\beta_{ij}$ es el coeficiente asociado a la interacción de los factores "i" y "j"(efecto sinérgico o antagónico) y $\beta_{123}$ es un coeficiente que representa la interacción simultánea entre los tres factores.

Cuando el análisis ANOVA detecta la existencia de curvatura en la respuesta de una variable, el modelo lineal no es el más adecuado para predecir su evolución ante la variación de los factores. Sin embargo, los coeficientes $\beta_i$ pueden utilizarse para evaluar la influencia relativa de los factores: cuanto mayor es el valor absoluto del coeficiente asociado al factor "i", mayor es la influencia que ejerce dicho factor sobre la variable, siempre que los factores estén expresados en términos codificados.

### *3.3.2. Experimentos de desulfuración*

Los factores de operación en las pruebas de desulfuración fueron los siguientes: (i) tipo de ceniza de lodo (ceniza de combustión o de gasificación); (ii) temperatura (600-800 ºC) (iii) gas alimentado (mezcla $H_2S/N_2$ o gas sintético de gasificación); y (iv) concentración de vapor de agua en el gas alimentado (0-30% vol.), lo que se traduce en una relación másica $H_2O/H_2S$ en el gas de 0 a 45 $g_{H2O} \cdot g^{-1}_{H2S}$. El error experimental se evaluó realizando tres réplicas bajo la

atmósfera gaseosa de $H_2S/N_2$ y, como en el estudio anterior, en valores intermedios de temperatura (700 ºC) y de la relación másica $H_2O/H_2S$ (22,5 $g \cdot g^{-1}$).

Con el fin de detectar cualquier efecto secundario causado por la propia configuración experimental, como por ejemplo la retención de $H_2S$ por su reacción con las partes metálicas calientes a la entrada y a la salida del reactor, se realizaron blancos sin utilizar lecho de ceniza bajo las diferentes condiciones de temperatura y atmósfera de reacción.

La Tabla 3.7 resume las condiciones de operación en los experimentos de desulfuración.

Tabla 3.7. Condiciones de operación en los experimentos de desulfuración.

| Núm. de experimento | Origen de la ceniza de lodo | Mezcla sintética de gas | T (ºC) | $H_2O/H_2S$ ($g \cdot g^{-1}$) | Duración del experimento (min) |
|---|---|---|---|---|---|
| 1 | Combustión | $H_2S/N_2$ | 600 | 0 | 300 |
| 2 | Combustión | $H_2S/N_2$ | 800 | 0 | 390 |
| 3 | Combustión | $H_2S/N_2$ | 600 | 45 | 120 |
| 4 | Combustión | $H_2S/N_2$ | 800 | 45 | 120 |
| 5,6,7 | Combustión | $H_2S/N_2$ | 700 | 22,5 | 120 |
| 8 | Gasificación | $H_2S/N_2$ | 600 | 0 | 120 |
| 9 | Gasificación | $H_2S/N_2$ | 800 | 0 | 390 |
| 10 | Gasificación | $H_2S/N_2$ | 600 | 45 | 120 |
| 11 | Gasificación | $H_2S/N_2$ | 800 | 45 | 120 |
| 12,13,14 | Gasificación | $H_2S/N_2$ | 700 | 22,5 | 120 |
| 15 | Sin sólido | $H_2S/N_2$ | 600 | 0 | 120 |
| 16 | Sin sólido | $H_2S/N_2$ | 800 | 0 | 120 |
| 17 | Sin sólido | $H_2S/N_2$ | 600 | 45 | 120 |
| 18 | Sin sólido | $H_2S/N_2$ | 800 | 45 | 120 |
| 19 | Sin sólido | $H_2S/N_2$ | 700 | 22,5 | 120 |
| 20 | Combustión | Gas de gasificación | 600 | 0 | 240 |
| 21 | Combustión | Gas de gasificación | 800 | 0 | 240 |
| 22 | Combustión | Gas de gasificación | 600 | 45 | 120 |
| 23 | Combustión | Gas de gasificación | 800 | 45 | 120 |
| 24 | Gasificación | Gas de gasificación | 600 | 0 | 120 |
| 25 | Gasificación | Gas de gasificación | 800 | 0 | 240 |
| 26 | Gasificación | Gas de gasificación | 600 | 45 | 120 |
| 27 | Gasificación | Gas de gasificación | 800 | 45 | 120 |
| 28 | Sin sólido | Gas de gasificación | 600 | 0 | 120 |
| 29 | Sin sólido | Gas de gasificación | 800 | 0 | 240 |
| 30 | Sin sólido | Gas de gasificación | 600 | 45 | 120 |
| 31 | Sin sólido | Gas de gasificación | 800 | 45 | 120 |

La influencia de los factores de operación en la cantidad de $H_2S$ eliminada del gas hasta el punto de ruptura se analizó estadísticamente mediante análisis ANOVA, utilizando un intervalo de confianza del 95% en el test F de Fischer.

Las pruebas de desulfuración realizadas en el laboratorio se simularon también de forma teórica, determinando así la máxima cantidad de $H_2S$ que podía ser eliminada del gas desde un punto de vista termodinámico. Para ello se utilizó el software HSC Chemistry 6.1. Este

programa utiliza el método de minimización de la energía de Gibbs para calcular la cantidad de cada producto en el equilibrio y en condiciones isotérmicas e isobáricas. El sistema de reacción debe ser especificado para los cálculos, incluyendo la temperatura, presión, cantidad de reactivos y posibles especies que cabría esperar como productos finales. Como reactivo sólido inicial se consideró sólo el contenido de hierro y de calcio de la ceniza, suponiendo que todo el contenido metálico se encontraba en forma de $Fe_2O_3$ y CaO, respectivamente. Entre las posibles especies que podían formar parte de los productos se consideraron las siguientes: $H_2S$, $SO_2$, COS, S, Ca, CaO, CaS, $CaCO_3$, $CaSO_4$, $CaSO_3$, Fe, $Fe_xO_y$, $Fe_xS_y$, $Fe_x(SO_4)_y$ y $Fe_x(SO_3)_y$, además de los propios compuestos gaseosos alimentados con cada mezcla gaseosa.

### *3.3.3. Ensayos de actividad de los catalizadores de níquel*

Los factores de estudio en los ensayos de actividad de los catalizadores de níquel fueron los siguientes: (i) promotor añadido (Ca, Cu, Fe o Mn); (ii) temperatura final de calcinación de los catalizadores (700 o 900 ºC); y (iii) procedimiento de reducción de los catalizadores, ya que en algunos casos los catalizadores se redujeron bajo una atmósfera de $H_2$ antes de comenzar los ensayos de actividad para transformar el NiO en Ni (900 ºC durante 1 h, con un caudal de 1 $LN \cdot min^{-1}$ de una mezcla $H_2/N_2$ al 50% vol.), mientras que en otros casos no se realizó esta reducción previa. La Tabla 3.8 resume las condiciones de operación en los ensayos de actividad de los catalizadores de níquel.

Tabla 3.8. Condiciones de operación en los ensayos de actividad de los catalizadores.

| Núm. de experimento | Catalizador | Temperatura final de calcinación (ºC) | Reducción previa del catalizador con $H_2$ |
|---|---|---|---|
| 1 | $Ni/Al_2O_3$ | 900 | sí |
| 2 | $Ni/Ca/Al_2O_3$ | 900 | sí |
| 3 | $Ni/Cu/Al_2O_3$ | 900 | sí |
| 4 | $Ni/Fe/Al_2O_3$ | 900 | sí |
| 5 | $Ni/Mn/Al_2O_3$ | 900 | sí |
| 6 | $Ni/Al_2O_3$ | 900 | no |
| 7 | $Ni/Ca/Al_2O_3$ | 900 | no |
| 8 | $Ni/Cu/Al_2O_3$ | 900 | no |
| 9 | $Ni/Fe/Al_2O_3$ | 900 | no |
| 10 | $Ni/Mn/Al_2O_3$ | 900 | no |
| 11 | $Ni/Al_2O_3$ | 700 | no |
| 12 | $Ni/Ca/Al_2O_3$ | 700 | no |
| 13 | $Ni/Cu/Al_2O_3$ | 700 | no |
| 14 | $Ni/Fe/Al_2O_3$ | 700 | no |
| 15 | $Ni/Mn/Al_2O_3$ | 700 | no |

El posible craqueo térmico de los alquitranes también se tuvo en cuenta realizando un blanco en el que se utilizó un material inerte como lecho sólido (SiC).

El efecto de la temperatura sobre la actividad del catalizador se estudió en todos los casos modificando la temperatura de reacción de acuerdo con la siguiente rampa: 900-850-800-900-750-700-900 ºC. Cada temperatura se mantuvo durante 3,5 h, por lo que la duración total de los experimentos fue de 24,5 h. La repetición de varios tramos a 900 ºC permite evaluar la tasa de desactivación del catalizador, comparando el nivel de conversión que se alcanza en todos ellos.

# 4. RESULTADOS Y DISCUSIÓN

En esta sección se muestran y se discuten los principales resultados obtenidos en los diferentes estudios que componen la presente Tesis. Los resultados experimentales de la gasificación de lodos de EDAR y de la gasificación de *char* se presentan en la sección 4.1, comparando los resultados obtenidos en ambos procesos y analizando la influencia de los factores de operación. En la sección 4.2 se realiza una evaluación energética de la gasificación de ambos materiales, analizando también la demanda energética del proceso de pirólisis en el que se produce el *char* y del secado térmico previo de los lodos para tener una idea global del rendimiento energético de ambos procesos: (i) secado y gasificación del lodo y (ii) secado, pirólisis del lodo y gasificación del *char*. Las secciones 4.3 y 4.4 muestran los resultados de los tratamientos secundarios de limpieza aplicados a diferentes gases sintéticos que simulan el gas de gasificación: estudio de la eliminación de $H_2S$ mediante el uso de las cenizas obtenidas en la combustión y gasificación del lodo (sección 4.3) y ensayos de actividad de diferentes catalizadores de níquel en el reformado de compuestos modelo de alquitrán (sección 4.4).

## 4.1. Gasificación de lodo y de *char*

El gas es el producto de interés de la gasificación, por lo que la mayoría de las variables respuesta analizadas están relacionadas con este producto: rendimiento o producción total de gas seco, composición del gas (relaciones $H_2/CO$ y $CO_2/CO$), rendimiento o producción de cada compuesto gaseoso, contenido de alquitrán en el gas, poder calorífico del gas y eficiencia energética de la gasificación. El rendimiento sólido y la distribución del carbono inicial entre los diferentes productos (sólido, gas y alquitrán) también fueron determinados después de los experimentos. Los resultados de todas estas variables respuesta obtenidos en la gasificación del lodo de EDAR se resumen en la Tabla 4.1 en función de las condiciones de operación (temperatura, relación gasificante y relación $H_2O/O_2$).

Tabla 4.1. Resultados obtenidos en los experimentos de gasificación de lodo de EDAR.

| Temperatura (ºC) | 850 | 770 | 850 | 770 | 850 | 770 | 850 | 770 | 810 |
|---|---|---|---|---|---|---|---|---|---|
| Relación gasificante, RG ($g \cdot g^{-1}_{org}$) | 1,1 | 1,1 | 0,8 | 0,8 | 1,1 | 1,1 | 0,8 | 0,8 | 0,95 |
| Relación molar $H_2O/O_2$ | 3 | 3 | 3 | 3 | 1 | 1 | 1 | 1 | 2 |
| Rendimiento a sólido ($g \cdot kg^{-1}_{lodo}$) | 368 | 401 | 401 | 407 | 356 | 392 | 384 | 400 | 382 ± 1 |
| Fracción de C remanente en el sólido (%) | 3 | 17 | 8 | 23 | 2 | 9 | 2 | 12 | 7 ± 1 |
| Fracción de C convertido en gas (%) | 76,4 | 61,3 | 65,1 | 61,8 | 89,7 | 74,8 | 83,1 | 65,7 | 73,1 ± 0,8 |
| Fracción de C convertido en alquitrán (%) | 4 | 7 | 5 | 5 | 4 | 7 | 4 | 6 | 5 ± 1 |
| Rendimiento a gas seco ($m^3N \cdot kg^{-1}_{lodo}$, sin $N_2$) | 0,72 | 0,51 | 0,65 | 0,53 | 0,72 | 0,52 | 0,71 | 0,49 | 0,61 ± 0,01 |
| Rendimiento a gas seco ($m^3N \cdot kg^{-1}_{org}$, sin $N_2$) | 1,32 | 0,94 | 1,20 | 0,97 | 1,32 | 0,96 | 1,30 | 0,89 | 1,13 ± 0,01 |
| Contenido de alquitrán en el gas ($g \cdot m^{-3}N$) | 19 | 44 | 19 | 44 | 12 | 22 | 11 | 45 | 15 ± 1 |
| Composición del gas (base seca) | | | | | | | | | |
| $H_2$ (% vol.) | 24,2 | 18,4 | 25,1 | 20,4 | 18,0 | 11,0 | 20,6 | 13,6 | 19,3 ± 0,1 |
| CO (% vol.) | 8,7 | 5,7 | 10,2 | 7,3 | 11,6 | 7,0 | 14,1 | 7,7 | 9,4 ± 0,1 |
| $CO_2$ (% vol.) | 17,1 | 18,6 | 12,6 | 15,5 | 20,7 | 23,8 | 16,0 | 19,8 | 18,1 ± 0,2 |
| $CH_4$ (% vol.) | 3,1 | 3,5 | 3,6 | 4,1 | 2,6 | 2,8 | 2,9 | 3,4 | 3,3 ± 0,1 |
| $C_2H_x$ (% vol.) | 1,7 | 2,1 | 1,4 | 2,2 | 1,3 | 1,6 | 1,4 | 2,0 | 1,7 ± 0,2 |
| $H_2S$ (% vol.) | 0,44 | 0,38 | 0,33 | 0,33 | 0,44 | 0,42 | 0,38 | 0,31 | 0,40 ± 0,02 |
| $N_2$ (% vol.) | 44,9 | 51,4 | 46,8 | 50,2 | 45,3 | 53,4 | 44,5 | 53,2 | 47,8 ± 0,2 |
| Producción de cada compuesto gaseoso ($g \cdot kg^{-1}_{org}$) | | | | | | | | | |
| $H_2$ | 51,8 | 31,8 | 50,4 | 36,5 | 38,6 | 20,1 | 43,1 | 23,2 | 37,2 ± 0,4 |
| CO | 260 | 137 | 287 | 182 | 351 | 179 | 414 | 183 | 253 ± 2 |
| $CO_2$ | 806 | 707 | 557 | 608 | 980 | 962 | 736 | 740 | 767 ± 7 |
| $CH_4$ | 53 | 49 | 59 | 59 | 45 | 41 | 49 | 46 | 51 ± 1 |
| $C_2H_x$ | 50 | 52 | 40 | 55 | 40 | 42 | 40 | 48 | 47 ± 4 |
| $H_2S$ | 16,0 | 11,2 | 11,4 | 10,0 | 16,1 | 13,1 | 13,5 | 9,0 | 13,0 ± 0,8 |
| Relación molar $H_2/CO$ en el gas producto | 2,79 | 3,25 | 2,46 | 2,81 | 1,54 | 1,57 | 1,46 | 1,77 | 2,06 ± 0,01 |
| Relación molar $CO/CO_2$ en el gas producto | 0,51 | 0,30 | 0,81 | 0,47 | 0,56 | 0,29 | 0,88 | 0,39 | 0,52 ± 0,01 |
| PCI del gas ($MJ \cdot m^{-3}N$) | 5,9 | 5,3 | 6,2 | 6,0 | 5,2 | 4,1 | 6,0 | 4,9 | 5,6 ± 0,1 |
| Eficiencia energética de la gasificación (%) | 65,8 | 47,7 | 64,7 | 55,3 | 58,4 | 39,1 | 64,7 | 43,4 | 55,8 ± 0,8 |

*Los datos de la última columna representan la media ± desviación estándar de las 3 réplicas del punto central.*

El ***rendimiento sólido*** (masa de producto sólido obtenida por unidad de masa de lodo alimentado) varió entre 356 y 407 $g \cdot kg^{-1}_{lodo}$. Los valores típicos para otros tipos de biomasa, como madera o paja, se encuentran habitualmente por debajo de 80 $g \cdot kg^{-1}$ (McKendry, 2002a). El alto contenido de ceniza en el lodo (39% en masa) explica esta diferencia. En algunos casos

la cantidad de sólido recogido después de los experimentos fue menor que el propio contenido de ceniza del lodo, lo que sugiere la volatilización de una pequeña fracción inorgánica del lodo durante la gasificación.

La ***distribución del contenido inicial de carbono*** en el lodo entre los diferentes productos fue la siguiente: (i) entre un 2% y un 23% del carbono se mantuvo en el sólido como consecuencia de su incompleta conversión (calculado a partir de los datos de rendimiento a sólido y análisis elemental del mismo); (ii) la fracción de carbono en forma de alquitrán varió entre un 4% y un 7% (calculado a partir de los datos de carbono orgánico total presente en el condensado); y (iii) la fracción de carbono convertido en gases no condensables fue la mayoritaria, variando entre un 61,3% y un 89,7% (calculado a partir del rendimiento a gas y la composición del mismo). Con estos datos, el balance de masa al carbono cierra al 78-95%. La posible formación de hidrocarburos ligeros no detectados por el cromatógrafo de gases ($C_3H_x$, $C_4H_x$...) o la escasa solubilidad de algunos compuestos del alquitrán en las disoluciones acuosas preparadas para la determinación del carbono orgánico total puede explicar la falta de carbono en el cierre de los balances.

El ***rendimiento a gas seco***, definido como el volumen de gas seco y libre de alquitrán producido por kilogramo de lodo orgánico, es decir en base seca y libre de ceniza, varió entre 0,89 y 1,32 $m^3N \cdot kg^{-1}_{org}$ (en base libre de $N_2$). Estos datos de producción de gas no difieren demasiado de los obtenidos por otros autores al gasificar otros tipos de biomasa bajo similares condiciones de operación (Campoy y cols., 2009; Gil y cols., 1999a; Pinto y cols., 2003). Como es habitual en un proceso de gasificación, los principales compuestos gaseosos producidos durante la gasificación de lodos de EDAR fueron $H_2$, CO, $CO_2$ e hidrocarburos ligeros, siendo el $CH_4$ el hidrocarburo mayoritario. También cabe destacar la formación de $H_2S$ debido a la presencia de un 1,3% de azufre en el lodo (Tabla 3.1). Además, como consecuencia de la alimentación del aire como parte del agente gasificante, el $N_2$ representó un 45-55% del volumen final de gas. En todos los experimentos se alimentó una cantidad muy similar de $N_2$ para evitar diferentes efectos de dilución del gas producto que pudiesen esconder o modificar el verdadero efecto de los factores de operación en determinadas variables respuesta.

La ***composición del gas*** ha mostrado importantes diferencias en función de las condiciones de operación. Tanto es así que los porcentajes volumétricos de $H_2$ (11,0-25,1%), CO (5,7-14,1%), $CO_2$ (12,6-23,8%) y $CH_4$ (2,6-4,1%) pueden llegar a duplicarse al modificar las condiciones de operación. Estos datos de composición dan lugar a unas relaciones molares $H_2/CO$ y $CO/CO_2$ de 1,46-3,25 y 0,29-0,88, respectivamente. La relación molar $H_2/CO$ es un parámetro importante de cara al posible uso del gas como gas de síntesis; valores de 2-3

suelen ser necesarios en procesos como la producción de metanol o la síntesis de líquidos Fischer Tropsch (Wender, 1996). Por otro lado, la relación $CO/CO_2$ da una idea de la distribución del carbono entre ambos compuestos. Valores altos de la relación $CO/CO_2$ son preferibles desde el punto de vista del contenido energético del gas.

El ***contenido de alquitrán*** en el gas varió desde 11 hasta 45 $g \cdot m^{-3}N$. Los valores más altos (22-45 $g \cdot m^{-3}N$) se corresponden con la temperatura de operación más baja (770 ºC), mientras que los valores más bajos (11-12 $g \cdot m^{-3}N$) se encuentran entre los valores habituales obtenidos en la gasificación de biomasa en lecho fluidizado (Han y Kim, 2008).

El ***poder calorífico inferior del gas*** (PCI) se calculó como $\Sigma$ ($x_i \cdot PCI_i$), donde $x_i$ y $PCI_i$ son la fracción volumétrica y el poder calorífico inferior de cada compuesto del gas, respectivamente. El PCI del gas osciló entre 4,1 y 6,2 $MJ \cdot m^{-3}N$, valor suficiente para su combustión en turbinas o motores (Bridgwater, 1995).

La ***eficiencia energética de la gasificación*** se define como el cociente entre la energía contenida en el gas frío (producto del rendimiento a gas por su PCI, sin tener en cuenta el calor sensible del gas) y la energía contenida en el lodo (PCI). La eficiencia energética así calculada varió en un amplio intervalo de valores, desde 39,1% hasta 65,8%.

Los resultados experimentales correspondientes a la gasificación del *char*, obtenidos bajo las mismas condiciones de operación que en la gasificación del lodo, se muestran en la Tabla 4.2.

Tabla 4.2. Resultados obtenidos en los experimentos de gasificación de *char*.

| Temperatura (ºC) | 850 | 770 | 850 | 770 | 850 | 770 | 850 | 770 | 810 |
|---|---|---|---|---|---|---|---|---|---|
| Relación gasificante, RG ($g \cdot g^{-1}_{org}$) | 1,1 | 1,1 | 0,8 | 0,8 | 1,1 | 1,1 | 0,8 | 0,8 | 0,95 |
| Relación molar $H_2O/O_2$ | 3 | 3 | 3 | 3 | 1 | 1 | 1 | 1 | 2 |
| Rendimiento a sólido ($g \cdot kg^{-1}_{char}$) | 757 | 785 | 750 | 785 | 731 | 771 | 752 | 813 | 775 ± 2 |
| Fracción de C remanente en el sólido (%) | 20 | 41 | 25 | 43 | 15 | 26 | 19 | 41 | 34 ± 3 |
| Fracción de C convertido en gas (%) | 71 | 56 | 62 | 48 | 83 | 67 | 72 | 56 | 62 ± 2 |
| Fracción de C convertido en alquitrán (%) | 1,3 | 0,7 | 2,9 | 3,3 | 1,0 | 5,7 | 3,2 | 5,8 | 2,8 ± 0,7 |
| Rendimiento a gas seco ($m^3N \cdot kg^{-1}_{char}$, sin $N_2$) | 0,36 | 0,27 | 0,31 | 0,24 | 0,35 | 0,28 | 0,32 | 0,24 | 0,29 ± 0,01 |
| Rendimiento a gas seco ($m^3N \cdot kg^{-1}_{org}$, sin $N_2$) | 1,47 | 1,12 | 1,30 | 0,99 | 1,46 | 1,15 | 1,31 | 1,00 | 1,21 ± 0,01 |
| Contenido de alquitrán en el gas ($g \cdot m^{-3}N$)* | 4 | 3 | 9 | 13 | 3 | 20 | 10 | 22 | 9 ± 2 |
| Composición del gas (base seca) | | | | | | | | | |
| $H_2$ (% vol.) | 29,3 | 26,3 | 27,8 | 24,8 | 21,5 | 19,0 | 22,0 | 20,2 | 25,2 ± 0,6 |
| CO (% vol.) | 19,5 | 12,0 | 20,2 | 12,8 | 22,7 | 14,0 | 23,7 | 15,2 | 15,9 ± 0,2 |
| $CO_2$ (% vol.) | 18,9 | 24,2 | 16,2 | 20,8 | 22,6 | 29,5 | 18,5 | 24,1 | 21,9 ± 0,1 |
| $CH_4$ (% vol.) | 0,76 | 0,91 | 0,77 | 0,92 | 0,59 | 0,70 | 0,64 | 0,84 | 0,88 ± 0,01 |
| $C_2H_x$ (ppm | 150 | 190 | 160 | 220 | 180 | 220 | 150 | 200 | 180 ± 10 |
| $H_2S$ (% vol.) | 0,25 | 0,12 | 0,14 | 0,07 | 0,17 | 0,08 | 0,12 | 0,06 | 0,10 ± 0,01 |
| $N_2$ (% vol.) | 31,3 | 36,5 | 34,9 | 40,7 | 32,5 | 36,7 | 35,0 | 39,6 | 36,1 ± 0,6 |
| Producción de cada compuesto gaseoso ($g \cdot kg^{-1}_{org}$) | | | | | | | | | |
| $H_2$ | 56,7 | 42,1 | 49,9 | 36,8 | 41,6 | 30,8 | 39,7 | 30,0 | 42,8 ± 0,3 |
| CO | 529 | 268 | 506 | 266 | 615 | 318 | 598 | 316 | 379 ± 10 |
| $CO_2$ | 808 | 853 | 637 | 679 | 960 | 1055 | 735 | 786 | 821 ± 20 |
| $CH_4$ | 11,7 | 11,7 | 11,0 | 10,9 | 9,1 | 9,0 | 9,2 | 9,9 | 11,9 ± 0,1 |
| $C_2H_x$ | 0,41 | 0,42 | 0,41 | 0,47 | 0,50 | 0,50 | 0,39 | 0,42 | 0,42 ± 0,04 |
| $H_2S$ | 8,2 | 3,2 | 4,1 | 1,8 | 5,7 | 2,3 | 3,7 | 1,5 | 2,8 ± 0,1 |
| Relación molar $H_2/CO$ en el gas producto | 1,50 | 2,20 | 1,38 | 1,93 | 0,95 | 1,36 | 0,93 | 1,33 | 1,58 ± 0,04 |
| Relación molar $CO/CO_2$ en el gas producto | 1,03 | 0,49 | 1,25 | 0,62 | 1,00 | 0,47 | 1,28 | 0,63 | 0,73 ± 0,01 |
| PCI del gas ($MJ \cdot m^{-3}N$) | 5,96 | 4,71 | 5,87 | 4,65 | 5,44 | 4,09 | 5,63 | 4,43 | 5,07 ± 0,07 |
| Eficiencia energética de la gasificación (%) | 62,9 | 41,1 | 57,2 | 37,6 | 57,4 | 36,2 | 55,3 | 35,7 | 47,0 ± 0,6 |

*Los datos de la última columna representan la media ± desviación estándar de las 3 réplicas del punto central.*

** La cantidad de alquitrán se ha aproximado a la cantidad de carbono orgánico detectado en el condensado.*

El ***rendimiento a sólido*** obtenido en la gasificación de *char* (731-813 $g \cdot kg^{-1}_{char}$) prácticamente se duplicó respecto al obtenido en la gasificación de lodo debido al mayor

contenido de materia inorgánica en el *char*. Según las especificaciones de la norma ISO-1171-1976, el 93-96% de este producto sólido era ceniza.

En cuanto a la ***distribución del contenido inicial de carbono*** en el *char*, la fracción de carbono remanente en el sólido osciló entre un 15% y un 43%, mientras que el valor máximo obtenido en la gasificación del lodo fue de aproximadamente un 23% (Tabla 4.1). Esta diferencia radica en la diferente estructura carbonosa del sólido. Sólo el 15% del contenido de carbono en el lodo se encuentra en forma de carbono fijo, mientras que este valor alcanza el 59% en el caso del *char* (Tabla 3.1). Las reacciones en las que se ve envuelto el carbono sólido son mucho más lentas que la liberación de la materia volátil y las reacciones en fase gas, lo que supone una reducción de la conversión total del carbono y, por tanto, de la fracción de carbono convertido a gas durante la gasificación de *char*. La fracción de carbono convertido en alquitrán durante la gasificación de *char* también se redujo en comparación con los resultados obtenidos en la gasificación de lodo, aunque no en la misma proporción que la reducción observada en el contenido de materia volátil de ambos sólidos (más de tres veces menor en el *char* que en el lodo, Tabla 3.1). Esto demuestra que parte de la materia volátil desprendida del lodo se descompone y reacciona para formar gases más ligeros.

Los datos de conversión de carbono durante la gasificación de *char* pueden recalcularse considerando conjuntamente la etapa previa de pirólisis de lodo y la posterior gasificación del *char*. Para ello ha de utilizarse como base de cálculo la cantidad de carbono alimentado inicialmente al proceso de pirólisis. Teniendo en cuenta que el rendimiento a *char* en la pirólisis de lodo se situó en torno a un 52% en masa (Gil-Lalaguna y cols., 2010), la fracción del carbono inicial que queda en forma de sólido después de la pirólisis del lodo y la gasificación del *char* se reduce a un 4-11%, lo que supone una mejora respecto a la gasificación directa del lodo bajo determinadas condiciones de operación.

El ***rendimiento a gas seco*** en la gasificación de *char* varió entre 0,24 y 0,36 $m^3N \cdot kg^{-1}_{char}$ (base libre de $N_2$), o entre 0,40 y 0,52 $m^3N \cdot kg^{-1}_{char}$ si se incluye la cantidad de $N_2$ en el volumen de gas. Estos datos suponen un reducción a la mitad de la producción de gas por kilogramo de materia prima en comparación con la gasificación de lodo (0,51-0,72 $m^3N \cdot kg^{-1}_{lodo}$ en base libre de $N_2$). El rendimiento a gas obtenido durante el proceso previo de pirólisis de lodo (0,07 $m^3_{STP} \cdot kg^{-1}_{lodo}$) no compensa esta diferencia ya que dicho proceso fue optimizado para maximizar la fracción de líquido. Sin embargo, si la producción de gas en las etapas de gasificación se calcula en base seca y libre de ceniza para el sólido, la gasificación de *char* (0,99-1,47 $m^3N \cdot kg^{-1}_{org}$) ofrece mejores resultados que la gasificación de lodo (0,89-1,32 $m^3N \cdot kg^{-1}_{org}$). Esto se debe a una mayor concentración del carbono en la fracción orgánica del sólido después

de la pirólisis (0,64 g $C \cdot g^{-1}_{org}$ en el *char* frente a 0,54 g $C \cdot g^{-1}_{org}$ en el lodo). La producción de gas por kilogramo de materia orgánica en el *char* de lodo de EDAR se encuentra en el mismo orden de magnitud que cuando se gasifica *char* de origen lignocelulósico, como *char* de bagazo (Chaudhari y cols., 2003) o de ramio (He y cols., 2012).

El ***contenido de alquitrán*** en el gas derivado de la gasificación de *char* se redujo a niveles de 3-4 $g \cdot m^{-3}N$ bajo ciertas condiciones de operación, mientras que el valor más bajo alcanzado en la gasificación de lodos de depuradora fue de 11-12 $g \cdot m^{-3}N$.

En cuanto a la ***composición del gas***, el $H_2$ (19,0-29,3% vol.), CO (12,0-23,7% vol.), $CO_2$ (16,2-29,5% vol.), $CH_4$ (0,59-0,92% vol.) y $N_2$ (31,3-40,7% vol.) fueron los compuestos mayoritarios detectados por el cromatógrafo de gases. La producción de CO (en términos de $g \cdot kg^{-1}_{org}$) se vio claramente incrementada al gasificar *char* en lugar de lodo (45-85% mayor), lo que puede estar relacionado con su mayor contenido de carbono fijo y con una mayor extensión de las reacciones *water-gas* (ec. 2.3) y de Boudouard (ec. 2.4). La producción de $CH_4$ en la gasificación de *char* se redujo en un 75-82% en comparación con la gasificación de lodo (en términos de $g \cdot kg^{-1}_{org}$), mientras que las variaciones en la producción de $H_2$ y $CO_2$ no fueron tan significativas. La relación molar $H_2$/CO en el gas producto de la gasificación de *char* (0,93-2,20) fue menor que la obtenida en la gasificación de lodo (1,46-3,25), mientras que la relación $CO/CO_2$ fue mayor en la gasificación de *char* (0,47-1,28). Sólo en la gasificación de *char*, y bajo determinadas condiciones de operación, se consigue favorecer la formación de CO frente a la de $CO_2$ ($CO/CO_2 > 1$).

Tanto el ***PCI del gas*** (4,09-5,96 $MJ \cdot m^{-3}N$) como la ***eficiencia energética*** (36,2-62,9%) de la gasificación de *char* oscilan en el mismo intervalo que los valores obtenidos en la gasificación del lodo.

La influencia de la temperatura (T), relación gasificante (RG) y composición del medio de gasificación (relación $H_2O/O_2$) en los resultados obtenidos en la gasificación de lodo y de *char* ha sido estadísticamente evaluada mediante análisis ANOVA. Las Tablas 4.3 y 4.4 muestran los coeficientes de regresión lineal obtenidos en el análisis ANOVA de las variables respuesta de ambos procesos. Estos coeficientes (β), obtenidos para valores codificados de los factores, resultan útiles para modelar la respuesta de las variables en el caso de una evolución lineal (ec. 3.1) y para determinar la influencia relativa de los factores, es decir, para establecer cuál es el factor con mayor impacto en cada variable.

Tabla 4.3. Coeficientes de regresión lineal (β) para las variables respuesta en la gasificación de lodo.

| | Valor medio | $\beta_T$ | $\beta_{RG}$ | $\beta_{H2O/O2}$ | $\beta_{T-RG}$ | $\beta_{T-H2O/O2}$ | $\beta_{RG-H2O/O2}$ | $\beta_{T-H2O/O2-RG}$ | Curvatura |
|---|---|---|---|---|---|---|---|---|---|
| Fracción de C remanente en el sólido (%) | 9,01 | -5,76 | -1,74 | 3,29 | * | -1,50 | * | * | * |
| Fracción de C convertido en gas (%) | 72,48 | 6,33 | 3,33 | -6,07 | * | * | * | * | * |
| Rendimiento a gas seco ($m^3N \cdot kg^{-1}_{org}$, sin $N_2$) | 1,12 | 0,17 | 0,02 | * | 0,02 | -0,02 | * | 0,03 | ** |
| Contenido de alquitrán ($g \cdot m^{-3}N$) | 27,03 | -11,91 | -2,78 | 4,35 | 3,15 | * | 2,62 | -2,89 | ** |
| Producción de cada compuesto gaseoso ($g \cdot kg^{-1}_{org}$) | | | | | | | | | |
| $H_2$ | 37,03 | 9,06 | -1,37 | 5,68 | * | * | * | * | * |
| CO | 250,10 | 78,79 | -17,51 | -32,67 | -5,03 | -21,95 | * | 9,65 | * |
| $CO_2$ | 763,42 | * | 101,57 | -92,53 | 21,59 | * | -14,93 | 15,91 | * |
| $CH_4$ | 50,23 | 1,49 | -3,13 | 4,80 | * | * | * | * | * |
| $C_2H_x$ | 46,13 | -3,28 | * | 3,35 | * | * | * | * | * |
| $H_2S$ | 12,66 | 1,73 | 1,56 | * | * | * | * | 0,62 | * |
| Relación molar $H_2$/CO en el gas producto | 2,21 | -0,14 | 0,08 | 0,62 | 0,02 | -0,06 | 0,11 | -0,05 | ** |
| Relación molar CO/$CO_2$ en el gas producto | 0,52 | 0,16 | -0,11 | * | -0,04 | -0,03 | * | * | * |
| PCI del gas ($MJ \cdot m^{-3}N$) | 5,49 | 0,37 | -0,31 | 0,40 | * | -0,17 | * | * | * |
| Eficiencia energética de la gasificación (%) | 55,12 | 8,51 | * | 3,47 | * | * | * | * | * |

** término no significativo; ** curvatura significativa*

Tabla 4.4. Coeficientes de regresión lineal (β) para las variables respuesta en la gasificación de *char*.

| | Valor medio | $\beta_T$ | $\beta_{RG}$ | $\beta_{H2O/O2}$ | $\beta_{T-RG}$ | $\beta_{T-H2O/O2}$ | $\beta_{RG-H2O/O2}$ | $\beta_{T-H2O/O2-RG}$ | Curvatura |
|---|---|---|---|---|---|---|---|---|---|
| Fracción de C remanente en el sólido (%) | 30,13 | -9,16 | -3,30 | 3,59 | * | * | * | * | * |
| Fracción de C convertido en gas (%) | 64,29 | 7,76 | 4,82 | -5,16 | * | * | * | * | ** |
| Rendimiento a gas seco ($m^3N \cdot kg^{-1}_{org}$, sin $N_2$) | 1,23 | 0,16 | 0,08 | * | * | * | * | * | ** |
| Contenido de alquitrán ($g \cdot m^{-3}N$) | 10,52 | -3,97 | -3,15 | -3,40 | * | 3,45 | * | * | * |
| Producción de cada compuesto gaseoso ($g \cdot kg^{-1}_{org}$) | | | | | | | | | |
| $H_2$ | 40,93 | 6,03 | 1,86 | 5,43 | 0,33 | 0,90 | 1,18 | * | ** |
| CO | 427,16 | 135,09 | * | -34,61 | * | -9,78 | * | * | ** |
| $CO_2$ | 815,96 | -29,09 | 104,91 | -69,95 | * | * | -18,75 | * | * |
| $CH_4$ | 10,33 | * | * | 1,01 | * | * | 0,32 | * | ** |
| $C_2H_x$ | 0,44 | * | * | * | * | * | -0,03 | * | * |
| $H_2S$ | 3,54 | 1,62 | 1,03 | * | * | * | * | * | * |
| Relación molar $H_2$/CO en el gas producto | 1,48 | -0,26 | * | 0,31 | * | * | * | * | * |
| Relación molar CO/$CO_2$ en el gas producto | 0,85 | 0,29 | -0,10 | * | -0,03 | * | 0,01 | * | ** |
| PCI del gas ($MJ \cdot m^{-3}N$) | 5,09 | 0,63 | * | 0,20 | * | * | 0,08 | * | * |
| Eficiencia energética de la gasificación (%) | 47,90 | 10,27 | 1,45 | 1,77 | 0,48 | * | 0,83 | * | ** |

** término no significativo; ** curvatura significativa*

La temperatura es el factor más influyente en la fracción del carbono inicial que queda en el subproducto sólido después de los procesos de gasificación. Esta fracción de carbono se reduce prácticamente a la mitad al aumentar la temperatura de gasificación desde 770 a 850 ºC (Figura 4.1). Por otro lado, el coeficiente positivo asociado a la la influencia de la relación $H_2O/O_2$ ($\beta_{H2O/O2} > 0$) sugiere una mayor reactividad del carbono con el oxígeno que con el vapor de agua. Nowicki y cols. (2011) mostraron un resultado similar al realizar ensayos de gasificación de *char* de lodo en una termobalanza bajo diferentes atmósferas gaseosas ($CO_2$, $H_2O$ y $O_2$), ya que la presencia de oxígeno en el medio de gasificación mejoraba la conversión del carbono. En el caso de la gasificación de lodo, el efecto de la composición del medio de gasificación se reduce considerablemente a alta temperatura (Figura 4.1.a). Además, como era de esperar, el aumento de la relación gasificante (RG) conlleva una reducción de la fracción de carbono que queda como subproducto sólido después de la gasificación ($\beta_{RG} < 0$).

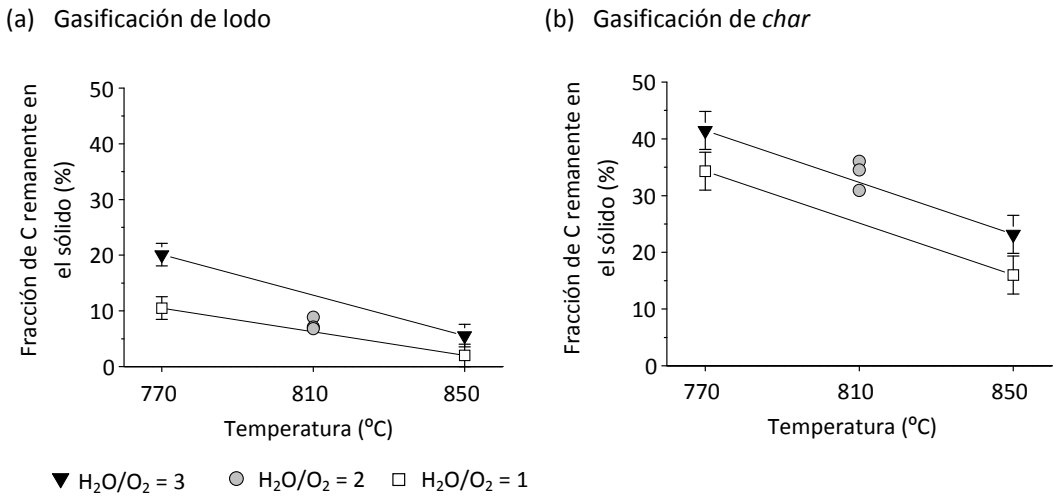


Figura 4.1. Fracción del carbono inicial que queda como subproducto sólido después de la (a) gasificación de lodo y (b) gasificación de *char* (RG = 0,95 $g \cdot g^{-1}_{org}$). Las barras de error en las figuras representan la mínima diferencia significativa.

Los resultados experimentales muestran una clara relación entre la fracción de carbono remanente en el sólido y la fracción de carbono convertido a gas: cuanto menor es la primera, mayor es la segunda. Por lo tanto, como se muestra en la Figura 4.2, la fracción de carbono convertido a gas se ve afectada positivamente por la temperatura ($\beta_T > 0$) y por la relación gasificante ($\beta_{RG} > 0$), y negativamente afectada por la relación $H_2O/O_2$ ($\beta_{H2O\ /\ O2} < 0$) en ambos casos.

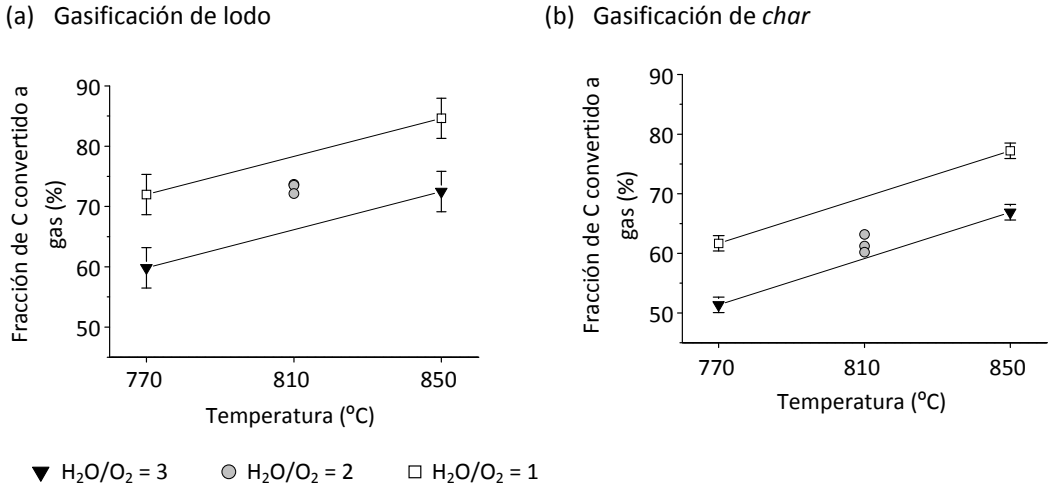


Figura 4.2. Fracción del carbono inicial convertido a gas en la (a) gasificación de lodo y (b) gasificación de *char* (RG = 0,95 $g \cdot g^{-1}_{org}$). Las barras de error en las figuras representan la mínima diferencia significativa.

Como muestran los coeficientes β de las Tablas 4.3 y 4.4, la temperatura es el factor con mayor impacto en el rendimiento a gas, afectándole de forma positiva ($\beta_T > 0$). Durante el proceso de gasificación, los compuestos gaseosos se producen en diferentes etapas que se ven favorecidas por el aumento de la temperatura, como la etapa inicial de pirólisis, el craqueo y reformado de los alquitranes y las reacciones de gasificación del carbono sólido, que son endotérmicas (Pinto y cols., 2003). El aumento de la relación gasificante también resulta favorable para la producción de gas ($\beta_{RG} > 0$), especialmente en la gasificación de *char*, mientras que la composición de la atmósfera reactiva no ejerce un efecto significativo en la producción de gas en la gasificación de ninguno de los dos materiales. Por lo tanto, el efecto negativo antes mencionado de la relación $H_2O/O_2$ sobre la fracción de carbono convertido a gas no se traduce en una variación significativa de la producción total de gas. Esto se explica teniendo en cuenta también la producción de $H_2$ que, como se discute más adelante, se ve favorecida con el aumento de la relación $H_2O/O_2$, contrarrestando así la disminución de la producción de gases carbonosos. Además de estas influencias, los factores han mostrado efectos sinérgicos y antagónicos estadísticamente significativos, pero mucho menos importantes que el efecto individual de la temperatura de gasificación.

La temperatura es de nuevo el factor más influyente en el contenido de alquitrán en el gas producto de la gasificación de lodo, mientras que los tres factores estudiados ejercen efectos similares durante la gasificación de *char*. El aumento de temperatura favorece tanto la producción total de gas como la descomposición de los alquitranes mediante reacciones de reformado, lo que se traduce en una menor concentración de alquitrán en el gas producto. El contenido de alquitrán en el gas también puede reducirse mediante el aumento de la relación

gasificante ($\beta_{RG} < 0$), aunque este efecto prácticamente desaparece cuando se opera a alta temperatura o con una alta relación $H_2O/O_2$ durante la gasificación del lodo. La relación $H_2O/O_2$ utilizada como agente gasificante ha mostrado efectos opuestos sobre el contenido de alquitrán en los gases producidos durante la gasificación de lodo y de *char*, mostrando un efecto positivo en el primer caso ($\beta_{H2O/O2} > 0$) y un efecto negativo en el segundo ($\beta_{H2O/O2} < 0$). En este último caso, tal como se muestra en la Figura 4.3, existe una clara interacción entre la temperatura y la relación $H_2O/O_2$ utilizada como agente gasificante, ya que el efecto de cada uno de ellos prácticamente desaparece al operar con el máximo valor del otro.

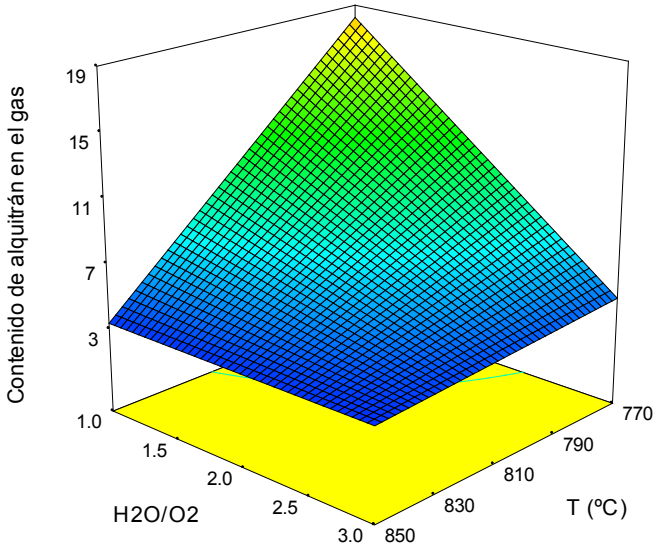


Figura 4.3. Contenido de alquitrán ($g \cdot m^{-3}N$) en el gas producto de la gasificación de *char* (RG=1,1 $g \cdot g^{-1}_{org}$).

El rendimiento o producción neta ($g \cdot kg^{-1}_{org}$) de los diferentes compuestos que forman parte del gas producto puede calcularse a partir de los datos de volumen total y composición del gas. Como muestran los coeficientes β mostrados en las Tablas 4.3 y 4.4, la temperatura de gasificación es de nuevo el factor más influyente en la producción de $H_2$ y de CO. Estos gases están involucrados en diversas reacciones tanto en forma de reactivos como de productos, pero el aumento de la temperatura favorece su producción frente a su consumo ($\beta_T > 0$). El reformado del alquitrán es una de las reacciones que contribuye a la formación de CO y $H_2$ a alta temperatura (ecs. 2.9 y 2.10). La evolución de la producción de CO con la temperatura ha mostrado variaciones insignificantes o incluso la tendencia opuesta en algunos estudios de la bibliografía (Gil y cols., 1997; Lv y cols., 2004), lo que demuestra la importancia de la naturaleza de la biomasa y de las demás condiciones de operación en la evolución de este compuesto. Aunque en menor medida, la composición de la atmósfera reactiva también ejerce un efecto significativo en la producción de $H_2$ y de CO. El aumento de la relación $H_2O/O_2$ conlleva un aumento de la producción de $H_2$ ($\beta_{H2O/O2} > 0$) y un descenso de la producción de CO

($\beta_{H2O/O2} < 0$). Ambas tendencias son consistentes con la reacción *water-gas shift* (ec. 2.6), que es una de las reacciones más influyentes en los procesos de gasificación con vapor de agua a temperaturas no demasiado altas, hasta unos 830 ºC (Franco y cols., 2003), y que se ve favorecida al aumentar la presencia de vapor de agua en el medio de reacción. A temperaturas más altas (830-900 ºC), las reacciones gas-sólido como la reacción *water-gas* (ec. 2.3) o la reacción de Boudouard (ec. 2.4) toman más importancia (Franco y cols., 2003), lo que contribuye a explicar el efecto positivo de la temperatura sobre la formación de CO (Figura 4.4.a). Aunque el aumento de la relación $H_2O/O_2$ conlleva, además de una mayor presencia de vapor de agua, una reducción de la disponibilidad de oxígeno en el medio de gasificación y una atenuación de las reacciones de combustión completa, el efecto negativo de la relación $H_2O/O_2$ en la producción neta de CO sugiere que el vapor de agua juega un papel más importante que el oxígeno en su consumo. Además, como se muestra en la Figura 4.4.a, el efecto positivo de la temperatura se ve aminorado con el aumento de la presencia de vapor de agua como consecuencia del desplazamiento de la reacción *water-gas shift* hacia el consumo de CO.

(a) Producción de CO en la gasificación de lodo (b) Producción de $CO_2$ en la gasificación de lodo

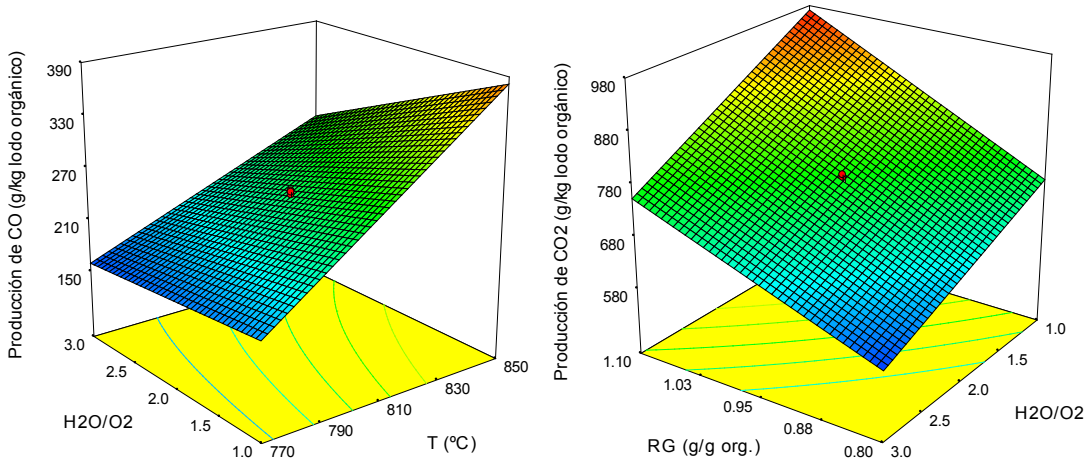


Figura 4.4. Producción neta de (a) CO ($g \cdot kg^{-1}_{org}$) y (b) $CO_2$ ($g \cdot kg^{-1}_{org}$) en la gasificación de lodo.

La relación gasificante (RG) ejerce la mayor influencia en la producción de $CO_2$, afectándole de forma positiva ($\beta_{RG} > 0$). El aumento de RG conlleva una mayor disponibilidad de oxígeno y de vapor de agua en el medio de reacción, por lo que la producción de $CO_2$ en reacciones de combustión y en reacciones promovidas por la presencia de vapor de agua (como por ejemplo la reacción *water-gas shift*) se ve favorecida. El efecto negativo de la relación $H_2O/O_2$ en la producción de $CO_2$ ($\beta_{H2O/O2} < 0$) revela que las reacciones de combustión son la principal fuente para la formación de este compuesto. Como se observa en la Figura 4.4.b, la mayor producción de $CO_2$ se corresponde con la mayor presencia de oxígeno en el

medio, que se obtiene con el mayor valor de RG y el menor valor de $H_2O/O_2$. La temperatura sólo aparece como un término estadísticamente significativo en la producción de $CO_2$ durante la gasificación de *char*. En este caso, el aumento de temperatura conlleva una reducción en la formación de $CO_2$ ($\beta_T < 0$) y, como se discutió anteriormente, favorece la producción de CO, lo que sugiere un aumento de la reactividad del *char* con el $CO_2$ a alta temperatura (reacción de Boudouard, ec. 2.4).

Los coeficientes β resultantes de los análisis ANOVA (Tablas 4.3 y 4.4) muestran que la producción neta de hidrocarburos ligeros ($CH_4$ y $C_2H_x$) se ve principalmente influenciada por la composición del medio de gasificación. Cuanto mayor es la relación $H_2O/O_2$, mayor es la producción de hidrocarburos ligeros ($\beta_{H2O/O2} > 0$), lo que sugiere una mayor reactividad de estos gases con oxígeno que con vapor de agua. Además, la mayor presencia de $H_2$ en la atmósfera gaseosa al aumentar la relación $H_2O/O_2$ puede contribuir a la formación de $CH_4$ a través de la reacción de metanización (ec. 2.5). En el caso de la gasificación del lodo, el rendimiento a $CH_4$ se ve negativamente afectado por la relación gasificante ($\beta_{RG} < 0$) y, a diferencia de los resultados mostrados por otros autores (Kim y cols., 2001; Pinto y cols., 2003), positivamente afectado por la temperatura ($\beta_T > 0$), lo que puede deberse a una mayor importancia de la reacción de metanización a alta temperatura. Por otro lado, el aumento de temperatura reduce la producción neta de $C_2H_x$ en la gasificción de lodo ($\beta_T < 0$). Ninguno de estos efectos ha resultado significativo en la producción de $C_2H_X$ en la gasificación de *char*, para la que se obtuvieron resultados muy similares en la mayoría de los experimentos (Tabla 4.2).

Por último, la producción de $H_2S$ en ambos procesos de gasificación se ve acrecentada a alta temperatura ($\beta_T > 0$) y/o alta relación gasificante ($\beta_{RG} > 0$).

Además de la producción específica de cada compuesto gaseoso, la evolución de las relaciones molares $H_2/CO$ y $CO/CO_2$ en el gas de salida resulta de especial interés para el posible uso del gas como materia prima para la producción de químicos. La relación molar $H_2/CO$ se puede incrementar mediante el aumento de la relación $H_2O/O_2$ utilizada como agente gasificante ($\beta_{H2O/O2} > 0$) y/o mediante la reducción de la temperatura de gasificación ($\beta_T < 0$). La influencia relativa de ambos factores es bastante similar en el gas producto de la gasificación de *char* (Tabla 4.4), pero el tipo de agente gasificante juega un papel más importante en la relación $H_2/CO$ del gas producto de la gasificación de lodo (Tabla 4.3). Por otro lado, la relación $CO/CO_2$ en ambos gases de salida se ve significativamente favorecida al aumentar la temperatura ($\beta_T > 0$) y/o al disminuir la relación gasificante ($\beta_{RG} < 0$), mientras que la composición del medio de gasificación no ejerce una influencia significativa en ella.

En cuanto al contenido energético del gas, el análisis ANOVA muestra que la temperatura es el factor más influyente en el PCI del gas cuando se gasifica *char* (Tabla 4.4), mientras que la influencia relativa de los tres factores estudiados en el PCI del gas es similar cuando se gasifica lodo (Tabla 4.3). Como se puede observar en la Figura 4.5, y a diferencia de los resultados mostrados por algunos autores (Pinto y cols., 2003), la temperatura ejerce un efecto positivo en el PCI de ambos productos gaseosos ($\beta_T > 0$). Dado que el contenido de hidrocarburos en el gas (en términos de composición volumétrica) disminuye al aumentar la temperatura, cabría esperar una reducción del PCI con la temperatura. Sin embargo, la concentración de $CO_2$ en el gas también disminuye con la temperatura, y lo hace en una mayor proporción que el contenido de hidrocarburos (Tablas 4.1 y 4.2), lo que al final se traduce en un aumento del PCI con la temperatura debido a la menor dilución del contenido energético del gas. El PCI de los gases también se ve favorecido con el aumento de la relación $H_2O/O_2$ ($\beta_{H2O/O2} > 0$) debido al aumento de la fracción de hidrocarburos y a la disminución simultánea del porcentaje de $CO_2$. En el caso de la gasificación del lodo, este efecto se ve claramente potenciado a baja temperatura (Figura 4.5.a).

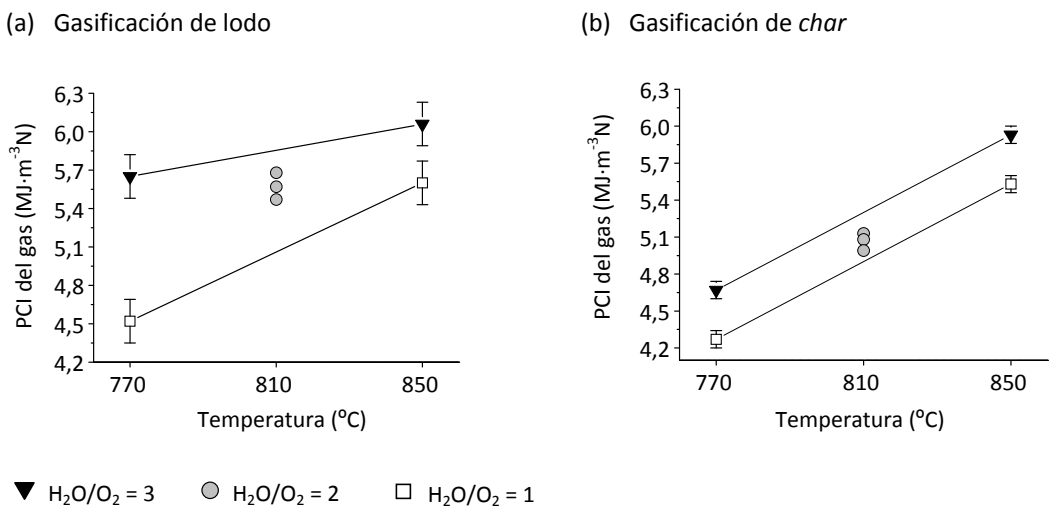


Figura 4.5. Poder calorífico inferior (MJ·m$^{-3}$N) del gas producto de la (a) gasificación de lodo y (b) gasificación de *char* (RG = 0,95 g·g$^{-1}_{org}$). Las barras de error en las figuras representan la mínima diferencia significativa.

Igual que ocurre con la producción de gas y con su PCI, la eficiencia energética de ambos procesos de gasificación depende principalmente de la temperatura de gasificación. Esta eficiencia puede mejorarse hasta casi en 20 puntos porcentuales mediante el aumento de la temperatura de 770 a 850 ºC ($\beta_T > 0$) (Figura 4.6) gracias al incremento del rendimiento a gas y de su PCI. La relación $H_2O/O_2$ también afecta positivamente a la eficiencia de gasificación ($\beta_{H2O/O2} > 0$), aunque en menor grado que la temperatura. Además, en el caso de la gasificación

de *char*, la relación gasificante es también un factor significativo ($\beta_{RG} > 0$), además de algunos efectos sinérgicos y antagónicos entre los factores, pero su influencia relativa es mucho menos importante que el efecto individual de la temperatura.

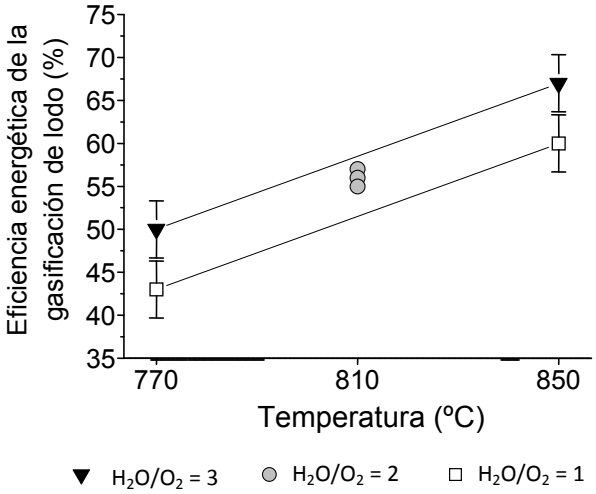


Figura 4.6. Eficiencia energética en la gasificación de lodo (%). Las barras de error en la figura representan la mínima diferencia significativa.

La composición del alquitrán recogido tras los experimentos de gasificación de lodo se analizó cualitativamente por cromatografía de gases. A modo de ejemplo, la Figura 4.7 muestra uno de los cromatogramas obtenidos con el detector de ionización de llama. El análisis de la composición de los alquitranes suele realizarse clasificando los compuestos en varias familias en función de su peso molecular y composición atómica (Li y Suzuki, 2009a). Las familias y compuestos considerados en este estudio han sido: (i) compuestos aromáticos con un solo anillo (estireno y benceno); (ii) compuestos poliaromáticos con 2 y 3 anillos (indeno, naftaleno, metil-naftaleno, bifenilo, bifenileno, fluoreno, antraceno y fenantreno) (iii) compuestos aromáticos heterocíclicos con átomos de N (incluyendo metil-piridina, benzonitrilo, metil-benzonitrilo, quinolina, metil-quinolina, indol, fenil-piridina, naftalenocarbonitrilo, benzoquinolina y 5H-indeno-[1,2-b]-piridina); (iv) compuestos aromáticos heterocíclicos con átomos de O (fenol y benzofurano); y (v) compuestos orgánicos con S (2-benzotiofeno y 3,3'-tiobis-propanonitrilo).

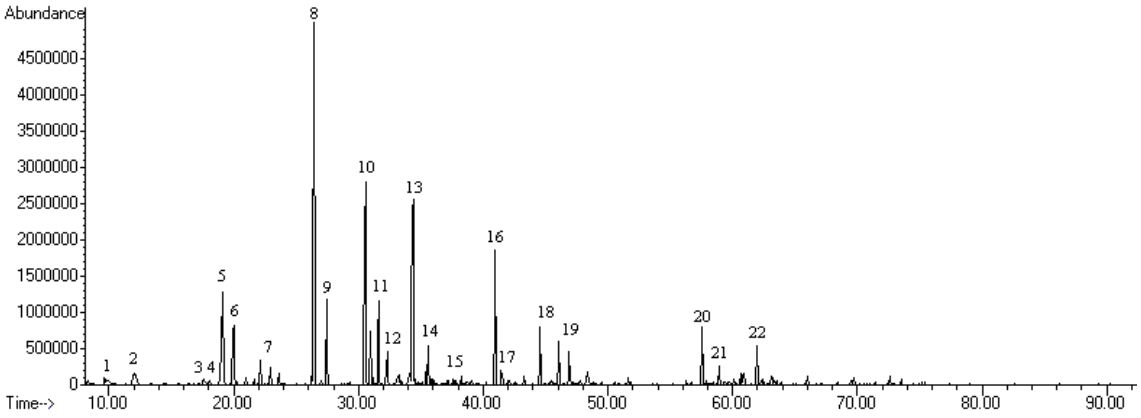


1. n-metil-piridina (9,6 min)
2. estireno (11,9 min)
3. fenol (17,5 min)
4. benzofurano (17,6 min)
5. benzonitrilo (19,2 min)
6. indeno (20,0 min)
7. n-metil-benzonitrilo (22,1 min)
8. naftaleno (26,4 min)
9. 2-benzotiofeno (27,5 min)
10. quinolina (30,6 min)
11. n-metil-naftaleno (31,0 min)
12. n-metil-quinolina (33,1 min)
13. indol (34,3 min)
14. bifenilo (35,6 min)
15. bifenileno (40,9 min)
16. n-fenil-piridina (41,4 min)
17. naftaleno-n-carbonitrilo (44,5 min)
18. fluoreno (46,9 min)
19. 3,3'-tiobis-propanonitrilo (48,4 min)
20. antraceno/fenantreno (57,6 min)
21. benzoquinolina (58,9 min)
22. 5H-indeno-[1,2-b]piridina (61,9 min)

Figura 4.7. Cromatograma de iones totales (TIC) de la muestra de alquitrán del experimento 3 (850 ºC, RG = 0,8 y $H_2O/O_2$ = 3.

Las áreas de los principales picos identificados en los cromatogramas TIC (especificados en su mayoría en la Figura 4.7) se han utilizado para evaluar la influencia de las condiciones de operación en la composición de las muestras de alquitrán. La Tabla 4.5 recoge estos porcentajes de área cromatográfica, agrupando los compuestos por familias. Cabe destacar que estos datos porcentuales no representan la composición real de las muestras, ya que el factor de respuesta área/concentración no es el mismo para todos los compuestos, pero estos datos son útiles para la comparación de las muestras y el análisis de la influencia de los factores.

Tabla 4.5. Porcentaje de área cromatográfica correspondiente a cada familia de compuestos del alquitrán.

| Temperatura (ºC) | 850 | 770 | 850 | 770 | 850 | 770 | 850 | 770 | 810 |
|---|---|---|---|---|---|---|---|---|---|
| Relación gasificante ($g \cdot g^{-1}_{org}$) | 1,1 | 1,1 | 0,8 | 0,8 | 1,1 | 1,1 | 0,8 | 0,8 | 0,95 |
| Relación molar $H_2O/O_2$ | 3 | 3 | 3 | 3 | 1 | 1 | 1 | 1 | 2 |
| Aromáticos con 1 anillo | 10 | 12 | 4 | 13 | 5 | 10 | 4 | 10 | 7 ± 2 |
| Poliaromáticos (2-3 anillos) | 9 | 9 | 34 | 5 | 40 | 42 | 45 | 23 | 36 ± 9 |
| Aromáticos con N | 75 | 68 | 57 | 69 | 46 | 44 | 44 | 61 | 50 ± 14 |
| Aromáticos con O | 3,0 | 7,7 | 0,3 | 7,7 | 0,6 | 2,1 | 1,0 | 6,0 | 2,6 ± 0,8 |
| Orgánicos con S | 4 | 3 | 4 | 5 | 8 | 3 | 6 | 1 | 5 ± 1 |

*Los datos de la última columna representan la media ± desviación estándar de las 3 réplicas del punto central.*

De acuerdo con el análisis ANOVA de los porcentajes de área cromatográfica (Tabla 4.6), la temperatura y la relación $H_2O/O_2$ son los únicos factores con un efecto significativo en la composición del alquitrán. Hay que destacar que la repetitividad de los resultados no fue todo lo buena que podría desearse, por lo que sólo los efectos con una clara influencia han resultado significativos en el análisis ANOVA.

Tabla 4.6. Coeficientes de regresión lineal (β) obtenidos del análisis ANOVA del área cromatográfica de las familias de compuestos en el alquitrán de la gasificación de lodo.

| | Valor medio | $\beta_T$ | $\beta_{RG}$ | $\beta_{H2O/O2}$ | $\beta_{T-RG}$ | $\beta_{T-H2O/O2}$ | $\beta_{RG-H2O/O2}$ | $\beta_{T-H2O/O2-RG}$ | Curvatura |
|---|---|---|---|---|---|---|---|---|---|
| Aromáticos con 1 anillo | 8,51 | -2,81 | * | * | * | * | * | * | * |
| Poliaromáticos (2-3 anillos) | 25,78 | * | * | -11,50 | * | * | * | * | * |
| Aromáticos con N | 58,04 | * | * | 9,11 | * | * | * | * | * |
| Aromáticos con O | 3,55 | -2,32 | * | * | * | * | * | * | * |
| Orgánicos con S | 4,14 | 1,26 | * | * | | -1,26 | -0.84 | * | * |

** término no significativo.*

Las familias de compuestos aromáticos más ligeros (1 anillo) y de aromáticos con átomos de O son las más sensibles a la variación de temperatura, disminuyendo su presencia con el aumento de la temperatura. Los compuestos fenólicos, parafinas, olefinas y aromáticos alquilados pueden ser fácilmente craqueados a altas temperaturas (Ponzio y cols., 2006). El aumento de la fracción de compuestos sulfurados con la temperatura puede ser sólo una consecuencia de la disminución de las otras fracciones de compuestos. Por otro lado, las familias de compuestos poliaromáticos y de aromáticos con N parecen las más sensibles a la relación $H_2O/O_2$ utilizada como agente gasificante. El aumento de la relación $H_2O/O_2$ conduce a una disminución en la fracción de poliaromáticos, lo que puede deberse a la interferencia del vapor de agua en las reacciones de polimerización. El peso molecular de los compuestos que forman parte del alquitrán depende de la presencia de radicales libres de H, relacionada con la disponibilidad de vapor de agua en el medio de gasificación (Qin y cols., 2010). La variación de la fracción de compuestos poliaromáticos se ha visto acompañada de una variación, en sentido opuesto, de la presencia de compuestos aromáticos con N, lo cual puede ser sólo una consecuencia del hecho de estar analizando datos porcentuales.

*Producción teórica de gases basada en datos de equilibrio*

El rendimiento o producción experimental de los distintos compuestos gaseosos obtenidos en la gasificación de lodo y de *char* se ha comparado con la producción teórica que cabría esperar en condiciones de equilibrio. Esta producción de gases en el equilibrio se ha

calculado con el software HSC Chemistry 6.1, que utiliza el método de minimización de la energía de Gibbs para calcular la composición de equilibrio en condiciones isotérmicas e isobáricas. El sistema de reacción debe ser especificado para los cálculos, incluyendo la temperatura de reacción, presión, cantidad de reactivos (agente gasificante y análisis elemental del sólido) y posibles especies que podrían formar parte de los productos. Las condiciones de temperatura, presión y alimentación de agente gasificante fueron las mismas que las estudiadas en el laboratorio. Como posibles especies que podrían formar parte de los productos en el equilibrio se especificaron todos los gases obtenidos en los experimentos ($H_2$, $N_2$, $O_2$, CO, $CO_2$, $H_2O$, $CH_4$, $C_2H_x$ y $H_2S$), además de $NH_3$, carbono sólido (C) y diversos compuestos modelo habituales en el alquitrán de gasificación (benceno, tolueno, naftaleno, y piridina). Los gases mayoritarios obtenidos en las simulaciones de equilibrio fueron $N_2$, $H_2$, CO, $CO_2$, $H_2O$, $CH_4$, $H_2S$ y $NH_3$. Los demás compuestos especificados aparecían en concentraciones insignificantes (% < $10^{-10}$).

En las Figuras 4.8 y 4.9 se comparan los datos teóricos y experimentales de la producción de $H_2$, CO, $CO_2$ y $CH_4$ en la gasificación de lodo y de *char*, respectivamente. Los rendimientos experimentales a $H_2$ y CO están claramente por debajo de sus correspondientes datos de equilibrio, mientras que los rendimientos experimentales a $CO_2$ y $CH_4$ son mayores que los valores teóricos de equilibrio. Estas diferencias ponen de manifiesto que el equilibrio químico no fue alcanzado en los experimentos de gasificación. Esto puede deberse a un insuficiente tiempo de residencia de los gases y vapores en el reactor y/o a que en el proceso existen reacciones limitantes controladas por la cinética o por la transferencia de masa.

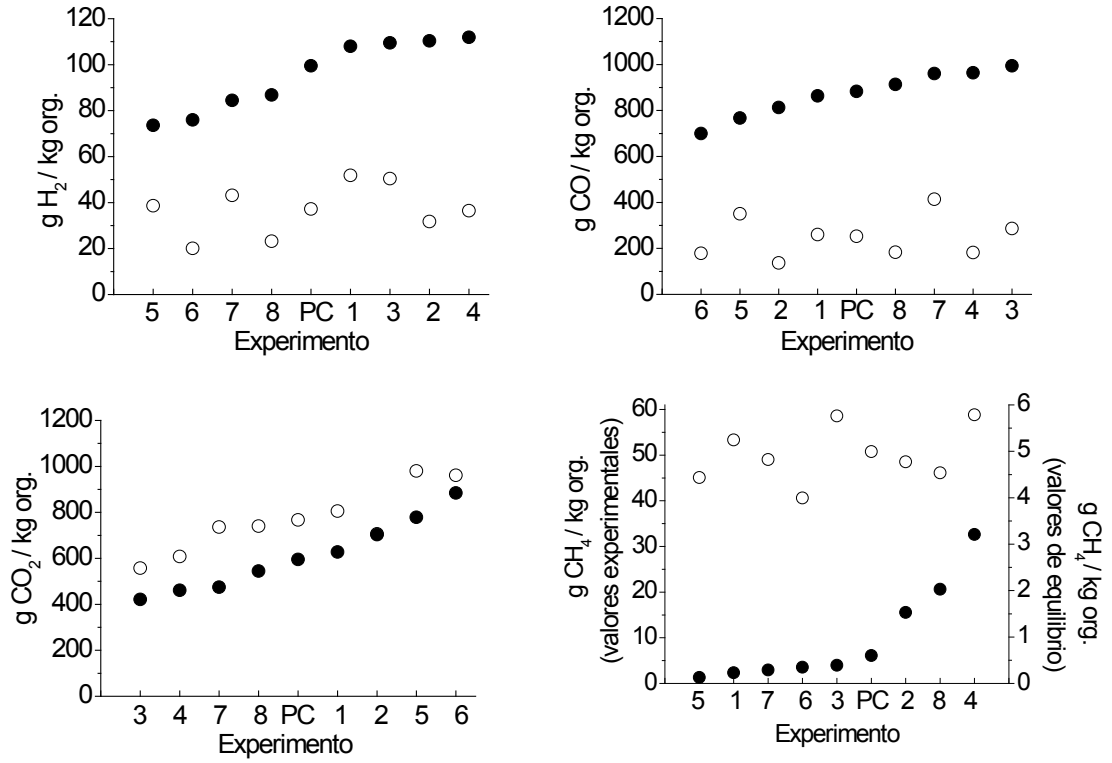


*PC: Punto central (media de los experimentos 9, 10 y 11).*

Figura 4.8. Producción teórica (●) y experimental (○) de $H_2$, CO, $CO_2$ y $CH_4$ en la gasificación de lodo.

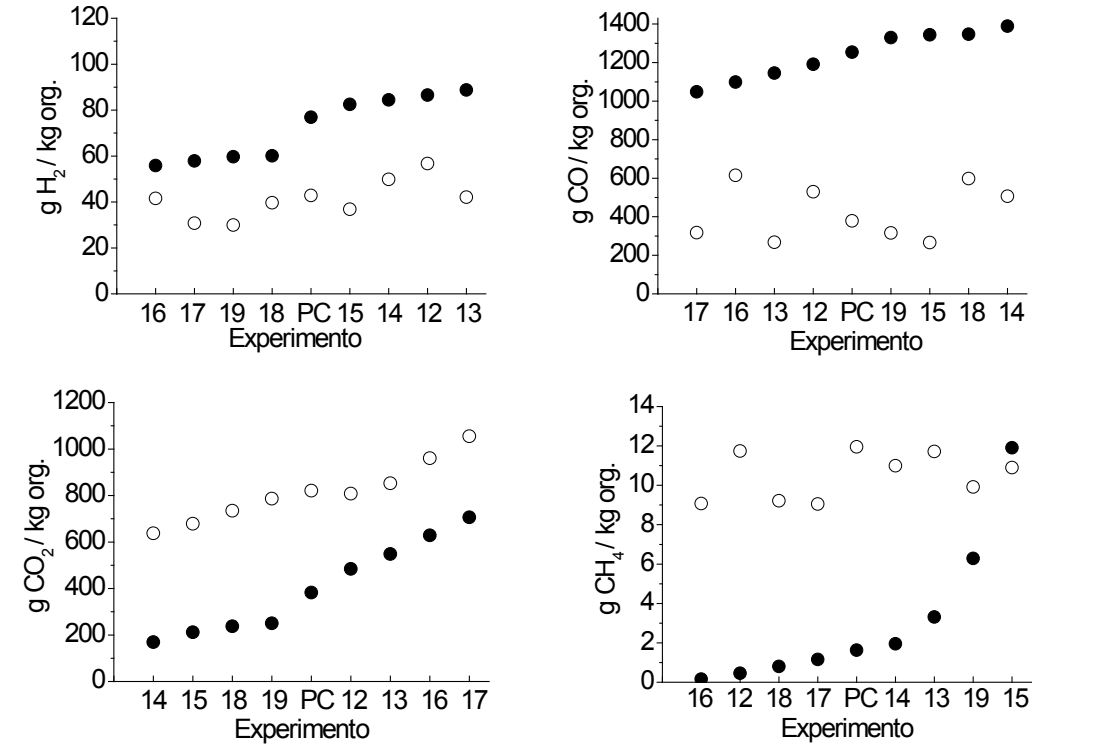


*PC: Punto central (media de los experimentos 20, 21 y 22).*

Figura 4.9. Producción teórica (●) y experimental (○) de $H_2$, CO, $CO_2$ y $CH_4$ en la gasificación de *char*.

La influencia de los factores de operación sobre los rendimientos teóricos a $H_2$, CO, $CO_2$ y $CH_4$ en el equilibrio ha sido analizada estadísticamente mediante análisis ANOVA. Los coeficientes de regresión lineal (β) obtenidos para los valores codificados de los factores se muestran en la Tabla 4.7.

Tabla 4.7. Coeficientes de regresión lineal (β) obtenidos del análisis ANOVA de los datos de producción de gases en el equilibrio.

| | Valor medio | $\beta_T$ | $\beta_{RG}$ | $\beta_{H2O/O2}$ | $\beta_{T\text{-}RG}$ | $\beta_{T\text{-}H2O/O2}$ | $\beta_{RG\text{-}H2O/O2}$ | $\beta_{T\text{-}H2O/O2\text{-}RG}$ | Curvatura |
|---|---|---|---|---|---|---|---|---|---|
| *Gasificación de lodo* | | | | | | | | | |
| $H_2$ ($g \cdot kg^{-1}_{org}$) | 95,04 | -1,15 | -3,20 | 14,80 | * | * | 2,37 | * | ** |
| CO ($g \cdot kg^{-1}_{org}$) | 873,07 | 24,65 | -87,22 | 36,38 | * | * | 15,83 | * | * |
| $CO_2$ ($g \cdot kg^{-1}_{org}$) | 610,16 | -36,50 | 138,61 | -58,31 | -8,80 | 7,52 | -24,41 | * | ** |
| $CH_4$ ($g \cdot kg^{-1}_{org}$) | 1,07 | -0,81 | -0,56 | 0,42 | 0,43 | -0,33 | -0,17 | 0,14 | ** |
| *Gasificación de char* | | | | | | | | | |
| $H_2$ ($g \cdot kg^{-1}_{org}$) | 71,97 | * | * | 13,58 | -0,82 | * | 1,81 | * | ** |
| CO ($g \cdot kg^{-1}_{org}$) | 1236,58 | 19,95 | -115,74 | 30,59 | * | * | 16,57 | * | * |
| $CO_2$ ($g \cdot kg^{-1}_{org}$) | 404,57 | -24,71 | 187,33 | -51,24 | -10,69 | * | -24,55 | * | ** |
| $CH_4$ ($g \cdot kg^{-1}_{org}$) | 3,25 | -2,41 | -1,98 | 1,15 | 1,45 | -0,79 | -0,54 | 0,32 | ** |

** término no significativo; ** curvatura significativa*

Los efectos de los factores de operación sobre la producción experimental y de equilibrio de $H_2$, CO, $CO_2$ y $CH_4$ muestran algunas diferencias importantes: (i) la temperatura era el factor más influyente en los rendimientos experimentales a $H_2$ y CO, pero no lo es en los datos de equilibrio; la relación $H_2O/O_2$ ejerce el efecto más significativo en la producción de equilibrio de $H_2$, mientras que la relación gasificante ejerce la mayor influencia en la producción teórica de CO; (ii) la producción de equilibrio de $H_2$ apenas se ve afectada por la temperatura; sólo se observa un pequeño efecto negativo de la temperatura en el caso de la gasificación de lodo; (iii) la producción de equilibrio de CO no se ve afectada negativamente por la relación $H_2O/O_2$ como ocurría con los datos experimentales, sino que le afecta positivamente; (iv) la producción de equilibrio de $CH_4$ no se ve afectada positivamente por la temperatura como ocurría con los datos experimentales en la gasificación de lodo, sino que se ve drásticamente reducida con el aumento de temperatura. A diferencia de lo que ocurre en un proceso controlado por la cinética o por fenómenos de difusión, en los que un aumento de temperatura favorece tanto la velocidad de reacción como la transferencia de masa, en el régimen de control termodinámico el aumento de temperatura no resulta favorable para el transcurso de las reacciones exotérmicas (principio de Le Châtelier). Esto justifica las diferencias observadas y pone de manifiesto la importancia de discernir entre control cinético o control termodinámico en un proceso de gasificación de cara a la optimización de las condiciones de operación.

## 4.2. Evaluación energética

En esta sección se plantea un estudio energético de las etapas de gasificación de lodo y de *char*, cuyos resultados experimentales han sido detallados en el apartado anterior. Además, esta sección incluye también un balance energético del proceso de pirólisis de lodo, en el que se genera el *char* como subproducto, y un análisis del consumo energético necesario para el secado térmico del lodo, previo a las etapas de pirólisis o gasificación. Los balances energéticos de las distintas etapas permiten tener una idea global del coste energético asociado al tratamiento termoquímico del lodo mediante: (i) secado y gasificación del lodo, y (ii) secado y pirólisis del lodo y gasificación del *char* (Figura 4.10).

(a) Secado y gasificación del lodo

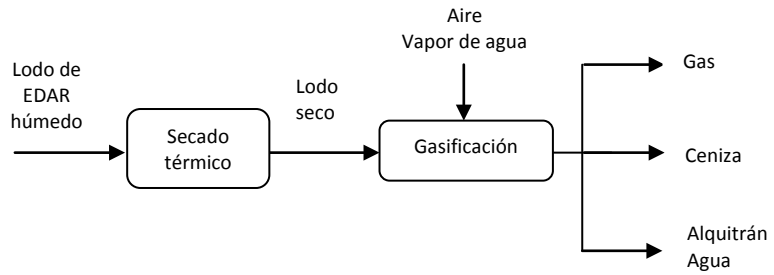


(b) Secado y pirólisis del lodo y gasificación del *char*.

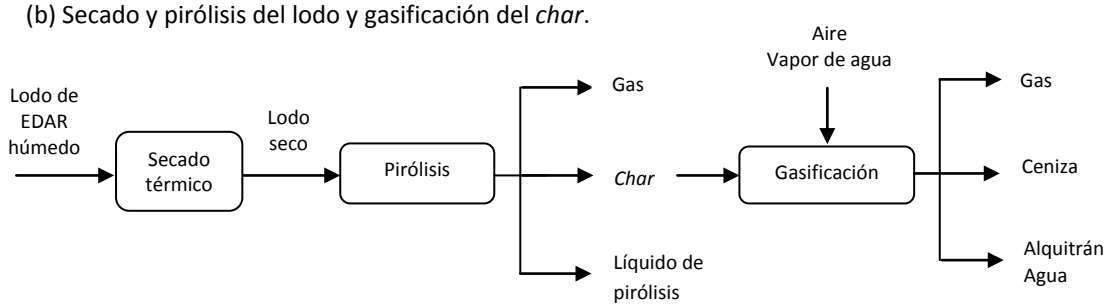


Figura 4.10. Diagrama de dos posibles tratamientos termoquímicos para la gestión de los lodos de EDAR.

La demanda energética de las etapas de gasificación y pirólisis se ha calculado utilizando los rendimientos experimentales a los distintos productos. Como se detalla más adelante, algunas de las propiedades de los reactantes y productos necesarias para los cálculos fueron medidas experimentalmente, mientras que otras se obtuvieron de datos bibliográficos. Los balances energéticos se han realizado considerando las siguientes hipótesis y simplificaciones:

- Reactor adiabático. No se consideran pérdidas de calor.
- La capacidad calorífica específica, Cp (T), de los reactivos y productos sólidos (lodo, *char* de pirólisis y cenizas de gasificación), que es una de las propiedades requeridas para los cálculos energéticos, se ha considerado constante con la temperatura. Aunque estas

capacidades caloríficas específicas fueron medidas experimentalmente por calorimetría diferencial de barrido, las limitaciones operacionales del equipo no permitieron obtener la función Cp (T) en el intervalo completo de temperatura requerido en cada caso (hasta 530 ºC para el *char* y hasta 850 ºC para las cenizas de gasificación), por lo que se optó por trabajar con valores constantes de Cp medidos en valores intermedios de dichos intervalos de temperatura (a 300 ºC para el char y a 500 ºC para a ceniza).

- Como se explica más adelante de forma más detallada, la composición de los condensados recogidos en ambos procesos (alquitrán de gasificación o líquido de pirólisis) se ha simplificado considerando sólo algunos de sus compuestos con el fin de obtener datos de propiedades de la bibliografía.

La demanda energética de los procesos de pirólisis y gasificación (Q) puede obtenerse por diferencia de las entalpías de las corrientes que entran ($\Delta H_{entra}$) y salen ($\Delta H_{sale}$) del reactor:

$$Q\ (MJ \cdot kg^{-1}_{\text{materia prima}}) = \Delta H_{sale} - \Delta H_{entra} \qquad \text{(ec. 4.1)}$$

De acuerdo con la ec. 4.1, Q < 0 se corresponde con un proceso exotérmico, mientras que Q > 0 hace referencia a un proceso endotérmico. La entalpía total de cada corriente de entrada o salida (ΔH), por kilogramo de materia prima alimentado, se calcula con la ec. 4.2.

$$\Delta H\ (MJ \cdot kg^{-1}_{\text{materia prima}}) = \sum_i m_i \cdot (\Delta H^o_{f,i} + \int_{T_{ref}}^{T} Cp_i\ (T) \cdot dT) \qquad \text{(ec. 4.2)}$$

donde:

- $m_i$ es el rendimiento másico de cada corriente o, en el caso de la corriente gaseosa, de cada compuesto gaseoso ya que se conocen los rendimientos individuales de cada uno. La base de cálculo utilizada ha sido de 1 kg de lodo en el proceso de pirólisis, y 1 kg de lodo o de *char* en el proceso de gasificación ($kg \cdot kg^{-1}_{\text{materia prima}}$).
- $T_{ref}$ es la temperatura de referencia (298 K) y T es la temperatura a la que se encuentra cada corriente (K). Todas las corrientes de entrada se consideran a temperatura ambiente (298 K), excepto el vapor de agua utilizado en los experimentos de gasificación que se alimentó a 150 ºC (448 K).
- $\Delta H^o_{f,i}$ es la entalpía estándar de formación ($MJ \cdot kg^{-1}$) de cada corriente o compuesto a la temperatura de referencia (298 K). Los datos de $\Delta H^o_f$ de los compuestos gaseosos se han obtenido de la literatura (Perry y Green, 1999), mientras que los correspondientes a los materiales sólidos y al líquido de pirólisis se han calculado a partir de los datos experimentales de análisis elemental y poder calorífico de acuerdo con la siguiente ecuación:

$$\Delta H^{o}_{f,i} = \left(\sum_j m_j \cdot \Delta H^{o}_{f,j}\right) + PCS_i \qquad \text{(ec. 4.3)}$$

donde 'j' representa cada producto derivado de la combustión completa del material ($CO_2$, $H_2O$, $SO_2$ y NO), $m_j$ es la masa de cada gas de combustión producido por kilogramo de material, $\Delta H^{o}_{f,j}$ es la entalpía estándar de formación de cada gas de combustión y $PCS_i$ es el poder calorífico superior del material. Esta forma de calcular la $\Delta H^{o}_{f}$ no incluye la entalpía correspondiente a la fracción inorgánica de los sólidos, pero este dato no es necesario para realizar los balances energéticos ya que la fracción inorgánica se considera inerte en el proceso.

- $Cp_i$ (T) es la capacidad calorífica específica de cada corriente o compuesto en función de la temperatura ($MJ \cdot kg^{-1} \cdot K^{-1}$). Como se ha comentado anteriormente, el Cp de los sólidos se midió experimentalmente por calorimetía diferencial de barrido, mientras que los datos de Cp (T) de los gases y vapores se obtuvieron de la bibliografía (*ChemSpider database*; Harrison y Seaton, 1988; Perry y Green, 1999). Si el intervalo de temperatura en la integral de la ec. 4.2 implica un cambio de fase, la entalpía de vaporización ($\Delta H_{vap}$) de los compuestos condensables y su Cp (T) en fase líquida también deben incluirse en la ecuación. Estos datos (para los compuestos condensables considerados en cada caso) se han obtenido de bases de datos y de estudios de la bibliografía (*ChemSpider database*; Chueh y Swanson, 1973).

A continuación se detallan los datos y consideraciones más específicas para el cálculo de la demanda energética en los procesos de pirólisis y gasificación.

*Pirólisis de lodo*

La distribución de productos resultante de la pirólisis de lodo, así como las propiedades de los mismos necesarias para el balance de energía, se recogen en la Tabla 4.8 (Gil-Lalaguna y cols., 2010). El líquido recogido después de la condensación de los vapores está compuesto de tres fases: fase orgánica ligera (FOL), fase orgánica pesada (FOP) y fase acuosa (FA). Las propiedades de las tres fases se midieron por separado, considerando cada fase líquida como un producto distinto para los cálculos.

Tabla 4.8. Rendimientos y propiedades de los productos de la pirólisis de lodo de EDAR.

| Rendimiento másico (%) | Composición | PCS ($MJ \cdot kg^{-1}$) | $\Delta H^o_f$ ($MJ \cdot kg^{-1}$) | Cp (T) ($kJ \cdot K^{-1} \cdot kg^{-1}$) | $\Delta H_{vap}$ ($MJ \cdot kg^{-1}$) |
|---|---|---|---|---|---|
| *Char* | | | | | |
| 51,9 ± 0,7 | *Análisis elemental (% en masa):*<br>C: 15,49; H: 0,97; N: 1,85; S: 0,35 | 5,2 ± 0,2 | -1,18 | 1,21 (300 °C) | --- |
| *Gases no condensables (sin incluir el $N_2$)* | | | | | |
| 10,1 ± 0,9 | *(% en masa)*<br>$CO_2$: 74,3 ± 0,9<br>CO: 13,2 ± 0,1<br>$H_2$: 1,7 ± 0,1<br>$CH_4$: 3,8 ± 0,1<br>$C_2H_6$: 1,4 ± 0,2<br>$C_2H_4$: 1,4 ± 0,1<br>$H_2S$: 4,3 ± 0,9 | 8,0 ± 0,3 | -7,39 | 1,18 (25 °C)<br>1,56 (530 °C) | --- |
| *Fase orgánica ligera (FOL)* | | | | | |
| 2,2 ± 0,2 | *Análisis elemental (% en masa):*<br>C: 85,92; H: 11,83: N: 1,80; S: 0,27<br>Agua: 0 (% en masa)<br>Orgánicos: 100 (% en masa) | 43,10 ± 0,04 | -1,74 | 1,85 (líquido)<br>3,07 (530 °C) | 0,18 |
| *Fase orgánica pesada (FOP)* | | | | | |
| 9,4 ± 0,2 | *Análisis elemental (% en masa):*<br>C: 69,54; H: 8,97; N: 9,44; S: 1,24<br>Agua: 6,4 ± 0,3 (% en masa)<br>Orgánicos: 93,6 ± 0,3 (% en masa) | 32 ± 2 | -3,49 | 2,13 (líquido)<br>2,36 (530 °C) | 0,55 |
| *Fase acuosa (FA)* | | | | | |
| 20,8 ± 0,2 | *Análisis elemental (% en masa):*<br>C: 11,17; H: 10,45; N: 6,52; S: 0,37<br>Agua: 73,8 ± 0,4 (% en masa)<br>Orgánicos: 26,2 ± 0,4 (% en masa) | 5,7 ± 0,3 | -12,44 | 3,59 (líquido)<br>2,12 (530 °C) | 1,77 |

*El error experimental se expresa como la media ± desviación estándar de 2 réplicas.*

El PCS de los sólidos y de las fases líquidas se midió experimentalmente con un calorímetro, mientras que el PCS del gas se calculó a partir de su composición. La $\Delta H^o_f$ de los sólidos y líquidos se puede calcular con la ec. 4.3, mientras que la $\Delta H^o_f$ de los distintos compuestos gaseosos puede obtenerse de la bibliografía (Perry y Green, 1999). Como se ha comentado anteriormente, se han utilizado valores constantes de Cp para los sólidos: $1{,}15 \cdot 10^{-3}$ $MJ \cdot kg^{-1} \cdot K^{-1}$ para el lodo y $1{,}21 \cdot 10^{-3}$ $MJ \cdot kg^{-1} \cdot K^{-1}$ para el *char*. La composición de las fases líquidas se ha simplificado considerando sólo su contenido de agua (determinado mediante el método Karl Fischer) y un compuesto representativo de toda la fracción orgánica en cada una de las fases: 4-colesteno para la FOL, 3-metil-fenol para la FOP y ácido acético para la FA. Estos compuestos fueron elegidos por ser algunos de los compuestos con mayor área cromatográfica en el análisis de las muestras por cromatografía con detector de ionización de

llama. La Cp y la $\Delta H_{vap}$ de las fracciones orgánicas de las fases líquidas se han equiparado a las de estos compuestos elegidos como representativos, cuyos datos han sido obtenidos de la bibliografía (*ChemSpider database*; Chueh y Swanson, 1973; Harrison y Seaton, 1988; Perry y Green, 1999). Los valores globales de Cp y $\Delta H_{vap}$ para cada fase pueden estimarse como un promedio ponderado de los datos correspondientes al agua y al compuesto orgánico elegido en cada fase.

Aplicando todos estos datos en la ec. 4.2, la entalpía total de las corrientes que entran al reactor ($\Delta H_{entra}$) es de -3,28 $MJ \cdot kg^{-1}_{lodo}$ y la entalpía total de los productos ($\Delta H_{sale}$) considerados a la temperatura de pirólisis (T = 803 K) es de -3,13 $MJ \cdot kg^{-1}_{lodo}$. La diferencia de estas entalpías (ec. 4.1) resulta en una demanda energética de 0,15 $MJ \cdot kg^{-1}_{lodo}$ para llevar a cabo la descomposición térmica del lodo durante el proceso de pirólisis. Este valor es algo menor que los datos encontrados en la bibliografía para la pirólisis de otros tipos de biomasa. Por ejemplo, la pirólisis de residuos de cosecha conlleva un coste energético de 0,3 $MJ \cdot kg^{-1}$ (Mangaro y cols., 2011). El mayor contenido de ceniza en el lodo, que no se descompone durante el proceso, puede explicar esta diferencia.

Si se considera el enfriamiento de los gases y vapores a la salida del reactor hasta temperatura ambiente (298 K) para aprovechar su energía térmica (calor sensible y latente), el proceso de pirólisis pasa a ser exotérmico, con un calor neto de -0,70 $MJ \cdot kg^{-1}_{lodo}$. Por lo tanto, bajo las hipótesis consideradas, la etapa de pirólisis podría ser un proceso autosuficiente desde el punto de vista energético.

*Gasificación de lodo y de char*

La distribución de productos obtenida experimentalmente en la gasificación del lodo de EDAR y de su *char* de pirólisis se mostró en las Tablas 4.1 y 4.2. Estos datos permiten calcular la demanda energética de ambos procesos bajo diferentes condiciones de operación.

La composición de las fracciones de alquitrán obtenidas en los experimentos se ha simplificado a una mezcla equimolar de benceno, naftaleno y piridina (compuestos presentes en la mayoría de las muestras). Así, los datos de $\Delta H^o_f$, Cp y $\Delta H_{vap}$ del alquitrán, necesarios para los balances energéticos, se han equiparado a los promedios ponderados de los valores correspondientes a estos tres compuestos, que se pueden encontrar en la bibliografía. Por otro lado, la Cp de los subproductos sólidos de la gasificación se ha aproximado en todos los casos a la de la ceniza del lodo, ya que estos sólidos están compuestos principalmente de ceniza (> 93% de su masa en la mayoría de los casos). La Cp (T) de la ceniza de lodo se midió experimentalmente por calorimetría diferencial de barrido, y el valor constante utilizado ha

sido $1{,}07 \cdot 10^{-3}$ MJ·K$^{-1}$·kg$^{-1}$ (medido a 500 ºC). La $\Delta H^{o}_{f}$ de los sólidos se ha calculado con la ec. 4.3, utilizando la fórmula de Dulong para calcular el PCS a partir de su análisis elemental [PCS (kJ·kg$^{-1}$) = 339·%C + 1430·(%H - %O/8 ) + 105·%S].

Todos estos datos se utilizan para calcular, con la ec. 4.2, las entalpías de las corrientes de entrada y de salida del reactor (considerando los productos a la temperatura de gasificación) y, con ellas, la demanda energética para las diferentes condiciones de operación estudiadas (ec. 4.1). Los resultados obtenidos se representan en la Figura 4.11 en función de la temperatura de gasificación (770-850 ºC) y de la composición del medio gasificante: RE (relación equivalente) y S/B (relación másica entre el vapor de agua y la cantidad de materia orgánica en el lodo o en el *char*).

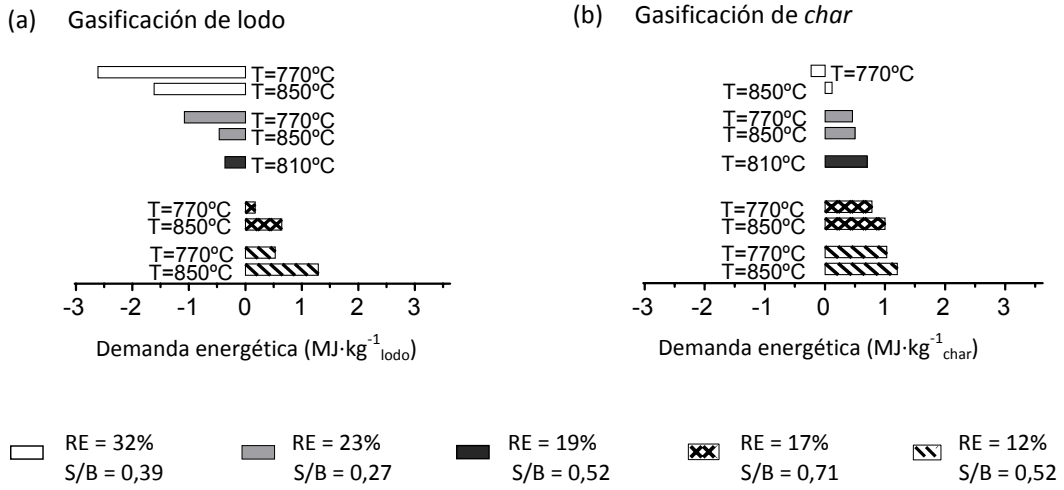


Figura 4.11. Demanda energética en la (a) gasificación de lodo y (b) gasificación de *char*, calculada con rendimientos experimentales y considerando los productos a la temperatura de gasificación.

Bajo las hipótesis realizadas, la demanda energética oscila entre -2,61 y 1,29 MJ·kg$^{-1}_{lodo}$ para la gasificación de lodo de EDAR y entre -0,23 y 1,20 MJ·kg$^{-1}_{char}$ para la gasificación de *char*. Por lo tanto, las condiciones de operación ejercen una mayor influencia en el balance energético de la gasificación del lodo. Por otro lado, a pesar de que el contenido orgánico del *char* es bastante menor que el del lodo (Tabla 3.1), gasificar 1 kg de *char* conlleva, en general, una mayor demanda de energía externa que gasificar 1 kg de lodo. Por ejemplo, la demanda energética en la gasificación de lodo cuando se opera con RE = 17%, S/B = 0,71 y T = 850ºC es de 0,64 MJ·kg$^{-1}_{lodo}$, mientras que alcanza 1,00 MJ·kg$^{-1}_{char}$ en la gasificación de *char*. Los cambios observados en la estructura carbonosa del sólido después del proceso de pirólisis permiten explicar esta diferencia. La fracción de materia volátil en el *char* es menor que en el lodo, mientras que su contenido en carbono fijo es mayor (Tabla 3.1). Por lo tanto, durante la gasificación del lodo, las reacciones de combustión de la materia volátil (reacciones rápidas

gas-gas) aportan buena parte de la energía necesaria para las reacciones endotérmicas, mientras que en el caso de la gasificación de *char*, la presencia de hidrocarburos en la atmósfera gaseosa es escasa, y las principales reacciones de combustión en fase gas involucran a otros gases como $H_2$ o CO, cuyo poder calorífico es bastante inferior al de los hidrocarburos. Como consecuencia de ello, la gasificación de *char* con mezclas de aire y vapor de agua aparece como un proceso endotérmico bajo la mayoría de las condiciones estudiadas, mientras que la gasificación de lodo es un proceso exotérmico cuando se trabaja simultáneamente con RE > 19% y S/B < 0,52.

Si se considera el enfriamiento de los gases y vapores a la salida del reactor hasta temperatura ambiente (298 K) para aprovechar su energía térmica (calor sensible y latente), el calor neto de los procesos de gasificación varía entre -5,80 y -1,65 $MJ \cdot kg^{-1}_{lodo}$ en la gasificación de lodo y entre -1,17 y 0,26 $MJ \cdot kg^{-1}_{char}$ en la gasificación de *char*. Por lo tanto, teniendo en cuenta las hipótesis realizadas, ambos procesos parecen autosuficientes desde el punto de vista energético (excepto la gasificación de *char* con RE = 12% y T = 850 ºC).

Además de calcular la demanda energética en los procesos de gasificación, se ha considerado interesante definir un parámetro (llamado eficiencia energética de la gasificación) para medir qué parte de la energía contenida inicialmente en la materia prima queda disponible en el gas producto tras cubrir la demanda energética del propio proceso de gasificación y el consumo energético en la generación del vapor de agua utilizado como agente gasificante (ec. 4.4).

$$\text{Eficiencia energética de la gasificación } (\%) = \frac{\text{Energía recuperada en el gas} - Q_{\text{gasificación}} - Q_{\text{vapor}}}{PCI_{\text{materia prima}}} \cdot 100 \quad \text{(ec. 4.4)}$$

donde:

- La energía recuperada en el gas incluye la energía asociada a su poder calorífico (producto del volumen de gas seco generado por su PCI) y el aprovechamiento de su calor sensible y latente, multiplicado por un factor de eficiencia de intercambio de calor del 70%.
- $Q_{gasificación}$ es la demanda de energía en la gasificación de lodo o de *char*, considerando los productos a la temperatura de gasificación (Figura 4.11).
- $Q_{vapor}$ es la energía necesaria para calentar y evaporar el agua, desde 25 ºC hasta 150 ºC (2,36 $MJ \cdot kg^{-1}_{H2O}$).
- $PCI_{materia\ prima}$ es la energía contenida en el lodo o en el *char*, expresada en forma de su poder calorífico inferior (Tabla 3.1).

Los datos de eficiencia energética de los procesos de gasificación de lodo y gasificación de *char*, calculados según la ec. 4.4, se muestran en la Tabla 4.9.

Tabla 4.9. Datos de eficiencia energética de la gasificación de lodo y de *char* basada en rendimientos experimentales a los productos.

| Temperatura | 850 | 770 | 850 | 770 | 850 | 770 | 850 | 770 | 810 |
|---|---|---|---|---|---|---|---|---|---|
| RE (%) | 17 | 17 | 12 | 12 | 32 | 32 | 23 | 23 | 19 |
| Relación másica S/B | 0,71 | 0,71 | 0,52 | 0,52 | 0,39 | 0,39 | 0,27 | 0,27 | 0,52 |
| Gasificación de lodo | | | | | | | | | |
| Energía recuperada en el gas ($MJ \cdot kg^{-1}_{lodo}$) | 10,23 | 7,91 | 9,63 | 8,41 | 9,10 | 6,77 | 9,56 | 6,93 | 8,72 ± 0,12 |
| Eficiencia energética (%) | 74 | 58 | 65 | 61 | 87 | 75 | 82 | 65 | 71 ± 2 |
| Gasificación de *char* | | | | | | | | | |
| Energía recuperada en el gas ($MJ \cdot kg^{-1}_{char}$) | 3,91 | 2,77 | 3,49 | 2,44 | 3,52 | 2,44 | 3,34 | 2,27 | 2,98 ± 0,05 |
| Eficiencia energética (%) | 51 | 32 | 40 | 23 | 64 | 49 | 54 | 33 | 40 ± 2 |

Los resultados de eficiencia energética varían del 58% al 87% en la gasificación de lodo y del 23% al 64% en la gasificación de *char*. Tanto la menor demanda de energía como el mayor rendimiento a gas obtenido en la gasificación de lodo en comparación con la gasificación de *char* contribuyen a su mejor eficiencia energética. Como se observa en la Tabla 4.9, la eficiencia energética de la gasificación (definida según la ec. 4.4) mejora al aumentar la temperatura de gasificación y, en ambos casos, los mejores resultados se obtienen al operar con la mayor RE (32%) y una relación S/B moderada (0,39 $g \cdot g^{-1}_{org}$).

*Estudio teórico de la gasificación de lodo y de char basado en datos de equilibrio*

Los resultados experimentales obtenidos en la gasificación de lodo y de *char* muestran que en ninguno de los procesos se alcanzó el equilibrio químico, sino que en ambos existían reacciones controladas por la cinética o por fenómenos difusionales. A pesar de ello, se ha considerado interesante incluir en el estudio energético la situación de equilibrio para evaluar sus límites desde un punto de vista termodinámico. El cálculo de la demanda energética para la gasificación de lodo y de *char* en la situación de equilibrio se lleva a cabo de forma análoga a la realizada con los datos experimentales, pero utilizando la distribución de productos calculada con el software HSC Chemistry 6.1 (Figuras 4.8 y 4.9) en lugar de los rendimientos experimentales. Los resultados obtenidos en las simulaciones de equilibrio, realizadas bajo las mismas condiciones de operación que las estudiadas en el laboratorio, se muestran en la Figura 4.12.

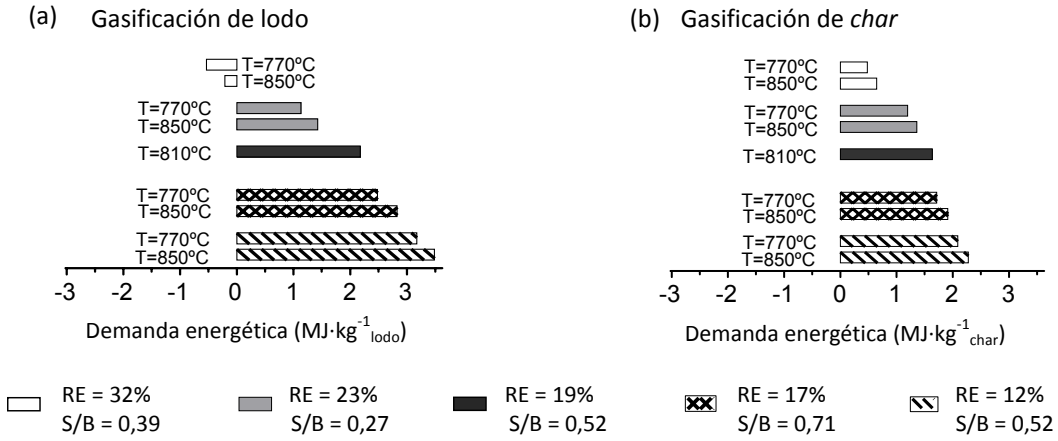


Figura 4.12. Demanda energética en la (a) gasificación de lodo y (b) gasificación de *char*, calculada con rendimientos de equilibrio y considerando los productos a la temperatura de gasificación.

La comparación de las Figuras 4.11 y 4.12 muestra que el hecho de alcanzar el equilibrio químico en ambos procesos de gasificación conlleva una demanda adicional de energía. La gasificación de lodos de EDAR en condiciones de equilibrio sólo aparece como un proceso exotérmico (en las condiciones experimentales simuladas) cuando la RE se aumenta hasta un 32%, mientras que la gasificación de *char* en condiciones de equilibrio es un proceso endotérmico en todas las situaciones simuladas. La razón es el predominio de las reacciones de equilibrio endotérmicas, como la reacción *water-gas* (ec. 2.3), la reacción de Boudouard (ec. 2.4), el reformado con vapor (ec. 2.7) y el reformado en seco (ec. 2.8), y la escasez de reacciones de equilibrio exotérmicas (reacción *water-gas shift*, ec. 2.6). Estas reacciones son llevadas a su máxima extensión cuando se alcanza el equilibrio químico, lo que implica un mayor consumo energético.

La eficiencia energética de ambos procesos de gasificación en situación de equilibrio se ha calculado de forma análoga al caso experimental (ec. 4.4). Estos resultados teóricos se recogen en la Tabla 4.10. A pesar de la energía adicional necesaria para alcanzar el equilibrio, los datos de eficiencia energética en condiciones de equilibrio son mayores que los datos experimentales: eficiencia del 90-94% en la gasificación de lodo en equilibrio y del 78-84% en la gasificación de *char* en equilibrio. Esto se debe a que en el equilibrio químico se obtiene un mayor rendimiento a gas que tiene, además, un mayor PCI, lo que permite recuperar más energía en el gas, contrarrestando así la mayor demanda energética.

Tabla 4.10. Datos de eficiencia energética de la gasificación de lodo y de *char* en condiciones de equilibrio.

| | | | | | | | | | |
|---|---|---|---|---|---|---|---|---|---|
| Temperatura | 850 | 770 | 850 | 770 | 850 | 770 | 850 | 770 | 810 |
| RE (%) | 17 | 17 | 12 | 12 | 32 | 32 | 23 | 23 | 19 |
| Relación másica S/B | 0,71 | 0,71 | 0,52 | 0,52 | 0,39 | 0,39 | 0,27 | 0,27 | 0,52 |
| Gasificación de lodo | | | | | | | | | |
| Energía recuperada en el gas ($MJ \cdot kg^{-1}_{lodo}$) | 14,37 | 14,11 | 14,95 | 14,72 | 11,34 | 11,09 | 12,86 | 12,64 | 13,70 |
| Eficiencia energética (%) | 90 | 91 | 91 | 92 | 94 | 94 | 94 | 94 | 92 |
| Gasificación de *char* | | | | | | | | | |
| Energía recuperada en el gas ($MJ \cdot kg^{-1}_{char}$) | 6,19 | 6,09 | 6,53 | 6,42 | 4,94 | 4,85 | 5,62 | 5,53 | 5,95 |
| Eficiencia energética (%) | 78 | 80 | 80 | 81 | 82 | 83 | 82 | 84 | 81 |

En los cálculos realizados hasta ahora la temperatura de gasificación ha sido una variable "impuesta", lo que podría conseguirse mediante el calentamiento o refrigeración externa del gasificador. Por otro lado, el ajuste de la composición del medio gasificante, es decir, de la disponibilidad de oxígeno y de vapor de agua, permite controlar la energía liberada en el proceso, lo que en un sistema adiabático y autotérmico se traduce en el control de la temperatura. La temperatura es, en este caso, la variable desconocida en el balance de energía que resulta de igualar las entalpías de las corrientes de entrada y de salida del reactor ($\Delta H_{entra} = \Delta H_{sale}$). La evolución de la temperatura en función de la composición del medio gasificante se ha calculado considerando datos de equilibrio. Este cálculo se ha realizado siguiendo un método iterativo, ya que $\Delta H_{sale}$ depende del rendimiento a los distintos productos (ec. 4.2) y éste, a su vez, depende de la temperatura de reacción (la temperatura debe especificarse en el software HSC Chemistry 6.1 para el cálculo de la cantidad de productos en equilibrio).

La Figura 4.13 muestra la evolución de la temperatura de equilibrio en función de RE (relación equivalente) y S/C (relación molar entre el vapor de agua alimentado y el carbono del sólido) en la gasificación de lodo y de *char* con mezclas de aire y vapor de agua.

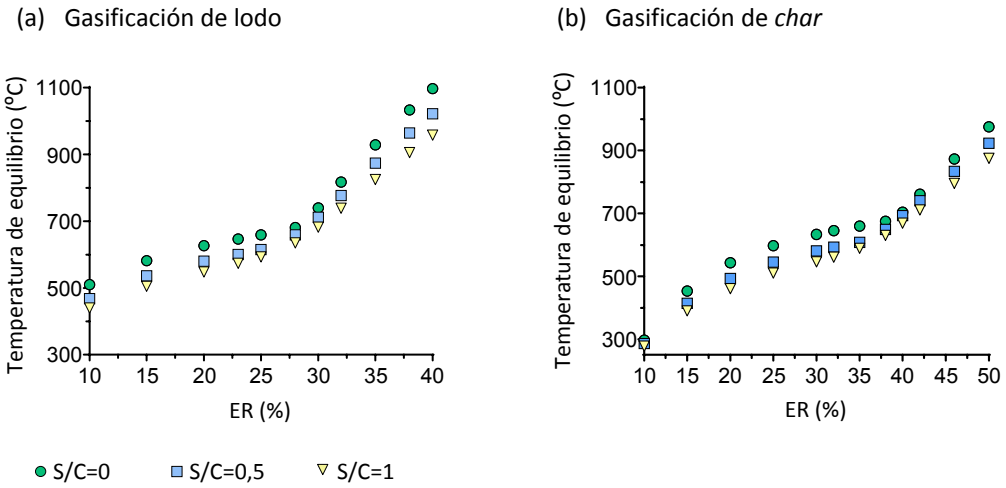


Figura 4.13. Temperatura de equilibrio en la (a) gasificación de lodo y (b) gasificación de *char* en función de la composición del medio de reacción.

Como era de esperar, la temperatura de equilibrio aumenta con RE y disminuye con S/C. El uso de bajas RE da lugar a temperaturas de equilibrio mucho menores que el intervalo de operación habitual en un gasificador (> 700 ºC). Esto indica que dichos datos de equilibrio se alejarán mucho del proceso real ya que, por ejemplo, en la realidad se obtendría una fracción de alquitrán muy alta, algo que no ocurre en el cálculo del equilibrio.

Como se puede observar en la Figura 4.13, la gasificación de *char* necesita una mayor RE que la gasificación de lodo para mantener la misma temperatura de operación en ambos procesos. Por ejemplo, en la gasificación de lodo se necesita una RE de 33% para operar de forma autotérmica a 800 ºC y con S/C = 0,5, mientras que este valor alcanza el 45% en la gasificación de *char*. El aumento de RE favorece las reacciones de combustión y, por tanto, la producción de $CO_2$. En este ejemplo, el 44% del contenido inicial de carbono en el lodo termina en forma de $CO_2$, mientras que este valor alcanza el 52% en la gasificación de *char*. La presencia de $CO_2$ en el gas de gasificación es indeseable debido al efecto de dilución del contenido energético del gas (PCI = 4,3 $MJ \cdot m^{-3}N$ en la gasificación de lodo y 3,1 $MJ \cdot m^{-3}N$ en la gasificación de *char* en el ejemplo planteado), y a la reducción de la formación de CO, ya que la formación de $CO_2$ y el consumo de CO, y viceversa, están ligados a través de varias reacciones, como la reacción *water-gas shift* (ec. 2.6) o la reacción de Boudouard (ec. 2.4).

*Secado térmico del lodo*

Antes del tratamiento termoquímico de los lodos de EDAR mediante pirólisis o gasificación, el secado térmico del mismo permite reducir su contenido de agua, disminuyendo así el volumen del residuo y facilitando la manipulación del sólido resultante. La energía necesaria para el secado térmico del lodo, por kilogramo de residuo final ($MJ \cdot kg^{-1}_{residuo\ final}$), puede calcularse con la ec. 4.5:

$$Q_{secado} = \frac{[m_{materia\ seca} \cdot Cp_{lodo\ seco} + m_{H_2O,lodo} \cdot Cp_{H_2O(l)}] \cdot \Delta T + m_{H_2O,evap} \cdot \Delta H_{vap,H_2O}}{\left({}^{kg\ residuo\ final}/_{kg\ lodo\ húmedo}\right)} \qquad \text{(ec. 4.5)}$$

donde:

- $m_{materia\ seca}$ es el contenido de materia seca en el lodo húmedo ($kg \cdot kg^{-1}_{lodo\ húmedo}$).
- $Cp_{lodo\ seco}$ es la capacidad calorífica específica del lodo seco lodo ($1{,}15 \cdot 10^{-3}$ $MJ \cdot kg^{-1} \cdot K^{-1}$). Este valor se obtuvo experimentalmente por calorimetría diferencial de barrido (a 25 ºC) y se ha considerado constante en el intervalo de temperatura del secado.
- $m_{H2O,lodo}$ es el contenido de agua en el lodo húmedo ($kg \cdot kg^{-1}_{lodo\ húmedo}$). Después de la deshidratación mecánica del lodo mediante filtros prensa o centrifugación, y antes del secado térmico, el contenido de humedad en el lodo se encuentra habitualmente en torno al 70% (Manara y Zabaniotou, 2012).
- $Cp_{H2O(l)}$ es la capacidad calorífica específica del agua líquida ($4{,}18 \cdot 10^{-3}$ $MJ \cdot kg^{-1} \cdot K^{-1}$), que es prácticamente constante en el intervalo de temperatura del secado (Perry y Green, 1999).
- $\Delta T$ es el incremento de temperatura durante el secado térmico (de 25 a 100 ºC).
- $m_{H2O,evap}$ es la cantidad de agua evaporada durante el proceso de secado ($kg \cdot kg^{-1}_{lodo\ húmedo}$).
- $\Delta H_{vap,H2O}$ es la entalpía de vaporización del agua a la temperatura final del proceso (2,26 $MJ \cdot kg^{-1}_{H2O}$ a 100 ºC) (Perry y Green, 1999).

La Figura 4.14 muestra la evolución de la energía necesaria para el secado térmico del lodo en función de su contenido de humedad inicial y final. Por ejemplo, se requieren casi 8 $MJ \cdot kg^{-1}_{residuo\ final}$ para reducir la fracción másica de agua del 77% al 6,5% (datos que se corresponden con el lodo utilizado). La energía necesaria para el secado térmico del lodo se reduce prácticamente a la mitad si el contenido de humedad inicial disminuye de un 77% a un 65%. Esta reducción podría lograrse mejorando la eficiencia de la etapa de deshidratación mecánica del lodo, anterior al secado térmico.

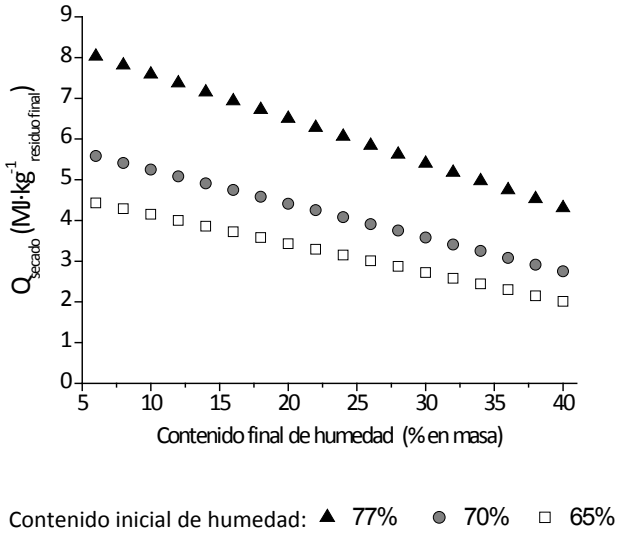


Figura 4.14. Energía necesaria para el secado térmico del lodo en función de su contenido de humedad inicial y final.

*Evaluación energética global de los procesos termoquímicos de dos y tres etapas*

El coste energético para el tratamiento termoquímico del lodo mediante los procesos de dos etapas (secado y gasificación del lodo) y de tres etapas (secado del lodo, pirólisis del lodo y gasificación del *char*) se ha calculado como la suma de la energía neta, requerida o liberada, en las etapas individuales. Este balance energético es sólo una primera aproximación, ya que sólo se ha tenido en cuenta la demanda energética de las etapas termoquímicas propiamente dichas, sin incluir otros consumos energéticos relacionados con el uso de bombas, compresores…ni rendimientos o eficiencias de combustión al considerar el aprovechamiento de los gases.

- *Secado térmico del lodo*. Se ha considerado una reducción del contenido de humedad en el lodo del 65% al 6,5%, lo que conlleva un coste energético de 4,4 MJ·kg$^{-1}_{lodo\ final}$ (Figura 4.14).

- *Pirólisis del lodo*. Si, como en la gasificación, se plantea la recuperación del contenido energético del gas producto de la pirólisis (PCI y calor sensible y latente de los gases y vapores, con una eficiencia de intercambio de calor del 70%), el calor neto del proceso de pirólisis es -1,17 MJ·kg$^{-1}_{lodo}$. El aprovechamiento del PCI del producto líquido (43 MJ·kg$^{-1}_{FOL}$ y 32 MJ·kg$^{-1}_{FOP}$) no se ha incluido en el balance de energía ya que algunas de sus propiedades, como su escasa estabilidad o alto contenido en nitrógeno, deben ser mejorados de cara a su posible uso como combustible (Fonts y cols., 2012).

- *Gasificación de lodo / gasificación de char*. El calor neto de las etapas de gasificación coincide con el numerador de la ec. 4.4. Para la comparación de los procesos de dos y tres etapas se requiere la misma base de cálculo en ambos, por ejemplo, 1 kg de lodo de EDAR a la salida del secado térmico para ser pirolizado o gasificado. Por lo tanto, los datos correspondientes a la gasificación de *char* ($MJ \cdot kg^{-1}_{char}$) deben convertirse a $MJ \cdot kg^{-1}_{lodo}$ teniendo en cuenta el rendimiento a *char* obtenido en la pirólisis ($0{,}52\ kg_{char} \cdot kg^{-1}_{lodo}$).

En la Figura 4.15 se muestran los datos de demanda total de energía para los procesos de dos y tres etapas en función de las distintas condiciones de operación estudiadas en las etapas de gasificación.

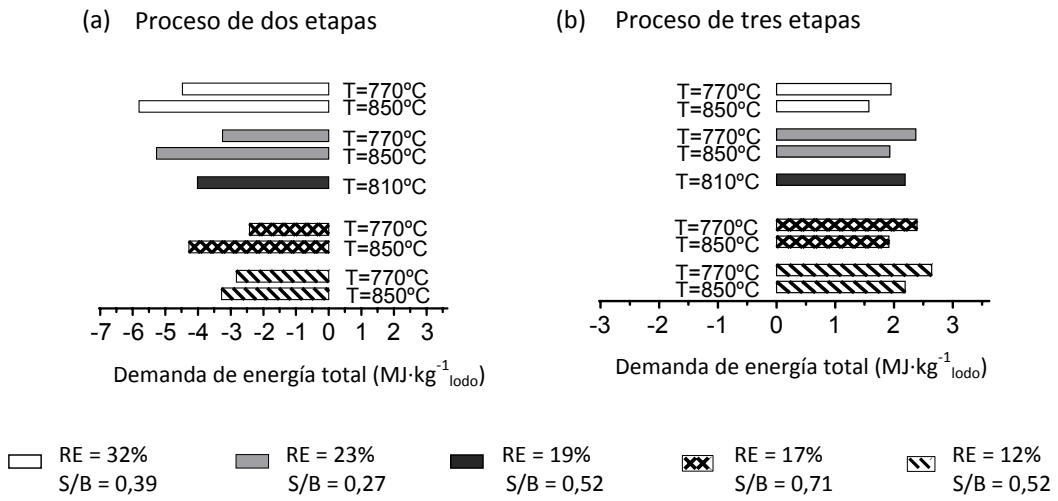


Figura 4.15. Demanda total de energía para el (a) proceso de dos etapas y (b) proceso de tres etapas.

La demanda total de energía en el proceso de dos etapas (secado y gasificación del lodo) varía entre -2,43 y -5,81 $MJ \cdot kg^{-1}_{lodo}$, es decir, la energía contenida en el gas producto de la gasificación de lodo es suficiente para cubrir la demanda energética del secado térmico y del proceso de gasificación en sí (proceso globalmente exotérmico). El balance de energía es todavía más favorable si se tiene en cuenta que parte de la humedad del lodo podría utilizarse como agente para la gasificación. La exigencia del secado térmico podría reducirse hasta dejar un contenido de humedad final en el lodo del 19-32% (lo que equivaldría a la alimentación de vapor de agua estudiada: S/B = 0,27-0,71), o visto de otro modo, el término $Q_{vap}$ del numerador de la ec. 4.4 (0,36-0,93 $MJ \cdot kg^{-1}_{lodo}$) podría evitarse si parte del secado del lodo se realizase en el propio gasificador.

Por otro lado, el coste energético del proceso de tres etapas (secado y pirólisis de lodo y gasificación de *char*) varía entre 1,57 y 2,64 $MJ \cdot kg^{-1}_{lodo}$ (proceso globalmente endotérmico), es decir, el aprovechamiento energético de los gases producto de la pirólisis de lodo y de la

gasificación de *char* no es suficiente para cubrir el secado térmico del lodo. Si en el balance energético se incluye también el aprovechamiento del poder calorífico de la fracción orgánica del líquido de pirólisis (-3,92 $MJ \cdot kg^{-1}_{lodo}$), el proceso de tres etapas se convierte en exotérmico, con un excedente de energía que varía desde -2,35 a -1,28 $MJ \cdot kg^{-1}_{lodo}$, siempre teniendo en mente las hipótesis y simplificaciones realizadas.

Los resultados energéticos globales más favorables se obtienen cuando en las etapas de gasificación se opera simultáneamente a la temperatura más alta (850 ºC), con la relación equivalente más alta (RE = 32%) y con una relación másica entre el vapor de agua y la materia orgánica moderada (S/B = 0,39).

## 4.3. Eliminación de $H_2S$ de diferentes gases con cenizas de lodo

En esta sección se presentan los resultados de la eliminación de $H_2S$ de diferentes gases sintéticos a alta temperatura (600-800 ºC) utilizando cenizas de combustión y de gasificación de lodos de EDAR. Uno de los gases utilizados contenía sólo $H_2S$ y $N_2$, mientras que el otro simulaba la composición de un gas de gasificación ($H_2$, CO, $CO_2$, $CH_4$, $C_2H_6$, $C_2H_4$, $C_2H_2$, $N_2$ y $H_2S$; Tabla 3.4). Ambos gases se alimentaron en forma seca y con cierto contenido de humedad (30% vol. en la mayoría de los casos) para analizar el efecto de la humedad.

Las curvas de ruptura del $H_2S$ obtenidas tras el paso de cada gas por el lecho de ceniza se representan en la Figura 4.16 en función de la atmósfera de gas, la temperatura de reacción y el tipo de ceniza.

(a) Mezcla $H_2S/N_2$ seca

b) Mezcla $H_2S/N_2$ húmeda (30% vol. humedad)

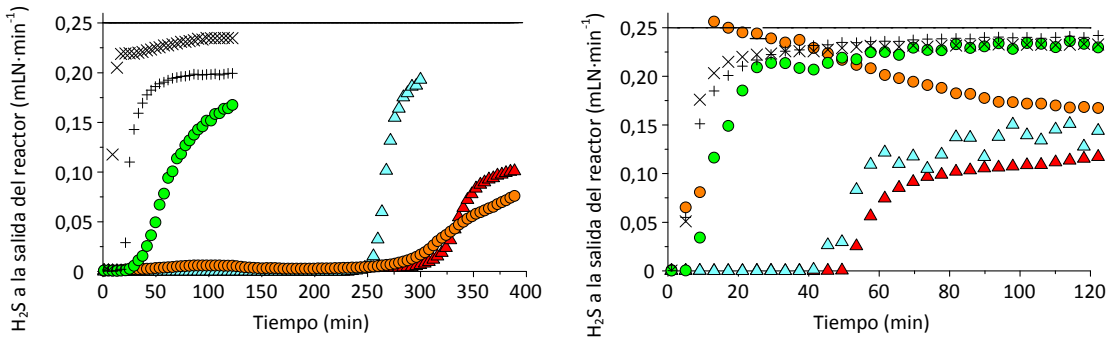


(c) Gas sintético de gasificación seco

d) Gas sintético de gasificación húmedo (30% vol. humedad)

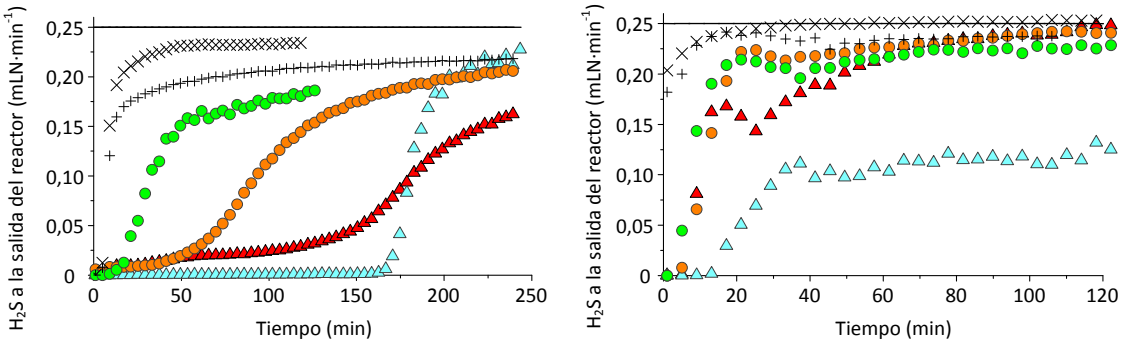


*$H_2S$ alimentado* ——

*$H_2S$ a la salida del reactor en los experimentos "blancos":* + *800 ºC* × *600 ºC*

*$H_2S$ a la salida del reactor cuando se utiliza la ceniza de combustión:* ▲ *800 ºC* △ *600 ºC*

*$H_2S$ a la salida del reactor cuando se utiliza la ceniza de gasificación:* ● *800 ºC* ● *600 ºC*

Figura 4.16. Curvas de ruptura para el $H_2S$: evolución del caudal de $H_2S$ ($mLN \cdot min^{-1}$) a la salida del reactor con el tiempo.

La concentración de $H_2S$ en el gas de salida del reactor se mantuvo por debajo de 100 ppm (lo que equivaldría a unos $5 \cdot 10^{-3}$ mLN·min$^{-1}$) durante 300 min y 260 min cuando se utilizaron las cenizas de combustión y de gasificación, respectivamente, para desulfurar la mezcla $H_2S/N_2$ seca a 800 ºC (Figura 4.16.a). Sin embargo, cuando se alimentó el gas sintético de gasificación seco (Figura 4.16.c), el punto de ruptura de las curvas se redujo a unos pocos minutos (< 20 min), excepto cuando se utilizó la ceniza de combustión a 600 ºC, con la que el punto de ruptura ($H_2S$ > 100 ppm) se retrasó hasta los 165 min, tiempo mucho menor que el obtenido con la mezcla $H_2S/N_2$ bajo las mismas condiciones de operación (245 min). Esto demuestra el efecto negativo que ejerce alguno de los componentes del gas de gasificación en el proceso de desulfuración. La reducción de los óxidos de hierro presentes en las cenizas del lodo (Figura 3.1) podría explicar este comportamiento. La presencia de $H_2$ y CO en el gas de gasificación crea una atmósfera reductora que puede causar la reducción del $Fe_3O_4$ y del $Fe_2O_3$ a FeO o incluso a Fe elemental en el intervalo de temperatura de 700-1000 ºC (Tamhankar y cols., 1981; Tseng y cols., 2008; Westmoreland y Harrison, 1976). Algunos estudios han mostrado una menor capacidad del FeO y del Fe para reaccionar con $H_2S$ (Tseng et al., 2008), lo que explicaría los peores resultados de eliminación de $H_2S$ obtenidos al alimentar el gas sintético de gasificación. La eficiencia del proceso de desulfuración dependerá, por tanto, de la competencia de las reacciones de reducción y de sulfuración (reacción con $H_2S$), que pueden verse afectadas en mayor o menor medida por las variaciones de temperatura.

La presencia de vapor de agua en la atmósfera de reacción también ha mostrado un impacto negativo en el proceso de eliminación de $H_2S$ de los gases (Figuras 4.16.b y 4.16.d). De acuerdo con la reacción general de los óxidos metálicos con $H_2S$ (ec. 4.6), la termodinámica predice un efecto negativo del vapor de agua en el proceso de retención de $H_2S$ debido a la regeneración simultánea de los sulfuros metálicos formados:

$$Me_xO_y\ (s) + y\ H_2S\ (g) \leftrightarrow Me_xS_y\ (s) + y\ H_2O\ (g) \qquad \Delta H < 0 \qquad \text{(ec. 4.6)}$$

Bajo control cinético, el mayor o menor efecto del vapor de agua dependerá de la diferencia de velocidad de las reacciones directa (formación del sulfuro metálico) e inversa (regeneración del óxido metálico), lo que a su vez depende del material utilizado y de las condiciones de operación (Cheah y cols., 2009). Por ejemplo, en su estudio de retención de $H_2S$ con un material basado en ZnO, Kim y cols. (2007) comprobaron que el tiempo de ruptura en la detección de $H_2S$ llegaba a reducirse a la mitad en presencia de un 45% vol. de vapor de agua a 360 ºC. El impacto negativo del vapor de agua ha sido todavía mayor en el presente estudio, observando una disminución del tiempo de ruptura del 85% cuando se utiliza la ceniza

de combustión a cualquiera de las dos temperaturas (600 o 800 ºC) con la mezcla $H_2S/N_2$, o una pérdida total de la actividad de la ceniza de gasificación.

Como se observa en la Figura 4.16, la cantidad de $H_2S$ detectada a la salida del reactor en los *blancos* (experimentos sin lecho de ceniza) también se vio afectada por la presencia de vapor de agua en la atmósfera de gas. La configuración experimental mostró cierta retención del $H_2S$ al alimentar los gases secos, y especialmente, al operar a 800 ºC, lo que puede ser debido a la reacción del $H_2S$ con las partes metálicas calientes a la entrada y salida del reactor. En condiciones de humedad, el caudal de $H_2S$ a la salida del reactor tiende hacia el valor de entrada, lo que significa que la presencia de vapor de agua evita la citada corrosión de las partes metálicas. Esto también demuestra que la posible absorción del $H_2S$ en la fracción acuosa recogida en el condensador no ocurre de forma importante.

La Tabla 4.11 resume los resultados de tiempo de ruptura ($t_{ruptura}$, tiempo en el que la concentración de $H_2S$ en el gas de salida supera las 100 ppm), cantidad de $H_2S$ eliminado del gas hasta dicho tiempo de ruptura y contenido de azufre en las muestras sólidas después de los experimentos, tanto los datos reales obtenidos con el analizador elemental, como la concentración que cabría esperar si todo el $H_2S$ eliminado del gas hubiese quedado retenido en el sólido.

La cantidad de $H_2S$ eliminado del gas hasta el $t_{ruptura}$ se ha calculado utilizando los datos de los experimentos blancos como referencia:

$$H_2S \text{ eliminado del gas hasta } t_{ruptura}\ (\text{mLN}) = V_{H_2S\ \text{blanco}} - V_{H_2S\ \text{experimento}} \qquad \text{(ec. 4.7)}$$

donde $V_{H2S\ experimento}$ es la cantidad de $H_2S$ (mLN) que sale del reactor hasta $t_{ruptura}$ en el experimento y $V_{H2S\ blanco}$ es la cantidad de $H_2S$ (mLN) que sale del reactor en el blanco realizado en las mismas condiciones de operación y durante el mismo tiempo que el experimento. El volumen de $H_2S$ que abandona el reactor se puede calcular por integración de las curvas de ruptura (Figura 4.16) y, gráficamente, se corresponde con el área que queda bajo cada curva hasta $t_{ruptura}$.

Tabla 4.11. Resultados experimentales de las pruebas de eliminación de $H_2S$.

| Tipo de ceniza | Relación $H_2O/H_2S$ ($g \cdot g^{-1}$) | T (ºC) | $t_{ruptura}$ (min) | $H_2S$ eliminado del gas hasta $t_{ruptura}$ (mLN) | Contenido de S real (mg $S \cdot g^{-1}_{ceniza}$)* | Contenido de S esperado (mg $S \cdot g^{-1}_{ceniza}$) |
|---|---|---|---|---|---|---|
| ***Gas alimentado: $H_2S/N_2$*** | | | | | | |
| Ceniza de combustión | 0 | 600 | 245 | 54 | 58 ± 1 | 92 |
| | 0 | 800 | 300 | 54 | 63 ± 4 | 100 |
| | 45 | 600 | 40 | 7 | 21,5 ± 0,8 | 29 |
| | 45 | 800 | 50 | 9 | 1,4 ± 0,1 | 32 |
| | 22,5 | 700 | 70 | 14 | 20,8 ± 0,6 | 38 |
| | 22,5 | 700 | 62 | 12 | 18,8 ± 0,2 | 37 |
| | 22,5 | 700 | 62 | 12 | 16,6 ± 0,6 | 36 |
| Ceniza de gasificación | 0 | 600 | 30 | 4 | 23,2 ± 0,5 | 27 |
| | 0 | 800 | 260 | 48 | 64,4 ± 0,7 | 100 |
| | 45 | 600 | 5 | 2 | 4,9 ± 0,2 | 7 |
| | 45 | 800 | 0 | 0 | 1,1 ± 0,1 | 8 |
| | 22,5 | 700 | 0 | 0 | 14,1 ± 0,5 | 17 |
| | 22,5 | 700 | 0 | 0 | 12,6 ± 0,5 | 18 |
| | 22,5 | 700 | 0 | 0 | 11,8 ± 0,4 | 17 |
| ***Gas alimentado: gas sintético de gasificación*** | | | | | | |
| Ceniza de combustión | 0 | 600 | 165 | 36 | 46,4 ± 0,6 | 64 |
| | 0 | 800 | 13 | 1 | 55 ± 4 | 53 |
| | 45 | 600 | 17 | 4 | 26,8 ± 0,5 | 32 |
| | 45 | 800 | 5 | 1 | 8,5 ± 0,5 | 11 |
| Ceniza de gasificación | 0 | 600 | 13 | 1 | 20 ± 1 | 19 |
| | 0 | 800 | 0 | 0 | 33,2 ± 0,6 | 31 |
| | 45 | 600 | 5 | 1 | 5,8 ± 0,2 | 11 |
| | 45 | 800 | 5 | 1 | 4,5 ± 0,5 | 8 |

** Valor medio ± desviación estándar de tres medidas.*

La cantidad de $H_2S$ eliminada del gas hasta $t_{ruptura}$ es la única variable que ofrece resultados comparables entre sí (Tabla 3.7). Esta variable respuesta ha sido, por tanto, la única utilizada para el análisis estadístico de la influencia de los factores de operación (temperatura, $H_2O/H_2S$ y tipo de ceniza) cuando se alimenta la mezcla $H_2S/N_2$. Los coeficientes de regresión lineal (β) obtenidos para los valores codificados de los factores se muestran en la Tabla 4.12. El término significativo de la curvatura impide el uso del modelo lineal obtenido, pero los coeficientes β pueden utilizarse para comparar la influencia relativa de los factores.

Tabla 4.12. Coeficientes de regresión lineal (β) obtenidos del análisis ANOVA para la cantidad de $H_2S$ (mLN) eliminada de la mezcla $H_2S/N_2$ hasta $t_{ruptura}$.

| Valor medio | $\beta_T$ | $\beta_{H2O/H2S}$ | $\beta_{tipo\ de\ ceniza}$ | $\beta_{T\text{-}H2O/H2S}$ | $\beta_{T\text{-}tipo\ de\ ceniza}$ | $\beta_{H2O/H2S\text{-}tipo\ de\ ceniza}$ | $\beta_{T\text{-}H2O/H2S\text{-}tipo\ de\ ceniza}$ | Curvatura |
|---|---|---|---|---|---|---|---|---|
| 22,36 | 5,46 | -17,76 | -8,91 | -5,36 | 4,94 | 5,16 | -5,89 | Significativa |

Los tres factores analizados (temperatura, relación $H_2O/H_2S$ y tipo de ceniza de lodo), así como sus interacciones, afectan de manera significativa a la cantidad de $H_2S$ que puede ser eliminada del gas hasta alcanzar el tiempo de ruptura. La Figura 4.17 muestra las superficies de respuesta obtenidas con cada tipo de ceniza según los coeficientes de la Tabla 4.12. Estas gráficas no se ajustan totalmente a la respuesta real de la variable debido a la existencia de curvatura, pero permiten ver, de forma muy clara, el efecto de los factores de operación.

(a) Ceniza de combustión (b) Ceniza de gasificación

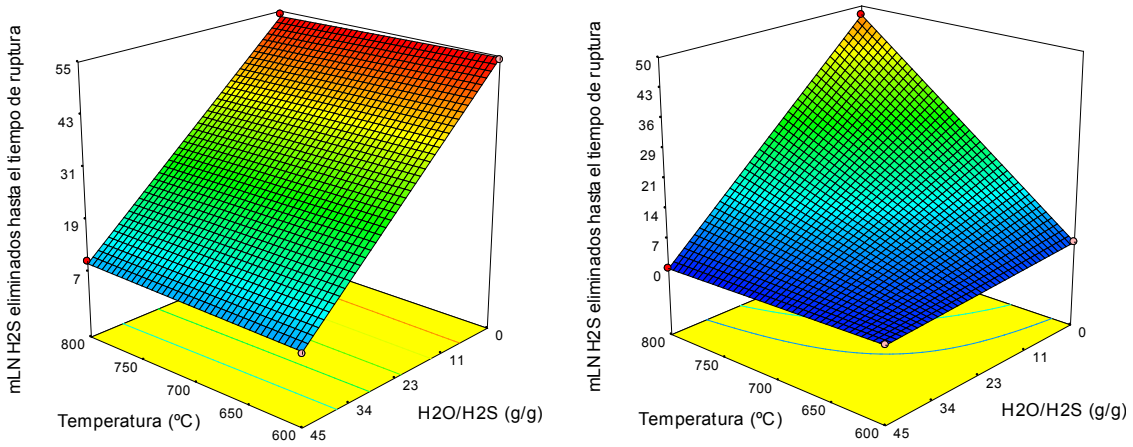


Figura 4.17. Cantidad de $H_2S$ (mLN) eliminada de la mezcla $H_2S/N_2$ hasta $t_{ruptura}$ con la (a) ceniza de combustión y (b) ceniza de gasificación de lodo.

Según los coeficientes β obtenidos del análisis ANOVA (Tabla 4.12), la relación $H_2O/H_2S$ es el factor más influyente y, en términos generales, su aumento afecta negativamente a la cantidad de $H_2S$ que puede ser eliminada del gas hasta alcanzar el punto de ruptura ($\beta_{H2O/H2S}$ = -17,76). Sin embargo, la existencia de interacciones significativas entre los factores pone de manifiesto que el impacto de la presencia de vapor de agua está fuertemente condicionado por la temperatura y el tipo de ceniza. Así, la relación $H_2O/H_2S$ es el único término significativo cuanto se utiliza la ceniza de combustión (Figura 4.17.a). En este caso, la cantidad de $H_2S$ eliminada del gas hasta la ruptura de la curva es independiente de la temperatura. Esto parece indicar que la variación observada en el $t_{ruptura}$ al modificar la temperatura es sólo una consecuencia de la mayor retención de $H_2S$ por parte de que la configuración experimental a 800 ºC que a 600 ºC, que se traduce en una disminución del caudal de $H_2S$ potencialmente

reactivo con la ceniza a 800 ºC y, por tanto, en un mayor tiempo de ruptura. Por otro lado, la temperatura y su interacción con la relación $H_2O/O_2$ sí que aparecen como términos significativos cuando se utiliza la ceniza de gasificación. Su capacidad de eliminación de $H_2S$ desaparece casi por completo al operar tanto a la menor temperatura (600 ºC) como con la mayor relación $H_2O/O_2$ (45 $g \cdot g^{-1}$), y presenta un claro máximo al operar a 800 ºC en atmósfera seca (Figura 4.17.b), alcanzando un resultado muy similar al de la ceniza de combustión.

El tipo de ceniza es, por tanto, otro factor clave en el proceso de eliminación de $H_2S$ ($\beta_{\text{tipo de ceniza}}$ = -8,91). El valor negativo de este coeficiente β representa un mejor comportamiento de la ceniza de combustión (denotado en términos codificados como -1) frente a la ceniza de gasificación (denotado como +1). La diferencia entre la actividad de ambas cenizas es más significativa a baja temperatura. Por ejemplo, la ceniza de combustión a 600 ºC fue capaz de eliminar 54 mLN de $H_2S$ de la mezcla $H_2S/N_2$ seca hasta alcanzar el tiempo de ruptura, mientras que la ceniza de gasificación apenas eliminó 4 mLN de $H_2S$ (Tabla 4.11). Puesto que las propiedades texturales de ambas cenizas son muy similares (Tabla 3.2), las diferencias observadas en su comportamiento están relacionadas con su composición química. La ceniza de gasificación contiene una pequeña cantidad de carbono (3,14% en masa) que podría contribuir a su peor rendimiento debido al obstáculo que puede suponer para el acceso del $H_2S$ a los centros metálicos reactivos. Sin embargo, esta cantidad de carbono no parece lo suficientemente alta como para ser la única causa de las diferencias observadas. Los distintos contenidos metálicos y especies detectadas en ambas cenizas (sección 3.1.2) como consecuencia de las diferentes atmósferas reactivas en la combustión y gasificación del lodo parecen la causa más razonable. El contenido de Fe (mayor en la ceniza de combustión) y su estado químico (en forma de $Fe_2O_3$ en la ceniza de combustión y como $Fe_3O_4$ en la ceniza de gasificación) son algunas de las principales diferencias. En el análisis por absorción de rayos X en estructura fina (EXAFS) de muestras de $Fe_2O_3$ y $Fe_3O_4$ tras su reacción con $H_2S$ a 400 ºC, Yoshimura y cols. (1995) observaron una menor intensidad del pico correspondiente a la coordinación Fe-S en la muestra sulfurada de $Fe_3O_4$ que en la de $Fe_2O_3$, indicando así una menor extensión de la reacción de $H_2S$ con $Fe_3O_4$. Este hecho puede explicar la escasa reactividad de la ceniza de gasificación con el $H_2S$ a la menor temperatura (600 ºC). La cinética de la reacción del $H_2S$ con $Fe_3O_4$ en condiciones secas parece mejorar sensiblemente a 800 ºC, alcanzando resultados muy similares a los del $Fe_2O_3$.

Además de la evolución del caudal de $H_2S$ a la salida del reactor, el contenido de azufre en las cenizas después de los experimentos de desulfuración se midió con un analizador elemental. Los resultados obtenidos están incluidos en la Tabla 4.11 (contenido de S real).

Todos estos datos no son directamente comparables entre sí porque el tiempo de los experimentos (y por tanto el grado de exposición a $H_2S$) no fue el mismo en todos los casos, por lo que la evolución de esta variable no ha sido analizada por análisis ANOVA. A pesar de ello, los datos de experimentos con la misma duración han mostrado un menor contenido de azufre en la ceniza de gasificación que en la ceniza de combustión cuando la temperatura de operación era 600 o 700 ºC, mientras que el contenido de azufre en ambos sólidos fue similar después de los experimentos realizados a 800 ºC. El máximo contenido de azufre detectado en las cenizas fue de 63-64 $mg \cdot g^{-1}_{ceniza}$ (tras 390 min de experimento) y se obtuvo al alimentar la mezcla $H_2S/N_2$ seca y al operar con cualquiera de las dos cenizas a 800 ºC. En condiciones de humedad, el contenido de azufre retenido finalmente en el sólido se vio favorecido con la disminución de la temperatura. Ante la situación más cercana a un proceso de desulfuración real (gas sintético de gasificación húmedo), la ceniza de combustión a 600 ºC mostró la mayor retención de azufre (26,8 $mg \cdot g^{-1}_{ceniza}$ después de 120 minutos).

Estos contenidos de azufre medidos experimentalmente se han comparado con los resultados que cabría esperar si toda la cantidad de $H_2S$ eliminada del gas hubiese quedado retenida en las cenizas tras los experimentos (ec. 4.8).

$$\text{Contenido de S esperado } (\text{mg S} \cdot \text{g}^{-1}_{\text{ceniza}}) = \text{S}_{\text{inicial}} + \frac{\text{V}_{\text{H}_2\text{S blanco}} - \text{V}_{\text{H}_2\text{S experimento}}}{22.4} \cdot 32 \qquad \text{(ec. 4.8)}$$

donde $S_{inicial}$ es el contenido inicial de azufre en la ceniza ($mg \cdot g^{-1}_{ceniza}$, Tabla 3.2), $V_{H2S\ blanco}$ es la cantidad de $H_2S$ (mLN) que abandona el reactor durante el blanco (extrapolando a la duración del experimento cuando ambas difieran), $V_{H2S\ experimento}$ es la cantidad total de $H_2S$ (mLN) que abandona el reactor tras un experimento completo, 22,4 ($mLN \cdot mmol^{-1}$) es el volumen de 1 mol de gas ideal en condiciones normales de presión (1 atm) y temperatura (0 ºC) y 32 ($mg \cdot mmol^{-1}$) es la masa atómica del azufre.

Los resultados de contenido de azufre calculados con la ec. 4.8 se han incluido en la última columna de la Tabla 4.11. Como se puede observar, los datos reales de concentración de azufre (medidos con el analizador elemental) son, en general, bastante más bajos que los datos calculados. Puesto que los blancos mostraron que el $H_2S$ no quedaba absorbido en la fracción de agua condensada a la salida del reactor, la justificación más probable para esta falta de azufre es que se encuentre formando parte de otros gases que no han sido detectados por el cromatógrafo a la salida del reactor, y cuya formación se haya visto potenciada por la presencia de las cenizas. Especialmente llamativa es la diferencia en los datos obtenidos para el experimento 4 (800 ºC y alimentación de la mezcla $H_2S/N_2$ húmeda), ya que el contenido de

azufre esperado en el sólido era de unos 32 $mg \cdot g^{-1}_{ceniza}$ y el analizador elemental sólo detectó 1,4 $mg \cdot g^{-1}_{ceniza}$.

Con el objetivo de explicar estas diferencias desde un punto de vista termodinámico, se realizaron simulaciones de equilibrio del proceso utilizando el software HSC Chemistry 6.1. Estas simulaciones resultaron bastante complejas debido a la propia configuración del sistema (lecho fijo de sólido y alimentación continua de gas), que hace que la composición del sólido cambie con el tiempo. Para hacer frente a esta situación se realizaron sucesivas simulaciones del equilibrio para pequeños intervalos de tiempo (10 min) hasta cubrir un tiempo de reacción de 300 min. El reactivo sólido considerado en la primera simulación fue la cantidad de Ca (en forma de CaO) y de Fe (en forma de $Fe_2O_3$) presente en 1 g de ceniza de combustión (Tabla 3.2). Tras el primer cálculo, los compuestos sólidos resultantes de cada simulación constituían el sólido reactivo para la siguiente. La cantidad de gas considerada como alimentación en cada simulación fue la correspondiente a 10 min de experimento en el laboratorio. De acuerdo con este procedimiento, las Figuras 4.18 y 4.19 muestran la evolución de la distribución del azufre entre los principales productos sulfurados formados en el equilibrio ($Fe_xS_y$, CaS, $H_2S$, $CaSO_4$ y $SO_2$) cuando se consideran la mezcla $H_2S/N_2$ y el gas de gasificación, respectivamente.

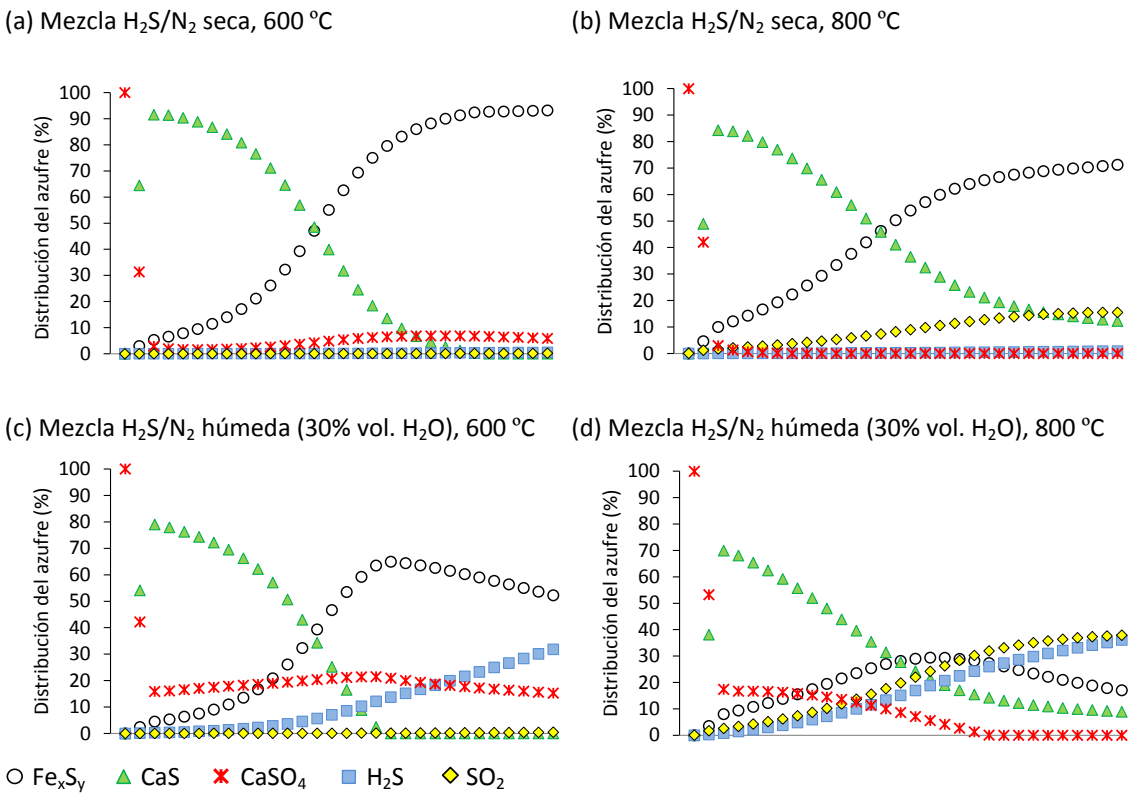


Figura 4.18. Evolución de la distribución del azufre entre los principales productos de equilibrio bajo la atmósfera de $H_2S/N_2$.

Bajo la atmósfera de $H_2S/N_2$, la formación de CaS se ve termodinámicamente favorecida frente a la formación de $Fe_xS_y$ en la primera parte de las simulaciones de equilibrio (Figura 4.18). A medida que disminuye la cantidad disponible de CaO, la formación de $Fe_xS_y$ va tomando más importancia. Además de la formación de ambos sulfuros metálicos, la termodinámica predice la formación de $SO_2$ y $CaSO_4$, éste último a consecuencia de la reacción del CaO con el $SO_2$ formado. La formación de $SO_2$ y $CaSO_4$, así como la fracción del $H_2S$ alimentado que permanece como tal, se ven favorecidas por la presencia de vapor de agua. El aumento de la temperatura desde 600 ºC hasta 800 ºC resulta favorable para la presencia de $SO_2$. La formación de este compuesto podría explicar la falta de azufre en las cenizas después de los experimentos. De acuerdo con estas simulaciones de equilibrio, los valores teóricos de retención de azufre en las cenizas de combustión serían de 107, 103, 42 y 38 $mg \cdot g^{-1}_{ceniza}$ para los experimentos 1, 2, 3 y 4, respectivamente. Los resultados experimentales, medidos con el analizador elemental, fueron un 46%, 39%, 49% y 96% más bajos que estos resultados teóricos, respectivamente.

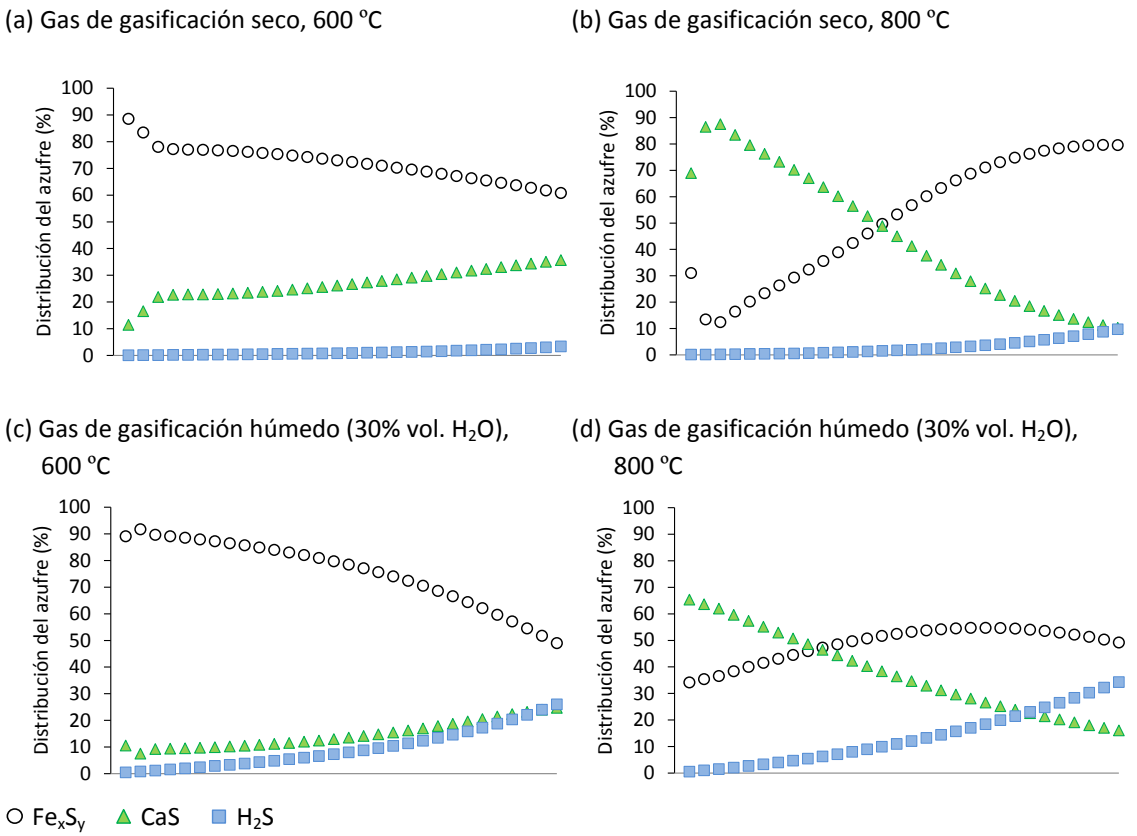


Figura 4.19. Evolución de la distribución de azufre entre los principales productos de equilibrio bajo la atmósfera del gas de gasificación.

Bajo la atmósfera reductora creada por el gas de gasificación (Figura 4.19), ni el $SO_2$ ni el $CaSO_4$ aparecen como productos de equilibrio. $H_2S$, CaS y $Fe_xS_y$ son las principales especies que

contienen azufre en el equilibrio. También se ha detectado la formación de COS, aunque en una proporción muy pequeña. La formación de COS en el ambiente reductor del gas de gasificación ($H_2S + CO_2 \leftrightarrow COS + H_2O$) ha sido observada por otros autores (Hepola y Simell, 1997a), lo que podría explicar la falta de azufre en las muestras de ceniza tras los experimentos con el gas sintético de gasificación. De acuerdo con las simulaciones de equilibrio realizadas, los valores teóricos de retención de azufre en las cenizas de combustión serían de 85, 84, 42 y 41 $mg \cdot g^{-1}_{ceniza}$ para los experimentos 20, 21, 22 y 23, respectivamente. Los resultados experimentales, medidos con el analizador elemental, fueron un 46%, 35%, 36% y 79% más bajos que estos resultados teóricos, respectivamente.

La comparación de las Figuras 4.18 y 4.19 muestra el importante efecto de la atmósfera gaseosa en la distribución del azufre entre CaS y $Fe_xS_y$. La presencia de $CO_2$ en el gas de gasificación puede explicar esta diferencia, ya que este gas es el responsable de la reacción de carbonatación del CaO ($CaO + CO_2 \leftrightarrow CaCO_3$). El exceso de $CO_2$ desplaza esta reacción hacia la formación de $CaCO_3$, especialmente a bajas temperaturas, lo que limita la formación de CaS a partir de CaO.

Por lo tanto, además de la competencia de las reacciones de sulfuración y reducción de los óxidos de hierro explicada anteriormente, la posible carbonatación del óxido de calcio es otro factor a tener en cuenta para justificar los diferentes resultados experimentales obtenidos para la mezcla $H_2S/N_2$ y para el gas de gasificación.

Una vez comprobada la posibilidad de retener azufre en las cenizas de lodo bajo ciertas condiciones de operación, la presencia de azufre en una de las cenizas (la del experimento 2) fue caracterizada mediante otras técnicas. La Figura 4.20 muestra una imagen obtenida por microscopía electrónica de barrido (SEM) mediante electrones retrodispersados. Los números en dicha figura indican los puntos superficiales sobre los que se analizó la composición elemental por espectroscopía de energía dispersiva de rayos X (EDX). Dichas fracciones atómicas se muestran en la Tabla 4.13.

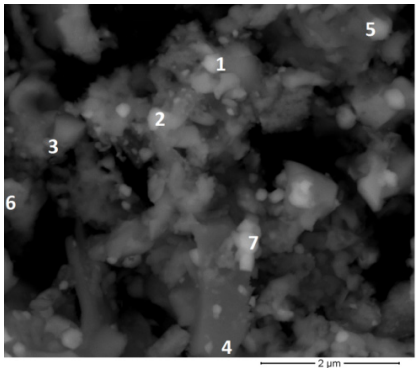


Figura 4.20. Imagen SEM obtenida mediante electrones retrodispersados.

Tabla 4.13. Composición elemental (SEM/EDX) en diferentes puntos superficiales de la ceniza resultante del experimento 2.

| Punto en la Figura 4.20 | Composición elemental (% atómico) | | | | | | | | | | |
|---|---|---|---|---|---|---|---|---|---|---|---|
| | C | O | Na | Mg | Al | Si | P | S | Ca | Fe | Zn |
| 1 | | 29,6 | | 1,0 | 2,0 | 1,7 | 4,3 | 23,8 | 1,6 | 35,9 | |
| 2 | 0,8 | 57,9 | | 3,4 | 3,7 | 2,4 | 13,3 | 1,1 | 6,6 | 10,6 | 0,3 |
| 3 | 2,2 | 45,9 | 0,5 | 1,5 | 5,7 | 9,2 | 11,5 | 8,6 | 6,3 | 8,8 | |
| 4 | 0,7 | 69,0 | 0,3 | 0,1 | 0,3 | 27,6 | 0,6 | | | 0,9 | |
| 5 | 0,9 | 50,7 | 0,3 | 3,3 | 6,2 | 9,3 | 12,2 | 4,6 | 7,0 | 5,6 | |
| 6 | 1,6 | 57,9 | | 2,4 | 1,4 | 4,0 | 11,7 | 0,4 | 4,1 | 16,1 | 0,4 |
| 7 | | 33,5 | | 0,8 | 1,3 | 7,8 | 3,5 | 23,7 | 4,1 | 25,3 | |

Los porcentajes de C, O, Na, Mg, Al, Si, P, S, Ca, Fe y Zn detectados en la superficie de la ceniza reflejan la heterogeneidad del material. Cabe destacar que los puntos con la mayor concentración de S (23,8% atómico en el punto 1 y 23,7% atómico en el punto 7) son también los que presentan una concentración de Fe más alta (35,9% y 25,3%, respectivamente), lo que sugiere la formación de sulfuros o sulfatos de hierro. Por otro lado, la presencia de S en otros puntos de la superficie fue prácticamente inexistente, como en el punto 4, formado principalmente por O y Si (probablemente en forma de $SiO_2$), o en el punto 6 en el que, a pesar de la importante presencia de Fe (16,1% atómico), sólo se encontró un 0,4% atómico de S. En este último punto, así como en los puntos 2 y 3, la alta presencia de Fe coincide con una alta concentración de P, que indica la presencia de fosfatos de hierro, también detectados por XRD (Figura 3.1).

Por último, la Figura 4.21 muestra el espectro XPS correspondiente al orbital 2p del S para la muestra de ceniza resultante del experimento 2, en el que se reflejan los diferentes entornos químicos del S. El pico localizado entre 160 y 164 eV refleja la presencia de sulfuros metálicos ($S_n^{-2}$) y el pico obtenido en torno a 169 eV se corresponde con estados más oxidados del S ($SO_4^{-2}$). La presencia de ambas especies fue predicha en las simulaciones del equilibrio.

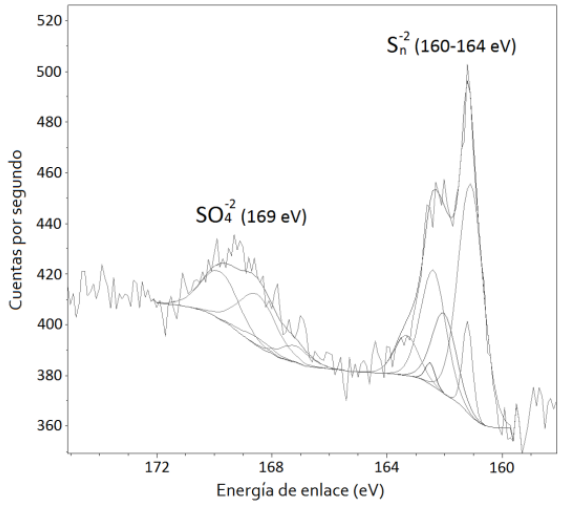


Figura 4.21. Espectro XPS correspondiente a la región S 2p para la ceniza resultante del experimento 2.

En resumen, los experimentos de desulfuración de gases sintéticos han demostrado la capacidad de las cenizas del lodo de EDAR, especialmente de las generadas en el proceso de combustión, para eliminar $H_2S$ de corrientes gaseosas bajo determinadas condiciones. Dado que el rendimiento de desulfuración se reduce drásticamente en presencia de vapor de agua, el uso de las cenizas para la eliminación de $H_2S$ resultará mucho más eficiente en la limpieza de un gas seco, como podría ser el gas de pirólisis de lodos de EDAR después de la condensación de los vapores. El uso de las cenizas resultantes de la combustión del *char* de pirólisis para la desulfuración del propio gas de pirólisis plantea una interesante opción para reintegrar el subproducto sólido en el proceso.

La retención de azufre con las cenizas de combustión de lodo a 600 ºC bajo el gas sintético de gasificación seco fue de 46 $mg \cdot g^{-1}_{ceniza}$ antes de su saturación (Tabla 4.11). Suponiendo un comportamiento similar de las cenizas resultantes de la combustión del *char* de pirólisis, y teniendo en cuenta los rendimientos másicos a ceniza (390 $g \cdot kg^{-1}_{lodo}$, Tabla 3.1) y a azufre gaseoso en forma de $H_2S$ (4,3 $g \cdot kg^{-1}_{lodo}$, Tabla 4.8), se puede concluir que la ceniza generada sería suficiente para retener todo el $H_2S$ producido en el proceso.

## 4.4. Estudio de la actividad de catalizadores de níquel en el reformado de alquitrán

En esta sección se presentan los resultados de la actividad de los distintos catalizadores de $Ni/Al_2O_3$, preparados y modificados con diferentes promotores metálicos (Ca, Fe, Mn y Cu), en el reformado de compuestos modelo de alquitrán e hidrocarburos ligeros. La atmósfera gaseosa de la gasificación se simuló mediante la mezcla de diferentes gases ($H_2$, CO, $CO_2$, $N_2$, $CH_4$, $C_2H_4$ y $H_2S$), vapor de agua y una mezcla de benceno ($C_6H_6$), tolueno ($C_7H_8$) y naftaleno ($C_{10}H_8$) como compuestos modelo de alquitrán (Tabla 3.5).

La Figura 4.22 muestra la evolución de las concentraciones de $C_{10}H_8$, $C_6H_6$+$C_7H_8$, $CH_4$ y $C_2H_4$ a la salida del reactor, cuando se utiliza el catalizador de $Ni/Al_2O_3$ sin promotores, calcinado a 900 ºC y reducido en una atmósfera de $H_2/N_2$ antes del experimento. En el eje superior de abscisas se ha especificado la rampa de temperatura seguida durante el experimento (3,5 h con cada temperatura).

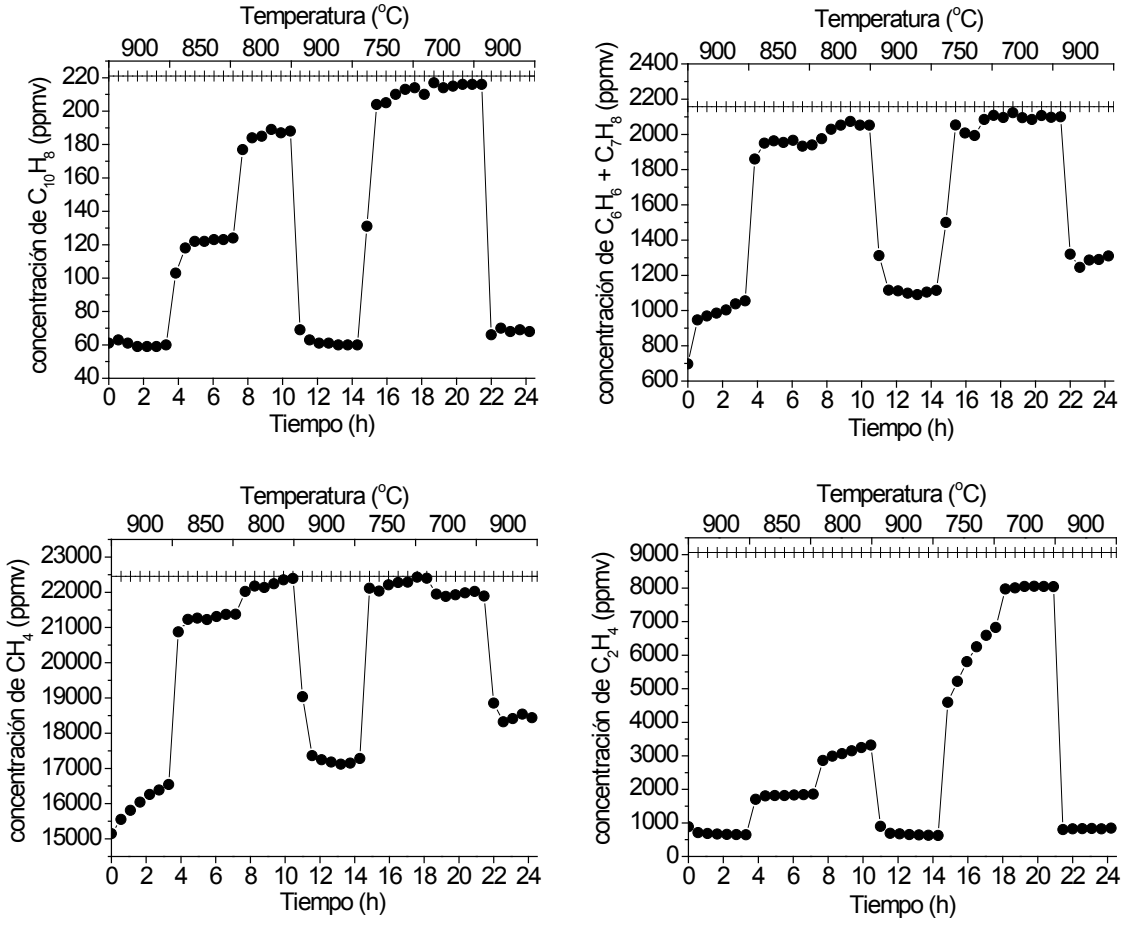


+ *Concentración de entrada;* ● *Concentración de salida*

Figura 4.22. Evolución de la concentración de $C_{10}H_8$, $C_6H_6 + C_7H_8$, $CH_4$ y $C_2H_4$ en el gas de salida del reactor con el catalizador de $Ni/Al_2O_3$ calcinado a 900 ºC y reducido previamente en atmósfera de $H_2/N_2$.

En el menor intervalo de temperatura (700-750 ºC), la concentración de $C_2H_4$ en el gas de salida fue la única que mostró una disminución apreciable respecto a su valor de entrada y, a la temperatura más alta (900 ºC), el $CH_4$ fue el hidrocarburo con menor tasa de conversión. Además, los sucesivos análisis realizados en cada intervalo de temperatura han mostrado cierta tendencia a la alza en la concentración de algunos de los hidrocarburos, lo que sugiere la progresiva pérdida de actividad del catalizador. Aunque la desactivación de los catalizadores de níquel por envenenamiento con $H_2S$ puede evitarse en gran medida al operar a altas temperaturas (Hepola y Simell, 1997a), el aumento gradual de la concentración de $CH_4$, y en menor medida de la concentración de $C_6H_6$ + $C_7H_8$, durante las 3,5 primeras horas de experimento a 900 ºC demuestran que, a pesar de la elevada temperatura, el catalizador de $Ni/Al_2O_3$ experimentó cierta pérdida de actividad en el reformado de estos compuestos. El $C_{10}H_8$ y el $C_2H_4$ no mostraron variación en su concentración cuando la temperatura era de 900 ºC, pero sí a menores temperaturas, siendo especialmente llamativo el rápido aumento de la concentración de $C_2H_4$ durante las 3,5 h a 750 ºC. Esto corrobora el mencionado efecto de la disminución de la temperatura sobre la desactivación del catalizador por envenenamiento con $H_2S$. Además, todos estos resultados ponen de manifiesto la diferente sensibilidad de los hidrocarburos ante la desactivación del catalizador de $Ni/Al_2O_3$ debido a la competencia de los mismos por los centros activos de la superficie del catalizador y a los diferentes mecanismos de descomposición.

La actividad de los distintos catalizadores ($Ni/Al_2O_3$, $Ni/Ca/Al_2O_3$, $Ni/Fe/Al_2O_3$, $Ni/Cu/Al_2O_3$ y $Ni/Mn/Al_2O_3$) calcinados a 900 ºC y reducidos previamente en una atmósfera de $H_2/N_2$ se muestra en la Figura 4.23. Los puntos representados en dicha figura muestran los valores medios de conversión obtenidos en cada intervalo de temperatura (ec. 4.9).

$$\text{Conversión}_{\,i}(\%) = \frac{n_{i,entra} - n_{i,sale}}{n_{i,entra}} \cdot 100 \qquad \text{(ec. 4.9)}$$

donde $n_{i,entra}$ y $n_{i,sale}$ representan el caudal molar del compuesto "i" que entra y sale del reactor, respectivamente. Puesto que la formación de $C_6H_6$ está generalmente ligada a la descomposición de $C_7H_8$ a través de diversas reacciones como la desalquilación con vapor de agua ($C_7H_8 + H_2O \leftrightarrow C_6H_6 + CO + 2H_2$) o la hidrodesalquilación ($C_7H_8 + H_2 \leftrightarrow C_6H_6 + CH_4$), los resultados de conversión de ambos compuestos mono-aromáticos se han analizado de forma conjunta.

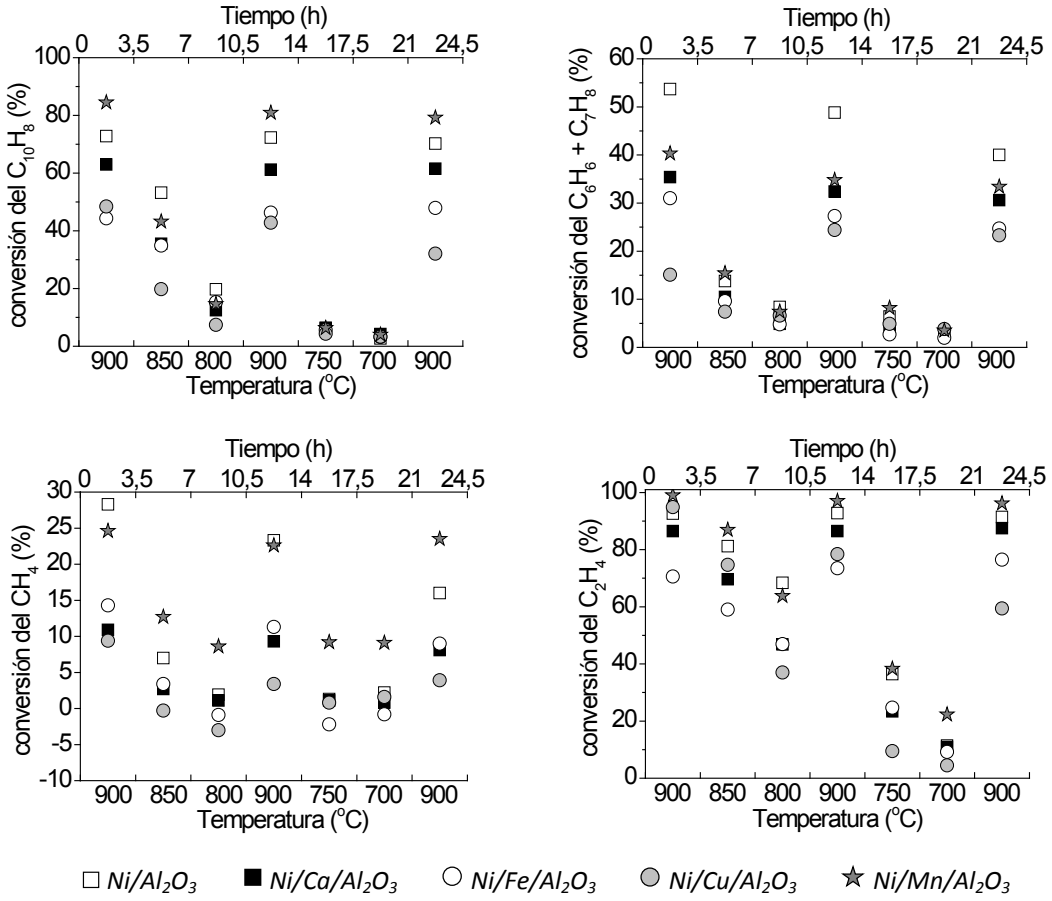


Figura 4.23. Conversión de los compuestos modelo de alquitrán y de los hidrocarburos ligeros obtenida con los distintos catalizadores calcinados a 900 °C y reducidos previamente en atmósfera de $H_2/N_2$.

Los resultados del blanco realizado con un lecho de material inerte (SiC) no se han representado en la Figura 4.23, pero evidenciaron una nula o escasa contribución del craqueo térmico en la descomposición de los hidrocarburos. Sólo la concentración de $C_2H_4$ fue ligeramente modificada, con una conversión que varió del 4,3% (700 °C) al 7,7% (900 °C).

En presencia de los catalizadores, tanto la conversión de los alquitranes como la de los hidrocarburos ligeros se vio claramente afectada por la temperatura. Como era de esperar, la disminución de la temperatura supuso una notable reducción de la conversión de todos ellos debido a la disminución de la velocidad de las reacciones de reformado con vapor de agua (ec. 2.9) o $CO_2$ (ec. 2.10). La conversión del $C_{10}H_8$ fue inferior al 20% al operar a temperaturas inferiores a 800 °C con todos los catalizadores, mientras que la conversión conjunta de $C_6H_6$ y $C_7H_8$ sólo se mantuvo por encima del 30% al operar a 900 °C con algunos de los catalizadores. Sólo la adición de Mn resultó ventajosa para la conversión del $C_{10}H_8$, que alcanzó un 80% a 900 °C, mejorando en 10 puntos porcentuales la conversión obtenida con el catalizador básico de $Ni/Al_2O_3$. La conversión de $C_2H_4$ también mejoró con la presencia de Mn, pasando de un 92%

en la primer etapa a 900 ºC con el catalizador $Ni/Al_2O_3$ a prácticamente un 100% con el catalizador $Ni/Mn/Al_2O_3$.

Por otro lado, la conversión máxima de $C_6H_6$ + $C_7H_8$ se obtuvo con el catalizador de $Ni/Al_2O_3$. En este caso, ni la adición de Mn ni la de ningún otro promotor consiguió mejorar la conversión inicial del catalizador, aunque sí su estabilidad en algunos casos. La conversión media de $C_6H_6$ + $C_7H_8$ con $Ni/Al_2O_3$ pasó de un 55% en la primera etapa a 900 ºC a un 49% en la segunda y a un 40% en la tercera etapa a 900 ºC, mostrando así una importante pérdida de actividad a lo largo del experimento. La incorporación de Mn mantuvo los niveles de conversión de $C_6H_6$ + $C_7H_8$ más cercanos entre sí en las tres etapas a 900 ºC (35-40%).

La importante pérdida de actividad del catalizador de $Ni/Al_2O_3$ también fue observada en los datos de conversión del $CH_4$, ya que se pasó de un valor promedio del 28% en la primera etapa a 900 ºC a un 16% en la tercera etapa a la misma temperatura. La incorporación de Mn en el catalizador permitió estabilizar la conversión del $CH_4$ en torno al 24-25% en las tres etapas a 900 ºC. En el caso del $CH_4$, también llaman la atención los valores negativos de conversión obtenidos con los catalizadores $Ni/Cu/Al_2O_3$ y $Ni/Fe/Al_2O_3$ a 700-800 ºC, lo que puede deberse a un aumento de la producción de este compuesto a través de las reacciones de metanización ($CO + 3H_2 \leftrightarrow CH_4 + H_2O$; $C + 2H_2 \leftrightarrow CH_4$).

En definitiva, sólo la adición de Mn resultó favorable para la actividad o estabilidad del catalizador de $Ni/Al_2O_3$ calcinado a 900 ºC y reducido en atmósfera de $H_2$ antes del experimento. La adición de los demás metales (Ca, Fe y Cu) resultó perjudicial para la conversión de todos los hidrocarburos analizados. La reducción de la superficie específica del catalizador al incorporar la segunda fase metálica (Tabla 3.3) parece la explicación más sencilla. Dado que esta reducción también se produjo al añadir el Mn, las mejoras observadas con la incorporación de dicho metal pueden estar relacionadas con una menor sinterización del catalizador en la fase previa de reducción, llevada a cabo a 900 ºC.

Los demás compuestos gaseosos que forman parte de la atmósfera reactiva ($H_2$, CO y $CO_2$) aparecen involucrados en diversas reacciones, tanto como en forma de reactivos como de productos, lo que hace que el caudal alimentado de cada uno de ellos pueda verse aumentado o disminuido al atravesar el lecho de catalizador. La Figura 4.24 muestra el cociente entre los caudales molares de $H_2$, CO y $CO_2$ medidos a la salida y a la entrada del reactor. Los datos representados reflejan los valores medios obtenidos en cada intervalo de temperatura. Los valores superiores a 1 indican una producción neta del compuesto y los inferiores a 1 se corresponden con un consumo neto.

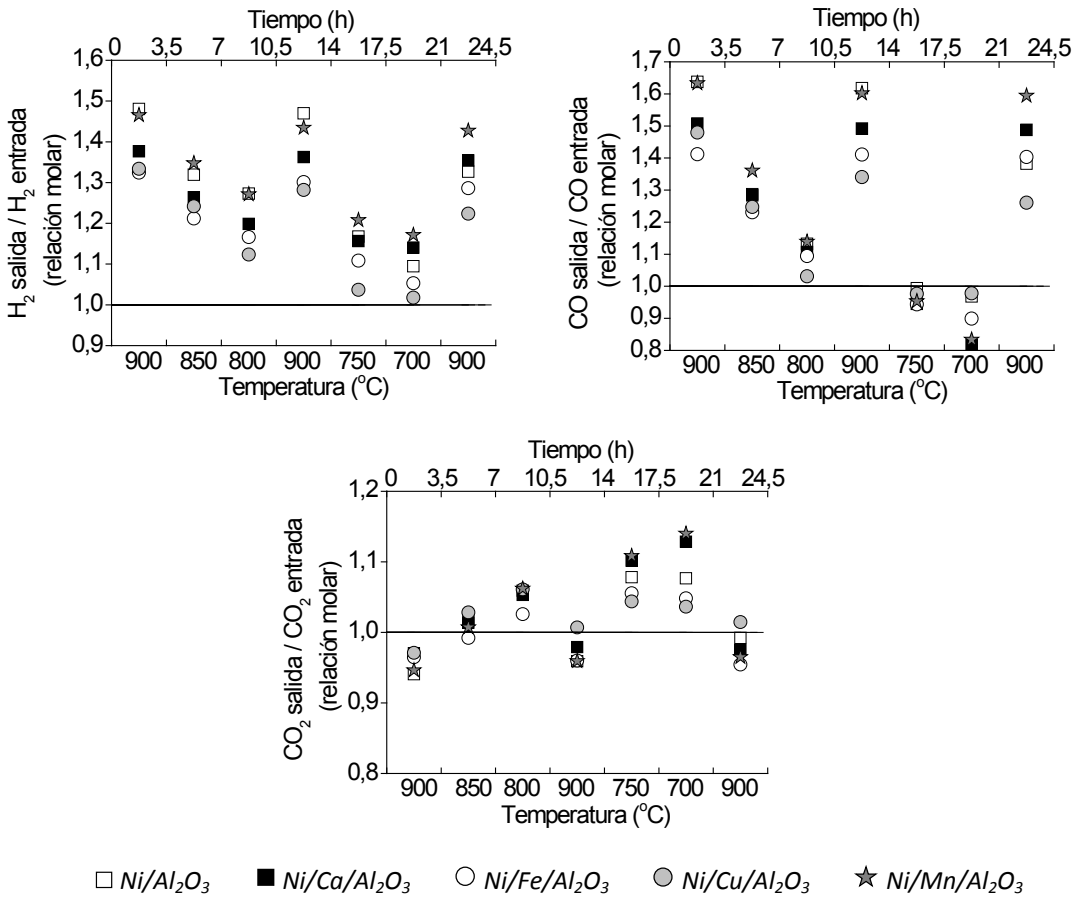


Figura 4.24. Cociente entre los caudales molares de $H_2$, CO y $CO_2$ a la salida y a la entrada del reactor para los distintos catalizadores calcinados a 900 ºC y reducidos previamente en atmósfera de $H_2/N_2$.

Como se puede observar en la Figura 4.24, el flujo de $H_2$ obtenido a la salida del reactor aumentó con respecto al valor de entrada con todos los catalizadores utilizados. Este aumento se vio favorecido al aumentar la temperatura de reacción, alcanzando un incremento cercano al 50% en algunos casos. Al igual que ocurrió con los datos de conversión del $CH_4$ y del $C_6H_6$ + $C_7H_8$, la producción de $H_2$ con el catalizador de $Ni/Al_2O_3$ se redujo en la última parte del experimento realizada a 900 ºC, reflejando la inestabilidad del catalizador. Por otro lado, el caudal de salida de CO también mostró un notable aumento respecto a su valor de entrada a temperaturas por encima de 800 ºC pero, a diferencia del flujo de $H_2$, su caudal se mantuvo prácticamente constante o incluso disminuyó con algunos de los catalizadores al operar a 700-750 ºC. Los resultados de $CO_2$ mostraron la tendencia opuesta, ya que los máximos en su producción se obtuvieron al reducir la temperatura de reacción. El aumento de la velocidad de las reacciones de reformado del alquitrán con la temperatura (control cinético) permite explicar estos resultados, ya que el $H_2$ y el CO son productos en estas reacciones (ec. 2.9 y 2.10), mientras que el $CO_2$ es el reactivo en las reacciones de reformado en seco (ec. 2.10). En cuanto a las demás reacciones en fase gas, el hecho de alcanzar o no el equilibrio químico es

un aspecto clave para explicar el efecto de la temperatura debido a la existencia de reacciones exotérmicas, como la reacción *water-gas shift* (ec. 2.6), que no se ven favorecidas con el aumento de la temperatura.

El equilibrio del proceso se ha calculado con el software HSC Chemistry 6.1 de forma análoga a como se hizo en la sección 4.1. Las simulaciones realizadas muestran que la presencia de alquitrán (naftaleno, benceno y tolueno) en el gas de equilibrio es prácticamente despreciable en todo el intervalo de temperatura analizado (700-900 ºC). El $H_2$, CO y $CO_2$ son los compuestos mayoritarios. La Tabla 4.14 muestra el cociente entre el caudal molar teórico de $H_2$, CO y $CO_2$ a la salida del reactor (en condiciones de equilibrio) y el caudal molar alimentado de cada uno de ellos.

Tabla 4.14. Cociente entre el caudal molar teórico de $H_2$, CO y $CO_2$ a la salida del reactor en condiciones de equilibrio y el caudal molar alimentado de cada uno.

| | 700 ºC | 750 ºC | 800 ºC | 850 ºC | 900 ºC |
|---|---|---|---|---|---|
| $H_{2\ salida}$ / $H_{2\ entrada}$ | 2,11 | 2,06 | 2,00 | 1,95 | 1,90 |
| $CO_{\ salida}$ / $CO_{\ entrada}$ | 1,72 | 1,86 | 1,99 | 2,10 | 2,20 |
| $CO_{2\ salida}$ / $CO_{2\ entrada}$ | 1,12 | 1,04 | 0,98 | 0,92 | 0,87 |

La comparación de los datos experimentales con los datos teóricos muestra que el uso de los catalizadores de níquel no fue suficiente para alcanzar el equilibrio químico, lo que puede tener su origen en la incompleta conversión del alquitrán. Los datos de producción de $H_2$ y CO en el equilibrio son considerablemente más altos que los valores experimentales, mientras que la producción de $CO_2$ en el equilibrio es ligeramente inferior o muy similar a los datos experimentales. Otra de las diferencias observadas es que la producción de $H_2$ en el equilibrio, sin presencia de alquitrán, se ve favorecida al disminuir la temperatura, lo cual pone de manifiesto el peso de la reacción *water-gas shift* (ec. 2.6) en la evolución de la composición de equilibrio del gas de gasificación.

*Efecto del procedimiento de reducción de los catalizadores*

La Figura 4.25 muestra los resultados de conversión de los compuestos modelo de alquitrán y de los hidrocarburos ligeros obtenidos con los catalizadores calcinados a 900 ºC y utilizados sin un tratamiento previo de reducción. La comparación de estos resultados con los datos de la Figura 4.23 (obtenidos tras la reducción previa de los catalizadores en atmósfera de $H_2/N_2$) permite analizar el efecto del tratamiento de reducción.

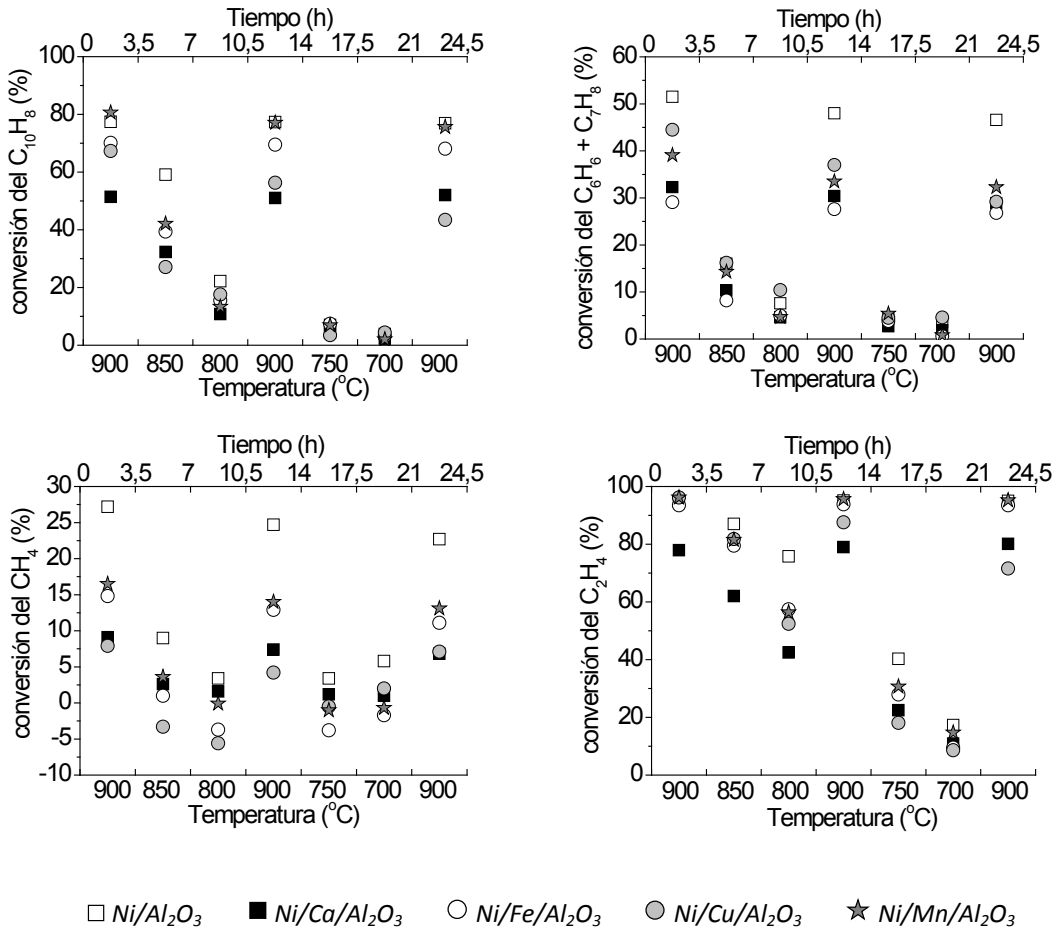


Figura 4.25. Conversión de los compuestos modelo de alquitrán y de los hidrocarburos ligeros obtenida con los distintos catalizadores calcinados a 900 ºC y utilizados sin pretratamiento de reducción.

La conversión media de $C_{10}H_8$ obtenida a 900 ºC en el primer tramo de los experimentos realizados sin reducción previa de los catalizadores de $Ni/Fe/Al_2O_3$, $Ni/Cu/Al_2O_3$ y $Ni/Al_2O_3$ mejoró en 25, 20 y 5 puntos porcentuales, respectivamente, con respecto a los resultados obtenidos tras la reducción de los catalizadores en atmósfera de $H_2/N_2$. Una posible explicación para esto puede ser la desactivación de dichos catalizadores durante la etapa previa de reducción, que se realizó a 900 ºC, pudiendo causar la sinterización de algunas partículas de níquel. Por otro lado, la conversión del $C_{10}H_8$ con el catalizador de $Ni/Mn/Al_2O_3$ se mantuvo en valores muy similares en ambos casos. Esto parece corroborar la hipótesis antes mencionada del efecto positivo de la adición de manganeso en la disminución de la sinterización de las partículas de níquel.

Los mejores resultados de conversión de $C_{10}H_8$ se obtuvieron con los catalizadores de $Ni/Al_2O_3$ y $Ni/Mn/Al_2O_3$, que no mostraron grandes diferencias para este compuesto (80% de conversión a 900 ºC). Sin embargo, igual que en el caso anterior, el catalizador básico de $Ni/Al_2O_3$ fue el más activo en la conversión de $C_6H_6 + C_7H_8$ y, en este caso también, en la

conversión de $CH_4$. En cuanto a la conversión de $C_2H_4$, el efecto más importante del procedimiento de reducción se observó en el catalizador de $Ni/Fe/Al_2O_3$, para el que la conversión media de $C_2H_4$ a 900 ºC pasó de un 70-75% cuando se redujo previamente en atmósfera de $H_2$, a un 95% cuando se evitó dicho pretratamiento, igualando en este último caso los resultados obtenidos con $Ni/Al_2O_3$ y $Ni/Mn/Al_2O_3$.

*Efecto de la temperatura de calcinación de los catalizadores*

La Figura 4.26 muestra los resultados de conversión de los compuestos modelo de alquitrán y de los hidrocarburos ligeros obtenidos con los catalizadores calcinados a 700 ºC y utilizados sin un tratamiento previo de reducción. La comparación de estos resultados con los datos de la Figura 4.25 (correspondientes a los catalizadores calcinados a 900 ºC y utilizados sin pretratamiento de reducción) permite analizar la influencia de la temperatura de calcinación.

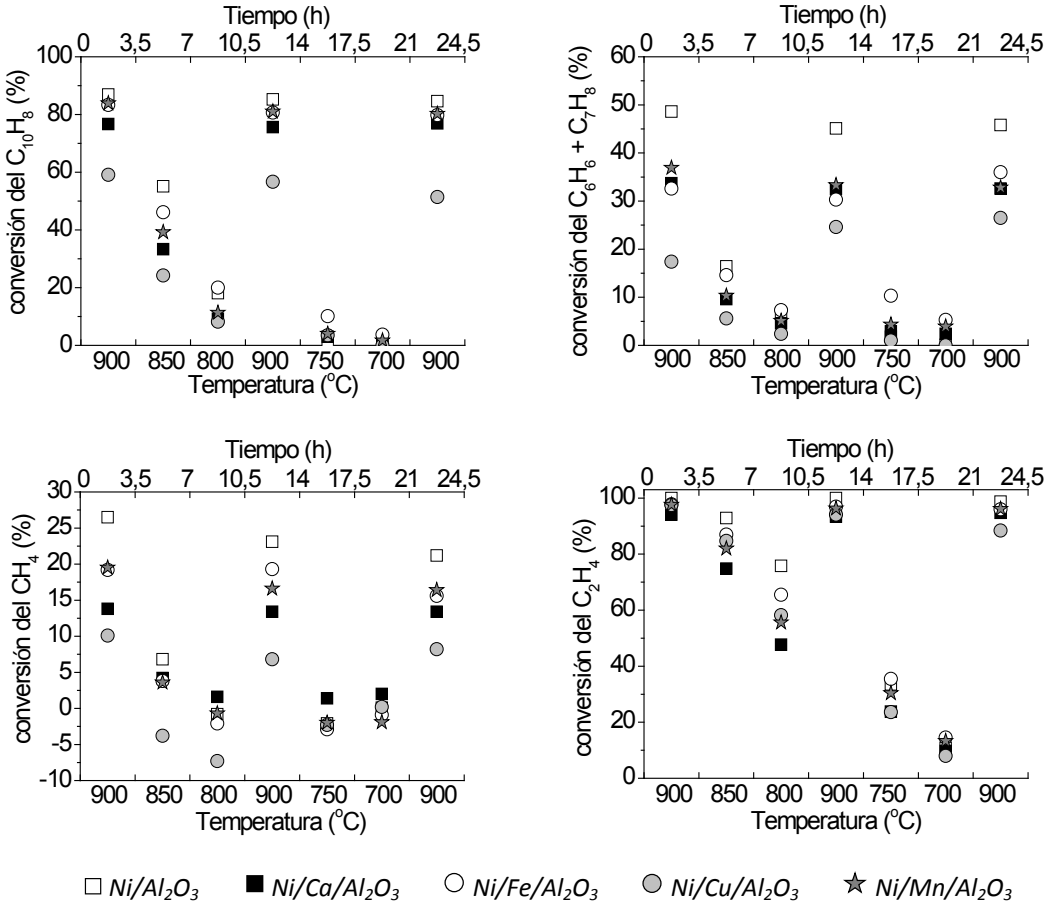


Figura 4.26. Conversión de los compuestos modelo de alquitrán y de los hidrocarburos ligeros obtenida con los distintos catalizadores calcinados a 700 ºC y utilizados sin pretratamiento de reducción.

Cuando los sólidos se calcinaron a 700 ºC, el catalizador básico de $Ni/Al_2O_3$ fue el más activo para la conversión de todos los compuestos, seguido muy de cerca por los catalizadores de $Ni/Mn/Al_2O_3$ y $Ni/Fe/Al_2O_3$ en la conversión de $C_{10}H_8$ y $C_2H_4$.

La disminución de la temperatura de calcinación de 900 a 700 ºC en los catalizadores de $Ni/Al_2O_3$, $Ni/Ca/Al_2O_3$ y $Ni/Fe/Al_2O_3$ supuso una mejora de 10, 25 y 15 puntos porcentuales, respectivamente, en el valor medio de conversión de $C_{10}H_8$ obtenido a 900 ºC. De hecho, si se comparan los resultados de todos los experimentos que forman este estudio catalítico, el catalizador básico de $Ni/Al_2O_3$ calcinado a 700 ºC fue el que dio lugar a la máxima conversión de $C_{10}H_8$ (87%). La influencia de la temperatura de calcinación en la conversión de $C_6H_6 + C7H_8$ no fue, en general, tan significativa como en el caso del $C_{10}H_8$. Por otro lado, la conversión de $CH_4$ a 900 ºC mejoró en torno a 5 puntos porcentuales con todos los sólidos al reducir la temperatura de calcinación de 900 a 700 ºC (salvo en el catalizador básico de $Ni/Al_2O_3$, que se mantuvo muy similar). Teniendo en cuenta que la máxima conversión alcanzada para el $CH_4$ fue de un 27%, dicha variación supone una mejora sustancial. Por último, los resultados de conversión de $C_2H_4$ obtenidos a 900 ºC con los catalizadores calcinados a 700 ºC fueron mucho más similares entre sí que en los casos anteriores, alcanzando valores de conversión superiores al 90% en todos los casos.

La variación de la superficie específica con la temperatura de calcinación (Tabla 3.3) parece la explicación más sencilla para justificar las diferencias observadas al utilizar los sólidos calcinados a 700 ºC y 900 ºC. Aunque la mayoría de los sólidos calcinados a 700 ºC mostraron mejores resultados de conversión, hubo algunas excepciones. Por eso, hay que tener en cuenta que la diferente temperatura de calcinación puede ocasionar cambios en la estructura química de los sólidos, dando lugar a especies más o menos activas que puedan contrarrestar la disminución de la superficie específica. Esto se intento comprobar con los análisis XRD mostrados a continuación, aunque los resultados obtenidos no fueron muy concluyentes.

*Caracterización de los catalizadores tras los experimentos*

Las muestras usadas de los catalizadores fueron caracterizadas después de los experimentos mediante análisis elemental y difracción de rayos X. La Tabla 4.15 presenta los contenidos de carbono y azufre detectados en todas las muestras.

Tabla 4.15. Contenidos de carbono y azufre en las muestras usadas de los catalizadores (% másico).

| Método de preparación | | $Ni/Al_2O_3$ | $Ni/Ca/Al_2O_3$ | $Ni/Fe/Al_2O_3$ | $Ni/Cu/Al_2O_3$ | $Ni/Mn/Al_2O_3$ |
|---|---|---|---|---|---|---|
| Calcinados a 900 ºC. Reducción previa en $H_2/N_2$ a 900 ºC. | % C | 1,7 ± 0,4 | 0,32 ± 0,01 | 0,39 ± 0,05 | 15,0 ± 0,2 | 0,23 ± 0,03 |
| | % S | 2,24 ± 0,06 | 1,6 ± 0,2 | 2,27 ± 0,04 | 3,1 ± 0,1 | 1,68 ± 0,06 |
| Calcinados a 900 ºC. Sin pretratamiento de reducción | % C | 2,4 ± 0,1 | 0,30 ± 0,06 | 0,40 ± 0,08 | 12,1 ± 0,2 | 0,40 ± 0,04 |
| | % S | 2,0 ± 0,3 | 1,8 ± 0,1 | 2,16 ± 0,03 | 3,44 ± 0,06 | 2,21 ± 0,01 |
| Calcinados a 700 ºC. Sin pretratamiento de reducción | % C | 2,8 ± 0,4 | 0,32 ± 0,07 | 0,17 ± 0,01 | 8,8 ± 0,3 | 0,12 ± 0,03 |
| | % S | 1,9 ± 0,3 | 2,06 ± 0,03 | 1,9 ± 0,2 | 3,74 ± 0,04 | 1,52 ± 0,07 |

*Los datos mostrados en la tabla se corresponden con la media ± desviación estándar de tres medidas.*

Los mayores contenidos de azufre y carbono se detectaron en las tres muestras usadas de $Ni/Cu/Al_2O_3$, independientemente de la temperatura de calcinación y del procedimiento de reducción. El contenido de carbono alcanzó el 15% (en masa) en la muestra de $Ni/Cu/Al_2O_3$calcinada a 900 ºC y reducida en atmósfera de $H_2/N_2$, lo que parece indicar que la deposición de carbono constituye un importante factor en la pérdida de actividad mostrada por este catalizador. El contenido de carbono se redujo a un 12% y a un 9% en las muestras no reducidas y calcinadas a 900 ºC y 700 ºC, respectivamente. Estos datos de formación de carbono, junto con la formación neta de $CH_4$ obtenida con este catalizador bajo ciertas temperaturas (Figuras 4.23, 4.25 y 4.26), ponen de manifiesto el importante papel del catalizador $Ni/Cu/Al_2O_3$ en la reacción de metanización heterogénea ($C + 2H_2 \leftrightarrow CH_4$). La incorporación de los demás promotores al catalizador de $Ni/Al_2O_3$ supuso una disminución en la deposición de carbono, aunque esta reducción puede ser sólo una consecuencia de la menor actividad de los catalizadores de $Ni/Fe/Al_2O_3$ y $Ni/Ca/Al_2O_3$. Sin embargo, en el caso del $Ni/Mn/Al_2O_3$, que mostró una actividad similar o incluso superior a la del $Ni/Al_2O_3$ en algunos casos, podría significar una buena capacidad del Mn para reducir la deposición de carbono (Koike y cols., 2013). En el caso en el que la incorporación del Mn resultó en una mejora más clara de la actividad y estabilidad del catalizador (calcinación a 900 ºC y reducción previa en atmósfera de $H_2/N_2$), el contenido final de carbono se redujo del 1,7% al 0,23% al incorporar el Mn. Respecto a la influencia de la temperatura de calcinación o del procedimiento de reducción sobre la deposición de carbono, no se ha encontrado una tendencia uniforme, sino que depende de la segunda fase metálica incorporada al catalizador. Lo mismo ocurre con el contenido final de azufre en los sólidos pero, igual que ocurrió con el contenido de carbono, el catalizador de $Ni/Cu/Al_2O_3$ fue el que presentó una mayor retención. La incorporación de los demás metales supuso la reducción del contenido de azufre en determinadas condiciones, aunque sin seguir un patrón general. Estos resultados por sí solos no permiten discernir si el

azufre quedó quimisorbido preferencialmente en los promotores o en los centros activos de níquel.

Para intentar identificar las posibles especies formadas, las muestras de los catalizadores se analizaron por difracción de rayos X (XRD). La Figura 4.27 muestra los difractogramas obtenidos para las muestras usadas de los catalizadores calcinados a 900 ºC y utilizados sin tratamiento previo de reducción. Los difractogramas obtenidos para las muestras sometidas al tratamiento previo de reducción fueron prácticamente idénticos a los que se muestran en esta figura.

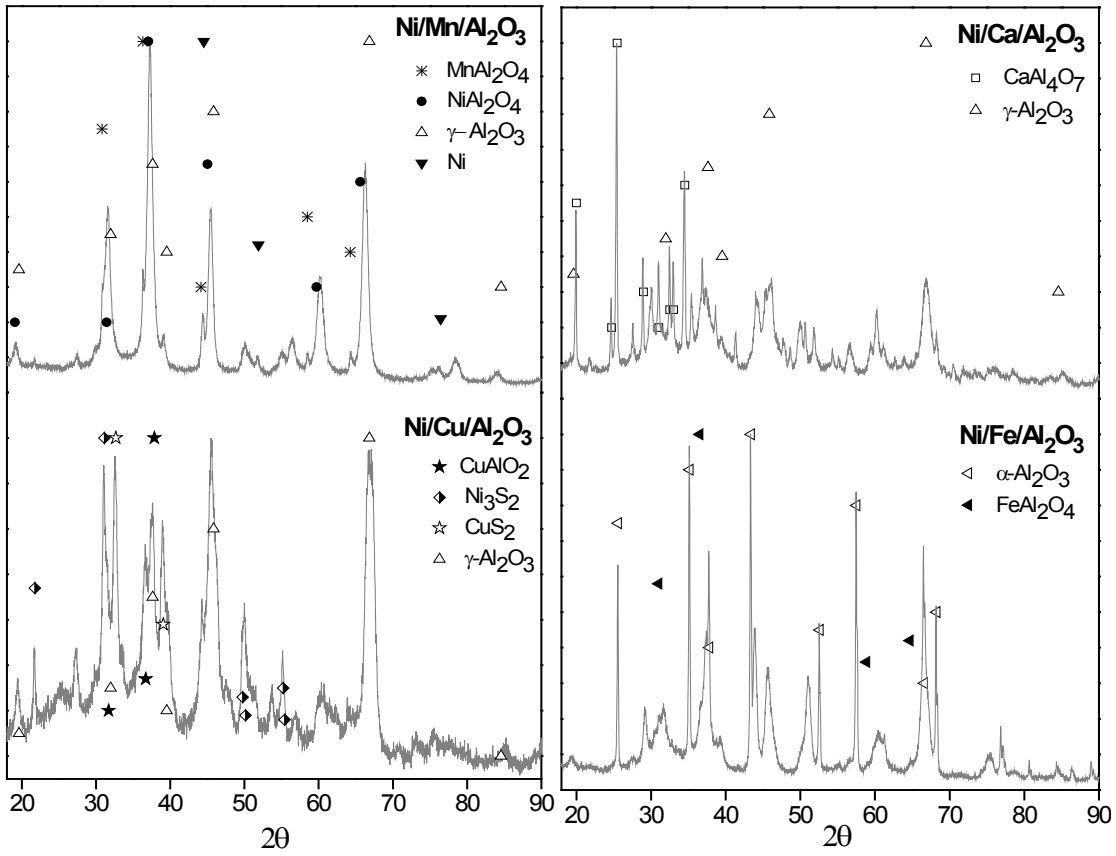


Figura 4.27. Difractogramas XRD de las muestras usadas de los catalizadores calcinados a 900 ºC y utilizados sin pretratamiento de reducción.

La comparación de los difractogramas de las muestras usadas (Figura 4.27) y sin usar (Figura 3.2) muestra claras diferencias. Tras los experimentos, las muestras parecen más cristalinas y el $NiAl_2O_4$ ya no es la fase principal detectada en todos ellos. Los difractogramas de las muestras usadas son más diferentes entre sí, permitiendo la detección de los metales añadidos como promotores, principalmente en forma de aluminatos: $MnAl_2O_4$, $CuAlO_4$, $FeAl_2O_4$ y $CaAl_4O_7$. Especial atención debe mostrarse también a la presencia de azufre, que sólo ha podido ser detectada en el catalizador de $Ni/Cu/Al_2O_3$ en forma de $Ni_3S_2$ y $CuS_2$.

# 5. CONCLUSIONES Y TRABAJOS FUTUROS

*Gasificación de lodo y de char con mezclas de vapor de agua y aire.*

Dado que el contenido de humedad de los lodos de EDAR antes de su secado térmico puede alcanzar el 70%, la gasificación de este residuo con la propia atmósfera de vapor creada a partir de su humedad parece una interesante opción para su valorización energética. Dada la endotermicidad del proceso, la adición de cierta cantidad de aire al medio de gasificación puede proporcionar la energía necesaria para el proceso a través de la combustión parcial de la materia prima.

La producción de gas durante la gasificación de lodos de EDAR con mezclas de aire y vapor de agua osciló entre 0,49 y 0,72 $m^3N \cdot kg^{-1}_{lodo}$ (gas seco y libre de $N_2$). El contenido energético de este gas es suficiente para su aprovechamiento en calderas, motores o turbinas (PCI = 4,1-6,2 $MJ \cdot m^{-3}N$). Además, la relación molar $H_2/CO$ en el gas producto también alcanzó el valor de 2 en algunos casos, valor requerido habitualmente para su uso como materia prima para la producción de químicos (Wender, 1996). El menor contenido de alquitrán obtenido en el gas fue de 11 $g \cdot m^{-3}N$, valor que se encuentra entre los resultados habituales para la gasificación de biomasa en lecho fluidizado (Corella y cols., 2006), y que supera los valores límite recomendados para el aprovechamiento del gas.

El *char* resultante de la pirólisis de lodos de EDAR aparece como una materia prima preferible para la gasificación desde el punto de vista de la formación de alquitrán. En este proceso, el contenido de alquitrán en el gas se redujo hasta niveles de 3 $g \cdot m^{-3}N$ en determinadas condiciones de operación. La reducción del contenido de materia volátil en el sólido después de la pirólisis explica esta diferencia. También la producción de gas seco por kilogramo de sólido se redujo prácticamente a la mitad al gasificar +*char* en lugar de lodo, siendo ésta la principal desventaja del proceso. Sin embargo, si el rendimiento a gas se calcula en base seca y libre de cenizas para el sólido, la gasificación de *char* ofrece un mayor rendimiento a gas (0,99-1,47 $m^3N \cdot kg^{-1}_{char\ org\acute{a}nico}$ frente a 0,89-1,32 $m^3N \cdot kg^{-1}_{lodo\ org\acute{a}nico}$), con un importante aumento de la producción de CO (45-85% mayor en términos de gramo por kilogramo de sólido seco y libre de cenizas) y una fuerte disminución de la producción de $CH_4$ y $C_2H_x$ (80% menor). A pesar de estas diferencias, el PCI de los gases de ambos procesos se mantuvo en el mismo orden de magnitud, y la relación molar $H_2/CO$ en el gas de gasificación de *char* también alcanzó el valor de 2 bajo algunas condiciones de operación.

La temperatura fue el factor más influyente para la mayoría de las variables analizadas en ambos procesos. El aumento de la temperatura resultó favorable para reducir el contenido de alquitrán y mejorar el rendimiento a gas y la producción específica de $H_2$, CO, así como la relación $CO/CO_2$ en el gas producto, el PCI del gas y la eficiencia energética de la gasificación. Por otro lado, el incremento de temperatura resultó desfavorable desde el punto de vista de la producción de $H_2S$, que se vio favorecida. La composición del medio de gasificación (relación $H_2O/O_2$) desempeñó un papel importante en la producción de $H_2$ y, en consecuencia, en la relación $H_2/CO$ del gas producto, que se vio favorecida con la mayor presencia de $H_2O$. La producción de $CH_4$ también aumentó al incrementar la relación $H_2O/O_2$, mientras que la conversión del carbono contenido inicialmente en los sólidos se vio perjudicada. Por último, el aumento del caudal de agente gasificante alimentado por gramo de sólido (RG) mostró una importante influencia en la producción de $CO_2$ y $H_2S$, que se vieron favorecidas. La Tabla 5.1 resume todas estas influencias de forma cualitativa (↓ y ↑ representan la disminución y el aumento de la variable respuesta al aumentar el valor del factor de operación, respectivamente).

Tabla 5.1. Impacto cualitativo de los factores de operación en la gasificación de lodo y de *char*.

| | *Gasificación de lodo* | | | *Gasificación de char* | | |
|---|---|---|---|---|---|---|
| | T | RG | $H_2O/O_2$ | T | RG | $H_2O/O_2$ |
| Fracción de C remanente en el sólido (%) | ↓↓↓ | ↓↓ | ↑↑↑ | ↓↓↓ | ↓↓ | ↑↑ |
| Fracción de C convertido en gas (%) | ↑ | ↑ | ↓ | ↑↑ | ↑ | ↓ |
| Rendimiento a gas seco ($m^3N \cdot kg^{-1}$, sin $N_2$) | ↑↑ | ↑ | --- | ↑↑ | ↑ | --- |
| Contenido de alquitrán en el gas ($g \cdot m^{-3}N$) | ↓↓↓↓ | ↓ | ↑↑ | ↓↓↓ | ↓↓↓ | ↓↓↓ |
| Producción de cada compuesto gaseoso ($g \cdot kg^{-1}_{sólido}$) | | | | | | |
| $H_2$ | ↑↑↑ | ↓ | ↑↑ | ↑↑ | ↑ | ↑↑ |
| CO | ↑↑↑ | ↓ | ↓↓ | ↑↑↑ | --- | ↓ |
| $CO_2$ | --- | ↑↑ | ↓↓ | ↓ | ↑↑ | ↓ |
| $CH_4$ | ↑ | ↓ | ↑↑ | --- | --- | ↑↑ |
| $C_2H_x$ | ↓ | --- | ↑ | --- | --- | --- |
| $H_2S$ | ↑↑ | ↑↑ | --- | ↑↑↑↑ | ↑↑↑ | --- |
| Relación molar $H_2/CO$ en el gas producto | ↓ | ↑ | ↑↑↑ | ↓↓ | --- | ↑↑ |
| Relación molar $CO/CO_2$ en el gas producto | ↑↑↑ | ↓↓ | --- | ↑↑↑ | ↓↓ | --- |
| PCI del gas ($MJ \cdot m^{-3}_{STP}$) | ↑ | ↓ | ↑ | ↑↑ | --- | ↑ |
| Eficiencia energética de gasificación (%) | ↑↑ | --- | ↑ | ↑↑ | ↑ | ↑ |

*Aspectos energéticos*

Dado el carácter endotérmico de muchas de las reacciones envueltas en el proceso de gasificación con vapor de agua, la composición de la mezcla de aire y vapor de agua utilizada como agente gasificante es clave para conseguir un balance energético favorable. Bajo las mismas condiciones y simplificaciones realizadas en los cálculos, la gasificación de *char* requiere un mayor aporte de energía externo que la gasificación de lodo para tener lugar. Entre los experimentos realizados, el uso de una relación equivalente de 19% fue suficiente para tener un proceso exotérmico de gasificación de lodo, mientras que esta relación tuvo que aumentarse hasta 32% en la gasificación de *char*. El hecho de alcanzar el equilibrio químico en el proceso conllevaría un mayor consumo energético pero, a su vez, la recuperación de energía en el gas producto podría ser mayor, de modo que la eficiencia energética de la gasificación mejoraría en condiciones de equilibrio.

Considerando la recuperación total e ideal del poder calorífico inferior y del calor sensible y latente de los gases, el contenido energético del gas obtenido en la gasificación de lodo podría ser suficiente para cubrir la demanda energética del propio proceso de gasificación y de la etapa previa de secado térmico. No ocurre lo mismo si se consideran de forma conjunta los productos gaseosos de la pirólisis de lodo y de la gasificación de *char*. La fracción líquida del proceso de pirólisis posee el contenido energético adicional necesario, pero algunas de sus propiedades, como su inestabilidad o alto contenido de nitrógeno, deben mejorarse antes de plantear su posible uso como combustible.

*Eliminación de $H_2S$ de gases calientes con cenizas de lodo*

Debido a su contenido en metales, especialmente hierro y calcio, las cenizas de lodos de EDAR plantean una interesante y económica opción para la eliminación de $H_2S$ de gases a alta temperatura. En los experimentos realizados con diferentes gases sintéticos, las cenizas de combustión de lodo mostraron mejores resultados que las cenizas de gasificación. Las diferencias en su composición pueden explicar su diferente comportamiento. Se detectó un menor contenido de hierro en la ceniza de gasificación, y en forma de distintas especies: $Fe_2O_3$ en la ceniza de combustión y $Fe_3O_4$ en la ceniza de gasificación.

Los mejores resultados de eliminación de $H_2S$ se obtuvieron al alimentar la mezcla de $H_2S/N_2$ seca (5000 ppm), obteniendo un gas de salida prácticamente libre de $H_2S$ (<100 ppm) durante 300 min con la ceniza de combustión a 800 ºC. En este caso, el contenido final de azufre en el sólido fue de 63 $mg \cdot g^{-1}_{ceniza}$. La eliminación de $H_2S$ del gas se vio claramente perjudicada por la presencia de vapor de agua en el medio de reacción debido a la

regeneración simultánea de los sulfuros metálicos formados. Además, los componentes del gas de gasificación también provocaron un efecto negativo en el proceso, tanto por la atmósfera reductora creada por el $H_2$ (que provoca la reducción de los óxidos de hierro), como por la presencia de $CO_2$ (que puede ocasionar la carbonatación de CaO). En las condiciones de operación más cercanas a lo que sería un proceso real, es decir, con el gas sintético de gasificación húmedo, la ceniza de combustión a 600 ºC mostró los mejores resultados: 50 min hasta alcanzar 100 ppm de $H_2S$ en el gas de salida y un contenido de azufre en el sólido de 27 $mg \cdot g^{-1}_{ceniza}$ después de 120 min de experimento.

Los análisis elementales realizados a las cenizas después de los experimentos revelaron que no toda la cantidad de $H_2S$ que había sido eliminada del gas estaba retenida en el sólido. Esto sugiere que el $H_2S$ no era el único compuesto con azufre en el gas de salida, sino que otros gases como $SO_2$ o COS parecen formarse durante la eliminación de $H_2S$ de corrientes gaseosas.

*Reformado de compuestos modelo de alquitrán con catalizadores de níquel*

El estudio catalítico consistió en la evaluación de la estabilidad y actividad de diferentes catalizadores de níquel soportados sobre alúmina y modificados con diferentes promotores (Fe, Ca, Mn y Cu) para el reformado de alquitrán e hidrocarburos ligeros en presencia de $H_2S$. Dada la afinidad de los óxidos de estos metales por el $H_2S$, con la incorporación de los promotores se buscaba un menor envenenamiento de los sitios activos de níquel y, por tanto, una mejora de la estabilidad del catalizador de $Ni/Al_2O_3$ ante la presencia de $H_2S$. En la mayoría de los casos no se obtuvieron dichos resultados, sino que la incorporación de los promotores resultó perjudicial para la actividad del catalizador debido, probablemente, a un exceso de carga metálica y a la reducción de la superficie específica (10-50% menor). De forma excepcional, los datos de conversión de naftaleno, metano y etileno mostraron una mejora de la actividad y estabilidad del catalizador de $Ni/Al_2O_3$ al incorporarle Mn, y tras haber sometido a los catalizadores a un pretratamiento de reducción en atmósfera de $H_2$. El análisis elemental de ambos catalizadores mostró un menor contenido de carbono depositado en el catalizador de $Ni/Mn/Al_2O_3$. Por lo tanto, aunque es necesario profundizar en el estudio, el Mn parece aportar cierta estabilidad al catalizador de $Ni/Al_2O_3$ para evitar la deposición de carbono y, también, el fenómeno de sinterización.

**TRABAJOS FUTUROS**

En base a los resultados obtenidos en este trabajo, se proponen las siguientes líneas de estudio para continuar la investigación relativa a la gasificación de lodos de EDAR y a la limpieza del gas producto:

- Gasificación de lodo de EDAR húmedo (con un contenido de humedad del 20-30%) para obtener la atmósfera de vapor de agua para su gasificación a partir del propio residuo. Esto requerirá, probablemente, el diseño de otro sistema de alimentación para el lodo húmedo.

- Gasificación de lodo de EDAR no digerido anaeróbicamente, con el fin de aprovechar toda la fracción orgánica acumulada durante el tratamiento de aguas residuales.

- Completar el estudio energético de los procesos de gasificación y pirólisis de lodo teniendo en cuenta factores exergéticos.

- Aplicación de las cenizas resultantes de la combustión del *char* de pirólisis de lodo para la eliminación de $H_2S$ del gas de pirólisis seco, tras la condensación de los vapores, reutilizando así el principal subproducto del proceso.

- Profundizar en el estudio del manganeso como aditivo para mejorar la estabilidad de los catalizadores de níquel. Aplicación del catalizador $Ni/Mn/Al_2O_3$ en el proceso real de gasificación de lodo, en un reactor aguas abajo del gasificador.

# 6. REFERENCIAS BIBLIOGRÁFICAS

Abu El-Rub Z., Bramer E.A., Brem G. (2004) *Review of catalysts for tar elimination in biomass gasification processes*. Industrial & Engineering Chemistry Research 43, 6911-6919.

Adegoroye A., Paterson N., Li X., Morgan T., Herod A.A., Dugwell D.R., Kandiyoti R. (2004) *The characterisation of tars produced during the gasification of sewage sludge in a spouted bed reactor*. Fuel 83, 1949-1960.

Álvarez-Rodríguez R., Clemente-Jul C. (2008) *Hot gas desulphurisation with dolomite sorbent in coal gasification*. Fuel 87, 3513-3521.

Anis S., Zainal Z.A. (2011) *Tar reduction in biomass producer gas via mechanical, catalytic and thermal methods: A review.* Renewable & Sustainable Energy Reviews 15, 2355-2377.

Antal M.J., Edwards W.E., Friedman K.L., Rogers F.E. (1979) *Final Progress Report to US Environmental Protection Agency*. Princeton University.

Asadullah M. (2014) *Barriers of commercial power generation using biomass gasification gas: A review*. Renewable & Sustainable Energy Reviews 29, 201-215.

Aznar M., González A.E., Manyà J.J., Sánchez J.L., Murillo M.B. (2007) *Understanding the effect of the transition period during the air gasification of dried sewage sludge in a fluidized bed reactor*. International Journal of Chemical Reactor Engineering 5, A18.

Aznar M., Manyà J.J., García G., Sánchez J.L., Murillo M.B. (2008) *Influence of freeboard temperature, fluidization velocity and particle size on tar production and composition during the air gasification of sewage sludge*. Energy & Fuels 22, 2840-2850.

Aznar M.P., Caballero M.A., Gil J., Martín J.A., Corella J. (1998). *Commercial steam reforming catalysts to improve biomass gasification with steam-oxygen mixtures. 2. Catalytic tar removal*. Industrial & Engineering Chemical Research 37, 2668-2680.

Bacaicoa P.G., Bilbao R., Uson C. (1995) *Sewage sludge gasification: first studies*. Proceedings of the Second Biomass Conference of the Americas: Energy, Environment, and Agricultural Industry, 685-694.

Bagreev A., Bandosz T.J. (2005) *On the mechanism of hydrogen sulfide removal from moist air on catalytic carbonaceous adsorbents*. Industrial & Engineering Chemistry Research 44, 530-538.

Bandosz T.J. (2002) *On the adsorption/oxidation of hydrogen sulfide on activated carbons at ambient temperatures*. Journal of Colloid and Interface Science 246, 1-20.

Bona S., Guillen P., Alcalde J.G., García L., Bilbao R. (2008) *Toluene steam reforming using coprecipitated Ni/Al catalysts modified with lanthanum or cobalt*. Chemical Engineering Journal 137, 587-597.

Brandt P., Henriksen U. (2000) *Decomposition of tar in gas from updraft gasifier by thermal cracking*. Proceedings of the first world conference on biomass for energy and industry.

Bridgwater A.V. (1995) *The technical and economic feasibility of biomass gasification for power generation*. Fuel 74, 631-653.

Bridgwater A.V., Peacocke G.V.C. (2000) *Fast pyrolysis processes for biomass*. Renewable & Sustainable Energy Reviews 4, 1-73.

Campoy M., Gómez-Barea A., Vidal F.B., Ollero P. (2009) *Air-steam gasification of biomass in a fluidised bed: Process optimisation by enriched air*. Fuel Processing Technology 90, 677-685.

Campoy M., Gómez-Barea A., Ollero P., Nilsson S. (2014) *Gasification of wastes in a pilot fluidized bed*. Fuel Processing Technology 121, 63-69.

Chaudhari S.T., Dalai A.K., Bakhshi N.N. (2003) *Production of hydrogen and/or syngas ($H_2$+ CO) via steam gasification of biomass-derived chars*. Energy & Fuels 17, 1062-1067.

Cheah S., Carpenter D.L., Magrini-Bair K.A. (2009) *Review of mid- to high- temperature sulfur sorbents for desulphurization of biomass- and coal-derived syngas*. Energy & Fuels 23, 5291-5307.

*ChemSpider database*. Royal Society of Chemistry. Disponible en www.chemspider.com. Consultado en enero de 2014.

Chueh C.F., Swanson A.C. (1973) *Estimation of liquid heat capacity*. The Canadian Journal of Chemical Engineering 51, 596-600.

Concha A., Andalaft A., Farías O. (2009) *Gasificación de carbón para generación de energía eléctrica: análisis con valoración de opciones reales*. Ingeniare. Revista chilena de ingeniería 17, 347-359.

Corella J., Toledo J.M., Molina G. (2006) *Calculation of the conditions to get less than 2 g tar/$Nm^3$ in a fluidized bed biomass gasifier.* Fuel Processing Technology 87, 841-846.

Courson C., Makaga E., Petit C., Kiennemann A. (2000) *Development of Ni catalysts for gas production from biomass gasification. Reactivity in steam- and dry-reforming*. Catalysis Today 63, 427-437.

De Andrés J.M., Narros A., Rodríguez M.E. (2011) *Behaviour of dolomite, olivine and alumina as primary catalysts in air-steam gasification ofsewage sludge*. Fuel 90, 521-527.

Decisión 2001/118/CE de la Comisión, de 16 de enero de 2001, por la que se modifica la Decisión 2000/532/CE en lo que se refiere a la lista de residuos. DOCE núm. L 47/1, de 16 de 16 de febrero de 2001.

De Lasa H., Salaices E., Mazumder J., Lucky R. (2011) *Catalytic steam gasification of biomass: catalysts, thermodynamics and kinetics*. Chemical Reviews 111, 5404-5433.

Delgado J., Aznar M.P., Corella J. (1997) *Biomass gasification with steam in fluidized bed: effectiveness of CaO, MgO and CaO-MgO for hot raw gas cleaning*. Industrial & Engineering Chemistry Research 36, 1535-1543.

Devi L., Ptasinski K.J., Janssen F.J.J.G. (2003) *A review of the primary measures for tar elimination in biomass gasification processes*. Biomass & Bioenergy 24, 125-140.

Di Blasi C. (2009) *Combustion and gasification rates of lignocellulosic chars*. Progress in Energy and Combustion Science 35, 121-140.

Directiva 86/278/CEE del Consejo, de 12 de junio de 1986, relativa a la protección del medio ambiente y, en particular, de los suelos, en la utilización de los lodos de depuradora en la agricultura. DOUE núm. L 181/6, de 4 de julio de 1986.

Directiva 91/271/CEE del Consejo, de 21 de mayo de 1991, sobre el tratamiento de aguas residuales urbanas. DOUE núm. L 135/40, de 30 de mayo de 1991.

Directiva 1999/31/CEE del Consejo, de 26 de abril de 1999, relativa al vertido de residuos. DOUE núm. L 182/1, de 16 de julio de 1999.

Directiva 2008/98/CE del Parlamento Europeo y del Consejo, de 19 de noviembre de 2008, sobre los residuos y por la que se derogan determinadas Directivas. DOUE núm. L 312/3, de 22 de noviembre de 2008.

Directiva 2010/75/UE del Parlamento Europeo y del Consejo, de 24 de noviembre de 2010, sobre las emisiones industriales (prevención y control integrados de la contaminación). DOUE núm. L 334/17, de 17 de dieciembre de 2010.

Domínguez A., Menéndez J.A., Pis J.J. (2006) *Hydrogen rich fuel gas production from the pyrolysis of wet sewage sludge at high temperature*. Journal of Analytical and Applied Pyrolysis 77, 127-132.

Dogru M., Midilli A., Howarth C.R. (2002) *Gasification of sewage sludge using a throated downdraft gasifier and uncertainty analysis*. Fuel Processing Technology 75, 55-82.

Dou B., Gao J., Sha X., Baek S.W. (2003) *Catalytic cracking of tar component from high-temperature fuel gas*. Applied Thermal Engineering 23, 2229-2239.

Elseviers W.F., Verelst H. (1999) *Transition metal oxides for hot gas desulphurization*. Fuel 78, 601-612.

Engelen K., Zhang Y.H., Draelants D.J., Baron G.V. (2003) *A novel catalytic filter for tar removal from biomass gasification gas: Improvement of the catalytic activity in presence of $H_2S$*. Chemical Engineering Science 58, 665-670.

Fonts I., Juan A., Gea G., Murillo M.B., Sánchez J.L. (2008) *Sewage sludge pyrolysis in fluidized bed. 1: Influence of operational conditions on the product distribution*. Industrial & Engineering Chemistry Research 47, 5376-5385.

Fonts I., Azuara M., Gea G., Murillo M.B. (2009) *Study of the pyrolysis liquids obtained from different sewage sludge*. Journal of Analytical and Applied Pyrolysis 85, 184-191.

Fonts I., Gea G., Azuara M., Ábrego J., Arauzo J. (2012) *Sewage sludge pyrolysis for liquid production: A review*. Renewable & Sustainable Energy Reviews 16, 2781-2805.

Franco C., Pinto F., Gulyurtlu I., Cabrita I. (2003) *The study of reactions influencing the biomass steam gasification process*. Fuel 82, 835-842.

Fytili D., Zabaniotou A. (2008) *Utilization of sewage sludge in EU application of old and new methods - A review*. Renewable & Sustainable Energy Reviews 12, 116-140.

García G., Cascarosa E., Ábrego J., Gonzalo A., Sánchez J.L. (2011) *Use of different residues for high temperature desulphurization of gasification gas*. Chemical Engineering Journal 174, 644-651.

Gil J., Aznar M.P., Caballero M.A., Francés E., Corella J. (1997) *Biomass gasification in fluidized bed at pilot scale with steam-oxygen mixtures. Product distribution for very different operating conditions*. Energy & Fuels 11, 1109-1118.

Gil J., Corella J., Aznar M.P., Caballero M.A. (1999a) Biomass gasification in atmospheric and bubbling fluidized bed: Effect of the type of gasifying agent on the product distribution. Biomass & Bioenergy 17, 389-403.

Gil J., Caballero M.A., Martín J.A., Aznar M.P., Corella J. (1999b) *Biomass gasification with air in fluidized bed: effect of in-bed use of dolomite under different operation conditions.* Industrial & Engineering Chemistry Research 38, 4226-4235.

Gil-Lalaguna N., Fonts I., Gea G., Murillo M.B., Lázaro L. (2010) *Reduction of water content in sewage sludge pyrolysis liquid by selective on-line condensation of the vapors*. Energy & Fuels 24, 6555-6564.

González J.F., Román S., Encinar J.M., Martínez G.J. (2009). *Pyrolysis of various biomass residues and char utilization for the production of activated carbons*. Journal of Analytical and Applied Pyrolysis 85, 134-141.

Gutiérrez-Ortiz F.J., Aguilera P.G., Ollero P. (2014) *Biogas desulfurization by adsorption on thermally treated sewage-sludge*. Separation and Purification Technology 123, 200-213.

Han J., Kim H. (2008) *The reduction and control technology of tar during biomass gasification/pyrolysis: An overview*. Renewable & Sustainable Energy Reviews 12, 397-406.

Harrison B.K., Seaton W.H. (1988) *Solution to missing group-problem for estimation of ideal-gas heat-capacities*. Industrial & Engineering Chemistry Research 27, 1536-1540.

Haykiri-Acma H., Yaman S., Kucukbayrak S. (2006) *Gasification of biomass chars in steam-nitrogen mixture*. Energy Conversion and Management 47, 1004-1013.

He P., Luo S., Cheng G., Xiao B., Cai L., Wang J. (2012) *Gasification of biomass char with air-steam in a cyclone furnace*. Renewable Energy 37, 398-402.

Hepola J., Simell P. (1997a) *Sulphur poisoning of nickel-based hot gas cleaning catalysts in synthetic gasification gas - I. Effect of different process parameters*. Applied Catalysis B: Environmental 14, 287-303.

Hepola J., Simell P. (1997b) *Sulphur poisoning of nickel-based hot gas cleaning catalysts in synthetic gasification gas - II. Chemisorption of hydrogen sulphide*. Applied Catalysis B: Environmental 14, 305-321.

Herguido J., Corella J., González-Saiz J. (1992) *Steam gasification of lignocellulosic residues in a fluidised bed at a small pilot scale. Effect of the type of feedstock.* Industrial & Engineering Chemistry Research 31, 1274-1282.

Inguanzo M., Domínguez A., Menéndez J.A., Blanco C.G., Pis J.J. (2002) *On the pyrolysis of sewage sludge: the influence of pyrolysis conditions on solid, liquid and gas fractions*. Journal of Analytical and Applied Pyrolysis 63, 209-222.

Judex J.W., Gaiffi M., Burgbacher H.C. (2012) *Gasification of dried sewage sludge: Status of the demonstration and the pilot plant*. Waste Management 32, 719-723.

Kelessidis A., Stasinakis A.S. (2012) *Comparative study of the methods used for treatment and final disposal of sewage sludge in European countries*. Waste Management 32, 1186-1195.

Kiely G. (1999) *Ingeniería ambiental. Fundamentos, entornos, tecnologías y sistemas de gestión*. Ed. McGraw-Hill: Buenos Aires.

Kim K., Jeon S.K., Vo C., Park C.S., Norbeck J.M. (2007) *Removal of $H_2S$ from steam-hydrogasifier product gas by zinc oxide sorbent*. Industrial & Engineering Chemistry Research 46, 5848-5854.

Kim Y.J., Lee S.H., Kim S.D. (2001) *Coal gasification characteristics in a downer reactor*. Fuel 80, 1915-1922.

Kimura T., Miyazawa T., Nishikawa J., Kado S., Okumura K., Miyao T., Naito S., Kunimori K., Tomishige K. (2006) *Development of Ni catalysts for tar removal by steam gasification of biomass*. Applied Catalysis B: Environmental 68, 160-170.

Kinoshita C.M., Wang Y., Zhou J. (1994) *Tar formation under different biomass gasification conditions*. Journal of Analytical and Applied Pyrolysis 29, 169-181.

Kinoshita C.M., Turn S.Q., Overend R.P., Bain R.L. (1997) *Power generation potential of biomass gasification systems*. Journal of Energy Engineering 123, 88-99.

Koike M., Ishikawa C., Li D., Wang L., Nakagawa Y., Tomishige K. (2013) *Catalytic performance of manganese-promoted nickel catalysts for the steam reforming of tar from biomass pyrolysis to synthesis gas*. Fuel 103, 122-129.

Kumar A., Jones D.D., Hanna M.A. (2009) *Thermochemical biomass gasification: a review of the current status of the technology*. Energies 2, 556-581.

Li C., Suzuki K. (2009a) *Tar property, analysis, reforming mechanism and model for biomass gasification - An overview*. Renewable & Sustainable Energy Reviews 13, 594-604.

Li C., Hirabayashi D., Suzuki K. (2009b) *Development of new nickel based catalyst for biomass tar steam reforming producing $H_2$-rich syngas*. Fuel Processing Technology 90, 790-796.

Lv P.M., Xiong Z.H., Chang J., Wu C.Z., Chen Y., Zhu J.X. (2004) *An experimental study on biomass air-steam gasification in a fluidized bed*. Bioresource Technology 95, 95-101.

Manara P., Zabaniotou A. (2012) *Towards sewage sludge based biofuels via thermochemical conversion - A review*. Renewable & Sustainable Energy Reviews 16, 2566-2582.

Manganaro J., Chen B., Adeosun J., Lakhapatri S., Favetta D., Lawal A. (2011) *Conversion of residual biomass into liquid transportation fuel: an energy analysis*. Energy & Fuels 25, 2711-2720.

Manyà J.J., Sánchez J.L., Gonzalo A., Arauzo J. (2005) *Air gasification of dried sewage sludge in a fluidized bed: Effect of the operating conditions and in-bed use of alumina*. Energy & Fuels 19, 629-636.

Manyà J.J, Sánchez J.L, Ábrego J., Gonzalo A., Arauzo J. (2006) *Influence of gas residence time and air ratio on the air gasification of dried sewage sludge in a bubbling fluidised bed*. Fuel 85, 2027-2033.

Márquez-Montesinos F., Cordero T., Rodríguez-Mirasol J., Rodríguez J.J. (2002) *$CO_2$ and steam gasification of a grapefuit skin char*. Fuel 81, 423-429.

Martínez J.D., Mahkamov K., Andrade R.V., Lora E.E.S. (2012) *Syngas production in downdraft biomass gasifiers and its application using internal combustion engines*. Renewable Energy 38, 1-9.

McKendry P. (2002a) *Energy production from biomass (part 1): overview of biomass*. Bioresource Technology 83, 37-46.

McKendry P. (2002b) *Energy production from biomass (part 3): gasification technologies*. Bioresource Technology 83, 55-63.

Meng X., Jong W., Pal R., Verkooijen A.H.M. (2010) *In bed and downstream hot gas desulphurization during solid fuel gasification: a review*. Fuel Processing Technology 91, 964-981.

Miccio F., Piriou B., Ruoppolo G., Chirone R. (2009) *Biomass gasification in a catalytic fluidized reactor with beds of different materials*.Chemical Engineering Journal 154, 369-374.

Midilli A., Dogru M., Howarth C.R., Ling M.J., Ayhan T. (2001) *Combustible gas production from sewage sludge with a downdraft gasifier*. Energy Conversion and Management 42, 157-172.

Miyazawa T., Kimura T., Nishikawa J., Kado S., Kunimori K., Tomishige K. (2006) *Catalytic performance of supported Ni catalysts in partial oxidation and steam reforming of tar derived from the pyrolysis of wood biomass*. Catalysis Today 115, 254-262.

Mondal P., Dang G.S., Garg M.O. (2011) *Syngas production through gasification and cleanup for downstream applications - Recent developments*. Fuel Processing Technology 92, 1395-1410.

Narváez I., Orio A., Aznar M.P., Corella J. (1996) *Biomass gasification with air in an atmospheric bubbling fluidized bed. Effect of six operational variables on the quality of the produced raw gas*. Industrial & Engineering Chemistry Research 35, 2110-2120.

Neeft J.P.A., Knoef H.A.M., Zielke U., Sjöstrom K., Hasler P., Simell P.A., Dorrington M.A., Thomas L., Abatzoglou N., Deutch S., Greil C., Buffinga G.J., Brage C., Suomalinen M. (2002) *Guideline for Sampling and Analysis of Tar and Particles in Biomass Producer Gases (Tar protocol).* Energy project EEN5-1999-00507.

Nilsson S., Gómez-Barea A., Fuentes-Cano D. (2012). *Gasification reactivity of char from dried sewage sludge in a fluidized bed*. Fuel 92, 346-353.

Nilsson S., Gómez-Barea A., Fuentes-Cano D., Campoy M. (2014) *Gasification kinetics of char from olive tree pruning in fluidized bed*. Fuel 125, 192-199.

Nipattummakul N., Ahmed I., Kerdsuwan S., Gupta A.K. (2010) *High temperature steam gasification of wastewater sludge*. Applied Energy 87, 3729-3734.

Nisbet I.C.T, Lagoy P.K. (1992) *Toxic equivalency factors (TEFs) for polycyclic aromatic-hydrocarbons (PAHs)*. Regulatory Toxicology and Pharmacology 16, 290-300.

Nishikawa J., Nakamura K., Asadullah M., Miyazawa T., Kunimori K., Tomishige K. (2008) *Catalytic performance of $Ni/CeO_2/Al_2O_3$ modified with noble metals in steam gasification of biomass*. Catalysis Today 131, 146-155.

Nowicki L., Antecka A., Bedyk T., Stolarek P., Ledakowicz S. (2011) *The kinetics of gasification of char derived from sewage sludge*. Journal of Thermal Analysis and Calorimetry 104, 693-700.

Olivares A., Aznar M.P., Caballero M.A., Gil J., Francés E., Corella J. (1997) *Biomass gasification: produced gas upgrading by in-bed use of dolomite*. Industrial & Engineering Chemistry Research 36, 5220-5226.

Park N.K., Lee D.H., Lee J.D., Chang W.C., Ryu S.O., Lee T.J. (2005) *Effects of reduction of metal oxide sorbents on reactivity and physical properties during hot gas desulphurization in IGCC*. Fuel 84, 2158-2164.

Park H.J., Park S.H., Sohn J.M., Park J., Jeon J.K., Kim S.S., Park Y.K. (2010) *Steam reforming of biomass gasification tar using benzene as a model compound over various Ni supported metal oxide catalysts*. Bioresource Technology 101, S101-S103.

Perry R.H., Green D.W. (1999) *Perry's Chemical Engineer's Handbook. 7th ed*. New York: McGraw-Hill.

Petersen I., Werther J. (2005) *Experimental investigation and modelling of gasification of sewage sludge in the circulating fluidized bed*. Chemical Engineering and Processing: Process Intensification 44, 717-736.

Pinto F., Franco C., André R.N., Tavares C., Dias M., Gulyurtlu I., Cabrita I. (2003) *Effect of experimental conditions on co-gasification of coal, biomass and plastics wastes with air/steam mixtures in a fluidized bed system*. Fuel 82, 1967-1976.

Pokorna E., Postelmans N., Jenicek P., Schreurs S., Carleer R., Yperman J. (2009) *Study of bio-oils and solids from flash pyrolysis of sewage sludges*. Fuel 88, 1344-1350.

Ponzio A., Kalisz S., Blasiak W. (2006) *Effect of operating conditions on tar and gas composition in high temperature air/steam gasification (HTAG) of plastic containing waste*. Fuel Processing Technology 87, 223-233.

Primavera A., Trovarelli A., Andreussi P., Dolcetti G. (1998) *The effect of water in the low-temperature catalytic oxidation of hydrogen sulfide to sulfur over activated carbon*. Applied Catalysis A: General 173, 185-192.

Qin Y.H., Feng J., Li W.Y. (2010) *Formation of tar and its characterization during air-steam gasification of sawdust in a fluidized bed reactor*. Fuel 89, 1344-1347.

Rapagnà S., Jand N., Kiennemann A., Foscolo P.U. (2000) *Steam-gasification of biomass in a fluidized-bed of olivine particles*. Biomass & Bioenergy 19, 187-197.

Raveendran K., Ganesh A. (1998) *Adsorption characteristics and pore-development of biomass-pyrolysis char*. Fuel 77, 769-781.

Richardson S.M., Gray M.R. (1997) *Enhancement of residue hydroprocessing catalysts by doping with alkali metals*. Energy & Fuels 11, 1119-1126.

Ros A., Montes-Morán M., Fuente E., Nevskaia D.M., Martin M.J. (2006) *Dried sludges and sludge-based chars for $H_2S$ removal at low temperature: influence of sewage sludge characteristics*. Environmental Science & Technology 40, 302-209.

Rulkens W. (2008) *Sewage sludge as a biomass resource for the production of energy: Overview and assessment of the various options*. Energy & Fuels 22, 9-15.

Salleh M.A.M, Kisiki N.H., Yusuf H.M., Ghani W.A.K. (2010) *Gasification of biochar from empty fruit bunch in a fluidized bed reactor*. Energies 3, 1344-1352.

Sato K., Fujimoto K. (2007) *Development of new nickel based catalyst for tar reforming with superior resistance to sulfur poisoning and coking in biomass gasification*. Catalysis Communications 8, 1697-1701.

Scott S.A., Davidson J.F., Dennis J.S., Fennell P.S., Hayhurst A.N. (2005) *The rate of gasification by $CO_2$ of chars from waste*. Proceedings of the Combustion Institute 30, 2151-2159.

Seok S., Choi S., Park E., Han S., Lee J. (2002) *Mn-promoted $Ni/Al_2O_3$ catalysts for stable carbon dioxide reforming of methane*. Journal of Catalysis 209, 6-15.

Shen L., Zhang D.K. (2003) *An experimental study of oil recovery from sewage sludge by low-temperature pyrolysis in a fluidised-bed*. Fuel 82, 465-472.

Smith K.M., Fowler G.D., Pullket S., Graham N.J.D. (2009) *Sewage sludge-based adsorbents: a review of their production, properties and use in water treatment applications*. Water Research 43, 2569-2594.

Spinosa L., Ayol A., Baudez J.C., Canziani R., Jenicek P., Leonard A., Rulkens W., Xu G., van Dijk L. (2011) *Sustainable and innovative solutions for sewage sludge management*. Water 3, 702-717.

Spliethoof H. (2001) *Status of biomass gasification for power production*. IFRF Combustion Journal, article number 200109. Delft University of Tecnology. The Netherlands.

Srinakruang J., Sato K., Vitidsant T., Fujimoto K. (2006) *Highly efficient sulfur and coking resistance catalysts for tar gasification with steam*. Fuel 85, 2419-2426.

Ståhl K., Neergaard M. (1998) *IGCC power plant for biomass utilisation, Värnamo, Sweden.* Biomass and Bioenergy 15, 205-211.

Struis R.P.W.J., Schildhauer T.J., Czekaj I., Janousch M., Biollaz S.M.A., Ludwig C. (2009) *Sulphur poisoning of Ni catalysts in the SNG production from biomass: a TPO/XPS/XAS study*. Applied Catalysis A: General 362, 121-128.

Sutton D., Kelleher B., Ross J.R.H. (2001a) *Review of literature on catalysts for biomass gasification*. Fuel Processing Technology 73, 155-173.

Sutton D., Kelleher B., Doyle A., Ross J.R.H. (2001b) *Investigation of nickel supported catalysts for the upgrading of brown peat derived gasification products*. Bioresource Technology 80, 111-116.

Swierczynski D., Libs S., Courson C., Kiennemann A. (2007) *Steam reforming of tar from a biomass gasification process over Ni/olivine catalyst using toluene as a model compound*. Applied Catalysis B: Environmental 74, 211-222.

Tae-Young M., Bo-Sung K., Joo-Sik K. (2009) *Production of a producer gas with high heating values and less tar from dried sewage sludge through air gasification using a two-stage gasifier and activated carbon*. Energy & Fuels 23, 3268-3276.

Tamhankar S.S., Hasatani M., Wen C.Y. (1981) *Kinetic studies on the reactions involved in the hot gas desulfurization using a regenerable iron oxide sorbent - I: Reduction and sulfidation of iron oxide*. Chemical Engineering Science 36, 1181-1191.

Tseng T.K., Chang H.C., Chu H., Chen H.T. (2008) *Hydrogen sulfide removal from coal gas by the metal-ferrite sorbents made from the heavy metal wastewater sludge*. Journal of Hazardous Materials 160, 482-488.

Van der Drift A., van Doorn J., Vermeulen J.W. (2001) *Ten residual biomass fuels for circulating fluidized-bed gasification*. Biomass & Bioenergy 20, 45-56

Wang T., Chang J., Lv P., Zhu J. (2005) *Novel catalyst for cracking of biomass tar*. Energy & Fuels 19, 22-27.

Wender I. (1996) *Reactions of synthesis gas*. Fuel Processing Technology 48, 189-297.

Westmoreland P.R., Harrison D.P. (1976) *Evaluation of candidate solids for high-temperature desulfurization of low-btu gases*. Environmental Science & Technology 10, 659-661.

Xie L., Li T., Gao J., Fei X., Wu X., Jiang Y. (2010) *Effect of moisture content in sewage sludge on air gasification*. Journal of Fuel Chemistry and Technology 38, 615-620.

Yan F., Luo S., Hu Z., Xiao B., Cheng G. (2010) *Hydrogen-rich gas production by steam gasification of char from biomass fast pyrolysis in a fixed bed reactor: Influence of temperature and steam on hydrogen yield and syngas composition*. Bioresource Technology 101, 5633-5637.

Yildirim O., Kiss A.A., Hüser N., Leßmann K., Kenig E.Y. (2012) *Reactive absorption in chemical process industry: a review on current activities*. Chemical Engineering Journal 213, 371-391.

Yoshimura Y., Yasuda H., Sato T., Shimada H. (1995) *Utilization of thermodynamic database in the systems using molybdate and iron based catalysis*. Coal Science and Technology 24, 1275-1278.

Yuan W., Bandosz T.J. (2007) *Removal of hydrogen sulfide from biogas on sludge-derived adsorbents*. Fuel 86, 2736-2746.

Yung M.M., Jablonski W.S., Magrini-Bair K.A. (2009) *Review of catalytic conditioning of biomass-derived syngas*. Energy & Fuels 23, 1874-1887.

Zhang R., Brown R.C., Suby A., Cummer K. (2004) *Catalytic destruction of tar in biomass derived producer gas*. Energy Conversion and Management 45, 995-1014.

Zhang R., Wang Y., Brown R.C. (2007) *Steam reforming of tar compounds over Ni/olivine catalysts doped with $CeO_2$*. Energy Conversion and Management 48, 68-77.

Zhang B., Xiong S., Xiao B., Yu D., Jia X. (2011) *Mechanism of a wet sewage sludge pyrolysis in a tubular furnace*. International Journal of Hydrogen Energy 36, 355-363.

# APÉNDICE. COPIA DE LOS ARTÍCULOS PUBLICADOS

# 7. APÉNDICE. COPIA DE LOS TRABAJOS PUBLICADOS

Las publicaciones que recogen los resultados de los estudios realizados en la presente Tesis Doctoral, y que se adjuntan en sucesivas páginas, son los siguientes:

i. **N. Gil-Lalaguna**, J.L. Sánchez, M.B. Murillo, E. Rodríguez, G. Gea. (2014) "*Air steam gasification of sewage sludge in a fluidized bed. Influence of some operating conditions*". **Chemical Engineering Journal** 248, 373-382.
Factor de impacto JCR de la revista *Chemical Engineering Journal* en 2013: 4,058. ISI ranking: 10 de 133 en el área de Ingeniería Química.

ii. **N. Gil-Lalaguna**, J.L. Sánchez, M.B. Murillo, V. Ruiz, G. Gea. (2014) "*Air steam gasification of char derived from sewage sludge pyrolysis. Comparison with the gasification of sewage sludge*". **Fuel** 129, 147-155.
Factor de impacto JCR de la revista *Fuel* en 2013: 3,406. ISI ranking: 11 de 133 en el área de Ingeniería Química.

iii. **N. Gil-Lalaguna**, J.L. Sánchez, M.B. Murillo, M. Atienza-Martínez, G. Gea. (2014) "*Energetic assessment of air-steam gasification of sewage sludge and of the integration of sewage sludge pyrolysis and air-steam gasification of char*". **Energy** 76, 652-662.
Factor de impacto JCR de la revista *Energy* en 2013: 4,159. ISI ranking: 14 de 81 en el área de Energía & Combustibles.

iv. **N. Gil-Lalaguna**, J.L. Sánchez, M.B. Murillo, G. Gea. (2015) "*Use of sewage sludge combustion ash and gasification ash for high-temperature desulphurization of different gas streams*". **Fuel** 141, 99-108.
Factor de impacto JCR de la revista *Fuel* en 2013: 3,406. ISI ranking: 11 de 133 en el área de Ingeniería Química.

La doctoranda ha sido la responsable de la experimentación, análisis de datos y redacción de todos los artículos.

Además, durante el desarrollo de la Tesis, la doctoranda ha tenido la oportunidad de presentar su trabajo en varios congresos internacionales, participando en algunos de ellos con ponencias orales:

**N. Gil-Lalaguna**, J.L. Sánchez, M.B. Murillo, G. Gea. "*Gas desulfurization with solid by-products from thermo-chemical conversion of sewage sludge*". 22nd European Biomass Conference & Exhibition. Hamburgo (Alemania), Junio 2014. ISBN: 978-88-89407-52-3.

**N. Gil-Lalaguna**, V. Ruiz, J.L. Sánchez, M.B. Murillo, G. Gea. *"Valorization of char from sewage sludge pyrolysis by means of gasification"*. 21st European Biomass Conference & Exhibition. Copenhague (Dinamarca), Junio 2013. ISBN: 978-88-89407-53-0.

**N. Gil-Lalaguna**, M. Atienza, I. Fonts, J.L. Sánchez, M.B. Murillo. *"Thermochemical valorization of sewage sludge by combination of fast pyrolysis and gasification"*. ANQUE International Congress of Chemical Engineering: Innovating for the future. Sevilla (España), Junio 2012.

**N. Gil-Lalaguna**, A. Moreno, J.L. Sánchez, M.B. Murillo, G. Gea. *"Catalytic steam reforming of model tar compounds over CaO-$Al_2O_3$ catalysts"*. 20th European Biomass Conference & Exhibition. Milán (Italia), Junio 2012. ISBN: 978-88-89407-54-7.

**N. Gil-Lalaguna**, J.L. Sánchez, M.B. Murillo, M. Azuara, G. Gea. *"Sewage sludge gasification. Effect of the type of gasifying agent".* 19th European Biomass Conference & Exhibition. Berlín (Alemania), Junio 2011. ISBN: 978-88-89407-55-7.

**N. Gil-Lalaguna**, J.L. Sánchez, M.B. Murillo. *"Preliminary study of gasification with steam/enriched air mixtures of sewage sludge and of the char obtained in its pyrolysis process".* BioEnergy III: Present and New Perspectives on Biorefineries. Lanzarote (España), Mayo 2011.

Chemical Engineering Journal 248 (2014) 373–382

Contents lists available at ScienceDirect

Chemical Engineering Journal

journal homepage: www.elsevier.com/locate/cej

# Air–steam gasification of sewage sludge in a fluidized bed. Influence of some operating conditions

N. Gil-Lalaguna *, J.L. Sánchez, M.B. Murillo, E. Rodríguez, G. Gea

*Thermo-chemical Processes Group, Aragón Institute of Engineering Research (I3A), Universidad de Zaragoza, c/Mariano Esquillor s/n., 50018 Zaragoza, Spain*

## HIGHLIGHTS

- Experimental work on air–steam gasification of sewage sludge in a fluidized bed.
- Temperature is the most influential factor for most of the variables analyzed.
- Steam presence favors the gas heating value and the $H_2$/CO in the product gas.
- Differences between kinetic and thermodynamic control in a gasification process.

## ARTICLE INFO

*Article history:*
Received 24 September 2013
Received in revised form 13 March 2014
Accepted 16 March 2014
Available online 24 March 2014

*Keywords:*
Air–steam gasification
Sewage sludge
Fluidized bed

## ABSTRACT

An experimental work was carried out to investigate the viability of energy recovery from the air–steam gasification of sewage sludge. The relative influence of different factors, as well as the effect of their possible interactions, has been determined by means of analysis of variance. Temperature was found to be the most influential factor for most of the variables analyzed. Solid yield (35–41 wt.%) and tar content (11–45 g/$m^3_{STP}$) were largely reduced with temperature, whereas gas production (0.89 – 1.32 $m^3_{STP}$/kg sewage sludge dry and ash free), carbon yield to gas phase (62–90 wt.%), gasification efficiency (39–66%), and $H_2$ and CO yields (20–52 and 137–414 g/kg sewage sludge dry and ash free, respectively) were improved at high temperature. Other important parameters for the end-use of the gas such as its heating value (4.12–6.20 MJ/$m^3_{STP}$) and its $H_2$/CO molar ratio (1.46–3.25) were greatly influenced by the composition of the gasification medium, since the increase in the steam to oxygen ratio was favorable for both. The comparison of experimental and theoretical results highlights that equilibrium was not reached during the experimental runs.



## 1. Introduction

Biomass is one of the most important primary renewable energy sources. The conversion of biomass to energy encompasses a wide range of materials, conversion technologies and end-use applications of the products, such as power/heat generation, transportation fuels and chemical feedstocks. Sewage sludge, which is the waste produced by wastewater treatment processes, can be considered an important renewable biomass energy source [1].

As a result of the application of the Urban Wastewater Treatment Directive (UWWTD) 91/271/EEC [2], new municipal wastewater treatment strategies have been developed during the last two decades in order to improve the quality of effluents. Existing treatment plants have been upgraded and new and more effective treatment plants have been designed and implemented. In parallel to the improvement of the effluent quality, environmental awareness about sewage sludge management has gained strength. The main commercial means of sewage sludge disposal include its use as fertilizer, land filling or incineration [3,4]. However, because of increasing legal limitations on sewage sludge land filling and agricultural reuse, energy recovery from sewage sludge remains an attractive and sustainable way of management. Thermal processes such as pyrolysis, gasification or combustion of sewage sludge have thus attracted considerable scientific interest. This paper presents an experimental work on sewage sludge gasification.

Gasification is the conversion of a carbonaceous material into a gas fuel by heating it in a gasification medium such as air, oxygen or steam. Gas from gasification consists of a mixture of carbon monoxide, carbon dioxide, hydrogen, methane and other light hydrocarbons, nitrogen (if air is used as gasifying agent) and steam. This gas can be used to power gas engines and gas turbines or used as a chemical feedstock to produce liquid fuels [5]. During gasification, a mixture of heavy and condensable hydrocarbons (tars) is

* Corresponding author. Tel.: +34 976762224.
*E-mail address:* noemigil@unizar.es (N. Gil-Lalaguna).

http://dx.doi.org/10.1016/j.cej.2014.03.055
1385-8947/

also produced. The presence of tar in the gas causes problems associated with condensation, formation of aerosols and polymerization leading to more complex structures which limit the subsequent utilization of the gas.

Operating conditions during gasification (such as the nature of the biomass, pressure, temperature, residence time or gasification medium) play an important role in both tar formation and gas quality. The higher the temperature, the lower the tar content in the product gas [6], but other factors such as the risk of ash sintering limit the operating temperature. The use of different gasifying agents such as air, steam, steam–oxygen mixtures or carbon dioxide has been reported in the literature. Both gas composition and gas heating value are noticeably affected by the gasification medium because of the variation of selectivity in the gasification reactions [7]. Generally, steam gasification enhances $H_2$ production compared to air gasification, and also leads to a higher gas heating value because the dilution of the gas with nitrogen is avoided [8]. However, the steam gasification reactions are endothermic and require a continuous supply of energy. Given this background, biomass gasification with mixtures of air and steam appears to be a potential solution from the economic point of view, since the partial combustion of biomass inside the gasifier can supply the required energy for the process, turning it into an autothermal process. The improvement in gas quality by feeding a flow of steam together with the air stream during biomass gasification has been reported in several experimental studies [9–12].

In the particular case of sewage sludge, experimental studies based on air gasification [13–17] and steam gasification [18] have been reported in the literature. In general, the gas composition and the gas heating value from sewage sludge gasification are close to typical values obtained from other kinds of biomass, which demonstrates the potential of sewage sludge as a raw material for the gasification process. However, tar formation and other additional problems such as the formation of other pollutants ($H_2S$, HCl or $NH_3$) hinder the development of sewage sludge gasification, so new efforts are required in order to optimize the process.

In this work, an experimental study (based on a $2^k$ factorial design) on sewage sludge gasification in a fluidized bed with mixtures of air and steam has been developed in order to find out the influence of several operating conditions (temperature, composition of the gasification medium and gasifying agent to biomass ratio) on the gasification performance. Furthermore, experimental results have been compared with theoretical data which were determined considering equilibrium conditions.

## 2. Materials and methods

### 2.1. Sewage sludge

Anaerobically digested and thermally dried sewage sludge (SS) was supplied by a Spanish urban wastewater treatment plant. Feedstock analyses were performed at the Instituto de Carboquímica (ICB-CSIC) in Zaragoza (Spain) according to standard methods: moisture according to ISO-589-1981, ash according to ISO-1171-1976, volatiles according to ISO-5623-1974, ultimate analysis (CHNS) using a Carlo Erba 1108 and heating value according to ISO-1928-89 (Table 1). More details about the sewage sludge characterization, such as FTIR and X-ray diffraction analyses, can be found elsewhere [19]. Sewage sludge was smashed and sieved to obtain a feed sample in the size range of 250–500 μm.

**Table 1**
Proximate and ultimate analyses and heating value of sewage sludge.

| | |
|---|---|
| *Proximate analysis (wt.%, wet basis)* | |
| Moisture | 6.48 |
| Ash | 39.04 |
| Volatiles | 50.09 |
| Fixed carbon | 4.39 |
| *Ultimate analysis (wt.%, wet basis)* | |
| C | 29.5 |
| H | 4.67 |
| N | 5.27 |
| S | 1.31 |
| HHV (MJ/kg) | 12.8 |
| LHV (MJ/kg) | 11.8 |

### 2.2. Experimental setup

Sewage sludge gasification runs have been carried out in a laboratory-scale fluidized bed reactor operating at atmospheric pressure, with continuous feed of solid and continuous removal of ash. The gasifier was a tubular reactor made of refractory steel (AISI 310) divided into two parts: a bed zone, with an inner diameter of 40 mm, and a freeboard zone, with an inner diameter of 63 mm. Sewage sludge was continuously fed to the reactor by a feeding system composed of a screw-feeder and a variable speed motor. The solid feed rate in each experiment was around 2.1 g/min. Ash from previous sewage sludge gasification tests constituted the solid bed by itself from the beginning of the runs. When the amount of bed material inside the reactor exceeded the height of the bed zone, it left the reactor by overflow through a lateral pipe and was collected in a separate vessel. The reactor was heated by an electrical furnace with three different heating zones (bed, free-board and cyclone), which could be controlled independently. The bed temperature was one of the factors under study, ranging between 770 and 850 °C (the same as in the free-board), while the cyclone temperature was set at 450 °C. A schematic diagram of the experimental setup can be found elsewhere [20].

The gasifying/fluidizing agent used in the process consisted of different mixtures of steam and enriched air (air + oxygen). Furthermore, an additional flow of nitrogen was necessary in two of the experiments (those with the lowest air requirement) in order to avoid differences in the dilution effect of the gas with nitrogen and in the fluidization rate (which was around 5–7 times greater than the minimum fluidization rate). The feed rate of these gases (air, oxygen and nitrogen) was adjusted by using mass flow controllers. The water was fed through a HPLC pump and vaporized before mixing into the gas stream. The composition and the amount of gasifying agent were the other factors under study in this work. The mixture of oxygen, steam and approximately 2/3 of the total air required was fed into the fluidized bed reactor through its distribution plate, while the remaining air was fed with the solid to facilitate its movement through the feeding pipe, which was externally refrigerated to prevent reactions taking place outside the bed.

The vapors and gases produced during gasification remained inside the reactor between 7 and 8 s and then passed through a cyclone and a hot filter, both at 450 °C, in which the solid particles swept by the gas were collected. Next, the gases and vapors passed through two ice-cooled condensers, where water and condensable organic compounds (tar) were collected. A cotton filter was situated after the condensers in order to remove small particulates and aerosols swept by the gas. The volume of particle- and tar-free gas was measured by a volumetric meter and its composition was analyzed on line using a micro gas chromatograph (Agilent 3000-A), which determined the volume percentages of $H_2$, $O_2$, CO, $CO_2$, $CH_4$, $C_2H_4$, $C_2H_6$, $C_2H_2$ and $H_2S$. Water content in the condensed fraction was analyzed off line by Karl Fischer titration (so the amount of tar was determined by difference) and the tar composition was analyzed by gas chromatography with mass spectroscopy and flame ionisation detectors (MS/FID GC). The experiments were

carried out during 90 min to ensure that the stationary state was reached [21].

### 2.3. Experimental design and data analysis

The influence of three operating factors (temperature, gasifying agent to biomass ratio and composition of the gasification medium) on sewage sludge gasification performance has been studied experimentally by means of a $2^k$ factorial design, where k indicates the number of factors studied (in this case 3) and $2^k$ represents the number of runs (in this case 8). Furthermore, three replicates at the center point (CP) were carried out in order to evaluate both the experimental error and the curvature shown by the evolution of each response variable, that is to say, whether this evolution is linear or not within the experimental range studied. This experimental design is suitable not only for studying the influence of operating conditions, but also the influence of their possible interactions. An interaction occurs when a factor influences a response variable in a different way depending on the value of another factor.

The three analyzed factors were: (i) bed reactor temperature (which ranges between 770 and 850 °C); (ii) gasifying ratio (GR) between the mass flow of gasifying agent (oxygen plus steam) and the mass flow of dry and ash-free basis (*daf*) sewage sludge (which ranges between 0.8 and 1.1 g/g SS *daf*); (iii) nature of the gasification medium, represented by the $H_2O/O_2$ molar ratio (which ranges between 1 and 3). The overall flow rate of gasifying agent was kept constant when the $H_2O/O_2$ molar ratio was modified. These three factors together with their respective ranges of study were chosen on the basis of works of other authors concerning gasification of different kinds of biomass in fluidized bed reactors [9–12].

As can be seen in Table 2, the experimental design consists of 8 runs plus 3 replicates at the center point (810 °C, 0.95 g/g SS *daf*, 2 mol $H_2O$/mol $O_2$). As usually occurs when an experimental design is planned, the lower and upper limits of the factors are coded as −1 (in this case T = 770 °C, GR = 0.8 and $H_2O/O_2$ = 1) and 1 (in this case T = 850 °C, GR = 1.1 and $H_2O/O_2$ = 3), respectively. The use of coded levels enables an easy identification of the term with the greatest influence on the response variable: the higher the coefficient, the more influential the factor.

The response variables analyzed were: (i) distribution of products (yields to the different gasification products: solid, gas and tar); (ii) gas composition, determined on line using a micro gas chromatograph; (iii) production of each gaseous component; (iv) lower heating value of the product gas ($LHV_{gas}$); (v) cold gasification efficiency; (vi) carbon yield to gas phase and (vii) tar composition.

Statistical analyses of the results have been carried out by analysis of variance (ANOVA), using the Design-Expert® 7 software (from Stat-Ease, Inc.). ANOVA analysis evaluates whether the effect of the factors, the interactions between them and the curvature have a significant influence or not on the response variables. A confidence level of 95% for the F-distribution was selected to determine the significant effects.

## 3. Results and discussion

### 3.1. Distribution of products

Experimental results for the distribution of products are presented in Table 3.

Furthermore, as a result of the ANOVA analysis, Table 4 shows the relative influence of each factor on the product distribution. In this table, the average data represent the average of the whole set of results obtained for each response variable, the coefficients associated to the different factors (T, GR and $H_2O/O_2$) show how the response variables evolve when varying each factor (considering the coded values for the factors within the studied range), and the coefficients associated to the interactions show whether a factor influences a response variable in a different way depending on the value of another factor.

#### 3.1.1. Solid yield and carbon content in the solid

The solid yield is defined as the mass (g) of solid product collected per 100 g of sewage sludge fed. Because of the high ash content in the sewage sludge (39 wt.%), the solid residue is an important by-product in its gasification process and its yield varied between 35 and 41 wt.%, whilst typical values for other kinds of biomass such as wood or straw are below 8 wt.% [22].

Carbon content in the solid product was analyzed using a Leco TruSpec Micro Elemental Analyzer (Table 3). According to the ANOVA results (Table 4), carbon content in the solid product is reduced by increasing both the gasification temperature (higher reaction rate) and the gasifying ratio, and by decreasing the $H_2O/O_2$ ratio (Fig. 1), which seems to indicate that carbon combustion is faster than its steam gasification. Although temperature is the most influential factor for the carbon reaction, its effect depends on other operating conditions, since its interaction with the $H_2O/O_2$ ratio is a significant term (Fig. 1a). This fact shows that carbon reactions with oxygen are more sensitive to temperature changes that the reactions with steam.

The results of the solid yield together with those of the carbon content in the solid (Table 3) suggest that inorganic ash compounds could have been released to the gas phase during the gasification process, since some data of solid yield are even below the original ash content of the sewage sludge (39 wt.%). Both the transformation and the release to gas phase of ash compounds during thermo-chemical processes have been shown in other studies [23,24], although this was usually found to take place at higher temperatures.

#### 3.1.2. Gas yield

The gas yield is defined as the volume of gas produced ($m^3_{STP}$ $N_2$-free basis, where STP means standard conditions of temperature and pressure at 0 °C and 1 atm) per kilogram of SS *daf* fed. The gas yield data from sewage sludge gasification varied between 0.89 and 1.32 $m^3_{STP}$/kg SS *daf*, so these values are close to the typical ones found in the literature for similar operating conditions and different kinds of biomass [7,9,12].

**Table 2**
Operating conditions of gasification tests.

| Experiment number | 1 | 2 | 3 | 4 | 5 | 6 | 7 | 8 | 9, 10, 11 |
|---|---|---|---|---|---|---|---|---|---|
| Coded values | 1,1,1 | −1,1,1 | 1,−1,1 | −1,−1,1 | 1,1,−1 | −1,1,−1 | 1,−1,−1 | −1,−1,−1 | 0,0,0 |
| Temperature (°C) | 850 | 770 | 850 | 770 | 850 | 770 | 850 | 770 | 810 |
| g gasifying agent/g sewage sludge *daf* | 1.1 | 1.1 | 0.8 | 0.8 | 1.1 | 1.1 | 0.8 | 0.8 | 0.95 |
| $H_2O/O_2$ molar ratio in the gasifying agent | 3 | 3 | 3 | 3 | 1 | 1 | 1 | 1 | 2 |
| Equivalence ratio (ER) | 0.17 | 0.17 | 0.12 | 0.12 | 0.32 | 0.32 | 0.23 | 0.23 | 0.19 |
| Steam to biomass *daf* mass ratio (S/B) | 0.71 | 0.71 | 0.52 | 0.52 | 0.39 | 0.39 | 0.27 | 0.27 | 0.52 |

**Table 3**
Experimental results: product distribution and gas composition.

| | 1,1,1 | −1,1,1 | 1,−1,1 | −1,−1,1 | 1,1,−1 | −1,1,−1 | 1,−1,−1 | −1,−1,−1 | 0,0,0[a] |
|---|---|---|---|---|---|---|---|---|---|
| *Product distribution* | | | | | | | | | |
| Solid yield (g solid/100 g SS) | 36.8 | 40.1 | 40.1 | 40.7 | 35.6 | 39.2 | 38.4 | 40.0 | 38.2 ± 0.1 |
| Carbon content in the solid product (wt.%) | 4.56 | 7.61 | 5.66 | 10.20 | 0.51 | 6.20 | 1.00 | 7.09 | 5.89 ± 0.33 |
| Gas yield ($m^3_{STP}$/kg SS) | 0.72 | 0.51 | 0.65 | 0.53 | 0.72 | 0.52 | 0.71 | 0.49 | 0.61 ± 0.01 |
| Gas yield ($m^3_{STP}$/kg SS *daf*) | 1.32 | 0.94 | 1.20 | 0.97 | 1.32 | 0.96 | 1.30 | 0.89 | 1.13 ± 0.01 |
| Tar content ($g/m^3_{STP}$) | 18.8 | 43.6 | 18.6 | 44.5 | 12.1 | 22.4 | 10.9 | 45.3 | 14.8 ± 1.4 |
| *Gas composition (vol.%, dry basis)* | | | | | | | | | |
| $H_2$ | 24.2 | 18.4 | 25.1 | 20.4 | 18.0 | 11.0 | 20.6 | 13.6 | 19.3 ± 0.1 |
| CO | 8.7 | 5.7 | 10.2 | 7.3 | 11.6 | 7.0 | 14.1 | 7.7 | 9.4 ± 0.1 |
| $CO_2$ | 17.1 | 18.6 | 12.6 | 15.5 | 20.7 | 23.8 | 16.0 | 19.8 | 18.1 ± 0.2 |
| $CH_4$ | 3.1 | 3.5 | 3.6 | 4.1 | 2.6 | 2.8 | 2.9 | 3.4 | 3.3 ± 0.1 |
| $C_2H_x$ | 1.7 | 2.1 | 1.4 | 2.2 | 1.3 | 1.6 | 1.4 | 2.0 | 1.7 ± 0.2 |
| $H_2S$ | 0.44 | 0.38 | 0.33 | 0.33 | 0.44 | 0.42 | 0.38 | 0.31 | 0.40 ± 0.02 |
| $N_2$ | 44.9 | 51.4 | 46.8 | 50.2 | 45.3 | 53.4 | 44.5 | 53.2 | 47.8 ± 0.2 |
| $H_2$/CO molar ratio | 2.79 | 3.25 | 2.46 | 2.81 | 1.54 | 1.57 | 1.46 | 1.77 | 2.06 ± 0.01 |
| CO/$CO_2$ molar ratio | 0.51 | 0.30 | 0.81 | 0.47 | 0.56 | 0.29 | 0.88 | 0.39 | 0.52 ± 0.01 |

[a] Mean value ± standard deviation.

**Table 4**
Relative influence of the significant factors on the carbon content in the solid product, gas yield, tar content in the gas, and $H_2$/CO and CO/$CO_2$ molar ratios in the product gas.

| | Carbon content in the solid (wt.%) | Gas yield ($m^3_{STP}$/kg SS *daf*) | Tar content in the gas ($g/m^3_{STP}$) | $H_2$/CO molar ratio in the gas | CO/$CO_2$ molar ratio in the gas |
|---|---|---|---|---|---|
| Average | 5.50 | 1.12 | 27.03 | 2.21 | 0.52 |
| T | −2.42 | 0.17 | −11.91 | −0.14 | 0.16 |
| GR | −0.63 | 0.019 | −2.78 | 0.081 | −0.11 |
| $H_2O/O_2$ | 1.65 | * | 4.35 | 0.62 | * |
| T-GR | * | 0.017 | 3.15 | 0.021 | −0.044 |
| T-($H_2O/O_2$) | 0.53 | −0.024 | * | −0.059 | −0.026 |
| GR-($H_2O/O_2$) | * | * | 2.62 | 0.11 | * |
| T-($H_2O/O_2$)-GR | * | 0.028 | −2.89 | −0.049 | * |
| Curvature | * | ** | ** | ** | * |

* Non-significant term.
** Curvature is significant.

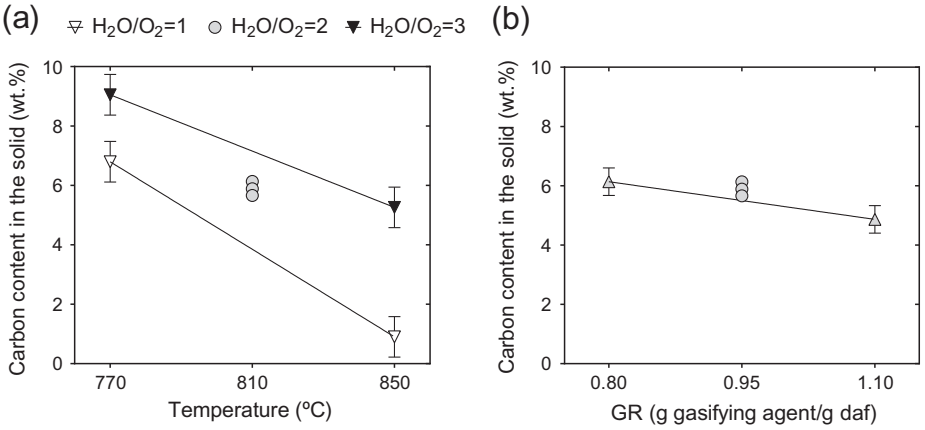


**Fig. 1.** Carbon content in the solid product (wt.%). (a) Interaction between temperature and $H_2O/O_2$ molar ratio (GR = 0.95). (b) Effect of the gasifying ratio (T = 810 °C; $H_2O/O_2$ = 2).

The ANOVA analysis (Table 4) shows that the gas yield does not follow a linear response within the studied range of the factors, since the curvature is a significant term. Temperature is clearly the most influential factor for the production of gas. The significant increase of the gas yield with temperature may be due to different processes that are favored by higher temperatures: greater production of gas in the initial stage of pyrolysis, cracking and steam reforming of tars and endothermic reactions of char gasification [12]. The increase of GR also favors the production of gas, although its effect is less significant than that corresponding to temperature. Significant interactions of temperature with both the GR and the $H_2O/O_2$ ratio have been found: the effect of temperature on the gas yield is intensified at the highest value of the GR (Fig. 2a) and at the lowest $H_2O/O_2$ ratio (Fig. 2b).

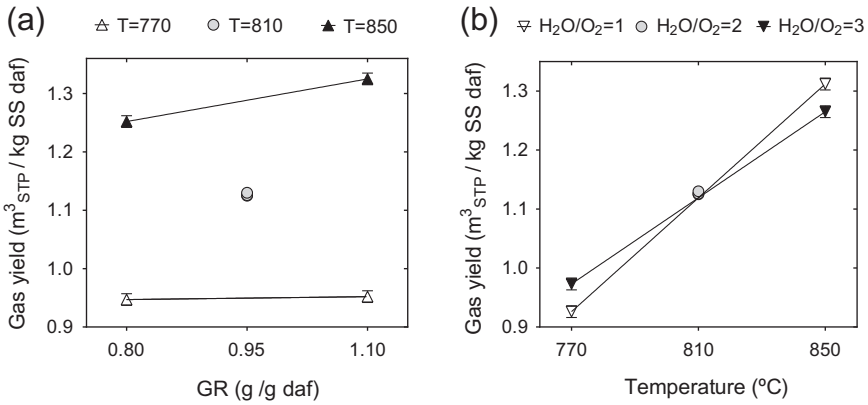


**Fig. 2.** Gas yield. (a) Interaction between temperature and gasifying ratio ($H_2O/O_2$ = 2). (b) Interaction between temperature and $H_2O/O_2$ molar ratio (GR = 0.95).

*3.1.3. Tar content in the product gas*

The tar content is defined as the mass (g) of condensable organic compounds collected in each experiment per $m^3_{STP}$ of dried gas measured after condensing the vapors. The lowest values of tar content obtained in this work are close to the typical values found for fluidized bed biomass gasifiers which, according to Corella et al. [25], usually range between 8 and 15 g/$m^3_{STP}$.

As occurred with the gas yield, the tar content in the gas does not follow a linear response within the studied range of the factors, as the curvature is a significant term. Temperature is also the most influential factor for tar content (Table 4). The rise in the gasification temperature from 770 to 850 °C causes a clear reduction in tar formation (Fig. 3a) because of the enhancement of tar cracking and reforming reactions [6]. The tar content is also reduced by decreasing the $H_2O/O_2$ ratio in the gasification medium, suggesting that tar combustion reactions are faster than tar steam reforming, and by increasing the GR, although the effect of the latter factor is less significant. The influence of the GR on the tar content disappears when working at the highest temperature (Fig. 3a) or at the highest $H_2O/O_2$ ratio (Fig. 3b).

*3.2. Gas composition*

The gas composition from a gasification process is the result of many complex and competing reactions. The most representative of these reactions are given below:

Oxidation $C + O_2 \leftrightarrow CO_2 \quad \Delta H < 0$ (1)

Partial oxidation $C + 1/2O_2 \leftrightarrow CO \quad \Delta H < 0$ (2)

Boudouard $C + CO_2 \leftrightarrow 2CO \quad \Delta H > 0$ (3)

Water–gas primary $C + H_2O \leftrightarrow CO + H_2 \quad \Delta H > 0$ (4)

Water–gas secondary $C + 2H_2O \leftrightarrow CO_2 + 2H_2 \quad \Delta H > 0$ (5)

Water–gas shift (WGS) $CO + H_2O \leftrightarrow CO_2 + H_2 \quad \Delta H < 0$ (6)

Methanation $C + 2H_2 \leftrightarrow CH_4 \quad \Delta H < 0$ (7)

Steam reforming $C_nH_x + nH_2O \leftrightarrow nCO + (x/2 + n)H_2 \quad \Delta H > 0$ (8)

Dry reforming $C_nH_x + nCO_2 \leftrightarrow 2nCO + (x/2)H_2 \quad \Delta H > 0$ (9)

Cracking $C_nH_x \leftrightarrow C + (x/2)H_2 \quad \Delta H > 0$ (10)

As usual in a biomass gasification process, the main gases produced during sewage sludge gasification are $H_2$, CO, $CO_2$ and light hydrocarbons, $CH_4$ being the most abundant of them. In addition, $H_2S$ is also released during the process due to the presence of sulfur-compounds in the sewage sludge (Table 1). Statistical analyses

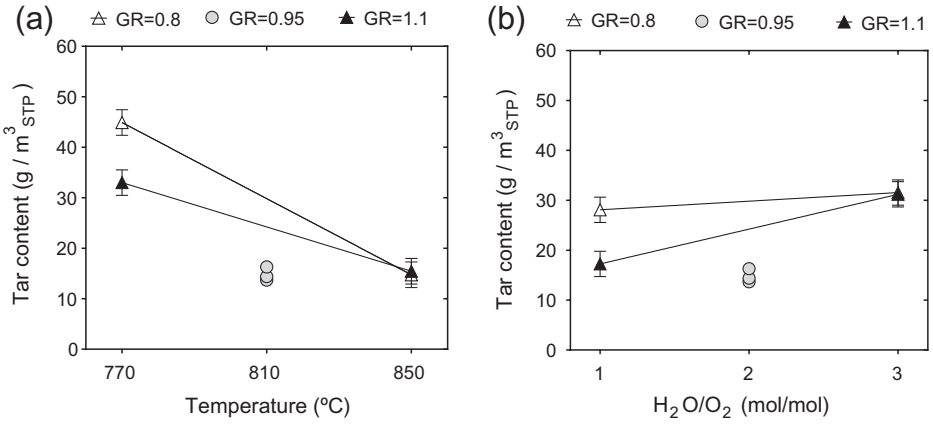


**Fig. 3.** Tar content in the gas. (a) Interaction between temperature and gasifying ratio ($H_2O/O_2$ = 2). (b) Interaction between $H_2O/O_2$ and gasifying ratio (T = 810 °C).

of gas composition have not been included in this work because it was considered preferable to analyze the production or the specific yield of each gaseous compound (g/kg SS *daf*), as detailed in the next section.

The average gas composition (dry basis) obtained in each experiment is reported in Table 3. Considerable differences in the fractions of the gaseous compounds have been found. For example, $H_2$ (11.0–25.1 vol.%), CO (5.7–14.1 vol.%), $CO_2$ (12.6–23.8 vol.%) or $CH_4$ (2.6–4.1 vol.%) can double or halve their percentages depending on the operating conditions. These volume percentages lead to $H_2$/CO and CO/$CO_2$ molar ratios in the exit gas ranging from 1.46–3.25 and 0.29–0.88, respectively. The $H_2$/CO molar ratio is an important parameter in view of possible end uses of the gas, and values close to 2 are usually required in processes such as methanol or Fischer Tropsch synthesis [26]. According to the ANOVA results (Table 4), the composition of the gasification medium is clearly the most influential factor for this ratio. The higher the $H_2O/O_2$ ratio used as gasifying agent, the higher the $H_2$/CO molar ratio obtained in the gas product. Working at lower temperatures also leads to an increase in the $H_2$/CO molar ratio.

The CO/$CO_2$ ratio shows how the carbon initially contained in the sewage sludge is distributed among both compounds. The higher the gasification temperature, the higher the CO/$CO_2$ ratio obtained in the product gas. Furthermore, the GR exerts a negative influence on the CO/$CO_2$ ratio, although its effect is less significant than that of the temperature.

### 3.3. Production of each gaseous compound

The production or yield of each analyzed gas ($H_2$, CO, $CO_2$, $CH_4$, $C_2H_x$ and $H_2S$) is defined as the mass (g) of each gas produced per kilogram of SS *daf* fed.

Both experimental and theoretical yields of gases are analyzed in this section. The theoretical production of each gas during sewage sludge gasification at equilibrium conditions has been determined using HSC Chemistry® 6.1 software, simulating the same operating conditions that had been previously tested in the laboratory, that is, following the same $2^k$ factorial design. According to the theoretical results obtained, the gas product from sewage sludge gasification at equilibrium conditions should only contain $H_2$, CO, $CO_2$, $CH_4$, $H_2S$ and $NH_3$.

The experimental and the theoretical yields of gases are compared in Fig. 4. The points in the same vertical line represent the results obtained under the same operating conditions. As can be seen, experimental and theoretical data appreciably differ one from the other, which means that equilibrium was not reached during the experimental runs, maybe due to insufficient residence time of the gases in the reactor. Experimental yields of $H_2$ and CO are clearly below their corresponding theoretical data (up to four and five times lower in the most unfavorable conditions, respectively). The lower the gasification temperature, the greater is the difference between the experimental and the theoretical data. In contrast, experimental yields of $CO_2$ and $CH_4$ are above their corresponding theoretical values. $CH_4$ is mainly produced during the pyrolysis step and is hardly reformed during the subsequent process.

The experimental and theoretical yields of gases have been analyzed statistically by means of ANOVA. In the case of the theoretical results, most of the yields revealed a curvature, so the design was augmented with central composite points in order to determine the evolution of the response variables in the studied ranges and to find out which factor(s) is (are) causing the curvature. Table 5 presents the ANOVA results for both the experimental and the theoretical results.

As can be seen in Table 5, temperature is the most influential factor for the experimental yield of $H_2$. Although this gas is involved in many reactions both as reactant and as product, the temperature rise leads to a global increase in its experimental yield. The same trend for $H_2$ production has usually been reported in the literature [11,12,27]. Although to a lesser extent, the $H_2$ experimental yield is also enhanced by increasing the $H_2O/O_2$ ratio. On the one hand, the increase in the steam presence favors $H_2$ formation (4, 5, 6, 8) and, on the other hand, $H_2$ combustion is mitigated by reducing the proportion of oxygen in the gasification medium. The GR affects the experimental production of $H_2$ in a negative way: $H_2$ consumption outweighs $H_2$ formation when both the ER and the S/B ratio are increased. In contrast to the experimental results, the $H_2O/O_2$ ratio is the most influential factor for the theoretical yield of $H_2$ (Table 5) and it is also the factor responsible for the curvature observed. The influence of the temperature is much less significant in this case and, unlike the experimental results, this factor adversely affects the theoretical production of $H_2$. The WGS reaction (6) may explain this observed trend at equilibrium conditions due to its exothermic nature.

As occurred with the $H_2$ experimental yield, temperature is the most influential factor for the experimental production of CO

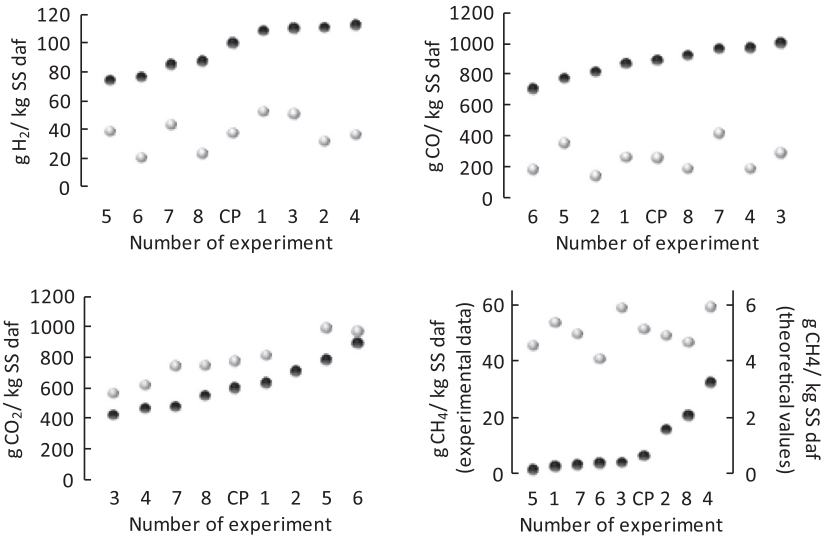


**Fig. 4.** Theoretical (●) and experimental (●) production of $H_2$, CO, $CO_2$ and $CH_4$.

**Table 5**
Relative influence of the significant factors on the yield of each gaseous compound, lower heating value of the gas, cold gasification efficiency and carbon yield to gas phase (experimental and theoretical results).

| | Yield of gaseous compounds (g/kg SS *daf*) | | | | | | $LHV_{gas}$ ($MJ/m^3_{STP}$) | Cold gasification efficiency (%) | Carbon yield to gas phase (%) |
|---|---|---|---|---|---|---|---|---|---|
| | $H_2$ | CO | $CO_2$ | $CH_4$ | $C_2H_x$ | $H_2S$ | | | |
| *Coefficients obtained for the experimental results* | | | | | | | | | |
| Average | 37.03 | 250.10 | 763.42 | 50.23 | 46.13 | 12.66 | 5.49 | 55.12 | 72.48 |
| T | 9.06 | 78.79 | * | 1.49 | −3.28 | 1.73 | 0.37 | 8.51 | 6.33 |
| GR | −1.37 | −17.51 | 101.57 | −3.13 | * | 1.56 | −0.31 | * | 3.33 |
| $H_2O/O_2$ | 5.68 | −32.67 | −92.53 | 4.80 | 3.35 | * | 0.40 | 3.47 | −6.07 |
| T-GR | * | −5.03 | 21.59 | * | * | * | * | * | * |
| T-($H_2O/O_2$) | * | −21.95 | * | * | * | * | −0.17 | * | * |
| GR-($H_2O/O_2$) | * | * | −14.93 | * | * | * | * | * | * |
| T-($H_2O/O_2$)-GR | * | 9.65 | 15.91 | * | * | 0.62 | * | * | * |
| Curvature | * | * | * | * | * | * | * | * | * |
| *Coefficients obtained for the theoretical results* | | | | | | | | | |
| Average | 99.53 | 883.23 | 595.21 | 0.60 | – | 25.54 | 6.56 | 98.47 | 100 |
| T | −1.19 | 24.54 | −36.44 | −0.76 | – | * | * | * | * |
| GR | −3.09 | −86.09 | 136.58 | −0.46 | – | * | −0.35 | −5.64 | * |
| $H_2O/O_2$ | 14.85 | 36.77 | −58.69 | 0.32 | – | * | 0.34 | 9.94 | * |
| T-GR | * | 4.96 | −8.85 | 0.38 | – | * | * | * | * |
| T-($H_2O/O_2$) | * | −4.34 | 7.57 | −0.27 | – | * | * | * | * |
| GR-($H_2O/O_2$) | 2.34 | 15.66 | −24.30 | * | – | * | 0.12 | 2.00 | * |
| T-($H_2O/O_2$)-GR | * | * | * | * | – | * | * | * | * |
| $(H_2O/O_2)^2$ | −4.44 | −11.12 | 16.84 | * | – | * | * | −2.39 | * |
| $T^2$ | * | * | * | 0.42 | – | * | * | * | * |
| $GR^2$ | * | * | * | * | – | * | * | * | * |

* Non-significant term.

(Table 5). Higher temperatures favor the production of CO through reactions such as steam and dry reforming (8, 9), the Boudouard reaction (3) or the water–gas primary reaction (4). However, negligible variations or even the opposite trend in CO production are found in the literature [10,11], which reveals the importance of the nature of the biomass and the operating conditions in the evolution of CO production. Both the GR and the $H_2O/O_2$ ratio affect the experimental yield of CO in a negative way. When the GR is increased, the higher amount of oxygen fed to the gasifier promotes the oxidation of CO to $CO_2$ and, in addition, the higher presence of steam favors CO consumption through the WGS reaction. Moreover, the negative effect of the $H_2O/O_2$ ratio might indicate that the consumption of CO in the WGS reaction outweighs its combustion process. Both negative effects are significantly intensified at higher temperatures. In contrast to the experimental results, the GR is the most influential factor for the theoretical production of CO (Table 5) and the $H_2O/O_2$ ratio shows a positive effect. The three interactions between the factors are significant terms in the theoretical production of CO: (i) the negative effect of the GR is slightly reduced when working at high temperatures, maybe due to the endothermic nature of the Boudouard reaction (in which CO is produced); (ii) the positive effect of the temperature is slightly reduced when working at high $H_2O/O_2$ ratios, since increasing the steam presence shifts the WGS equilibrium towards CO consumption; (iii) the negative effect of the GR is intensified when the highest $H_2O/O_2$ ratio is used as gasification medium.

Regarding the production of $CO_2$, the GR is the most influential factor for both the experimental and the theoretical yields (Table 5). When the GR is increased more oxygen and steam are fed to the gasifier, thus the increased production of $CO_2$ can be attributed to a higher extent of combustion reactions, as well as to other reactions promoted by the presence of steam, such as the WGS reaction (6) or the secondary water–gas reaction (5), in which $CO_2$ is produced. The positive effect of the GR on the experimental yield of $CO_2$ is intensified at higher temperatures and lower $H_2O/O_2$ ratios. Although to a lesser extent, the increase in the $H_2O/O_2$ ratio negatively affects the production of $CO_2$. This trend suggests that combustion reactions are the main source of $CO_2$. In contrast to the theoretical results, the experimental yield of $CO_2$ is not significantly influenced by the temperature. Theoretical results show that $CO_2$ and CO yields are influenced by the same significant factors and interactions, but all of them show opposite effects since CO production is normally linked with $CO_2$ consumption, and vice versa (3, 6, 9).

Regarding the experimental production of light hydrocarbons ($CH_4$ and $C_2H_x$), the $H_2O/O_2$ ratio is the most influential factor for it (Table 5). Increasing the $H_2O/O_2$ ratio in the gasification medium enhances the production of both $CH_4$ and $C_2H_x$, thus suggesting that the steam reforming of light hydrocarbons occurs more slowly than its combustion process. The formation of $CH_4$ via the methanation reaction (7) may also be promoted by increasing the $H_2O/O_2$ ratio due to an increased presence of $H_2$ in the gasification medium. Although to a lesser extent, $CH_4$ production is negatively affected by the increase in the GR, as its combustion and steam reforming reactions are promoted by increasing the ER and the S/B ratio, respectively. This expected effect is not observed for the $C_2H_x$ experimental yield probably because of its large experimental variability. Unlike the results shown by other authors [12,27], the experimental yield of $CH_4$ is found to increase slightly with the temperature, maybe as a result of the thermal cracking of heavier hydrocarbons, while the experimental yield of $C_2H_x$ follows the opposite trend with temperature. In relation to the theoretical results, the presence of $C_2H_x$ in the equilibrium gas is practically negligible. $CH_4$ is produced at equilibrium conditions, but its theoretical yield is much lower than its experimental yield. Temperature is the most influential factor for the theoretical yield of $CH_4$ (Table 5). It has a negative effect due to the enhancement of the endothermic reactions in which $CH_4$ is consumed, such as steam and dry reforming (8, 9), and the restriction of the methanation reaction (7) due to its exothermic nature. The negative effect of the temperature on the theoretical yield of $CH_4$ is intensified by increasing the $H_2O/O_2$ ratio and/or decreasing the GR. The temperature also seems to be the factor responsible for the curvature shown by the theoretical yield of $CH_4$.

Lastly, according to the ANOVA results, the experimental production of $H_2S$ is favored by increasing both the temperature and

the GR, although the effect of the latter is slightly smaller than that of the temperature (Table 5). In contrast to the experimental results, non-significant influences of the studied factors on the theoretical production of $H_2S$ have been found within the studied intervals. $H_2S$ is the only sulfured-compound considered in the equilibrium gas, thus a constant yield of $H_2S$ has been obtained for all the simulated conditions (25.54 g/kg SS *daf*).

### 3.4. Lower heating value of the product gas

The lower heating value of the gas ($LHV_{gas}$) is calculated as $\sum(x_i \cdot LHV_i)$, where $x_i$ and $LHV_i$ are the volumetric fraction and the lower heating value ($MJ/m^3_{STP}$) of each gaseous component, respectively. The LHV of the product gas obtained from the sewage sludge gasification ranged between 4.12 and 6.20 $MJ/m^3_{STP}$, thus this gas can be considered as a low heating value gas. Similar values of $LHV_{gas}$ are usually reported in the literature for air gasification or air–steam gasification of other kinds of biomass [5].

As a result of the ANOVA analysis, Table 5 presents the coded coefficients that explain the influence of the factors on the theoretical and experimental gas heating values. As can be seen, the theoretical gas heating values are higher than those obtained experimentally under the same operating conditions. The lower production of $CO_2$ obtained at equilibrium conditions compared to its experimental production leads to a lower dilution effect of the gas from the energy point of view, which outweighs the lower production of light hydrocarbons (gas components with the highest heating value) at equilibrium conditions.

The composition of the gasification medium is the most influential factor for the experimental $LHV_{gas}$. When the $H_2O/O_2$ ratio is increased, the hydrocarbon content increases and the $CO_2$ content decreases, so both effects contribute to improve the $LHV_{gas}$. The influence of temperature on the experimental $LHV_{gas}$ is almost as important as that of the composition of the gasification medium. Although the experimental production of $CO_2$ (in terms of g/kg SS *daf*) is not affected by the temperature, this result is not the same when considering the concentration data, since a clear reduction in the $CO_2$ fraction with temperature is observed (Table 3). The effect of this reduced fraction of $CO_2$ on the gas calorific value is more significant than that of the reduced fraction of light hydrocarbons, so a global positive effect of temperature on the $LHV_{gas}$ has been found in this study. In contrast to this, results in the literature usually show a negative effect of the temperature on the $LHV_{gas}$ [12], thus showing that the evolution of the gas composition depends on the raw material and the operating conditions. Although its effect is slightly smaller, the GR negatively affects the experimental $LHV_{gas}$, since both the production of $CO_2$ and the consumption of light hydrocarbons are favored at higher GR.

The theoretical results show that the GR and the $H_2O/O_2$ ratio have almost the same relative influence on the $LHV_{gas}$, whereas the gasification temperature does not affect it significantly (Table 5).

### 3.5. Cold gasification efficiency

The cold gasification efficiency is defined as the ratio between the energy contained in the gas product ($m^3_{STP}$ gas $\cdot LHV_{gas}$) and the energy contained in the mass of sewage sludge fed ($kg_{SS} \cdot LHV_{SS}$). Cold gasification efficiency assumes a temperature of 25 °C of the product gases, so the sensible heat of the gas is not taken into account.

The experimental values of cold gasification efficiency varied between 39% and 66% and, according to the ANOVA results (Table 5), the temperature and the $H_2O/O_2$ ratio are the only factors that affect it significantly. Temperature is the most influential factor and its variation from 770 to 850 °C improves the cold gasification efficiency by 17%. This enhancement is based on the increase of both $LHV_{gas}$ and gas production with temperature. Although to a lesser extent, the $H_2O/O_2$ ratio also affects the experimental gasification efficiency in a positive way, since the $LHV_{gas}$ increases with the $H_2O/O_2$ ratio and the production of gas is not affected by it.

The theoretical cold gasification efficiencies are much higher than the experimental data. Unlike the experimental results, the $H_2O/O_2$ ratio is the most influential factor for the theoretical cold gasification efficiency, as well as being the factor responsible for the curvature exhibited by the results. As occurred with the theoretical $LHV_{gas}$, increasing the GR negatively affects the theoretical cold gasification efficiency, whereas the gasification temperature does not affect it significantly.

### 3.6. Carbon yield to gas phase

The carbon yield to gas phase is defined as the ratio between the mass of carbon contained in the product gas and the mass of carbon contained in the sewage sludge fed. The conversion of solid carbon during the sewage sludge gasification reached 76–98 wt.%. However, not all the solid carbon leads to the formation of gaseous compounds, as tar is also produced. Therefore, the experimental results of carbon yield to gas phase are slightly lower than the aforementioned range (62–90 wt.%), whereas a carbon yield to gas phase of 100% is expected at equilibrium conditions.

According to the ANOVA results (Table 5), carbon yield to gas phase shows a linear response with the factors within the studied intervals. Temperature is the most influential factor, and its variation from 770 to 850 °C improves the carbon yield to gas phase by 13 wt.%. The rise in temperature not only favors the heterogeneous reactions between the carbon contained in the sewage sludge and the gas compounds (3–5), but also enhances the tar cracking and reforming reactions, so a greater amount of carbon leaves the gasifier as part of the product gas. The effect of the gasification medium is slightly lower than that of the temperature. Carbon yield to gas phase is increased at higher fractions of oxygen and lower fractions of steam, which suggests that carbon oxidation reactions (1, 2) take place faster than the heterogeneous water–gas reactions (4, 5). To a lesser extent, carbon yield to gas phase is also favored by the GR, since a greater amount of gasifying agent is available to react with the carbon contained in the sewage sludge.

### 3.7. Tar composition

The tar composition was analyzed by gas chromatography (MS/FID GC). Fig. 5 shows a representative chromatogram of the components detected in most of the tar samples. Some researchers have divided tar components into several groups based on their molecular weight [28]. A similar classification of tar compounds has been considered in this work in order to analyze the effect of the operating conditions on the fractions of the following families of compounds: heterocyclic aromatics containing N (including n-methyl-pyridine, benzonitrile, n-methyl-benzonitrile, quinoline, n-methyl-quinoline, indole, n-phenyl-pyridine, n-naphthalenecarbonitrile, benzoquinoline and 5H-indeno[1,2-b]pyridine); heterocyclic aromatics containing O (phenol and benzofuran); compounds containing S (2-benzothiophene and propanenitrile, 3,3′-thiobis-); light aromatics with 1 ring (styrene) and light PAH compounds with 2 or 3 rings (indene, naphthalene, n-methylnaphthalene, biphenyl, biphenylene, fluorene, anthracene and phenantrene).

The areas of the main peaks shown by the GC-FID have been used to compare the composition of the different samples. Therefore, the results presented in this work do not represent actual compositions of the tar samples, but they are useful for analyzing

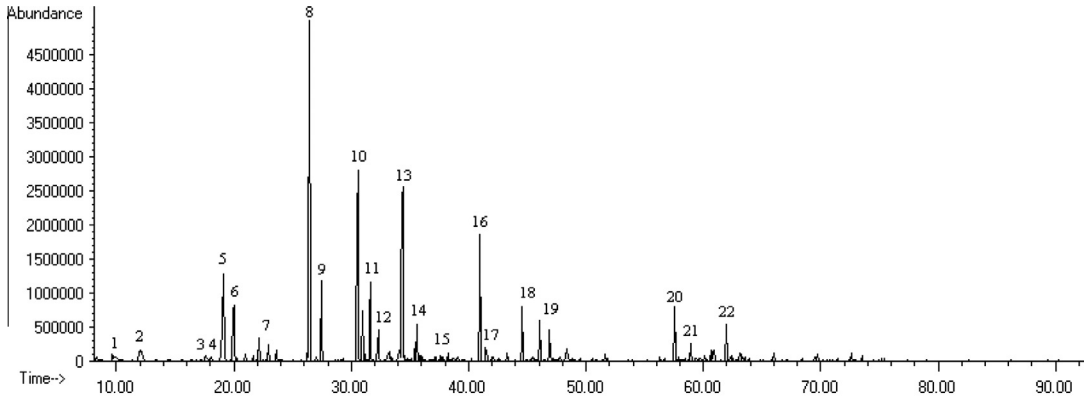


| | | |
|---|---|---|
| 1. Pyridine, n-methyl- (9.6) | 9. 2-Benzothiophene (27.5) | 17. n-Naphthalenecarbonitrile (44.5) |
| 2. Styrene (11.9) | 10. Quinoline (30.6) | 18. Fluorene (46.9) |
| 3. Phenol (17.5) | 11. Naphthalene, n-methyl- (31.0) | 19. Propanenitrile, 3,3'-thiobis- (48.4) |
| 4. Benzofuran (17.6) | 12. Quinoline, n-methyl- (33.1) | 20. Anthracene / Phenantrene (57.6) |
| 5. Benzonitrile (19.2) | 13. Indole (34.3) | 21. Benzoquinoline (58.9) |
| 6. Indene (20.0) | 14. Biphenyl (35.6) | 22. 5H-Indeno[1,2-b]pyridine (61.9) |
| 7. Benzonitrile, n-methyl- (22.1) | 15. Biphenylene (40.9) | |
| 8. Naphthalene (26.4) | 16. Pyridine, n-phenyl- (41.4) | |

**Fig. 5.** Total ion chromatogram (TIC) of a tar sample obtained at 850 °C, GR = 0.8 and $H_2O/O_2$ molar ratio = 3.

**Table 6**
Tar composition (percentage of area in the GC-FID signal of each family of tar compounds).

| Experiment | 1,1,1 | −1,1,1 | 1,−1,1 | −1,−1,1 | 1,1,−1 | −1,1,−1 | 1,−1,−1 | −1,−1,−1 | 0,0,0[a] |
|---|---|---|---|---|---|---|---|---|---|
| N-aromatics | 74.6 | 68.2 | 57.1 | 68.7 | 46.5 | 44.0 | 44.7 | 60.5 | 50.0 ± 14.4 |
| O-aromatics | 3.0 | 7.7 | 0.34 | 7.7 | 0.6 | 2.1 | 1.0 | 6.0 | 2.6 ± 0.8 |
| S-compounds | 3.6 | 2.9 | 4.4 | 5.1 | 7.9 | 2.5 | 5.7 | 1.0 | 4.9 ± 0.1 |
| Light aromatics (1 ring) | 9.7 | 12.2 | 4.4 | 13.4 | 5.1 | 9.9 | 3.6 | 9.8 | 6.5 ± 1.8 |
| Light PAH compounds (2–3 rings) | 9.1 | 9.1 | 33.8 | 5.14 | 39.9 | 41.5 | 45.0 | 22.7 | 36.0 ± 8.8 |

[a] Mean value ± standard deviation.

how the factors influence the fraction of each family of compounds. The percentages of the GC-FID-areas obtained for each sample are shown in Table 6. According to the ANOVA results, the temperature and the $H_2O/O_2$ ratio are the only factors affecting tar composition. Light aromatics and O-aromatics are the most sensitive families to temperature. Their fractions are found to decrease with temperature. Similar results have been reported by other researchers [29], showing that phenolic compounds, paraffines, olefins and alkylated aromatics are easily cracked at high temperatures. The S-compounds fraction has been found to increase with temperature, probably as a result of the aforementioned decrease in the fractions of other compounds.

On the other hand, N-aromatics and light PAH fractions are the most sensitive families to the $H_2O/O_2$ ratio. The increase in this ratio leads to a decrease in the fraction of light PAHs, thus the presence of steam seems to prevent the polymerization reactions. According to Corella et al. [30], tars generated in gasification with steam are easier to eliminate than tars generated in gasification with air. Tar molecular weight depends on the presence of H free radicals, which is related to the steam added during gasification [31]. A simultaneous increase in the fraction of N-aromatics was found, but this may only be a consequence of the aforementioned decrease in the light PAH fraction.

## 4. Conclusions

Temperature was found to be the most influential factor for most of the response variables analyzed during sewage sludge gasification. Higher temperatures are favorable for reducing the tar content and improving the gas yield, the gasification efficiency and the carbon yield to gas phase. On the other hand, the gas heating value and the $H_2/CO$ molar ratio in the product gas are clearly favored by increasing the steam presence and reducing the oxygen presence in the gasification medium. The significant differences between the theoretical and the experimental yields of gases, as well as the differences in the effects of the factors, show how important it is to distinguish between kinetic and thermodynamic control in a gasification process.

## Acknowledgements

The financial support received from the Spanish Ministry of Science and Technology (Research Project CTQ2010-20137) and from the Spanish Ministry of Education (pre-doctoral grant awarded to N. Gil-Lalaguna, AP2009-3446) is gratefully appreciated.

## References

[1] D. Fytili, A. Zabaniotou, Utilization of sewage sludge in EU application of old and new methods – a review, Renew. Sustain. Energy Rev. 12 (2008) 116–140.
[2] EC. European Commission Council Directive 91/271/EEC of May 21, 1991, on the treatment of urban waste water.
[3] W. Rulkens, Sewage sludge as a biomass resource for the production of energy: overview and assessment of the various options, Energy Fuel 22 (2008) 9–15.
[4] J. Werther, T. Ogada, Sewage sludge combustion, Prog. Energy Combust. Sci. 25 (1999) 55–116.
[5] P. McKendry, Energy production from biomass (part 3): gasification technologies, Bioresour. Technol. 83 (2002b) 55–63.

[6] L. Devi, K.J. Ptasinski, F.J.J.G. Janssen, A review of the primary measures for tar elimination in biomass gasification processes, Biomass Bioenergy 24 (2003) 125–140.
[7] J. Gil, J. Corella, M.P. Aznar, M.A. Caballero, Biomass gasification in atmospheric and bubbling fluidized bed: effect of the type of gasifying agent on the product distribution, Biomass Bioenergy 17 (1999) 389–403.
[8] G. Schuster, G. Löffler, K. Weigl, H. Hofbauer, Biomass steam gasification – an extensive parametric modeling study, Bioresour. Technol. 77 (2001) 71–79.
[9] M. Campoy, A. Gómez-Barea, F.B. Vidal, P. Ollero, Air–steam gasification of biomass in a fluidised bed: process optimisation by enriched air, Fuel Process. Technol. 90 (2009) 677–685.
[10] J. Gil, M.P. Aznar, M.A. Caballero, E. Francés, J. Corella, Biomass gasification in fluidized bed at pilot scale with steam–oxygen mixtures. Product distribution for very different operating conditions, Energy Fuel 11 (1997) 1109–1118.
[11] P.M. Lv, Z.H. Xiong, J. Chang, C.Z. Wu, Y. Chen, J.X. Zhu, An experimental study on biomass air–steam gasification in a fluidized bed, Bioresour. Technol. 95 (2004) 95–101.
[12] F. Pinto, C. Franco, R.N. André, C. Tavares, M. Dias, I. Gulyurtlu, I. Cabrita, Effect of experimental conditions on co-gasification of coal, biomass and plastics wastes with air/steam mixtures in a fluidized bed system, Fuel 82 (2003) 1967–1976.
[13] M. Dogru, A. Midilli, C.R. Howarth, Gasification of sewage sludge using a throated downdraft gasifier and uncertainty analysis, Fuel Process. Technol. 75 (2002) 55–82.
[14] B. Gross, C. Eder, P. Grziwa, J. Horst, K. Kimmerle, Energy recovery from sewage sludge by means of fluidised bed gasification, Waste Manage. 28 (2008) 1819–1826.
[15] J.J. Manyá, J.L. Sánchez, J. Ábrego, A. Gonzalo, J. Arauzo, Influence of gas residence time and air ratio on the air gasification of dried sewage sludge in a bubbling fluidised bed, Fuel 85 (2006) 2027–2033.
[16] A. Midilli, M. Dogru, C.R. Howarth, M.J. Ling, T. Ayhan, Combustible gas production from sewage sludge with a downdraft gasifier, Energy Convers. Manage. 42 (2001) 157–172.
[17] I. Petersen, J. Werther, Experimental investigation and modelling of gasification of sewage sludge in the circulating fluidized bed, Chem. Eng. Process. 44 (2005) 717–736.
[18] N. Nipattummakul, I. Ahmed, S. Kerdsuwan, A.K. Gupta, High temperature steam gasification of wastewater sludge, Appl. Energy 87 (2010) 3729–3734.
[19] N. Gil-Lalaguna, I. Fonts, G. Gea, M.B. Murillo, L. Lázaro, Reduction of water content in sewage sludge pyrolysis liquid by selective on-line condensation of the vapors, Energy Fuel 24 (2010) 6555–6564.
[20] G. García, E. Cascarosa, J. Ábrego, A. Gonzalo, J.L. Sánchez, Use of different residues for high temperature desulphurization of gasification gas, Chem. Eng. J. 174 (2011) 644–651.
[21] M. Aznar, A.E. González, J.J. Manyà, J.L. Sánchez, M.B. Murillo, Understanding the effect of the transition period during the air gasification of dried sewage sludge in a fluidized bed reactor, Int. J. Chem. React. Eng. 5 (2007) A18.
[22] P. McKendry, Energy production from biomass (part 1): overview of biomass, Bioresour. Technol. 83 (2002a) 37–46.
[23] M. Bläsing, M. Müller, Release of alkali metal, sulphur, and chlorine species from high temperature gasification of high- and low-rank coals, Fuel Process. Technol. 106 (2013) 289–294.
[24] P.A. Jensen, F.J. Frandsen, K. Dam-Johansen, B. Sander, Experimental investigation of the transformation and release to gas phase of potassium and chlorine during straw pyrolysis, Energy Fuel 14 (2000) 1280–1285.
[25] J. Corella, J.M. Toledo, G. Molina, Calculation of the conditions to get less than 2 g tar/Nm$^3$ in a fluidized bed biomass gasifier, Fuel Process. Technol. 87 (2006) 841–846.
[26] I. Wender, Reactions of synthesis gas, Fuel Process. Technol. 48 (1996) 189–297.
[27] Y.J. Kim, S.H. Lee, S.D. Kim, Coal gasification characteristics in a downer reactor, Fuel 80 (2001) 1915–1922.
[28] C. Li, K. Suzuki, Tar property, analysis, reforming mechanism and model for biomass gasification – an overview, Renew. Sustain. Energy Rev. 13 (2009) 594–604.
[29] A. Ponzio, S. Kalisz, W. Blasiak, Effect of operating conditions on tar and gas composition in high temperature air/steam gasification (HTAG) of plastic containing waste, Fuel Process. Technol. 87 (2006) 223–233.
[30] J. Corella, A. Orio, J.M. Toledo, Biomass gasification with air in a fluidized bed: exhaustive tar elimination with commercial steam reforming catalysts, Energy Fuel 13 (1999) 702–709.
[31] Y.H. Qin, J. Feng, W.Y. Li, Formation of tar and its characterization during air–steam gasification of sawdust in a fluidized bed reactor, Fuel 89 (2010) 1344–1347.

Fuel 129 (2014) 147–155

Contents lists available at ScienceDirect

Fuel

journal homepage: www.elsevier.com/locate/fuel

# Air-steam gasification of char derived from sewage sludge pyrolysis. Comparison with the gasification of sewage sludge

N. Gil-Lalaguna *, J.L. Sánchez, M.B. Murillo, V. Ruiz, G. Gea

*Thermo-chemical Processes Group, Aragón Institute of Engineering Research (I3A), Universidad de Zaragoza, c/Mariano Esquillor s/n, 50018 Zaragoza, Spain*

## HIGHLIGHTS

- Increased content of fixed carbon in the solid after sewage sludge pyrolysis.
- Higher gas yield from dried and ash-free (*daf*) char than from sewage sludge (*daf*).
- Average tar yield decreased by 45% when gasifying char instead of sewage sludge.
- Average CO yield was 70% higher when gasifying char (*daf* basis for solids).
- Temperature was the most influential factor for most of the studied variables.

## ARTICLE INFO

*Article history:*
Received 16 January 2014
Received in revised form 24 March 2014
Accepted 25 March 2014
Available online 13 April 2014

*Keywords:*
Air-steam gasification
Sewage sludge
Char
Fast pyrolysis
Fluidized bed

## ABSTRACT

Air-steam gasification of char derived from fast pyrolysis of sewage sludge has been experimentally evaluated in a fluidized bed as a route towards a full recovery of energy from sewage sludge. The results have been compared with those obtained from the direct gasification of sewage sludge in order to evaluate how the previous pyrolysis stage affects the subsequent gasification process. The fixed carbon content in the solid increased after the pyrolysis stage so that heterogeneous reactions of carbon with steam or $CO_2$ assumed greater importance during char gasification than during sewage sludge gasification. Furthermore, char gasification led to an improvement in the gas yield -calculated on a dry and ash-free basis (*daf*)- due to the increased concentration of carbon in the organic fraction of the solid after the pyrolysis step, with an increase in the average CO yield of about 70% -in terms of g/kg solid *daf*-. The reduction in the fraction of carbon which forms tar is another advantage of char gasification over the direct gasification of sewage sludge, with an average decrease of about 45%. Regarding the influence of the operating conditions, the response variables were mainly controlled by the same factors in both processes.



## 1. Introduction

Sewage sludge is the waste generated during successive treatment stages of urban wastewaters. In recent years the production of sewage sludge in the EU has considerably increased due to the expansion in the amount and capacity of wastewater treatment plants [1,2]. For instance, the production of sewage sludge in Spain increased by 41% in the period 2000–2009 [3]. For this reason, the economical and environmentally-friendly treatment of sewage sludge has become an important issue. The traditional methods of treatment or disposal of sewage sludge include its use as fertilizer on croplands, incineration and landfilling [1,2,4]. However, as a result of the environmental and health problems caused by the application of these techniques, energy recovery from sewage sludge by thermo-chemical treatments such as pyrolysis or gasification technologies could be an interesting alternative [2].

A large number of lab-scale studies on sewage sludge pyrolysis for liquid production (fast pyrolysis) can be found in the literature [5–11]. The liquid yield and its physicochemical properties depend on the operational conditions (mainly on the temperature) and on the composition of the sewage sludge [6]. Char is the main by-product of sewage sludge fast pyrolysis. Common solid yields of around 35–55 wt.% are found in the literature [8–11], but it should be noted that the ash content in these solids is much higher than those of lignocellulosic origin. The use of this solid by-product as adsorbent material has been investigated by some authors. The results show that char obtained from sewage sludge pyrolysis is not a very porous material (its surface area ranges 50–150 $m^2/g$) because of its high inorganic content [12]. Despite this, some

* Corresponding author. Tel.: +34 976762224; fax: +34 976762043.
*E-mail address:* noemigil@unizar.es (N. Gil-Lalaguna).

http://dx.doi.org/10.1016/j.fuel.2014.03.059
0016-2361/

authors have reported a certain capacity of this kind of material to remove contaminants such as $H_2S$, $NO_x$, metals, dyes and phenols [12–16]. Physical activation of this kind of char was proposed as part of a three-stage thermo-chemical treatment of sewage sludge in a previous work in our group [17].

On the other hand, the remaining organic fraction in char gives it a moderate calorific value which could be further exploited through thermo-chemical processes. In fact, the gasification of char resulting from fast pyrolysis of different types of biomass is being investigated by some authors as a route towards an integral valorization of biomass [18–22]. Furthermore, as part of volatile matter is removed from biomass during pyrolysis, the gasification of char obtained from pyrolysis instead of the direct gasification of biomass should lead to a reduction in the formation of tar during the process, which is one of the main hurdles for the development of gasification technology.

The present work is focused on the gasification of char obtained from sewage sludge fast pyrolysis. An experimental study has been carried out in a lab-scale fluidized bed reactor in order to evaluate the feasibility of gasifying this kind of char. The influence of several operating conditions (temperature, composition of the gasification medium and gasifying agent to biomass ratio) on the gasification performance has been analyzed statistically in order to determine the relative influence of each factor. Moreover, results from char gasification have been compared with those obtained from the direct gasification of sewage sludge under the same operating conditions [23] in order to evaluate how the previous pyrolysis stage affects the subsequent gasification process.

## 2. Materials and methods

### 2.1. Char obtained from sewage sludge pyrolysis

Char obtained from the fast pyrolysis of anaerobically digested and thermally dried sewage sludge is the feedstock for the gasification experiments performed in this work. Table 1 presents the results of the proximate and ultimate analyses and heating value of the char, as well as the results obtained for the original sewage sludge. The fixed carbon content in this kind of char is considerably lower than in other types of biomass chars [18–22] as the composition of sewage sludge and lignocellulosic materials are quite different.

### 2.2. Experimental setup

Char was produced during sewage sludge fast pyrolysis in a lab-scale fluidized bed reactor operating at a temperature of 530 °C. The pyrolysis plant and the operating conditions are described in detail elsewhere [24].

**Table 1**
Proximate and ultimate analyses and lower heating value of both the char derived from sewage sludge pyrolysis and the sewage sludge itself (SS).

| | | Char | SS |
|---|---|---|---|
| *Proximate analysis (wt.%, wet basis)* | | | |
| Moisture | ISO-589-1981 | 1.70 | 6.48 |
| Ash | ISO-1171-1976 | 74.20 | 39.04 |
| Volatiles | ISO-5623-1974 | 15.02 | 50.09 |
| Fixed carbon | By difference | 9.08 | 4.39 |
| *Ultimate analysis (wt.%, wet basis. Carlo Erba 1108 elemental analyzer)* | | | |
| C | | 15.49 | 29.50 |
| H | | 0.97 | 4.67 |
| N | | 1.85 | 5.27 |
| S | | 0.35 | 1.31 |
| LHV (MJ/kg) | IKA C-2000 calorimeter | 5.0 | 11.8 |

Char gasification experiments have also been carried out in a lab-scale fluidized bed reactor operating at atmospheric pressure, with continuous feed of solid (around 2.1 g/min of char) and continuous removal of ash. Ash from previous gasification tests constituted the solid bed by itself from the beginning of the runs. The gasifying/fluidizing agent used in the process consisted of different mixtures of steam and enriched air (air + oxygen). Air flow was kept constant in all the experiments and different flows of pure oxygen were fed together with the air, thus enriching the air at different percentages.

The vapors and gases produced during the gasification process remained inside the reactor around 17–18 s and then passed through a cyclone and a hot filter (both at 450 °C) in which the solid particles swept by the gas were collected. Water and condensable organic compounds (tar) were collected in two ice-cooled condensers. The volume of particle- and tar-free gas was measured by a volumetric meter and its composition was analyzed on-line using a micro gas chromatograph (Agilent 3000-A). The experiments were carried out during 60 min. Fig. 1 shows a diagram of the laboratory installation. A more detailed description of the plant can be found elsewhere [23].

Ash content in the solid by-product was determined according to ISO-1171-1976 and its carbon content was analyzed using a Leco TruSpec Micro Elemental Analyzer. Water content in the condensed fraction was analyzed off-line by Karl Fischer titration in order to determine the amount of tar by difference. However, tar production was almost negligible and all the results from the Karl Fischer titration were about 100 wt.% of water, so non-significant differences in tar production were found by this way. Therefore, in order to evaluate the effect of the factors, tar production from char gasification was approximated to the amount of organic carbon present in the condensate (g $C_{condensate}$), measured by means of a total organic carbon analyzer (TOC-L CSH/CSN Shimadzu analyzer).

### 2.3. Experimental design and data analysis

A $2^k$ factorial experimental design was planned in order to determine the influence of some operating factors on the char gasification performance. This kind of experimental design allows the existence of interactions between the factors to be identified. In other words, it can be seen whether a factor influences a response variable in a different way depending on the value of another factor.

Three factors have been studied in this work: (i) gasification temperature, measured inside the bed (ranging between 770 and 850 °C); (ii) gasifying ratio (*GR*) between the mass flow of gasifying agent (oxygen plus steam) and the mass flow of dry and ash-free (*daf*) basis char (ranging between 0.8 and 1.1 g/g char *daf*) and (iii) composition of the gasification medium, represented by the $H_2O/O_2$ molar ratio (ranging between 1 and 3). The three studied factors, together with their respective ranges of study, were chosen based on our previous work on sewage sludge gasification [23] in order to compare the performance of both processes and evaluate how a previous pyrolysis stage affects the subsequent gasification process. The temperature and the ratio between the flow of oxygen or steam and the feed of biomass are among the most studied factors in the air-steam gasification of biomass [22,25].

As seen in Table 2, the experimental design consisted of 8 runs ($2^k$ runs, where $k$ is the number of factors, in this case 3). Furthermore, three replicates at the center point (CP) were added to the experimental design in order to evaluate the experimental variability as well as to determine if the response of each variable was linear or not within the studied range. Coded values of the factors were used to identify the term with the greatest influence on each response variable, that is, −1 for the lower limits ($T$ = 770 °C, $GR$ = 0.8

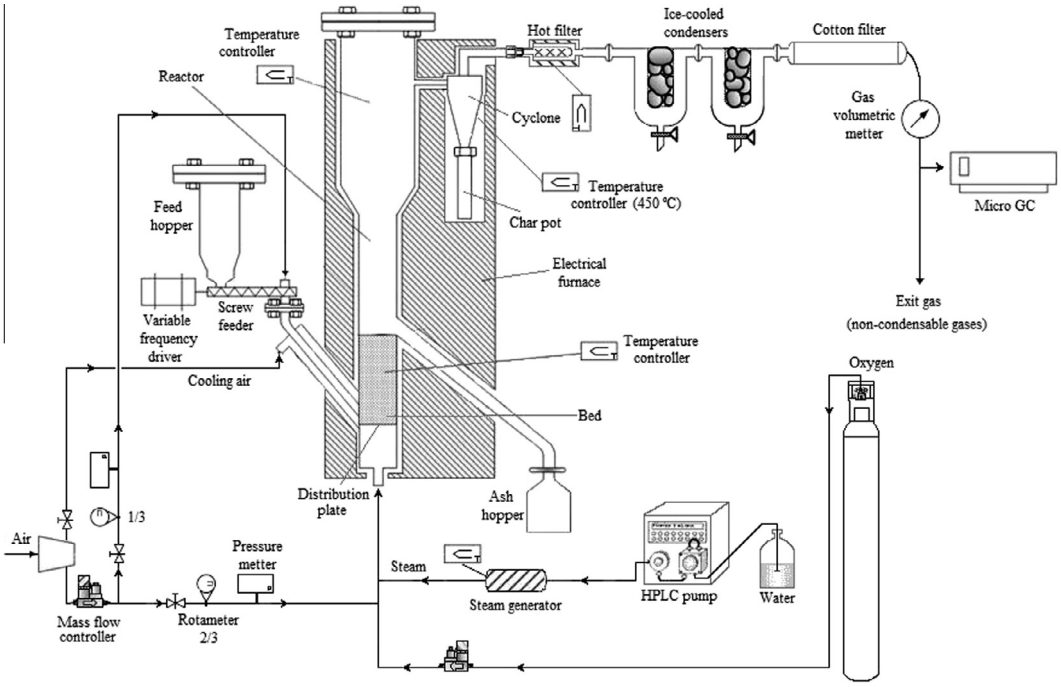


**Fig. 1.** Laboratory-scale gasification setup.

**Table 2**
Operating conditions in the char gasification experiments.

| Experiment number | 1 | 2 | 3 | 4 | 5 | 6 | 7 | 8 | CP (9, 10, 11) |
|---|---|---|---|---|---|---|---|---|---|
| Coded values (*T*, *GR*, $H_2O/O_2$) | 1,1,1 | −1,1,1 | 1,−1,1 | −1,−1,1 | 1,1,−1 | −1,1,−1 | 1,−1,−1 | −1,−1,−1 | 0,0,0 |
| Temperature (°C) | 850 | 770 | 850 | 770 | 850 | 770 | 850 | 770 | 810 |
| g gasifying agent/g char *daf* (*GR*) | 1.1 | 1.1 | 0.8 | 0.8 | 1.1 | 1.1 | 0.8 | 0.8 | 0.95 |
| $H_2O/O_2$ molar ratio in the gasifying agent | 3 | 3 | 3 | 3 | 1 | 1 | 1 | 1 | 2 |
| Equivalence ratio (*ER*) | 0.17 | 0.17 | 0.12 | 0.12 | 0.32 | 0.32 | 0.23 | 0.23 | 0.19 |
| Steam to char *daf* mass ratio (*S*/*B*) | 0.71 | 0.71 | 0.52 | 0.52 | 0.39 | 0.39 | 0.27 | 0.27 | 0.52 |

and $H_2O/O_2$ = 1) and +1 for the upper ones (*T* = 850 °C, *GR* = 1.1 and $H_2O/O_2$ = 3).

The response variables analyzed were the following: (i) distribution of products (solid, gas and tar); (ii) gas composition, determined on-line using a micro-gas chromatograph; (iii) production of each gaseous component, based on the amount of char *daf* fed; (iv) lower heating value of the product gas ($LHV_{gas}$); (v) cold gasification efficiency and (vi) carbon yield to gas phase.

The experimental results have been analyzed statistically by means of analysis of variance (ANOVA), using a confidence level of 95% for the F-distribution to identify the terms that significantly affect each response variable. Design-Expert® 7 software (from Stat-Ease, Inc.) was used for the analyses.

## 3. Results and discussion

Experimental results obtained from the char gasification tests are shown in Table 3. Furthermore, as a result of the ANOVA analyses, Table 4 presents the relative influence of each factor on the response variables. Average data represent the average of the whole set of results obtained, whereas the coefficients associated to the different factors (*T*, *GR* and $H_2O/O_2$) show the effect that the change of each factor has on the studied responses (in terms of coded values for the factors); the existence of significant interactions between the factors is also denoted by means of coefficients. In order to compare these results with those corresponding to the direct gasification of sewage sludge, Table 5 presents a summary of the ANOVA results obtained when sewage sludge was the feedstock for the gasification process [23]. This comparative study is based on a single type of sewage sludge and char. Therefore, although the expected trends for other kind of materials will be similar, extrapolation of the results should be done carefully.

### 3.1. Product distribution

#### 3.1.1. Solid yield and carbon fraction remaining as solid

The solid fraction was the most abundant by-product during char gasification because of the high ash content in the char. The solid yield varied between 73 and 82 wt.% (based on the amount of char fed), though this solid was mainly composed of ash (93–96 wt.%). Its carbon content ranged between 3.8 and 6.2 wt.% (Table 3). The fraction of carbon remaining as solid after char gasification can be calculated from the above data as follows:

$$\text{Carbon fraction as solid (wt.\%)} = gC_{\text{solid by-product}}/gC_{\text{char fed}} \cdot 100 \quad (1)$$

It should be noted that the amount of solid introduced in the reactor as initial bed (ash from previous gasification tests) was also part of the solid collected after the experiments and contained a small amount of carbon (between 3 and 5 wt.%). This amount of carbon is not included in g $C_{\text{solid by-product}}$.

The fraction of carbon remaining as solid after char gasification ranged between 15 and 43 wt.% (Table 3), whereas the maximum

**Table 3**
Experimental results from char gasification.

| | 1,1,1 | −1,1,1 | 1,−1,1 | −1,−1,1 | 1,1,−1 | −1,1,−1 | 1,−1,−1 | −1,−1,−1 | 0,0,0[a] |
|---|---|---|---|---|---|---|---|---|---|
| Solid yield (g solid/100 g char) | 75.7 | 78.5 | 75.0 | 78.5 | 73.1 | 77.1 | 75.2 | 81.3 | 77.5 ± 1.7 |
| Carbon content in the solid product (wt.%) | 3.9 | 6.2 | 4.5 | 6.1 | 3.9 | 4.5 | 3.9 | 5.8 | 5.6 ± 0.6 |
| Carbon fraction remaining as solid (wt.%) | 19.5 | 41.3 | 25.4 | 43.1 | 14.7 | 26.2 | 18.8 | 40.9 | 33.8 ± 2.6 |
| Gas yield ($m^3_{STP}$/kg char) | 0.36 | 0.27 | 0.31 | 0.24 | 0.35 | 0.28 | 0.32 | 0.24 | 0.29 ± 0.01 |
| Gas yield ($m^3_{STP}$/kg char *daf*) | 1.47 | 1.12 | 1.30 | 0.99 | 1.46 | 1.15 | 1.31 | 1.00 | 1.21 ± 0.01 |
| Carbon fraction forming tar (wt.%) | 1.3 | 0.7 | 2.9 | 3.3 | 1.0 | 5.7 | 3.2 | 5.8 | 2.8 ± 0.7 |
| *Gas composition (dry basis)* | | | | | | | | | |
| $H_2$ (vol.%) | 29.3 | 26.3 | 27.8 | 24.8 | 21.5 | 19.0 | 22.0 | 20.2 | 25.2 ± 0.6 |
| CO (vol.%) | 19.5 | 12.0 | 20.2 | 12.8 | 22.7 | 14.0 | 23.7 | 15.2 | 15.9 ± 0.2 |
| $CO_2$ (vol.%) | 18.9 | 24.2 | 16.2 | 20.8 | 22.6 | 29.5 | 18.5 | 24.1 | 21.9 ± 0.1 |
| $CH_4$ (vol.%) | 0.76 | 0.91 | 0.77 | 0.92 | 0.59 | 0.70 | 0.64 | 0.84 | 0.88 ± 0.01 |
| $C_2H_x$ (ppmv) | 150 | 190 | 160 | 220 | 180 | 220 | 150 | 200 | 180 ± 10 |
| $H_2S$ (vol.%) | 0.25 | 0.12 | 0.14 | 0.07 | 0.17 | 0.08 | 0.12 | 0.06 | 0.10 ± 0.01 |
| $N_2$ (vol.%) | 31.3 | 36.5 | 34.9 | 40.7 | 32.5 | 36.7 | 35.0 | 39.6 | 36.1 ± 0.6 |
| $H_2$/CO molar ratio | 1.50 | 2.20 | 1.38 | 1.93 | 0.95 | 1.36 | 0.93 | 1.33 | 1.58 ± 0.04 |
| CO/$CO_2$ molar ratio | 1.03 | 0.49 | 1.25 | 0.62 | 1.00 | 0.47 | 1.28 | 0.63 | 0.73 ± 0.01 |
| $LHV_{gas}$ ($MJ/m^3_{STP}$) | 5.96 | 4.71 | 5.87 | 4.65 | 5.44 | 4.09 | 5.63 | 4.43 | 5.07 ± 0.07 |
| Cold gasification efficiency (%) | 62.9 | 41.1 | 57.2 | 37.6 | 57.4 | 36.2 | 55.3 | 35.7 | 47.0 ± 0.6 |
| Carbon yield to gas phase (wt.%) | 71.0 | 55.5 | 62.1 | 47.9 | 82.9 | 67.1 | 72.2 | 55.7 | 61.5 ± 1.5 |

[a] Mean value ± standard deviation.

**Table 4**
Relative influence of the studied factors on the response variables for char gasification.

| | Average | *T* | *GR* | $H_2O/O_2$ | *T*–*GR* | *T*–$H_2O/O_2$ | *GR*-$H_2O/O_2$ | *T*–$H_2O/O_2$–*GR* | Curvature |
|---|---|---|---|---|---|---|---|---|---|
| Carbon fraction remaining as solid (wt.%) | 30.13 | −9.16 | −3.30 | 3.59 | [a] | [a] | [a] | [a] | [a] |
| Gas yield ($m^3_{STP}$/kg char *daf*) | 1.23 | 0.16 | 0.08 | [a] | [a] | [a] | [a] | [a] | [b] |
| Carbon fraction forming tar (wt. %) | 2.94 | −0.90 | −0.81 | −0.93 | | 0.95 | | [a] | [a] |
| $H_2$/CO molar ratio in the product gas | 1.48 | −0.26 | [a] | 0.31 | [a] | [a] | [a] | [a] | [a] |
| CO/$CO_2$ molar ratio in the product gas | 0.85 | 0.29 | −0.10 | [a] | −0.03 | [a] | 0.01 | [a] | [b] |
| *Yield of gaseous compounds (g/kg char daf)* | | | | | | | | | |
| $H_2$ | 40.93 | 6.03 | 1.86 | 5.43 | 0.33 | 0.90 | 1.18 | [a] | [b] |
| CO | 427.16 | 135.09 | [a] | −34.61 | [a] | −9.78 | [a] | [a] | [b] |
| $CO_2$ | 815.96 | −29.09 | 104.91 | −69.95 | [a] | [a] | −18.75 | [a] | [a] |
| $CH_4$ | 10.33 | [a] | [a] | 1.01 | [a] | [a] | 0.32 | [a] | [b] |
| $C_2H_4$ | 0.28 | −0.023 | [a] | [a] | [a] | [a] | [a] | [a] | [a] |
| $H_2S$ | 3.54 | 1.62 | 1.03 | [a] | [a] | [a] | [a] | [a] | [a] |
| $LHV_{gas}$ ($MJ/m^3_{STP}$) | 5.09 | 0.63 | [a] | 0.20 | [a] | [a] | 0.08 | [a] | [a] |
| Cold gasification efficiency (%) | 47.90 | 10.27 | 1.45 | 1.77 | 0.48 | [a] | 0.83 | [a] | [b] |
| Carbon yield to gas phase (wt.%) | 64.29 | 7.76 | 4.82 | −5.16 | [a] | [a] | [a] | [a] | [b] |

[a] Non-significant term.
[b] Significant curvature.

**Table 5**
Relative influence of the studied factors on the response variables for sewage sludge gasification.

| | Average | *T* | *GR* | $H_2O/O_2$ | *T*–*GR* | *T*–$H_2O/O_2$ | *GR*–$H_2O/O_2$ | *T*–$H_2O/O_2$–*GR* | Curvature |
|---|---|---|---|---|---|---|---|---|---|
| Carbon fraction remaining as solid (wt.%) | 9.01 | −5.76 | −1.74 | 3.29 | [a] | −1.50 | [a] | [a] | [a] |
| Gas yield ($m^3_{STP}$/kg SS *daf*) | 1.12 | 0.17 | 0.02 | [a] | 0.02 | −0.02 | [a] | 0.03 | [b] |
| Carbon fraction forming tar (wt.%) | 5.28 | −1.11 | [a] | [a] | −0.56 | [a] | [a] | [a] | [a] |
| $H_2$/CO molar ratio in the product gas | 2.21 | −0.14 | 0.08 | 0.62 | 0.02 | −0.06 | 0.11 | −0.05 | [b] |
| CO/$CO_2$ molar ratio in the product gas | 0.52 | 0.16 | −0.11 | [a] | −0.04 | −0.03 | [a] | [a] | [a] |
| *Yield of gaseous compounds (g/kg SS daf)* | | | | | | | | | |
| $H_2$ | 37.03 | 9.06 | −1.37 | 5.68 | [a] | [a] | [a] | [a] | [a] |
| CO | 250.10 | 78.79 | −17.51 | −32.67 | −5.03 | −21.95 | [a] | 9.65 | [a] |
| $CO_2$ | 763.42 | [a] | 101.57 | −92.53 | 21.59 | [a] | −14.93 | 15.91 | [a] |
| $CH_4$ | 50.23 | 1.49 | −3.13 | 4.80 | [a] | [a] | [a] | [a] | [a] |
| $C_2H_x$ | 46.13 | −3.28 | [a] | 3.35 | [a] | [a] | [a] | [a] | [a] |
| $H_2S$ | 12.66 | 1.73 | 1.56 | [a] | [a] | [a] | [a] | 0.62 | [a] |
| $LHV_{gas}$ ($MJ/m^3_{STP}$) | 5.49 | 0.37 | −0.31 | 0.40 | [a] | −0.17 | [a] | [a] | [a] |
| Cold gasification efficiency (%) | 55.12 | 8.51 | [a] | 3.47 | [a] | [a] | [a] | [a] | [a] |
| Carbon yield to gas phase (wt.%) | 72.48 | 6.33 | 3.33 | −6.07 | [a] | [a] | [a] | [a] | [a] |

[a] Non-significant term.
[b] Significant curvature.

value for sewage sludge gasification was about 24 wt.%. This difference may be explained by the different structure of the carbonaceous matter in the solids. Most of the carbon in sewage sludge is in the form of volatile matter (85 wt.% of the carbon content) which can be easily released during the gasification stage. However, the volatile matter in sewage sludge was considerably

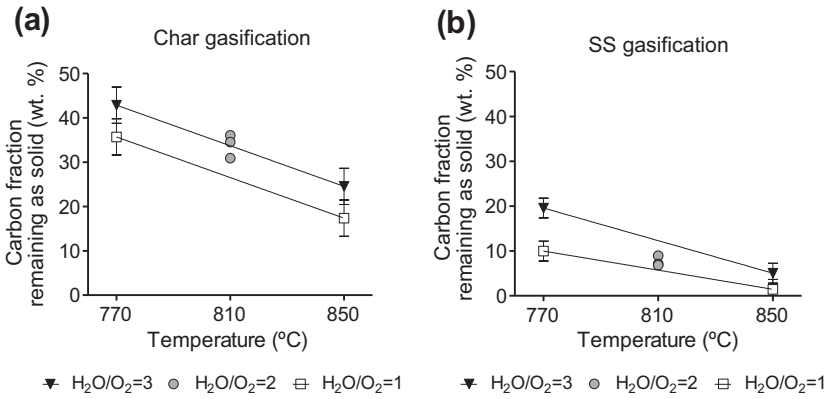


**Fig. 2.** Carbon fraction remaining as solid after (a) char gasification and (b) sewage sludge gasification (gasifying ratio = 0.95 g/g solid *daf*).

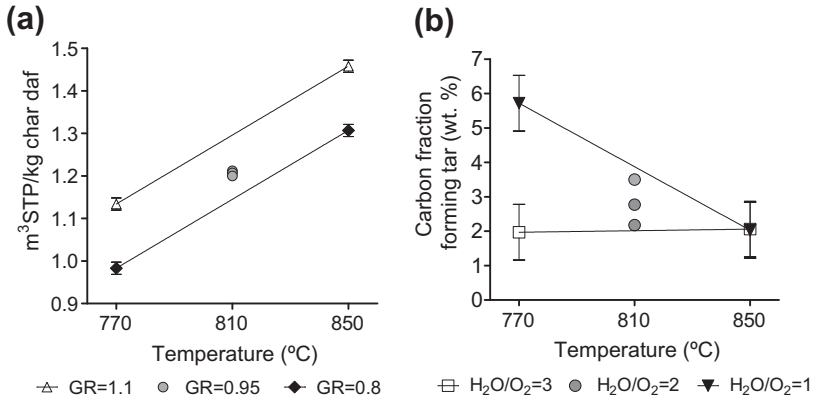


**Fig. 3.** (a) Gas yield during char gasification ($H_2O/O_2$ = 2). (b) Carbon fraction forming tar during char gasification (gasifying ratio = 0.95 g/g char *daf*).

reduced during the pyrolysis stage and about 59 wt.% of the carbon in char is in the form of fixed carbon, which is more difficult to gasify than the volatile matter.

According to the ANOVA results (Table 4), temperature is the most influential factor on the carbon fraction remaining as solid. Higher reaction temperatures favor carbon gasification [26], so that the carbon fraction remaining as solid was reduced by as much as half when the temperature increased from 770 to 850 °C (Fig. 2a). Carbon conversion is also enhanced by increasing the gasifying ratio (*GR*) and/or decreasing the $H_2O/O_2$ ratio, thus indicating that carbon reactivity with oxygen is greater than its reactivity with steam. The same trends were observed in the direct gasification of sewage sludge (Table 5), although the carbon fraction remaining as solid was even more sensitive to the variation of the factors in that case. Furthermore, the interaction between the temperature and the $H_2O/O_2$ ratio was denoted as a significant term, with negligible influence of the gasification medium composition at the higher temperature (Fig. 2b). The error bars shown in the figures of results (Figs. 2, 3 and 5) correspond to the least significant difference (LSD).

As mentioned above, carbon conversion was higher for sewage sludge gasification than for char gasification. However, results for char gasification can be recalculated considering both stages (pyrolysis + gasification) as a whole and taking the initial amount of carbon in sewage sludge as a reference for calculating the carbon conversion. In this way, the fraction of carbon remaining as solid after char gasification is reduced to 4–11 wt.%, thus improving the carbon conversion obtained in the direct gasification of sewage sludge.

*3.1.2. Gas production*

The gas yield from char gasification varied between 0.24 and 0.36 $m^3_{STP}$/kg char ($N_2$-free basis), or between 0.40 and 0.52 $m^3_{STP}$/kg char if $N_2$ is included (where STP means standard conditions of temperature and pressure at 0 °C and 1 atm). Comparing these data with those corresponding to sewage sludge gasification (0.49–0.72 $m^3_{STP}$ $N_2$-free/kg SS) [23], it can be observed that the production of gas has been reduced by half, mainly due to the higher ash content in char. The production of gas during the pyrolysis stage (around 0.06–0.07 $m^3_{STP}$ $N_2$-free/kg SS) is not high enough to offset the difference in the production of gas from the gasification of both materials.

On the other hand, if the gas yield ($N_2$-free basis) is calculated taking into account only the organic content in the raw material, it ranged between 0.99 and 1.47 $m^3_{STP}$/kg char *daf* for char gasification and 0.89–1.32 $m^3_{STP}$/kg SS *daf* for sewage sludge gasification [23], thus indicating that the previous pyrolysis stage leads to structural changes in the organic fraction of the solid that improve the production of gas. Gas yield results obtained from the gasification of sewage sludge-derived char (expressed on a $N_2$-free and *daf* basis) are in the same range as those obtained from char derived from lignocellulosic materials, such as bagasse char [18] or char derived from ramie residues [22].

As with the gasification of sewage sludge, temperature is the most influential factor on the production of gas during char gasification (Table 4). An average gas yield improvement of about 30% was obtained when the temperature varied from 770 to 850 °C in the gasification of char (Fig. 3a). Although to a lesser extent, the increase in the gasifying ratio (*GR*) is also favorable for the production of gas, whereas the nature of the gasification medium does not exert a significant influence on the gas yield obtained from the

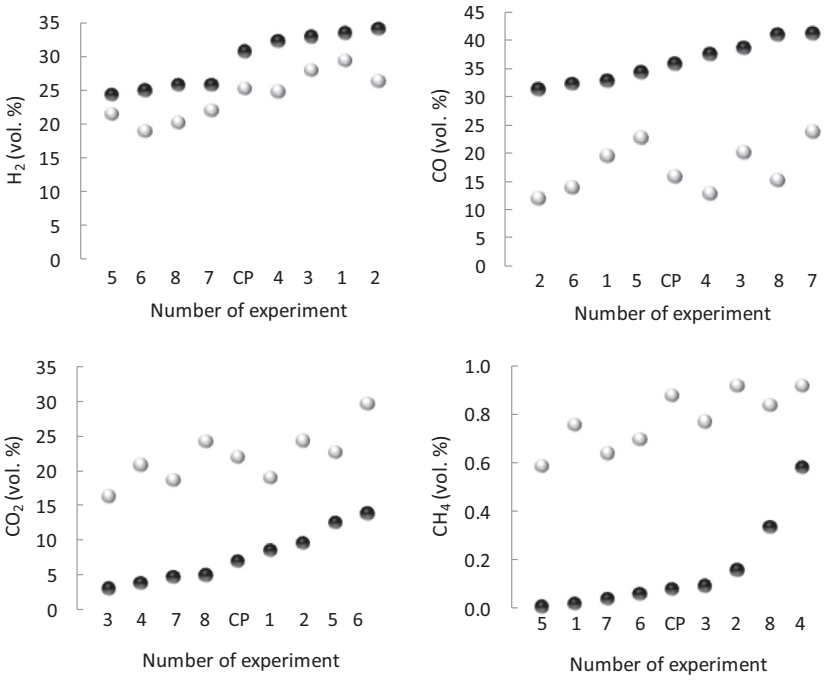


**Fig. 4.** Equilibrium (●) and experimental (◔) fractions of $H_2$, CO, $CO_2$ and $CH_4$ in the product gas from char gasification.

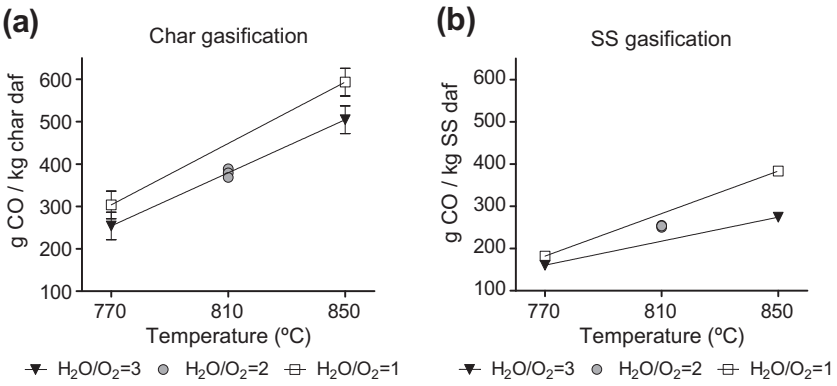


**Fig. 5.** CO production during (a) char gasification and (b) sewage sludge gasification (gasifying ratio = 0.95 g/g solid *daf*).

gasification of either char or sewage sludge. Therefore, as can be noted, the negative effect of $H_2O/O_2$ on the gasified carbon fraction (discussed in the previous section) does not result in a significant gas yield decrease. The production of $H_2$ may be the major reason for this disagreement because, as discussed below, $H_2$ formation is promoted by increasing the $H_2O/O_2$ ratio (mainly through the water–gas shift reaction), thus counteracting the decrease in the production of gaseous carbon-compounds.

Gas yield does not follow a linear trend with all factors, as curvature appears as a significant term in the ANOVA analysis. This means that at least one of the three factors has a quadratic effect on the evolution of gas production. Some studies reported in the literature show that excess steam is not favorable for the production of gas during steam gasification and suggest optimal values for steam to carbon ratios in order to maximize it [20,22,25,27]. The observed curvature may therefore be associated with the presence of steam in the gasification medium.

### 3.1.3. Tar production

The fraction of carbon which forms tar can be calculated as follows:

$$\text{Carbon fraction as tar (wt.\%)} = gC_{condensate}/gC_{char\ fed} \cdot 100 \quad (2)$$

The fraction of carbon which formed tar during char gasification ranged between 0.7 and 5.8 wt.% (Table 3) and according to the ANOVA results (Table 4), it can be reduced by increasing any of the studied factors, though the effect of temperature disappears at the higher $H_2O/O_2$ ratio and the effect of $H_2O/O_2$ is negligible at the higher temperature (Fig. 3b). On the other hand, the average carbon fraction forming tar during sewage sludge gasification was about 1.8 times higher than during char gasification and only the temperature and its interaction with the gasifying ratio were found to be significant terms (Table 5).

The production rates of tar and gas allow the tar content in the product gas to be calculated (g tar/$m^3_{STP}$). The tar content in the gas from char gasification (by approximation of the amount of tar to the amount of organic carbon present in the condensate) ranged between 2 and 13 g tar/$m^3_{STP}$ under most operating conditions, while the results for sewage sludge gasification ranged between 11 and 45 g tar/$m^3_{STP}$ [23].

### 3.2. Gas composition

The composition of the product gas from a gasification process is the result of many complex and competing reactions. The most representative reactions include the water–gas shift reaction (WGS), oxidation reactions, water–gas reactions (reactions of carbon with steam), steam and dry reforming of hydrocarbons, the methanation reaction and the Boudouard reaction [25–27].

As can be seen in Table 3, $H_2$ (19.0–29.3 vol.%), CO (12.0–23.7 vol.%), $CO_2$ (16.2–29.5 vol.%), $CH_4$ (0.59–0.92 vol.%) and $N_2$ (31.3–40.7 vol.%) were the main gases detected by the micro GC during char gasification. Other minor compounds were also detected in the gas, such as $C_2H_x$ hydrocarbons (mainly $C_2H_4$) or $H_2S$, which is released during the process due to the presence of sulfur-compounds in the char (Table 1). Statistical results from the analysis of gas composition have not been included in this work because it was preferred to analyze the yield of each gaseous compound in terms of g/kg char *daf* (Section 3.3). However, the variation of the product gas composition has been evaluated through two molar ratios: $H_2$/CO and CO/$CO_2$. On the one hand, the $H_2$/CO ratio in the product gas is increased by reducing the temperature and/or increasing $H_2O/O_2$ in the gasification medium, this last factor being the most influential (Table 4). These trends are consistent with those obtained for sewage sludge gasification (Table 5), although in that case the gasifying ratio also played a significant role in the evolution of the $H_2$/CO ratio (positive effect), as well as the interactions between the factors and the curvature term. Higher values of $H_2$/CO were obtained from sewage sludge gasification (1.46–3.25) than from char gasification (0.93–2.20). On the other hand, temperature is the most influential factor on the CO/$CO_2$ ratio in the exit gas in both processes. The CO/$CO_2$ ratio can be improved by increasing the temperature and/or reducing the amount of gasifying agent fed to the reactor (Table 4). The curvature has been denoted as a significant term in the evolution of CO/$CO_2$, as well as some interactions between the factors. The same trends were observed for sewage sludge gasification, although in that case the CO/$CO_2$ ratio followed a linear response. Higher values of CO/$CO_2$ have been obtained from char gasification (0.49–1.28) than from sewage sludge gasification (0.30–0.88).

The theoretical composition of the gas at equilibrium conditions was also calculated in order to determine if the gasification process was kinetically or thermodynamically controlled. The HSC Chemistry® 6.1 software was used to obtain the theoretical composition of the gas under the same operating conditions tested in the laboratory. The results from the theoretical simulations varied within the following ranges: $H_2$ (24.3–33.9 vol.%), CO (31.3–41.1 vol.%), $CO_2$ (3.0–13.8 vol.%), $N_2$ (24.8–28.7 vol.%), $CH_4$ (87–5801 ppmv), $H_2S$ (0.35–0.40 vol.%) and $NH_3$ (17–42 ppmv). The $H_2$/CO and CO/$CO_2$ ratios at equilibrium conditions ranged 0.62–1.09 and 2.33–12.90, respectively. Experimental fractions of $H_2$ and CO were lower than their corresponding theoretical values, whereas experimental fractions of $CO_2$ and $CH_4$ were above their corresponding theoretical values (Fig. 4). The significant differences observed in the concentration ranges reveal that chemical equilibrium was not reached during the experimental tests.

### 3.3. Production of each gaseous compound

The production or yield of each gas ($H_2$, CO, $CO_2$, $CH_4$, $C_2H_4$ and $H_2S$) is expressed in terms of mass of gas (g) produced per kilogram of char *daf* fed.

According to the ANOVA results (Table 4), gasification temperature is the most influential factor on the production of both $H_2$ and CO during char gasification. These gases are involved in many reactions both as reactants and as products, but the temperature rise seems to enhance their formation rather than their consuming reactions. Although to a lesser extent, the production of $H_2$ is also improved by increasing the $H_2O/O_2$ ratio, unlike the CO yield which decreases with $H_2O/O_2$. Both trends are consistent with the WGS reaction ($CO + H_2O \leftrightarrow H_2 + CO_2$), which is one of the most representative reactions for a steam gasification process. Besides increasing the steam presence, the oxygen presence is reduced with the increase in $H_2O/O_2$, so combustion reactions should be mitigated. The negative effect of $H_2O/O_2$ on the production of CO suggests that the WGS reaction outweighs the combustion reactions in the evolution of the CO yield. The same trend was found when directly gasifying the sewage sludge (Table 5). Similarly, Franco et al. [27] found that the WGS reaction appeared to be the most dominant reaction in the steam gasification of biomass for the temperature range of 730–830 °C. For higher temperatures (830–900 °C), steam reforming of carbon (water–gas reactions) prevailed, although these reactions also appeared to contribute significantly at temperatures lower than 830 °C for some types of biomass. In the present study, an upward trend in CO production with increasing temperature was found. As the process is controlled by kinetics, this behavior cannot be explained through the WGS reaction alone, but through the steam reforming of carbon ($C + H_2O \leftrightarrow CO + H_2$), the Boudouard reaction ($C + CO_2 \leftrightarrow 2\ CO$) and the steam and dry reforming of hydrocarbons in which CO is formed, which seem to gain importance at higher temperatures. As shown in Fig. 5, the positive effect of temperature on the CO yield slightly diminishes with increased steam presence due to the enhancement of the WGS reaction.

The gasifying ratio (*GR*) does not significantly affect the CO yield and only slightly influences the $H_2$ yield in a positive way during char gasification (Table 4). However, the amount of gasifying agent is the most influential factor on the production of $CO_2$: the higher the gasifying ratio, the greater the amount of $CO_2$ produced. Increasing the gasifying ratio means more oxygen and more steam fed to the gasifier, so combustion reactions, as well as $CO_2$ formation through other reactions promoted by the presence of steam (such as the WGS reaction), take place to a greater extent. The gasification temperature and the composition of the gasification medium also exert a significant influence on the production of $CO_2$. The temperature rise reduces the formation of $CO_2$ and, as discussed above, favors the production of CO, thus suggesting once again the importance of the Boudouard reaction at high temperatures. The negative effect of $H_2O/O_2$ on the $CO_2$ yield reveals that combustion is the main source of $CO_2$ in the process.

Regarding the production of light hydrocarbons ($CH_4$ and $C_2H_4$) during char gasification, the experimental variability was considerable (15% for $C_2H_4$), so only those factors with a very clear effect were denoted as significant terms in the ANOVA analysis. The composition of the gasification medium was found to be the only factor affecting the production of $CH_4$: increasing $H_2O/O_2$ involves greater $CH_4$ production, thus suggesting that its consumption through combustion reactions outweighs its steam reforming process. Methane formation via the methanation reaction ($C + 2H_2 \leftrightarrow CH_4$) may also be promoted by increasing the $H_2O/O_2$ ratio due to an increased presence of $H_2$ in the gasification medium. On the other hand, temperature is the only factor affecting the $C_2H_4$ yield (Table 4) and, as expected, a downward trend with increasing temperature was found, since higher temperatures provide more favorable conditions for thermal cracking and reforming reactions [25].

Lastly, according to the ANOVA results (Table 4), the production of $H_2S$ during the gasification of char is significantly affected by the gasification temperature and the gasifying ratio, although the effect of the latter factor is less significant. The production of $H_2S$ is promoted by the temperature rise (process controlled by kinetics). Moreover, the production of $H_2S$ is favored by the steam presence ($COS + H_2O \leftrightarrow H_2S + CO_2$) [28].

Some other conclusions can be drawn by comparing the results derived from char gasification and sewage sludge gasification:

- Average yield to $H_2$ was very similar for both feedstocks (41 g/kg char *daf* and 37 g/kg SS *daf*), whereas average yields to CO and $CO_2$ (g/kg *daf*) were 70% and 6% higher in the gasification of char, respectively. The production of light hydrocarbons and $H_2S$ was much lower when char was gasified due to the previous release of these compounds in the pyrolysis stage (about 4–5 mg $H_2S$/g sewage sludge released during the pyrolysis step). However, it should be noted that if gas yields are calculated with respect to the whole feedstock and not only considering the dry and ash-free material, the production of all the gas components is clearly greater during the gasification of sewage sludge.
- The production of each gas is mainly controlled by the same factor in both processes. The gasification temperature is the most influential factor on the production of $H_2$, CO and $H_2S$; the gasifying ratio is the most significant factor on the $CO_2$ yield, and the composition of the gasification medium exerts the greatest influence on the $CH_4$ yield. However, some differences related to minor influences of the factors have also been found. For example, temperature did not affect the production of $CO_2$ in the gasification of sewage sludge while it had a negative effect during char gasification. An increased reactivity of char with $CO_2$ (Boudouard reaction) may explain this difference. Furthermore, the gasifying ratio did not affect the production of CO in the gasification of char, but it had a negative effect during the gasification of sewage sludge. This implies that the consumption of CO through combustion or through the WGS reaction during char gasification is offset by an increased production of CO from heterogeneous reactions between carbon and steam (water–gas reactions) or carbon and $CO_2$ (Boudouard reaction), since the fixed carbon content is higher in char (9.08 wt.%) than in sewage sludge (4.39 wt.%).
- The production of each gas during the gasification of sewage sludge follows a linear response with the factors, whereas curvature appears as a significant term in the production of some gases during char gasification.

### 3.4. Lower heating value of the product gas

The lower heating value of the gas is calculated as follows:

$$LHV_{gas} = \Sigma(x_i \cdot LHV_i) \quad (3)$$

where $x_i$ and $LHV_i$ are the volumetric fraction and the lower heating value ($MJ/m^3_{STP}$) of each gaseous component, respectively. Therefore, the variation in the gas heating value only depends on the gas composition evolution.

The lower heating value of the product gas from char gasification ranged between 4.09 and 5.96 $MJ/m^3_{STP}$ (Table 3), thus defining this gas as a low heating value gas [26]. According to the ANOVA results (Table 4), the gas heating value follows a linear trend with the gasification temperature and the $H_2O/O_2$ ratio, the temperature being the most influential factor. As remarked above, the temperature rise leads to a decrease in the production of $CO_2$ and a simultaneous increase in the yields of $H_2$ and CO. These variations outweigh the decrease in the content of light hydrocarbons, thus resulting in a positive effect of the temperature on the gas heating value. The composition of the gasification medium also exerts a significant influence on the gas heating value: when $H_2O/O_2$ is increased, the content of $CH_4$ increases and the content of $CO_2$ decreases, so both effects contribute to improve the $LHV_{gas}$. The effect of the gasification medium is intensified when more gasifying agent is fed to the reactor (significant interaction between the gasifying ratio and $H_2O/O_2$).

Despite feeding different flows of nitrogen to the reactor, gas lower heating values from char gasification (4.09–5.96 $MJ/m^3_{STP}$) are in the same range as those obtained from sewage sludge gasification (4.12–6.20 $MJ/m^3_{STP}$) [23]. Temperature plays the most important role in the evolution of the gas heating value when char is gasified (Table 4), while the three studied factors exerted similar relative influences on the gas heating value from sewage sludge gasification (Table 5).

### 3.5. Cold gasification efficiency

The cold gasification efficiency, without taking into account the sensible heat of the gases, is defined as follows:

$$\text{Gasification efficiency}\ (\%) = (Gas_{volume} \cdot LHV_{gas})/(Char_{mass} \cdot LHV_{char}) \cdot 100 \quad (4)$$

where $Gas_{volume}$ is the total production of gas ($m^3_{STP}$, including the amount of $N_2$), $Char_{mass}$ is the amount of char fed during each experiment (kg), and $LHV_{gas}$ and $LHV_{char}$ are the lower heating values of the product gas and of the char expressed on $MJ/m^3_{STP}$ and MJ/kg, respectively.

The cold efficiency for char gasification ranged between 36% and 63% (Table 3). These values are quite similar to those obtained for the gasification of sewage sludge (39–66%) [23]. According to the ANOVA results (Table 4), the response of char gasification efficiency does not follow a linear trend with all the factors since the curvature was denoted as a significant term. Temperature is clearly the most influential factor on the gasification efficiency, and its variation from 770 to 850 °C improved the char gasification efficiency by about 20%. As remarked above, both the gas heating value and the gas yield were enhanced at high temperatures. The other factors ($H_2O/O_2$ and gasifying ratio) also have a positive effect on the char gasification efficiency, but play a less important role in its variation. Moreover, some interactions between the factors appear as significant terms in the evolution of the char gasification efficiency: the positive effects of temperature and $H_2O/O_2$ are intensified by increasing the gasifying ratio.

Temperature and $H_2O/O_2$ also have a positive effect on the sewage sludge gasification efficiency (Table 5), the temperature being the most influential factor. However, the gasifying ratio did not exert a significant influence in this case because its positive effect on the production of gas was counteracted by its negative effect on the gas heating value. The response of the sewage sludge gasification efficiency was linear with its two significant factors.

### 3.6. Carbon yield to gas phase

The carbon yield to gas phase is defined as follows:

$$\text{Carbon yield to gas phase}\ (\%) = gC_{product\ gas}/gC_{char\ fed} \cdot 100 \quad (5)$$

Although the conversion of solid carbon during char gasification reached 57–85 wt.%, the carbon yield to gas phase was slightly lower (between 48 and 83 wt.%), since not all the converted carbon produced gaseous compounds. However, both variables are linked since a decreased carbon fraction remaining as solid led to an increased production of carbon-containing gases. This link is shown by the ANOVA results, as the same factors that affected the carbon fraction remaining as solid also affect the carbon fraction which forms gas, but in opposite directions. The same trends were observed when gasifying sewage sludge (Table 5), though the difference between carbon conversion (76–98 wt.%) and carbon yield to gas phase (62–90 wt.%) was more significant because of the greater formation of tar.

Although carbon yield to gas phase achieved in sewage sludge gasification was higher than that for char gasification, gas

production calculated on a *daf* basis was better for char gasification. This may be explained by the increased concentration of carbon in the dried and ash-free fraction of the solid after the pyrolysis step (0.64 g C/g char *daf* vs. 0.54 g C/g SS *daf*).

## 4. Conclusions

Gasification of char obtained from fast pyrolysis of sewage sludge has been experimentally studied in this work. The results have been compared with those obtained from the direct gasification of sewage sludge in order to evaluate how the previous pyrolysis stage affects the subsequent gasification process. Most of the carbon in the sewage sludge was in the form of volatile matter (85 wt.%), while almost 60 wt.% of the carbon in char was in the form of fixed carbon, thus causing differences in the gasification performances of both materials. The carbon fraction remaining as solid after char gasification was higher than that for sewage sludge gasification. Despite this, gas production (expressed on a dry and ash-free basis, *daf*) was improved when gasifying char due to the increased concentration of carbon in the dried and ash-free fraction of the solid after the pyrolysis step (0.64 g C/g char *daf* vs. 0.54 g C/g SS *daf*).

The comparison of theoretical and experimental results showed that equilibrium conditions were not reached during the gasification experiments of either char or sewage sludge, so both processes were controlled by kinetics. The average yield to $H_2$ (expressed as g/kg solid *daf*) was very similar for both feedstocks, whereas average yields to CO and $CO_2$ (g/kg solid *daf*) were 70% and 6% higher in the gasification of char, respectively. On the other hand, the production of light hydrocarbons and tar was significantly reduced during char gasification due to the reduction in the volatile matter of the solid after the pyrolysis step. The gasification efficiency and the gas heating value varied in similar ranges in both processes.

All the studied variables were mainly controlled by the same operating factor (temperature, composition of the gasification medium or gasifying agent to biomass ratio) in both char gasification and sewage sludge gasification. Temperature was the most influential factor on the carbon conversion, gasification efficiency, gas yield, production of $H_2$, CO and $H_2S$ and $CO/CO_2$ ratio in the product gas from both processes, affecting all of them positively. The gasifying ratio was the most significant factor on the production of $CO_2$ (positive effect), whereas the composition of the gasification medium exerted the greatest influence on the $CH_4$ yield and $H_2/CO$ ratio in the product gas (enhanced by the presence of steam). Temperature also played the most important role in the evolution of the gas heating value when char was gasified, while the three studied factors exerted similar relative influences on the gas heating value from sewage sludge gasification.

In summary, results show how the increased content of fixed carbon in the solid after the pyrolysis step leads to a greater importance of heterogeneous reactions at high temperatures, such as the steam reforming of carbon or the Boudouard reaction.

## Acknowledgements

The authors gratefully acknowledge the financial support provided by the Spanish Ministry of Science and Technology (research project CTQ2010-20137) and the Spanish Ministry of Education (pre-doctoral grant awarded to N. Gil-Lalaguna, AP2009-3446).

## References

[1] Fytili D, Zabaniotou A. Utilization of sewage sludge in EU application of old and new methods – a review. Renew Sust Energy Rev 2008;12:116–40.
[2] Rulkens W. Sewage sludge as a biomass resource for the production of energy: overview and assessment of the various options. Energy Fuel 2008;22:9–15.
[3] Statistical Office of the European Communities (Eurostat). Water statistics: total sewage sludge production from urban wastewater (2009). Retrieved from epp.eurostat.ec.europa.eu.
[4] Werther J, Ogada T. Sewage sludge combustion. Prog Energy Combust Sci 1999;25:55–116.
[5] Fonts I, Gea G, Azuara M, Ábrego J, Arauzo J. Sewage sludge pyrolysis for liquid production: a review. Renew Sustain Energy Rev 2012;16:2781–805.
[6] Fonts I, Azuara M, Gea G, Murillo MB. Study of the pyrolysis liquids obtained from different sewage sludge. J Anal Appl Pyrol 2009;85:184–91.
[7] Kim Y, Parker W. A technical and economic evaluation of the pyrolysis of sewage sludge for the production of bio-oil. Bioresoure Technol 2008;99:1409–16.
[8] Shen L, Zhang DK. An experimental study of oil recovery from sewage sludge by low-temperature pyrolysis in a fluidised-bed. Fuel 2003;82:465–72.
[9] Fonts I, Juan A, Gea G, Murillo MB, Sánchez JL. Sewage sludge pyrolysis in fluidized bed. 1: influence of operational conditions on the product distribution. Ind Eng Chem Res 2008;47:5376–85.
[10] Inguanzo M, Domínguez A, Menéndez JA, Blanco CG, Pis JJ. On the pyrolysis of sewage sludge: the influence of pyrolysis conditions on solid, liquid and gas fractions. J Anal Appl Pyrol 2002;63:209–22.
[11] Pokorna E, Postelmans N, Jenicek P, Schreurs S, Carleer R, Yperman J. Study of bio-oils and solids from flash pyrolysis of sewage sludges. Fuel 2009;88:1344–50.
[12] Smith KM, Fowler GD, Pullket S, Graham NJD. Sewage sludge-based adsorbents: a review of their production, properties and use in water treatment applications. Water Res 2009;43:2569–94.
[13] Lu GQ, Lau DD. Characterisation of sewage sludge-derived adsorbents for $H_2S$ removal. 2. Surface and pore structural evolution in chemical activation. Gas Sep Purif 1996;10:103–11.
[14] Jindarom C, Meeyoo V, Kitiyanan B, Rirksomboon T, Rangsunvigit P. Surface characterization and dye adsorptive capacities of char obtained from pyrolysis/gasification of sewage sludge. Chem Eng J 2007;133:239–46.
[15] Pietrzak R, Bandosz TJ. Reactive adsorption of $NO_2$ at dry conditions on sewage sludge-derived materials. Environ Sci Technol 2007;41:7516–22.
[16] García G, Cascarosa E, Ábrego J, Gonzalo A, Sánchez JL. Use of different residues for high temperature desulphurisation of gasification gas. Chem Eng J 2011;174:644–51.
[17] Ábrego J, Sánchez JL, Arauzo J, Fonts I, Gil-Lalaguna N, Atienza-Martínez M. Technical and energetic assessment of a three-stage thermochemical treatment for sewage sludge. Energy Fuel 2013;27:1026–34.
[18] Chaudhari ST, Dalai AK, Bakhshi NN. Production of hydrogen and/or syngas ($H_2$+CO) via steam gasification of biomass-derived chars. Energy Fuel 2003;17:1062–7.
[19] Haykiri-Acma H, Yaman S, Kucukbayrak S. Gasification of biomass chars in steam-nitrogen mixture. Energy Convers Manage 2006;47:1004–13.
[20] Yan F, Luo S, Hu Z, Xiao B, Cheng G. Hydrogen-rich gas production by steam gasification of char from biomass fast pyrolysis in a fixed bed reactor: influence of temperature and steam on hydrogen yield and syngas composition. Bioresoure Technol 2010;101:5633–7.
[21] Mohd Salleh MA, Kisiki NH, Yusuf HM, Ghani WAK. Gasification of biochar from empty fruit bunch in a fluidized bed reactor. Energies 2010;3:1344–52.
[22] He P, Luo S, Cheng G, Xiao B, Cai L, Wang J. Gasification of biomass char with air-steam in a cyclone furnace. Renew Energy 2012;37:398–402.
[23] Gil-Lalaguna N, Sánchez JL, Murillo MB, Rodríguez E, Gea G. Air-steam gasification of sewage sludge in a fluidized bed. Influence of some operating conditions. Chem. Eng. J. 2014. In press; doi: 10.1016/j.cej.2014.03.055.
[24] Gil-Lalaguna N, Fonts I, Gea G, Murillo MB, Lázaro L. Reduction of water content in sewage sludge pyrolysis liquid by selective on-line condensation of the vapors. Energy Fuels 2010;24:6555–64.
[25] Lv PM, Xiong ZH, Chang J, Wu CZ, Chen Y, Zhu JX. An experimental study on biomass air-steam gasification in a fluidized bed. Bioresoure Technol 2004;95:95–101.
[26] McKendry P. Energy production from biomass (part 3): gasification technologies. Bioresoure Technol 2002;83:55–63.
[27] Franco C, Pinto F, Gulyurtlu I, Cabrita I. The study of reactions influencing the biomass steam gasification process. Fuel 2003;82:835–42.
[28] Hepola J, Simell P, Kurkela E, Stahlberg P. Sulphur poisoning of nickel catalyst in catalytic hot gas cleaning conditions of biomass gasification. In: Proceedings of the 6th International Symposium. Catalyst deactivation 1994. p. 499–506.

Energy 76 (2014) 652–662

Contents lists available at ScienceDirect

Energy

journal homepage: www.elsevier.com/locate/energy

# Energetic assessment of air-steam gasification of sewage sludge and of the integration of sewage sludge pyrolysis and air-steam gasification of char

N. Gil-Lalaguna*, J.L. Sánchez, M.B. Murillo, M. Atienza-Martínez, G. Gea

*Thermo-chemical Processes Group, Aragón Institute of Engineering Research (I3A), Universidad de Zaragoza, c/Mariano Esquillor s/n., 50018 Zaragoza, Spain*

ARTICLE INFO

*Article history:*
Received 23 March 2014
Received in revised form
25 July 2014
Accepted 17 August 2014
Available online 15 September 2014

*Keywords:*
Sewage sludge
Char
Air-steam gasification
Pyrolysis
Thermal drying

ABSTRACT

Thermo-chemical treatment of sewage sludge is an interesting option for recovering energy and/or valuable products from this waste. This work presents an energetic assessment of pyrolysis and gasification of sewage sludge, also considering the prior sewage sludge thermal drying and the gasification of the char derived from the pyrolysis stage. Experimental data obtained from pyrolysis of sewage sludge, gasification of sewage sludge and gasification of char (all of these performed in a lab-scale fluidized reactor) were used for the energetic calculations. The results show that the energy contained in the product gases from pyrolysis and char gasification is not enough to cover the high energy consumption for thermal drying of sewage sludge. Additional energy could be obtained from the calorific value of the pyrolysis liquid, but some of its properties must be improved facing towards its use as fuel. On the other hand, the energy contained in the product gas of sewage sludge gasification is enough to cover the energy demand for both the sewage sludge thermal drying and the gasification process itself. Furthermore, a theoretical study included in this work shows that the gasification efficiency is improved when the chemical equilibrium is reached in the process.



## 1. Introduction

Sewage sludge is the major by-product of wastewater treatment. The sludge stemming from the wastewater treatment usually appears in the form of a dilute suspension, which typically contains from 0.25 to 12 wt.% of dry solid matter, depending on the operation and process used [1]. The generated amount of this waste has increased in recent years due to the stricter European legislation concerning urban wastewater treatment [2], which has led to an increase in the number of wastewater treatment plants. As a consequence, sewage sludge management has become an important issue [3].

Sewage sludge has been traditionally used as fertilizer due to its organic matter and nutrient content. However, the presence of various contaminant elements in the sludge such as heavy metals, organic contaminants and pathogenic bacteria limits this practice, which is regulated by European environmental legislation [4]. Landfill disposal and incineration are other common ways of sewage sludge management, but they are not exempt from drawbacks [1]. Thus, different energy valorization technologies are currently being developed. Among them, thermo-chemical processes such us gasification and pyrolysis represent interesting options since they could provide energy and/or valuable products from sewage sludge [5,6]. A large number of lab-scale studies on sewage sludge pyrolysis for liquid production (fast pyrolysis) can be found in the literature [7–9]. In addition to the liquid fraction, a gas stream and a carbonaceous solid by-product (char) are also obtained in the process. The remaining organic fraction in char gives it a moderate calorific value which could be further exploited through thermo-chemical processes such as combustion or gasification, thus providing a route towards the complete energetic valorization of the biomass [10–12]. In addition to the pyrolysis works, sewage sludge gasification has been studied since mid-1990s [13]. Since then, numerous studies have been performed at laboratory plants [14–17] and the process has even been tried at demonstration and pilot scale [18–20]. Most of these studies used air as a gasification medium, but steam gasification or supercritical water gasification of sewage sludge have also been performed in order to enhance $H_2$ production and improve gas quality [21,22]. However, the addition of steam into a gasification process accelerates a series of

* Corresponding author. Tel.: +34 976762224.
*E-mail address:* noemigil@unizar.es (N. Gil-Lalaguna).

http://dx.doi.org/10.1016/j.energy.2014.08.061
0360-5442/

**Abbreviations**

| | |
|---|---|
| $\Delta H$ | total enthalpy |
| $\Delta H_{cond}$ | enthalpy of condensation |
| $\Delta H_f^{\circ}$ | standard enthalpy of formation at 298 K |
| $\Delta H_{vap}$ | enthalpy of vaporization |
| AP | aqueous phase |
| Cp | specific heat capacity |
| *daf* | dry and ash-free |
| DSC | differential scanning calorimetry |
| ER | equivalence ratio |
| HHV | higher heating value |
| HOP | heavy organic phase |
| LHV | lower heating value |
| LOP | light organic phase |
| $m$ | mass flow rate |
| $\eta_{gas}$ | dry gas yield |
| $Q$ | heat of reaction |
| $Q_{drying}$ | heat for thermal drying |
| S/B | steam to dry and ash-free biomass mass ratio |
| S/C | steam to carbon molar ratio |
| SS | sewage sludge |
| STP | standard conditions of temperature and pressure (273 K, 1 atm) |
| $T_b$ | boiling point |
| $T_{ref}$ | reference temperature (298 K) |

endothermic reactions that result in a temperature decrease, making it more difficult to achieve an autothermal process [23,24]. Therefore, not only technical and operational aspects should be taken into account for the development of a gasification process. Energetic assessment is also a key issue, especially when steam is used as a gasifying agent.

The energy needed for steam gasification can be achieved by the addition of oxygen (or air, since the use of pure oxygen raises the process cost) together with the steam into the gasification medium, which causes the combustion of part of the organic matter and the release of energy. The gasification temperature is controlled by the oxygen supply itself in an autothermal gasifier, while the transfer of external heat is required in an allothermal gasifier to maintain a suitable temperature during the process.

Several works reported in the literature describe energetic aspects related to the gasification and pyrolysis of different types of biomass [25–29], but not specifically refer to the use of sewage sludge. Given this background, this paper presents an energetic assessment of two potential treatments for sewage sludge: (i) two-stage process: sewage thermal drying + air-steam gasification of sewage sludge and (ii) three-stage process: sewage sludge thermal drying + pyrolysis of sewage sludge + air-steam gasification of the char derived from the pyrolysis stage. Fig. 1 shows a schematic overview of both treatments. The objective of this study is to determine the overall energy demand of these thermo-chemical processes by considering the individual energy requirement of each stage (drying, pyrolysis and gasification). Experimental data resulting from the pyrolysis and gasification stages were used in the energy balances. Furthermore, theoretical simulations of the gasification stages (performed with the HSC Chemistry® 6.1 software and based on the Gibbs energy minimization method) were also conducted in order to evaluate the thermodynamic restrictions of the process under different scenarios.

## 2. Materials and methods

### 2.1. Sewage sludge and char

Table 1 provides a brief characterization of both the anaerobically digested and thermally dried SS (sewage sludge), on which the study is based, and the char obtained experimentally from the pyrolysis of this sewage sludge. Proximate analyses were performed according to standard methods (ISO-589-1981 for moisture, ISO-1171-1976 for ash and ISO-5623-1974 for volatiles), while the ultimate analyses were determined with a Carlo Erba EA1108 elemental analyzer. The heating values of the solids were measured with an IKA C-2000 calorimeter and their specific heat capacities were determined by differential scanning calorimetry using a Netzsch DSC 200 Maia Thermobalance (inert atmosphere: 40 mL $min^{-1}$ of nitrogen).

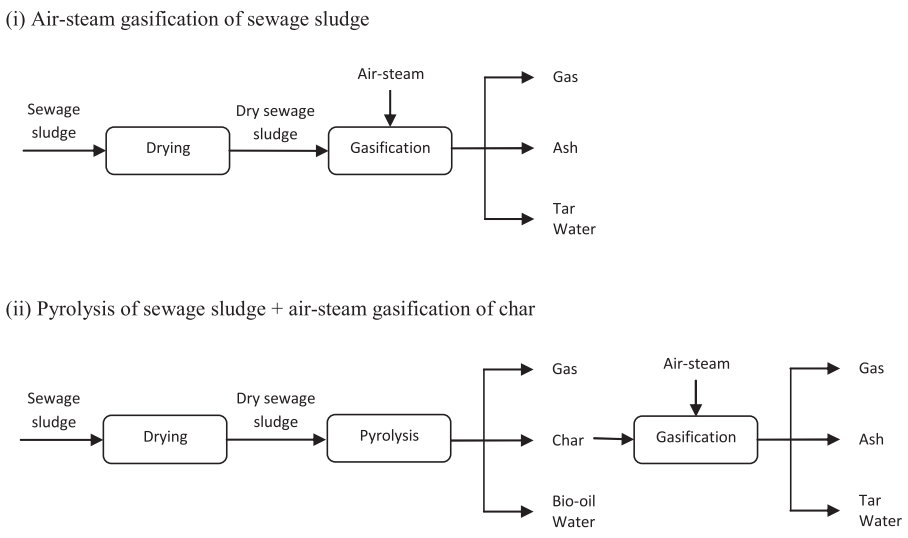


**Fig. 1.** Schematic overview of the thermo-chemical processes proposed for sewage sludge treatment.

**Table 1**
Characterization of sewage sludge (SS) and char derived from sewage sludge pyrolysis.

| | SS | Char |
|---|---|---|
| *Proximate analysis (wt.%, wet basis)* | | |
| Moisture | 6.48 | 1.70 |
| Ash | 39.04 | 74.20 |
| Volatiles | 50.09 | 15.02 |
| Fixed carbon | 4.39 | 9.08 |
| *Ultimate analysis (wt.%, wet basis)* | | |
| C | 29.50 | 15.49 |
| H | 4.67 | 0.97 |
| N | 5.27 | 1.85 |
| S | 1.31 | 0.35 |
| *LHV (MJ kg$^{-1}$)* | *11.8* | *5.0* |
| *$Cp_{25\,^{\circ}C}$ (kJ kg$^{-1}$ K$^{-1}$)* | *1.15* | *0.82* |

### 2.2. Experimental setup

Sewage sludge fast pyrolysis was performed in a lab-scale fluidized bed reactor operating at 530 °C and using 4.5 $m^3_{STP}$ min$^{-1}$ of nitrogen (where STP means standard conditions of temperature and pressure at 0 °C and 1 atm) as fluidizing agent. Two ice-cooled condensers and an electrostatic precipitator were used to condensate the produced vapors. The composition of the dry product gas was analyzed on-line with a micro gas chromatograph (Agilent 3000). The pyrolysis plant and the operating conditions are described in detail elsewhere [30]. The liquid collected after condensation of the vapors was separated into three phases: LOP (light organic phase), HOP (heavy organic phase) and AP (aqueous phase). The water content of each phase was analyzed by Karl Fischer titration (Mettler Toledo titrator), while its composition was qualitatively determined by gas chromatography-mass spectrometry (Hewlett Packard HP 5890 A). Ultimate analysis and higher heating value of each liquid phase were determined with a Carlo Erba EA1108 elemental analyzer and an IKA C-2000 analytical calorimeter, respectively. As commented above, the solid by-product resulting from the pyrolysis process was also characterized and used as a raw material for the gasification process.

The experiments of sewage sludge gasification and char gasification were carried out in a lab-scale fluidized bed reactor operating at atmospheric pressure and in a temperature range of 770–850 °C. More details about the gasification setup can be found elsewhere [31,32]. Different mixtures of steam and air (or enriched air in order to ensure similar fluidization rates) were used as gasifying/fluidizing agent. The equivalence ratio (ER: ratio of the actual fuel-to-oxygen ratio to the stoichiometric fuel-to-oxygen ratio) varied from 12% to 32%, while the steam to *daf* (dry and ash-free) biomass ratio (S/B) varied from 0.27 to 0.71 kg kg$^{-1}$ in both cases. The produced mixture of steam and tar was condensed in two ice-cooled condensers. The water content and the qualitative composition of the mixture were determined using the aforementioned equipment. The composition of the dry product gas was analyzed on-line with a micro gas chromatograph (Agilent 3000). The ultimate analyses of the solid by-products resulting from the gasification processes were determined with a Leco TruSpec Micro elemental analyzer and their higher heating values were calculated according to Dulong formula [HHV (kJ kg$^{-1}$) = 339% C + 1430·(%H − %O/8) + 105% S].

## 3. Results and discussion

This section includes the results of the energetic assessment of the individual stages forming part of the processes shown in Fig. 1: sewage sludge drying, sewage sludge gasification, sewage sludge pyrolysis and char gasification. An overview of the total energy requirement for the two-stage and three-stage processes is also included at the end of the section.

### 3.1. Sewage sludge thermal drying

Prior to the thermo-chemical treatment of sewage sludge by means of pyrolysis or gasification, sewage sludge thermal drying allows reduction of water content in the waste. Thermal drying of sewage sludge is not a waste elimination method, but waste volume is considerably reduced and handling of the dry biosolids is easier.

The heat needed for the sewage sludge thermal drying can be calculated as follows:

$$Q_{drying} = \left(m_{dried\ SS} \cdot Cp_{SS} + m_{H_2O,SS} \cdot Cp_{H_2O(l)}\right) \cdot \Delta T + m_{H_2O,evap} \cdot \Delta H_{vap,H_2O} \quad (1)$$

where:

- $Q_{drying}$ is the heat needed for sewage sludge thermal drying (MJ $kg^{-1}_{dried\ SS}$).
- $m_{dried\ SS}$ is the mass of dried sewage sludge (1 kg as calculation basis).
- $m_{H2O,SS}$ is the mass of water present in the sewage sludge before the thermal drying (kg $kg^{-1}_{dried\ SS}$).
- $\Delta T$ is the difference between the temperature of the sewage sludge at the beginning and at the end of the drying process (from 25 to 100 °C).
- $Cp_{SS}$ is the specific heat capacity of the dried sewage sludge. This value was experimentally obtained at 25 °C ($1.15 \cdot 10^{-3}$ MJ kg$^{-1}$ K$^{-1}$) and has been considered constant with temperature for the calculations. The variation of $Cp_{SS}$ with temperature could not be obtained in the upper range of temperature because of the sewage sludge thermal decomposition observed during the measurement.
- $Cp_{H2O(l)}$ is the commonly used specific heat capacity for the liquid water ($4.18 \cdot 10^{-3}$ MJ kg$^{-1}$ K$^{-1}$). $Cp_{H2O(l)}$ is virtually constant in the temperature range considered (25–100 °C), only varying from $4.18 \cdot 10^{-3}$ to $4.22 \cdot 10^{-3}$ MJ kg$^{-1}$ K$^{-1}$ [33].
- $m_{H2O,evap}$ is the mass of water evaporated during the sewage sludge thermal drying (kg $kg^{-1}_{dried\ SS}$).
- $\Delta H_{vap,H2O}$ is the enthalpy of vaporization of water at the exit temperature (2.26 MJ $kg^{-1}_{H_2O}$ at 100 °C) [33].

Fig. 2 shows the evolution of the heat needed for sewage sludge drying as a function of the initial and final moisture contents, based on calculations performed with equation (1). For instance, almost 8 MJ $kg^{-1}_{dried\ SS}$ are required for reducing the water content from 77 wt.% to 6.5 wt.%, which represent the actual data of the wastewater treatment plant in which the used sewage sludge was

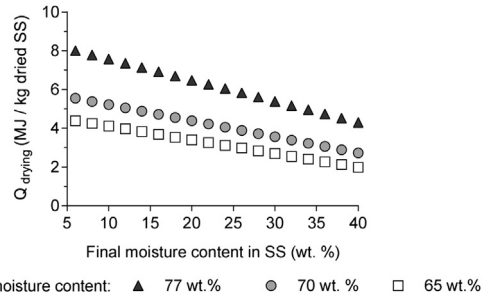


**Fig. 2.** Heat demand for the thermal drying of sewage sludge (SS) as a function of the initial and final moisture contents.

generated. However, the heat required for the sewage sludge thermal drying could be reduced by half if the initial moisture content is reduced from 77 to 65 wt.% by improving the efficiency of the prior mechanical dewatering of sewage sludge.

### 3.2. Sewage sludge pyrolysis

If negligible heat losses are considered in the reactor (adiabatic reactor), the heat of reaction for the pyrolysis of sewage sludge can be calculated from the enthalpies of the streams entering and exiting the reactor as follows:

$$Q = \Delta H_{out} - \Delta H_{in} \quad (2)$$

where $Q$ is the heat of pyrolysis reaction (MJ $kg_{SS}^{-1}$), and $\Delta H_{in}$ and $\Delta H_{out}$ represent the enthalpies of the streams entering and exiting the reactor, respectively. According to equation (2), $Q < 0$ corresponds to an exothermic process, while $Q > 0$ refers to an endothermic process.

The total enthalpy of each stream ($\Delta H$) can be calculated from equation (3):

$$\Delta H = \sum_i m_i \cdot (\Delta H^o_{f,i} + \int_{T_{ref}}^{T} Cp_i(T) \cdot dT) \quad (3)$$

where:

- $m_i$ is the mass flow rate of each compound (kg $kg_{SS}^{-1}$). 1 kg of sewage sludge was used as calculation basis. The mass flow rates of the products have been calculated according to the experimental yields obtained in the pyrolysis process (Table 2).
- $T_{ref}$ is the reference temperature (298 K) and $T$ (K) is the temperature of each stream. The inlet streams (sewage sludge and nitrogen) were at ambient temperature (298 K), the same as the outlet stream of gases and vapors, which was cooled down to ambient temperature in order to take advantage of their sensible and latent heats. The solid product (char) was supposed to leave the reactor at the pyrolysis temperature (803 K).
- $\Delta H^\circ_{f,i}$ is the standard enthalpy of formation (MJ $kg^{-1}$) of each compound at the reference temperature (298 K). The $\Delta H^\circ_f$ data of the gases involved in the process can be easily found in the literature [33]. The $\Delta H^\circ_f$ data corresponding to the solid materials (sewage sludge and char) and to the liquid phases (LOP, HOP and AP) have been calculated from their ultimate analyses and heating values according to the following equation:

$$\Delta H^o_{f,i} = \left( \sum_j m_j \cdot \Delta H^o_{f,j} \right) + HHV \quad (4)$$

where '$j$' represents each product derived from the complete combustion of the material ($CO_2$, $H_2O$, $SO_2$ and NO), $m_j$ is the mass of each combustion gas produced per kilogram of material, $\Delta H^\circ_{f,j}$ is the standard enthalpy of formation of each combustion gas and HHV is the higher heating value of the solid material or liquid phase (Table 2). This way of calculating the $\Delta H^\circ_f$ does not include the $\Delta H^\circ_f$ corresponding to the ash content in the solids, but this is not necessary for the calculations because ash is considered an inert material during the process and the contribution of its $\Delta H^\circ_f$ is simplified in the energy balance. The $\Delta H^\circ_f$ of the sewage sludge was found to be −3.28 MJ $kg_{SS}^{-1}$ (note that this value does not include the $\Delta H^\circ_f$ of the ash content). The $\Delta H^\circ_f$ of the pyrolysis products are summarized in Table 2.
- $Cp_i$ ($T$) is the specific heat capacity of each compound as a function of the temperature (MJ $kg^{-1}$ $K^{-1}$). Only the temperature of the solid product (803 K) is different from the reference value (298 K), thus only the Cp ($T$) of char contributes to the energy balance. However, the Cp ($T$) function could not be obtained up to the pyrolysis temperature (803 K) because of operational limitations of the thermobalance used. Therefore, the Cp of char has been considered constant with temperature for the calculations, using an experimental value obtained at an intermediate temperature ($1.21 \cdot 10^{-3}$ MJ $kg^{-1}$ $K^{-1}$ at 573 K).

According to this procedure, the heat of pyrolysis reaction (including the cooling and condensation of the vapors) was found

**Table 2**
Yields and properties of the products of the sewage sludge fast pyrolysis.

| Yield (wt.%) | Composition | HHV (MJ $kg^{-1}$) | $\Delta H^\circ_f$ (MJ $kg^{-1}$) | Cp ($T$) (kJ $K^{-1}$ $kg^{-1}$) | $\Delta H_{vap}$ (MJ $kg^{-1}$) |
|---|---|---|---|---|---|
| *Char* | | | | | |
| 51.9 ± 0.7 | – | 5.2 ± 0.2 | −1.18 | 0.82 (25 °C)<br>1.21 (300 °C) | – |
| *Non-condensable gas ($N_2$-free)* | | | | | |
| 10.1 ± 0.9 | *(%, mass fraction)*<br>$CO_2$: 74.3 ± 0.9<br>CO: 13.2 ± 0.1<br>$H_2$: 1.7 ± 0.1<br>$CH_4$: 3.8 ± 0.1<br>$C_2H_6$: 1.4 ± 0.2<br>$C_2H_4$: 1.4 ± 0.1<br>$H_2S$: 4.3 ± 0.9 | 8.0 ± 0.3 | −7.39 | 1.18 (25 °C)<br>1.56 (530 °C) | – |
| *Light organic phase (LOP)* | | | | | |
| 2.2 ± 0.2 | *Elemental analysis (wt.%, wet basis)*<br>C:85.9; H:11.8: N:1.8; S:0.2<br>100 wt.% of organic compounds | 43.10 ± 0.04 | −1.74 | 1.85 (liquid)<br>3.07 (530 °C) | 0.18 |
| *Heavy organic phase (HOP)* | | | | | |
| 9.4 ± 0.2 | *Elemental analysis (wt.%, wet basis)*<br>C:69.5; H:9.0: N:9.4; S:1.2<br>Water: 6.4 ± 0.3 wt.%<br>Organics: 93.6 ± 0.3 wt.% | 32 ± 2 | −3.49 | 2.13 (liquid)<br>2.36 (530 °C) | 0.55 |
| *Aqueous phase (AP)* | | | | | |
| 20.8 ± 0.2 | *Elemental analysis (wt.%, wet basis)*<br>C:11.2; H:10.5: N:6.5; S:0.4<br>Water: 73.8 ± 0.4 wt.%<br>Organics: 26.2 ± 0.4 wt.% | 5.7 ± 0.3 | −12.44 | 3.59 (liquid)<br>2.12 (530 °C) | 1.77 |

Experimental uncertainty is expressed as mean ± deviation standard (two replicates were performed).

to be around −0.70 MJ $kg_{SS}^{-1}$. This indicates that, in the absence of significant heat losses and if the heat released from the cooling and condensation of the gases and vapors could be efficiently used, sewage sludge pyrolysis could be an autothermal process.

The energy demand corresponding only to the thermal decomposition of sewage sludge, without including the energy recovery from gases and vapors, has also been approximately calculated. In this case, gases and vapors were supposed to leave the reactor at the pyrolysis temperature, that is, in gas phase. The following assumptions have been considered for performing the energy balance:

- The composition of each liquid phase was simplified considering only its water content and one representative organic compound: cholest-4-ene for the LOP, 3-methyl-phenol for the HOP and acetic acid for the AP. These were some of the compounds detected by GC–MS with the largest chromatographic area. The mass of the representative organic compound in each phase was equated to the whole organic fraction in the phase. This assumption slightly affects the actual values of Cp and $\Delta H_{vap}$ of the liquid phases, but this should not result in misleading conclusions since the properties of the main organic compounds present in each phase are similar to each other.
- Although the aforementioned organic compounds were in gas phase in the outlet stream, Cp of these compounds in liquid phase are also required, as well as their enthalpies of vaporization, since the temperature range in the integral equation (3) involves a phase change for the produced vapors ($T_{ref} = 298$ K, $T = 803$ K).
- The equation of Harrison and Seaton [34] was used for calculating the Cp of the representative organic compounds in liquid phase (considered constant with temperature), while the Cp data of the compounds in gas phase were found in the literature as a function of temperature. The global Cp of each phase (both in liquid and gas phases) can be estimated as a weighted average of the specific heat capacities of water (or steam) and of the representative organic compound. The results are presented in Table 2.
- In the same way, the enthalpy of vaporization of the liquid phases ($\Delta H_{vap}$) was estimated as a weighted average of the enthalpies of vaporization of the water and of the representative organic compound of each phase at their boiling temperatures. These results are also presented in Table 2.

According to this procedure, the energy demand for the thermal decomposition of sewage sludge was around 0.15 MJ $kg_{SS}^{-1}$. This value is lower than the decomposition heats found in the literature for other types of biomass. For example, a decomposition heat of 0.3 MJ $kg^{-1}$ has been reported for pyrolysis of crop residues [29]. The higher ash content in sewage sludge, which is not decomposed during the process, can explain this difference. The variation in the water content of sewage sludge will also affect the energy demand for its thermal decomposition.

### 3.3. Air-steam gasification of both sewage sludge and char

In addition to the energetic assessment based on experimental data from sewage sludge gasification and char gasification, a theoretical study based on equilibrium data is also presented in this section in order to further study the gasification stages and find their thermodynamic restrictions. Experimental and equilibrium data are compared.

#### 3.3.1. Energetic assessment according to experimental results

Gasification experiments were performed under allothermal conditions since the gasifier required external heat to maintain the gasification temperature. If negligible heat losses are considered in the gasifier, the heat of reaction for the air-steam gasification of both raw materials, sewage sludge and char, can be calculated according to equation (2). The total $\Delta H$ of each stream was calculated as shown in equation (3), considering the following data:

- 1 kg of raw material (sewage sludge or char) has been used as calculation basis in both gasification processes. The amount of gasifying agent varied depending on the ER and S/B defined in each case. Tables 3 and 4 present the mass flow rates of the products obtained from the experiments of sewage sludge gasification and char gasification under different operating conditions, respectively [31,32].
- The raw material (sewage sludge or char) and the air stream were at ambient temperature (298 K) at the gasifier inlet, while steam was generated and fed at 448 K. All the products (gas, solid, steam and tar) left the gasifier at the gasification temperature (1043–1123 K).
- The collected amount of tar was simplified to an equimolar mixture of benzene, naphthalene and pyridine, since these were some of the main compounds detected in the tar mixtures by GC–MS [31]. As tar yield was much lower than the yields of other products, its contribution to the energy balance is also less important and this simplification should not result in misleading calculations.
- The $\Delta H_f^\circ$ and Cp ($T$) of the gases and vapors involved in the process ($N_2$, $O_2$, $H_2$, CO, $CO_2$, $CH_4$, $C_2H_2$, $C_2H_4$, $C_2H_6$, $H_2S$, steam, benzene, naphthalene and pyridine) were taken from the literature [33]. The $\Delta H_f^\circ$ of the solid by-products were calculated according to equation (4).
- The Cp ($T$) of the solid by-products were approximated to that of sewage sludge combustion ash since these solids were mainly composed of ash (>93 wt.% in most cases) [31,32]. The Cp ($T$) of the sewage sludge ash was experimentally measured by DSC but, because of operational limitations of the thermobalance used, the variation of Cp with temperature could not be obtained up to 1043–1123 K, which is the upper limit in the integral equation (3). Thus, the Cp of the solid by-products were considered constant with temperature and an experimental value measured at an intermediate temperature ($1.07 \cdot 10^{-3}$ MJ $kg^{-1}$ $K^{-1}$ at 773 K) was used for calculations.

The experimental heats of reaction for the gasification of sewage sludge and char under different operating conditions are depicted in Fig. 3a and b. Despite the lower organic content in the char than in the sewage sludge (Table 1), the external energy demand for gasifying 1 kg of char was higher than that for gasifying 1 kg of sewage sludge. For instance, the heat of reaction for sewage sludge gasification with ER = 17% and S/B = 0.71 was 0.64 MJ $kg^{-1}$ at 850 °C and 0.17 MJ $kg^{-1}$ at 770 °C, while it reached 1.00 MJ $kg^{-1}$ and 0.78 MJ $kg^{-1}$ for char gasification at 850 and 770 °C, respectively. This behavior could be related to the observed changes in the organic structure of sewage sludge after carrying out the pyrolysis process. The fraction of volatile matter in the sewage sludge was higher than in the char, while the fraction of fixed carbon was higher in the char (Table 1). This means that combustion reactions in gas phase, which usually show less diffusional resistance than the solid–gas reactions, involve vaporized hydrocarbons during the sewage sludge gasification. However, in the case of char gasification, the main combustion reactions in gas phase involve gases such as $H_2$ or CO (produced from the fixed carbon), whose calorific value is lower than that of hydrocarbons. As a consequence, char gasification was an endothermic process under most of the experimental conditions used (Fig. 3b), while sewage sludge gasification was an

**Table 3**
Experimental results from the gasification of sewage sludge [31].

| Temperature | 850 | 770 | 850 | 770 | 850 | 770 | 850 | 770 | 810[a] |
|---|---|---|---|---|---|---|---|---|---|
| ER (%) | 17 | 17 | 12 | 12 | 32 | 32 | 23 | 23 | 19[a] |
| $O_2$ in enriched-air (vol.%) | 21 | 21 | 21 | 21 | 33 | 33 | 27 | 27 | 23[a] |
| S/B (mass ratio) | 0.71 | 0.71 | 0.52 | 0.52 | 0.39 | 0.39 | 0.27 | 0.27 | 0.52[a] |
| Solid product (g $kg_{SS}^{-1}$) | 368 | 401 | 401 | 407 | 356 | 392 | 384 | 400 | 382 ± 1 |
| Tar (g $kg_{SS}^{-1}$) | 25 | 46 | 23 | 49 | 16 | 25 | 14 | 47 | 17 ± 2 |
| $H_2O$ (g $kg_{SS}^{-1}$) | 451 | 515 | 356 | 391 | 352 | 451 | 270 | 336 | 414 ± 8 |
| $CO_2$ (g $kg_{SS}^{-1}$) | 439 | 385 | 304 | 332 | 534 | 524 | 401 | 403 | 418 ± 4 |
| CO (g $kg_{SS}^{-1}$) | 142 | 75 | 156 | 99 | 191 | 97 | 226 | 100 | 138 ± 1 |
| $H_2$ (g $kg_{SS}^{-1}$) | 28.2 | 17.3 | 27.5 | 19.9 | 21.1 | 10.9 | 23.5 | 12.6 | 20.3 ± 0.2 |
| $CH_4$ (g $kg_{SS}^{-1}$) | 29.1 | 26.5 | 31.9 | 32.1 | 24.6 | 22.1 | 26.7 | 25.1 | 27.7 ± 0.8 |
| $C_2H_6$ (g $kg_{SS}^{-1}$) | 4.0 | 4.9 | 3.2 | 4.2 | 2.1 | 1.9 | 2.4 | 4.3 | 2.9 ± 0.4 |
| $C_2H_4$ (g $kg_{SS}^{-1}$) | 22 | 23 | 18 | 25 | 19 | 20 | 19 | 21 | 22 ± 2 |
| $C_2H_2$ (g $kg_{SS}^{-1}$) | 0.9 | 0.9 | 0.4 | 0.9 | 1.1 | 1.1 | 1.0 | 1.0 | 1.0 ± 0.1 |
| $H_2S$ (g $kg_{SS}^{-1}$) | 8.7 | 6.1 | 6.2 | 5.5 | 8.8 | 7.1 | 7.4 | 4.9 | 7.1 ± 0.4 |
| $N_2$ (g $kg_{SS}^{-1}$) | 734 | 677 | 533 | 502 | 742 | 747 | 711 | 690 | 703 ± 6 |
| $\eta_{gas}$ ($m_{STP}^3$ $kg_{SS}^{-1}$) | 1.31 | 1.06 | 1.23 | 1.09 | 1.31 | 1.12 | 1.28 | 1.04 | 1.18 ± 0.01 |
| $LHV_{gas}$ (MJ $m_{STP}^{-3}$) | 5.9 | 5.3 | 7.1 | 6.9 | 5.2 | 4.1 | 6.0 | 4.9 | 5.6 ± 0.1 |

[a] Three replicates were performed at the center point of the experimental design. Mean ± standard deviation of these replicates is shown.

**Table 4**
Experimental results from the gasification of char [32].

| Temperature | 850 | 770 | 850 | 770 | 850 | 770 | 850 | 770 | 810[a] |
|---|---|---|---|---|---|---|---|---|---|
| ER (%) | 17 | 17 | 12 | 12 | 32 | 32 | 23 | 23 | 19[a] |
| $O_2$ in enriched-air (vol.%) | 27 | 27 | 21 | 21 | 40 | 40 | 33 | 33 | 29[a] |
| S/B (mass ratio) | 0.71 | 0.71 | 0.52 | 0.52 | 0.39 | 0.39 | 0.27 | 0.27 | 0.52[a] |
| Solid product (g $kg_{char}^{-1}$) | 757 | 785 | 750 | 785 | 731 | 771 | 752 | 813 | 775 ± 2 |
| Tar (g $kg_{char}^{-1}$) | 2 | 12 | 2 | 5 | 2 | 9 | 5 | 7 | 5 ± 1 |
| $H_2O$ (g $kg_{char}^{-1}$) | 119 | 160 | 78 | 99 | 88 | 99 | 59 | 69 | 112 ± 11 |
| $CO_2$ (g $kg_{char}^{-1}$) | 195 | 206 | 154 | 164 | 232 | 254 | 177 | 190 | 198 ± 5 |
| CO (g $kg_{char}^{-1}$) | 128 | 65 | 122 | 64 | 148 | 77 | 144 | 76 | 91 ± 3 |
| $H_2$ (g $kg_{char}^{-1}$) | 13.7 | 10.1 | 12.0 | 8.9 | 10.0 | 7.4 | 9.6 | 7.2 | 10.3 ± 0.1 |
| $CH_4$ (g $kg_{char}^{-1}$) | 2.8 | 2.8 | 2.6 | 2.6 | 2.2 | 2.2 | 2.2 | 2.4 | 2.9 ± 0.1 |
| $C_2H_4$ (g $kg_{char}^{-1}$) | 0.07 | 0.07 | 0.06 | 0.08 | 0.06 | 0.08 | 0.05 | 0.07 | 0.07 ± 0.01 |
| $H_2S$ (g $kg_{char}^{-1}$) | 1.97 | 0.76 | 0.99 | 0.44 | 1.38 | 0.56 | 0.90 | 0.36 | 0.68 ± 0.03 |
| $N_2$ (g $kg_{char}^{-1}$) | 205 | 197 | 211 | 204 | 212 | 201 | 213 | 198 | 207 ± 8 |
| $\eta_{gas}$ ($m_{STP}^3$ $kg_{char}^{-1}$) | 0.52 | 0.43 | 0.48 | 0.40 | 0.52 | 0.44 | 0.49 | 0.40 | 0.46 ± 0.01 |
| $LHV_{gas}$ (MJ $m_{STP}^{-3}$) | 6.0 | 4.7 | 5.9 | 4.7 | 5.4 | 4.1 | 5.6 | 4.4 | 5.1 ± 0.1 |

[a] Three replicates were performed at the center point of the experimental design. Mean ± standard deviation of these replicates is shown.

exothermic process when simultaneously working with ER > 19% and S/B < 0.52 (Fig. 3a). The heat of reaction (based on experimental data) ranged from −2.61 to +1.29 MJ $kg_{SS}^{-1}$ for sewage sludge gasification and from −0.23 to +1.20 MJ $kg_{char}^{-1}$ for char gasification. Therefore, the temperature and the gasification medium play a larger role in the energy balance of sewage sludge gasification.

The energy demand for carrying out an endothermic gasification process may be obtained from the product gas, either from its thermal energy (for example by using the product gas to preheat the inlet air stream in a heat exchanger) or from the combustion of part of the gas. The gasification efficiency can be defined as the fraction of the energy initially contained in the raw material that could be recovered from the product gas after carrying out the gasification process (5):

$$\text{Efficiency}\ (\%) = \frac{\text{Energy in gas} - Q_{\text{gasification}} - Q_{\text{steam}}}{\text{LHV}_{\text{raw material}}} \cdot 100 \qquad (5)$$

where:

- "Energy in gas" is the energy that could be recovered from the thermal and calorific values of the gasification product gas (MJ $kg_{raw\ material}^{-1}$)(equation 6). A heat exchange efficiency of 70% has been considered when taking advantage of the sensible and latent heats of the gas stream [35].

$$\begin{aligned}\text{Energy in gas} = {} & \eta_{gas}\cdot \text{LHV}_{gas} + 0.7\cdot\left[\sum_i m_{i,gas}\cdot\int_{T_{ref}}^{T} \text{Cp}_{i,gas}\,(T)\cdot dT\right] \\ & + 0.7\cdot m_{H_2O}\cdot\left[\text{Cp}_{H_2O(l)}\cdot\left(T_{b,\,H_2O} - T_{ref}\right)\right. \\ & \left. + \Delta H_{cond.\,H_2O} + \int_{T_{b,H_2O}}^{T} \text{Cp}_{H_2O(v)}(T)\cdot dT\right] \\ & + 0.7\cdot\sum_{i,tar} m_{i,tar}\cdot\left[\text{Cp}_{i,tar(l)}\cdot\left(T_{b\,i,\,tar} - T_{ref}\right)\right. \\ & \left. + \cdot H_{cond.i,tar} + \int_{T_{b\,i,\,tar}}^{T} \text{Cp}_{i,tar(v)}(T)\cdot dT\right]\end{aligned} \qquad (6)$$

being $\eta_{gas}$ the dry gas yield ($m_{STP}^3$ $kg_{raw\ material}^{-1}$, Tables 3 and 4), $LHV_{gas}$ the lower heating value of the dry gas (MJ $m_{STP}^{-3}$, Tables 3 and 4), $m_{i,gas}$ the mass flow rate of the non-condensable gases (kg $kg_{raw\ material}^{-1}$, Tables 3 and 4), $T_{ref} = 298$ K, $T$ the gasification temperature (K), $\text{Cp}_{i,gas}\,(T)$ the specific heat capacity of the non-condensable gases as a function of temperature (MJ $kg^{-1}$ $K^{-1}$)

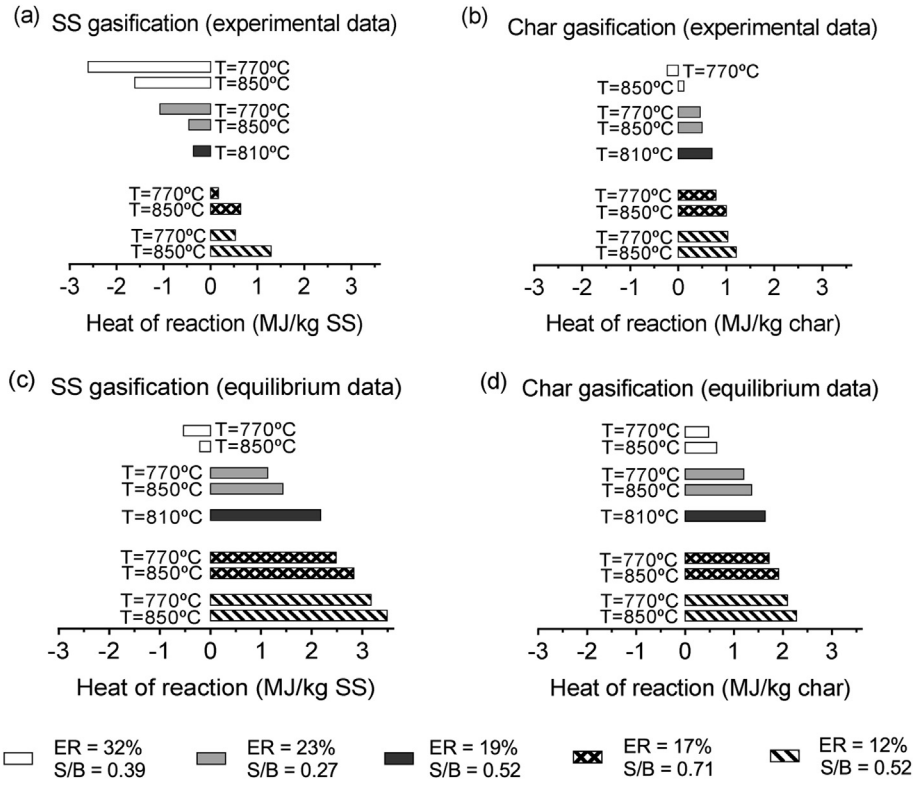


**Fig. 3.** Heats of reaction for sewage sludge (SS) gasification (a, c) and char gasification (b, d) based on both experimental and equilibrium data.

[33], $m_{H2O}$ the mass flow rate of produced water (kg $kg^{-1}_{raw\ material}$, Tables 3 and 4), $Cp_{H2O(l)}$ the specific heat capacity of liquid water ($4.18 \cdot 10^{-3}$ MJ $kg^{-1}$ $K^{-1}$), $T_{b,H2O}$ the boiling point of water (373 K), $\Delta H_{cond.H2O}$ the enthalpy of condensation of water at its boiling point (2.26 MJ $kg^{-1}$), $Cp_{H2O(v)}(T)$ the specific heat capacity of steam as a function of temperature [33], $m_{i,tar}$ the mass flow rates of tar compounds (kg $kg^{-1}_{raw\ material}$), $Cp_{i,tar(l)}$ the specific heat capacity of tar compounds in liquid phase (calculated according to [34]), $T_{bi,tar}$ the boiling point of tar compounds, $\Delta H_{cond.i,tar}$ the enthalpy of condensation of tar compounds at their boiling points (0.39, 0.34 and 0.44 MJ $kg^{-1}$ for benzene, naphthalene and pyridine, respectively) and $Cp_{i,tar(v)}(T)$ the specific heat capacity of tar compounds in gas phase as a function of temperature. The obtained results of "Energy in gas" are shown in Table 5.

- $Q_{gasification}$ is the heat of reaction for the gasification process (MJ $kg^{-1}_{raw\ material}$), previously calculated according to equation (2) under different experimental conditions (Fig. 3a and b).
- $Q_{steam}$ (MJ $kg^{-1}_{raw\ material}$) is the energy demand for heating and evaporating the inlet flow of water from 25 °C to 150 °C (2.36 MJ $kg^{-1}_{H_2O}$).
- $LHV_{raw\ material}$ (MJ $kg^{-1}_{raw\ material}$) is the energy initially contained in the raw material, expressed as its lower heating value (Table 1).

The efficiency results for sewage sludge gasification and char gasification are presented in Table 5. Experimental efficiency data varied from 58% to 87% for sewage sludge gasification and from 23% to 64% for char gasification. Better efficiency results were obtained for the sewage sludge gasification as a consequence of its lower heat of reaction and higher gas yield (Tables 3 and 4). The gasification efficiency (based on experimental data) improved at higher temperatures, higher ER and lower S/B.

### 3.3.2. Energetic assessment according to equilibrium data

The heat of reaction for the air-steam gasification of sewage sludge and char when reaching the chemical equilibrium is determined in this section. The calculation has been carried out analogously to Section 3.3.1, but in this case the product mass flows were not experimental data, but equilibrium data. HSC Chemistry® 6.1 software was used to determine the mass flow rates of the products at equilibrium conditions. This software uses the Gibbs energy minimization method to calculate the amounts of products at equilibrium in isothermal and isobaric conditions. Therefore, the reaction system (temperature, pressure, feed of gasifying agent, amounts of C, H, O, S and N that form part of the raw material and species expected to be part of the products) must be specified for the calculations.

The main compounds found in the product gas at equilibrium conditions were $H_2$, CO, $CO_2$, $CH_4$, $H_2S$, $NH_3$, $N_2$ and steam. Neither tar nor light hydrocarbons, except $CH_4$, were formed at equilibrium conditions. In addition to gas production, a small fraction of the initial carbon contained in the raw material (sewage sludge or char) remained in the solid by-product under some of the simulated conditions.

The heats of reaction at chemical equilibrium under the same operating conditions used in the laboratory are depicted in Fig. 3c and d as a comparison to the experimental data (Fig. 3a and b). As can be observed, reaching the chemical equilibrium in both gasification processes entails additional energy consumption. The reason may be the predominance of endothermic reactions during the gasification equilibrium, such as steam reforming ($C + H_2O \leftrightarrow CO + H_2$, $\Delta H_{298K} = 131.4$ kJ $mol^{-1}$), dry reforming ($CH_4 + CO_2 \leftrightarrow 2CO + 2H_2$, $\Delta H_{298K} = 246.8$ kJ $mol^{-1}$) or the Boudouard reaction ($C + CO_2 \leftrightarrow 2CO$, $\Delta H_{298K} = 172.3$ kJ $mol^{-1}$), against the exothermic equilibrium reactions, such as the water-gas shift reaction ($CO + H_2O \leftrightarrow CO_2 + H_2$, $\Delta H_{298K} = -40.9$ kJ $mol^{-1}$). These reactions

**Table 5**
Energy recovery from the product gas and efficiency of sewage sludge gasification and char gasification according to experimental and equilibrium data.

| | | | | | | | | | |
|---|---|---|---|---|---|---|---|---|---|
| Temperature | 850 | 770 | 850 | 770 | 850 | 770 | 850 | 770 | 810 |
| ER (%) | 17 | 17 | 12 | 12 | 32 | 32 | 23 | 23 | 19 |
| S/B (mass ratio) | 0.71 | 0.71 | 0.52 | 0.52 | 0.39 | 0.39 | 0.27 | 0.27 | 0.52 |
| *Sewage sludge gasification (experimental results)* | | | | | | | | | |
| Energy in gas (MJ $kg_{SS}^{-1}$) | 10.23 | 7.91 | 9.63 | 8.41 | 9.10 | 6.77 | 9.56 | 6.93 | 8.72 ± 0.12 |
| Gasification efficiency (%) | 74 | 58 | 65 | 61 | 87 | 75 | 82 | 65 | 71 ± 2 |
| *Sewage sludge gasification (equilibrium results)* | | | | | | | | | |
| Energy in gas (MJ $kg_{SS}^{-1}$) | 14.37 | 14.11 | 14.95 | 14.72 | 11.34 | 11.09 | 12.86 | 12.64 | 13.70 |
| Gasification efficiency (%) | 90 | 91 | 91 | 92 | 94 | 94 | 94 | 94 | 92 |
| *Char gasification (experimental results)* | | | | | | | | | |
| Energy in gas (MJ $kg_{char}^{-1}$) | 3.91 | 2.77 | 3.49 | 2.44 | 3.52 | 2.44 | 3.34 | 2.27 | 2.98 ± 0.05 |
| Gasification efficiency (%) | 51 | 32 | 40 | 23 | 64 | 49 | 54 | 33 | 40 ± 2 |
| *Char gasification (equilibrium results)* | | | | | | | | | |
| Energy in gas (MJ $kg_{char}^{-1}$) | 6.19 | 6.09 | 6.53 | 6.42 | 4.94 | 4.85 | 5.62 | 5.53 | 5.95 |
| Gasification efficiency (%) | 78 | 80 | 80 | 81 | 82 | 83 | 82 | 84 | 81 |

occur to a greater extent at equilibrium, which shows the thermodynamic limit of the process.

As can be seen in Fig. 3c and d, the gasification of sewage sludge at equilibrium conditions only resulted in an exothermic process when ER was increased to 32%, while char gasification at equilibrium conditions was an endothermic process in all the simulated cases. However, the gas heating value and the gas yield calculated for equilibrium conditions were higher than those obtained experimentally [31,32], so more energy could be recovered from the equilibrium product gas (Table 5). This latter difference outweighs the difference observed in the experimental and equilibrium data of heat of reaction (Fig. 3), so the gasification efficiency is improved at equilibrium conditions: 90–94% for sewage sludge gasification and 78–84% for char gasification (Table 5).

As an extension of the theoretical study, Fig. 4 shows the evolution of the heat of reaction for air-steam gasification of both sewage sludge and char as a function of the feed of oxygen and steam, which are represented by ER and S/C (steam to carbon molar ratio), respectively. Two different gasification temperatures (800 and 850 °C) have been used for the calculations. Operating temperatures above 800 °C are usually preferred in gasification processes in order to achieve high carbon conversion and low tar content in the product gas [36]. The heat of reaction for both gasification processes at equilibrium conditions decreases with the availability of oxygen (higher ER enhances the combustion reactions) and/or with the reduced presence of steam (lower S/C restricts the endothermic steam reforming reactions). For example, for ER = 20% and S/C = 0–1, an external heat transfer of 2.01–2.43 MJ $kg_{SS}^{-1}$ and 1.36–1.86 MJ $kg_{char}^{-1}$ would be required in order to maintain a temperature of 850 °C during the gasification of sewage sludge and char at equilibrium conditions, respectively. In the lower range of ER (up to 25%), the energy demand for gasifying 1 kg of char is lower than that required for gasifying 1 kg of sewage sludge, but this trend is reversed in the upper range of ER since the energy released from the in situ combustion of sewage sludge becomes more important.

If the gasifier operates at autothermal conditions instead of being heated by external heat transfer, the gasification temperature is the output variable from balancing out the enthalpies of the streams entering and exiting the gasifier ($\Delta H_{in} = \Delta H_{out}$, assuming negligible heat losses). The equilibrium temperature has been calculated under different gasification mediums following an iterative method: $\Delta H_{out}$ depends on the mass flow rates of the products (equation 3), and these in turn depend on the gasification temperature (temperature has to be specified in the HSC Chemistry software to calculate the amounts of products at equilibrium). Fig. 5 shows the evolution of the equilibrium temperature as a function of ER and S/C for the air-steam gasification of both sewage sludge and char. Obviously, the equilibrium temperature is increased with ER and decreased with S/C. Furthermore, the required ER to maintain a specific reaction temperature is higher in char gasification than in sewage sludge gasification. For instance, an ER of 33% would be required for the autothermal operation of sewage sludge gasification at 800 °C and S/C = 0.5 under equilibrium conditions, while this value reaches 45% in the case of char gasification. The higher the ER, the greater the production of $CO_2$ through combustion reactions. The presence of $CO_2$ in the gasification gas is undesirable since it implies both a dilution effect of the gas heating value and a reduction in the formation of CO (production and consumption of CO and $CO_2$ are connected by reactions such as the water-gas shift or the Boudouard reaction). In addition to the gas calorific value, the $H_2$/CO ratio in the product gas is an important parameter for using this gas as a feedstock in the synthesis of chemicals such as methanol or Fischer Tropsch fuels. Values of this ratio close to 2 are usually required in these processes [37]. For the aforementioned example (ER of 33% for sewage sludge gasification and 45% for char gasification to maintain 800 °C with S/C = 0.5), 44% of the initial carbon contained in the sewage sludge produces $CO_2$, while this value reaches 52% in the case of char gasification. Both the heating value and the $H_2$/CO ratio in the product gas of sewage sludge gasification ($LHV_{gas}$ = 4.27 MJ $m_{STP}^{-3}$, $H_2$/CO = 1.47) are higher than those obtained from char gasification ($LHV_{gas}$ = 3.05 MJ $m_{STP}^{-3}$, $H_2$/CO = 0.89).

### 3.4. Energetic assessment of the whole processes

This last section presents an overall energetic assessment of the two thermo-chemical processes proposed in Fig. 1 for sewage sludge treatment: (i) sewage sludge drying + sewage sludge gasification (two-stage process) and (ii) sewage sludge drying + sewage sludge pyrolysis + char gasification (three-stage process). The total energy demand for the whole processes is the sum of the net heats required or released in the involved stages (positive term for endothermic processes and negative value for exothermic processes). Experimental data resulting from the pyrolysis and gasification stages have been used for the calculations:

- Sewage sludge drying. The water content in sewage sludge is assumed to be reduced from 65 wt.% (typical moisture content before thermal drying) to 6.5 wt.% during the thermal drying. For this case, $Q_{drying}$ is around 4 MJ $kg_{dried\ SS}^{-1}$ (Fig. 2).
- Sewage sludge pyrolysis. The energy contained in the produced gases and vapors could be recovered to be used in the thermal decomposition of sewage sludge itself and in the prior thermal drying. This energy was calculated analogously to the

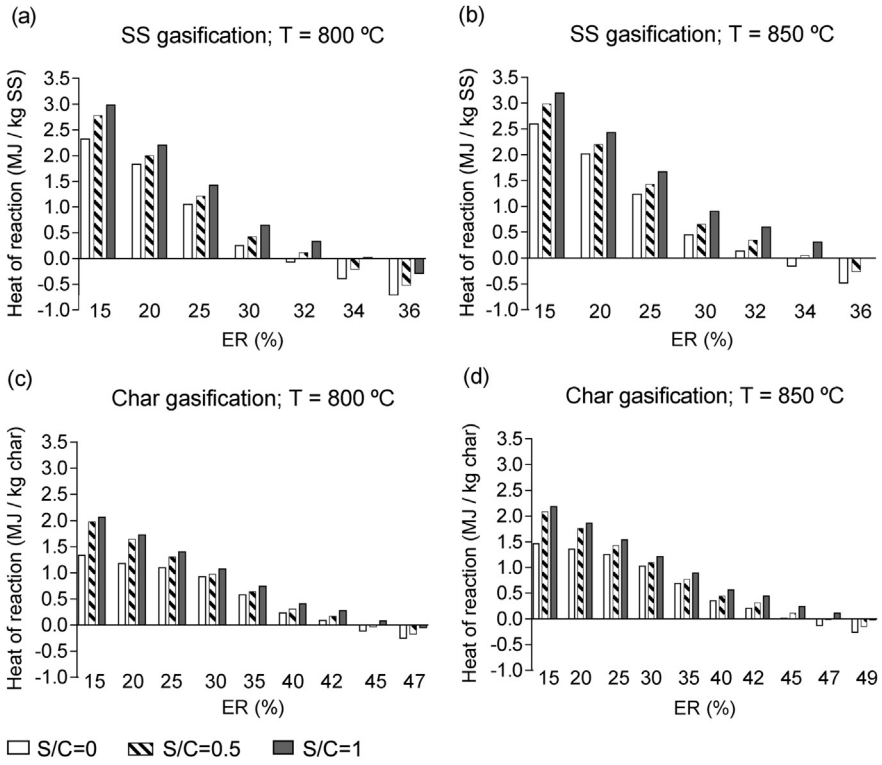


**Fig. 4.** Heats of reaction for sewage sludge (SS) gasification (a, b) and char gasification (c, d) at 800 °C and 850 °C according to equilibrium data.

gasification gas energy according to equation (6). An energy recovery of −1.32 MJ $kg_{SS}^{-1}$ was obtained, which turns into −1.17 MJ $kg_{SS}^{-1}$ if the thermal decomposition heat is subtracted (+0.15 MJ $kg_{SS}^{-1}$). The use of the calorific value of the organic liquid product (43 MJ $kg_{LOP}^{-1}$ and 32 MJ $kg_{HOP}^{-1}$) has not been included in the energy balance, as some important properties such as its poor stability or its high nitrogen content must be improved facing toward its use as fuel [7].

- Sewage sludge gasification/char gasification. The net heats of the gasification stages correspond to the numerator of the equation (5). As the same calculation basis is required for the comparison of the two-stage and three-stage processes (1 kg of dried sewage sludge), data corresponding to the gasification of char (MJ $kg_{char}^{-1}$) must be turned into MJ $kg_{SS}^{-1}$ by means of the char yield obtained during the pyrolysis of sewage sludge (0.519 $kg_{char}$ $kg_{SS}^{-1}$).

Fig. 6 shows the total energy requirement for the whole processes, considering the different experimental conditions used in the gasification stages. The total energy demand ranged between −2.83 and −6.21 MJ $kg_{SS}^{-1}$ for the two-stage process (exothermic process) and between +1.17 and +2.24 MJ $kg_{SS}^{-1}$ for the three-stage process (endothermic process). Thus, if the energy contained in the product gas of sewage sludge gasification could be efficiently used, it would be enough to cover the energy demand for both the sewage sludge thermal drying and the gasification process itself. It should be noted that the flow of water required for the air-steam gasification of sewage sludge could directly come from the own moisture content in the sludge, thus the energy required for thermal drying would be reduced and the total energy balance would be even more favorable (between −3.70 and −6.69 MJ $kg_{SS}^{-1}$). On the other hand, the energy balance shows that the three-stage treatment is globally an endothermic process (note that the use

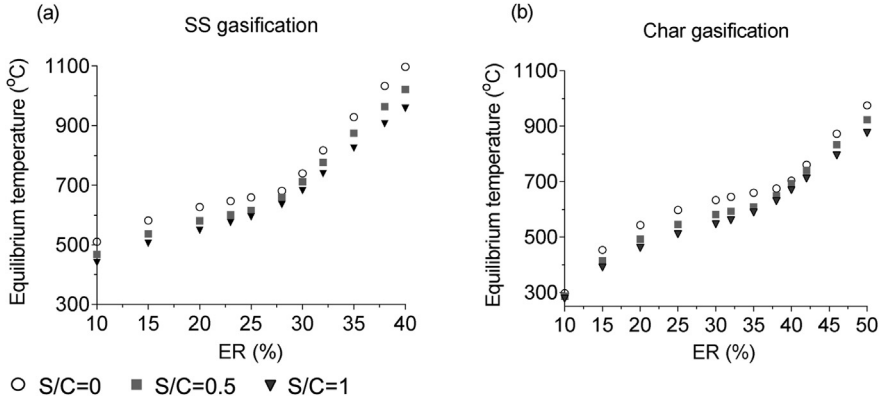


**Fig. 5.** Equilibrium temperature as a function of the equivalence ratio (ER) and the steam to carbon molar ratio (S/C) during sewage sludge (SS) gasification and char gasification.

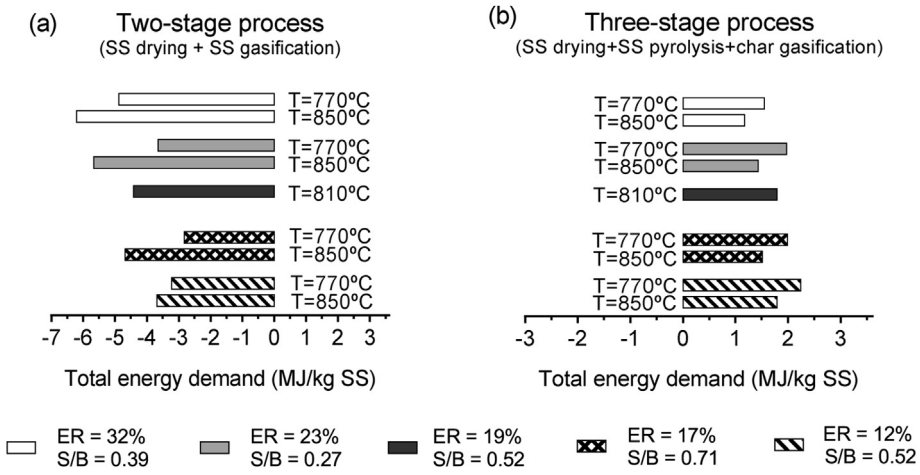


**Fig. 6.** Total energy demand for the two-stage and three-stage processes for sewage sludge (SS) treatment (experimental data).

of the calorific value of the pyrolysis liquid is not considered), so that an additional energy input would be needed to carry out this treatment. However, assuming a direct and efficient use of the calorific value of the organic pyrolysis liquid (3.92 MJ $kg_{SS}^{-1}$), a favorable energetic assessment of the three-stage process is also obtained, with a total energy demand ranging from −2.75 to −1.68 MJ $kg_{SS}^{-1}$ (exothermic process). Therefore, the use of the calorific value of the produced pyrolysis liquid is a key issue for reaching an autothermal three-stage process that does not require external heat to take place.

Regarding the influence of the gasification operating conditions on the total energy demand of the whole processes, the energy balance was more favorable at the highest gasification temperature (850 °C), the highest ER (32%) and a moderate S/B (0.39).

## 4. Conclusions

This paper presents an energetic assessment of two potential thermo-chemical treatments for sewage sludge: (i) sewage sludge thermal drying + air-steam gasification of sewage sludge (two-stage process) and (ii) sewage sludge thermal drying + pyrolysis of sewage sludge + air-steam gasification of the char derived from the pyrolysis (three-stage process). The sewage sludge thermal drying can drastically reduce the waste volume, which facilitates handling of the biosolids, but it involves high energy consumption. For example, 4 MJ $kg_{dried\ SS}^{-1}$ are required for reducing water content from 65 wt.% to 6.5 wt.%. Regarding the pyrolysis stage, energetic calculations based on experimental yields showed that the energy needed for thermal decomposition of sewage sludge (+0.15 MJ $kg_{SS}^{-1}$ at 530 °C) could be covered by the energy contained in the product stream of gases and vapors. An energy output of −1.17 MJ $kg_{SS}^{-1}$ could be recovered from the calorific value and the thermal energy of the product gas (heat exchange efficiency of 70%) after covering the energy demand in the pyrolysis reaction. Despite the lower organic content in the char (24.1 wt.%) than in the sewage sludge (54.5 wt.%), higher external energy demand was found for gasifying 1 kg of char than for gasifying 1 kg of sewage sludge (based on experimental yields). This means that less energy is released from the in-situ combustion reactions during char gasification. Depending on the operating conditions, sewage sludge gasification was an exothermic or endothermic process and its heat of reaction varied from −2.61 MJ $kg_{SS}^{-1}$ ($T$ = 770 °C, ER = 32%, S/B = 0.39) to +1.29 MJ $kg_{SS}^{-1}$ ($T$ = 850 °C, ER = 12%, S/B = 0.52). Char gasification was an endothermic process in most of the experimental conditions and its heat of reaction varied from −0.23 MJ $kg_{char}^{-1}$ ($T$ = 770 °C, ER = 32%, S/B = 0.39) to +1.20 MJ $kg_{char}^{-1}$ ($T$ = 850 °C, ER = 12%, S/B = 0.52). A theoretical study performed with equilibrium data (according to Gibbs energy minimization method) showed that both gasification processes require more energy to take place at equilibrium conditions. However, the equilibrium gasification efficiency was higher than the experimental results because more energy could be recovered from the equilibrium product gas.

In summary, the energy balances showed that the energy contained in the product gas of sewage sludge gasification is enough to cover the energy demand for both the sewage sludge thermal drying and the gasification process itself. However, an additional energy input is required to carry out the three-stage process. This energy demand could be provided by the calorific value of the bio-oil produced in the pyrolysis stage, but some important properties such as its poor stability or its high nitrogen content must be improved facing toward its use as fuel.

## Acknowledgments

The authors gratefully acknowledge the financial support provided by the Spanish Ministry of Science and Technology (CTQ2010-20137) and the Spanish Ministry of Education (AP2009-3446).

## References

[1] Werther J, Ogada T. Sewage sludge combustion. Prog Energy Combust Sci 1999;25:55–116.
[2] Council Directive 91/271/EEC of 21 May 1991 concerning urban waste water treatment.
[3] Fytili D, Zabaniotou A. Utilization of sewage sludge in EU application of old and new methods – a review. Renew Sustain Energy Rev 2008;12:116–40.
[4] Council Directive 86/278/EEC of 12 June 1986 on the protection of the environment, and in particular of the soil, when sewage sludge is used in agriculture.
[5] Furness DT, Hoggett LA, Judd SJ. Thermochemical treatment of sewage sludge. J Chart Inst Water Environ Manage 2000;14:57–65.
[6] Rulkens W. Sewage sludge as a biomass resource for the production of energy: overview and assessment of the various options. Energy Fuels 2008;22:9–15.
[7] Fonts I, Gea G, Azuara M, Ábrego J, Arauzo J. Sewage sludge pyrolysis for liquid production: a review. Renew Sustain Energy Rev 2012;16:2781–805.
[8] Kim Y, Parker W. A technical and economic evaluation of the pyrolysis of sewage sludge for the production of bio-oil. Bioresour Technol 2008;99:1409–16.
[9] Pokorna E, Postelmans N, Jenicek P, Schreurs S, Carleer R, Yperman J. Study of bio-oils and solids from flash pyrolysis of sewage sludges. Fuel 2009;88:1344–50.
[10] Chaudhari ST, Dalai AK, Bakhshi NN. Production of hydrogen and/or syngas ($H_2$+CO) via steam gasification of biomass-derived chars. Energy Fuels 2003;17:1062–7.

[11] Haykiri-Acma H, Yaman S, Kucukbayrak S. Gasification of biomass chars in steam-nitrogen mixture. Energy Convers Manage 2006;47:1004–13.
[12] He P, Luo S, Cheng G, Xiao B, Cai L, Wang J. Gasification of biomass char with air-steam in a cyclone furnace. Renew Energy 2012;37:398–402.
[13] Bacaicoa PG, Bilbao R, Uson C. Sewage sludge gasification: first studies. In: Proceedings of the Second Biomass Conference of the Americas: Energy, Environment, and Agricultural Industry; 1995. p. 685–94.
[14] Adegoroye A, Paterson N, Li X, Morgan T, Herod AA, Dugwell DR, et al. The characterisation of tars produced during the gasification of sewage sludge in a spouted bed reactor. Fuel 2004;83:1949–60.
[15] Manyá JJ, Sánchez JL, Gonzalo A, Arauzo J. Air gasification of dried sewage sludge in a fluidized bed: effect of the operating conditions and in-bed use of alumina. Energy Fuels 2005;19:629–36.
[16] Aznar M, Manyá JJ, García G. Influence of freeboard temperature, fluidization velocity and particle size on tar production and composition during the air gasification of sewage sludge. Energy Fuels 2008;22:2840–50.
[17] Tae-Young M, Bo-Sung K, Joo-Sik K. Production of a producer gas with high heating values and less tar from dried sewage sludge through air gasification using a two-stage gasifier and activated carbon. Energy Fuels 2009;23:3268–76.
[18] Dogru M, Midilli A, Howarth CR. Gasification of sewage sludge using a throated downdraft gasifier and uncertainty analysis. Fuel Process Technol 2002;75:55–82.
[19] Petersen I, Werther J. Experimental investigation and modelling of gasification of sewage sludge in the circulating fluidized bed. Chem Eng Process 2005;44:717–36.
[20] Judex JW, Gaiffi M, Burgbacher HC. Gasification of dried sewage sludge: status of the demonstration and the pilot plant. Waste Manage 2012;32:719–23.
[21] Nipattummakul N, Ahmed I,I, Kerdsuwan S, Gupta AK. High temperature steam gasification of wastewater sludge. Appl Energy 2010;87:3729–34.
[22] Xu ZR, Zhu W, Li M. Influence of moisture content on the direct gasification of dewatered sludge via supercritical water. Int J Hydrogen Energy 2012;37:6527–35.
[23] McKendry P. Energy production from biomass (part 3): gasification technologies. Bioresour Technol 2002;83:55–63.
[24] Franco C, Pinto F, Gulyurtlu I, Cabrita I. The study of reactions influencing the biomass steam gasification process. Fuel 2003;82:835–42.
[25] Hosseini M, Dincer I, Rosen MA. Steam and air fed biomass gasification: comparisons based on energy and exergy. Int J Hydrogen Energy 2012;37:16446–52.
[26] Karamarkovic R, Karamarkovic V. Energy and exergy analysis of biomass gasification at different temperatures. Energy 2010;35:537–49.
[27] Ptasinski KJ, Prins MJ, Pierik A. Exergetic evaluation of biomass gasification. Energy 2007;32:568–74.
[28] Zhang Y, Li B, Li H, Zhang B. Exergy analysis of biomass utilization via steam gasification and partial oxidation. Thermochim Acta 2012;538:21–8.
[29] Manganaro J, Chen B, Adeosun J, Lakhapatri S, Favetta D, Lawal A. Conversion of residual biomass into liquid transportation fuel: an energy analysis. Energy Fuels 2011;25:2711–20.
[30] Gil-Lalaguna N, Fonts I, Gea G, Murillo MB, Lázaro L. Reduction of water content in sewage sludge pyrolysis liquid by selective on-line condensation of the vapors. Energy Fuels 2010;24:6555–64.
[31] Gil-Lalaguna N, Sánchez JL, Murillo MB, Rodríguez E, Gea G. Air-steam gasification of sewage sludge in a fluidized bed. Influence of some operating conditions. Chem Eng J 2014;248:373–82.
[32] Gil-Lalaguna N, Sánchez JL, Murillo MB, Ruiz V, Gea G. Air-steam gasification of char derived from sewage sludge pyrolysis. Comparison with the gasification of sewage sludge. Fuel 2014;129:147–55.
[33] Perry RH, Green DW. Perry's chemical engineer's handbook. 7th ed. New York: McGraw-Hill; 1999.
[34] Harrison BK, Seaton WH. Solution to missing group-problem for estimation of ideal-gas heat-capacities. Ind Eng Chem Res 1988;27:1536–40.
[35] Çengel YA. Heat and mass transfer: a practical approach. 3rd ed. Mexico: McGraw-Hill Science/Engineering/Math; 2005.
[36] Devi L, Ptasinski KJ, Janssen FJJG. A review of the primary measures for tar elimination in biomass gasification processes. Biomass Bioenergy 2003;24:125–40.
[37] Wender I. Reactions of synthesis gas. Fuel Process Technol 1996;48:189–297.

Fuel 141 (2015) 99–108

Contents lists available at ScienceDirect

Fuel

journal homepage: www.elsevier.com/locate/fuel

# Use of sewage sludge combustion ash and gasification ash for high-temperature desulphurization of different gas streams

N. Gil-Lalaguna *, J.L. Sánchez, M.B. Murillo, G. Gea

*Thermo-chemical Processes Group, Aragón Institute of Engineering Research (I3A), Universidad de Zaragoza, c/Mariano Esquillor s/n, 50018 Zaragoza, Spain*

## HIGHLIGHTS

- Hot gas desulphurization (600–800 °C) by using different sewage sludge ash.
- Better results obtained with the combustion ash than with the gasification ash.
- Different metal content and crystalline phases detected in both solids.
- Negative impact of steam and gasification gas components on $H_2S$ removal.
- The total amount of $H_2S$ removed from gas was only partially captured in the ash.

## ARTICLE INFO

*Article history:*
Received 27 May 2014
Received in revised form 29 August 2014
Accepted 15 October 2014
Available online 29 October 2014

*Keywords:*
$H_2S$ removal
Hot gas cleaning
Sewage sludge
Combustion ash
Gasification ash

## ABSTRACT

Due to its metal content, sewage sludge ash appears as a potential sorbent material for $H_2S$ removal at high temperature. The desulphurization ability of the solid by-products of combustion and gasification of sewage sludge has been evaluated in this work. Ash characterization results revealed that metal fraction in sewage sludge did not remained completely inert during combustion and gasification processes. Iron content was lower in the gasification ash and X-ray patterns showed different crystalline phases in the solids: $Fe_2O_3$ in the combustion ash and $Fe_3O_4$ in the gasification ash. These differences resulted in a lower sulphur capture capacity of the gasification ash. Desulphurization tests were carried out in a lab-scale fixed bed reactor operating at 600–800 °C. Different gases containing 5000 ppmv $H_2S$ ($H_2S/N_2$ mixture and synthetic gasification gas) were used. The $H_2S$ breakthrough curves were negatively affected by the reducing atmosphere created by the gasification gas and by the presence of steam in the reaction medium. However, $H_2S$ breakthrough curves alone do not provide enough information to evaluate the sulphur capture capacity of the sorbent materials. Ultimate analyses of the spent solid samples showed that the total amount of $H_2S$ removed from the gas was only partially captured in the ash. Thermodynamic data pointed to a significant fraction of sulphur forming part of other gases, such as $SO_2$. In the best operating conditions, an outlet gas with less than 100 ppmv $H_2S$ was obtained during 300 min, thus resulting in a sulphur loading of 63 mg S $g_{ash}^{-1}$. This experimental sulphur content was 39% lower than the maximum value predicted by equilibrium simulations.



## 1. Introduction

Sewage sludge has become an increasingly important residue needing effective management. Due to the organic nature of sewage sludge, thermal processes such as pyrolysis, gasification or combustion have attracted considerable scientific interest as a potential route to its energy valorization [1–3]. However, as occurs in most thermo-chemical treatments of wastes and solid fuels, various impurities are found in the products of interest deriving from these processes, which significantly limits their final uses. One of these impurities is $H_2S$, present in the gaseous products of both the pyrolysis and the gasification of sewage sludge due to its initial content of sulphur compounds [4]. As is well known, $H_2S$ emissions to the atmosphere (or $SO_2$ emissions in the case of burning a $H_2S$-containing gas) entail environmental problems related to acid rain. In addition, the presence of $H_2S$ in the gas leads to operational problems such as corrosion in pipes, engines or turbines, as well as the deactivation of the common catalysts used for tar cracking and gas reforming after gasification processes [5].

Several low and high temperature processes for $H_2S$ removal from products or off-gases have been described and developed at

* Corresponding author. Tel.: +34 976762224.
*E-mail address:* noemigil@unizar.es (N. Gil-Lalaguna).

http://dx.doi.org/10.1016/j.fuel.2014.10.036
0016-2361/

various stages. Wet scrubbing with selected solvents has been a widely used low-temperature process in the chemical process industry [6]. The use of activated carbons for $H_2S$ removal at low temperature has also been extensively studied [7–9]. Given the combination of their unique surface features (high specific surface and pore volume) and surface chemistry improved by the addition of functional groups, activated carbon-based materials have been proved to work efficiently as adsorbents of sulphur-containing gases such as $H_2S$, $SO_2$ or methyl mercaptans. As a result of surface reactions, $H_2S$ can be oxidized to either sulphur or $SO_2$ [8]. Some activated carbons of different characteristics have been prepared from sewage sludge pyrolysis or carbonization [10–13], obtaining in some cases pollutant removal efficiencies comparable to those corresponding to commercial activated carbons [13].

On the other hand, high temperature desulphurization processes are advantageous from an energy standpoint as a result of the elimination of gas cooling and the associated heat exchangers [14]. Different studies concerning the use of metal oxide based sorbents for hot gas desulphurization can be found in the literature [14–20]. Zinc, manganese, copper, iron, rare earth, and calcium sorbents are among the most promising and most extensively studied [14,15]. Typically, metal oxides are converted to sulphides during a sulphur loading stage under reducing hot gas conditions. After sulphidation, the spent metal sulphides can be regenerated back to metal oxides by using oxygen, steam, $SO_2$ or a combination of these [14].

Ash residues derived from thermo-chemical treatment of biomass or wastes are known to contain metal oxides in different proportions, so its use as sorbent materials for $H_2S$ removal from hot gases could be an attractive alternative due to its low cost. This is the case of sewage sludge ash, in which this work focuses. An integrated process could be proposed to remove the $H_2S$ produced during thermo-chemical treatment of sewage sludge by using the own ash resulting from these processes in a downstream cleaning stage. The desulphurization capacity of the solid by-products derived from the combustion and gasification of sewage sludge has been evaluated in this work. Desulphurization tests were carried out in a lab-scale fixed bed reactor and the effects of temperature, type of sewage sludge ash, presence of steam and type of $H_2S$-containing gas were studied, thus extending an earlier work performed by our group [20].

## 2. Materials and methods

### 2.1. Sewage sludge ash

The raw material used to obtain the ash samples was anaerobically digested and thermally dried sewage sludge. Sewage sludge combustion was performed under air atmosphere in a heating muffle furnace at 900 °C (heating rate of 20 °C $min^{-1}$) during two hours. The sewage sludge gasification ash was obtained in a previous gasification study performed in a lab-scale fluidized bed reactor at 850 °C, using a mixture of steam and air as gasifying agent ($H_2O/O_2$ molar ratio = 1) [4].

Both ash samples were characterized before the desulphurization tests by various techniques. Ultimate analyses were performed using a Leco TruSpec Micro elemental analyzer. Textural properties such as the BET surface area and the average pore size and volume (BJH method) were calculated from $N_2$ physisorption isotherms (BET volumetric method) using a Micromeritics TriStar II 3000 analyzer. The $N_2$ adsorption–desorption isotherms were obtained at −196 °C and room temperature, respectively, over the whole range of relative pressures. The samples were previously degasified at 200 °C during 8 h in a $N_2$ flow. Powder X-ray diffraction (XRD) patterns of the fresh samples were acquired with a D-Max Rigaku diffractometer equipped with a copper anode (voltage of 40 kV and current of 80 mA). The measurements were completed in the Bragg's angle ($2\theta$) range from 5° to 95°, using a scanning rate of 0.03° $s^{-1}$. Phases present in the solid samples were defined according to the JCPDS-International Centre for Diffraction Data 2000 database. Lastly, metal content in the ash samples was analyzed by inductively coupled plasma combined with optical emission spectroscopy (ICP-OES), using a Thermo Elemental IRIS Intrepid ICP–OES spectrometer. The samples were dissolved by microwave-assisted acid digestion in a CEM MARS microwave reaction system.

### 2.2. Experimental setup and operating conditions

Desulphurization tests were performed at atmospheric pressure in a fixed-bed quartz tubular reactor of 1.2 cm inner diameter and 40 cm length. A diagram of the installation used for the desulphurization tests is shown in Fig. 1. The reactor was packed with 1 g of the solid material (combustion ash or gasification ash), which was supported on a fibreglass fleece located 18.5 cm from the top of the reactor. The reactor was electrically heated and a K-type thermocouple located in the middle of the solid bed was used to measure and control the temperature. The flow rate of the $H_2S$-containing gas was adjusted to 50 $mL_{STP}$ $min^{-1}$ (STP: standard conditions of temperature and pressure at 0 °C and 1 atm) by means of a previously calibrated mass flow controller. Two different inlet gases containing 5000 ppmv $H_2S$ were used to evaluate the effect of the gas components on the desulphurization process: (i) a gas mixture only containing $H_2S$ and $N_2$ and (ii) a synthetic gasification gas, similar to the dry product gas of sewage sludge gasification [4]. Table 1 shows the composition of both gas mixtures. On the

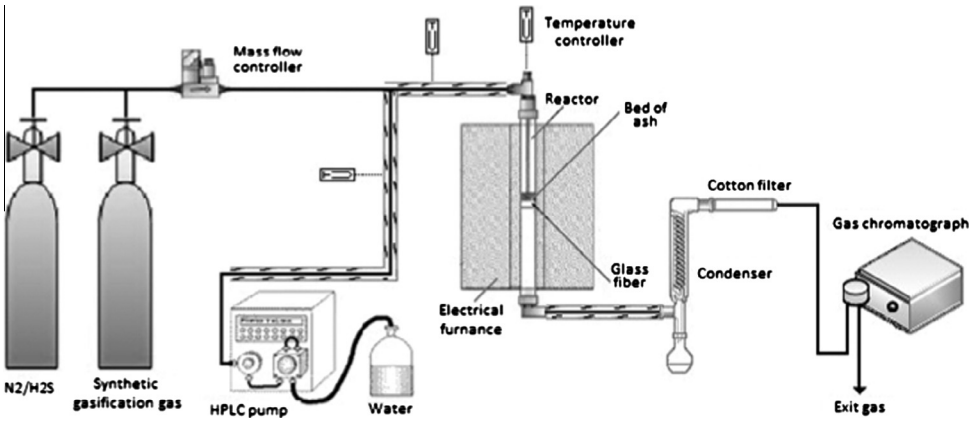


**Fig. 1.** Experimental setup for desulphurization tests.

**Table 1**
Composition of the gas mixtures (dry basis).

| Gas component | $H_2S/N_2$ mixture (vol.%) | Synthetic gasification gas (vol.%) |
|---|---|---|
| CO | – | 10.0 |
| $CO_2$ | – | 15.0 |
| $H_2$ | – | 10.0 |
| $CH_4$ | – | 4.0 |
| $C_2H_6$ | – | 0.2 |
| $C_2H_4$ | – | 1.5 |
| $C_2H_2$ | – | 0.2 |
| $H_2S$ | 0.5 | 0.5 |
| $N_2$ | 99.5 | 58.6 |

one hand, the $H_2S/N_2$ mixture allows the assessment of the desulphurization process without involving any interference from other gases. On the other hand, the synthetic gasification gas simulates more real conditions for $H_2S$ removal. Steam was also added in some tests in order to evaluate its effect on the desulphurization ability of the solids. The required flow of liquid water (0–1 g $h^{-1}$) was accurately adjusted by a HPLC pump and was evaporated before entering the reactor. Steam concentration in the gas entering the reactor varied from 0 to 30 vol.%, which led to a $H_2O/H_2S$ mass ratio varying from 0 to 45 g $H_2O$/g $H_2S$. The weight hourly space velocity during the experiments ranged between 3.7 $h^{-1}$ and 4.7 $h^{-1}$ depending on the steam feed rate. The gas–solid contact time was chosen after preliminary experiments and based on earlier studies [20].

The reactor containing the ash sample was flushed with a $N_2$ flow while heating. The experiment started when the desired temperature was reached in the solid bed. Just then the $N_2$ flow was replaced by the synthetic gasification gas or by the $H_2S/N_2$ mixture. The composition of the outlet gas was continuously analyzed during the experiments by means of an Agilent Micro-GC 3000 (sample injection every four minutes). The $H_2S$ outlet flow ($mL_{STP}$ $min^{-1}$) was calculated from the gas composition data taking $N_2$ of the gas mixture as an internal standard. The evolution of the $H_2S$ outlet flow with time is depicted in the $H_2S$ breakthrough curves. Initially, the established time for the experiments was two hours, but reaction time had to be extended in some cases to 240 or 390 min (Table 2) in order to reach the $H_2S$ breakthrough time.

After the desulphurization tests, sulphur content in the ash samples was determined with a Leco TruSpec Micro elemental analyzer. Furthermore, one of the ash samples was morphologically and chemically characterized by scanning electron microscopy combined with energy dispersive X-ray spectroscopy (SEM/EDX) and by X-ray photoelectron spectroscopy (XPS). A FEI Inspect F50 microscope was used for the SEM/EDX analysis. External metal coating was not applied to the solid sample. The back-scattered electron imaging mode was used in the EDX analysis (acquisition time of 1 min). The XPS measurements were perfomed with a Kratos AXIS Ultra DLD spectrometer by using monochromatic Al Kα (1486.6 eV) X-ray source and a chamber pressure of around $3{\cdot}10^{-8}$ Pa. The quantification of the XPS spectra was carried out with the help of the CasaXPS software and spectra were deconvoluted by applying Gaussian-Lorentzian line-shapes with Shirley-type background.

Table 2 summarizes the operating conditions for the desulphurization tests. The operating factors studied were the following: bed temperature (600–800 °C), $H_2O/H_2S$ mass ratio in the inlet gas (0–45 g/g), type of sewage sludge ash (combustion ash or gasification ash) and type of $H_2S$-containing gas ($H_2S/N_2$ mixture or synthetic gasification gas). Blank tests (with no bed material) were performed at the different temperatures and gas atmospheres in order to assess any side effect of the experimental setup caused, for example, by the reaction of $H_2S$ with the hot metal parts (made of steel) at the reactor inlet and outlet. Experimental uncertainty was evaluated through three replicates performed at intermediate values of temperature (700 °C) and $H_2O/H_2S$ mass ratio (22.5 g/g) when feeding the $H_2S/N_2$ mixture. The impact of the factors was

**Table 2**
Operating conditions in the desulphurization tests.

| Experiment | Origin of sewage sludge ash | Synthetic gas mixture | Temperature (°C) | $H_2O/H_2S$ mass ratio | Test duration (min) |
|---|---|---|---|---|---|
| 1 | Combustion | $H_2S/N_2$ | 600 | 0 | 300 |
| 2 | Combustion | $H_2S/N_2$ | 800 | 0 | 390 |
| 3 | Combustion | $H_2S/N_2$ | 600 | 45 | 120 |
| 4 | Combustion | $H_2S/N_2$ | 800 | 45 | 120 |
| 5, 6, 7 | Combustion | $H_2S/N_2$ | 700 | 22.5 | 120 |
| 8 | Gasification | $H_2S/N_2$ | 600 | 0 | 120 |
| 9 | Gasification | $H_2S/N_2$ | 800 | 0 | 390 |
| 10 | Gasification | $H_2S/N_2$ | 600 | 45 | 120 |
| 11 | Gasification | $H_2S/N_2$ | 800 | 45 | 120 |
| 12, 13, 14 | Gasification | $H_2S/N_2$ | 700 | 22.5 | 120 |
| 15 | Blank run | $H_2S/N_2$ | 600 | 0 | 120 |
| 16 | Blank run | $H_2S/N_2$ | 800 | 0 | 120 |
| 17 | Blank run | $H_2S/N_2$ | 600 | 45 | 120 |
| 18 | Blank run | $H_2S/N_2$ | 800 | 45 | 120 |
| 19 | Blank run | $H_2S/N_2$ | 700 | 22.5 | 120 |
| 20 | Combustion | Gasification gas | 600 | 0 | 240 |
| 21 | Combustion | Gasification gas | 800 | 0 | 240 |
| 22 | Combustion | Gasification gas | 600 | 45 | 120 |
| 23 | Combustion | Gasification gas | 800 | 45 | 120 |
| 24 | Gasification | Gasification gas | 600 | 0 | 120 |
| 25 | Gasification | Gasification gas | 800 | 0 | 240 |
| 26 | Gasification | Gasification gas | 600 | 45 | 120 |
| 27 | Gasification | Gasification gas | 800 | 45 | 120 |
| 28 | Blank run | Gasification gas | 600 | 0 | 120 |
| 29 | Blank run | Gasification gas | 800 | 0 | 240 |
| 30 | Blank run | Gasification gas | 600 | 45 | 120 |
| 31 | Blank run | Gasification gas | 800 | 45 | 120 |

**Table 3**
Characterization of the ash samples obtained in the combustion and gasification of sewage sludge.

| | Sewage sludge combustion ash | Sewage sludge gasification ash |
|---|---|---|
| *Ultimate analysis* | | |
| C (wt.%) | 0.15 | 3.14 |
| H (wt.%) | n.d.[a] | n.d.[a] |
| N (wt.%) | 0.28 | 0.77 |
| S (wt.%) | 0.46 | 0.41 |
| BET surface ($m^2\ g^{-1}$) | 6.5 | 6.7 |
| Pore volume ($cm^3\ g^{-1}$) | 0.02 | 0.02 |
| Average pore size (nm) | 12.0 | 10.9 |
| *Metal content ($mg\ g_{ash}^{-1}$)* | | |
| Al | 52 | 61 |
| Ca | 65 | 84 |
| Fe | 192 | 116 |
| K | 14 | n.a.[b] |
| P | 63 | 51 |
| Mg | 17 | n.a.[b] |
| Na | 4 | n.a.[b] |
| Si | 122 | n.a.[b] |
| Ti | 4 | n.a.[b] |

[a] Not detected.
[b] Not analyzed.

statistically analyzed by means of analysis of variance ANOVA (confidence level of 95% for the F-distribution). Design-Expert® 7 software (from Stat-Ease, Inc.) was used for this purpose. The use of coded levels for the factors (−1 for the lower limits and +1 for the upper limits) in the ANOVA analysis enables an easy identification of the term with the greatest influence: the higher the absolute value of the coefficient, the more influential the factor. Although the type of sewage sludge ash is not a numerical factor, a coded value of −1 was assigned to the combustion ash and +1 to the gasification ash in order to obtain comparable coefficients from the ANOVA analysis.

The desulphurization tests performed at the laboratory were also theoretically simulated to determine the maximum amount of $H_2S$ that could be removed from the gas from a thermodynamic point of view. HSC Chemistry® 6.1 software was used for this purpose. This software uses the Gibbs energy minimization method to calculate the amounts of products at equilibrium in isothermal and isobaric conditions. The reaction system must be specified for the calculations.

## 3. Results and discussion

The characterization results of the fresh ash samples are presented in Section 3.1. After that, desulphurization performance results are shown and discussed in two different sections according to the gas mixture used (Sections 3.2 and 3.3). The $H_2S$ breakthrough curves and the sulphur content in the solid samples (expected and measured data) are the main results evaluated.

### 3.1. Characterization of the fresh ash samples

Table 3 summarizes some characterization results of the ash samples resulting from combustion and gasification of sewage sludge. Both solids contained a small fraction of sulphur and some amount of carbon was also present in the gasification ash (around 3 wt.%). The surface properties of sewage sludge ash are not good enough for its use as an adsorbent material, but its desulphurization potential is based on its metallic content. The main metals detected by ICP–OES were Fe, Si, Ca and Al. According to the thermodynamic study reported by Westmoreland and Harrison [21] concerning the desulphurization potential of different metal oxides, Ca and Fe oxides are able to react with $H_2S$ to form metal sulphides, so both ash samples are potential sulphur sorbents. Some differences were found in the metal content of the solids, which might indicate that the ash fraction of sewage sludge did not remained completely inert during the combustion and gasification processes. Heterogeneity of sewage sludge may also explain these differences. Particularly striking is the case of Fe content which was much lower in the gasification ash. Part of the Fe content in the raw sewage sludge could be in the form of iron chloride ($FeCl_3$) as a result of the use of this compound as a coagulant agent during the wastewater treatment. During combustion, excess oxygen appears to favour the retention of Fe in the ash in the oxide form. However, during the gasification process, the reduced presence of oxygen prevents the total conversion of $FeCl_3$ to iron oxides, so some amount of Fe could leave the reactor in the gas phase, as $FeCl_3$ evaporates at 315 °C [22].

Fig. 2 shows the XRD patterns of the combustion ash and gasification ash before the desulphurization tests. Species such as quartz, calcite, iron oxides and different calcium and iron phosphates were detected in the ash samples. The oxidation state of Fe is one of the main differences in the XRD patterns: Fe appears in the form of hematite ($Fe_2O_3$) in the combustion ash and in the form of magnetite ($Fe_3O_4$) in the gasification ash. Concordantly, the reddish colour characteristic of hematite was only observed on the combustion ash.

### 3.2. Desulphurization performance: $H_2S/N_2$ mixture as inlet gas

Different tolerable sulphur levels can be found in the literature depending on the gas application. For instance, the $H_2S$ concentration limit ranges between 20 and 750 ppmv for gas turbine application [14]. An intermediate value of 100 ppmv has been used in this work to define the $H_2S$ breakthrough time.

The $H_2S$ breakthrough curves obtained at the reactor outlet when feeding the dry and moist $H_2S/N_2$ mixtures are depicted in Fig. 3 as a function of temperature and type of ash. An exit gas essentially free of $H_2S$ was obtained during 300 min and 260 min by using the combustion ash and the gasification ash, respectively, at 800 °C and under dry conditions (Fig. 3a). However, when steam was present in the reaction medium, the $H_2S$ breakthrough time corresponding to the combustion ash was reduced to 50 min, while the gasification ash showed a complete loss of its capacity to remove $H_2S$ (Fig. 3b). According to the general reaction of metal oxides with $H_2S$ (1), thermodynamics predicts a negative effect of steam on the equilibrium between $H_2S$ and metal oxide sorbents because of the simultaneous regeneration of the spent metal sulphides:

$$Me_xO_y\ (s) + y\ H_2S\ (g) \leftrightarrow Me_xS_y\ (s) + y\ H_2O\ (g) \quad \Delta H < 0 \qquad (1)$$

Experimental results reported in the literature show different steam impact levels on the sulphidation rate depending on the sorbent material and the operating conditions [15]. For instance, Kim et al. studied the effect of steam on $H_2S$ removal by a ZnO sorbent and found that the presence of 45% steam reduced the $H_2S$ breakthrough time by almost half at 363 °C [23]. In general, the effect of steam on the sulphur sorbent performance is expected to be more severe at higher temperatures, but there are not many studies concerning this effect [15]. In the present work, the $H_2S$ breakthrough time was reduced by 85% in the presence of 30% steam when testing the combustion ash at 600–800 °C, while the gasification ash showed even higher loss in its sulphur capture capacity as a consequence of their different metallic phases. The presence of carbon in the gasification ash also seemed to slightly affect its desulphurization performance. The downward trend

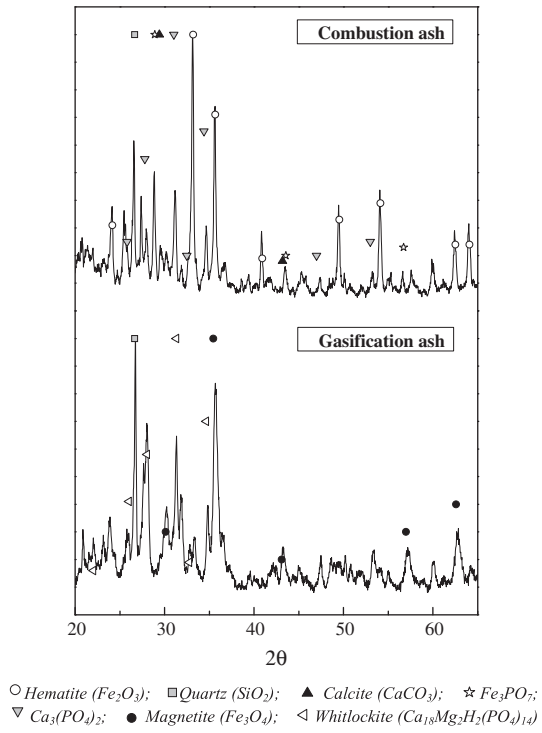


**Fig. 2.** XRD patterns of the fresh samples of sewage sludge combustion ash and sewage sludge gasification ash.

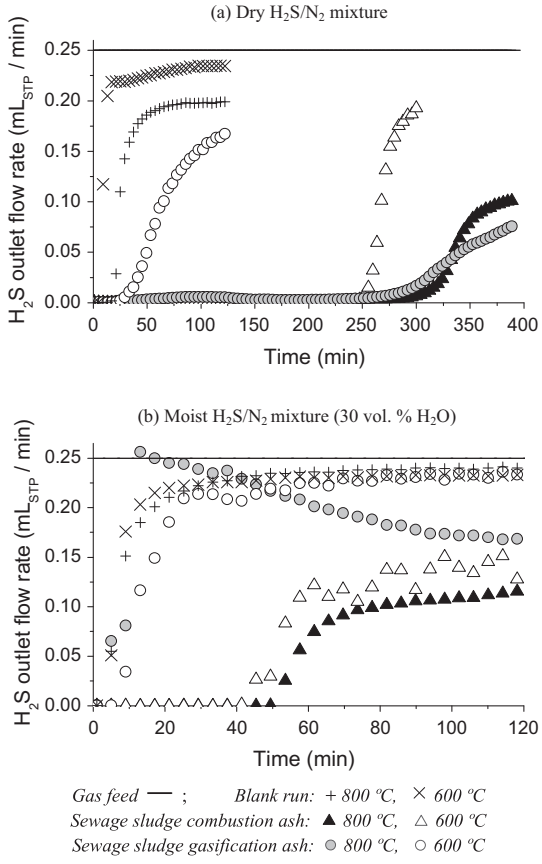


**Fig. 3.** $H_2S$ breakthrough curves: evolution of the $H_2S$ flow rate ($mL_{STP}\ min^{-1}$) leaving the reactor when feeding the $H_2S/N_2$ mixture.

observed in the $H_2S$ outlet flow at 800 °C (Fig. 3b) could be related to the steam gasification of the carbon present in the gasification ash. Ultimate analyses of the gasification ash before and after the experiment confirm this, as the carbon content was reduced from 3.14 to 0.25 wt.%.

The presence of steam in the gas atmosphere also affected the blank run results. As is well known, susceptible alloys, especially steels, react with $H_2S$ forming metal sulphides as corrosion by-products. This could explain the reduced $H_2S$ outlet flow rate in the blank runs with respect to the inlet gas, particularly at 800 °C and under dry operating conditions (Fig. 3a). The hot metal parts in the experimental setup did not appear to react with $H_2S$ under wet conditions (Fig. 3b) since, as discussed above, the formation of metal sulphides from metal oxides is restricted by the presence of steam.

The amount of $H_2S$ ($mL_{STP}$) removed from the gas up to the breakthrough time was calculated using data from the blank runs as a reference:

$$V_{H_2S\ \text{removed up to breakthrough time}} = V_{H_2S\ \text{blank}} - V_{H_2S\ \text{experiment}} \quad (2)$$

where $V_{H_2S\ \text{experiment}}$ is the amount of $H_2S$ ($mL_{STP}$) leaving the reactor up to the $H_2S$ breakthrough time during each experiment and $V_{H_2S\ \text{blank}}$ is the amount of $H_2S$ ($mL_{STP}$) leaving the reactor in the blank run during the same experimental time. These $H_2S$ outlet volumes were calculated by integration of the area under the breakthrough curves (Fig. 3), considering only the flow rate data up to the breakthrough time. The amounts of $H_2S$ removed from the gas up to the breakthrough time are included in Table 4. These data have been statistically evaluated by analysis of variance (Table 5). Although the presence of a significant curvature prevents the use of the linear regression model obtained from the experimental design used, the relative influence of the factors can be assessed by the coefficients shown in Table 5. The existence of curvature appears to be due to the sharp reduction of the $H_2S$ breakthrough time when steam was present in the reaction medium. The three studied factors (temperature, $H_2O/H_2S$ and ash type), as well as their interactions, significantly affect the amount of $H_2S$ removed from the gas up to the breakthrough time ($p$-value < 0.0001). The $H_2O/H_2S$ ratio is the most influential factor ($\beta_{H_2O/H_2S} = -17.76$). The higher the presence of steam, the smaller the amount of $H_2S$ removed from gas. The origin of the sewage sludge ash is also a key factor in the $H_2S$ removal process ($\beta_{\text{Ash type}} = -8.91$). Larger amounts of $H_2S$ can be removed from the gas with the combustion ash than with the gasification ash, especially at the lowest temperature. For instance, 54 $mL_{STP}$ of $H_2S$ were removed from the dry gas up to the breakthrough time using the combustion ash at 600 °C, while the gasification ash only removed 4 $mL_{STP}$ of $H_2S$ before reaching the breakthrough time (Table 4). Non-significant differences in the surface features of both solids were found (Table 3), so that the difference in their desulphurization performances must be related to ash composition. On the one hand, gasification ash contains some amount of carbon that could hinder the access of $H_2S$ to the metallic sites. However, this amount of carbon (3.14 wt.%) does not appear large enough to be the only cause for the observed differences. As discussed in Section 3.1, metal content and metallic species detected in both types of sewage sludge ash were not exactly the same as a consequence of the different reactive atmospheres in the combustion and gasification processes. As discussed above, one of the main differences in the composition of the ash samples was related to Fe content, which was detected in the form of $Fe_2O_3$ in the combustion ash and as $Fe_3O_4$ in the gasification ash. Yoshimura et al. [24] analyzed $Fe_2O_3$ and $Fe_3O_4$ samples after sulphidation with $H_2S$ at 400 °C and the patterns obtained by Extended X-ray Absorption Fine Structure (EXAFS) showed that the intensity of the peak corresponding to Fe–S coordination after sulphidation of $Fe_3O_4$ was lower than that in the sulphided sample

**Table 4**
Desulphurization performance results: $H_2S$ removed from the gas up to the breakthrough time and sulphur content in the solid samples after the desulphurization tests (measured and expected data).

| Gas mixture | Ash type | $H_2O/H_2S$ mass ratio | Temperature (°C) | $V_{H_2S\ removed\ to\ breakthrough\ time}$ ($mL_{STP}$) | Sulphur content by ultimate analysis (mg S $g_{ash}^{-1}$) [a] | Expected sulphur content (mg S $g_{ash}^{-1}$) |
|---|---|---|---|---|---|---|
| $H_2S/N_2$ | Sewage sludge combustion ash | 0 | 600 | 54 | 58 ± 1 | 92 |
| | | 0 | 800 | 54 | 63 ± 4 | 100 |
| | | 45 | 600 | 7 | 21.5 ± 0.8 | 29 |
| | | 45 | 800 | 9 | 1.4 ± 0.1 | 32 |
| | | 22.5 | 700 | 14 | 20.8 ± 0.6 | 38 |
| | | 22.5 | 700 | 12 | 18.8 ± 0.2 | 37 |
| | | 22.5 | 700 | 12 | 16.6 ± 0.6 | 36 |
| $H_2S/N_2$ | Sewage sludge gasification ash | 0 | 600 | 4 | 23.2 ± 0.5 | 27 |
| | | 0 | 800 | 48 | 64.4 ± 0.7 | 100 |
| | | 45 | 600 | 2 | 4.9 ± 0.2 | 7 |
| | | 45 | 800 | 0 | 1.1 ± 0.1 | 8 |
| | | 22.5 | 700 | 0 | 14.1 ± 0.5 | 17 |
| | | 22.5 | 700 | 0 | 12.6 ± 0.5 | 18 |
| | | 22.5 | 700 | 0 | 11.8 ± 0.4 | 17 |
| Synthetic gasification gas | Sewage sludge combustion ash | 0 | 600 | 36 | 46.4 ± 0.6 | 64 |
| | | 0 | 800 | 1 | 55 ± 4 | 53 |
| | | 45 | 600 | 4 | 26.8 ± 0.5 | 32 |
| | | 45 | 800 | 1 | 8.5 ± 0.5 | 11 |
| Synthetic gasification gas | Sewage sludge gasification ash | 0 | 600 | 1 | 20 ± 1 | 19 |
| | | 0 | 800 | 0 | 33.2 ± 0.6 | 31 |
| | | 45 | 600 | 1 | 5.8 ± 0.2 | 11 |
| | | 45 | 800 | 1 | 4.5 ± 0.5 | 8 |

[a] Mean value ± standard deviation.

**Table 5**
ANOVA results and linear regression coefficients for the amount of $H_2S$ removed from the gas up to the breakthrough time under the $H_2S/N_2$ atmosphere.

| | Sum of squares (SS) | Degrees of freedom | *p*-Value | Coefficient ($\beta$)[a] |
|---|---|---|---|---|
| Model | 4544.22 | 7 | <0.0001 | – |
| Intercept | – | 1 | – | 22.36 ± 1.20 |
| T | 238.71 | 1 | <0.0001 | 5.46 ± 1.20 |
| $H_2O/H_2S$ | 2524.05 | 1 | <0.0001 | −17.76 ± 1.20 |
| Ash type | 635.46 | 1 | <0.0001 | −8.91 ± 1.20 |
| T-$H_2O/H_2S$ | 230.05 | 1 | <0.0001 | −5.36 ± 1.20 |
| T-ash type | 195.03 | 1 | <0.0001 | 4.94 ± 1.20 |
| $H_2O/H_2S$-ash type | 213.21 | 1 | <0.0001 | 5.16 ± 1.20 |
| T-$H_2O/H_2S$-ash type | 277.30 | 1 | <0.0001 | −5.89 ± 1.20 |
| Curvature | 883.20 | 2 | <0.0001 | – |
| Pure error | 2.67 | 4 | – | – |
| Corrected total | 5430.09 | 13 | – | – |
| $R^2$ = 0.84 (=$SS_{model}/SS_{corrected\ total}$) | | | | |

[a] 95% Confidence interval for the regression coefficients.

of $Fe_2O_3$, thus indicating more difficulty in sulphiding $Fe_3O_4$ at low temperatures. This fact, as well as the lower Fe content detected in the gasification ash, may explain the rapid saturation of the gasification ash. The difference in the desulphurization performance of both solids was reduced with increasing temperature, probably due to a significant increase in the $Fe_3O_4$ sulphidation reaction rate.

As the desulphurization process is based on gas–solid reactions, the sulphidation rate is expected to be controlled by chemical reaction kinetics or by mass transfer. The effect of the reaction temperature on the amount of $H_2S$ removed from the gas up to the breakthrough time is clearly dependent on the ash type and presence of moisture in the gas ($\beta_T = 5.46$, $\beta_{T\text{-Ash type}} = 4.94$, $\beta_{T\text{-}H_2O/H_2S} = -5.36$). Thus, temperature hardly affected the removed amount of $H_2S$ under wet operating conditions and/or when using the combustion ash, whereas a great positive impact was observed when the gasification ash was used at dry conditions.

In addition to the evaluation of the $H_2S$ breakthrough curves, sulphur content in the solid samples was measured after the desulphurization tests by means of an elemental analyzer. These results are included in Table 4. Only a few of these data are directly comparable with each other because they refer to the total amount of sulphur removed in each complete experiment and the duration of the experiments was not the same in all cases. Comparable data show lower sulphur content in the gasification ash than in the combustion ash after the experiments performed at 600 and 700 °C, while similar sulphur contents were detected in both solids after the experiments performed at 800 °C, pointing to similar sulphidation reaction rates of $Fe_2O_3$ and $Fe_3O_4$ at higher temperatures. The highest sulphur content detected in both types of ash was around 63–64 mg S $g_{ash}^{-1}$ after operating at 800 °C and dry conditions during 390 min.

In order to check the sulphur mass balance, the expected sulphur content in the used ash samples has been calculated assuming that all the amount of $H_2S$ removed from the gas remained in the solid after the desulphurization test:

$$\text{Expected sulphur content (mg S } g_{ash}^{-1}) = \frac{V_{H_2S\ blank} - V_{H_2S\ experiment}}{22.4} \cdot 32 \quad (3)$$

where $V_{H_2S\ experiment}$ is the amount of $H_2S$ ($mL_{STP}$) leaving the reactor during each complete experiment, $V_{H2S\ blank}$ is the amount of $H_2S$ ($mL_{STP}$) leaving the reactor during the blank run (extrapolating to the duration of the experiment where this differs), 22.4 is the

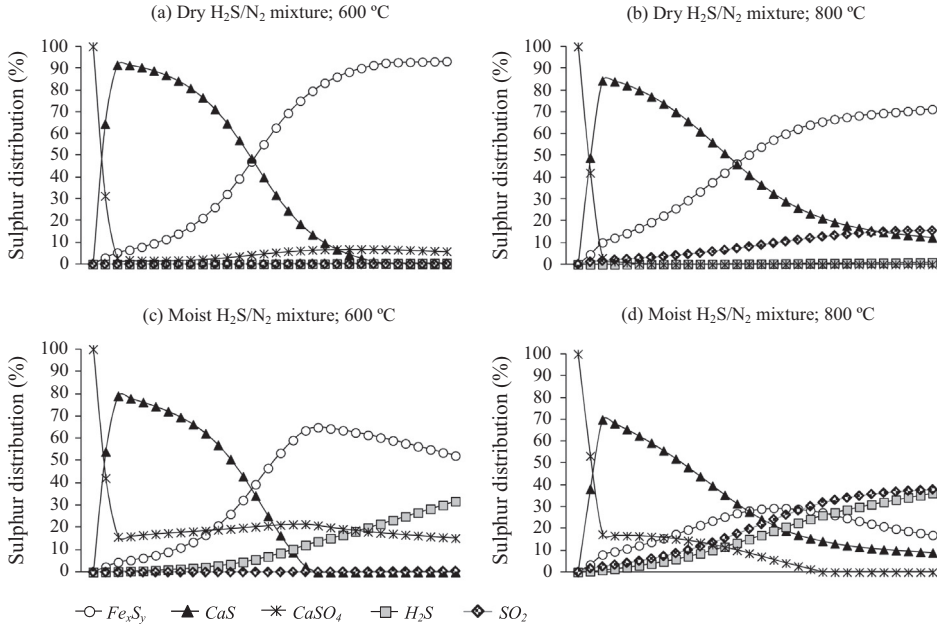


**Fig. 4.** Evolution of the sulphur distribution into the main sulphur-containing species at equilibrium conditions ($H_2S/N_2$ mixture as inlet gas).

volume of one ideal gas mole at STP ($mL_{STP}$ $mmol^{-1}$) and 32 is the sulphur atomic mass (mg $mmol^{-1}$). The expected sulphur contents are included in Table 4. These calculated data are higher than the experimental results obtained from the elemental analyzer. This suggests that other sulphur-containing gases not detected by the micro GC could be formed during the desulphurization tests. Especially striking is the difference between the results obtained in experiment 4 (800 °C and moist $H_2S/N_2$ mixture), for which the expected sulphur content in the solid was around 32 mg S $g_{ash}^{-1}$, while the elemental analyzer only detected 1.4 mg S $g_{ash}^{-1}$. This latter value was significantly lower than that detected at 600 °C (21.5 mg S $g_{ash}^{-1}$), so the final sulphur content of the solid under wet conditions was favoured at low temperatures.

Equilibrium simulations were conducted in order to try to explain these observed differences from a thermodynamic point of view. Fig. 4 shows the evolution of the theoretical distribution of sulphur into the main sulphur-containing species resulting from the equilibrium simulation: $Fe_xS_y$, CaS, $H_2S$, $CaSO_4$ and $SO_2$. As the composition of the solid evolves over time (discontinuous bed of solid and continuous feed of gas), successive simulations for small time intervals (10 min) were performed in order to obtain an approximation to the real process during 300 min. The amount of Ca (in the form of CaO) and Fe (in the form of $Fe_2O_3$) present in 1 g of sewage sludge ash was the initial solid for the first simulation. The gas input for each equilibrium calculation was the amount of gas fed during 10 min of experiment, while the solid input was the solid resulting from the previous simulation. Successive gas–solid contact intervals of 10 min are represented in Fig. 4. As can be noted, the formation of CaS is thermodynamically favoured over the formation of $Fe_xS_y$ in the early stage of the desulphurization process. The available amount of Ca decreases and $Fe_xS_y$ formation becomes more significant while the desulphurization process progresses. The remaining fraction of $H_2S$ in the gas stream increases at high temperature (exothermic nature of the sulphidation reaction) and in the presence of steam. Besides the formation of metal sulphides, thermodynamics predicts the formation of $SO_2$ and $CaSO_4$ (as a result of the reaction of the formed $SO_2$ with CaO). The formation of both $SO_2$ and $CaSO_4$ is favoured at the presence of steam. The temperature increase shifts the reaction to $SO_2$ formation. Thus, $SO_2$ formation may be the reason for the observed differences in the expected and measured sulphur contents in the ash samples. Maximum sulphur loadings of 107, 103, 42 and 38 mg S $g_{ash}^{-1}$ were predicted for experiments 1, 2, 3 and 4, respectively. Experimental results obtained with the elemental analyzer were 46%, 39%, 49% and 96% lower than the theoretical results, respectively (Table 4).

Fig. 5 shows a back-scattered electron image of the ash resulting from experiment 2. Numbers in Fig. 5 indicate the points where the elemental composition was analyzed. The atomic fractions obtained by EDX in the different superficial points are shown in Table 6. As can be noted, ash presents a heterogeneous surface. C, O, Na, Mg, Al, Si, P, S, Ca, Fe and Zn are detected along the surface in different fractions. It should be noted that the points with the highest atomic percentage of S (23.8% in point 1 and 23.7% in point 7) are also those with the highest Fe content (35.9% and 25.3%, respectively), thus suggesting the formation of either iron sulphides or iron sulphates. On the other hand, S was hardly detected in other points, such as in point 4 (mainly formed by O and Si in the form of $SiO_2$) or in point 6 in which, despite of the high fraction of Fe (16.1%), only 0.4 atomic % S was found. In this case, as well as in points 2 and 3, the high presence of Fe is linked with a high presence of P, which indicates the presence of iron phosphates.

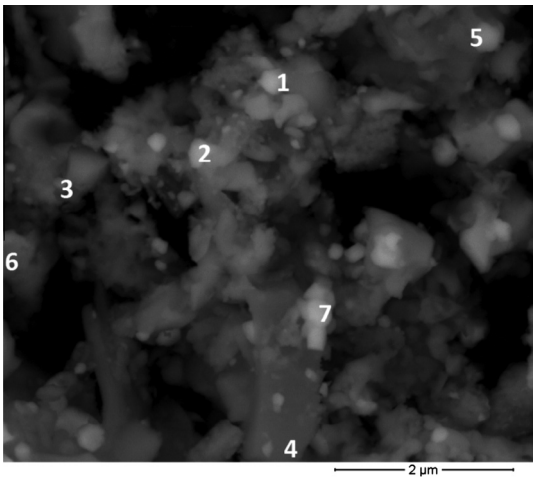


**Fig. 5.** Back-scattered electron image of the ash resulting from experiment 2.

**Table 6**
Elemental composition (SEM/EDX) on different superficial points of the ash resulting from experiment 2.

| Point in Fig. 5 | Elemental composition (atomic percentage) | | | | | | | | | | |
|---|---|---|---|---|---|---|---|---|---|---|---|
| | C | O | Na | Mg | Al | Si | P | S | Ca | Fe | Zn |
| 1 | | 29.6 | | 1.0 | 2.0 | 1.7 | 4.3 | 23.8 | 1.6 | 35.9 | |
| 2 | 0.8 | 57.9 | | 3.4 | 3.7 | 2.4 | 13.3 | 1.1 | 6.6 | 10.6 | 0.3 |
| 3 | 2.2 | 45.9 | 0.5 | 1.5 | 5.7 | 9.2 | 11.5 | 8.6 | 6.3 | 8.8 | |
| 4 | 0.7 | 69.0 | 0.3 | 0.1 | 0.3 | 27.6 | 0.6 | | | 0.9 | |
| 5 | 0.9 | 50.7 | 0.3 | 3.3 | 6.2 | 9.3 | 12.2 | 4.6 | 7.0 | 5.6 | |
| 6 | 1.6 | 57.9 | | 2.4 | 1.4 | 4.0 | 11.7 | 0.4 | 4.1 | 16.1 | 0.4 |
| 7 | | 33.5 | | 0.8 | 1.3 | 7.8 | 3.5 | 23.7 | 4.1 | 25.3 | |

Fig. 6 shows the XPS spectra in S 2p region of the ash resulting from experiment 2. Several doublets can be fitted to the experimental signal, indicating different chemical states of sulphur in the ash surface. The peak located between 160 and 164 eV is indicative of $S_n^{2-}$ (metal sulphides), but other oxidized sulphur forms have also been detected (169 eV: $SO_4^{2-}$).

### 3.3. Desulphurization performance: synthetic gasification gas as inlet gas

The $H_2S$ breakthrough curves obtained when feeding the dry and moist (30 vol.% $H_2O$) synthetic gasification gases are depicted in Fig. 7 as a function of temperature and type of ash. The $H_2S$ concentration in the outlet gasification gas remained below 100 ppmv for less time than in the previous case ($H_2S/N_2$ mixture). Unlike occurring with the $H_2S/N_2$ mixture, a significant amount of $H_2S$ was detected in the outlet gasification gas from almost the beginning of all the experiments (Fig. 7). In this case, the $H_2S$ breakthrough time was longer than 20 min only by using the combustion ash at 600 °C and dry conditions (165 min). This breakthrough time was in turn significantly lower than that obtained for the $H_2S/N_2$ mixture under the same operating conditions (260 min). Reduction of iron oxides present in sewage sludge ash may explain this observed behaviour. As discussed in the literature [17,21,25], the presence of CO and $H_2$ in the gasification gas creates a reducing atmosphere that causes the conversion of $Fe_3O_4$ and $Fe_2O_3$ to FeO or even to Fe in the temperature range of 700–1000 °C. FeO and Fe show less favourable sulphidation equilibrium, which led to a reduction in the sulphur capture capacity [25]. The temperature rise from 600 to 800 °C was found to be detrimental for the $H_2S$ removal capacity of the combustion ash, probably as a consequence of the higher reduction rate of $Fe_2O_3$ to FeO at 800 °C (Fig. 7a). However, the $H_2S$ removal capacity of the gasification ash improved at higher temperature. Thus, the impact of temperature on $H_2S$ removal from the gasification gas is the result of the competition of reduction and sulphidation reaction rates. The influence of the other factors (presence of steam and type of sludge ash) on $H_2S$ removal from the synthetic gasification gas was similar to the previous case.

Table 4 shows the results of the sulphur content measured in the ash samples after the experiments performed with the synthetic gasification gas, as well as data calculated according to the sulphur mass balance (Eq. 3). Even though the longest $H_2S$ breakthrough time was obtained for the combustion ash at 600 °C, the highest sulphur loading was detected in the ash used at 800 °C (46 vs. 55 mg S $g_{ash}^{-1}$ after 240 min). The different shape of the $H_2S$ breakthrough curves explains this result. After the desulphurization of the moist gasification gas, the highest sulphur content was found in the combustion ash operating at 600 °C (26.8 mg S $g_{ash}^{-1}$ after 120 min). This value was slightly higher than that obtained after the desulphurization of the moist $H_2S/N_2$ mixture.

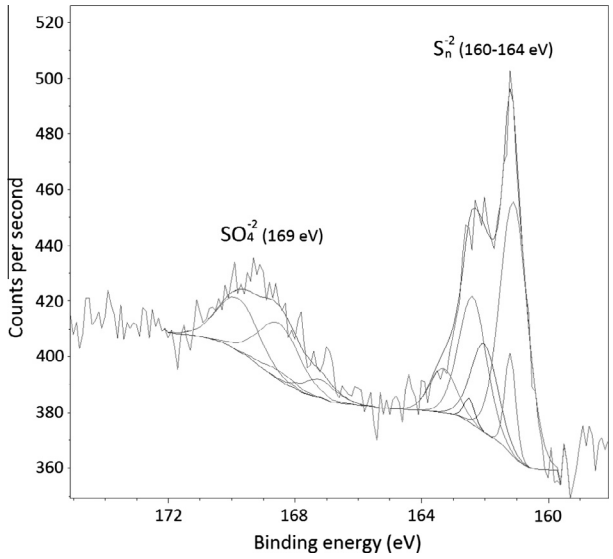


**Fig. 6.** XPS spectra in the S 2p region corresponding to the ash resulting from experiment 2.

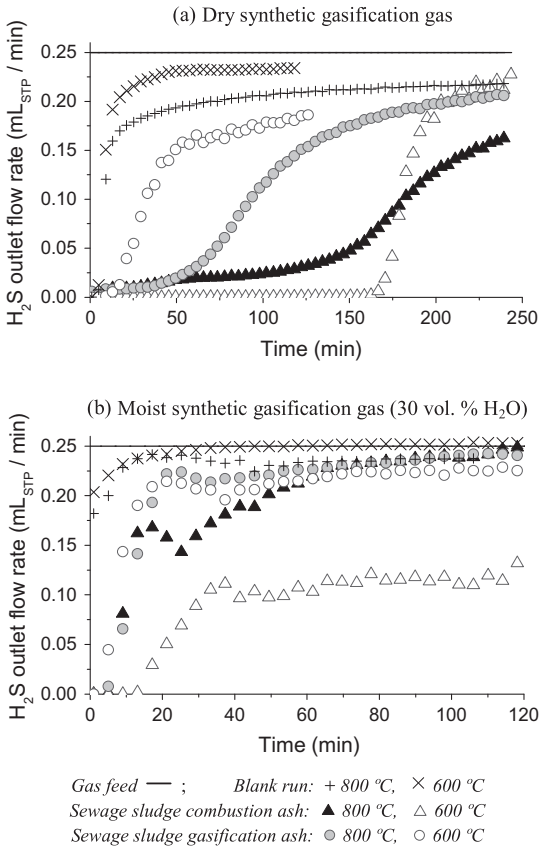


**Fig. 7.** $H_2S$ breakthrough curves: evolution of the $H_2S$ flow rate ($mL_{STP}$ $tmin^{-1}$) leaving the reactor when feeding the synthetic gasification gas.

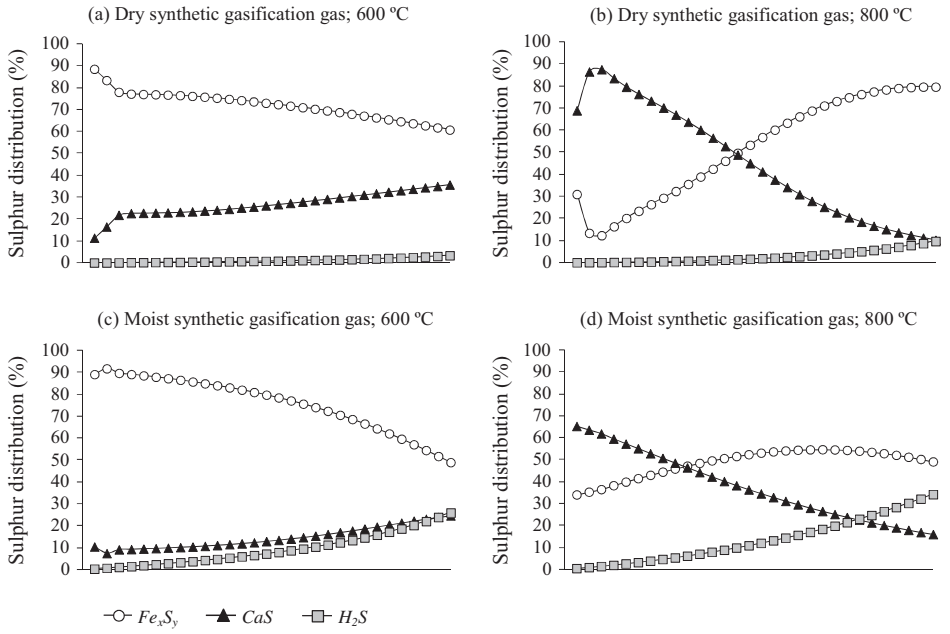


**Fig. 8.** Evolution of the sulphur distribution into the main sulphur-containing species at equilibrium conditions (synthetic gasification gas as inlet gas).

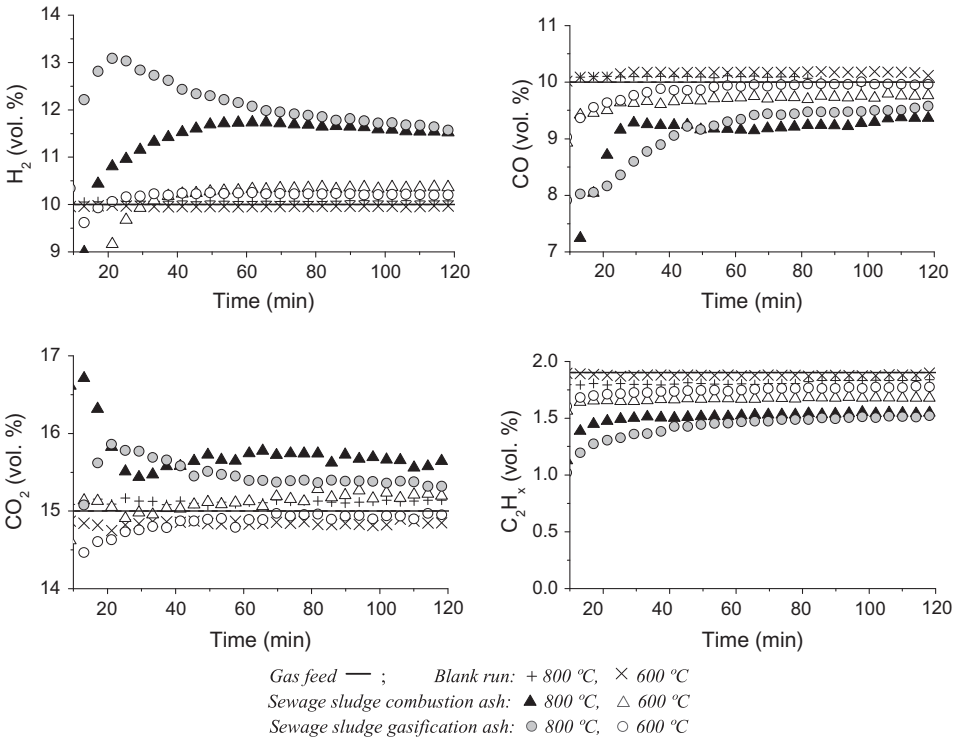


**Fig. 9.** Evolution of the outlet fractions of $H_2$, CO, $CO_2$ and $C_2H_x$ (dry basis) when feeding the moist synthetic gasification gas.

Thermodynamic data obtained for the synthetic gasification gas feed are shown in Fig. 8. In this case, neither $SO_2$ nor $CaSO_4$ are present at equilibrium conditions since the reducing atmosphere created by the gasification gas prevents its formation. $H_2S$, CaS and $Fe_xS_y$ are the main sulphur-containing species and COS is also formed in a very low proportion. Some authors have experimentally detected the formation of COS in the reducing environment of the gasification gas ($H_2S + CO_2 \leftrightarrow COS + H_2O$) [26], which could explain the observed differences in the expected and measured sulphur contents in the ash samples. Maximum sulphur loadings of 85, 84, 42 and 41 mg S $g_{ash}^{-1}$ are theoretically predicted for experiments 20, 21, 22 and 23, respectively. Experimental results measured with the elemental analyzer were 46%, 35%, 36% and 79% lower than the theoretical results, respectively (Table 4). Comparison of Figs. 4 and 8 shows a great impact of the gas atmosphere on the distribution of sulphur between CaS and $Fe_xS_y$. The presence of $CO_2$ in the gasification gas can explain this difference since this is the responsible gas for the carbonation reaction of CaO ($CaO + CO_2 \leftrightarrow CaCO_3$). Excess $CO_2$ shifts the reaction to the formation of $CaCO_3$, especially at low temperature, thus limiting the formation of CaS from CaO. Thus, besides the reduction of the iron oxides, carbonation of CaO may also contribute to the

different results obtained for the $H_2S/N_2$ mixture and the synthetic gasification gas.

In addition to $H_2S$ removal, the composition of the inlet gasification gas was modified during some desulphurization tests, thus suggesting some catalytic activity of sewage sludge ash. The evolution of the outlet concentrations of $H_2$, CO, $CO_2$ and $C_2H_x$ when feeding the moist synthetic gasification gas is depicted in Fig. 9. As can be noted, the use of both types of sewage sludge ash at 800 °C led to a slight increase in the fractions of $H_2$ and $CO_2$ and a decrease in the percentage of CO with respect to the inlet values. This could be attributed to an enhancement of the water–gas shift reaction ($CO + H_2O \leftrightarrow CO_2 + H_2$). Fe content in sewage sludge ash may explain this catalytic activity [27]. Furthermore, the fraction of $C_2H_x$ was slightly reduced, suggesting an enhancement of steam reforming reactions. The fraction of $CH_4$ (not shown in Fig. 9) was not modified in any case (4.0 vol.%). As shown in Fig. 9, the composition of the synthetic gasification gas was hardly modified during the blank runs and during the experiments performed at 600 °C.

## 4. Conclusions

The use of the solid by-products of combustion and gasification of sewage sludge for high-temperature desulphurization (600–800 °C) of different gases containing 5000 ppmv $H_2S$ has been evaluated in this work. In general, the gasification ash showed worse desulphurization ability than the combustion ash. Some differences in the composition of both solids may explain their different behaviour. Lower iron content was detected in the gasification ash (116 mg Fe $g_{ash}^{-1}$) than in the combustion ash (192 mg Fe $g_{ash}^{-1}$). Furthermore, iron was forming part of different crystalline species: $Fe_2O_3$ in the combustion ash and $Fe_3O_4$ in the gasification ash.

In the absence of interferences from other gases (gas atmosphere only composed of $H_2S$ and $N_2$), the $H_2S$ breakthrough time (<100 ppmv $H_2S$) was around 300 min by using the combustion ash at 800 °C. A final sulphur content of around 63 mg S $g_{ash}^{-1}$ was detected in this spent ash. The $H_2S$ breakthrough time was drastically reduced to a few minutes in the presence of 30% steam as a consequence of the simultaneous regeneration of the spent metal sulphides. Thus, the use of sewage sludge ash for $H_2S$ removal at 600–800 °C is only suitable for dry gas cleaning. The desulphurization process was also negatively affected by the reducing atmosphere created by the gasification gas due to the simultaneous reduction of $Fe_2O_3$ and $Fe_3O_4$ to FeO, whose sulphur capture capacity has been proved to be lower, and by the presence of $CO_2$ which causes the carbonation of CaO. Combustion ash at 600 °C led to the best results during desulphurization of the moist synthetic gasification gas (most realistic conditions), showing a $H_2S$ breakthrough time of 50 min and a final sulphur content of 27 mg S $g_{ash}^{-1}$ after 120 min of experiment.

$H_2S$ was the only sulphur-containing gas analyzed during the experiments. However, thermodynamic data pointed to the possible formation of other sulphur-containing gases during the desulphurization process, such as $SO_2$ or COS (this latter in a very low proportion). Therefore, the analysis of the $H_2S$ breakthrough curves alone can lead to misleading conclusions about the sulphur capture capacity of a sorbent material. In most cases, sulphur content detected by the elemental analyzer in the spent combustion ash was 35–50% lower than the maximum thermodynamic data calculated assuming that the total content of calcium and iron in the solid was in the form of CaO and $Fe_2O_3$, respectively.

## Acknowledgements

The authors gratefully acknowledge the financial support provided by the Spanish Ministry of Science and Technology (research project CTQ2010-20137) and the Spanish Ministry of Education (pre-doctoral grant awarded to N. Gil-Lalaguna, AP2009-3446). Authors also wish to thank the Servicio General de Apoyo a la Investigación at Universidad de Zaragoza and Laboratorio de Microscopías Avanzadas at Instituto de Nanociencia de Aragón for the XRD, ICP-OES, XPS and SEM/EDX analyses.

## References

[1] Rulkens W. Sewage sludge as a biomass resource for the production of energy: overview and assessment of the various options. Energy Fuel 2008;22:9–15.
[2] Fytili D, Zabaniotou A. Utilization of sewage sludge in EU application of old and new methods – a review. Renew Sust Energy Rev 2008;12:116–40.
[3] Manara P, Zabaniotou A. Towards sewage sludge based biofuels via thermochemical conversion – a review. Renew Sust Energy Rev 2012;16:2566–82.
[4] Gil-Lalaguna N, Sánchez JL, Murillo MB, Rodríguez E, Gea G. Air-steam gasification of sewage sludge in a fluidized bed. Influence of some operating conditions. Chem Eng J 2014;248:373–82.
[5] Abu El-Rub Z, Bramer EA, Brem G. Review of catalysts for tar elimination in biomass gasification processes. Ind Eng Chem Res 2004;43:6911–9.
[6] Yildirim O, Kiss AA, Hüser N, Leßmann K, Kenig EY. Reactive absorption in chemical process industry: a review on current activities. Chem Eng J 2012;213:371–91.
[7] Bagreev A, Bandosz TJ. On the mechanism of hydrogen sulfide removal from moist air on catalytic carbonaceous adsorbents. Ind Eng Chem Res 2005;44:530–8.
[8] Bandosz TJ. On the adsorption/oxidation of hydrogen sulfide on activated carbons at ambient temperatures. J Colloid Interface Sci 2002;246:1–20.
[9] Primavera A, Trovarelli A, Andreussi P, Dolcetti G. The effect of water in the low-temperature catalytic oxidation of hydrogen sulfide to sulfur over activated carbon. Appl Catal A-Gen 1998;173:185–92.
[10] Gutiérrez-Ortiz FJ, Aguilera PG, Ollero P. Biogas desulfurization by adsorption on thermally treated sewage-sludge. Sep Purif Technol 2014;123:200–13.
[11] Ros A, Montes-Morán M, Fuente E, Nevskaia DM, Martin MJ. Dried sludges and sludge-based chars for $H_2S$ removal at low temperature: influence of sewage sludge characteristics. Environ Sci Technol 2006;40:302–9.
[12] Ansari A, Bagreev A, Bandosz TJ. Effect of adsorbent composition on $H_2S$ removal on sewage sludge-based materials enriched with carbonaceous phase. Carbon 2005;43:1039–48.
[13] Yuan W, Bandosz TJ. Removal of hydrogen sulfide from biogas on sludge-derived adsorbents. Fuel 2007;86:2736–46.
[14] Meng X, Jong W, Pal R, Verkooijen AHM. In bed and downstream hot gas desulphurization during solid fuel gasification: a review. Fuel Process Technol 2010;91:964–81.
[15] Cheah S, Carpenter DL, Magrini-Bair KA. Review of mid- to high- temperature sulfur sorbents for desulphurization of biomass- and coal-derived syngas. Energy Fuel 2009;23:5291–307.
[16] Park NK, Lee DH, Lee JD, Chang WC, Ryu SO, Lee TJ. Effects of reduction of metal oxide sorbents on reactivity and physical properties during hot gas desulphurization in IGCC. Fuel 2005;84:2158–64.
[17] Tamhankar SS, Hasatani M, Wen CY. Kinetic studies on the reactions involved in the hot gas desulfurization using a regenerable iron oxide sorbent – I: Reduction and sulfidation of iron oxide. Chem Eng Sci 1981;36:1181–91.
[18] Álvarez-Rodríguez R, Clemente-Jul C. Hot gas desulphurisation with dolomite sorbent in coal gasification. Fuel 2008;87:3513–21.
[19] Elseviers WF, Verelst H. Transition metal oxides for hot gas desulphurization. Fuel 1999;78:601–12.
[20] García G, Cascarosa E, Ábrego J, Gonzalo A, Sánchez JL. Use of different residues for high temperature desulphurisation of gasification gas. Chem Eng J 2011;174:644–51.
[21] Westmoreland PR, Harrison DP. Evaluation of candidate solids for high-temperature desulfurization of low-btu gases. Environ Sci Technol 1976;10:659–61.
[22] Perry RH, Green DW. Perry's chemical engineer's handbook. 7th ed. New York: McGraw-Hill; 1999.
[23] Kim K, Jeon SK, Vo C, Park CS, Norbeck JM. Removal of $H_2S$ from steam-hydrogasifier product gas by zinc oxide sorbent. Ind Eng Chem Res 2007;46:5848–54.
[24] Yoshimura Y, Yasuda H, Sato T, Shimada H. Utilization of thermodynamic database in the systems using molybdate and iron based catalysis. Coal Sci Technol 1995;24:1275–8.
[25] Tseng TK, Chang HC, Chu H, Chen HT. Hydrogen sulfide removal from coal gas by the metal–ferrite sorbents made from the heavy metal wastewater sludge. J Hazard Mater 2008;160:482–8.
[26] Hepola J, Simell P. Sulphur poisoning of nickel-based hot gas cleaning catalysts in synthetic gasification gas. I. Effect of different process parameters. Appl Catal B-Environ 1997;14:287–303.
[27] Liu QS, Zhang QC, Ma WP, He RX, Kou LJ, Mou ZJ. Progress in water–gas-shift catalyst. Prog Chem 2005;17:389–98.

## ELSEVIER LICENSE
## TERMS AND CONDITIONS

Nov 18, 2014

This is a License Agreement between Noemí Gil ("You") and Elsevier ("Elsevier") provided by Copyright Clearance Center ("CCC"). The license consists of your order details, the terms and conditions provided by Elsevier, and the payment terms and conditions.

**All payments must be made in full to CCC. For payment instructions, please see information listed at the bottom of this form.**

| | |
|---|---|
| Supplier | Elsevier Limited<br>The Boulevard,Langford Lane<br>Kidlington,Oxford,OX5 1GB,UK |
| Registered Company Number | 1982084 |
| Customer name | Noemí Gil |
| Customer address | C/Mariano Esquillor s/n<br>Zaragoza, 50018 |
| License number | 3511870187669 |
| License date | Nov 18, 2014 |
| Licensed content publisher | Elsevier |
| Licensed content publication | Chemical Engineering Journal |
| Licensed content title | Air–steam gasification of sewage sludge in a fluidized bed. Influence of some operating conditions |
| Licensed content author | N. Gil-Lalaguna,J.L. Sánchez,M.B. Murillo,E. Rodríguez,G. Gea |
| Licensed content date | 15 July 2014 |
| Licensed content volume number | 248 |
| Licensed content issue number | n/a |
| Number of pages | 10 |
| Start Page | 373 |
| End Page | 382 |
| Type of Use | reuse in a thesis/dissertation |
| Portion | full article |
| Format | both print and electronic |
| Are you the author of this Elsevier article? | Yes |
| Will you be translating? | Yes |
| Number of languages | 1 |
| Languages | Spanish |
| Title of your thesis/dissertation | Estudio de la gasificación de lodos de EDAR en lecho fluidizado. Efecto de la atmósfera reactiva, evaluación energética y limpieza del gas producto |
| Expected completion date | Jan 2015 |
| Estimated size (number of pages) | 150 |

## ELSEVIER LICENSE
## TERMS AND CONDITIONS

Nov 18, 2014

This is a License Agreement between Noemí Gil ("You") and Elsevier ("Elsevier") provided by Copyright Clearance Center ("CCC"). The license consists of your order details, the terms and conditions provided by Elsevier, and the payment terms and conditions.

**All payments must be made in full to CCC. For payment instructions, please see information listed at the bottom of this form.**

| | |
|---|---|
| Supplier | Elsevier Limited<br>The Boulevard,Langford Lane<br>Kidlington,Oxford,OX5 1GB,UK |
| Registered Company Number | 1982084 |
| Customer name | Noemí Gil |
| Customer address | C/Mariano Esquillor s/n<br>Zaragoza, 50018 |
| License number | 3511870438485 |
| License date | Nov 18, 2014 |
| Licensed content publisher | Elsevier |
| Licensed content publication | Fuel |
| Licensed content title | Air-steam gasification of char derived from sewage sludge pyrolysis. Comparison with the gasification of sewage sludge |
| Licensed content author | N. Gil-Lalaguna,J.L. Sánchez,M.B. Murillo,V. Ruiz,G. Gea |
| Licensed content date | 1 August 2014 |
| Licensed content volume number | 129 |
| Licensed content issue number | n/a |
| Number of pages | 9 |
| Start Page | 147 |
| End Page | 155 |
| Type of Use | reuse in a thesis/dissertation |
| Intended publisher of new work | other |
| Portion | full article |
| Format | both print and electronic |
| Are you the author of this Elsevier article? | Yes |
| Will you be translating? | Yes |
| Number of languages | 1 |
| Languages | Spanish |
| Title of your thesis/dissertation | Estudio de la gasificación de lodos de EDAR en lecho fluidizado. Efecto de la atmósfera reactiva, evaluación energética y limpieza del gas producto |
| Expected completion date | Jan 2015 |

## ELSEVIER LICENSE
## TERMS AND CONDITIONS

Nov 18, 2014

This is a License Agreement between Noemí Gil ("You") and Elsevier ("Elsevier") provided by Copyright Clearance Center ("CCC"). The license consists of your order details, the terms and conditions provided by Elsevier, and the payment terms and conditions.

**All payments must be made in full to CCC. For payment instructions, please see information listed at the bottom of this form.**

| | |
|---|---|
| Supplier | Elsevier Limited<br>The Boulevard,Langford Lane<br>Kidlington,Oxford,OX5 1GB,UK |
| Registered Company Number | 1982084 |
| Customer name | Noemí Gil |
| Customer address | C/Mariano Esquillor s/n<br>Zaragoza, 50018 |
| License number | 3511870675551 |
| License date | Nov 18, 2014 |
| Licensed content publisher | Elsevier |
| Licensed content publication | Energy |
| Licensed content title | Energetic assessment of air-steam gasification of sewage sludge and of the integration of sewage sludge pyrolysis and air-steam gasification of char |
| Licensed content author | N. Gil-Lalaguna,J.L. Sánchez,M.B. Murillo,M. Atienza-Martínez,G. Gea |
| Licensed content date | 1 November 2014 |
| Licensed content volume number | 76 |
| Licensed content issue number | n/a |
| Number of pages | 11 |
| Start Page | 652 |
| End Page | 662 |
| Type of Use | reuse in a thesis/dissertation |
| Intended publisher of new work | other |
| Portion | full article |
| Format | both print and electronic |
| Are you the author of this Elsevier article? | Yes |
| Will you be translating? | Yes |
| Number of languages | 1 |
| Languages | Spanish |
| Title of your thesis/dissertation | Estudio de la gasificación de lodos de EDAR en lecho fluidizado. Efecto de la atmósfera reactiva, evaluación energética y limpieza del gas producto |

## ELSEVIER LICENSE
## TERMS AND CONDITIONS

Nov 18, 2014

This is a License Agreement between Noemí Gil ("You") and Elsevier ("Elsevier") provided by Copyright Clearance Center ("CCC"). The license consists of your order details, the terms and conditions provided by Elsevier, and the payment terms and conditions.

**All payments must be made in full to CCC. For payment instructions, please see information listed at the bottom of this form.**

| | |
|---|---|
| Supplier | Elsevier Limited<br>The Boulevard,Langford Lane<br>Kidlington,Oxford,OX5 1GB,UK |
| Registered Company Number | 1982084 |
| Customer name | Noemí Gil |
| Customer address | C/Mariano Esquillor s/n<br>Zaragoza, 50018 |
| License number | 3511870874837 |
| License date | Nov 18, 2014 |
| Licensed content publisher | Elsevier |
| Licensed content publication | Fuel |
| Licensed content title | Use of sewage sludge combustion ash and gasification ash for high-temperature desulphurization of different gas streams |
| Licensed content author | N. Gil-Lalaguna,J.L. Sánchez,M.B. Murillo,G. Gea |
| Licensed content date | 1 February 2015 |
| Licensed content volume number | 141 |
| Licensed content issue number | n/a |
| Number of pages | 10 |
| Start Page | 99 |
| End Page | 108 |
| Type of Use | reuse in a thesis/dissertation |
| Intended publisher of new work | other |
| Portion | full article |
| Format | both print and electronic |
| Are you the author of this Elsevier article? | Yes |
| Will you be translating? | Yes |
| Number of languages | 1 |
| Languages | Spanish |
| Title of your thesis/dissertation | Estudio de la gasificación de lodos de EDAR en lecho fluidizado. Efecto de la atmósfera reactiva, evaluación energética y limpieza del gas producto |
| Expected completion date | Jan 2015 |

Departamento de Ingeniería Química y Tecnologías del Medio Ambiente
Universidad Zaragoza

instituto de investigación en ingeniería de Aragón
Universidad de Zaragoza

# GASIFICATION OF SEWAGE SLUDGE IN A FLUIDIZED BED REACTOR. EFFECT OF THE REACTIVE ATMOSPHERE, ENERGETIC ASSESSMENT AND CLEAN-UP OF THE PRODUCT GAS

**PhD Thesis**

by

**NOEMÍ GIL LALAGUNA**

November 2014, Zaragoza

Supervisors: Dr. José Luis Sánchez Cebrián / Dr. María Benita Murillo Esteban

**Dr. Sánchez Cebrián** and **Dr. Murillo Esteban**,

Associate Professors at the University of Zaragoza in the Department of Chemical Engineering and Environmental Technologies, and research team members of the Thermo-chemical Processes Group of the Aragón Institute of Engineering Research (I3A)

**INFORM** that:

This PhD report entitled

***"Gasification of sewage sludge in a fluidized bed reactor. Effect of the reactive atmosphere, energetic assessment and clean-up of the product gas"***

has been developed by Ms. Gil Lalaguna under our supervision in the Department of Chemical Engineering and Environmental Technologies.

We authorize the presentation of this report.

In witness whereof, we sign this certificate in Zaragoza on November 24, 2014.

Dr. José Luis Sánchez Cebrián

Dr. María Benita Murillo Esteban

# OUTLINE

# 1. PREFACE

This PhD thesis has been developed in the Thermochemical Processes Group, belonging to the Aragón Institute of Engineering Research (I3A). This group focuses on various research areas, including thermo-chemical treatment of biomass and organic waste by pyrolysis and gasification, biodiesel production and improvement of its properties, pollutants removal from combustion gases such as $NO_x$ or soot and hydrogen production from catalytic reforming of aqueous streams.

The present work falls within the energetic valorization of organic waste and, in particular, is focused on sewage sludge gasification. Sewage sludge is the waste produced by wastewater treatment processes. The generated amount of this waste has increased in recent years due to a stricter European legislation concerning urban wastewater treatment (Directive 91/271/CEE). As a consequence, environmentally and healthy safe management of sewage sludge before final disposal has become a significant challenge in municipal wastewater treatment. Thermo-chemical processes such as gasification or pyrolysis are potential routes for the energetic valorization of this organic waste. Gasification involves the thermal conversion of a carbonaceous material into combustible gas and ash in a reducing atmosphere. The product gas from gasification consists of a mixture of CO, $CO_2$, $H_2$, $CH_4$ and other light hydrocarbons, steam and $N_2$ (if air is used as gasification medium), which could be used for power generation in gas engines or turbines or as a chemical feedstock to produce chemicals (Wender, 1996).

The Thermochemical Processes Group started to study the gasification of sewage sludge in the mid-1990s, when the first tests were conducted at the laboratory in cooperation with the company Cadagua S.A. Based on the earlier experimental results, a fluidized bed pilot plant of 100 $kg \cdot h^{-1}$ was designed and developed for sewage sludge gasification during the years 2001-2003. Some experiments were conducted in the pilot plant during 2003, but problems arising from the large scale work raised the need to further study the process at lab scale in order to evaluate the influence of the operating conditions. Since then, both sewage sludge gasification and sewage sludge pyrolysis at lab scale have attracted special attention in the Thermochemical Processes Group. Financial support has been provided by the Spanish Ministry during the last decade for this research area. Specifically, this PhD thesis has been developed with financial support from the Spanish Ministry of Science and Technology through the research project "*Sewage sludge valorization by means of pyrolysis: study and improvement of the products use (CTQ2010-20137)"*, as well as from the Spanish Ministry of

Education through the pre-doctoral grant awarded to the PhD student during the last four years (AP2009-3446).

Most of the published studies concerning sewage sludge gasification (Adegoroye et al., 2004; Campoy et al., 2014; Dogru et al., 2002; Midilli et al., 2001; Petersen and Werther, 2005; Tae-Young et al., 2009; van der Drift et al., 2001), as well as the previous work carried out in the Thermochemical Processes Group (Aznar et al., 2007; Aznar et al., 2008; Manyà et al., 2005; Manyà et al., 2006), used air to gasify the dried waste. However, after the mechanical dewatering by filter pressing or centrifugation, the moisture content of the waste still exceeds 70% (Manara and Zabaniotou, 2012), so steam gasification could make sense in such waste. Thus, part of the experimental work carried out in this PhD thesis aims to extend the knowledge about the effect of the reactive atmosphere on the gasification of sewage sludge, using different mixtures of air and steam as gasification medium. Steam gasification is an endothermic process, so the addition of air into the gasifying medium can provide the necessary energy through the partial combustion of the feedstock.

The pyrolysis (thermal decomposition under inert atmosphere) of sewage sludge has also been widely studied in the Thermochemical Processes Group during the last years (Fonts et al., 2008; Fonts et al., 2009; Gil-Lalaguna et al., 2010). Fast pyrolysis of sewage sludge is focused on maximizing the bio-oil production, but a significant fraction of char (around 50 wt. %) is also obtained. The remaining organic fraction in char gives it a moderate calorific value which could be further exploited through combustion or gasification processes, thus leading to an integral valorization of the raw material. Compared to the raw biomass, char resulting from biomass pyrolysis appears as a preferable feedstock for gasification from the point of view of tar formation since most of the volatile matter, responsible for tar formation, is eliminated during pyrolysis. Air-steam gasification of the char obtained in the pyrolysis of sewage sludge has been experimentally studied in this PhD thesis, comparing the results with those obtained in the direct gasification of sewage sludge.

In addition to the operational and technical feasibility of thermo-chemical processes, the energetic assessment of such processes is a key factor to be considered before their industrial development. An energetic study of both the air-steam gasification of sewage sludge and the integration of sewage sludge pyrolysis and air-steam gasification of char has been performed. Prior to the thermo-chemical treatment of sewage sludge by means of pyrolysis or gasification, sewage sludge thermal drying allows the reduction of water content in the waste, thus reducing the waste volume and facilitating handling of the biosolids. As the thermal drying of sewage sludge involves high energy consumption, it is interesting to evaluate if the energy that

could be recovered from the products of sewage sludge gasification and pyrolysis (together with char gasification) is enough to cover such energy demand.

One of the major issues in biomass gasification is to deal with the tar formed during the process. Tar is a complex mixture of condensable organic compounds including single- to multiple-ring aromatic compounds. The presence of tar in the gasification gas leads to operational problems associated with condensation, formation of aerosols and polymerization, such as the blocking of downstream pipelines and fouling of engines and turbines. To date, tar removal from gasification gas has not been solved satisfactorily, so many studies in the gasification research area are still focused on tar removal, especially by means of catalytic cracking (Anis and Zainal, 2011; De Lasa et al., 2011). In the particular case of sewage sludge gasification, an additional trouble is found as a consequence of the significant sulphur content of this waste. This leads to the formation of sulphur-containing gases during the gasification process, being hydrogen sulphide ($H_2S$) the most abundant. The presence of $H_2S$ in the gasification gas entails both environmental and operational problems. On the one hand, combustion of a $H_2S$-containing gas leads to $SO_2$ emissions, partially responsible for acid rain. On the other hand, the presence of $H_2S$ causes corrosion in pipes, engines or turbines, as well as the poisoning of the common catalysts used for tar cracking and gas reforming after gasification processes, which are usually based on Ni. These difficulties motivated the subsequent studies developed in this PhD thesis, focused on the gas clean-up.

High-temperature desulphurization of various synthetic $H_2S$-containing gases was studied in order to evaluate the effect of the operating conditions (temperature and reactive atmosphere) on the sulphur capture process. This process is based on the chemical reaction of $H_2S$ with metal oxides to form metal sulphides. Due to its metallic content, sewage sludge ash derived from the combustion and gasification processes of this waste were chosen as sorbent materials in the desulphurization tests. The use of ash residues for $H_2S$ removal from hot gases could be an attractive alternative due to its low cost. Furthermore, an integrated process could be proposed to remove the $H_2S$ produced during the thermo-chemical treatment of sewage sludge (gasification or pyrolysis) by using the own ash resulting from these processes in a downstream cleaning stage.

The last part of the PhD thesis was developed during a research stay at the VTT-Technical Research Centre of Finland. This work includes a study of catalytic reforming of tar model compounds present in a $H_2S$-containing synthetic gasification gas by using modified Ni-based catalysts. Different promoters (Ca, Fe, Mn and Cu) were added to a Ni-$Al_2O_3$ catalyst to evaluate their impact on the tar reforming activity and sulphur poisoning resistance of the

catalysts. From a thermodynamic standpoint, these chosen promoters would be able to react with $H_2S$ to form metal sulphides (Westmoreland and Harrison, 1976). Thus, it could be expected that sulphur chemisorption on nickel active sites, and the consequent activity loss, would be hindered by sulphur chemisorption on the promoter sites.

In summary, the main objective of this work is to improve the quality of the gas product obtained from sewage sludge gasification through the optimization of the operating conditions in the gasifier and the application of downstream gas cleaning treatments. Various tasks have been developed for that purpose:

- Study of the impact of some operating conditions on the sewage sludge gasification performance, using mixtures of air and steam as gasification medium.
- Study of the use of the char obtained in the pyrolysis of sewage sludge as a raw material for the gasification process in order to reduce tar formation.
- Energetic assessment of the air-steam gasification of sewage sludge and of the combination of sewage sludge pyrolysis and char gasification.
- Study of $H_2S$ removal from gases at high temperature by using sewage sludge ash obtained in thermo-chemical treatments of this waste.
- Study of the activity and stability of nickel-alumina catalysts modified with different promoters for the reforming of tar model compounds in presence of $H_2S$.

Much of the work developed in this PhD thesis has already been published or accepted for publication in journals with high impact factor:

- N. Gil-Lalaguna, J.L. Sánchez, M.B. Murillo, E. Rodríguez, G. Gea. (2014) *"Air steam gasification of sewage sludge in a fluidized bed. Influence of some operating conditions"*. **Chemical Engineering Journal** 248, 373-382.
- N. Gil-Lalaguna, J.L. Sánchez, M.B. Murillo, V. Ruiz, G. Gea. (2014) *"Air steam gasification of char derived from sewage sludge pyrolysis. Comparison with the gasification of sewage sludge"*. **Fuel** 129, 147-155.
- N. Gil-Lalaguna, J.L. Sánchez, M.B. Murillo, M. Atienza-Martínez, G. Gea. (2014) *"Energetic assessment of air-steam gasification of sewage sludge and of the integration of sewage sludge pyrolysis and air-steam gasification of char"*. **Energy** 76, 652-662.
- N. Gil-Lalaguna, J.L. Sánchez, M.B. Murillo, G. Gea. (2015) *"Use of sewage sludge combustion ash and gasification ash for high-temperature desulphurization of different gas streams"*. **Fuel** 141, 99-108.

# 2. INTRODUCTION

Biomass is one of the most important primary renewable energy sources and its thermo-chemical conversion encompasses a wide range of materials, conversion technologies and end-uses of the products, such as power/heat generation, transportation fuels and chemical feedstock. Sewage sludge produced by wastewater treatment processes can be considered a special case of biomass due to its substantial organic fraction and high enough calorific value (Fytili and Zabaniotou, 2008; Rulkens, 2008). This sludge is enlisted as a non-hazardous waste in the European Waste Catalogue (Decision 2001/118/EC).

The sludge stemming from wastewater treatment usually is in the form of a dilute suspension and its composition is strongly influenced by the original pollution load and the purification treatment applied in the process. As a rough guide, this composition includes: (i) water, varying from a small percentage to more than 95%; (ii) a substantial fraction of non-toxic organic material (about 60% dry basis) including biological constituents such as nucleic acids, proteins, carbohydrates and lipids, as well as organic material undigested in the process, such as cellulose; (iii) a fraction of inorganic material that comprises silicates, aluminates, calcium- and magnesium-containing compounds and nutrients such as nitrogen, phosphorus and potassium; (iv) toxic pollutants as a result of the industrial activity, including persistent organic compounds (pesticides, industrial solvents, dyes, plasticizers, surfactants, etc.) and heavy metals (Zn, Cr, Pb, Cu, Cd, Ni, As and Hg), whose concentration can vary from less than 1 ppm to more than 1000 ppm; (v) pathogens and other microbiological pollutants (Fytili and Zabaniotou, 2008; Rulkens, 2008; Manara and Zabaniotou, 2012). These toxic pollutants and pathogens entail environmental and human health risks in the case of poor sludge management.

The production of sewage sludge has considerably increased during the last two decades as a consequence of the stricter European legislation concerning urban wastewater treatment (Directive 91/271/EEC). This Directive requires all cities above 2000 population equivalent to implement secondary treatment of wastewater. Thus, new municipal wastewater treatment plants and renewed technologies have been developed in order to improve the quality of the effluents. As a result, the annual production of sewage sludge in the European Union almost doubled in the period 1992-2005, increasing from 6.5 to 10.9 million tonnes of dry matter per year (Kelessidis y Stasinakis, 2012). Spain is among the five European countries with highest annual sludge production, with about 1.2 million tons of dry matter per year (Eurostat).

In addition to the production of large quantities of sewage sludge, the costs of its treatment often represent more than 50% of the total wastewater treatment costs (Rulkens, 2008), so environmentally and healthy safe management of sewage sludge before final disposal has become a significant challenge in municipal wastewater treatment.

Policy and legislation regarding sludge application and management are heavily dependent upon local, national, and regional conditions. However, sewage sludge is catalogued as non-hazardous waste and, according to European waste policy (Directive 2008/98/CE), the following hierarchy shall always apply as a priority order in waste management: (i) prevention, (ii) reuse, (iii) recycling, (iv) other recovery forms, such as energy recovery, and (v) disposal. Currently, the most common options for sewage sludge management in the European Union include its reuse in agriculture, land reclamation and restoration, incineration and landfill disposal (Fytili and Zabaniotou, 2008; Rulkens, 2008; Manara and Zabaniotou, 2012). On the one hand, sewage sludge contains components of agricultural value such as organic matter and nutrients (nitrogen, phosphorus and potassium), thus its use as a fertilizer appears as an interesting option. Sewage sludge reuse by direct agricultural application or composting is the predominant choice for sludge management in the European Union (53% of produced sludge) (Kelessidis and Stasinakis, 2012). However, the presence of harmful substances in the sludge such as heavy metals, toxins and pathogens has sparked some controversy over its agricultural reuse because of the possible adverse effects of these toxic pollutants and pathogens on the food chain. This practice is regulated by European legislation (Directive 86/278/EEC), but more stringent legislation has been adopted for sludge disposal in soil by several European countries, setting lower limit values for heavy metals as well as limit values for pathogens and organic micro-pollutants. The degree of flexibility varies from country to country (Kelessidis and Stasinakis, 2012). Landfilling has been another conventional route for sewage sludge disposal, but this practice is on decline in the European Union because of the prohibition of landfilling of both liquid and untreated wastes, as well as restrictions for bio-degradable solid wastes (Directive 99/31/EC). Sewage sludge landfilling showed a significant and continuing decline between 1992 and 2005, from 33% to 17% of the produced sludge, while incineration has been almost doubled (from 11 to 21%) (Kelessidis and Stasinakis, 2012).

As agricultural use is increasingly regarded as an insecure handling route, thermo-chemical valorization of sewage sludge seems an interesting alternative. Thermo-chemical processes (combustion, pyrolysis and gasification) are considered one of the most promising ways to produce energy and valuable products from waste by removing the organic part and leaving only the mineral component for final disposal. In the particular case of dry sewage sludge, its

calorific value (12-20 $MJ \cdot kg^{-1}$) is comparable to that of coal (14.6-26.7 $MJ \cdot kg^{-1}$) (Manara and Zabaniotou, 2012). This work focuses on sewage sludge gasification.

Gasification involves the thermal conversion of a carbonaceous material into combustible gas and ash in a reducing atmosphere. The product gas from gasification consists of a mixture of CO, $CO_2$, $H_2$, $CH_4$ and other light hydrocarbons, steam and $N_2$ (if air is used as gasification medium), whose proportions depend on the composition of the raw material and the operating conditions. The gas produced can be used in more versatile ways than the original biomass, for example for power generation in gas engines or turbines, or as a chemical feedstock to produce chemicals (methanol, Fischer-Tropchs liquids…) (Wender, 1996). Gasification technology appears to offer attractive options for medium to large scale applications, for example by integration of gasification in combined heat and power units (IGCC) to efficiently convert the energy carried in the fuel to electricity (Manara and Zabaniotou, 2012). Furthermore, compared to combustion, gasification is a more friendly way of using biomass for energy purposes since pollutant emissions are reduced in the presence of non-oxidizing conditions (Franco et al., 2003).

The gasification medium is an important parameter influencing the gaseous product quality. Air is the most widely used gasifying agent due to its low cost, but $N_2$ introduced with the air dilutes the product gas ($N_2$ content around 50 vol. %), giving a poor-quality gas in terms of calorific value (lower heating value of 4-6 $MJ \cdot m^{-3}_{STP}$, being STP standard conditions of temperature and pressure at 25 ºC and 1 atm). This gas is suitable for boiler, engine and turbine operation, but not for pipeline transportation due to its low energy density (Bridgwater, 1995). Gasification with pure $O_2$ prevents the dilution of the gas, increasing its lower heating value to 10-14 $MJ \cdot m^{-3}_{STP}$, but the cost of the process increases because of the required air separation unit for the production of pure $O_2$. Instead of air/$O_2$, steam can also be used as gasification medium, thus improving $H_2$ production for the use of the gas in fuel cells or as feedstock for the synthesis of chemicals. Synthetic fuel production requires a high quality syngas with high concentration of CO + $H_2$ and sufficient high $H_2$/CO ratio. $H_2$ concentration as high as 60 vol. % has been reported from steam gasification of biomass (Herguido et al., 1992). However, unlike the reaction with $O_2$, the reaction of carbon with steam is endothermic, requiring heat to be transferred at high temperatures, which is difficult to achieve. The addition of some amount of $O_2$ to the gasifying medium can provide the necessary energy for steam gasification through the partial combustion of the feedstock. Hence, the joint use of steam and $O_2$ (or air) as gasification medium seems an attractive option. Some studies on air-steam gasification of biomass are reported in the literature (Campoy et al., 2009; Gil et al.,

1997; Lv et al., 2004; Pinto et al., 2003), but more efforts are required to assess both the operational and energetic aspects of the process.

In the particular case of sewage sludge gasification, the first published studies date back to mid-1990s (Bacaicoa et al., 1995). Since then, several studies have been performed at laboratory facilities (Adegoroye et al., 2004; Aznar et al., 2007; Aznar et al., 2008; Manyà et al., 2005; Manyà et al., 2006; Tae-Young et al., 2009) and the process has even been tried at demonstration and pilot scale (Campoy et al., 2014; Dogru et al., 2002; Judex et al., 2012; Midilli et al., 2001; Petersen and Werther, 2005; van der Drift et al., 2001) showing the feasibility of obtaining a fuel gas from such waste. Most of the published studies use air to gasify the dried waste. Steam has been scarcely used as gasification medium (Domínguez et al., 2006; Nipattummakul et al., 2010; Xie et al., 2010; Zhang et al., 2011). Nipattummakul et al. (2010) found that $H_2$ production during steam gasification of sewage sludge was three times higher than that obtained in the air gasification of dried sludge.

After stabilization and mechanical dewatering of sewage sludge by filter pressing or centrifugation, water content can be further reduced by means of thermal drying in order to reduce the waste volume and facilitate its handling. However, this stage consumes a large amount of energy and raises the cost of sewage sludge disposal. Before thermal drying, the moisture content of sludge still exceeds 70% (Manara and Zabaniotou, 2012), so steam gasification seems to make sense in such waste. Thus, wet sewage sludge can be assumed as an interesting feedstock to manufacture $H_2$ (Fytili and Zabaniotou, 2008). The high moisture content of sewage sludge generates, at high temperatures, a steam-rich atmosphere, leading consequently to an in situ steam reforming of the volatile compounds and to a partial gasification of the solid char, which contributes to the production of $H_2$-rich fuel gas (Domínguez et al., 2006). Hence, drying, pyrolysis and partial gasification of the raw sludge take place in the same process.

It is generally referred by different authors that the process of biomass gasification occurs through various steps (Antal et al., 1979): initial drying of the raw material, subsequent pyrolysis or thermal decomposition that produces volatile matter and a carbonaceous solid residue (*char*), followed by secondary reactions involving the volatile products and finally, gasification reactions of the remaining carbonaceous residue with steam and $CO_2$. These latter reactions are slow compared to devolatilization and gas phase reactions. The sequence and duration of the stages vary with the type of reactor used.

The main gas-solid reactions taking place in the gasifier can be summarized as follows (Mondal et al., 2011):

| | | | |
|---|---|---|---|
| Partial oxidation: | $C + ½\ O_2 \rightarrow CO$ | $\Delta H_{298K} = -110\ kJ \cdot mol^{-1}$ | (eq. 2.1) |
| Complete oxidation: | $C + O_2 \rightarrow CO_2$ | $\Delta H_{298K} = -393\ kJ \cdot mol^{-1}$ | (eq. 2.2) |
| Water gas reaction: | $C + H_2O \leftrightarrow CO + H_2$ | $\Delta H_{298K} = 131\ kJ \cdot mol^{-1}$ | (eq. 2.3) |
| Boudouard reaction: | $C + CO_2 \leftrightarrow 2CO$ | $\Delta H_{298K} = 172\ kJ \cdot mol^{-1}$ | (eq. 2.4) |
| Methanation: | $C + 2H_2 \leftrightarrow CH_4$ | $\Delta H_{298K} = -75\ kJ \cdot mol^{-1}$ | (eq. 2.5) |

As commented above, the produced gases can undergo further reactions as follows:

| | | | |
|---|---|---|---|
| Water-gas shift reaction: | $CO + H_2O \leftrightarrow CO_2 + H_2$ | $\Delta H_{298K} = -41\ kJ \cdot mol^{-1}$ | (eq. 2.6) |
| Steam reforming: | $CH_4 + H_2O \leftrightarrow CO + 3H_2$ | $\Delta H_{298K} = 205\ kJ \cdot mol^{-1}$ | (eq. 2.7) |
| Dry reforming: | $CH_4 + CO_2 \leftrightarrow 2CO + 2H_2$ | $\Delta H_{298K} = 247\ kJ \cdot mol^{-1}$ | (eq. 2.8) |

Most of these reactions are equilibria and can proceed in either direction, depending on the temperature, pressure and concentration of the reacting species.

One of the major issues in biomass gasification is to deal with the tar formed during the process. Tar is a complex mixture of condensable hydrocarbons produced during the thermal decomposition of biomass, which includes single- to multiple-ring aromatic compounds along with other oxygen-containing hydrocarbons and complex polycyclic aromatic hydrocarbons (PAHs). In the context of gasification, tar is usually defined as all the organic contaminants with a molecular weight larger than benzene, except soot and char (Neeft et al., 2002). The presence of tar in the gasification gas leads to operational problems associated with condensation (< 450 $^{o}$C), formation of aerosols and polymerization of tar compounds to form more complex structures that block downstream pipelines and foul engines and turbines, thus restricting the direct use of the gas (McKendry, 2002b). Moreover, tar compounds entail serious environmental problems due to their persistent and toxic nature (Nisbet and Lagoy, 1992). The minimum allowable limit for tar is highly dependent on the kind of process and the gas end-use. Several researchers state that internal combustion gas engines are more tolerant of contaminants than gas turbines. In particular, it is possible to have tar content up to 50-100 $mg \cdot m^{-3}_{STP}$ for internal combustion engines, but less than 5 $mg \cdot m^{-3}_{STP}$ is preferable for gas turbines (Anis and Zainal, 2011). However, if the gas is fed at the turbine at high temperature, tar content can be not a problem at all (Ståhl and Neergaard, 1998).

The tar content in the product gas from biomass gasification usually greatly exceeds the allowable limits, ranging between 0.5 and 100 $g \cdot m^{-3}_{STP}$ depending on the feedstock, the

operating conditions and the gasifier type (Devi et al., 2003). Various gasification reactors types exist, among which the fixed bed (downdraft or updraft), fluidized bed and entrained flow gasifiers are the most widely used (Mondal et al., 2011). Fluidized bed configuration (which is the gasification technology used in the present work) presents higher gasification efficiency compared to fixed bed gasifiers since mass and heat transfer phenomena are enhanced. However, the product gas usually has increased content in solid particulates and tar with respect to downdraft fixed bed reactors (Han and Kim, 2008). The typical range of tar content in fluidized bed gasifiers is around 8-15 $g \cdot m^{-3}_{STP}$ (Corella et al., 2006). Hence, tar removal becomes one of the most necessary and urgent problems during biomass gasification.

Tar removal technologies can be broadly divided into two approaches: treatments inside the gasifier (primary methods) and gas cleaning downstream the gasifier (secondary methods). Primary methods can be defined as all the measures taken in the gasification step itself to prevent or convert tar formed in the gasifier. The presence of an active material in the gasifier can largely improve the product gas distribution. Tar contents as low as 1-2 $g \cdot m^{-3}_{STP}$ have been obtained by adding bed materials such as dolomite and olivine in fluidized beds (Gil et al., 1999a; Olivares et al., 1997; Rapagnà et al., 2000). On the other hand, a proper selection of the operating conditions (temperature, pressure, gasification medium, amount of gasifying agent, residence time…) is critical to reduce tar formation (Devi et al., 2003).

It is generally referred by different authors that an increasing temperature promotes the formation of gaseous products at the expense of total tar. Different tar decomposition mechanisms are proposed in the literature, suggesting kinetically controlled processes that are enhanced with increasing temperature (Li and Suzuki, 2009a). An operating temperature above 800 $^{o}C$ is usually preferred to achieve high carbon conversion and low tar content in the resultant product gas. However, there are other factors that limit the operating temperature, such as are the reduced gas heating value and the risk of ash sintering (Devi et al., 2003). Tar composition is also affected by temperature. The increase in temperature drastically reduces the amount of oxygen-containing components and substituted 1-ring and 2-ring aromatics, while formation of 3- and 4-ring aromatics increases rapidly, resulting in an increase in the tar dew point. In summary, higher temperatures favor the formation of fewer aromatic tar species without substituent groups such as benzene, naphthalene and phenanthrene (Kinoshita et al., 1994).

Selectivity of the gasification reactions varies with the gasification medium, thus affecting both gas composition and tar formation. Air gasification produces slow-reacting tar, while steam gasification produces tar with a lower molecular weight (McKendry, 2002b). Likewise,

Gil et al. (1999b) found that tar generated during steam gasification was "easier to destroy'' with Ni-based catalysts or with dolomites than tar generated during air gasification. They found higher tar contents in steam gasification (30-80 $g \cdot m^{-3}_{STP}$) than in air gasification (2-20 $g \cdot m^{-3}_{STP}$), but the reduced operating temperature set in the first case may influence this result. More studies are necessary to increase knowledge of this effect. The ratio between the gasifying agent flow rate and the biomass feed rate also influences tar content in the gas. In the case of air/$O_2$ gasification, the equivalence ratio (ER: ratio between the actual fuel-to-$O_2$ ratio and the stoichiometric fuel-to-$O_2$ ratio) usually varies from 0.20 to 0.40 (Narváez et al., 1996). An ER increase means more availability of oxygen to react with the volatile matter, thus reducing the tar content in the gas (Kinosita et al., 1994; Narváez et al., 1996). Tar content of about 2-4 $g \cdot m^{-3}_{STP}$ was obtained by Narváez et al. (1996) when the ER was increased up to 0.45 in the gasification of pine sawdust at 800 ºC. However, gas composition is also affected by ER and an increase in the fractions of $CO_2$ and $N_2$ (if gasifying with air) is expected at higher ER, which means a reduced gas heating value.

Compared to the raw biomass, char resulting from biomass pyrolysis appears as a preferable feedstock for gasification from the point of view of tar formation. The product gas from the direct gasification of raw biomass is usually rich in tar because of the high volatile matter content of the solid. However, in the case of char gasification, a product gas with lower tar content can be obtained, since most of volatile matter is eliminated during the pyrolysis process. Fast pyrolysis of biomass focuses on the production of bio-oil, being char the main by-product of the process. This remaining solid char shows different properties than the raw biomass as a consequence of the thermal treatment. The most remarkable differences are related to surface area, pore structure and chemical composition (ultimate and proximate analyses). As a route towards an integral valorization of biomass, the solid by-product of pyrolysis can be reused as a material for activated carbon preparation (González et al., 2009) or be further exploited through thermo-chemical processes such as combustion (Di Blasi, 2009) or gasification (Chaudhari et al., 2003; Haykiri-Acma et al., 2006; He et al., 2012; Nilsson et al., 2014; Salleh et al., 2010; Yan et al., 2010).

In the particular case of sewage sludge pyrolysis, common solid yields are around 35-55 wt. % (Fonts et al., 2008; Fonts et al., 2012; Inguanzo et al., 2002; Pokorna et al., 2009; Shen and Zhang, 2003). The use of sewage sludge char as an adsorbent material has been investigated by some authors and the results showed a reduced porosity (surface area of 50-150 $m^2 \cdot g^{-1}$) compared to that of commercial active carbons (> 500 $m^2 \cdot g^{-1}$) because of the high inorganic content in the sewage sludge char (Smith et al., 2009). Studies on gasification of

sewage sludge char are scarce and they are mainly focused on kinetic aspects (Nilsson et al., 2012; Nowicki et al., 2011; Scott et al., 2005).

In addition to the primary methods for tar removal, downstream cleaning treatments are usually required in the gasification processes to further improve gas quality. The different secondary methods for tar removal are classified into mechanical/physical methods, thermal cracking and catalytic cracking. Mechanical cleanup systems include the use of cyclones, electrostatic precipitators, filters (fabric filters, ceramic filters…), activated carbon adsorbents and scrubbers (Abu El-Rub et al., 2004; Anis and Zainal, 2011). These methods are considerably efficient in removing solid particles accompanied by tar liquid droplets. Tar removal cannot be separated from solid particles removal at temperatures below its dew point, while tar vapors are hardly removed at higher temperatures. Tar removal efficiencies of 40-70% and 0-50% have been reported by using electrostatic precipitators and fabric filters, respectively, while higher removal efficiencies can be achieved by using venturi scrubbers (60-90%). Tar removal in the range of 70% can be expected with tar adsorbents based on activated carbon (Anis and Zainal, 2011; Han and Kim, 2008). Tar management is an important drawback in such cleaning treatments that remove tar from the gas without destroying it.

Tar conversion into lighter gases such as $H_2$, CO and $CH_4$ appears as the most effective method for tar removal. These reactions are known to be kinetically limited (Abu El-Rub et al., 2004; Anis and Zainal, 2011), so either extremely high temperatures or the use of catalysts are required for tar cracking reactions. Biomass-derived tar is very refractory and hard to crack by thermal treatment alone (Bridgwater, 1995). Brandt and Henriksen (2000) found that a temperature as high as 1250 $^{o}$C and a residence time of 0.5 s were necessary to achieve a high tar cracking efficiency. The use of catalysts allows a lower operating temperature, thus reducing the energy demand for tar cracking. Due to the advantages of converting tar into useful gases and adjusting the composition of the product gas, catalytic cracking has attracted scientific interest since the mid-1980s. Hydrocarbons may be reformed on the catalyst surface with either steam (eq. 2.9) or $CO_2$ (eq. 2.10) to produce additional CO and $H_2$. The reaction mechanism involves the dissociative adsorption of the hydrocarbon onto a metal site where dehydrogenation occurs (Han and Kim, 2008).

Steam reforming: $C_nH_m + n\,H_2O \leftrightarrow n\,CO + (n + m/2)\,H_2$ $\Delta H > 0$ (eq. 2.9)

Dry reforming: $C_nH_m + n\,CO_2 \leftrightarrow 2n\,CO + (m/2)\,H_2$ $\Delta H > 0$ (eq. 2.10)

Various types of catalysts such as minerals and calcined rocks (dolomite, olivine…), alkali metal catalysts and transition metal catalysts have been widely tested for tar removal during

biomass gasification (Abu El-Rub et al., 2004; Anis and Zainal, 2011; De Lasa et al., 2011; Sutton et al., 2001a). Among these, Ni-based catalysts appear to be the most suitable choice for both technical and economic reasons. An increase in $H_2$ and CO content of the exit gas, as well as the elimination or reduction of the hydrocarbon and $CH_4$ content, is usually observed when using these catalysts at temperatures above 740 $^oC$ (Sutton et al., 2001a). Heavy tar destruction efficiencies of 98-99% have been reported with commercial steam reforming Ni-catalysts (Aznar et al., 1998; Zhang et al., 2004). Not only the active metal, but also the catalyst support plays an important role in the catalyst activity since it affects the dispersion of the active phase. The use of different metal oxides such as $Al_2O_3$, MgO, $ZrO_2$, $TiO_2$, $CeO_2$ or $SiO_2$, and natural materials such as dolomite, olivine or activated charcoal as supports for Ni-catalysts has been extensively reviewed in the literature (Courson et al., 2000; Kimura et al., 2006; Li et al., 2009b; Miyazawa et al., 2006; Park et al., 2010; Sato and Fujimoto, 2007; Srinakruang et al., 2006; Sutton et al., 2001b; Swierczynski et al., 2007; Wang et al., 2005). Of these, alumina ($Al_2O_3$) is the most commonly used support (Anis and Zainal, 2011). Some studies point to $Ni/Al_2O_3$ as one of the most efficient catalysts for tar removal (Sutton et al., 2001b), but this is not stable and eventually deactivates (Swierczynski et al., 2007).

Several deactivation mechanisms have been reported for Ni-based catalysts including poisoning by sulphur, chlorine and alkali metals, sintering of Ni particles and coke formation (Abu El-Rub et al., 2004; Anis and Zainal, 2011; De Lasa et al., 2011; Sutton et al., 2001a). The modification of Ni catalysts with promoters can positively affect catalyst activity, reducibility, regenerability and coke resistance, as well as mechanical strength and attrition resistance (Yung et al., 2009). The addition of a wide variety of metals (Na, K, Ru, Rh, Mn, Mo, W, Zr, Mn, La, Ce…) to Ni-catalysts has been studied by many researchers (Bona et al., 2008; Dou et al., 2003; Nishikawa et al., 2008; Richardson and Grey, 1997; Seok et al., 2002; Zhang et al., 2007), showing in some cases good anti-coking ability and improved durability and activity of the catalysts. In addition to coke deposition, conventional Ni-based catalysts are very sensitive to poisoning by sulphur compounds (Yung et al., 2009). Strong metal-sulphur chemisorption occurs during sulphur poisoning, thus leading to saturation of the metal active sites. This poisoning effect has been studied by many researchers (Engelen et al., 2003; Hepola and Simell, 1997; Struis et al., 2009), using low concentrations of sulphur in the gas. However, during the gasification of sulphur-containing raw materials, such as coal or sewage sludge, sulphur concentration in the gas can easily exceed 1000 ppmv, especially in the form of $H_2S$.

The presence of $H_2S$ in the gasification gas entails both environmental and operational problems. On the one hand, combustion of a $H_2S$-containing gas leads to $SO_2$ emissions,

partially responsible for acid rain. On the other hand, the presence of $H_2S$ in gas causes corrosion in pipes, engines or turbines, as well as deactivation of the common catalysts used for tar cracking and gas reforming after gasification processes. Several low and high temperature processes for $H_2S$ removal from products and off-gases have been described and developed at various stages. Wet scrubbing with selected solvents has been a widely used low-temperature process in the chemical process industry (Yildirim et al., 2012). The use of activated carbons for $H_2S$ removal at low temperature has also been extensively studied (Bagreev and Bandosz, 2005; Bandosz, 2002; Primavera et al., 1998). Given the combination of their unique surface features (high specific surface and pore volume) and surface chemistry improved by the addition of functional groups, activated carbon-based materials have been proved to work efficiently as adsorbents of sulphur-containing species such as $H_2S$, $SO_2$ or methyl mercaptans. As a result of surface reactions, $H_2S$ can be oxidized to either sulphur or $SO_2$ (Bandosz, 2002). Some adsorbents materials have been prepared from the solid by-products of sewage sludge pyrolysis or carbonization (Gutiérrez-Ortiz et al., 2014; Ros et al., 2006; Yuan and Bandosz, 2007), obtaining in some cases pollutant removal efficiencies comparable to those corresponding to commercial catalytic activated carbons.

On the other hand, high temperature desulphurization processes are advantageous from an energy standpoint as a result of the elimination of gas cooling and the associated heat exchangers (Meng et al., 2010). Furthermore, tar condensation after a gasification process can be prevented by desulphurization at high temperature. The high temperature desulphurization process is based on the chemical reaction of $H_2S$ with metal oxides. Typically, metal oxides are converted to sulphides during a sulphur loading stage under reducing hot gas conditions. After sulphidation, the spent metal sulphides can be regenerated back to metal oxides by using oxygen, steam, $SO_2$ or a combination of these (Meng et al., 2010). Different studies on the use of metal oxide based sorbents for hot gas desulphurization can be found in the literature (Álvarez-Rodríguez and Clemente-Jul, 2008; Cheah et al., 2009; Elseviers and Verelst, 1999; García et al., 2011; Meng et al., 2010; Park et al., 2005; Tamhankar et al., 1981; Westmoreland and Harrison, 1976). Several metal oxides can be used for high temperature sulphur capture downstream the gasifier, but each solid has its own advantages and limitations at the same time. Sorbents based on zinc, manganese, copper, iron or calcium are some of the most studied and promising materials (Cheah et al., 2009; Meng et al., 2010; Westmoreland and Harrison, 1976). Ash residues derived from thermo-chemical treatment of biomass or wastes are known to contain metal oxides in different proportions, so its use as sorbent materials for $H_2S$ removal from hot gases could be an attractive alternative due to its low cost.

# 3. MATERIALS AND METHODS

## 3.1. Materials

### *3.1.1. Raw materials for gasification: sewage sludge and sewage sludge char*

The raw material for gasification was anaerobically digested and thermally dried sewage sludge (SS), as well as the char resulting from its pyrolysis process. The sewage sludge was supplied by a Spanish urban wastewater treatment plant located in Madrid. Table 3.1 presents a brief characterization of both materials. The proximate analyses were performed according to standard methods (ISO-589-1981 for moisture, ISO-1171-1976 for ash and ISO-5623-1974 for volatiles); the ultimate analyses (CHNS) were determined with a Carlo Erba EA1108 elemental analyzer *(Analysis Service of Instituto de Carboquímica)*; the higher heating values (HHV) of the solids were measured using an IKA C-2000 calorimeter and their specific heat capacities (Cp) were determined by differential scanning calorimetry with a Netzsch DSC 200 Maia (inert atmosphere, 40 mL $N_2 \cdot min^{-1}$). Sewage sludge was ground and sieved before the experiments to obtain a feed sample in the size range of 250-500 μm.

Table 3.1. Sewage sludge and char characterization.

| | Sewage sludge | Char |
|---|---|---|
| Proximate analysis (wt. % wet basis) | | |
| Moisture | 6.48 | 1.70 |
| Ash | 39.04 | 74.20 |
| Volatiles | 50.09 | 15.02 |
| Fixed carbon | 4.39 | 9.08 |
| Ultimate analysis (wt. % wet basis) | | |
| C | 29.50 | 15.49 |
| H | 4.67 | 0.97 |
| N | 5.27 | 1.85 |
| S | 1.31 | 0.35 |
| HHV ($MJ \cdot kg^{-1}$) | 12.8 | 5.2 |
| LHV ($MJ \cdot kg^{-1}$) | 11.8 | 5.0 |
| $Cp_{25^oC}$ ($kJ \cdot kg^{-1} \cdot K^{-1}$) | 1.15 | 0.82 |

Only 15 wt. % of the carbon content of sewage sludge is in the form of fixed carbon, while it reaches 59 wt. % in the sewage sludge char because of the structural changes occurring during the pyrolysis process. In terms of mass, the amount of fixed carbon is doubled after pyrolysis (4.39 vs. 9.08 wt. %).

*3.1.2. Sewage sludge ash for $H_2S$ removal*

The ash obtained from the gasification and combustion of sewage sludge was used as sorbent material in the desulphurization tests. Sewage sludge combustion was performed under air atmosphere in a heating muffle furnace at 900 ºC (20 ºC·min$^{-1}$) during two hours. Gasification ash was the solid by-product obtained in one of the sewage sludge gasification experiments (experiment 5 in Table 3.6). Both ash samples were characterized before the experiments by various techniques (Table 3.2). Ultimate analyses were performed using a Leco TruSpec Micro elemental analyzer. Textural properties such as BET surface area and average pore size and volume (BJH method) were calculated from $N_2$ physisorption isotherms using a Micromeritics TriStar II 3000 analyzer. The samples were previously degasified at 200 ºC during 8 h in a $N_2$ flow. Then, $N_2$ adsorption-desorption isotherms were obtained at -196 ºC and room temperature, respectively, over the whole range of relative pressures. Metal content in the ash samples was analyzed by inductively coupled plasma combined with optical emission spectroscopy (ICP-OES), using a Thermo Elemental IRIS Intrepid ICP-OES spectrometer *(Chemical Analysis Service of the Universidad de Zaragoza)*. The samples were dissolved by microwave-assisted acid digestion in a CEM MARS microwave reaction system.

Table 3.2. Characterization results of sewage sludge combustion ash and sewage sludge gasification ash.

| | Combustion ash | Gasification ash |
|---|---|---|
| Ultimate analysis (wt. % wet basis) | | |
| C | 0.15 | 3.14 |
| H | n.d. | n.d. |
| N | 0.28 | 0.77 |
| S | 0.46 | 0.41 |
| BET surface ($m^2 \cdot g^{-1}$) | 6.5 | 6.7 |
| Pore volume ($cm^3 \cdot g^{-1}$) | 0.02 | 0.02 |
| Average pore size (nm) | 12.0 | 10.9 |
| Metal content ($mg \cdot g^{-1}_{ash}$) | | |
| Al | 52 | 61 |
| Ca | 65 | 84 |
| Fe | 192 | 116 |
| K | 14 | n.a. |
| P | 63 | 51 |
| Mg | 17 | n.a. |
| Na | 4 | n.a. |
| Si | 122 | n.a. |
| Ti | 4 | n.a. |

n.d.: not detected; n.a.: not analyzed.

Both solids initially contained a small fraction of sulphur. Some amount of carbon was also present in the gasification ash (around 3 wt. %). The surface properties of sewage sludge ash

are not good enough for its use as an adsorbent material, but its desulphurization potential is based on its metallic content. The main metallic elements detected by ICP-OES were Fe, Si, Ca and Al. According to the thermodynamic study reported by Westmoreland and Harrison (1976) concerning the desulphurization potential of different metal oxides, Ca and Fe oxides are able to react with $H_2S$ to form metal sulphides, so both ash samples are potential sulphur sorbents. Some differences have been found in the metal content of the solids, which might indicate that the initial ash fraction does not remain completely inert during the combustion and gasification processes. Heterogeneity of sewage sludge may also explain these differences. Particularly striking is the case of Fe content which was much lower in the gasification ash. Part of the Fe content in the raw sewage sludge could be in the form of iron chloride ($FeCl_3$) as a consequence of the use of this compound as a coagulant agent during the wastewater treatment. During combustion, excess oxygen appears to favor the retention of Fe in the ash in the oxide form. However, during the gasification process, the reduced presence of oxygen prevents the total conversion of $FeCl_3$ to iron oxides, so some amount of Fe could leave the reactor in the gas phase, as $FeCl_3$ evaporates at 315 $^oC$.

Powder X-ray diffraction (XRD) patterns of the fresh samples were acquired with a D-Max Rigaku diffractometer *(Service of X-Ray Diffraction and Fluorescence Analysis of the Universidad de Zaragoza)* equipped with a copper anode (voltage of 40 kV and current of 80 mA). The measurements were completed in the Bragg's angle (2θ) range from 5º to 95º, using a scanning rate of $0.03^o \cdot s^{-1}$. Phases present in the solid samples were defined according to the JCPDS-International Centre for Diffraction Data 2000 database. The obtained XRD patterns are shown in Fig. 3.1. Species such as quartz, calcite, iron oxides and different calcium and iron phosphates have been detected in the ash samples. The oxidation state of Fe is one of the main differences in the XRD patterns: Fe appears in the form of hematite ($Fe_2O_3$) in the combustion ash and in the form of magnetite ($Fe_3O_4$) in the gasification ash. Concordantly, the reddish color characteristic of hematite was only observed on the combustion ash.

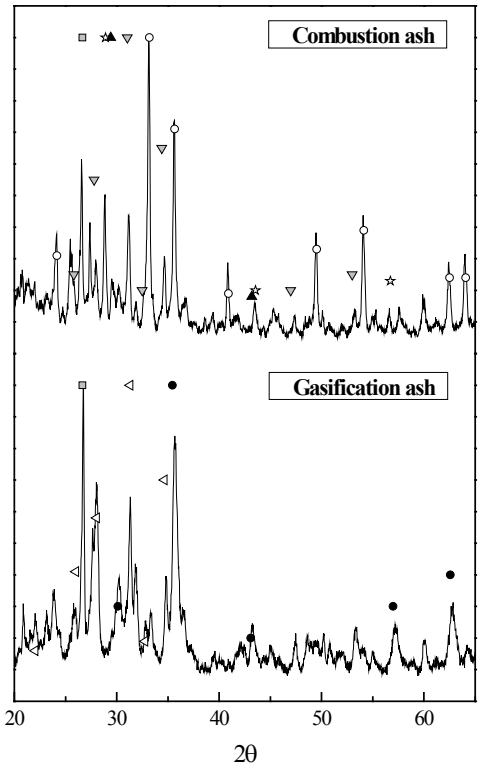


Figure 3.1. XRD patterns of the sewage sludge ash samples. ○ Hematite ($Fe_2O_3$); □ Quartz ($SiO_2$); ▲ Calcite ($CaCO_3$); ☆ $Fe_3PO_7$; ▽ $Ca_3(PO_4)_2$; ● Magnetite ($Fe_3O_4$); ◁ Whitlockite ($Ca_{18}Mg_2H_2(PO_4)_{14}$).

*3.1.3. Nickel-based catalysts*

Nickel-based catalysts were prepared and modified by adding different metals (Fe, Ca, Mn and Cu) in order to evaluate the effect of these promoters on the catalyst stability and activity for tar reforming. From a thermodynamic standpoint, these chosen promoters are able to react with $H_2S$ to form metal sulphides (Westmoreland and Harrison, 1976). Thus, it could be expected that sulphur chemisorption on nickel active sites, and the consequent activity loss, would be hindered by sulphur chemisorption on the promoter sites.

The catalysts were prepared by incipient wetness impregnation of γ-alumina (250-315 μm size) with aqueous solutions of nitrates of the metal of interest: $Ni(NO_3)_2{\cdot}6H_2O$, $Ca(NO_3)_2{\cdot}4H_2O$, $Fe(NO_3)_3{\cdot}9H_2O$, $Cu(NO_3)_2{\cdot}3H_2O$ and $Mn(NO_3)_2{\cdot}4H_2O$. Both the nickel nitrate and the promoter nitrate were solved and impregnated in one step. After impregnation the catalysts were dried at 110 ºC for 24 h, followed by calcination under air atmosphere according to the following temperature ramp: 120 ºC for 20 min, 200 ºC for 30 min, 320 ºC for 90 min and final calcination temperature (700 ºC or 900 ºC) for 120 min. Two different calcination temperatures were used in order to evaluate their influence on the catalyst activity and stability. Metal loading in the calcined samples was around 8 wt. % of Ni and 8 wt. % of promoter (Ca, Fe, Cu or Mn). Textural properties (Table 3.3) and XRD patterns (Fig. 3.2) of the calcined powder catalysts

were obtained analogously to that described in section 3.1.2 for the sewage sludge ash. A significant decrease in the BET surface area (reduced by 10-50%), as well as a decrease in the pore volume, was found when promoters were incorporated into the catalysts. This could be attributed to plugging of part of the micropores in the support due to an excess of metal loading. Adding Ca resulted in the greatest loss of surface area, as well as the greatest average pore size and the smallest pore volume. The surface area was also reduced when the calcination temperature was increased from 700 to 900 ºC. Pore volume did not show evident changes in any case, but the pore diameter increased with the calcination temperature probably as a result of sintering of metal particulates.

Table 3.3. Textural properties of the fresh calcined catalysts.

| | Final calcination temperature | $Ni/Al_2O_3$ | $Ni/Ca/Al_2O_3$ | $Ni/Fe/Al_2O_3$ | $Ni/Cu/Al_2O_3$ | $Ni/Mn/Al_2O_3$ |
|---|---|---|---|---|---|---|
| Surface area ($m^2 \cdot g^{-1}$) | 700 ºC | 120.5 | 61.7 | 108.1 | 105.1 | 96.6 |
| | 900 ºC | 96.4 | 52.7 | 72.6 | 62.4 | 71.2 |
| Pore volume ($cm^3 \cdot g^{-1}$) | 700 ºC | 0.35 | 0.24 | 0.31 | 0.32 | 0.28 |
| | 900 ºC | 0.33 | 0.22 | 0.25 | 0.25 | 0.25 |
| Average pore size nm) | 700 ºC | 11.1 | 15.1 | 11.0 | 11.8 | 11.3 |
| | 900 ºC | 13.2 | 16.3 | 13.5 | 15.7 | 13.7 |

As an example, Fig. 3.2 shows the XRD patterns of two of the fresh catalysts calcined at 700 and 900 ºC ($Ni/Mn/Al_2O_3$ and $Ni/Cu/Al_2O_3$). The XRD patterns show quite low crystallinity of the samples. Non-significant differences are found in the patterns of the catalysts prepared at the same calcination temperature, regardless of the metal added as promoter. All the samples calcined at 700 ºC showed wide and asymmetric peaks mainly corresponding to the γ-$Al_2O_3$ phase. As an exception, the $Ni/Cu/Al_2O_3$ sample calcined at 700 ºC showed two diffraction peaks at 35.6º and 38.8º corresponding to CuO. Peaks corresponding to other expected metal oxides, such as NiO, were not clearly shown by this technique because of the wide peaks forming the pattern. When the calcination temperature was increased to 900 ºC, the width of the peaks decreased, pointing to more crystalline phases. $NiAl_2O_4$ was the main phase detected in all the samples calcined at 900 ºC. Other aluminates might also be present in the catalysts, but both the aluminates and the γ- $Al_2O_3$ are spinel-type phases and their X-ray patterns are very similar, so their presence cannot be confirmed by the results of this technique alone.

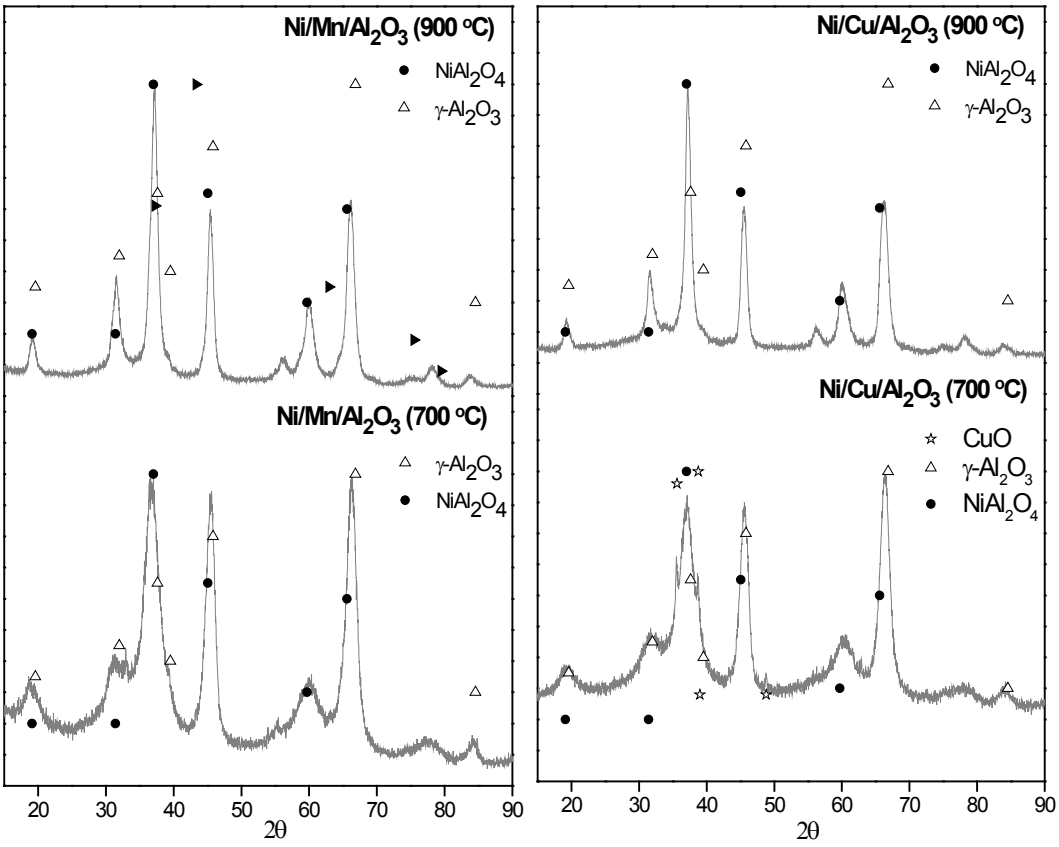


Figure 3.2. XRD patterns of the fresh samples of $Ni/Mn/Al_2O_3$ and $Ni/Cu/Al_2O_3$ calcined at 700 and 900ºC.

## 3.2. Experimental facilities and procedures

### *3.2.1. Gasification setup*

Sewage sludge and char gasification experiments were carried out in a lab-scale fluidized bed reactor operating at atmospheric pressure. Fig. 3.3 shows a diagram of the gasification experimental setup.

Sewage sludge fast pyrolysis, in which the used char was obtained as solid by-product, was conducted in a similar experimental setup to that shown in Fig. 3.3. $N_2$ was used as inert atmosphere and fluidizing agent, providing a fluidizing velocity around 8 times greater than the minimum fluidization rate. The pyrolysis temperature was 530 ºC. The average residence time of the solid-byproduct and the produced gases and vapors in the reactor was around 8 min and 1 s, respectively.

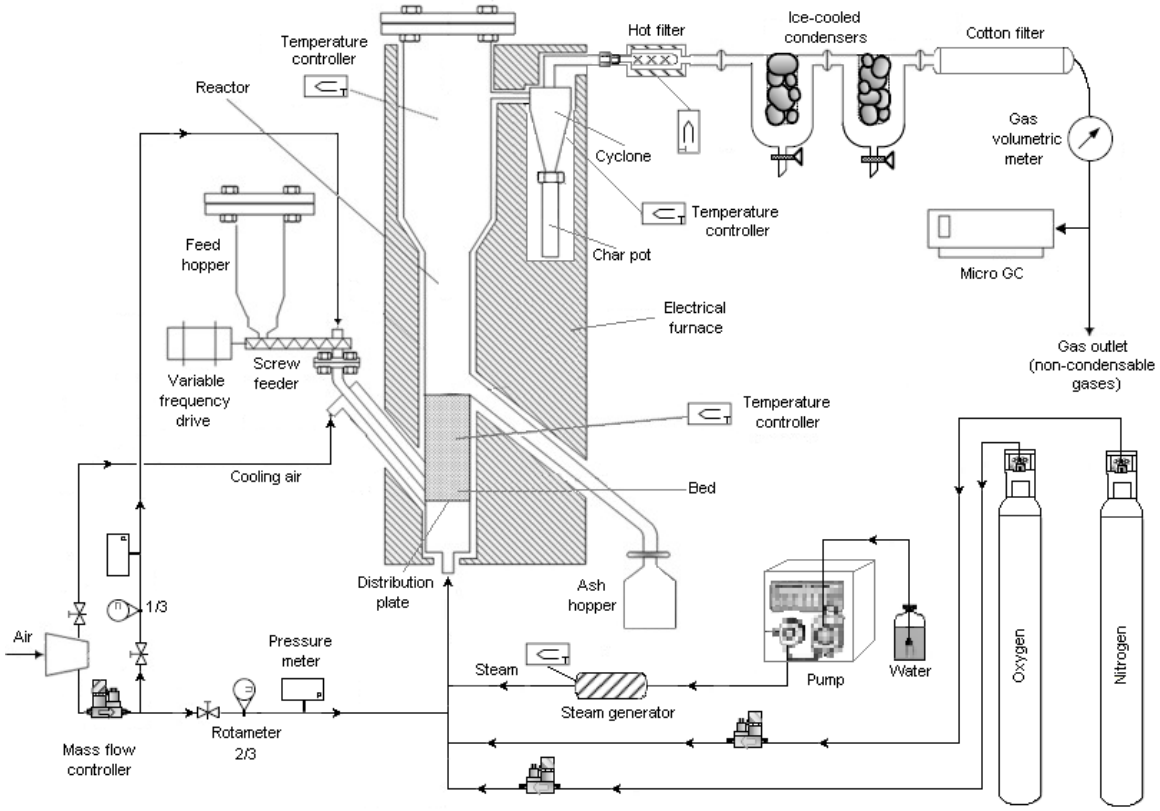


Figure 3.3. Lab-scale gasification experimental setup.

The gasifier was a tubular reactor (1270 mm height) made of refractory steel (AISI 310) divided into two parts: a bed zone (40 mm inner diameter) and a freeboard zone (70 mm inner diameter). The reactor was heated by an electrical furnace with three different heating zones which can be controlled independently (bed, free-board and cyclone). Temperature in each zone was measured by a K-type thermocouple. A feeding system composed of a hopper and a screw-feeder controlled by a variable frequency drive allowed continuous feed of the solid raw material. The solid feed rate was around 2.1 $g \cdot min^{-1}$ in all the gasification experiments (minimum value that could be obtained with the variable frequency drive). The feed pipe was cooled down by an air flow through an outer jacket to prevent reactions occurring out of solid bed. The solid bed at the beginning of the experiment was composed of ash from previous gasification tests (around 120 g). When the amount of accumulated solid in the reactor exceeded the height of the bed zone (310 mm), excess solid left the reactor by overflow through a lateral pipe and was collected in a separate vessel.

Different mixtures of steam and air (or enriched air) were used as gasifying/fluidizing agent. The air stream was enriched with pure oxygen in the experiments with the highest demand of oxygen to avoid an abrupt change in the fluidization rate. Fluidizing velocity was 5-7

times greater than the minimum fluidization rate during sewage sludge gasification and 2-3 times greater during char gasification. The lower organic content in the char is the reason for this difference.

The flow rate of gases (air and oxygen) was adjusted by means of mass flow controllers, while the required flow of liquid water was accurately adjusted by a HPLC pump. Water was evaporated before entering the reactor. Most of the gasifying agent was fed through the distribution plate located at the bottom of the reactor, but part of the required air (around one third) was diverted to the screw feeder to improve the movement of the solid through the feeding pipe. The residence time of the produced vapors and gases was around 7-8 s in the case of sewage sludge gasification, and a bit higher during char gasification (17-18 s) because of the lower flow rate of gasifying agent used.

The product gas passed through a cyclone and a hot filter, both at 450 $^{o}$C, in which the solid particles swept by the gas were collected. Next, gases and vapors passed through two ice-cooled condensers, where water and condensable organic compounds (tar) were collected. A cotton filter was situated after the condensers in order to remove small particulates and aerosols still present in the gas. The volume of particle-free and tar-free gas was measured with a volumetric meter (G4 Gallus 2000 gas meter) and its composition was analyzed on-line using a micro gas chromatograph (Agilent 3000-A) which determined the volume percentages of $H_2$, $N_2$, CO, $CO_2$, $CH_4$, $C_2H_4$, $C_2H_6$, $C_2H_2$ and $H_2S$. The experiments were carried out during 60-90 min to ensure the stationary state (Aznar et al., 2007).

The produced amount of solid and liquid products was determined after the experiments by gravimetry, that is, by weight difference of the collecting devices before and after the experiment. Methanol was used to wash the condensers when collecting the liquid. Water content in the condensed fraction was analyzed off line by Karl Fischer titration (Mettler Toledo V20 Karl Fischer titrator), so that tar fraction could be determined by difference. The amount of organic carbon in condensates can also give an idea of the tar content. This carbon content was determined with an analyzer of total organic carbon (TOC-L CSH/CSN analyzer Shimadzu), which measures the amount of $CO_2$ produced during the catalytic combustion of the liquid sample. Tar composition from sewage sludge gasification was qualitatively determined by gas chromatography combined with mass spectroscopy and flame ionization detection (Agilent 5975C inert GC/MSD complemented by Agilent 7890A GC system). Ultimate analyses of the solid by-products were performed with a Leco TruSpec Micro elemental analyzer and their ash contents were determined according to a standard method (ISO 1171-1976).

### *3.2.2. Desulphurization setup*

Desulphurization tests were performed at atmospheric pressure in a fixed-bed quartz tubular reactor of 1 cm inner diameter and 40 cm length. A schematic diagram of the experimental setup is shown in Fig. 3.4.

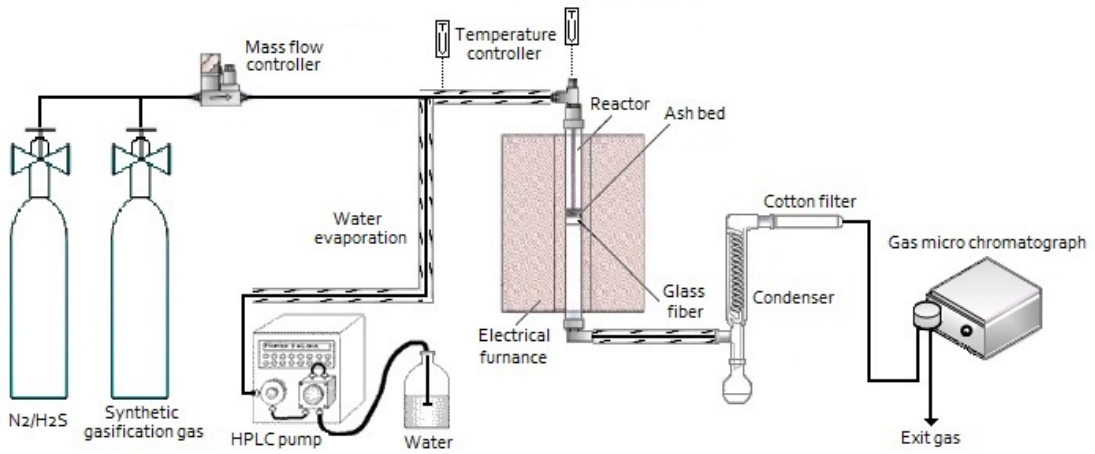


Figure 3.4. Experimental setup for desulphurization tests.

The reactor was packed with 1 g of the sorbent material (sewage sludge combustion ash or gasification ash), which was supported on a fibreglass fleece located 18.5 cm from the top of the reactor. The system was electrically heated to the desired temperature. A K-type thermocouple was used to measure and control the temperature in the middle of the solid bed. Two different inlet gases containing 5000 ppmv of $H_2S$ were used to evaluate the effect of the gas components on the desulphurization process (Table 3.4). The gas containing only $H_2S$ and $N_2$ allows the assessment of the desulphurization process without involving any interference from other gases, while the synthetic gasification gas simulates the composition of the gas from sewage sludge gasification, thus representing more real conditions for $H_2S$ removal.

Table 3.4. Composition of the gas mixtures used in the desulphurization tests (dry basis).

| Gas component | $H_2S/N_2$ mixture (vol. %) | Synthetic gasification gas (vol. %) |
|---|---|---|
| CO | -- | 10.0 |
| $CO_2$ | -- | 15.0 |
| $H_2$ | -- | 10.0 |
| $CH_4$ | -- | 4.0 |
| $C_2H_6$ | -- | 0.2 |
| $C_2H_4$ | -- | 1.5 |
| $C_2H_2$ | -- | 0.2 |
| $H_2S$ | 0.5 | 0.5 |
| $N_2$ | 99.5 | 58.6 |

The flow rate of the $H_2S$-containing gases was adjusted to 50 $mL_{STP}·min^{-1}$ by means of a previously calibrated mass flow controller. Steam was also added in some tests in order to evaluate its effect on the desulphurization ability of the solids. The required flow of liquid water was accurately adjusted by a HPLC pump and was evaporated before entering the reactor. The weight hourly space velocity during the experiments ranged between 3.7 $h^{-1}$ and 4.7 $h^{-1}$ depending on the steam feed rate. The gas-solid contact time was chosen after preliminary experiments and based on earlier studies (García et al., 2011).

The composition of the outlet gas was continuously analyzed during the experiments by means of a gas micro chromatograph (Agilent 3000). The $H_2S$ outlet flow was calculated from the gas composition data taking $N_2$ of the gas mixture as an internal standard. Initially, the established experimental time was two hours, but reaction time had to be extended in some cases to 240 or 390 min in order to reach the $H_2S$ breakthrough time.

Different tolerable levels of sulphur in gases can be found in the literature depending on the gas application. For instance, the $H_2S$ concentration limit ranges between 20 and 750 ppmv for gas turbine applications (Meng et al., 2010). An intermediate value of 100 ppmv has been used in this work to define the $H_2S$ breakthrough time.

After the desulphurization tests, sulphur content in the ash samples was determined with a Leco TruSpec Micro elemental analyzer. One of the ash samples was morphologically and chemically characterized by scanning electron microscopy combined with energy dispersive X-ray spectroscopy (SEM/EDX) and by X-ray photoelectron spectroscopy (XPS). A FEI Inspect F50 microscope *(Advanced Microscopy Laboratory of the Instituto de Nanociencia de Aragón)* was used for the SEM/EDX analysis. External metal coating was not applied to the solid sample. The back-scattered electron imaging mode was used in the EDX analysis (acquisition time of 1 min). The XPS measurements were performed with a Kratos AXIS ultra DLD spectrometer *(Laboratory of Microstructural Characterization and Spectroscopy of the Instituto de Nanociencia de Aragón)* by using monochromatic Al Kα (1486.6 eV) X-ray source and a chamber pressure of around $3·10^{-8}$ Pa. The quantification of the XPS spectra was carried out with the help of the CasaXPS software and spectra were deconvoluted by applying Gaussian-Lorentzian line-shapes with Shirley-type background.

### *3.2.3. Catalyst testing setup*

This part of the work was developed during a research stay at the VTT-Technical Research Centre of Finland. Tar reforming activity and stability of several Ni-based catalysts prepared with different promoters were evaluated. The activity tests were performed in a lab-scale

fixed-bed quartz reactor (1 cm inner diameter with 0.4 cm thermocouple pocket) operating at atmospheric pressure and in a temperature range of 700-900 ºC. The diagram of the experimental setup is shown in Fig. 3.5. The reactor was packed with 2 g of the solid powder catalyst (supported on a quartz frit) and placed in an electrical furnace. The reaction temperature was monitored with a K-type thermocouple located in the middle of the catalyst bed.

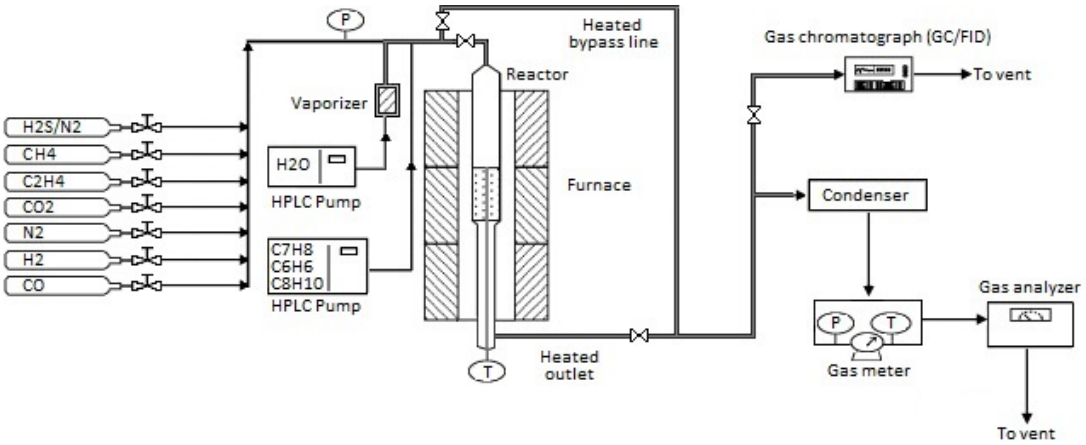


Figure 3.5. Experimental setup for catalyst activity tests.

A mixture of various gases (CO, $CO_2$, $H_2$, $N_2$, $C_2H_4$, $C_2H_4$ and steam) was used to simulate the composition of a typical gas resulting from the air-steam gasification of sewage sludge. Benzene, toluene and naphthalene were used as model compounds to simulate the presence of tar in the gasification gas, with a concentration of 15 $g \cdot m^{-3}_{STP}$. The composition of the resulting gas is shown in Table 3.5. The gas feed rate was adjusted to 1 $L_{STP} \cdot min^{-1}$ by means of independent mass flow controllers. The liquid reactants (water and the model tar mixture) were fed independently through HPLC pumps and vaporized before entering the reactor. All the gas lines were heated to 200 ºC to avoid condensation of the vapors. The gas space velocity (STP) was around 25000 $h^{-1}$.

Table 3.5. Composition of the synthetic gas used in catalysts testing (wet basis).

| Gas component | vol. % |
|---|---|
| $H_2O$ | 30 |
| CO | 6.6 |
| $CO_2$ | 12.5 |
| $H_2$ | 13.6 |
| $CH_4$ | 2.2 |
| $C_2H_4$ | 1.1 |
| $H_2S$ | 0.3 |
| $N_2$ | 33.4 |
| Tar content | 15 $g \cdot m^{-3}_{STP}$ |
| Tar composition toluene/naphthalene/benzene | 80/10/10 wt. % |

The product gas from the reactor was analyzed on-line with a gas chromatograph (Agilent 7980A) equipped with a flame ionization detector (FID) calibrated for benzene, toluene, naphthalene, methane and ethylene (analysis every 33 min). The condensable compounds were then removed by a cold trap consisting of isopropanol and water in series in an ice bath. The flow rate and temperature of the dry gas thus obtained were measured and the gas was directed to an on-line gas analyzer (Sick Maihak S710) which continuously measured the volumetric composition of the permanent gas components (CO, $CO_2$ and $H_2$). The accurate composition of the inlet gas was also determined before each test using the same equipment. Possible thermal cracking of tar compounds was taken into account by performing a blank run with a SiC bed.

The used samples of catalyst were characterized by X-ray diffraction and ultimate analysis, using the same equipment that was mentioned in section 3.1.2 for characterization of sewage sludge ash.

## 3.3. Operating conditions and experimental design

### *3.3.1. Gasification experiments*

The influence of some operating factors on the distribution of products and quality of the gas obtained from the gasification of sewage sludge and char has been evaluated and compared, using a two-level factorial experimental design ($2^k$ design, where k indicates the number of factors studied and $2^k$ represents the number of runs). This experimental design allows the assessment of the effect of the operating conditions, as well as of the existence of interactions between the factors, which occur when a factor influences a response variable in a different way depending on the value of another factor.

The analyzed factors were, in both cases, the following: (i) gasification temperature (770-850 $^oC$); (ii) gasifying ratio (GR), which is the ratio between the mass flow rate of gasifying agent ($H_2O+O_2$) and the feed rate of biomass on a dry and ash-free basis (0.8-1.1 $g \cdot g^{-1}_{daf}$); (iii) nature of the gasification medium, represented by the $H_2O/O_2$ molar ratio (1-3). The total flow rate of gasifying agent was kept constant when the $H_2O/O_2$ molar ratio was modified. These three factors together with their respective ranges of study were chosen according to other published studies concerning air-steam gasification of biomass in a fluidized bed reactor (Campoy et al., 2009; Gil et al., 1997; Lv et al., 2004; Pinto et al., 2003).

The operating conditions in the gasification tests are shown in Table 3.6. Three replicates at the average points in the studied range of the factors were carried out in order to evaluate

both the experimental error and the linearity/curvature in the response of the analyzed variables (experiments 9, 10 and 11 in sewage sludge gasification and 20, 21 and 22 in char gasification). The two levels of the factors in the $2^k$ experimental designs are usually represented as -1 (for the first or the lowest level) and +1 (for the second or the highest level), using 0 for the center points (average values).

Table 3.6. Operating conditions in the gasification tests.

| **SEWAGE SLUDGE GASIFICATION** | | | | | | | |
|---|---|---|---|---|---|---|---|
| Exp. | Coded values (T, GR, $H_2O/O_2$) | T ($^oC$) | GR ($g \cdot g^{-1}_{daf}$) | $H_2O/O_2$ | ER (%) | S/B ($g_{H2O} \cdot g^{-1}_{daf}$) | vol. % $O_2$ in air/enriched air |
| 1 | 1,1,1 | 850 | 1.1 | 3 | 17 | 0.71 | 21 |
| 2 | -1,1,1 | 770 | 1.1 | 3 | 17 | 0.71 | 21 |
| 3 | 1,-1,1 | 850 | 0.8 | 3 | 12 | 0.52 | 21 |
| 4 | -1,-1,1 | 770 | 0.8 | 3 | 12 | 0.52 | 21 |
| 5 | 1,1,-1 | 850 | 1.1 | 1 | 32 | 0.39 | 33 |
| 6 | -1,1,-1 | 770 | 1.1 | 1 | 32 | 0.39 | 33 |
| 7 | 1,-1,-1 | 850 | 0.8 | 1 | 23 | 0.27 | 27 |
| 8 | -1,-1,-1 | 770 | 0.8 | 1 | 23 | 0.27 | 27 |
| 9,10,11 | 0,0,0 | 810 | 0.95 | 2 | 19 | 0.52 | 23 |
| **CHAR GASIFICATION** | | | | | | | |
| Exp. | Coded values (T, GR, $H_2O/O_2$) | T ($^oC$) | GR ($g \cdot g^{-1}_{daf}$) | $H_2O/O_2$ | ER (%) | S/B ($g_{H2O} \cdot g^{-1}_{daf}$) | vol. % $O_2$ in air/enriched air |
| 12 | 1,1,1 | 850 | 1.1 | 3 | 17 | 0.71 | 27 |
| 13 | -1,1,1 | 770 | 1.1 | 3 | 17 | 0.71 | 27 |
| 14 | 1,-1,1 | 850 | 0.8 | 3 | 12 | 0.52 | 21 |
| 15 | -1,-1,1 | 770 | 0.8 | 3 | 12 | 0.52 | 21 |
| 16 | 1,1,-1 | 850 | 1.1 | 1 | 32 | 0.39 | 40 |
| 17 | -1,1,-1 | 770 | 1.1 | 1 | 32 | 0.39 | 40 |
| 18 | 1,-1,-1 | 850 | 0.8 | 1 | 23 | 0.27 | 33 |
| 19 | -1,-1,-1 | 770 | 0.8 | 1 | 23 | 0.27 | 33 |
| 20,21,22 | 0,0,0 | 810 | 0.95 | 2 | 19 | 0.52 | 29 |

*ER (%) = fraction of the stoichiometric oxygen that has been actually fed.*
*S/B = ratio between the mass flow rate of steam and the feed rate of biomass on a dry and ash-free basis.*

Experimental results obtained for each response variable have been statistically analyzed by means of analysis of variance (ANOVA), which compares the experimental variance associated with error with the variance caused by the modification of the factors. This comparison is performed using the F-test (Fischer's test) and allows to discriminate whether the observed effect is statistically significant compared to error with a predetermined confidence level (95% in this case). The Design-Expert® 7 software (from Stat-Ease, Inc.) was used for the analyses. The evolution of each response variable with the variation of the factors

can be empirically modeled using only the significant effects shown by the ANOVA analysis according to the following equation:

$$RV = \alpha+\beta_1 \cdot F_1+\beta_2 \cdot F_2+\beta_3 \cdot F_3+\beta_{12} \cdot F_1 \cdot F_2+\beta_{13} \cdot F_1 \cdot F_3+\beta_{23} \cdot F_2 \cdot F_3+\beta_{123} \cdot F_1 \cdot F_2 \cdot F_3 \quad \text{(eq. 3.1)}$$

where RV represent an experimental value of the response variable, α is the average value of the whole set of experimental results obtained for this response variable, $F_i$ is the coded value of factor "i", $\beta_i$ is the linear coefficient associated to factor "i", $\beta_{ij}$ is the coefficient associated to the interaction of factors "i" and "j" (synergic or antagonistic effect) and $\beta_{123}$ is the coefficient that represents a simultaneous interaction between the three factors. Coefficients of the non-significant effects do not appear in this equation. Although the existence of a significant curvature prevents the use of the linear regression model, the relative influence of the factors can be still assessed by comparison of coefficients $\beta_i$. Expressing the equation in terms of coded values of the factors (from -1 to +1) enables an easier identification of the term with the greatest influence on the response variable: the higher the absolute value of the coefficient, the more influential the factor.

### *3.3.2. Desulphurization tests*

Table 3.7 summarizes the operating conditions for the desulphurization tests. The operating factors studied were the following: (i) temperature (600-800 ºC); (ii) type of sewage sludge ash (combustion ash or gasification ash); (iii) type of $H_2S$-containing gas ($H_2S/N_2$ mixture or synthetic gasification gas); (iv) steam concentration in the inlet gas (0-30 vol. %), which resulted in a $H_2O/H_2S$ mass ratio ranging between 0 and 45 $g_{H2O} \cdot g^{-1}_{H2S}$. Experimental uncertainty was evaluated through three replicates performed when feeding the $H_2S/N_2$ mixture and operating at the average values of temperature (700 ºC) and $H_2O/H_2S$ mass ratio (22.5 $g \cdot g^{-1}$). The impact of the factors on the $H_2S$ breakthrough curves was statistically analyzed by ANOVA analysis (confidence level of 95% for the F-distribution).

Blank tests (with no bed material) were also performed at the different temperatures and gas atmospheres in order to assess any side effect of the experimental setup caused, for example, by the reaction of $H_2S$ with the hot metal parts (made of steel) at the reactor inlet and outlet.

Table 3.7. Operating conditions in the desulphurization tests.

| Experiment | Origin of sewage sludge ash | Synthetic gas mixture | Temperature (ºC) | $H_2O/H_2S$ mass ratio | Test duration (min) |
|---|---|---|---|---|---|
| 1 | Combustion | $H_2S/N_2$ | 600 | 0 | 300 |
| 2 | Combustion | $H_2S/N_2$ | 800 | 0 | 390 |
| 3 | Combustion | $H_2S/N_2$ | 600 | 45 | 120 |
| 4 | Combustion | $H_2S/N_2$ | 800 | 45 | 120 |
| 5,6,7 | Combustion | $H_2S/N_2$ | 700 | 22.5 | 120 |
| 8 | Gasification | $H_2S/N_2$ | 600 | 0 | 120 |
| 9 | Gasification | $H_2S/N_2$ | 800 | 0 | 390 |
| 10 | Gasification | $H_2S/N_2$ | 600 | 45 | 120 |
| 11 | Gasification | $H_2S/N_2$ | 800 | 45 | 120 |
| 12,13,14 | Gasification | $H_2S/N_2$ | 700 | 22.5 | 120 |
| 15 | Blank run | $H_2S/N_2$ | 600 | 0 | 120 |
| 16 | Blank run | $H_2S/N_2$ | 800 | 0 | 120 |
| 17 | Blank run | $H_2S/N_2$ | 600 | 45 | 120 |
| 18 | Blank run | $H_2S/N_2$ | 800 | 45 | 120 |
| 19 | Blank run | $H_2S/N_2$ | 700 | 22.5 | 120 |
| 20 | Combustion | Gasification gas | 600 | 0 | 240 |
| 21 | Combustion | Gasification gas | 800 | 0 | 240 |
| 22 | Combustion | Gasification gas | 600 | 45 | 120 |
| 23 | Combustion | Gasification gas | 800 | 45 | 120 |
| 24 | Gasification | Gasification gas | 600 | 0 | 120 |
| 25 | Gasification | Gasification gas | 800 | 0 | 240 |
| 26 | Gasification | Gasification gas | 600 | 45 | 120 |
| 27 | Gasification | Gasification gas | 800 | 45 | 120 |
| 28 | Blank run | Gasification gas | 600 | 0 | 120 |
| 29 | Blank run | Gasification gas | 800 | 0 | 240 |
| 30 | Blank run | Gasification gas | 600 | 45 | 120 |
| 31 | Blank run | Gasification gas | 800 | 45 | 120 |

The desulphurization tests performed at the laboratory were theoretically simulated to determine the maximum amount of $H_2S$ that could be removed from the gas from a thermodynamic point of view. HSC Chemistry® 6.1 software was used for this purpose. This software uses the Gibbs energy minimization method to calculate the amounts of products at equilibrium in isothermal and isobaric conditions. The reaction system (temperature, pressure, reactants and expected species to be part of the products) must be specified for the calculations. The expected species to be part of the products were the following: fed gases, sulphur-containing gases ($H_2S$, $SO_2$, COS), elemental sulphur (S), calcium-containing species (Ca, CaO, CaS, $CaCO_3$, $CaSO_4$ and $CaSO_3$), and iron-containing species (Fe, $Fe_xO_y$, $Fe_xS_y$, $Fe_x(SO_4)_y$ and $Fe_x(SO_3)_y$).

### *3.3.3. Catalyst testing*

Table 3.8 summarizes the operating conditions in the activity tests of the Ni-based catalysts. The effects of the added promoter (Ca, Cu, Fe or Mn), calcination temperature (700

or 900 ºC) and reduction procedure were evaluated. In order to obtain the metallic nickel active sites, the catalysts were reduced in some cases before starting the activity tests in a $H_2/N_2$ atmosphere at 900 ºC for 1 h (1 $L_{STP}$·$min^{-1}$, 50/50 vol. %). In other cases, the reduction was performed during the activity test itself in the reducing atmosphere created by the synthetic gasification gas.

Table 3.8. Operating conditions in the catalyst activity tests.

| Experiment | Catalyst | Calcination temperature (ºC) | Reduction pretreatment in $H_2/N_2$ atmosphere |
|---|---|---|---|
| 1 | $Ni/Al_2O_3$ | 900 | yes |
| 2 | $Ni/Ca/Al_2O_3$ | 900 | yes |
| 3 | $Ni/Cu/Al_2O_3$ | 900 | yes |
| 4 | $Ni/Fe/Al_2O_3$ | 900 | yes |
| 5 | $Ni/Mn/Al_2O_3$ | 900 | yes |
| 6 | $Ni/Al_2O_3$ | 900 | no |
| 7 | $Ni/Ca/Al_2O_3$ | 900 | no |
| 8 | $Ni/Cu/Al_2O_3$ | 900 | no |
| 9 | $Ni/Fe/Al_2O_3$ | 900 | no |
| 10 | $Ni/Mn/Al_2O_3$ | 900 | no |
| 11 | $Ni/Al_2O_3$ | 700 | no |
| 12 | $Ni/Ca/Al_2O_3$ | 700 | no |
| 13 | $Ni/Cu/Al_2O_3$ | 700 | no |
| 14 | $Ni/Fe/Al_2O_3$ | 700 | no |
| 15 | $Ni/Mn/Al_2O_3$ | 700 | no |

The effect of the reaction temperature on the catalyst activity was also studied by modifying the temperature during the tests. The temperature was programmed according to the following ramp: 900-850-800-900-750-700-900 ºC. Each temperature was maintained for 3.5 h, so the duration of the complete runs was 24.5 h. The loss of catalyst activity may be evaluated by comparing the conversion results obtained in the successive steps at 900 ºC.

# 4. DISCUSSION OF THE MAIN RESULTS

The main results obtained in the different studies of this PhD thesis are discussed in this section. Experimental results from sewage sludge gasification and char gasification, as well as the impact analysis of the operating factors, are presented in section 4.1. An energetic assessment of both gasification stages is included in section 4.2, also considering the pyrolysis process in which the char is produced and the prior thermal drying of the sewage sludge. Section 4.3 shows the results concerning desulphurization of various synthetic gases by using ash derived from the combustion and gasification of sewage sludge. Finally, the results obtained in the activity tests of nickel-catalysts prepared with different promoters for tar reforming under a $H_2S$-containing atmosphere are detailed in section 4.4.

## 4.1. Sewage sludge and char gasification

Gas is the product of interest from gasification, so most of the analyzed response variables are related to this product: gas production (dry gas yield) and specific yield of each non-condensable gas compound ($g \cdot kg^{-1}_{solid\ daf}$), gas composition ($H_2$/CO and CO/$CO_2$ ratios), tar content in the gas, lower heating value of the gas ($LHV_{gas}$) and gasification efficiency. The solid yield and the carbon distribution into the different products (solid, gas and tar) was also determined after the gasification runs. All these experimental results corresponding to sewage sludge gasification are summarized in Table 4.1, as a function of the operating conditions.

The ***solid yield***, defined as the mass (g) of solid product obtained per kilogram of sewage sludge fed, varied between 356 and 407 $g \cdot kg^{-1}_{SS}$. Typical values for other types of biomass such as wood or straw are usually below 80 $g \cdot kg^{-1}$ (McKendry, 2002a). The high ash content in the sewage sludge (39 wt. %) explains this difference. The solid yield was found to be lower than the initial ash content of sewage sludge in some cases, suggesting some transformations and release of ash compounds to gas phase.

The ***distribution of initial carbon content*** of sewage sludge into the different products was determined from different analysis of the products: the fraction of carbon remaining as solid (2-23%) was calculated from the ultimate analyses of the solid samples; the fraction of carbon forming tar (4-7%) was calculated from the total organic carbon present in the liquid fractions, and the fraction of carbon converted into non-condensable gases (61.3-89.7%) was calculated from the gas composition experimental results. Carbon mass balances closed to 78-95%. The possible formation of light hydrocarbons not detected by the micro-GC ($C_3H_x$, $C_4H_x$...) or the

poor solubility of tar compounds in the aqueous solutions for determination of the total organic carbon may explain the observed defect carbon.

Table 4.1. Experimental results from sewage sludge gasification.

| Temperature (°C) | 850 | 770 | 850 | 770 | 850 | 770 | 850 | 770 | 810 |
|---|---|---|---|---|---|---|---|---|---|
| Gasifying ratio ($g \cdot g^{-1}_{daf}$) | 1.1 | 1.1 | 0.8 | 0.8 | 1.1 | 1.1 | 0.8 | 0.8 | 0.95 |
| $H_2O/O_2$ molar ratio | 3 | 3 | 3 | 3 | 1 | 1 | 1 | 1 | 2 |
| Solid yield ($g \cdot kg^{-1}_{SS}$) | 368 | 401 | 401 | 407 | 356 | 392 | 384 | 400 | 382 ± 1 |
| Carbon fraction remaining as solid (%) | 3 | 17 | 8 | 23 | 2 | 9 | 2 | 12 | 7 ± 1 |
| Carbon fraction converted into gas (%) | 76.4 | 61.3 | 65.1 | 61.8 | 89.7 | 74.8 | 83.1 | 65.7 | 73.1 ± 0.8 |
| Carbon fraction forming tar (%) | 4 | 7 | 5 | 5 | 4 | 7 | 4 | 6 | 5 ± 1 |
| Dry gas yield ($N_2$-free, $m^3_{STP} \cdot kg^{-1}_{SS}$) | 0.72 | 0.51 | 0.65 | 0.53 | 0.72 | 0.52 | 0.71 | 0.49 | 0.61 ± 0.01 |
| Dry gas yield ($N_2$-free, $m^3_{STP} \cdot kg^{-1}_{SS\ daf}$) | 1.32 | 0.94 | 1.20 | 0.97 | 1.32 | 0.96 | 1.30 | 0.89 | 1.13 ± 0.01 |
| Tar content ($g \cdot m^{-3}_{STP}$) | 19 | 44 | 19 | 44 | 12 | 22 | 11 | 45 | 15 ± 1 |
| Gas composition (dry basis) | | | | | | | | | |
| $H_2$ (vol. %) | 24.2 | 18.4 | 25.1 | 20.4 | 18.0 | 11.0 | 20.6 | 13.6 | 19.3 ± 0.1 |
| CO (vol. %) | 8.7 | 5.7 | 10.2 | 7.3 | 11.6 | 7.0 | 14.1 | 7.7 | 9.4 ± 0.1 |
| $CO_2$ (vol. %) | 17.1 | 18.6 | 12.6 | 15.5 | 20.7 | 23.8 | 16.0 | 19.8 | 18.1 ± 0.2 |
| $CH_4$ (vol. %) | 3.1 | 3.5 | 3.6 | 4.1 | 2.6 | 2.8 | 2.9 | 3.4 | 3.3 ± 0.1 |
| $C_2H_x$ (vol. %) | 1.7 | 2.1 | 1.4 | 2.2 | 1.3 | 1.6 | 1.4 | 2.0 | 1.7 ± 0.2 |
| $H_2S$ (vol. %) | 0.44 | 0.38 | 0.33 | 0.33 | 0.44 | 0.42 | 0.38 | 0.31 | 0.40 ± 0.02 |
| $N_2$ (vol. %) | 44.9 | 51.4 | 46.8 | 50.2 | 45.3 | 53.4 | 44.5 | 53.2 | 47.8 ± 0.2 |
| Mass yield of each gas compound ($g \cdot kg^{-1}_{SS\ daf}$) | | | | | | | | | |
| $H_2$ | 51.8 | 31.8 | 50.4 | 36.5 | 38.6 | 20.1 | 43.1 | 23.2 | 37.2 ± 0.4 |
| CO | 260 | 137 | 287 | 182 | 351 | 179 | 414 | 183 | 253 ± 2 |
| $CO_2$ | 806 | 707 | 557 | 608 | 980 | 962 | 736 | 740 | 767 ± 7 |
| $CH_4$ | 53 | 49 | 59 | 59 | 45 | 41 | 49 | 46 | 51 ± 1 |
| $C_2H_x$ | 50 | 52 | 40 | 55 | 40 | 42 | 40 | 48 | 47 ± 4 |
| $H_2S$ | 16.0 | 11.2 | 11.4 | 10.0 | 16.1 | 13.1 | 13.5 | 9.0 | 13.0 ± 0.8 |
| $H_2$/CO molar ratio in the product gas | 2.79 | 3.25 | 2.46 | 2.81 | 1.54 | 1.57 | 1.46 | 1.77 | 2.06 ± 0.01 |
| $CO/CO_2$ molar ratio in the product gas | 0.51 | 0.30 | 0.81 | 0.47 | 0.56 | 0.29 | 0.88 | 0.39 | 0.52 ± 0.01 |
| LHV gas ($MJ \cdot m^{-3}_{STP}$) | 5.9 | 5.3 | 6.2 | 6.0 | 5.2 | 4.1 | 6.0 | 4.9 | 5.6 ± 0.1 |
| Cold gasification efficiency (%) | 65.8 | 47.7 | 64.7 | 55.3 | 58.4 | 39.1 | 64.7 | 43.4 | 55.8 ± 0.8 |

*Data in the last column show the "mean ± standard deviation" obtained from the 3 replicates at the center point.*

The ***dry gas yield*** from sewage sludge varied between 0.89 and 1.32 $m^3_{STP} \cdot kg^{-1}_{SS\ daf}$, expressing the volume of gas on $N_2$-free basis and the mass of sewage sludge on a dry and ash-free basis (*daf*). These values are in the same range as those obtained from the gasification of

other types of biomass under similar operating conditions (Campoy et al., 2009; Gil et al., 1999b; Pinto et al., 2003). As usual in a biomass gasification process, the main gases produced during sewage sludge gasification were $H_2$, CO, $CO_2$ and light hydrocarbons, $CH_4$ being the most abundant hydrocarbon. $H_2S$ was also released during the process due to the presence of sulphur-compounds in the sewage sludge (Table 3.1). As a consequence of the use of air, the presence of $N_2$ accounted for 45-55% of the total gas volume. The same amount of $N_2$ was fed in all tests to avoid different dilution effects.

Considerable differences in the ***gas composition*** have been found. The concentration of $H_2$ (11.0-25.1 vol. %), CO (5.7-14.1 vol. %), $CO_2$ (12.6-23.8 vol. %) or $CH_4$ (2.6-4.1 vol. %) was doubled or halved depending on the operating conditions. These volume percentages led to a $H_2$/CO molar ratio in the exit gas ranging between 1.46 and 3.25 and a CO/$CO_2$ molar ratio ranging between 0.29 and 0.88. The ***$H_2$/CO molar ratio*** is an important parameter in view of possible end uses of the gas, and values close to 2 are usually required in processes such as methanol production or Fischer Tropsch synthesis (Wender, 1996). On the other hand, the ***CO/$CO_2$ ratio*** shows how the carbon content of sewage sludge is distributed among both compounds. Higher CO/$CO_2$ are preferred from an energy standpoint.

The ***tar content*** in the product gas varied from 11 to 45 $g \cdot m^{-3}_{STP}$. The highest values (22-45 $g \cdot m^{-3}_{STP}$) were obtained at the lowest operating temperature (770 ºC), while the lowest values (< 19 $g \cdot m^{-3}_{STP}$) are among the reported values for bubbling fluidized bed gasifiers (Han and Kim, 2008).

The ***lower heating value of the gas*** ($LHV_{gas}$) was calculated as $\Sigma$ ($x_i \cdot LHV_i$), where $x_i$ and $LHV_i$ are the volumetric fraction and the lower heating value ($MJ \cdot m^{-3}_{STP}$) of each gaseous compound, respectively. The LHV of the product gas of sewage sludge gasification ranged between 4.1 and 6.2 $MJ \cdot m^{-3}_{STP}$. The prevailing dilution effect of $N_2$ causes the gas calorific value from the air-steam gasification to be in the same range as that reported for biomass gasification when only air is used as gasifying agent (McKendry, 2002b).

The ***cold gasification efficiency*** is defined as the ratio between the energy contained in the gas product (gas volume · $LHV_{gas}$), not taking into account its sensible heat, and the energy contained in the mass of sewage sludge fed (mass of SS · $LHV_{SS}$). A wide range of experimental values was obtained, ranging from 39.1 and 65.8%.

Experimental results corresponding to char gasification, obtained at the same operating conditions that those of sewage sludge gasification, are summarized in Table 4.2.

Table 4.2. Experimental results from char gasification.

| Temperature (ºC) | 850 | 770 | 850 | 770 | 850 | 770 | 850 | 770 | 810 |
|---|---|---|---|---|---|---|---|---|---|
| Gasifying ratio ($g \cdot g^{-1}_{daf}$) | 1.1 | 1.1 | 0.8 | 0.8 | 1.1 | 1.1 | 0.8 | 0.8 | 0.95 |
| $H_2O/O_2$ molar ratio | 3 | 3 | 3 | 3 | 1 | 1 | 1 | 1 | 2 |
| Solid yield ($g \cdot kg^{-1}_{char}$) | 757 | 785 | 750 | 785 | 731 | 771 | 752 | 813 | 775 ± 2 |
| Carbon fraction remaining as solid (%) | 20 | 41 | 25 | 43 | 15 | 26 | 19 | 41 | 34 ± 3 |
| Carbon fraction converted into gas (%) | 71 | 56 | 62 | 48 | 83 | 67 | 72 | 56 | 62 ± 2 |
| Carbon fraction forming tar (%) | 1.3 | 0.7 | 2.9 | 3.3 | 1.0 | 5.7 | 3.2 | 5.8 | 2.8 ± 0.7 |
| Dry gas yield ($N_2$-free, $m^3_{STP} \cdot kg^{-1}_{char}$) | 0.36 | 0.27 | 0.31 | 0.24 | 0.35 | 0.28 | 0.32 | 0.24 | 0.29 ± 0.01 |
| Dry gas yield ($N_2$-free, $m^3_{STP} \cdot kg^{-1}_{char\ daf}$) | 1.47 | 1.12 | 1.30 | 0.99 | 1.46 | 1.15 | 1.31 | 1.00 | 1.21 ± 0.01 |
| Tar content ($g \cdot m^{-3}_{STP}$)* | 4 | 3 | 9 | 13 | 3 | 20 | 10 | 22 | 9 ± 2 |
| Gas composition (dry basis) | | | | | | | | | |
| $H_2$ (vol. %) | 29.3 | 26.3 | 27.8 | 24.8 | 21.5 | 19.0 | 22.0 | 20.2 | 25.2 ± 0.6 |
| CO (vol. %) | 19.5 | 12.0 | 20.2 | 12.8 | 22.7 | 14.0 | 23.7 | 15.2 | 15.9 ± 0.2 |
| $CO_2$ (vol. %) | 18.9 | 24.2 | 16.2 | 20.8 | 22.6 | 29.5 | 18.5 | 24.1 | 21.9 ± 0.1 |
| $CH_4$ (vol. %) | 0.76 | 0.91 | 0.77 | 0.92 | 0.59 | 0.70 | 0.64 | 0.84 | 0.88 ± 0.01 |
| $C_2H_x$ (ppmv) | 150 | 190 | 160 | 220 | 180 | 220 | 150 | 200 | 180 ± 10 |
| $H_2S$ (vol. %) | 0.25 | 0.12 | 0.14 | 0.07 | 0.17 | 0.08 | 0.12 | 0.06 | 0.10 ± 0.01 |
| $N_2$ (vol. %) | 31.3 | 36.5 | 34.9 | 40.7 | 32.5 | 36.7 | 35.0 | 39.6 | 36.1 ± 0.6 |
| Mass yield of each gas compound ($g \cdot kg^{-1}_{char\ daf}$) | | | | | | | | | |
| $H_2$ | 56.7 | 42.1 | 49.9 | 36.8 | 41.6 | 30.8 | 39.7 | 30.0 | 42.8 ± 0.3 |
| CO | 529 | 268 | 506 | 266 | 615 | 318 | 598 | 316 | 379 ± 10 |
| $CO_2$ | 808 | 853 | 637 | 679 | 960 | 1055 | 735 | 786 | 821 ± 20 |
| $CH_4$ | 11.7 | 11.7 | 11.0 | 10.9 | 9.1 | 9.0 | 9.2 | 9.9 | 11.9 ± 0.1 |
| $C_2H_x$ | 0.41 | 0.42 | 0.41 | 0.47 | 0.50 | 0.50 | 0.39 | 0.42 | 0.42 ± 0.04 |
| $H_2S$ | 8.2 | 3.2 | 4.1 | 1.8 | 5.7 | 2.3 | 3.7 | 1.5 | 2.8 ± 0.1 |
| $H_2$/CO molar ratio in the product gas | 1.50 | 2.20 | 1.38 | 1.93 | 0.95 | 1.36 | 0.93 | 1.33 | 1.58 ± 0.04 |
| CO/$CO_2$ molar ratio in the product gas | 1.03 | 0.49 | 1.25 | 0.62 | 1.00 | 0.47 | 1.28 | 0.63 | 0.73 ± 0.01 |
| $LHV_{gas}$ ($MJ \cdot m^{-3}_{STP}$) | 5.96 | 4.71 | 5.87 | 4.65 | 5.44 | 4.09 | 5.63 | 4.43 | 5.07 ± 0.07 |
| Cold gasification efficiency (%) | 62.9 | 41.1 | 57.2 | 37.6 | 57.4 | 36.2 | 55.3 | 35.7 | 47.0 ± 0.6 |

*Data in the last column show the "mean ± standard deviation" obtained from the 3 replicates at the center point.*
** The amount of tar was approximated to the amount of organic carbon detected in the condensed liquid fraction.*

The ***solid yield*** from char gasification varied from 731 to 813 $g \cdot kg^{-1}_{char}$, though this solid was mainly composed of ash (93-96 wt. % according to ISO-1171-1976 analysis).

Regarding the ***distribution of initial carbon content*** into the different products, the fraction of initial carbon remaining as solid after char gasification ranged between 15 and 43%,

while the maximum value for sewage sludge gasification was about 23% (Table 4.1). This difference may be explained by the different structure of the carbonaceous matter in the solid. Only 15% of the carbon content was in the form of fixed carbon in the sewage sludge, while this value reached 59% in the char (Table 3.1). Gasification reactions of solid carbon are slower than devolatilization and gas phase reactions, which results in both an increased fraction of initial carbon remaining as solid and a reduced fraction of carbon forming non-condensable gases during char gasification (48-83%). However, results of carbon conversion during char gasification can be recalculated considering both the previous pyrolysis of sewage sludge and the subsequent gasification of char as a whole. The initial carbon content of sewage sludge (29.5 wt. %) has to be used as a reference for recalculating the carbon conversion in this case. Given a char yield of around 52 wt. % during sewage sludge pyrolysis (Gil-Lalaguna et al., 2010), the fraction of initial carbon remaining as solid after sewage sludge pyrolysis and char gasification is reduced to 4-11%, thus improving in some cases the conversion results obtained from the direct gasification of sewage sludge.

***Tar formation*** during char gasification declined compared to the results obtained in sewage sludge gasification but, in general, this reduction was not as high as the reduction in the initial volatile content of both raw materials (Table 3.1). The tar content in the gas from char gasification was as low as 3-4 $g \cdot m^{-3}_{STP}$ under some operating conditions, while the lowest value achieved in sewage sludge gasification was about 11-12 $g \cdot m^{-3}_{STP}$.

The ***dry gas yield*** from char gasification varied between 0.24 and 0.36 $m^3_{STP} \cdot kg^{-1}_{char}$ ($N_2$-free basis), or between 0.40 and 0.52 $m^3_{STP} \cdot kg^{-1}_{char}$ if $N_2$ is included in the gas volume. The production of gas per kilogram of raw material during char gasification was halved compared to that from sewage sludge gasification (0.51-0.72 $m^3_{STP} \cdot kg^{-1}_{SS}$, $N_2$-free basis) due to the higher ash content of char. The production of gas during the previous fast pyrolysis process of sewage sludge (around 0.07 $m^3_{STP} \cdot kg^{-1}_{SS}$) is not high enough to offset this difference since that process was focused on maximizing the liquid fraction. On the other hand, the gas yield expressed on a dry and ash-free basis for the solid was improved by gasifying the char (0.99-1.47 $m^3_{STP} \cdot kg^{-1}_{char}$) instead of the sewage sludge (0.89-1.32 $m^3_{STP} \cdot kg^{-1}_{SS}$) since carbon content was more concentrated in the dry and ash-free fraction of the solid after pyrolysis (0.64 g $C \cdot g^{-1}_{char\ daf}$ vs. 0.54 g $C \cdot g^{-1}_{SS\ daf}$). The dry gas yield ($N_2$-free and *daf* basis) from the gasification of char derived from sewage sludge is in the same range as those obtained from lignocellulosic chars, such as bagasse char (Chaudhari et al., 2003) or char derived from ramie residues (He at al., 2012).

Regarding ***gas composition***, $H_2$ (19.0-29.3 vol. %), CO (12.0-23.7 vol. %), $CO_2$ (16.2-29.5 vol. %), $CH_4$ (0.59-0.92 vol. %) and $N_2$ (31.3-40.7 vol. %) were the main gases detected by the micro

GC during char gasification. The CO mass yield (in terms of $g \cdot kg^{-1}_{solid\ daf}$) was clearly improved by gasifying char instead of sewage sludge (45-85% higher in most cases), while $CH_4$ production was reduced by 75-82%. Variations in the production of $H_2$ and $CO_2$ (in terms of $g \cdot kg^{-1}_{solid\ daf}$) were not so significant. However, it should be noted that gas yields calculated with respect to the whole feedstock and not on a dry and ash-free basis are considerably higher for sewage sludge gasification. The ***$H_2$/CO molar ratio*** obtained from char gasification (0.93-2.20) was lower than that obtained from sewage sludge gasification (1.46-3.25), while the ***$CO/CO_2$ molar ratio*** was higher for char gasification (0.47-1.28) than for sewage sludge gasification (0.29-0.88). Thus, CO formation was only favored rather than $CO_2$ formation ($CO/CO_2 > 1$) under some operating conditions in char gasification. The ***lower heating value of the gas*** (4.09-5.96 $MJ \cdot m^{-3}_{STP}$) and the ***cold gasification efficiency*** (36.2-62.9%) of char gasification were in the same range as those obtained for sewage sludge gasification.

The influence of temperature (T), gasifying ratio (GR) and composition of the gasification medium ($H_2O/O_2$ molar ratio) on the aforementioned response variables has been statistically evaluated. Tables 4.3 and 4.4 show the linear regression coefficients obtained from the ANOVA analysis of the experimental results of sewage sludge gasification and char gasification, respectively. These coefficients are expressed in terms of coded values for the factors.

Table 4.3. Linear regression coefficients (β) from ANOVA analysis of sewage sludge gasification results.

| | Average | $\beta_T$ | $\beta_{GR}$ | $\beta_{H2O/O2}$ | $\beta_{T\text{-}GR}$ | $\beta_{T\text{-}H2O/O2}$ | $\beta_{GR\text{-}H2O/O2}$ | $\beta_{T\text{-}H2O/O2\text{-}GR}$ | Curvature |
|---|---|---|---|---|---|---|---|---|---|
| Carbon fraction remaining as solid (%) | 9.01 | -5.76 | -1.74 | 3.29 | * | -1.50 | * | * | * |
| Carbon fraction converted into gas (%) | 72.48 | 6.33 | 3.33 | -6.07 | * | * | * | * | * |
| Dry gas yield ($N_2$-free, $m^3_{STP} \cdot kg^{-1}_{SS\ daf}$) | 1.12 | 0.17 | 0.02 | * | 0.02 | -0.02 | * | 0.03 | ** |
| Tar content ($g \cdot m^{-3}_{STP}$) | 27.03 | -11.91 | -2.78 | 4.35 | 3.15 | * | 2.62 | -2.89 | ** |
| Yield of gaseous compounds ($g \cdot kg^{-1}_{SS\ daf}$) | | | | | | | | | |
| $H_2$ | 37.03 | 9.06 | -1.37 | 5.68 | * | * | * | * | * |
| CO | 250.10 | 78.79 | -17.51 | -32.67 | -5.03 | -21.95 | * | 9.65 | * |
| $CO_2$ | 763.42 | * | 101.57 | -92.53 | 21.59 | * | -14.93 | 15.91 | * |
| $CH_4$ | 50.23 | 1.49 | -3.13 | 4.80 | * | * | * | * | * |
| $C_2H_x$ | 46.13 | -3.28 | * | 3.35 | * | * | * | * | * |
| $H_2S$ | 12.66 | 1.73 | 1.56 | * | * | * | * | 0.62 | * |
| $H_2$/CO molar ratio in the product gas | 2.21 | -0.14 | 0.08 | 0.62 | 0.02 | -0.06 | 0.11 | -0.05 | ** |
| $CO/CO_2$ molar ratio in the product gas | 0.52 | 0.16 | -0.11 | * | -0.04 | -0.03 | * | * | * |
| $LHV_{gas}$ ($MJ \cdot m^{-3}_{STP}$) | 5.49 | 0.37 | -0.31 | 0.40 | * | -0.17 | * | * | * |
| Cold gasification efficiency (%) | 55.12 | 8.51 | * | 3.47 | * | * | * | * | * |

** non-significant term; ** significant curvature*

Table 4.4. Linear regression coefficients (β) from ANOVA analysis of char gasification results.

| | Average | $\beta_T$ | $\beta_{GR}$ | $\beta_{H2O/O2}$ | $\beta_{T\text{-}GR}$ | $\beta_{T\text{-}H2O/O2}$ | $\beta_{GR\text{-}H2O/O2}$ | $\beta_{T\text{-}H2O/O2\text{-}GR}$ | Curvature |
|---|---|---|---|---|---|---|---|---|---|
| Carbon fraction remaining as solid (%) | 30.13 | -9.16 | -3.30 | 3.59 | * | * | * | * | * |
| Carbon fraction converted into gas (%) | 64.29 | 7.76 | 4.82 | -5.16 | * | * | * | * | ** |
| Dry gas yield ($N_2$-free, $m^3_{STP}\cdot kg^{-1}_{char\ daf}$) | 1.23 | 0.16 | 0.08 | * | * | * | * | * | ** |
| Tar content ($g\cdot m^{-3}_{STP}$) | 10.52 | -3.97 | -3.15 | -3.40 | * | 3.45 | * | * | * |
| Yield of gaseous compounds ($g\cdot kg^{-1}_{char\ daf}$) | | | | | | | | | |
| $H_2$ | 40.93 | 6.03 | 1.86 | 5.43 | 0.33 | 0.90 | 1.18 | * | ** |
| CO | 427.16 | 135.09 | * | -34.61 | * | -9.78 | * | * | ** |
| $CO_2$ | 815.96 | -29.09 | 104.91 | -69.95 | * | * | -18.75 | * | * |
| $CH_4$ | 10.33 | * | * | 1.01 | * | * | 0.32 | * | ** |
| $C_2H_x$ | 0.44 | * | * | * | * | * | -0.03 | * | * |
| $H_2S$ | 3.54 | 1.62 | 1.03 | * | * | * | * | * | * |
| $H_2$/CO molar ratio in the product gas | 1.48 | -0.26 | * | 0.31 | * | * | * | * | * |
| $CO/CO_2$ molar ratio in the product gas | 0.85 | 0.29 | -0.10 | * | -0.03 | * | 0.01 | * | ** |
| $LHV_{gas}$ ($MJ\cdot m^{-3}_{STP}$) | 5.09 | 0.63 | * | 0.20 | * | * | 0.08 | * | * |
| Cold gasification efficiency (%) | 47.90 | 10.27 | 1.45 | 1.77 | 0.48 | * | 0.83 | * | ** |

** non-significant term; ** significant curvature*

Temperature is the most influential factor on the fraction of initial carbon remaining as solid after the gasification processes. This carbon fraction can be practically halved by increasing the gasification temperature from 770 to 850 ºC (Fig. 4.1). Furthermore, the positive coefficient associated to the $H_2O/O_2$ ratio ($\beta_{H2O/O2} > 0$) suggests a higher reactivity of carbon with $O_2$ compared to its reactivity with steam. The similar conclusion was drawn by Nowicki et al. (2011) by conducting some gasification tests in a thermobalance with different gas atmospheres ($CO_2$, $H_2O$ and $O_2$). The gaseous mixtures containing $O_2$ were found to be the most efficient gasifying agents. In the case of sewage sludge gasification, the effect of the gasification medium seems to be mitigated at high temperatures (Fig. 4.1.a). As expected, the increase in the gasifying ratio also leads to a reduction in the fraction of initial carbon that remains in the solid by-product after gasification ($\beta_{GR} < 0$).

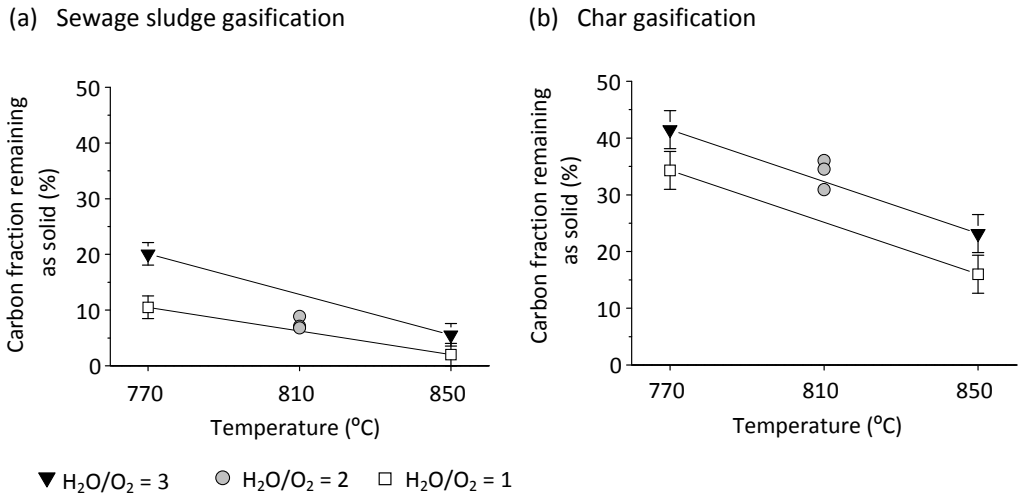


Figure 4.1. Fraction of initial carbon remaining in the solid-byproduct after (a) sewage sludge gasification and (b) char gasification (GR = 0.95 $g \cdot g^{-1}_{solid\ daf}$). Error bars in the figures represent the least significant difference (LSD).

Experimental results show a clear connection between the fraction of carbon remaining as solid and the fraction of carbon converted into gases: the lower the carbon fraction remaining as solid, the higher the carbon fraction converted into non-condensable gases. Hence, the formation of non-condensable carbonaceous gases is positively affected by the temperature ($\beta_T > 0$) and by the gasifying ratio ($\beta_{GR} > 0$), and negatively affected by the $H_2O/O_2$ ratio ($\beta_{H2O/O2} < 0$) (Fig. 4.2).

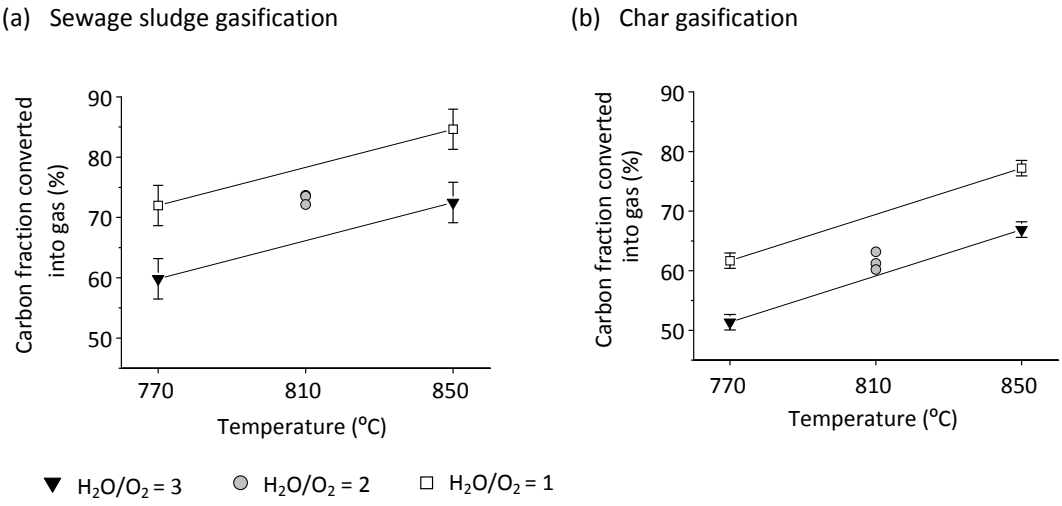


Figure 4.2. Fraction of initial carbon converted into gas during (a) sewage sludge gasification and (b) char gasification (GR = 0.95 $g \cdot g^{-1}_{solid\ daf}$). Error bars in the figures represent the least significant difference.

Dry gas yield is strongly dependent on the reaction temperature ($\beta_T > 0$). During the gasification process, gas is produced at different stages that are favored at higher

temperatures, such as the initial stage of pyrolysis, the cracking and steam reforming of tars and the endothermic gasification reactions of the carbonaceous solid (Pinto et al., 2003). The increase of the gasifying ratio (GR) is also favorable for gas production ($\beta_{GR} > 0$), especially during char gasification, whereas the composition of the gasification medium does not exert a significant influence on the dry gas yield obtained from the gasification of either char or sewage sludge. Hence, the above mentioned negative effect of $H_2O/O_2$ on the gasified carbon fraction does not result in a significant variation of the dry gas yield. Different production rates of $H_2$ may explain this disagreement since, as discussed below, $H_2$ formation is promoted by increasing the $H_2O/O_2$ ratio, thus counteracting the observed decrease in the production of carbon-containing gases at high $H_2O/O_2$ ratios. Some synergic and antagonistic effects between the factors are statistically significant on the evolution of the gas yield from sewage sludge gasification, but these are much less important than the individual effect of gasification temperature.

Temperature is also the most influential factor on the tar content of sewage sludge gasification gas, while the three studied factors exert similar effects during char gasification. The rise in temperature not only favors the gasification reactions of solid carbon, but also the tar reforming reactions rate. The tar content is also reduced by increasing the gasifying ratio ($\beta_{GR} < 0$), but this effect practically disappears when operating at high temperatures or high $H_2O/O_2$ ratios during sewage sludge gasification. The composition of the gasification medium has shown opposite effects on the tar content of the gases produced during sewage sludge gasification and char gasification: the decrease of the $H_2O/O_2$ ratio is favorable for reducing the tar content during sewage sludge gasification ($\beta_{H2O/O2} > 0$), while this reduction involves an increase of the tar content during char gasification ($\beta_{H2O/O2} < 0$). In this latter case, the effect of the $H_2O/O_2$ ratio is significantly mitigated at high temperatures. Thus, the surface response of tar content cannot be modelled by a horizontal plane due to the importance of the interaction between the temperature and the $H_2O/O_2$ ratio (Fig. 4.3).

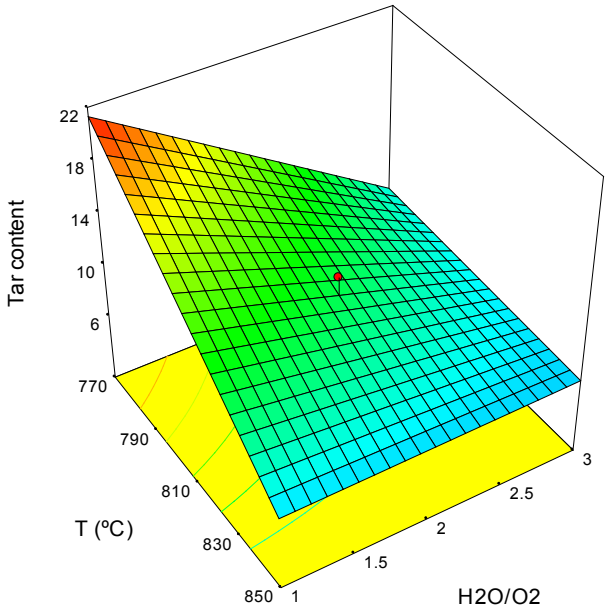


Figure 4.3. Tar content ($g \cdot m^{-3}_{STP}$) in the product gas from char gasification (GR = 0.95 $g \cdot g^{-1}_{daf}$).

The production or mass yield ($g \cdot kg^{-1}_{solid\ daf}$) of each non-condensable gaseous compound was calculated from gas volume and gas composition data. As can be noted from β coefficients shown in Tables 4.3 and 4.4, gasification temperature is again the most influential factor on the production of both $H_2$ and CO. These gases are involved in many reactions both as reactants and as products, but the temperature rise seems to enhance their formation rather than their consuming reactions ($\beta_T > 0$). Tar reforming also contributes to the increase of $H_2$ and CO production at high temperatures (eq. 2.9 and 2.10). Other studies in the literature have shown negligible variations or even the opposite trend on the CO production when varying the temperature (Gil et al., 1997; Lv et al., 2004), which reveals the importance of the biomass nature and the operating conditions on the evolution of this compound.

Although to a lesser extent, the production of $H_2$ is also improved by increasing the $H_2O/O_2$ ratio ($\beta_{H2O/2} > 0$), unlike the CO yield which decreases with $H_2O/O_2$ ($\beta_{H2O/2} < 0$). Both observed trends are consistent with the water-gas shift reaction (eq. 2.6), which seems one of the most representative reactions for a steam gasification process for temperatures up to 830 ºC (Franco et al., 2003). Franco et al. (2003) found that, at higher temperatures (830-900 ºC), solid-gas reactions such as the water gas reaction (eq. 2.3) and the Boudouard reaction (eq. 2.4) appeared to prevail, which can explain the positive effect of temperature on CO formation. This positive effect is mitigated by increasing the presence of steam (Fig. 4.4.a), probably due to the shift of the water-gas shift reaction to CO consumption. Besides increasing the presence of steam, the increase of the $H_2O/O_2$ ratio entails a reduction of the availability of oxygen in

the gasification medium, which should mitigate the combustion reactions. However, the negative effect of $H_2O/O_2$ on the production of CO suggests that steam plays a more significant role than $O_2$ in CO consumption.

(a) CO yield from sewage sludge gasification (b) $CO_2$ yield from sewage sludge gasification

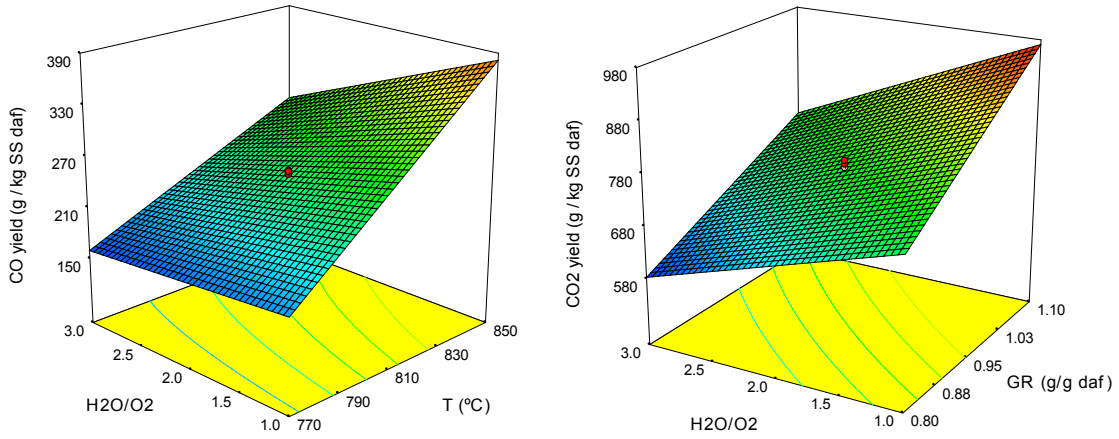


Figure 4.4 (a) CO yield ($g \cdot kg^{-1}_{SS\ daf}$) and (b) $CO_2$ yield ($g \cdot kg^{-1}_{SS\ daf}$) during sewage sludge gasification.

As observed in Fig. 4.4.b, the $CO_2$ yield is mainly affected by the gasifying ratio ($\beta_{GR} > 0$). The increase of the gasifying ratio (GR) involves larger amounts of both oxygen and steam in the gasification medium, so combustion reactions, as well as other reactions promoted by the presence of steam in which $CO_2$ is produced (such as the water-gas shift reaction), take place to a greater extent. The negative effect of the $H_2O/O_2$ ratio ($\beta_{H2O/O2} < 0$) reveals that combustion reactions are the main source of $CO_2$. On the other hand, temperature only appears as a statistically significant term on $CO_2$ production in the case of char gasification. In this case, the temperature rise leads to a reduction in the formation of $CO_2$ ($\beta_T < 0$) and, as discussed above, favors the production of CO, thus suggesting an increased reactivity of char with $CO_2$ at high temperatures (Boudouard reaction, eq. 2.4). The surface response of neither CO production nor $CO_2$ production can be modelled as horizontal planes due to the significant synergic and antagonistic effects between the factors (Fig. 4.4).

As can be noted from β coefficients resulting from the ANOVA analyses (Tables 4.3 and 4.4), the production of light hydrocarbons ($CH_4$ and $C_2H_x$) is mainly influenced by the composition of the gasification medium. The higher the $H_2O/O_2$ ratio, the higher the light hydrocarbons yield ($\beta_{H2O/O2} > 0$). This suggests a higher reactivity of these gases with $O_2$ compared to their reactivity with steam. Furthermore, the formation of $CH_4$ via the methanation reaction (eq. 2.5) may be partly responsible of the positive effect of the $H_2O/O_2$ ratio, since the presence of $H_2$ in the gasification medium is increased at high $H_2O/O_2$ ratios. In

the case of sewage sludge gasification, the $CH_4$ yield is negatively affected by the gasifying ratio ($\beta_{GR} < 0$) and, unlike the results shown by other authors (Kim et al., 2001; Pinto et al., 2003), positively influenced by the temperature ($\beta_T > 0$), maybe because of the increase of the methanation reaction rate. On the other hand, the temperature rise leads to a reduction in the $C_2H_x$ formation during the sewage sludge gasification ($\beta_T < 0$) due to the increased reforming reactions rate. Lastly, the production of $H_2S$ is favored in both gasification processes at high temperature ($\beta_T > 0$) and high gasifying ratio ($\beta_{GR} > 0$).

In addition to the production of each gaseous compound, the evolution of the $H_2/CO$ and $CO/CO_2$ molar ratios in the exit gas has been analyzed due to their importance for the gas use as a feedstock for chemical processes. The $H_2/CO$ molar ratio in the product gas can be enhanced by increasing the $H_2O/O_2$ ratio used as gasification medium ($\beta_{H2O/O2} > 0$) and/or reducing the gasification temperature ($\beta_T < 0$). The relative influence of both factors is quite similar in the gasification of char (Table 4.4), but the gasifying agent plays a more important role in the gasification of sewage sludge (Table 4.3). On the other hand, the higher the gasification temperature, the higher the $CO/CO_2$ molar ratio in the exit gas ($\beta_T > 0$). The $CO/CO_2$ ratio can also be improved by reducing the gasifying ratio ($\beta_{GR} < 0$), while the composition of the gasification medium does not exert a significant influence on this ratio.

ANOVA analyses have revealed that temperature plays the most important role in the evolution of the gas heating value when char is gasified, while the three studied factors exert similar effects on the gas heating value from sewage sludge gasification (see β coefficients in Tables 4.3 and 4.4). As shown in Fig. 4.5, and in contrast to some results shown in the literature (Pinto et al., 2003), temperature shows a positive effect on the gas lower heating value from both gasification processes ($\beta_T > 0$). The hydrocarbons content of the gas decreases with increasing temperature, so a reduction in the gas heating value would be expected. However, $CO_2$ concentration in the gas decreases with temperature in a greater proportion than the hydrocarbons content (see gas composition data in Tables 4.1 and 4.2), thus reducing the dilution effect of the gas and resulting in an increase of the gas heating value. The $LHV_{gas}$ can also be improved by increasing the $H_2O/O_2$ ratio used as gasifying agent ($\beta_{H2O/O2} > 0$), since both an increase in the hydrocarbon content and a decrease in the $CO_2$ fraction are found when the presence of steam in the gasification medium is increased and the availability of oxygen is reduced simultaneously. In the case of sewage sludge gasification, the gasifying ratio (GR) exerts a significant negative effect on the $LHV_{gas}$ ($\beta_{GR} < 0$) and, as shown in Fig. 4.5.a, the effect of the gasification medium is significantly mitigated at high temperatures.

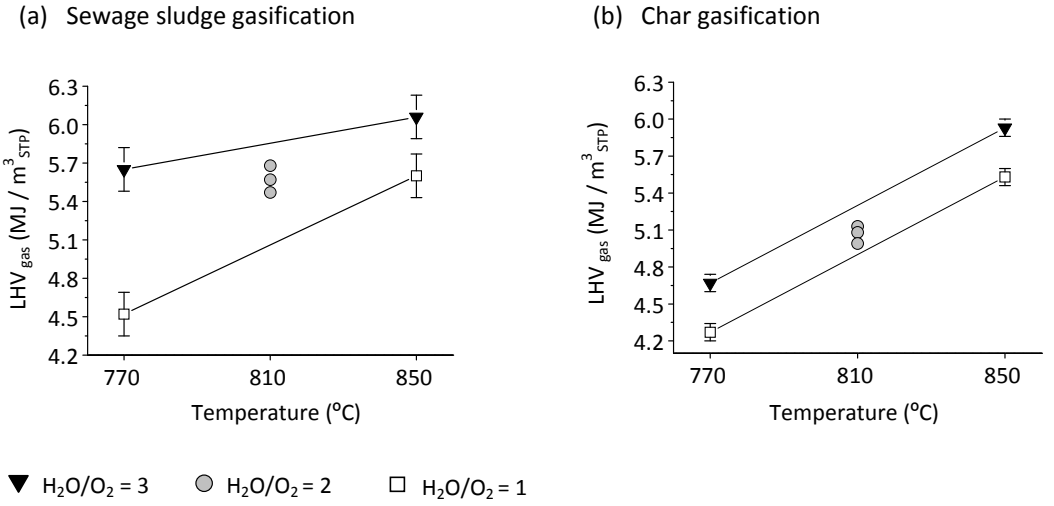


Figure 4.5. Lower heating value of the gas ($MJ \cdot m^{-3}_{STP}$) from (a) sewage sludge gasification and (b) char gasification (GR = 0.95 $g \cdot g^{-1}_{solid\ daf}$).

As occurring with the dry gas yield and the gas heating value, the cold gasification efficiency is mainly dependent on gasification temperature. This efficiency can be improved in 20 percentage points by increasing the gasification temperature from 770 to 850 ºC in both processes ($\beta_T > 0$). This improvement is based on the increase of both the $LHV_{gas}$ and the gas yield. The $H_2O/O_2$ ratio positively affects the cold gasification efficiency ($\beta_{H2O/O2} > 0$) to a lesser extent than the temperature. In the case of char gasification, the gasifying ratio ($\beta_{GR} > 0$) and some synergic and antagonistic effects between the factors are statistically significant on the gasification efficiency evolution, but these are much less important than the individual effect of temperature.

The composition of the tar formed during sewage sludge gasification was analyzed by gas chromatography (MS/FID GC). Fig. 4.6 shows a representative chromatogram with the main compounds detected in most of the tar samples. Some researchers have divided tar components into different families based on their molecular weight and atomic composition (Li and Suzuki, 2009a). A similar classification of tar compounds has been considered in this work: (i) light aromatics with 1 ring (styrene); (ii) PAH compounds with 2 or 3 rings (indene, naphthalene, n-methyl-naphthalene, biphenyl, biphenylene, fluorene, anthracene and phenantrene) (iii) heterocyclic aromatics containing N (including n-methyl-pyridine, benzonitrile, n-methyl-benzonitrile, quinoline, n-methyl-quinoline, indole, n-phenyl-pyridine, n-naphthalenecarbonitrile, benzoquinoline and 5H-indeno[1,2-b]pyridine); (iv) heterocyclic aromatics containing O (phenol and benzofuran); and (v) compounds containing S (2-benzothiophene and propanenitrile, 3,3'-thiobis-).

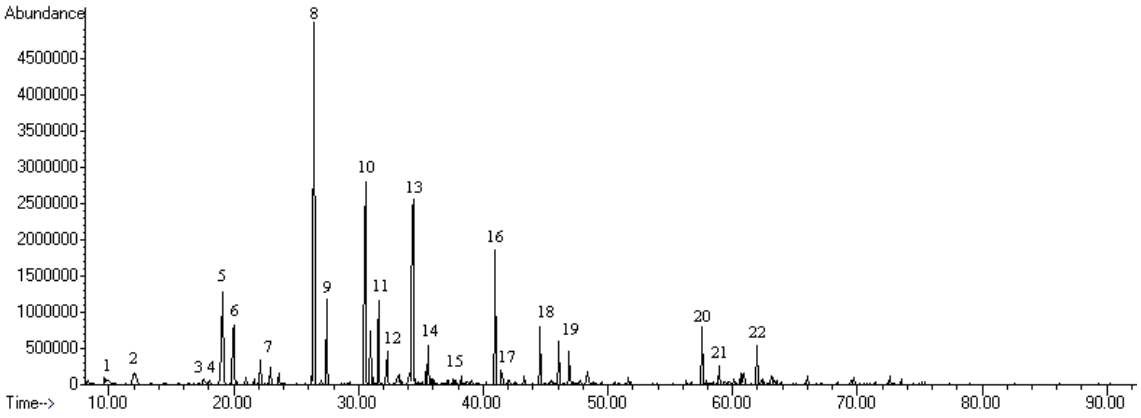


| | | |
|---|---|---|
| 1. Pyridine, n-methyl- (9.6) | 9. 2-Benzothiophene (27.5) | 17. n-Naphthalenecarbonitrile (44.5) |
| 2. Styrene (11.9) | 10. Quinoline (30.6) | 18. Fluorene (46.9) |
| 3. Phenol (17.5) | 11. Naphthalene, n-methyl- (31.0) | 19. Propanenitrile, 3,3'-thiobis- (48.4) |
| 4. Benzofuran (17.6) | 12. Quinoline, n-methyl- (33.1) | 20. Anthracene / Phenantrene (57.6) |
| 5. Benzonitrile (19.2) | 13. Indole (34.3) | 21. Benzoquinoline (58.9) |
| 6. Indene (20.0) | 14. Biphenyl (35.6) | 22. 5H-Indeno[1,2-b]pyridine (61.9) |
| 7. Benzonitrile, n-methyl- (22.1) | 15. Biphenylene (40.9) | |
| 8. Naphthalene (26.4) | 16. Pyridine, n-phenyl- (41.4) | |

Figure 4.6. Total ion chromatogram (TIC) of a tar sample obtained at 850 ºC, GR = 0.8 and $H_2O/O_2$ = 3.

The areas of the main peaks detected by the GC-FID have been used to compare the composition of the different samples. Hence, results presented in this work do not represent the actual composition of the tar samples, but the peak areas are useful for comparing how the factors influence the formation of each family of compounds. The percentages of the GC-FID-areas are shown in Table 4.5.

Table 4.5. Percentage of area in the GC-FID signal of each family of tar compounds.

| Temperature (ºC) | 850 | 770 | 850 | 770 | 850 | 770 | 850 | 770 | 810 |
|---|---|---|---|---|---|---|---|---|---|
| Gasifying ratio ($g \cdot g^{-1}_{daf}$) | 1.1 | 1.1 | 0.8 | 0.8 | 1.1 | 1.1 | 0.8 | 0.8 | 0.95 |
| $H_2O/O_2$ molar ratio | 3 | 3 | 3 | 3 | 1 | 1 | 1 | 1 | 2 |
| Light aromatics (1 ring) | 9.7 | 12.2 | 4.4 | 13.4 | 5.1 | 9.9 | 3.6 | 9.8 | 6.5 ± 1.8 |
| PAH compounds (2-3 rings) | 9.1 | 9.1 | 33.8 | 5.14 | 39.9 | 41.5 | 45.0 | 22.7 | 36.0 ± 8.8 |
| N-aromatics | 74.6 | 68.2 | 57.1 | 68.7 | 46.5 | 44.0 | 44.7 | 60.5 | 50.0 ± 14.4 |
| O-aromatics | 3.0 | 7.7 | 0.34 | 7.7 | 0.6 | 2.1 | 1.0 | 6.0 | 2.6 ± 0.8 |
| S-compounds | 3.6 | 2.9 | 4.4 | 5.1 | 7.9 | 2.5 | 5.7 | 1.0 | 4.9 ± 0.1 |

*Data in the last column show the "mean ± standard deviation" obtained from the 3 replicates at the center point.*

Temperature and $H_2O/O_2$ ratio are the only significant factors affecting tar composition. Light aromatics and O-aromatics are the most sensitive families to temperature, and their fractions are found to decrease with temperature. Similar results have been reported by other researchers (Ponzio et al., 2006), showing that phenolic compounds, paraffines, olefins and alkylated aromatics are easily cracked at high temperatures. The S-compounds fraction has

been found to increase with temperature, maybe as a result of the aforementioned decrease in the fractions of other compounds. On the other hand, N-aromatics and PAH fractions are the most sensitive families to the $H_2O/O_2$ ratio. The increase in this ratio leads to a decrease in the fraction of PAHs, so the presence of steam seems to prevent polymerization reactions. Tar molecular weight depends on the presence of H free radicals, which is related to the steam added during gasification (Qin et al., 2010). According to Corella et al. (1999), tars generated in gasification with steam are easier to crack than tars generated in gasification with air. A simultaneous increase in the fraction of N-aromatics has been observed, but this may be only a consequence of the aforementioned decrease in the PAH fraction.

*Theoretical production of gases based on equilibrium data*

The experimental production of gaseous compounds has been compared to the expected production of gases at equilibrium conditions, which has been determined with the HSC Chemistry 6.1 software. This software uses the Gibbs energy minimization method to calculate the amounts of products at equilibrium in isothermal and isobaric conditions. Therefore, the reaction system (temperature, pressure, feed rate of gasifying agent, amount of C, H, O, S and N that form part of the raw material and expected species to be part of the products) must be specified for the calculations. The same operating conditions studied at the laboratory were defined for the equilibrium simulations. $H_2$, CO, $CO_2$, $CH_4$, $H_2S$ and $NH_3$ are the main compounds in the equilibrium gases. Neither light hydrocarbons (except $CH_4$) nor tar should be present in the equilibrium product gas.

Fig. 4.7 (sewage sludge gasification) and Fig. 4.8 (char gasification) compare equilibrium and experimental yields of $H_2$, CO, $CO_2$ and $CH_4$. Experimental yields of $H_2$ and CO are clearly below their corresponding equilibrium data, while the experimental yields of $CO_2$ and $CH_4$ are above the equilibrium values. These differences reveal that chemical equilibrium was not reached during the gasification runs. Insufficient residence time of gases and vapors in the reactor and/or mass transfer control or kinetic control in gas-solid reactions could explain why the chemical equilibrium was not reached in the gasification experiments.

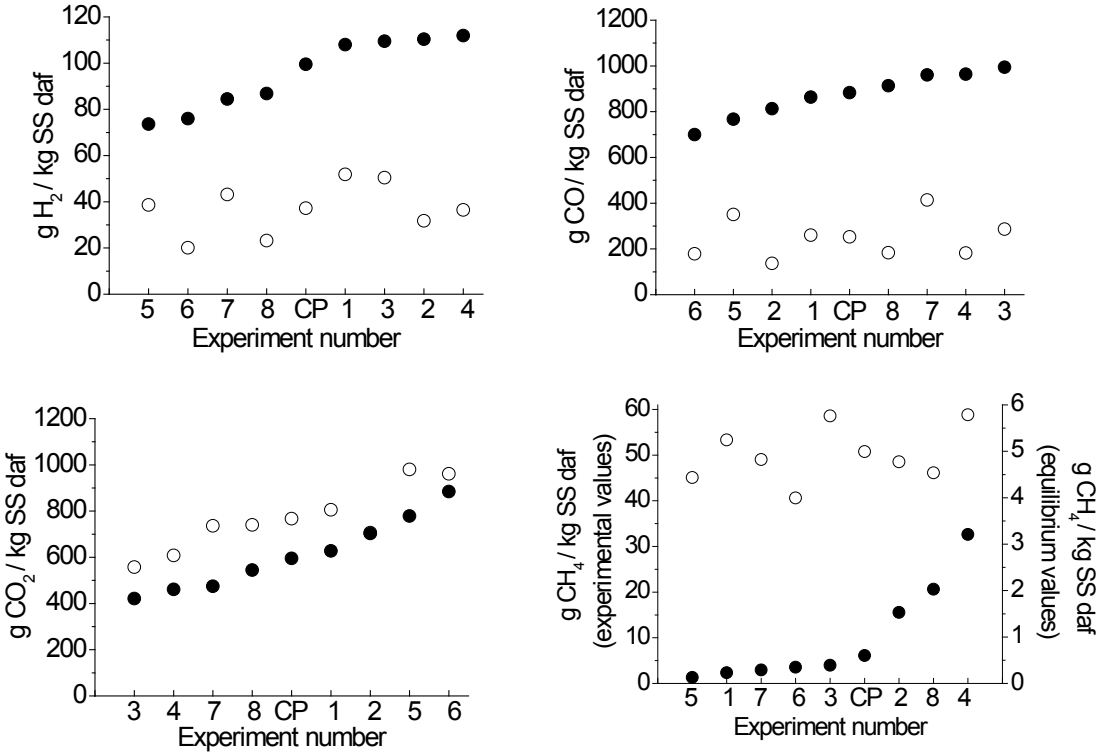


*CP: Center point (mean value from experiments 9, 10, 11).*

Figure 4.7. Theoretical (●) and experimental (○) production of $H_2$, CO, $CO_2$ and $CH_4$ during sewage sludge gasification.

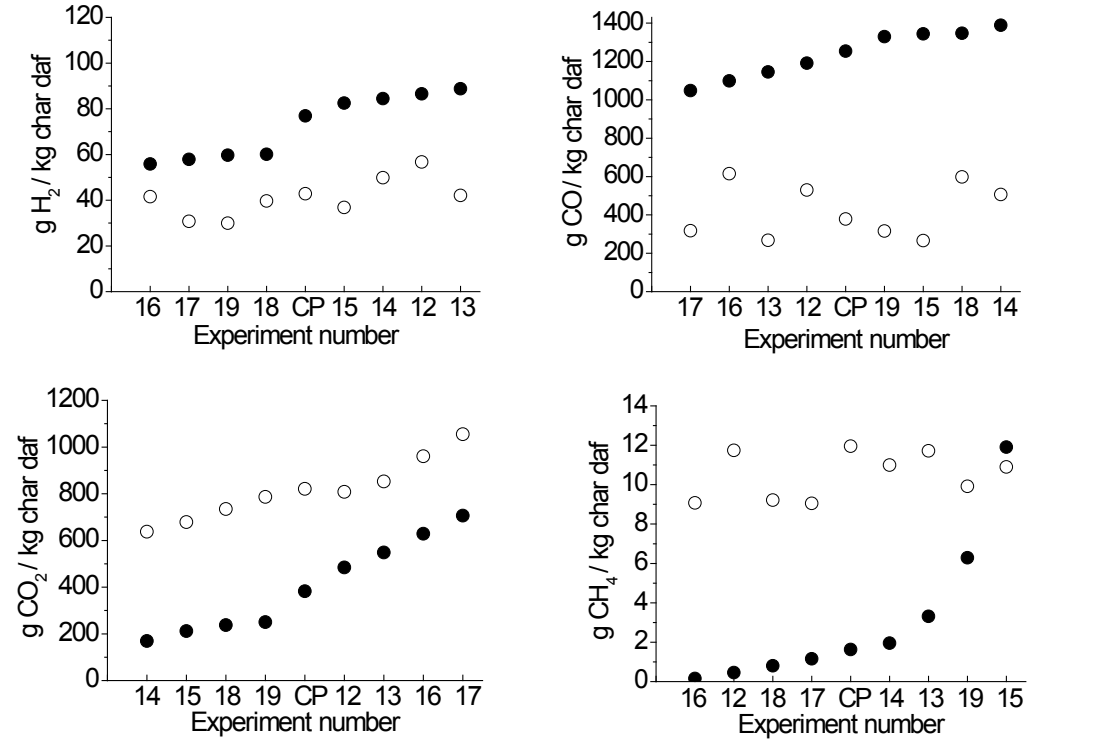


*CP: Center point (mean value from experiments 20, 21, 22).*

Figure 4.8. Theoretical (●) and experimental (○) production of $H_2$, CO, $CO_2$ and $CH_4$ during char gasification.

The influence of the studied operating factors on the evolution of the equilibrium gas yields has been statistically analyzed by ANOVA analysis. The linear regression coefficients (β) in terms of coded values of the factors are shown in Table 4.6.

Table 4.6. Linear regression coefficients (β) from ANOVA analysis of equilibrium gas yields.

| | Average | $\beta_T$ | $\beta_{GR}$ | $\beta_{H2O/O2}$ | $\beta_{T-GR}$ | $\beta_{T-H2O/O2}$ | $\beta_{GR-H2O/O2}$ | $\beta_{T-H2O/O2-GR}$ | Curvature |
|---|---|---|---|---|---|---|---|---|---|
| *Sewage sludge gasification* | | | | | | | | | |
| $H_2$ ($g \cdot kg^{-1}_{SS\ daf}$) | 95.04 | -1.15 | -3.20 | 14.80 | * | * | 2.37 | * | ** |
| CO ($g \cdot kg^{-1}_{SS\ daf}$) | 873.07 | 24.65 | -87.22 | 36.38 | * | * | 15.83 | * | * |
| $CO_2$ ($g \cdot kg^{-1}_{SS\ daf}$) | 610.16 | -36.50 | 138.61 | -58.31 | -8.80 | 7.52 | -24.41 | * | ** |
| $CH_4$ ($g \cdot kg^{-1}_{SS\ daf}$) | 1.07 | -0.81 | -0.56 | 0.42 | 0.43 | -0.33 | -0.17 | 0.14 | ** |
| *Char gasification* | | | | | | | | | |
| $H_2$ ($g \cdot kg^{-1}_{char\ daf}$) | 71.97 | * | * | 13.58 | -0.82 | * | 1.81 | * | ** |
| CO ($g \cdot kg^{-1}_{char\ daf}$) | 1236.58 | 19.95 | -115.74 | 30.59 | * | * | 16.57 | * | * |
| $CO_2$ ($g \cdot kg^{-1}_{char\ daf}$) | 404.57 | -24.71 | 187.33 | -51.24 | -10.69 | * | -24.55 | * | ** |
| $CH_4$ ($g \cdot kg^{-1}_{char\ daf}$) | 3.25 | -2.41 | -1.98 | 1.15 | 1.45 | -0.79 | -0.54 | 0.32 | ** |

Some important differences with respect to the experimentally observed effects of the factors can be highlighted: (i) Temperature is not further the most influential factor on the equilibrium production of $H_2$ and CO; the $H_2O/O_2$ ratio exerts the most significant effect on the equilibrium production of $H_2$, while the gasifying ratio is the most influential factor on the equilibrium CO production; (ii) Equilibrium $H_2$ production is not positively affected by the temperature, but slightly reduced (sewage sludge gasification) or not affected (char gasification); (iii) Equilibrium CO production is not negatively influenced by the $H_2O/O_2$ ratio, but positively affected; (iv) Equilibrium $CH_4$ production is not positively affected by the temperature, but strongly decreased with temperature. Unlike occurring in a kinetically controlled process in which the temperature rise favors both mass transfer and chemical reaction rates, the endothermic or exothermic nature of reactions has to be considered to explain the evolution of the gases at equilibrium conditions.

## 4.2. Energetic assessment

This section presents the energetic assessment of two potential thermo-chemical treatments for sewage sludge management which include the studied stages of gasification. One of these processes involves the direct gasification of sewage sludge, while the other includes the pyrolysis of sewage sludge and the gasification of the char produced in it (Fig. 4.9).

(a) Air-steam gasification of sewage sludge

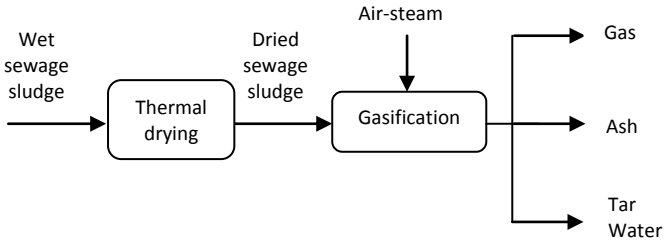


(b) Pyrolysis of sewage sludge + air-steam gasification of char

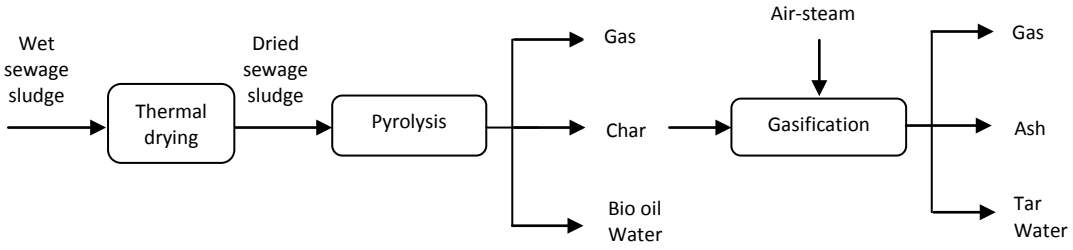


Figure 4.9. Schematic overview of two thermo-chemical processes for sewage sludge management.

The individual energy requirement of each stage (drying, pyrolysis and gasification) has been calculated to determine the overall energy demand of each process.

Experimental data concerning mass yields of solid, liquid and gas products and some of their properties (higher heating value and ultimate analysis of liquid and solid streams, specific heat capacity of solids and gases composition) have been used for calculating the enthalpy of reaction of the gasification and pyrolysis processes. As detailed below, the other required properties of gases and liquid compounds were taken from literature. Some general assumptions and simplifications have been considered:

- Adiabatic reactor.
- The specific heat capacity (Cp) of the solid materials (char and ash) was considered constant with temperature. Although these specific heat capacities were experimentally measured by differential scanning calorimetry (DSC), the function of Cp with temperature could not be obtained in the whole range of temperature required in each case because

of operational limitations of the equipment used. Thus, constant Cp values corresponding to intermediate values of temperature were used for calculations.

- As detailed below, the composition of the liquid fractions obtained from both processes (bio-oil from pyrolysis and tar from gasification) was simplified in order to obtain some of their required properties (specific heat capacity, enthalpy of vaporization and standard enthalpy of formation in the case of tar) from literature.

If negligible heat losses are considered in the reactor (adiabatic reactor), the enthalpy of reaction for the pyrolysis or the gasification processes (Q) can be calculated from the enthalpies of the streams entering ($\Delta H_{in}$) and exiting ($\Delta H_{out}$) the reactor as follows:

$$Q\ (MJ \cdot kg^{-1}) = \Delta H_{out} - \Delta H_{in} \qquad \text{(eq. 4.1)}$$

According to eq. 4.1, Q < 0 corresponds to an exothermic process, while Q > 0 refers to an endothermic process. The total enthalpy of each stream (ΔH) can be calculated as follows:

$$\Delta H\ (MJ \cdot kg^{-1}) = \sum_i m_i \cdot (\Delta H^o_{f,i} + \int_{T_{ref}}^{T} Cp_i\ (T) \cdot dT) \qquad \text{(eq. 4.2)}$$

where:

- $m_i$ is the mass yield of each gas compound, liquid stream or solid stream ($kg \cdot kg^{-1}_{solid}$). 1 kg of raw material (dried sewage sludge or char) has been used as calculation basis.
- $T_{ref}$ is the reference temperature (298 K) and T is the temperature of each stream (K). All the inlet streams were at ambient temperature (298 K), except the steam used in the gasification experiments, which was generated and fed at 448 K.
- $\Delta H^o_{f,i}$ is the standard enthalpy of formation ($MJ \cdot kg^{-1}$) of each compound at the reference temperature (298 K). The $\Delta H^o_f$ data of the gases involved in the process can be easily found in the literature (Perry and Green, 1999). The $\Delta H^o_f$ data corresponding to the solid materials (sewage sludge, pyrolysis char and solid by-products from gasification) and to the pyrolysis liquid fractions have been calculated from their ultimate analyses and heating values according to the following equation:

$$\Delta H^o_{f,i} = \left(\sum_j m_j \cdot \Delta H^o_{f,j}\right) + HHV_i \qquad \text{(eq. 4.3)}$$

where 'j' represents each product derived from the complete combustion of the material ($CO_2$, $H_2O$, $SO_2$ and NO), $m_j$ is the mass of each combustion gas produced per kilogram of material, $\Delta H^o_{f,j}$ is the standard enthalpy of formation of each combustion gas and $HHV_i$ is the higher heating value of the solid or liquid phases.

- $Cp_i$ (T) is the specific heat capacity as a function of temperature ($MJ \cdot kg^{-1} \cdot K^{-1}$). Cp of the solid materials was experimentally measured by DSC, while Cp (T) of the gases and vapors involved in the processes were taken from literature (*ChemSpider database*; Harrison and Seaton, 1988; Perry and Green, 1999). If the range of temperature in the integral of eq. 4.2 involves a phase change, both the enthalpy of vaporization and the Cp of the condensable compounds in the liquid phase have to be included to calculate the total enthalpy. These data can be also found in the literature (*ChemSpider database*; Chueh and Swanson, 1973).

Specific assumptions and energetic results for the pyrolysis of sewage sludge and the gasification of sewage sludge and char are detailed below.

*Enthalpy of reaction of sewage sludge pyrolysis*

The experimental product yields obtained in the pyrolysis of sewage sludge (Gil-Lalaguna et al., 2010), as well as the properties of the products required for the energy balance, are included in Table 4.7. The liquid collected after condensation of the vapors was separated into three phases: light organic phase (LOP), heavy organic phase (HOP) and aqueous phase (AP).

The higher heating values (HHV) of char and liquid phases were experimentally measured with a calorimeter, while the gas heating value was calculated from its composition. $\Delta H^o_f$ of solid and liquid products was calculated from eq. 4.3, while $\Delta H^o_f$ of gases was taken from literature (Perry and Green, 1999).

As mentioned above, constant values of Cp were used for the solids: $1.15 \cdot 10^{-3}$ $MJ \cdot kg^{-1} \cdot K^{-1}$ for sewage sludge and $1.21 \cdot 10^{-3}$ $MJ \cdot kg^{-1} \cdot K^{-1}$ for char (measured at an average temperature, 300 $^oC$). The composition of the liquid phases was simplified to determine their Cp by considering only its water content and one representative organic compound: cholest-4-ene for the LOP, 3-methyl-phenol for the HOP and acetic acid for the AP. These were some of the main compounds with the largest chromatographic area detected by GC-MS. The mass of the representative species in each phase was equated to the whole organic fraction in the phase. The global Cp of each phase (both in liquid and gas phases) can be estimated as a weighted average of the specific heat capacities of water (or steam) and of the representative organic compound of each phase.

In the same way, the enthalpy of vaporization of the liquid phases ($\Delta H_{vap}$) was estimated as a weighted average of the enthalpies of vaporization of water and of the representative organic compound of each phase at their boiling temperatures.

Table 4.7. Yields and properties of the products of sewage sludge fast pyrolysis.

| Mass yield (wt. %) | Composition | HHV ($MJ \cdot kg^{-1}$) | $\Delta H^o_f$ ($MJ \cdot kg^{-1}$) | Cp (T) ($kJ \cdot K^{-1} \cdot kg^{-1}$) | $\Delta H_{vap}$ ($MJ \cdot kg^{-1}$) |
|---|---|---|---|---|---|
| *Char* | | | | | |
| 51.9 ± 0.7 | *Elemental analysis (wt. %, wet basis)*<br>C:15.49; H:0.97; N:1.85; S:0.35 | 5.2 ± 0.2 | -1.18 | 0.82 (25 ºC)<br>1.21 (300 ºC) | --- |
| *Non-condensable gas ($N_2$-free)* | | | | | |
| 10.1 ± 0.9 | *(%, mass fraction)*<br>$CO_2$: 74.3 ± 0.9<br>CO: 13.2 ± 0.1<br>$H_2$: 1.7 ± 0.1<br>$CH_4$: 3.8 ± 0.1<br>$C_2H_6$: 1.4 ± 0.2<br>$C_2H_4$: 1.4 ± 0.1<br>$H_2S$: 4.3 ± 0.9 | 8.0 ± 0.3 | -7.39 | 1.18 (25 ºC)<br>1.56 (530 ºC) | --- |
| *Light organic phase (LOP)* | | | | | |
| 2.2 ± 0.2 | *Elemental analysis (wt. %, wet basis)*<br>C:85.92; H:11.83: N:1.80; S:0.27<br>Water: 0 wt. %<br>Organics: 100 wt. % | 43.10 ± 0.04 | -1.74 | 1.85 (liquid)<br>3.07 (530 ºC) | 0.18 |
| *Heavy organic phase (HOP)* | | | | | |
| 9.4 ± 0.2 | *Elemental analysis (wt. %, wet basis)*<br>C:69.54; H:8.97; N:9.44; S:1.24<br>Water: 6.4 ± 0.3 wt. %<br>Organics: 93.6 ± 0.3 wt. % | 32 ± 2 | -3.49 | 2.13 (liquid)<br>2.36 (530 ºC) | 0.55 |
| *Aqueous phase (AP)* | | | | | |
| 20.8 ± 0.2 | *Elemental analysis (wt. %, wet basis)*<br>C:11.17; H:10.45; N:6.52; S:0.37<br>Water: 73.8 ± 0.4 wt. %<br>Organics: 26.2 ± 0.4 wt. % | 5.7 ± 0.3 | -12.44 | 3.59 (liquid)<br>2.12 (530 ºC) | 1.77 |

*Experimental uncertainty is expressed as mean ± standard deviation (two replicates were performed).*

Thus, considering all the product streams at the pyrolysis temperature at the reactor exit (T = 803 K), the enthalpies of the streams entering ($\Delta H_{in}$) and exiting ($\Delta H_{out}$ ) the reactor have been found to be -3.28 $MJ \cdot kg^{-1}_{SS}$ and -3.13 $MJ \cdot kg^{-1}_{SS}$, respectively (eq. 4.2). The difference of these enthalpies (eq. 4.1) results in an energy demand of 0.15 $MJ \cdot kg^{-1}_{SS}$ for the thermal decomposition of sewage sludge during the pyrolysis process. This value is significantly lower than decomposition heats found in the literature for other types of biomass. For example, 0.3 $MJ \cdot kg^{-1}$ has been reported for the pyrolysis of crop residues (Mangaro et al., 2011). The higher ash content in sewage sludge, which is hardly decomposed during the process, can explain this difference.

If the outlet stream of gases and vapors is cooled down to ambient temperature (298 K) in order to take advantage of their sensible and latent heats, the net heat of the process is

reduced to -0.70 $MJ \cdot kg^{-1}_{SS}$. This indicates that in the absence of significant heat losses, and keeping in mind the considered assumptions, the pyrolysis of sewage sludge could be an autothermal process if the cooling and condensation of the gases and vapors could be efficiently used.

*Enthalpy of reaction of sewage sludge gasification and char gasification*

The mass yields of the products obtained in the gasification of sewage sludge and char under the different operating conditions were presented in Tables 4.1 and 4.2, respectively.

The collected amount of tar has been simplified to an equimolar mixture of benzene, naphthalene and pyridine (typical compounds found in the tar mixtures from sewage sludge gasification) for determination of their Cp and $\Delta H_{vap}$. On the other hand, Cp (T) of all the solid gasification by-products has been approximated to that of sewage sludge ash because these solids were mainly composed of ash (> 93 wt. % in most cases). The constant value used for sewage sludge ash was $1.07 \cdot 10^{-3}$ $MJ \cdot kg^{-1} \cdot K^{-1}$ (experimentally measured at an average temperature, 500 ºC).

The enthalpy of reaction of the gasification of sewage sludge and char under the tested operating conditions can be calculated according to eq. 4.1. The results are depicted in Fig. 4.10, considering the products at the gasification temperature (770-850 ºC) and as a function of the gasification medium: ER (equivalence ratio) and S/B (steam to biomass *daf* mass ratio).

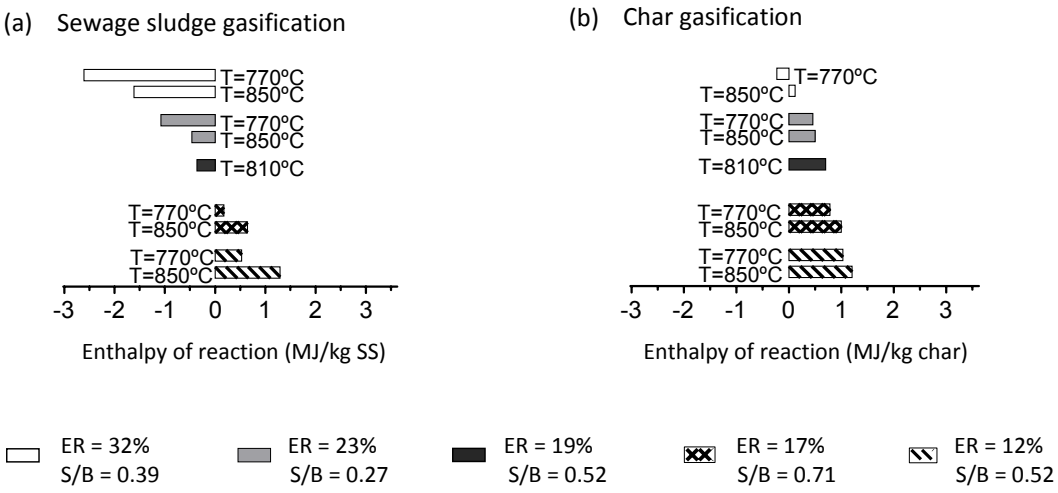


Figure 4.10. Enthalpy of reaction of (a) sewage sludge gasification and (b) char gasification based on experimental data (products at the gasification temperature).

As shown in Fig. 4.10, the enthalpy of reaction ranges between -2.61 and 1.29 $MJ \cdot kg^{-1}_{SS}$ for sewage sludge gasification and between -0.23 and 1.20 $MJ \cdot kg^{-1}_{char}$ for char gasification under the tested conditions. Thus, enthalpy of reaction is more affected by the operating conditions

in the case of sewage sludge gasification. Despite the lower organic content in the char than in the sewage sludge, the external energy demand for gasifying 1 kg of char is higher than that for gasifying 1 kg of sewage sludge. For instance, the enthalpy of reaction of sewage sludge gasification at ER = 17% and S/B = 0.71 is 0.64 $MJ \cdot kg^{-1}$ at 850 ºC and 0.17 $MJ \cdot kg^{-1}$ at 770 ºC, while it reaches 1.00 $MJ \cdot kg^{-1}$ and 0.78 $MJ \cdot kg^{-1}$ for char gasification at the same temperature, respectively. This behavior could be related to the observed changes in the carbonaceous structure of sewage sludge after carrying out the pyrolysis process. The fraction of volatile matter in the sewage sludge was higher than in the char, while the fraction of fixed carbon was higher in the char (Table 3.1). Thus, combustion reactions in gas phase, which usually show less diffusional resistance than the solid-gas reactions, involve vaporized hydrocarbons during the sewage sludge gasification, while the main combustion reactions in gas phase during char gasification involve gases such as $H_2$ or CO (produced from fixed carbon reactions), whose calorific value is lower than those of hydrocarbons. As a consequence, air-steam gasification of char was an endothermic process under most of the experimental conditions used, while air-steam gasification of sewage sludge was an exothermic process when simultaneously working with ER > 19% and S/B < 0.52.

If the outlet stream of gases and vapors is cooled down to ambient temperature (298 K) in order to take advantage of their sensible and latent heats, the net heat of the gasification processes varies from -5.80 to -1.65 $MJ \cdot kg^{-1}_{SS}$ in the case of sewage sludge gasification and from -1.17 to 0.26 $MJ \cdot kg^{-1}_{char}$ in the case of char gasification. This shows that the required energy for carrying out the endothermic gasification processes may be obtained from the product gas, either from its thermal energy (for example by using the product gas to preheat the inlet air stream in a heat exchanger) or from the combustion of part of the gas. In this context, a parameter called “gasification efficiency” has been defined as the fraction of the energy initially contained in the raw material that could be still recovered from the product gas after carrying out the gasification reaction:

$$\text{Gasification efficency } (\%) = \frac{\text{Energy recovery from gas} - Q_{\text{gasification}} - Q_{\text{steam}}}{LHV_{\text{raw material}}} \cdot 100 \qquad \text{(eq. 4.4)}$$

where:

- “Energy recovery from gas” includes the gas calorific value (Dry gas yield · $LHV_{gas}$) and the sensible and latent heats of gases and vapors ( $\sum_i m_i \cdot \left[\Delta H_{cond,i} + \int Cp_i\,(T)\right]$, where “i” represents each gas or vapor compound). A heat exchange efficiency of 70% has been considered for the thermal energy recovery from gases.

- $Q_{gasification}$ is the enthalpy of reaction of the gasification stages, considering the products at the gasification temperature (Fig. 4.10).
- $Q_{steam}$ is the energy demand for heating and evaporating the inlet flow of water from 25 to 150 ºC (2.36 $MJ \cdot kg^{-1}_{H2O}$).
- $LHV_{raw\ material}$ is the energy contained in the raw material (sewage sludge or char), expressed as its lower heating value (Table 3.1).

Gasification efficiency data obtained for sewage sludge gasification and char gasification, calculated according to eq. 4.4, are presented in Table 4.8. Efficiency results vary from 58% to 87% for sewage sludge gasification and from 23% to 64% for char gasification. Better efficiency results have been obtained for sewage sludge gasification as a consequence of its lower enthalpy of reaction and higher gas yield. The gasification efficiency improves at higher temperatures, higher ER and lower S/B.

Table 4.8. Experimental data of sewage sludge gasification efficiency and char gasification efficiency.

| Temperature | 850 | 770 | 850 | 770 | 850 | 770 | 850 | 770 | 810 |
|---|---|---|---|---|---|---|---|---|---|
| ER (%) | 17 | 17 | 12 | 12 | 32 | 32 | 23 | 23 | 19 |
| S/B (mass ratio, *daf* basis) | 0.71 | 0.71 | 0.52 | 0.52 | 0.39 | 0.39 | 0.27 | 0.27 | 0.52 |
| ***Sewage sludge gasification*** | | | | | | | | | |
| Energy recovery from gas ($MJ \cdot kg^{-1}_{SS}$) | 10.23 | 7.91 | 9.63 | 8.41 | 9.10 | 6.77 | 9.56 | 6.93 | 8.72 ± 0.12 |
| Gasification efficiency (%) | 74 | 58 | 65 | 61 | 87 | 75 | 82 | 65 | 71 ± 2 |
| ***Char gasification*** | | | | | | | | | |
| Energy recovery from gas ($MJ \cdot kg^{-1}_{char}$) | 3.91 | 2.77 | 3.49 | 2.44 | 3.52 | 2.44 | 3.34 | 2.27 | 2.98 ± 0.05 |
| Gasification efficiency (%) | 51 | 32 | 40 | 23 | 64 | 49 | 54 | 33 | 40 ± 2 |

*Theoretical enthalpy of reaction of the gasification of sewage sludge and char at equilibrium conditions*

The theoretical enthalpy of reaction for the air-steam gasification of sewage sludge and char at equilibrium conditions has also been determined in order to evaluate the thermodynamic restrictions of the processes under different scenarios. HSC Chemistry 6.1 software was used to determine the mass flow rates of the products at equilibrium conditions. These theoretical enthalpies of reaction are depicted in Fig. 4.11, simulating the same operating conditions that were tested at the laboratory.

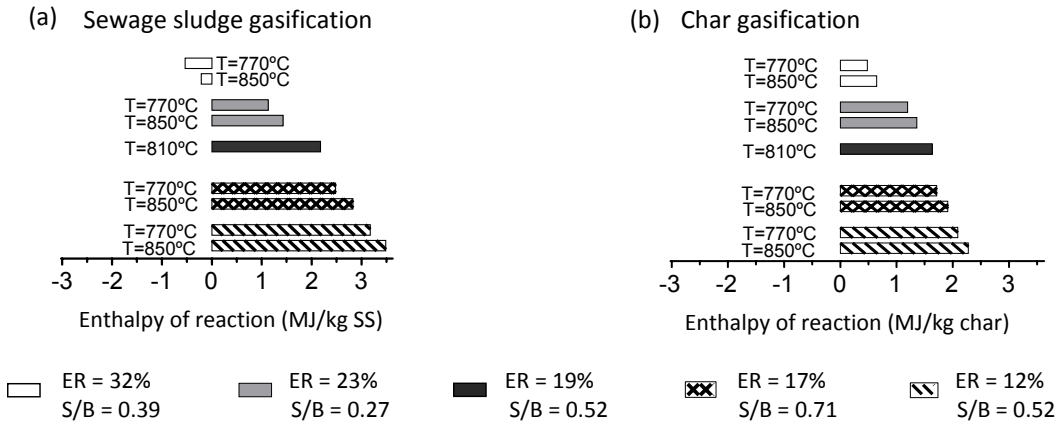


Figure 4.11. Enthalpy of reaction of (a) sewage sludge gasification and (b) char gasification based on equilibrium data (products at the gasification temperature).

As can be seen in Fig. 4.11, gasification of sewage sludge at equilibrium conditions only results in an exothermic process when ER is increased up to 32%. Char gasification is an endothermic process in all the simulated cases.

Comparison of Figs. 4.10 and 4.11 shows that reaching the chemical equilibrium in both gasification processes entails additional energy consumption. The reason may be the predominance of endothermic equilibrium reactions during the gasification, such as the water gas reaction (eq. 2.3), the Boudouard reaction (eq. 2.4), steam reforming (eq. 2.7) and dry reforming (eq. 2.8), against the exothermic equilibrium reactions, such as the water-gas shift reaction (eq. 2.6). These reactions occur to a greater extent at equilibrium, which shows the thermodynamic limit of the process. However, the gas heating value and the gas yield calculated at equilibrium conditions are higher than those obtained experimentally, so more energy could be recovered from the equilibrium product gas (Table 4.9). This latter difference outweighs the difference observed in the experimental and equilibrium data of enthalpy of reaction, so the gasification efficiency is improved at equilibrium conditions: 90-94% for sewage sludge gasification and 78-84% for char gasification (Table 4.9).

Table 4.9. Theoretical data of sewage sludge gasification efficiency and char gasification efficiency at equilibrium conditions.

| Temperature | 850 | 770 | 850 | 770 | 850 | 770 | 850 | 770 | 810 |
|---|---|---|---|---|---|---|---|---|---|
| ER (%) | 17 | 17 | 12 | 12 | 32 | 32 | 23 | 23 | 19 |
| S/B (mass ratio, *daf* basis) | 0.71 | 0.71 | 0.52 | 0.52 | 0.39 | 0.39 | 0.27 | 0.27 | 0.52 |
| ***Sewage sludge gasification*** | | | | | | | | | |
| Energy recovery from gas ($MJ \cdot kg^{-1}_{SS}$) | 14.37 | 14.11 | 14.95 | 14.72 | 11.34 | 11.09 | 12.86 | 12.64 | 13.70 |
| Gasification efficiency (%) | 90 | 91 | 91 | 92 | 94 | 94 | 94 | 94 | 92 |
| ***Char gasification*** | | | | | | | | | |
| Energy recovery from gas ($MJ \cdot kg^{-1}_{char}$) | 6.19 | 6.09 | 6.53 | 6.42 | 4.94 | 4.85 | 5.62 | 5.53 | 5.95 |
| Gasification efficiency (%) | 78 | 80 | 80 | 81 | 82 | 83 | 82 | 84 | 81 |

If the gasifier operates at autothermal conditions instead of being heated by external heat transfer, the gasification temperature is the output variable from balancing out the enthalpies of the streams entering and exiting the gasifier ($\Delta H_{in} = \Delta H_{out}$, assuming negligible heat losses). The equilibrium temperature has been calculated under different gasification mediums following an iterative method: $\Delta H_{out}$ depends on the mass of products (eq. 4.2) and these in turn depend on the gasification temperature (temperature has to be specified in the HSC Chemistry software to calculate the amounts of products at equilibrium). Fig. 4.12 shows the evolution of the equilibrium temperature as a function of ER (equivalence ratio) and S/C (steam to carbon molar ratio) for the air-steam gasification of both sewage sludge and char.

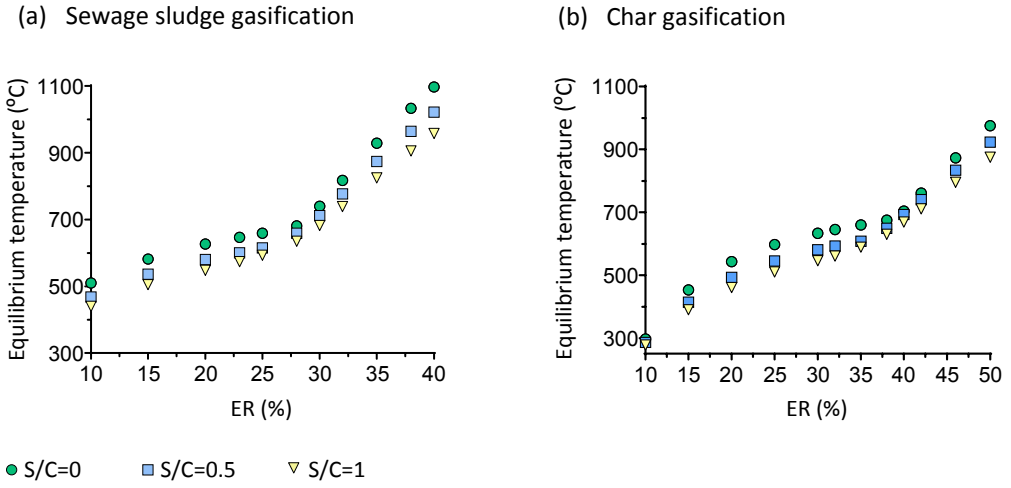


Figure 4.12. Equilibrium temperature as a function of the equivalence ratio (ER) and the steam to carbon molar ratio (S/C) during (a) sewage sludge gasification and (b) char gasification.

The equilibrium temperature obviously increases with ER and decreases with S/C. It should be noted that equilibrium temperature obtained at low ER is too low for a gasification process,

so it does not make sense to think on a tar-free gas product under these conditions, which has been supposed to occur at equilibrium conditions.

The required ER to maintain a specific reaction temperature during char gasification is higher than that in sewage sludge gasification. For instance, an ER of 33 % would be required for autothermal operation of sewage sludge gasification at 800 ºC and S/C = 0.5 under equilibrium conditions, while this value reaches 45% in the case of char gasification. The higher the ER, the greater the production of $CO_2$ through combustion reactions. The presence of $CO_2$ in the gasification gas is undesirable since it implies both a dilution effect of the gas heating value and a reduction in the formation of CO (production and consumption of CO and $CO_2$ are connected by reactions such as the water-gas shift or the Boudouard reaction). In addition to the gas calorific value, the $H_2$/CO ratio in the product gas is an important parameter for using this gas as a feedstock in the synthesis of chemicals such as methanol or Fischer Tropsch fuels. Values of this ratio close to 2 are usually required in these processes (Wender, 1996). For the aforementioned example (ER of 33% for sewage sludge gasification and 45% for char gasification to maintain 800 ºC when S/C = 0.5), 44% of the initial carbon contained in the sewage sludge produces $CO_2$, while this value reaches 52% in the case of char gasification. Both the heating value and the $H_2$/CO ratio in the product gas of sewage sludge gasification ($LHV_{gas}$ = 4.27 $MJ \cdot m^{-3}_{STP}$, $H_2$/CO = 1.47) are higher than those obtained for char gasification ($LHV_{gas}$ = 3.05 $MJ \cdot m^{-3}_{STP}$, $H_2$/CO = 0.89).

*Sewage sludge drying*

Prior to the thermo-chemical treatment of sewage sludge by means of pyrolysis or gasification, sewage sludge thermal drying allows reduction of water content in the waste, thus reducing the waste volume and facilitating handling of the biosolids. The heat needed for the sewage sludge thermal drying ($Q_{drying}$) can be calculated as follows:

$$Q_{drying}\ (MJ \cdot kg^{-1}_{final\ SS}) = \frac{[m_{dry\ SS} \cdot Cp_{SS} + m_{H_2O,SS} \cdot Cp_{H_2O(l)}] \cdot \Delta T + m_{H_2O,evap} \cdot \Delta H_{vap,H_2O}}{\left(kg_{final\ SS} / kg_{wet\ SS}\right)} \qquad \text{(eq. 4.5)}$$

where:

- $m_{dry\ SS}$ is the dry matter content of the wet sludge ($kg \cdot kg^{-1}_{wet\ SS}$).
- $m_{H2O,SS}$ is the water content of the wet sludge ($kg \cdot kg^{-1}_{wet\ SS}$). After the mechanical dewatering of sewage sludge by filter pressing or centrifugation (just before thermal drying) moisture content of sewage sludge is around 70% (Manara and Zabaniotou, 2012).
- ΔT is the temperature difference between the beginning and the end of the drying process (from 25 to 100 ºC).

- $Cp_{SS}$ is the specific heat capacity of the dried sewage sludge ($1.15 \cdot 10^{-3}$ MJ·kg$^{-1}$·K$^{-1}$). This value was experimentally obtained at 25 ºC by differential scanning calorimetry and has been considered constant with temperature for calculations.
- $Cp_{H2O(l)}$ is the specific heat capacity of liquid water ($4.18 \cdot 10^{-3}$ MJ·kg$^{-1}$·K$^{-1}$), which is virtually constant in the considered temperature range (Perry and Green, 1999).
- $m_{H2O,evap}$ is the mass of evaporated water per kilogram of wet sludge (kg·kg$^{-1}_{wet\ SS}$).
- $\Delta H_{vap,H2O}$ is the enthalpy of vaporization of water at the exit temperature (2.26 MJ·kg$^{-1}_{H2O}$ at 100 ºC) (Perry and Green, 1999).

Fig. 4.13 shows the evolution of the heat needed for sewage sludge drying as a function of the initial and final moisture contents, based on calculations performed with eq. 4.5. For instance, an energy input of 8 MJ·kg$^{-1}_{final\ SS}$ is required for reducing the water content from 77 wt. % to 6.5 wt. %, which represent the actual data of the wastewater treatment plant in which the used sewage sludge was generated. However, the heat required for the sewage sludge thermal drying is reduced by half if the initial moisture content is reduced from 77 to 65 wt. %. This reduction could be achieved by improving the efficiency of the prior mechanical dewatering of sewage sludge.

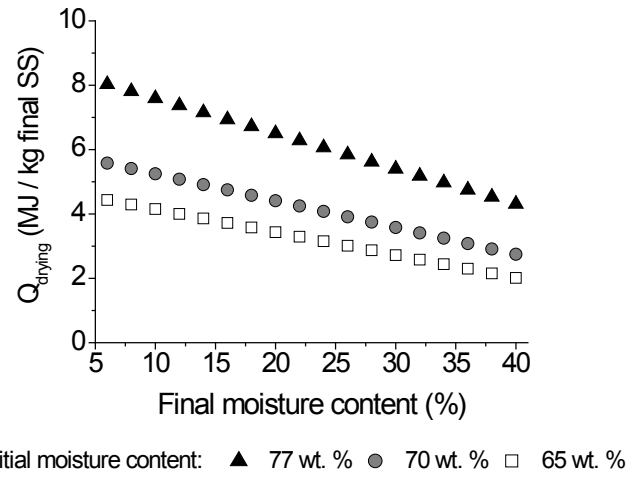


Figure 4.13. Heat demand for the thermal drying of sewage sludge as a function of the initial and final moisture contents.

*Energetic assessment of the two-stage and three-stages processes*

The energy demand for the two-stage (sewage sludge drying + sewage sludge gasification) and three-stage processes (sewage sludge drying + sewage sludge pyrolysis + char gasification) is the sum of the net energy required or released in the individual stages (positive terms for endothermic processes and negative values for exothermic processes). Note that energy

consumptions related to the use of pumps, compressors, motors, etc. have not been included in this study. Only energetic aspects related to the thermo-chemical stages have been considered.

- *Sewage sludge drying*. Water content in the sewage sludge is assumed to be reduced from 65 wt. % (typical content of moisture in sewage sludge before its thermal drying) to 6.5 wt. % during the thermal drying. Thus, $Q_{drying}$ is around 4.4 $MJ \cdot kg^{-1}_{dried\ SS}$ (Fig. 4.13).

- *Sewage sludge pyrolysis.* As occurs in the gasification processes, the energy contained in the produced gases and vapors could be recovered to be used in the thermal decomposition of sewage sludge itself and in the prior thermal drying. Taking advantage of the gas lower heating value and the sensible and latent heats of gases and vapors (given 70% of exchange efficiency for thermal energy recovery), a net heat of -1.17 $MJ \cdot kg^{-1}_{SS}$ is obtained for the pyrolysis process. The use of the calorific value of the liquid product (43 $MJ \cdot kg^{-1}_{LOP}$ and 32 $MJ \cdot kg^{-1}_{HOP}$) is not included in the energy balance, as some important properties such as its poor stability or its high nitrogen content must be improved facing toward its use as fuel (Fonts et al., 2012).

- *Sewage sludge gasification/char gasification.* The net heats of the gasification stages (based on experimental data) can be calculated according to the numerator in eq. 4.4. As the same calculation basis is required for the comparison of the two-stage and three-stage processes (1 kg of dried sewage sludge fed initially), data corresponding to the gasification of char ($MJ \cdot kg^{-1}_{char}$) must be turned into $MJ \cdot kg^{-1}_{SS}$ by means of the char yield obtained in the pyrolysis of sewage sludge (0.519 $kg_{char} \cdot kg^{-1}_{SS}$).

Fig. 4.14 shows the total energy demand for the two-stage and three-stage processes, considering the different experimental conditions used in the gasification stages.

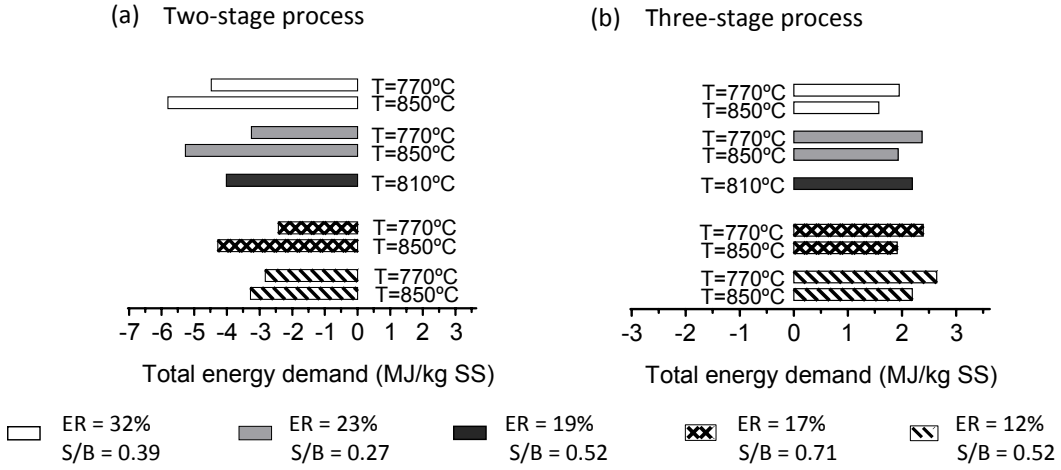


Figure 4.14. Total energy demand for the (a) two-stage and (b) three-stage processes.

The energy demand ranges between -2.43 and -5.81 MJ·kg$^{-1}_{SS}$ for the two-stage process (exothermic process) and between 1.57 and 2.64 MJ·kg$^{-1}_{SS}$ for the three-stage process (endothermic process). Thus, energy contained in the product gas of sewage sludge gasification would be enough to cover the energy demand for both the sewage sludge thermal drying and the gasification process itself if this energy would be efficiently used. Moreover, it should be noted that the flow of water required for the air-steam gasification of sewage sludge could be directly obtained from the own moisture content of the sludge, so the final moisture of the sewage sludge after the drying stage could be increased up to 19-32% (depending on the S/B ratio defined in the gasification stage). Hence, the energy demand during the thermal drying stage could be reduced around 0.36-0.93 MJ·kg$^{-1}_{dried\ SS}$, resulting in a more favorable energy balance. On the other hand, the three-stage treatment is globally an endothermic process (note that the use of the pyrolysis liquid calorific value is not considered), so that an additional energy input would be needed for this treatment. However, assuming a direct and efficient use of calorific value of organic liquid phases obtained from pyrolysis (3.92 MJ·kg$^{-1}_{SS}$), a favorable energetic assessment is also obtained for the three-stage process, with a total energy release ranging from -2.35 to -1.28 MJ·kg$^{-1}_{SS}$ (exothermic process). Thus, the use of the calorific value of the produced pyrolysis liquid is a key issue for reaching an autothermal three-stage process.

Lastly, regarding the influence of the gasification conditions on the total energy demand of the processes, the best energetic results are obtained when operating simultaneously at the highest gasification temperature (850 ºC), the highest equivalence ratio (32%) and a moderate steam to biomass *daf* ratio (0.39).

## 4.3. Desulphurization of different gas streams

This section presents the results of the desulphurization tests at high temperature (600-800 ºC). $H_2S$ was removed from different synthetic gases by using sewage sludge combustion ash and gasification ash as sorbent materials. One of these gases only contained $H_2S$ and $N_2$, while the other was a synthetic gasification gas containing $H_2$, CO, $CO_2$, $CH_4$, $C_2H_6$, $C_2H_4$, $C_2H_2$, $N_2$ and $H_2S$ (Table 3.4). Steam was added in some experiments together with gas in order to evaluate its impact on the desulphurization performance.

The $H_2S$ breakthrough curves obtained at the ash bed exit ($H_2S$ outlet flow as a function of experiment time) are depicted in Fig. 4.15 as a function of the type of gas atmosphere, temperature and type of ash.

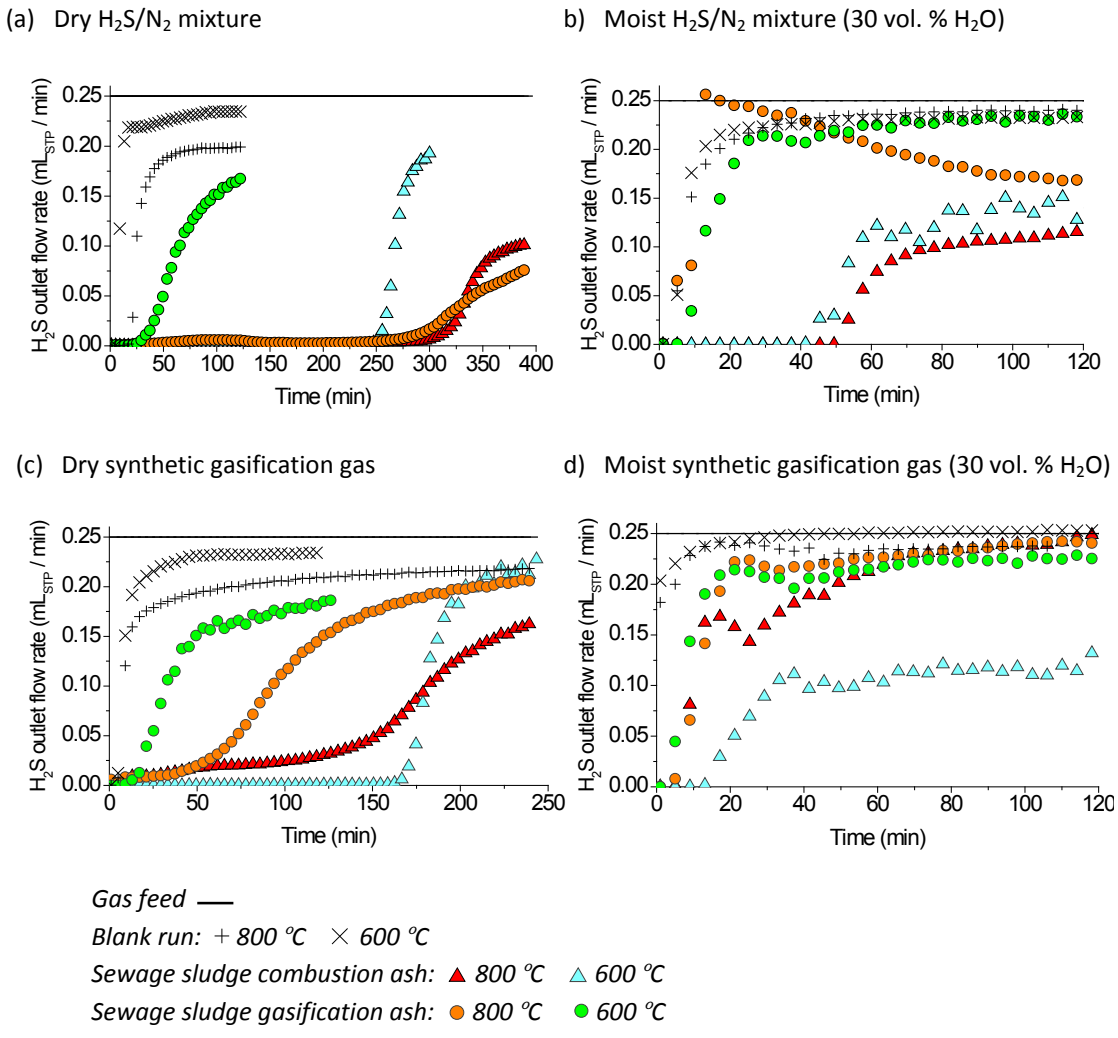


Figure 4.15. $H_2S$ breakthrough curves: evolution of the $H_2S$ flow rate leaving the reactor ($mL_{STP} \cdot min^{-1}$).

An exit gas essentially free of $H_2S$ was obtained during 300 min and 260 min by using the combustion ash and the gasification ash at 800 ºC under the dry $H_2S/N_2$ gas atmosphere,

respectively (Fig. 4.15.a). On the other hand, unlike occurring with the $H_2S/N_2$ mixture, a significant $H_2S$ flow was detected in the exit synthetic gasification gas from almost the beginning of all the experiments. In this case, the $H_2S$ breakthrough time was longer than 20 min only when operating with the combustion ash at 600 $^oC$ under dry conditions (165 min, Fig. 4.15.c). This breakthrough time was in turn significantly lower than that obtained for the $H_2S/N_2$ mixture under the same operating conditions (245 min, Fig. 4.15.a). The reduction of the iron oxides present in the sewage sludge ash may explain this observed behavior. As discussed in the literature (Tamhankar et al., 1981; Tseng et al., 2008; Westmoreland and Harrison, 1976), the presence of CO and $H_2$ in the gasification gas creates a reducing atmosphere that may cause the conversion of $Fe_3O_4$ and $Fe_2O_3$ to FeO or even to elemental Fe in the temperature range of 700-1000 $^oC$. FeO and Fe show less favorable sulphidation equilibrium, which led to a reduction in the sulphur capture capacity of the ash (Tseng et al., 2008). Thus, the impact of temperature on the $H_2S$ removal from the gasification gas is the result of the competition of reduction and sulphidation reaction rates.

The presence of 30 vol. % of steam in the reaction medium also affected negatively the $H_2S$ breakthrough time. According to the general reaction of metal oxides with $H_2S$ (eq. 4.6), thermodynamics predicts a negative effect of steam on the equilibrium between the $H_2S$ and the metal oxide sorbents because of the simultaneous regeneration of the spent metal sulphides:

$$Me_xO_y\,(s) + y\,H_2S\,(g) \leftrightarrow Me_xS_y\,(s) + y\,H_2O\,(g) \qquad \Delta H < 0 \qquad \text{(eq. 4.6)}$$

Experimental results reported in the literature show different steam impact levels on the sulphidation rate depending on the sorbent material and the operating conditions (Cheah at al., 2009). For instance, Kim et al. (2007) studied the effect of steam on $H_2S$ removal by a ZnO sorbent and found that the presence of 45% steam halved the $H_2S$ breakthrough time at 363 $^oC$. In general, the effect of steam on the sulphur sorbent performance is expected to be more severe at higher temperatures, but there are not many studies concerning this effect (Cheah at al., 2009). In the present work, the $H_2S$ breakthrough time was reduced by 85% in the presence of 30% steam when testing the combustion ash at 600-800 $^oC$ ($H_2S/N_2$ mixture), while the gasification ash showed a complete loss of its capacity to remove $H_2S$.

The presence of steam in the gas atmosphere also affected the blank run results. As it is well known, susceptible alloys, especially steels, react with $H_2S$ to form metal sulphides as corrosion by-products. This could explain the reduced $H_2S$ outlet flow rate in the blank runs with respect to the inlet gas, particularly at 800 $^oC$ and under dry operating conditions (Figs.

4.15.a and 4.15.c). The hot metal parts in the experimental setup do not appear to react with $H_2S$ under wet conditions (Fig. 4.15.b and 4.15.d) since, as discussed above, the formation of metal sulphides from metal oxides is restricted by the presence of steam.

Table 4.10 summarizes the $H_2S$ breakthrough times (time in which the $H_2S$ concentration exceeds 100 ppmv), as well as other experimental results such as the amount of $H_2S$ removed up to the breakthrough time or the sulphur content in the solid samples, which are discussed below.

Table 4.10. Experimental results from the desulphurization tests.

| | $H_2O/H_2S$ mass ratio | T (ºC) | $H_2S$ breakthrough time (min) | $H_2S$ removed up to breakthrough time ($mL_{STP}$) | S content (ultimate analysis, mg $S \cdot g^{-1}_{ash}$) [a] | Expected S content (mg $S \cdot g^{-1}_{ash}$) |
|---|---|---|---|---|---|---|
| *$H_2S/N_2$ mixture feed* | | | | | | |
| Sewage sludge combustion ash | 0 | 600 | 245 | 54 | 58 ± 1 | 92 |
| | 0 | 800 | 300 | 54 | 63 ± 4 | 100 |
| | 45 | 600 | 40 | 7 | 21.5 ± 0.8 | 29 |
| | 45 | 800 | 50 | 9 | 1.4 ± 0.1 | 32 |
| | 22.5 | 700 | 70 | 14 | 20.8 ± 0.6 | 38 |
| | 22.5 | 700 | 62 | 12 | 18.8 ± 0.2 | 37 |
| | 22.5 | 700 | 62 | 12 | 16.6 ± 0.6 | 36 |
| Sewage sludge gasification ash | 0 | 600 | 30 | 4 | 23.2 ± 0.5 | 27 |
| | 0 | 800 | 260 | 48 | 64.4 ± 0.7 | 100 |
| | 45 | 600 | 5 | 2 | 4.9 ± 0.2 | 7 |
| | 45 | 800 | 0 | 0 | 1.1 ± 0.1 | 8 |
| | 22.5 | 700 | 0 | 0 | 14.1 ± 0.5 | 17 |
| | 22.5 | 700 | 0 | 0 | 12.6 ± 0.5 | 18 |
| | 22.5 | 700 | 0 | 0 | 11.8 ± 0.4 | 17 |
| *Synthetic gasification gas feed* | | | | | | |
| Sewage sludge combustion ash | 0 | 600 | 165 | 36 | 46.4 ± 0.6 | 64 |
| | 0 | 800 | 13 | 1 | 55 ± 4 | 53 |
| | 45 | 600 | 17 | 4 | 26.8 ± 0.5 | 32 |
| | 45 | 800 | 5 | 1 | 8.5 ± 0.5 | 11 |
| Sewage sludge gasification ash | 0 | 600 | 13 | 1 | 20 ± 1 | 19 |
| | 0 | 800 | 0 | 0 | 33.2 ± 0.6 | 31 |
| | 45 | 600 | 5 | 1 | 5.8 ± 0.2 | 11 |
| | 45 | 800 | 5 | 1 | 4.5 ± 0.5 | 8 |

[a] *mean value ± standard deviation*

The amount of $H_2S$ removed from gas up to the breakthrough time was calculated using the blank runs data as a reference:

$$H_2S \text{ removed up to breakthrough time } (mL_{STP}) = V_{H_2S \text{ blank}} - V_{H_2S \text{ experiment}} \quad \text{(eq. 4.7)}$$

where $V_{H2S\ experiment}$ is the amount of $H_2S$ ($mL_{STP}$) leaving the reactor up to the $H_2S$ breakthrough time during each experiment and $V_{H2S\ blank}$ is the amount of $H_2S$ ($mL_{STP}$) leaving the reactor in the blank run during the same experimental time. These $H_2S$ outlet volumes were calculated by integration of the area under the breakthrough curves (Fig. 4.15), considering only the flow rate data up to the breakthrough time. These results have been statistically compared by analysis of variance. The regression linear coefficients (β) in terms of coded values of the factors are shown in Table 4.11. Although the significant curvature prevents the use of the linear regression model obtained, the relative influence of the factors can be easily evaluated by comparison of the absolute values of coefficients β.

Table 4.11. Linear regression coefficients (β) from ANOVA analysis of the amount of $H_2S$ removed from the $H_2S/N_2$ mixture up to the breakthrough time ($mL_{STP}$).

| Average | $\beta_T$ | $\beta_{H2O/H2S}$ | $\beta_{ash\ type}$ | $\beta_{T\text{-}H2O/H2S}$ | $\beta_{T\text{-}ash\ type}$ | $\beta_{H2O/H2S\text{-}ash\ type}$ | $\beta_{T\text{-}H2O/H2S\text{-}ash\ type}$ | Curvature |
|---|---|---|---|---|---|---|---|---|
| 22.36 | 5.46 | -17.76 | -8.91 | -5.36 | 4.94 | 5.16 | -5.89 | Significant |

The three studied factors (temperature, $H_2O/H_2S$ and ash type), as well as their interactions, significantly affect the amount of $H_2S$ removed from the gas up to the breakthrough time. Fig. 4.16 shows the surface response obtained from the ANOVA analysis of the amount of $H_2S$ removed from the $H_2S/N_2$ mixture by each solid.

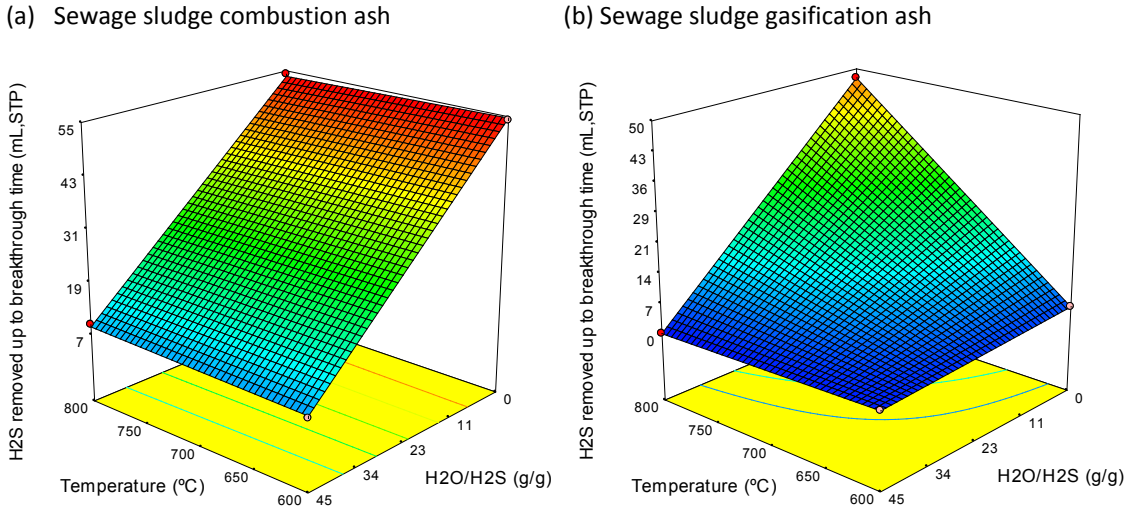


Figure 4.16. $H_2S$ removed from the $H_2S/N_2$ mixture up to the breakthrough time ($mL_{STP}$) by using (a) sewage sludge combustion ash and (b) sewage sludge gasification ash.

The $H_2O/H_2S$ ratio is the most influential factor ($\beta_{H2O/H2S}$ = -17.76). The higher the presence of steam, the smaller the amount of $H_2S$ removed from gas. The origin of the sewage sludge ash is also a key factor in the $H_2S$ removal process ($\beta_{ash\ type}$ = -8.91). Larger amounts of $H_2S$ can

be removed from the gas with the combustion ash than with the gasification ash, especially at the lowest temperature. For instance, 54 $mL_{STP}$ of $H_2S$ were removed from the dry $H_2S/N_2$ mixture up to the breakthrough time by using the combustion ash at 600 $^oC$, while the gasification ash only removed 4 $mL_{STP}$ of $H_2S$ before reaching the breakthrough time (Table 4.10). Non-significant differences in the surface features of both solids were found (Table 3.2), so that the difference in their desulphurization performances must be related to ash composition. On the one hand, gasification ash contains some amount of carbon that could hinder the access of $H_2S$ to the metallic sites. However, this amount of carbon (3.14 wt. %) does not appear large enough to be the only cause for the observed differences. As discussed in section 3.1.2, metal content and metallic species detected in both types of sewage sludge ash were not exactly the same as a consequence of the different reactive atmospheres in the combustion and gasification processes. One of the main differences in the composition of the ash samples was related to Fe content, which was detected in the form of $Fe_2O_3$ in the combustion ash and as $Fe_3O_4$ in the gasification ash. Yoshimura et al. (1995) analyzed $Fe_2O_3$ and $Fe_3O_4$ samples after sulphidation with $H_2S$ at 400 $^oC$ and the patterns obtained by Extended X-ray Absorption Fine Structure (EXAFS) showed that the intensity of the peak corresponding to Fe-S coordination after sulphidation of $Fe_3O_4$ was lower than that in the sulphided sample of $Fe_2O_3$, thus indicating more difficulty in sulphiding $Fe_3O_4$ at low temperature. This fact, as well as the lower Fe content detected in the gasification ash, may explain the rapid saturation of the gasification ash. The difference in the desulphurization performance of both solids was reduced with increasing temperature, probably due to a rapid increase in the $Fe_3O_4$ sulphidation reaction rate.

As the desulphurization process is based on gas-solid reactions, the sulphidation rate is expected to be controlled by chemical reaction kinetics or by mass transfer. The effect of the reaction temperature on the amount of $H_2S$ removed from the $H_2S/N_2$ mixture up to the breakthrough time is clearly dependent on the ash type and presence of moisture in the gas ($\beta_T$ = 5.46, $\beta_{T\text{-ash type}}$ = 4.94, $\beta_{T\text{-H2O/H2S}}$ = -5.36). Thus, temperature hardly affected the removed amount of $H_2S$ up to the breakthrough time when using the combustion ash, whereas a great positive temperature impact was observed when the gasification ash was used at dry conditions (Fig. 4.16).

In addition to the evaluation of the $H_2S$ breakthrough curves, sulphur content in the solid samples was measured after the desulphurization tests by means of an elemental analyzer. The obtained results are included in Table 4.10 (column denoted as S content, ultimate analysis). Only a few of these data are directly comparable with each other because they refer

to the total amount of sulphur removed in each complete experiment and the duration of the experiments was not the same in all cases. Comparable data show lower sulphur content in the gasification ash than in the combustion ash after the experiments performed at 600 and 700 ºC, while similar sulphur contents were detected in both solids after the experiments performed at 800 ºC with the $H_2S/N_2$ mixture, pointing to similar sulphidation reaction rates of $Fe_2O_3$ and $Fe_3O_4$ at high temperature. These latter values were around 63-64 mg $S{\cdot}g^{-1}_{ash}$ after 390 min of test, being the highest sulphur loading detected in the solids. However, in the presence of steam, sulphur capture was improved at low temperature. Combustion ash operating at 600 ºC showed the best sulphur capture ability (26.8 mg $S{\cdot}g^{-1}_{ash}$ after 120 min) under the most realistic operating conditions ($H_2S$ removal from the moist synthetic gasification gas).

In order to check the sulphur mass balance, the expected sulphur content in the spent ash samples has been calculated assuming that all the amount of $H_2S$ removed from the gas remained in the solid after the desulphurization test:

$$\text{Expected sulphur content (mg S} \cdot g^{-1}\text{ash)} = \frac{V_{H_2S\ blank} - V_{H_2S\ experiment}}{22.4} \cdot 32 \qquad \text{(eq. 4.8)}$$

where $V_{H2S\ experiment}$ is the amount of $H_2S$ ($mL_{STP}$) leaving the reactor during each complete experiment, $V_{H2S\ blank}$ is the amount of $H_2S$ ($mL_{STP}$) leaving the reactor during the blank run (extrapolating to the duration of the experiment where this differs), 22.4 is the volume of one ideal gas mole at STP ($mL_{STP}{\cdot}mmol^{-1}$) and 32 is the sulphur atomic mass ($mg{\cdot}mmol^{-1}$). The expected sulphur contents are included in the last column of Table 4.10. As can be observed, these calculated data are higher than the experimental results obtained from the elemental analyzer. This suggests that other sulphur-containing gases not detected by the micro GC could be formed during the desulphurization tests. Especially striking is the difference between the results obtained in experiment 4 (800 ºC and moist $H_2S/N_2$ mixture), for which the expected sulphur content in the solid was around 32 mg $S{\cdot}g^{-1}_{ash}$, while the elemental analyzer only detected 1.4 mg $S{\cdot}g^{-1}_{ash}$.

Equilibrium simulations were conducted in order to try to explain these observed differences from a thermodynamic point of view. As the composition of the solid evolves over time (discontinuous bed of solid and continuous feed of gas), successive simulations for small time intervals (10 min) were performed in order to obtain an approximation to the real process during 300 min. The amount of Ca (in the form of CaO) and Fe (in the form of $Fe_2O_3$) present in 1 g of sewage sludge ash was the initial solid for the first simulation. The gas input

for each equilibrium simulation was the amount of gas fed during 10 min of experiment, while the solid input was the solid resulting from the previous simulation.

Figs. 4.17 and 4.18 show the evolution of the theoretical distribution of sulphur into the main sulphur-containing species resulting from the equilibrium simulations: $Fe_xS_y$, CaS, $H_2S$, $CaSO_4$ and $SO_2$. Successive gas-solid contact intervals of 10 min are represented.

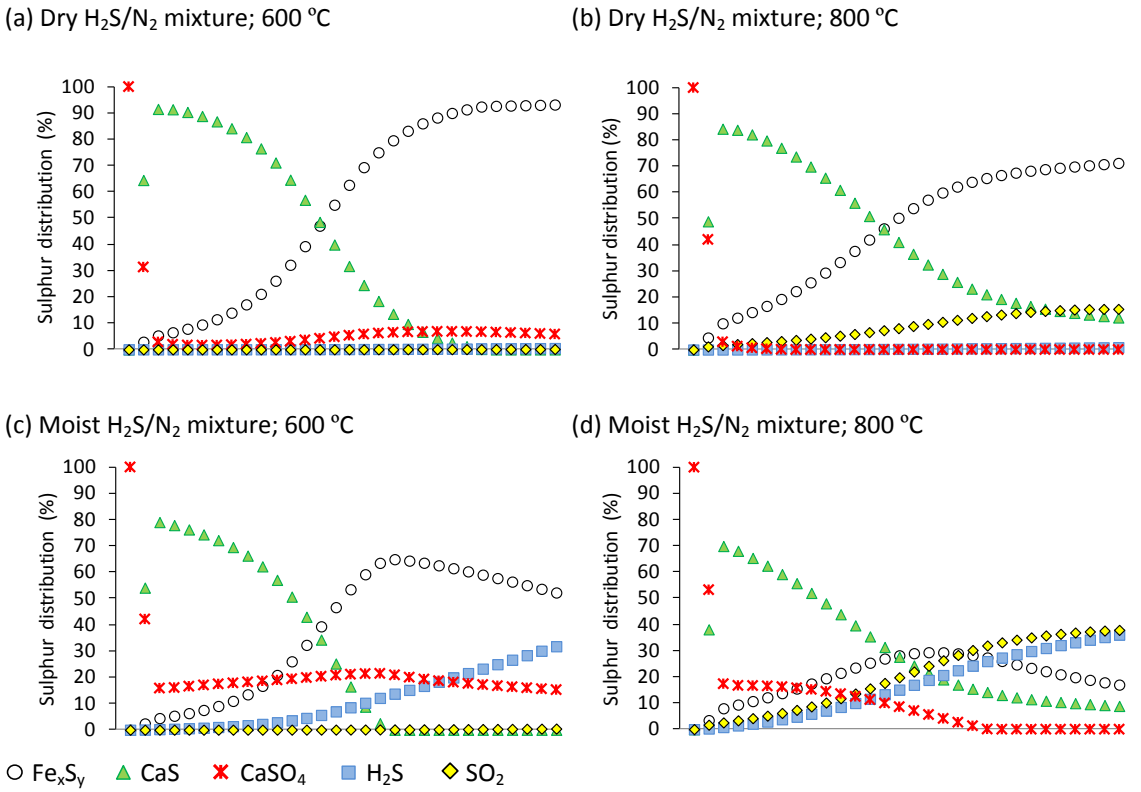


Figure 4.17. Evolution of the sulphur distribution into the main sulphur-containing species at equilibrium conditions when considering the $H_2S/N_2$ mixture as inlet gas.

The formation of CaS is thermodynamically favored over the formation of $Fe_xS_y$ in the early stage of the desulphurization process when feeding the $H_2S/N_2$ mixture (Fig. 4.17). The available amount of Ca decreases and $Fe_xS_y$ formation becomes more significant while the desulphurization process progresses. The remaining fraction of $H_2S$ in gas increases at the presence of steam (Figs. 4.17.b and 4.17.d). Besides the formation of metal sulphides, thermodynamics predicts the formation of $SO_2$ and $CaSO_4$ as a result of the reaction of the formed $SO_2$ with CaO. The formation of both $SO_2$ and $CaSO_4$ is favored at the presence of steam. The temperature increase shifts the reaction to $SO_2$ formation. Thus, $SO_2$ formation may be the reason for the observed differences in the expected and measured sulphur contents in the ash samples. Maximum sulphur loadings of 107, 103, 42 and 38 mg $S \cdot g^{-1}_{ash}$ are theoretically predicted for experiments 1, 2, 3 and 4, respectively. Experimental results

measured with the elemental analyzer (Table 4.10) were 46%, 39%, 49% and 96% lower than the theoretical results, respectively.

Thermodynamic data obtained for the synthetic gasification gas feed are shown in Fig. 4.18.

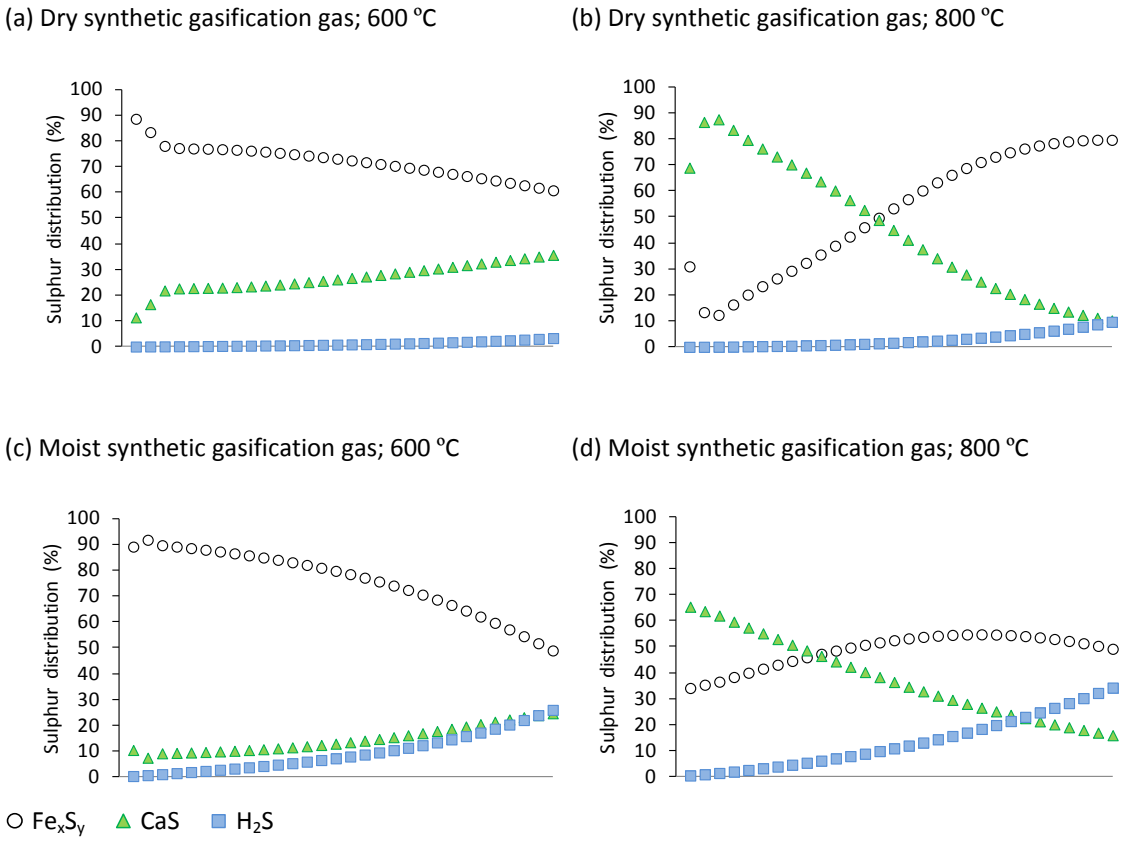


Figure 4.18. Evolution of the sulphur distribution into the main sulphur-containing species at equilibrium conditions when considering the synthetic gasification gas as inlet gas.

In this case, neither $SO_2$ nor $CaSO_4$ are present at equilibrium conditions since the reducing atmosphere created by the gasification gas prevents its formation. $H_2S$, CaS and $Fe_xS_y$ are the main sulphur-containing species at equilibrium conditions. COS is also formed in a very low proportion. Some authors have detected the formation of COS in the reducing environment of the gasification gas ($H_2S + CO_2 \leftrightarrow COS + H_2O$) (Hepola and Simell, 1997), which could explain the observed differences in the expected and measured sulphur contents in the ash samples. Maximum sulphur loadings of 85, 84, 42 and 41 mg $S \cdot g^{-1}_{ash}$ are theoretically predicted for experiments 20, 21, 22 and 23, respectively. Experimental results measured with the elemental analyzer (Table 4.10) were 46%, 35%, 36% and 79% lower than the theoretical results, respectively.

Comparison of Figs. 4.17 and 4.18 shows a great impact of the gas atmosphere on the distribution of sulphur between CaS and $Fe_xS_y$. The presence of $CO_2$ in the gasification gas can explain this difference since this is the responsible gas for the carbonation reaction of CaO ($CaO + CO_2 \leftrightarrow CaCO_3$). Excess $CO_2$ shifts the reaction to the formation of $CaCO_3$, especially at low temperatures, thus limiting the formation of CaS from CaO. Thus, besides the reduction of the iron oxides, carbonation of CaO may also contribute to the different results obtained for the $H_2S/N_2$ mixture and the synthetic gasification gas.

In addition to the elemental analysis of solid samples, other characterization techniques were applied. Fig. 4.19 shows a back-scattered electron image of the combustion ash resulting from experiment 2. Numbers in Fig. 4.19 indicate the points where the elemental composition was analyzed. The atomic fractions obtained by EDX on the different superficial points are shown in Table 4.12.

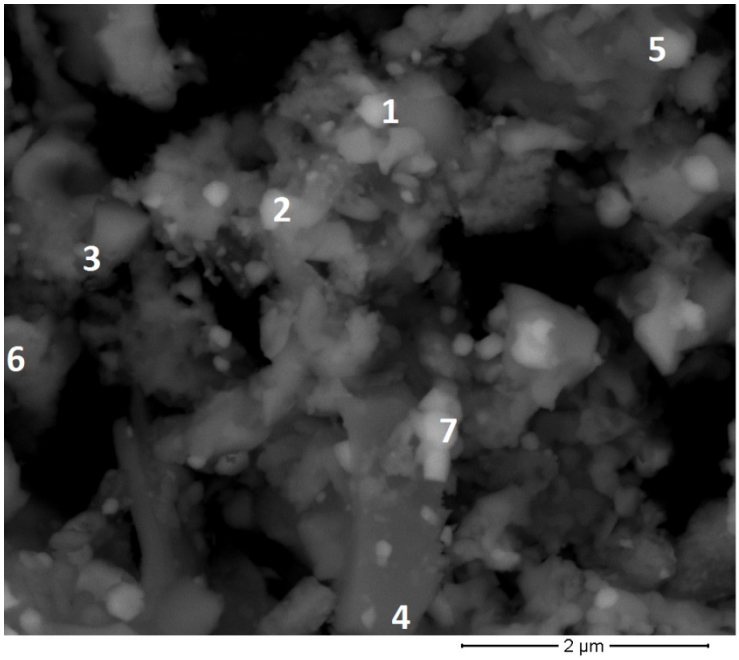


Figure 4.19. Back-scattered electron image of the ash resulting from experiment 2.

Table 4.12. Elemental composition (SEM/EDX) on different superficial points of the ash resulting from experiment 2.

| Point in Fig. 4.19 | Elemental composition (atomic percentage) | | | | | | | | | | |
|---|---|---|---|---|---|---|---|---|---|---|---|
| | C | O | Na | Mg | Al | Si | P | S | Ca | Fe | Zn |
| 1 | | 29.6 | | 1.0 | 2.0 | 1.7 | 4.3 | 23.8 | 1.6 | 35.9 | |
| 2 | 0.8 | 57.9 | | 3.4 | 3.7 | 2.4 | 13.3 | 1.1 | 6.6 | 10.6 | 0.3 |
| 3 | 2.2 | 45.9 | 0.5 | 1.5 | 5.7 | 9.2 | 11.5 | 8.6 | 6.3 | 8.8 | |
| 4 | 0.7 | 69.0 | 0.3 | 0.1 | 0.3 | 27.6 | 0.6 | | | 0.9 | |
| 5 | 0.9 | 50.7 | 0.3 | 3.3 | 6.2 | 9.3 | 12.2 | 4.6 | 7.0 | 5.6 | |
| 6 | 1.6 | 57.9 | | 2.4 | 1.4 | 4.0 | 11.7 | 0.4 | 4.1 | 16.1 | 0.4 |
| 7 | | 33.5 | | 0.8 | 1.3 | 7.8 | 3.5 | 23.7 | 4.1 | 25.3 | |

As can be noted from data in Table 4.12, the composition of the sewage sludge ash surface is quite heterogeneous. C, O, Na, Mg, Al, Si, P, S, Ca, Fe and Zn are detected along the surface in different fractions. It should be noted that the points with the highest atomic percentage of S (23.8% in point 1 and 23.7% in point 7) are also those with the highest Fe content (35.9% and 25.3%, respectively), thus suggesting the formation of either iron sulphides or iron sulphates. On the other hand, S was hardly detected in other points, such as in point 4 (mainly formed by O and Si in the form of $SiO_2$) or in point 6 in which, despite of the high fraction of Fe (16.1%), only 0.4 atomic % S was found. In this case, as well as in points 2 and 3, the high presence of Fe is linked with a high presence of P, which indicates the presence of iron phosphates.

Fig. 4.20 shows the XPS spectra in S 2p region of the ash resulting from experiment 2. Several doublets can be fitted to the experimental signal, indicating different chemical states of sulphur in the ash surface. The peak located between 160 and 164 eV is indicative of $S_n^{-2}$ (metal sulphides), but other oxidized sulphur forms have also been detected (169 eV: $SO_4^{-2}$).

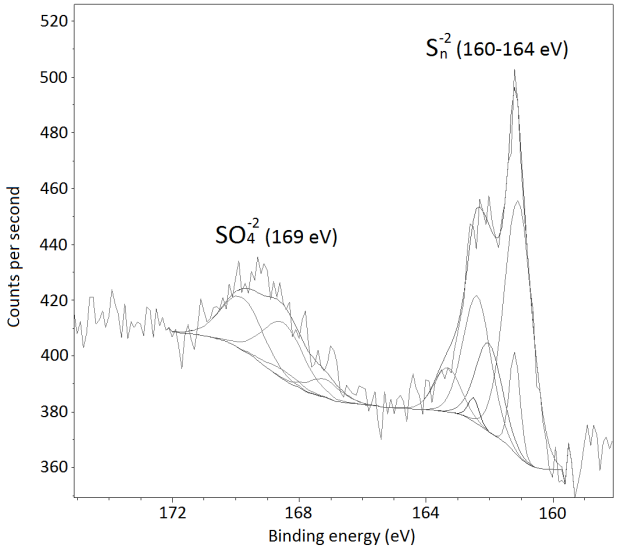


Figure 4.20. XPS spectra in the S 2p region corresponding to the ash resulting from experiment 2.

In summary, results from desulphurization tests have shown some sulphur capture capacity of sewage sludge ash, especially in the case of the solid by-product derived from the combustion process. The desulphurization performance is dramatically reduced in the presence of steam, so the use of this solid by-product as sorbent material for $H_2S$ could be further exploited for dry gas cleaning, such as the sewage sludge pyrolysis gas after condensation of water and vapors.

## 4.4. Catalyst activity tests

This section presents the results obtained in the Ni-based catalysts activity tests for tar reforming. The Ni-$Al_2O_3$ catalysts were modified by adding different metallic promoters: Ca, Fe, Mn and Cu. A synthetic gasification gas containing $H_2$, CO, $CO_2$, $N_2$, $CH_4$, $C_2H_4$, $H_2O$, $H_2S$ (3000 ppmv, wet basis) and a mixture of benzene, toluene and naphthalene as tar model compounds (Table 3.5) was used as reactive atmosphere in the experiments.

Fig. 4.21 shows the evolution of the outlet concentration of naphthalene ($C_{10}H_8$), mono-aromatic tar ($C_6H_6$+$C_7H_8$), methane ($CH_4$) and ethylene ($C_2H_4$) when using the non-modified catalyst (Ni-$Al_2O_3$) calcined at 900 ºC and pre-reduced in a $H_2/N_2$ atmosphere. The temperature ramp followed during the experiment is shown in the upper x-axis. Ethylene was the only hydrocarbon significantly converted below 800 ºC. In the upper temperature range (800-900 ºC), naphthalene conversion rate was higher than those of methane and mono-aromatic tar.

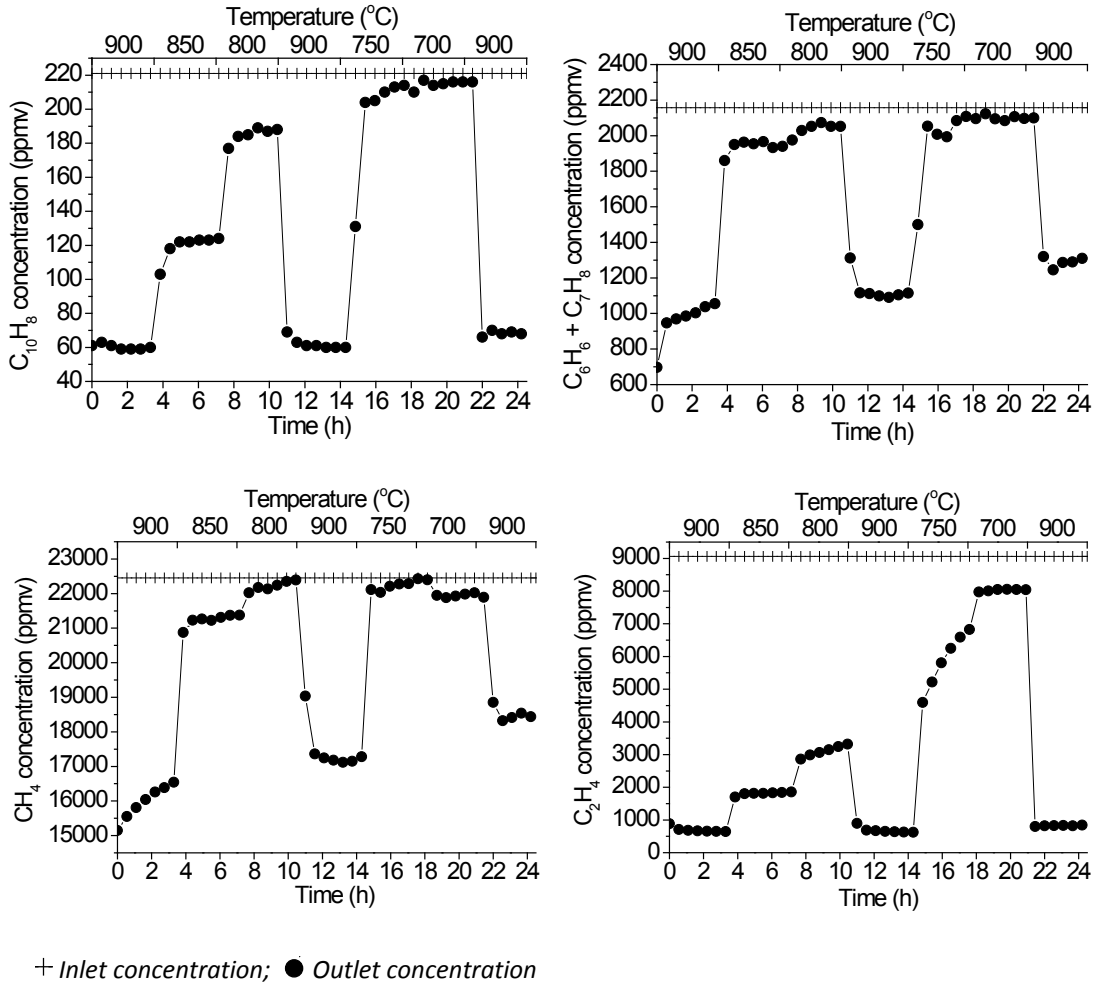


Figure 4.21. Evolution of the concentration of naphthalene, mono-aromatic tar (benzene + toluene), methane and ethylene with the pre-reduced sample of Ni/$Al_2O_3$ calcined at 900 ºC.

The concentration of tar and hydrocarbons in the outlet gas was not totally stable in the temperature range in which the catalyst remained active, but a slight upward trend was observed in most of them as a consequence of a progressive activity loss. Hepola and Simell (1997) found that catalyst deactivation by $H_2S$ was reduced by increasing the operating temperature and decreasing the system pressure. However, despite the high temperature used in the first 3.5 h of experiment (900 ºC), the observed gradual increase in the concentration of methane and mono-aromatic suggests a quick reforming-activity loss of the catalyst in the first stage of experiment. Naphthalene and ethylene concentrations obtained at 900 ºC were not affected by catalyst deactivation as much as methane and mono-aromatic tar conversions. The aforementioned effect of temperature on catalyst deactivation by $H_2S$ poisoning can be clearly observed in the ethylene concentration, which shows the most abrupt increase in the stage at 750 ºC. The different behavior of mono-aromatic tar, naphthalene, methane and ethylene conversions can be attributed to the different decomposition mechanisms and to the competition of reactants for active reaction sites on the catalyst surface.

Performance of the promoted catalysts calcined at 900 ºC and pre-reduced in a $H_2/N_2$ atmosphere is shown in Fig. 4.22. The depicted points represent the conversion average data obtained at each temperature. The conversion of the tar model compounds, methane and ethylene can be calculated from the reactor mass balance as follows:

$$\text{Conversion}_{\,i}(\%) = \frac{n_{i,in} - n_{i,out}}{n_{i,in}} \cdot 100 \qquad \text{(eq. 4.9)}$$

where $n_{i,in}$ and $n_{i,out}$ are the molar flows of compound “i” at the reactor inlet and outlet, respectively. The formation of benzene is usually linked to the decomposition of toluene through reactions such as the steam dealkylation ($C_7H_8 + H_2O \leftrightarrow C_6H_6 + CO + 2H_2$) or hydrodealkylation ($C_7H_8 + H_2 \leftrightarrow C_6H_6 + CH_4$), so a global conversion for both compounds has been calculated and named “mono-aromatic tar conversion”.

The blank run results are not depicted in Fig. 4.22, but they evidenced that thermal cracking hardly contributed to the decomposition of tar compounds and light hydrocarbons under the tested operating conditions. Conversion of methane, naphthalene and mono-aromatic tar was found to be virtually zero in the blank run, while ethylene conversion varied from 4.3% (700 ºC) to 7.7% (900 ºC).

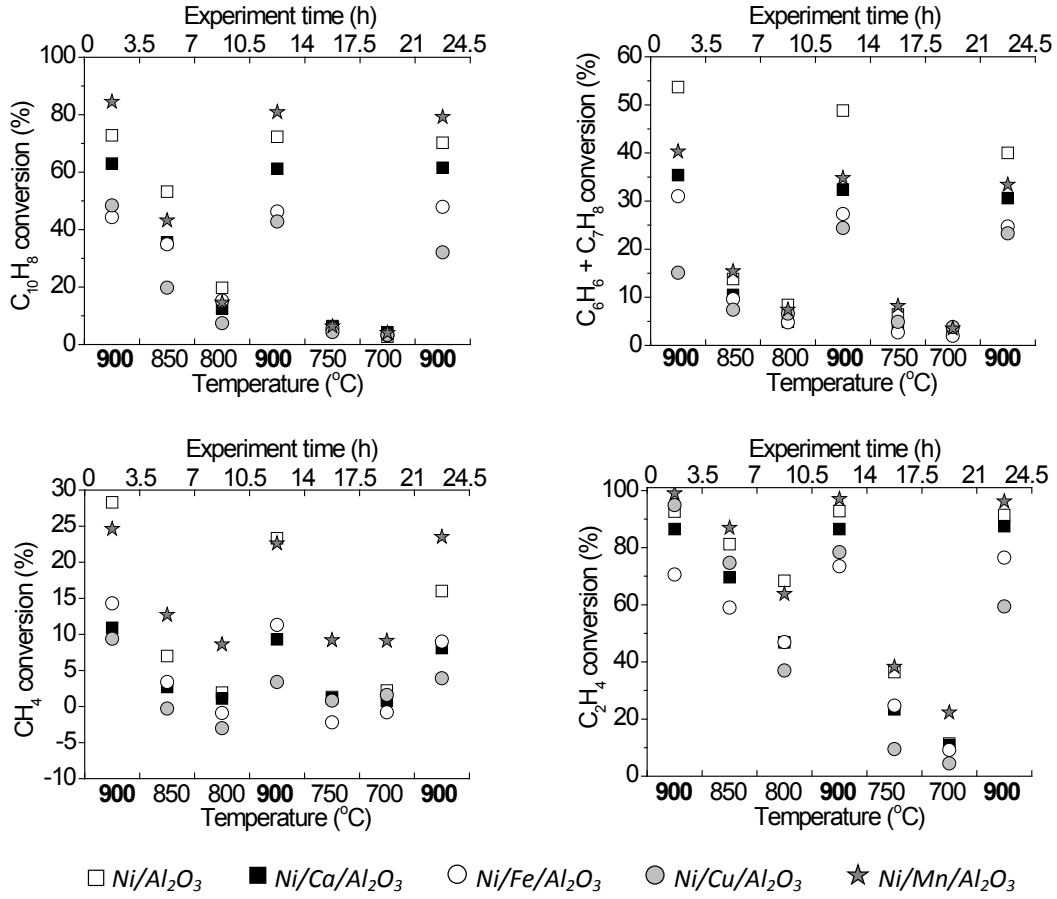


Figure 4.22. Conversion of tar model compounds and light hydrocarbons as a function of the catalyst temperature and added promoter in the solid samples calcined at 900 ºC and pre-reduced in a $H_2/N_2$ atmosphere.

As observed in Fig. 4.22, tar conversion was significantly reduced as the catalyst temperature decreased. This is obvious as both the reaction rate of tar decomposition and the mass transfer rate are favored at higher temperatures. Naphthalene conversion was lower than 20% for temperatures below 800 ºC with all the catalysts. At 900 ºC, the presence of Mn in the catalyst led to a naphthalene conversion of 80%, thus improving the conversion obtained with $Ni/Al_2O_3$ by 10 percentage points. Adding the other metals (Ca, Fe and Cu) was found to be detrimental to naphthalene conversion, as well as to mono-aromatic tar, methane and ethylene conversions. The reduced surface area obtained when the promoters were added (Table 3.3) may explain the worse performance of the promoted catalysts.

The maximum mono-aromatic tar conversion was obtained with $Ni/Al_2O_3$, obtaining an average value of 55% in the first step of 900 ºC. However, this average conversion decreased to 49% and 40% in the following temperature steps at 900 ºC, being the most significant reduction among the tested catalysts. The activity loss of $Ni/Al_2O_3$ was also clearly observed in methane conversion data, as the average value was reduced from 28% in the first step at 900

ºC to 16% in the third step at the same temperature. Mn addition allowed a stable methane conversion in the three temperature steps at 900 ºC (around 24%). Negative values of methane conversion were even found with $Ni/Cu/Al_2O_3$ and $Ni/Fe/Al_2O_3$ at temperatures between 700 and 800 ºC, indicating an increased production of this compound through methanation reactions ($CO + 3H_2 \leftrightarrow CH_4 + H_2O$; $C + 2H_2 \leftrightarrow CH_4$). Mn addition also improved ethylene conversion, as this was above 90% with $Ni/Al_2O_3$ and close to 100% with $Ni/Mn/Al_2O_3$ in the successive steps at 900 ºC.

Regarding the evolution of the other permanent gases, Fig. 4.23 shows the ratio between the outlet and the inlet molar flows of $H_2$, CO and $CO_2$ as a function of the catalyst temperature and added promoter. The depicted points represent the average ratio obtained at each temperature. Values above 1 indicate that the outlet flow exceeds the inlet flow of the gas component.

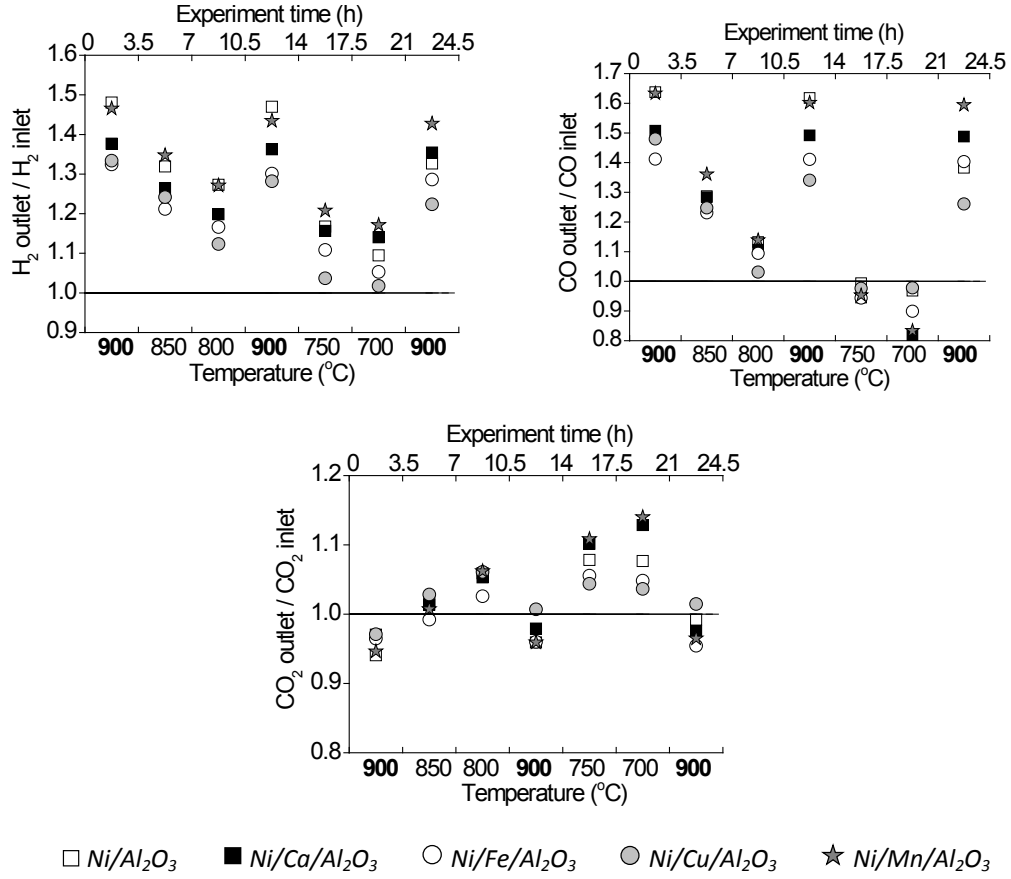


Figure 4.23. Molar ratio between the outlet and inlet molar flows of $H_2$, CO and $CO_2$ as a function of the catalyst temperature and added promoter in the samples calcined at 900 ºC and pre-reduced in a $H_2/N_2$ atmosphere.

$H_2$, CO and $CO_2$ are involved in many reactions both as reactant and as product. As can be observed in Fig. 4.23, the outlet $H_2$ flow increased with respect to the inlet value in the whole temperature range with all the catalysts tested, which means that $H_2$ formation rate was higher than its consumption rate. The higher the temperature, the higher the $H_2$ production. However, as occurred with the conversion of mono-aromatic tar and methane, the downward trend in the $H_2$ outlet flow in the successive steps at 900 ºC also demonstrates the instability of $Ni/Al_2O_3$. The CO outlet flow also increased with the catalyst temperature but, unlike the $H_2$ flow, it was also found to slightly decrease with respect to the inlet value at temperatures below 750 ºC. An opposite trend was found for $CO_2$, as its outlet molar flow decreased with temperature. The improved conversion of tar at high temperatures may partly explain the observed evolution of these permanent gases, since CO and $H_2$ are products of the reforming reactions (eq. 2.9 and 2.10), while $CO_2$ is consumed during dry reforming reactions (eq. 2.10).

Endothermic reactions are favored at high temperatures from both a kinetic and thermodynamic standpoint, but exothermic reactions are thermodynamically restricted at high temperatures given equilibrium conditions. Therefore, it is necessary to know if the process is controlled by thermodynamics or kinetics to justify the results. HSC Chemistry® 6.1 software was used to determine the mass flow rates of the products at equilibrium conditions. Table 4.13 shows the ratio between the outlet and inlet flows of $H_2$, CO and $CO_2$ when the equilibrium is reached at different temperatures. Tar (naphthalene, benzene and toluene) was found to be totally converted in the equilibrium simulation in the whole temperature range (700-900 ºC).

Table 4.13. Equilibrium ratio between the outlet and inlet molar flows of $H_2$, CO and $CO_2$.

| | 700 ºC | 750 ºC | 800 ºC | 850 ºC | 900 ºC |
|---|---|---|---|---|---|
| $H_{2\ outlet}$ / $H_{2\ inlet}$ | 2.11 | 2.06 | 2.00 | 1.95 | 1.90 |
| $CO_{\ outlet}$ / $CO_{\ inlet}$ | 1.72 | 1.86 | 1.99 | 2.10 | 2.20 |
| $CO_{2\ outlet}$ / $CO_{2\ inlet}$ | 1.12 | 1.04 | 0.98 | 0.92 | 0.87 |

Comparison of the experimental and theoretical data shows that chemical equilibrium was not reached in the process: equilibrium production of $H_2$ and CO is considerable higher than the experimental values, while equilibrium production of $CO_2$ is slightly lower than experimental data, especially in the temperature range of 800-900 ºC. The evolution of the equilibrium production of CO, $CO_2$ and $H_2$ may be explained by shifting the equilibrium reactions according to their exothermic or endothermic nature.

*Effect of the reduction procedure*

Fig. 4.24 shows the performance of the promoted catalysts calcined at 900 ºC and tested without a reduction pre-treatment. The impact of the reduction procedure on the catalyst activity can be evaluated by a comparison of Figs. 4.22 and 4.24.

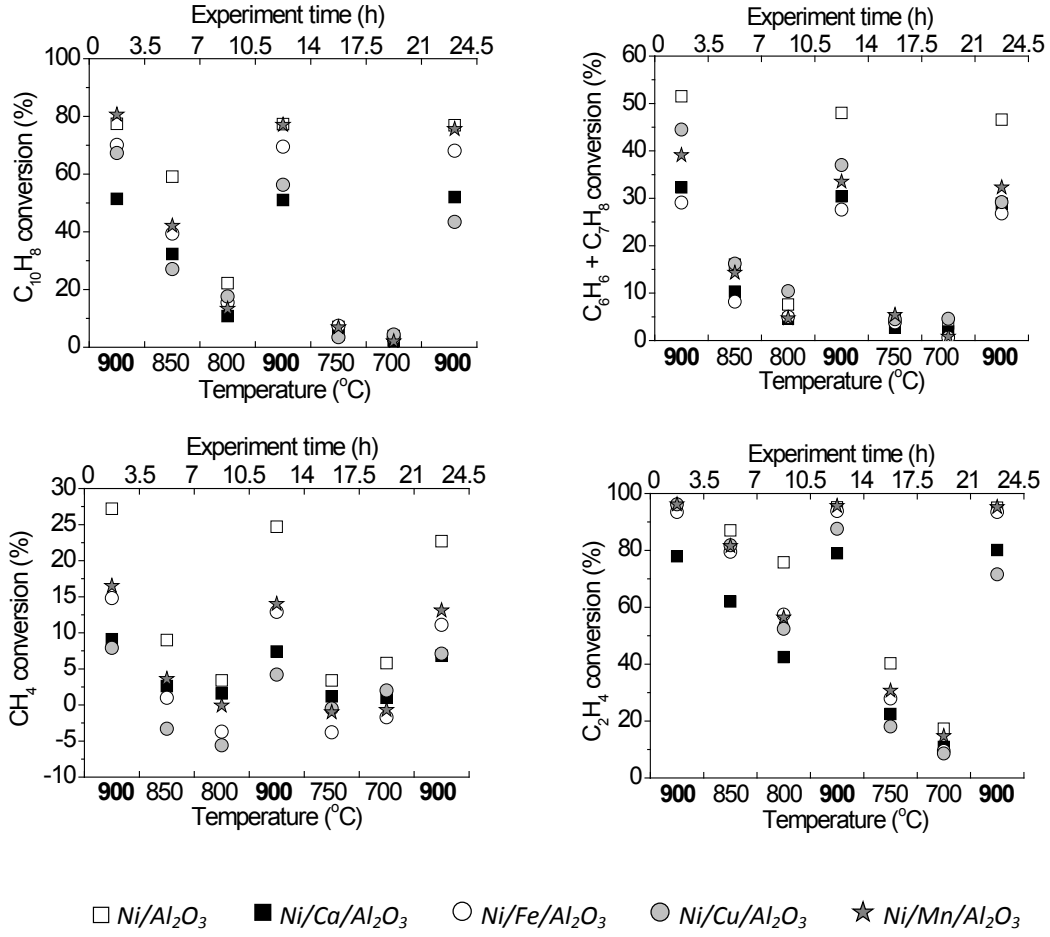


Figure 4.24. Conversion of tar model compounds and light hydrocarbons as a function of the catalyst temperature and added promoter in the solid samples calcined at 900 ºC and tested without reduction pre-treatment.

In the absence of a reduction pre-treatment, the average naphthalene conversion obtained in the first step at 900 ºC with $Ni/Fe/Al_2O_3$, $Ni/Cu/Al_2O_3$ and $Ni/Al_2O_3$ improved by 25, 20 and 5 percentage points with respect to the results obtained when the samples were pre-reduced, respectively. Further sintering of the catalysts during the reduction pre-treatment at 900 ºC could explain this observed trend, since the pre-reduced samples were exposed to a high temperature for a longer time. However, the activity of $Ni/Mn/Al_2O_3$ for naphthalene conversion was almost the same regardless of the reduction procedure, while the performance of $Ni/Ca/Al_2O_3$ was slightly better for the reduced sample. Both $Ni/Al_2O_3$ and $Ni/Mn/Al_2O_3$ led to the maximum naphthalene conversion at 900 ºC (80%). The non-modified catalyst ($Ni/Al_2O_3$)

showed again the best results for mono-aromatic tar conversion. Regarding methane conversion, only the activity of $Ni/Mn/Al_2O_3$ was significantly affected by the reduction procedure: the average methane conversion in the first step at 900 ºC dropped from 25% with the pre-reduced sample to 16% with the non-reduced sample. In the case of ethylene conversion, the most significant difference was observed for $Ni/Fe/Al_2O_3$, as the average ethylene conversion in the first step at 900 ºC increased from 70% with the pre-reduced sample to 95% with the non-reduced sample.

The decline in the average conversion of methane and mono-aromatic tar in the successive steps at 900 ºC was less pronounced when avoiding the pre-reduction stage of the $Ni/Al_2O_3$ catalyst.

*Effect of the calcination temperature*

Fig. 4.25 shows the performance of the promoted catalysts calcined at 700 ºC and tested without a reduction pre-treatment. The influence of the calcination temperature on the catalyst activity can be evaluated by a comparison of Figs. 4.24 and 4.25.

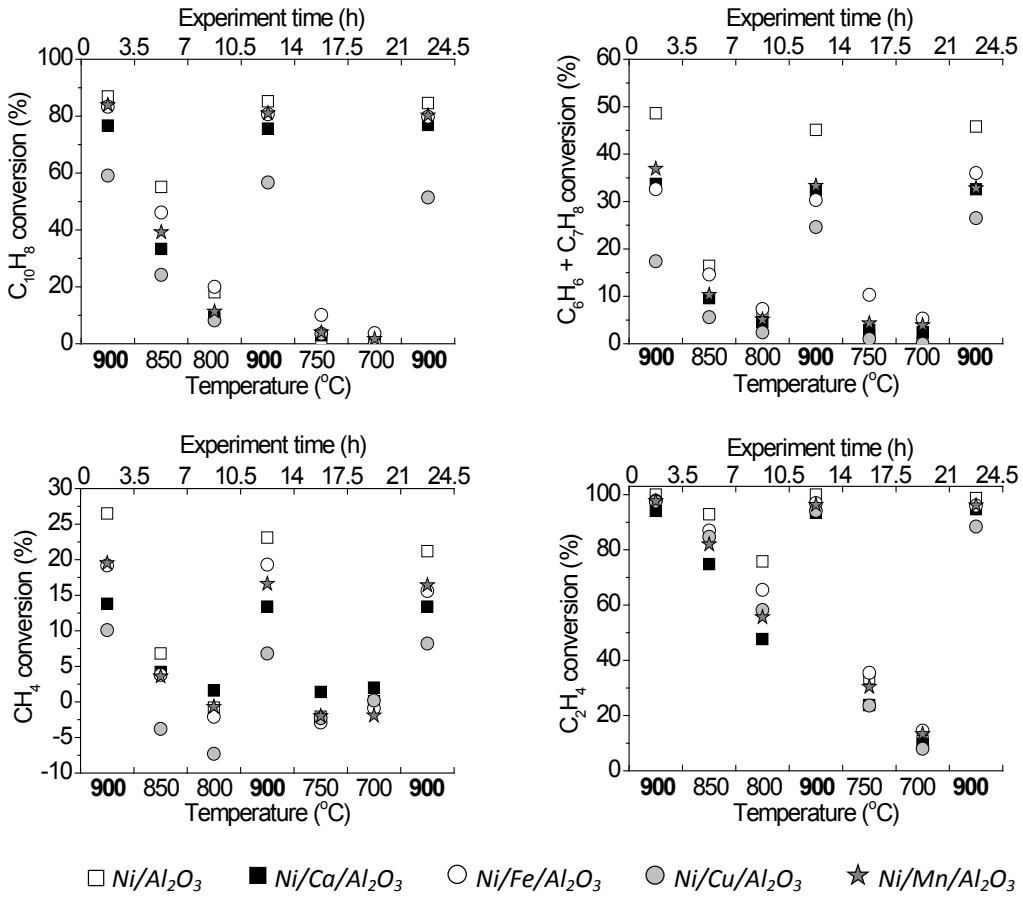


Figure 4.25. Conversion of tar model compounds and light hydrocarbons as a function of the catalyst temperature and added promoter in the solid samples calcined at 700 ºC and tested without reduction pre-treatment.

The average naphthalene conversion obtained in the first step at 900 ºC with the samples of $Ni/Al_2O_3$, $Ni/Ca/Al_2O_3$ and $Ni/Fe/Al_2O_3$ calcined at 700 ºC were 10, 25 and 15 percentage points higher than those obtained for the samples calcined at 900 ºC, respectively. As discussed in section 3.1.3, the reduction in the surface area of the catalysts while increasing the calcination temperature may explain this trend (Table 3.3). However, naphthalene conversion with $Ni/Mn/Al_2O_3$ was hardly influenced by the calcination temperature, while $Ni/Cu/Al_2O_3$ even showed a slightly lower naphthalene conversion when calcined at 700 ºC. Therefore, not only does the surface area affect naphthalene conversion, but also the different metallic phases formed when varying the calcination temperature.

The maximum naphthalene conversion was obtained with the $Ni/Al_2O_3$ sample calcined at 700 ºC (85%), but very similar results were obtained with the $Ni/Mn/Al_2O_3$ and $Ni/Fe/Al_2O_3$ samples calcined at the same temperature. Mono-aromatic tar conversion was hardly affected by the calcination temperature, except for $Ni/Cu/Al_2O_3$ which, as occurred with the naphthalene conversion, showed worse results when calcined at 700 ºC, especially at the beginning of the experiment. Regarding methane conversion, all the promoted catalysts calcined at 700 ºC led to an initial average conversion around 5 percentage points higher than that obtained when calcined at 900 ºC. Considering that the maximum conversion of methane was around 25%, the observed increase is a significant improvement. Lastly, ethylene conversion results obtained at 900 ºC with the catalysts calcined at 700 ºC were more similar to each other than in the previous cases. Conversions above 90% were obtained in all cases.

*Catalyst characterization*

The spent catalysts were characterized by XRD and ultimate analysis after the activity tests. Table 4.14 presents the sulphur and carbon contents detected in the spent catalyst samples.

Table 4.14. Carbon and sulphur fractions (wt. %) in the spent catalyst samples.

| Catalyst preparation | | $Ni/Al_2O_3$ | $Ni/Ca/Al_2O_3$ | $Ni/Fe/Al_2O_3$ | $Ni/Cu/Al_2O_3$ | $Ni/Mn/Al_2O_3$ |
|---|---|---|---|---|---|---|
| Calcined at 900 ºC. With reduction pre-treatment | % C | 1.7 ± 0.4 | 0.32 ± 0.01 | 0.39 ± 0.05 | 15.0 ± 0.2 | 0.23 ± 0.03 |
| | % S | 2.24 ± 0.06 | 1.6 ± 0.2 | 2.27 ± 0.04 | 3.1 ± 0.1 | 1.68 ± 0.06 |
| Calcined at 900 ºC. Without reduction pre-treatment | % C | 2.4 ± 0.1 | 0.30 ± 0.06 | 0.40 ± 0.08 | 12.1 ± 0.2 | 0.40 ± 0.04 |
| | % S | 2.0 ± 0.3 | 1.8 ± 0.1 | 2.16 ± 0.03 | 3.44 ± 0.06 | 2.21 ± 0.01 |
| Calcined at 700 ºC. Without reduction pre-treatment | % C | 2.8 ± 0.4 | 0.32 ± 0.07 | 0.17 ± 0.01 | 8.8 ± 0.3 | 0.12 ± 0.03 |
| | % S | 1.9 ± 0.3 | 2.06 ± 0.03 | 1.9 ± 0.2 | 3.74 ± 0.04 | 1.52 ± 0.07 |

*mean value ± standard deviation.*

The highest sulphur and carbon contents were found in the spent samples of $Ni/Cu/Al_2O_3$, irrespective of the method of preparation and reduction of the catalysts. Carbon content reached 15% in the pre-reduced sample calcined at 900 ºC. Thus carbon deposition seems to contribute significantly to the striking deactivation of this catalyst sample. The carbon content was reduced to 12% in the non-reduced sample calcined at 900 ºC and to 9% in the non-reduced sample calcined at 700 ºC. Given this high carbon deposition and the net formation of $CH_4$ detected with $Ni/Cu/Al_2O_3$ (Figs. 4.22, 4.24, 4.25), this catalyst seems to play an important role in the heterogeneous methanation reaction ($C + 2H_2 \leftrightarrow CH_4$). The addition of the other promoters to $Ni/Al_2O_3$ resulted in a decreased content of carbon. This reduction might be related to the lower activity of the $Ni/Fe/Al_2O_3$ and $Ni/Ca/Al_2O_3$ catalysts, but in the case of $Ni/Mn/Al_2O_3$ which showed even higher activity than $Ni/Al_2O_3$. As suggested by other researchers, this could mean a good anti-coking ability of Mn (Koike et al., 2013). For instance, the carbon content was reduced from 1.7% in the pre-reduced sample of $Ni/Al_2O_3$ to 0.23% in the pre-reduced sample of $Ni/Mn/Al_2O_3$. No correlation was found between the deposited carbon amount and the calcination temperature or the reduction treatment of the catalysts, but this depends on the promoter added. The same occurs with the sulphur content. However, adding Cu to $Ni/Al_2O_3$ always resulted in an increase in the sulphur content, regardless of the preparation method of the catalysts. The sulphur content in the other modified catalysts was very similar or even slightly lower than in $Ni/Al_2O_3$, although these results alone cannot confirm whether the sulphur was preferentially chemisorbed on nickel sites or on the promoter sites.

Fig. 4.26 shows the XRD patterns of the spent catalysts calcined at 900 ºC and tested without reduction pre-treatment. The patterns obtained for the pre-reduced spent samples calcined at 900 ºC were exactly the same as those presented in Fig. 4.26.

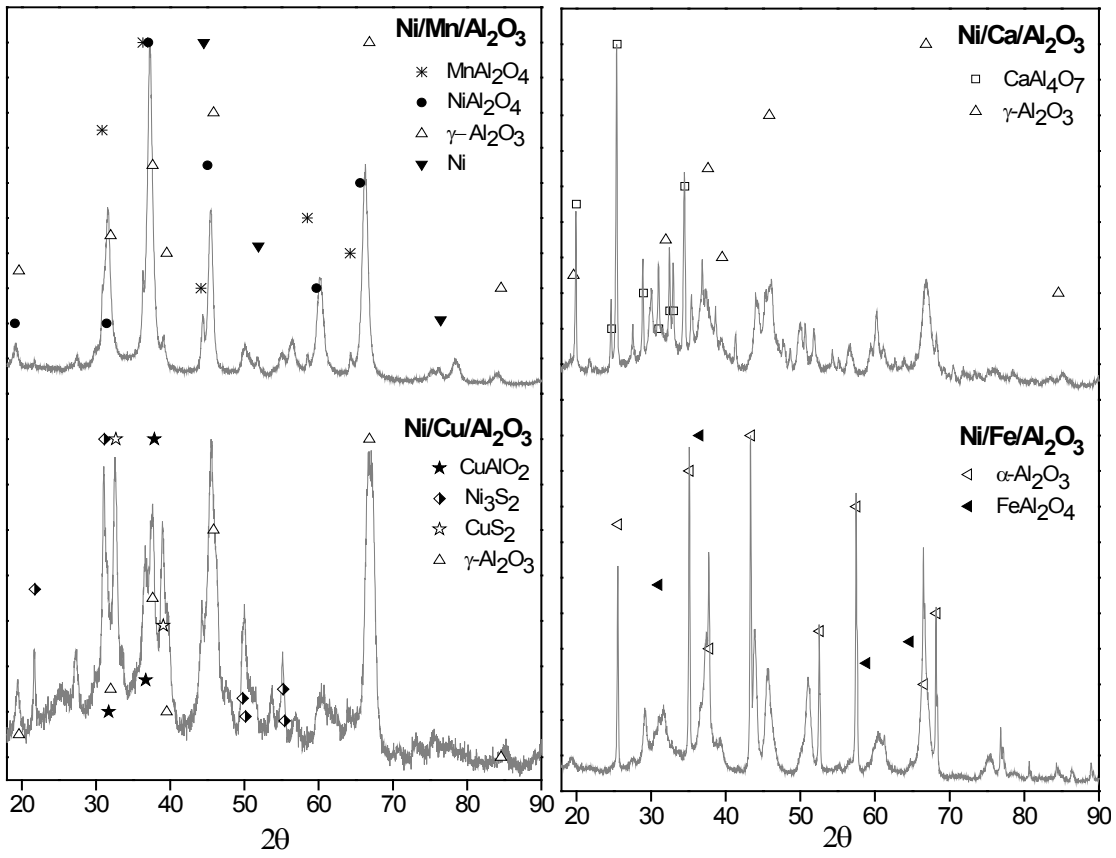


Figure 4.26. XRD patterns of the spent catalysts calcined at 900 °C and tested without reduction pre-treatment.

Significant changes can be found by comparing the XRD patterns of the spent (Fig. 4.26) and fresh catalysts (Fig. 3.2).The spent samples were considerably more crystalline and $NiAl_2O_4$ was not the main phase detected in all of them. As the peaks are narrower in the spent samples, the presence of the promoter metals in different phases can be confirmed. This leads to XRD patterns more different from each other than those of the fresh samples. Despite the reducing atmosphere created by the gasification gas, aluminates of the metal promoters ($MnAl_2O_4$, $CuAlO_4$, $FeAl_2O_4$ and $CaAl_4O_7$) were still present in the spent catalysts. Special attention should also be drawn to the detection of sulphur-containing phases in the $Ni/Cu/Al_2O_3$ spent sample, such as $Ni_3S_2$ and $CuS_2$, and to the high crystallinity of the $Ni/Fe/Al_2O_3$ spent sample due to a change in the structure of alumina.

In summary, only Mn addition resulted in improved stability and activity of the $Ni/Al_2O_3$ catalyst when the catalysts were pre-reduced in a $H_2/N_2$ atmosphere before the activity tests. Results suggest suppression of carbon deposition and reduction of sintering phenomena by addition of Mn, but further studies are required to confirm these results, as well as to clarify the role of Mn in sulphur poisoning.

# 5. CONCLUSIONS AND FUTURE WORK

*Air-steam gasification of sewage sludge and char*

Air-steam gasification appears as an interesting option for energy recovery from sewage sludge. The sludge can contain up to 70% of water prior to thermal drying, so a steam rich atmosphere can be created by the own moisture content of the sludge for the steam reforming and gasification reactions at high temperature. The addition of air into the gasification medium provides the necessary energy for the endothermic process of steam gasification through the partial combustion of the raw material.

The dry gas production during the air-steam gasification of sewage sludge ranged between 0.89 and 1.32 $m^3_{STP}\cdot kg^{-1}_{SS\ daf}$ ($N_2$-free basis). This gas could be suitable for boiler, engine and turbine operation from the calorific value standpoint ($LHV_{gas}$ = 4.1-6.2 $MJ\cdot m^{-3}_{STP}$). The $H_2$/CO molar ratio in the gas also reached a suitable value for its use as a chemical feedstock ($H_2$/CO = 2) when using a $H_2O/O_2$ molar ratio of 3 as gasification medium. The lowest tar content in the product gas obtained during the air-steam gasification of sewage sludge was around 11 $g\cdot m^{-3}_{STP}$.

Char obtained in the pyrolysis of sewage sludge appears as a preferable feedstock for gasification from the point of view of tar formation. In this case, tar content was reduced as much as 3 $g\cdot m^{-3}_{STP}$ under some specific operating conditions. The reduction in the volatile matter content of the solid after pyrolysis (50 wt. % in the sewage sludge and 15 wt. % in the pyrolysis char) explains the reduced tar formation during char gasification. The dry gas yield per kilogram of solid material was practically reduced by half when gasifying char instead of sewage sludge. This is the main drawback of char gasification. However, if gas production is calculated on a dry and ash-free basis (*daf*) for the solid, the gas yield is increased in the case of char gasification (0.99-1.47 $m^3_{STP}\cdot kg^{-1}_{char\ daf}$, $N_2$-free basis). It is worth mentioning that the production of CO during char gasification increased by 45-85% (in terms of $g\cdot kg^{-1}_{solid\ daf}$) compared to that obtained from sewage sludge gasification. This increased production of CO seems to be related to the higher fixed carbon content in the char (9.08 wt. %) than in the sewage sludge (4.36 wt. %). Heterogeneous reactions such as the water gas reaction or the Boudouard reaction, in which CO is formed at high temperatures, take place to a greater extent in solids with higher fixed carbon content. On the other hand, the production of light hydrocarbons ($CH_4$, $C_2H_x$) decreased by around 80% (in terms of $g\cdot kg^{-1}_{solid\ daf}$) when gasifying char instead of sewage sludge. Despite these differences, the lower heating value of the gases

resulting from both processes remained in the same order of magnitude (4-6 $MJ \cdot m^{-3}_{STP}$). The $H_2/CO$ molar ratio in the gas from char gasification also exceeded 2 under some operating conditions.

Table 5.1 summarizes qualitatively the impact of the studied operating factors (temperature, gasifying ratio and $H_2O/O_2$ ratio used as gasification medium) on the response of the analyzed variables.

Table 5.1. Qualitative impact of the operating factors on sewage sludge gasification and char gasification.

| | *Sewage sludge gasification* | | | *Char gasification* | | |
|---|---|---|---|---|---|---|
| | T | GR | $H_2O/O_2$ | T | GR | $H_2O/O_2$ |
| Carbon fraction remaining as solid (%) | ↓↓↓↓ | ↓↓ | ↑↑↑ | ↓↓↓ | ↓↓ | ↑↑ |
| Carbon fraction converted into gas (%) | ↑ | ↑ | ↓ | ↑↑ | ↑ | ↓ |
| Dry gas yield ($N_2$-free, $m^3_{STP} \cdot kg^{-1}_{solid}$) | ↑↑ | ↑ | --- | ↑↑ | ↑ | --- |
| Tar content ($g \cdot m^{-3}_{STP}$) | ↓↓↓↓ | ↓ | ↑↑ | ↓↓↓ | ↓↓↓ | ↓↓↓ |
| Mass yield of each gas ($g \cdot kg^{-1}_{solid}$) | | | | | | |
| $H_2$ | ↑↑↑ | ↓ | ↑↑ | ↑↑ | ↑ | ↑↑ |
| CO | ↑↑↑ | ↓ | ↓↓ | ↑↑↑ | --- | ↓ |
| $CO_2$ | --- | ↑↑ | ↓↓ | ↓ | ↑↑ | ↓ |
| $CH_4$ | ↑ | ↓ | ↑↑ | --- | --- | ↑↑ |
| $C_2H_x$ | ↓ | --- | ↑ | --- | --- | --- |
| $H_2S$ | ↑↑ | ↑↑ | --- | ↑↑↑↑ | ↑↑↑ | --- |
| $H_2/CO$ molar ratio in the product gas | ↓ | ↑ | ↑↑↑ | ↓↓ | --- | ↑↑ |
| $CO/CO_2$ molar ratio in the product gas | ↑↑↑ | ↓↓ | --- | ↑↑↑ | ↓↓ | --- |
| $LHV_{gas}$ ($MJ \cdot m^{-3}_{STP}$) | ↑ | ↓ | ↑ | ↑↑ | --- | ↑ |
| Cold gasification efficiency (%) | ↑↑ | --- | ↑ | ↑↑ | ↑ | ↑ |

- ↓, ↓↓, ↓↓↓ and ↓↓↓↓: an increase of the operating factor leads to a decrease of the response variable at different impact levels: slight, medium, high and very high, respectively.
- ↑, ↑↑, ↑↑↑ and ↑↑↑↑: an increase of the operating factor leads to an increase of the response variable at different impact levels: slight, medium, high and very high, respectively.

Although both processes have shown some differences in the relative importance of the factors on the evolution of the response variables, the same trends have been found in most of them. Temperature was the most influential factor for most of the response variables analyzed. Higher temperatures were favorable for reducing the tar content in the gas and improving the carbon conversion, the gas yield, the production of $H_2$, CO and $H_2S$, the $CO/CO_2$ ratio in the product gas, the gas heating value and the cold gasification efficiency in both processes. The gasification medium ($H_2O/O_2$ ratio) played an important role in the $H_2$

production and, consequently, in the $H_2$/CO ratio in the product gas, being favored by the presence of steam. The $CH_4$ production was also improved at high $H_2O/O_2$ ratio. However, the increase of the $H_2O/O_2$ ratio was detrimental for carbon conversion. On the other hand, the increase of the gasifying ratio (GR) showed a great impact on the production of $CO_2$ and $H_2S$, affecting them positively. Based on these results, the best conditions from the point of view of gas use seem to be a high gasification temperature (850 ºC), an average gasification ratio (0.95) and a high $H_2O/O_2$ ratio as gasification medium (3).

The energetic assessment of the air-steam gasification processes is a key issue since the presence of steam in the gasification medium involves a series of endothermic reactions. Energy balances based on the experimental product yields were conducted. Despite the lower organic content in the char (24.1 wt. %) than in the sewage sludge (54.5 wt. %), greater external energy demand is required for gasifying 1 kg of char than that for gasifying 1 kg of sewage sludge under the same operating conditions. In the studied range of the factors, the air-steam gasification of sewage sludge can be either an exothermic or endothermic process depending on the operating conditions, showing an enthalpy of reaction ranging between -2.6 $MJ \cdot kg^{-1}_{SS}$ and 1.3 $MJ \cdot kg^{-1}_{SS}$ (considering the products at the gasification temperature). However, the air-steam gasification of char was an endothermic process in most of the experimental conditions, and its enthalpy of reaction varied from -0.2 $MJ \cdot kg^{-1}_{char}$ to 1.2 $MJ \cdot kg^{-1}_{char}$ (products at the gasification temperature). A theoretical study based on equilibrium simulations showed that both gasification processes require more energy to take place at equilibrium conditions, but further energy may be recovered in turn from the equilibrium gas, so that the gasification efficiency is improved at equilibrium conditions.

If the lower heating value and the sensible and latent heats of gases and vapors could be efficiently recovered and used, the energy contained in the gas product of sewage sludge gasification would be enough to cover the energy demand for both the thermal drying of sewage sludge and the gasification process itself.

The energy required for the thermal decomposition of sewage sludge during the pyrolysis process (0.15 $MJ \cdot kg^{-1}_{SS}$ at 530 ºC) can be supplied by an efficient use of the energy contained in the product stream of gases and vapors ($LHV_{gas}$ and sensible and latent heats). However, the remaining energy in the gas products of both sewage sludge pyrolysis and char gasification is not enough for the prior thermal drying of sewage sludge. An additional energy input is required to carry out this three-stage process. This energy demand could be provided by the calorific value of the bio-oil produced during pyrolysis, but some important properties such as its poor stability or its high nitrogen content must be improved facing toward its use as fuel.

*High-temperature desulphurization of gases with sewage sludge ash*

Due to its metal content, especially iron and calcium, sewage sludge ash appears as a potential sorbent material for $H_2S$ removal at high temperature. In general, sewage sludge gasification ash showed worse desulphurization ability than the combustion ash. Some differences in the composition of both solids may explain their different behavior. Lower iron content was detected in the gasification ash (116 mg $Fe \cdot g^{-1}_{ash}$) than in the combustion ash (192 mg $Fe \cdot g^{-1}_{ash}$). Furthermore, iron was forming part of different crystalline species: $Fe_2O_3$ in the combustion ash and $Fe_3O_4$ in the gasification ash.

In the absence of interferences from other gases (gas atmosphere only composed of 5000 ppm $H_2S$ and $N_2$), the $H_2S$ breakthrough time (< 100 ppmv $H_2S$) was around 300 min by using the combustion ash at 800 ºC, and a final sulphur content of around 63 mg $S \cdot g^{-1}_{ash}$ was detected in the spent ash (1 g of ash, 50 $mL_{STP} \cdot min^{-1}$).

The $H_2S$ breakthrough time was drastically reduced to a few minutes (50 min in the best conditions) in the presence of 30% steam as a consequence of the simultaneous regeneration of the spent metal sulphides. Thus, the use of sewage sludge ash for $H_2S$ removal at 600-800 ºC is only suitable for dry gas cleaning. The desulphurization process was also negatively affected by the reducing atmosphere created by the gasification gas (CO, $H_2$) due to the simultaneous reduction of $Fe_2O_3$ and $Fe_3O_4$ to FeO, whose sulphur capture capacity has been proved to be lower, and by the presence of $CO_2$ which causes the carbonation of CaO. Combustion ash at 600 ºC led to the best results during desulphurization of the moist synthetic gasification gas (most realistic conditions), showing a $H_2S$ breakthrough time of 50 min and a final sulphur content of 27 mg $S \cdot g^{-1}_{ash}$ after 120 min of experiment.

Ultimate analyses of the spent ash samples showed that the total amount of $H_2S$ removed from gas was only partially captured in the ash. $H_2S$ was the only sulphur-containing gas analyzed during the experiments, but sulphur mass balances suggest that it is probably not the only sulphur-containing compound in the exit gas. Theoretical simulations based on thermodynamic data showed the formation of other sulphur-containing gases such as $SO_2$ or COS (this latter in a very low proportion). Therefore, the analysis of the $H_2S$ breakthrough curves alone can lead to misleading conclusions about the sulphur capture capacity of a sorbent material. In most cases, sulphur content detected by the elemental analyzer in the spent combustion ash was 35-50% lower than the maximum thermodynamic data calculated assuming that the total content of calcium and iron in the solid was in the form of CaO and $Fe_2O_3$, respectively.

*Catalytic reforming of tar model compounds with Ni-based catalysts*

Several nickel-alumina catalysts were prepared and modified by adding different metals (Fe, Ca, Mn and Cu) in order to evaluate the effect of these promoters on the catalyst stability and activity for the reforming of tar and hydrocarbons. A synthetic gasification gas containing high sulphur content (3000 ppmv $H_2S$, wet basis) and a mixture of benzene, toluene and naphthalene as tar model compounds was used in the experiments. Sulphur chemisorption on nickel active sites was expected to decrease with the addition of the aforementioned promoters because of their ability to react with $H_2S$. However, this effect was not observed at all along the duration of the experiments, but the catalyst activity was found to decrease with the addition of most of the promoters. This could be explained by the significant reduction in the catalyst surface area observed when the promoters were added (10-50% lower compared to $Ni/Al_2O_3$). Exceptionally, Mn addition to $Ni/Al_2O_3$ improved the catalytic performance, although this improvement was only observed when the catalysts were pre-reduced before the activity tests ($H_2/N_2$ atmosphere at 900 $^oC$) and not when the catalysts were reduced during the experiments with the gasification gas itself. Despite the reduced surface area, the presence of Mn led to an increase in naphthalene conversion up to 80% at 900 $^oC$, which was 10 percentage points higher than that obtained with $Ni/Al_2O_3$. Mono-aromatic tar conversion was not improved by adding Mn, but gas composition was considerably more stable over time. This higher stability may be related to the lower carbon content deposited on $Ni/Mn/Al_2O_3$ (0.23 wt. %) compared to that on $Ni/Al_2O_3$ (1.7 wt. %). As Mn addition was not favorable for catalyst activity when the catalysts were not pre-reduced in a $H_2$ atmosphere, the aforementioned improvement could be related to a good anti-sintering ability of Mn. More work is required to prove this theory.

Regarding the addition of the other promoters, none of them resulted in an improved activity for tar reforming. It should be noted that the addition of Cu and Fe favored the net production of methane in the lower temperature range (700-800 $^oC$). This fact together with the high carbon content detected in the spent samples of $Ni/Cu/Al_2O_3$ suggests an important role of this catalyst in the methanation reaction ($C + 2H_2 \leftrightarrow CH_4$).

**FUTURE WORK**

Based on the results obtained in this study, some future work can be proposed in order to further study the air-steam gasification of sewage sludge and the gas cleaning at lab-scale:

- Use of sewage sludge with higher moisture content (20-30%) to obtain the steam-rich atmosphere from the own moisture content of the sludge. This will probably require the design of a different feeding system for the wet sludge.
- Use of non-digested sewage sludge as raw material for the gasification process in order to take advantage of the whole organic fraction removed and accumulated during the wastewater treatment.
- Since sewage sludge combustion ash has proved some capacity for $H_2S$ removal at dry conditions, the use of the ash resulting from the pyrolysis char combustion for desulphurization of the pyrolysis gas (after the condensation of water and bio-oil) can be an interesting option in order to reuse the main by-product of the process.
- Further study of Mn as a promoter for Ni-catalysts.
- Use of the Ni/Mn catalyst in a downstream reactor during the sewage sludge gasification in order to evaluate its activity and stability under the gas atmosphere resulting from the gasifier.

# 6. REFERENCES

Abu El-Rub Z., Bramer E.A., Brem G. (2004) *Review of catalysts for tar elimination in biomass gasification processes*. Industrial & Engineering Chemistry Research 43, 6911-6919.

Adegoroye A., Paterson N., Li X., Morgan T., Herod A.A., Dugwell D.R., Kandiyoti R. (2004) *The characterisation of tars produced during the gasification of sewage sludge in a spouted bed reactor*. Fuel 83, 1949-1960.

Álvarez-Rodríguez R., Clemente-Jul C. (2008) *Hot gas desulphurisation with dolomite sorbent in coal gasification*. Fuel 87, 3513-3521.

Anis S., Zainal Z.A. (2011) *Tar reduction in biomass producer gas via mechanical, catalytic and thermal methods: A review.* Renewable & Sustainable Energy Reviews 15, 2355-2377.

Antal M.J., Edwards W.E., Friedman K.L., Rogers F.E. (1979) *Final Progress Report to US Environmental Protection Agency*. Princeton University.

Aznar M., González A.E., Manyà J.J., Sánchez J.L., Murillo M.B. (2007) *Understanding the effect of the transition period during the air gasification of dried sewage sludge in a fluidized bed reactor*. International Journal of Chemical Reactor Engineering 5, A18.

Aznar M., Manyà J.J., García G., Sánchez J.L., Murillo M.B. (2008) *Influence of freeboard temperature, fluidization velocity and particle size on tar production and composition during the air gasification of sewage sludge*. Energy & Fuels 22, 2840-2850.

Aznar M.P., Caballero M.A., Gil J., Martín J.A., Corella J. (1998). *Commercial steam reforming catalysts to improve biomass gasification with steam-oxygen mixtures. 2. Catalytic tar removal*. Industrial & Engineering Chemical Research 37, 2668-2680.

Bacaicoa P.G., Bilbao R., Uson C. (1995) *Sewage sludge gasification: first studies*. In: Proceedings of the Second Biomass Conference of the Americas: Energy, Environment, and Agricultural Industry, 685-694.

Bagreev A., Bandosz T.J. (2005) *On the mechanism of hydrogen sulfide removal from moist air on catalytic carbonaceous adsorbents*. Industrial & Engineering Chemistry Research 44, 530-538.

Bandosz T.J. (2002) *On the adsorption/oxidation of hydrogen sulfide on activated carbons at ambient temperatures*. Journal of Colloid and Interface Science 246, 1-20.

Bona S., Guillen P., Alcalde J.G., García L., Bilbao R. (2008) *Toluene steam reforming using coprecipitated Ni/Al catalysts modified with lanthanum or cobalt*. Chemical Engineering Journal 137, 587-597.

Brandt P., Henriksen U. (2000) *Decomposition of tar in gas from updraft gasifier by thermal cracking*. In: Proceedings of the first world conference on biomass for energy and industry.

Bridgwater A.V. (1995) *The technical and economic feasibility of biomass gasification for power generation*. Fuel 74, 631-653.

Campoy M., Gómez-Barea A., Vidal F.B., Ollero P. (2009) *Air-steam gasification of biomass in a fluidised bed: Process optimisation by enriched air*. Fuel Processing Technology 90, 677-685.

Campoy M., Gómez-Barea A., Ollero P., Nilsson S. (2014) *Gasification of wastes in a pilot fluidized bed*. Fuel Processing Technology 121, 63-69.

Chaudhari S.T., Dalai A.K., Bakhshi N.N. (2003) *Production of hydrogen and/or syngas ($H_2$+ CO) via steam gasification of biomass-derived chars*. Energy & Fuels 17, 1062-1067.

Cheah S., Carpenter D.L., Magrini-Bair K.A. (2009) *Review of mid- to high- temperature sulfur sorbents for desulphurization of biomass- and coal-derived syngas*. Energy & Fuels 23, 5291-5307.

Chueh C.F., Swanson A.C. (1973) *Estimation of liquid heat capacity*. The Canadian Journal of Chemical Engineering 51, 596-600.

Commission of the European Communities (2001). *Decision 2001/118/EC of 16 January 2001 amending Decision 2000/532/EC as regards the list of wastes*. Official Journal of the European Communities No. L 47/1.

Corella J., Orio A., Toledo J.M. (1999) *Biomass gasification with air in a fluidized bed: Exhaustive tar elimination with commercial steam reforming catalysts*. Energy & Fuels 13, 702-709.

Corella J., Toledo J.M., Molina G. (2006) *Calculation of the conditions to get less than 2 g tar/$Nm^3$ in a fluidized bed biomass gasifier.* Fuel Processing Technology 87, 841-846.

Council of the European Communities (1986). *Council Directive 86/278/EEC of 12 June 1986 on the protection of the environment, and in particular of the soil, when sewage sludge is used in agriculture.* Official Journal of the European Communities No. L 181/6.

Council of the European Communities (1991). *Council Directive 91/271/EEC of 21 May 1991 concerning urban waste water treatment*. Official Journal of the European Communities No. L 135/40.

Council of the European Union (1999). *Council Directive 99/31/EC of 26 April 1999 on the landfill of waste*. Official Journal of the European Communities No. L 182/1.

Council of the European Union and European Parliament (2008). *Directive 2008/98/EC of 19 November 2008 on waste and repealing certain Directives*. Official Journal of the European Union No. L 312/3.

Council of the European Union and European Parliament (2010). *Directive 2010/75/EU of 24 November 2010 on industrial emissions (integrated pollution prevention and control)*. Official Journal of the European Union No. L 334/17.

Courson C., Makaga E., Petit C, Kiennemann A. (2000) *Development of Ni catalysts for gas production from biomass gasification. Reactivity in steam- and dry-reforming*. Catalysis Today 63, 427-437.

De Lasa H., Salaices E., Mazumder J., Lucky R. (2011) *Catalytic steam gasification of biomass: catalysts, thermodynamics and kinetics*. Chemical Reviews 111, 5404-5433.

Devi L., Ptasinski K.J., Janssen F.J.J.G. (2003) *A review of the primary measures for tar elimination in biomass gasification processes*. Biomass & Bioenergy 24, 125-140.

Di Blasi C. (2009) *Combustion and gasification rates of lignocellulosic chars*. Progress in Energy and Combustion Science 35, 121-140.

Domínguez A., Menéndez J.A., Pis J.J. (2006) *Hydrogen rich fuel gas production from the pyrolysis of wet sewage sludge at high temperature*. Journal of Analytical and Applied Pyrolysis 77, 127-132.

Dogru M., Midilli A., Howarth C.R. (2002) *Gasification of sewage sludge using a throated downdraft gasifier and uncertainty analysis*. Fuel Processing Technology 75, 55-82.

Dou B., Gao J., Sha X., Baek S.W. (2003) *Catalytic cracking of tar component from high-temperature fuel gas*. Applied Thermal Engineering 23, 2229-2239.

Elseviers W.F., Verelst H. (1999) *Transition metal oxides for hot gas desulphurization*. Fuel 78, 601-612.

Engelen K., Zhang Y.H., Draelants D.J., Baron G.V. (2003) *A novel catalytic filter for tar removal from biomass gasification gas: Improvement of the catalytic activity in presence of $H_2S$*. Chemical Engineering Science 58, 665-670.

Fonts I., Juan A., Gea G., Murillo M.B., Sánchez J.L. (2008) *Sewage sludge pyrolysis in fluidized bed. 1: Influence of operational conditions on the product distribution*. Industrial & Engineering Chemistry Research 47, 5376-5385.

Fonts I., Azuara M., Gea G., Murillo M.B. (2009) *Study of the pyrolysis liquids obtained from different sewage sludge*. Journal of Analytical and Applied Pyrolysis 85, 184-191.

Fonts I., Gea G., Azuara M., Ábrego J., Arauzo J. (2012) *Sewage sludge pyrolysis for liquid production: A review*. Renewable & Sustainable Energy Reviews 16, 2781-2805.

Franco C., Pinto F., Gulyurtlu I., Cabrita I. (2003) *The study of reactions influencing the biomass steam gasification process*. Fuel 82, 835-842.

Fytili D., Zabaniotou A. (2008) *Utilization of sewage sludge in EU application of old and new methods - A review*. Renewable & Sustainable Energy Reviews 12, 116-140.

García G., Cascarosa E., Ábrego J., Gonzalo A., Sánchez J.L. (2011) *Use of different residues for high temperature desulphurization of gasification gas*. Chemical Engineering Journal 174, 644-651.

Gil J., Aznar M.P., Caballero M.A., Francés E., Corella J. (1997) *Biomass gasification in fluidized bed at pilot scale with steam-oxygen mixtures. Product distribution for very different operating conditions*. Energy & Fuels 11, 1109-1118.

Gil J., Caballero M.A., Martín J.A., Aznar M.P., Corella J. (1999a) *Biomass gasification with air in fluidized bed: effect of in-bed use of dolomite under different operation conditions.* Industrial & Engineering Chemistry Research 38, 4226-4235.

Gil J., Corella J., Aznar M.P., Caballero M.A. (1999b) *Biomass gasification in atmospheric and bubbling fluidized bed: Effect of the type of gasifying agent on the product distribution*. Biomass & Bioenergy 17, 389-403.

Gil-Lalaguna N., Fonts I., Gea G., Murillo M.B., Lázaro L. (2010) *Reduction of water content in sewage sludge pyrolysis liquid by selective on-line condensation of the vapors*. Energy & Fuels 24, 6555-6564.

González J.F., Román S., Encinar J.M., Martínez G.J. (2009). *Pyrolysis of various biomass residues and char utilization for the production of activated carbons*. Journal of Analytical and Applied Pyrolysis 85, 134-141.

Gutiérrez-Ortiz F.J., Aguilera P.G., Ollero P. (2014) *Biogas desulfurization by adsorption on thermally treated sewage-sludge*. Separation and Purification Technology 123, 200-213.

Han J., Kim H. (2008) *The reduction and control technology of tar during biomass gasification/pyrolysis: An overview*. Renewable & Sustainable Energy Reviews 12, 397-406.

Harrison B.K., Seaton W.H. (1988) *Solution to missing group-problem for estimation of ideal-gas heat-capacities*. Industrial & Engineering Chemistry Research 27, 1536-1540.

Haykiri-Acma H., Yaman S., Kucukbayrak S. (2006) *Gasification of biomass chars in steam-nitrogen mixture*. Energy Conversion and Management 47, 1004-1013.

He P., Luo S., Cheng G., Xiao B., Cai L., Wang J. (2012) *Gasification of biomass char with air-steam in a cyclone furnace*. Renewable Energy 37, 398-402.

Hepola J., Simell P. (1997) *Sulphur poisoning of nickel-based hot gas cleaning catalysts in synthetic gasification gas - I. Effect of different process parameters*. Applied Catalysis B: Environmental 14, 287-303.

Herguido J., Corella J., González-Saiz J. (1992) *Steam gasification of lignocellulosic residues in a fluidised bed at a small pilot scale. Effect of the type of feedstock.* Industrial & Engineering Chemistry Research 31, 1274-1282.

Inguanzo M., Domínguez A., Menéndez J.A., Blanco C.G., Pis J.J. (2002) *On the pyrolysis of sewage sludge: the influence of pyrolysis conditions on solid, liquid and gas fractions*. Journal of Analytical and Applied Pyrolysis 63, 209-222.

Judex J.W., Gaiffi M., Burgbacher H.C. (2012) *Gasification of dried sewage sludge: Status of the demonstration and the pilot plant*. Waste Management 32, 719-723.

Kelessidis A., Stasinakis A.S. (2012) *Comparative study of the methods used for treatment and final disposal of sewage sludge in European countries*. Waste Management 32, 1186-1195.

Kim K., Jeon S.K., Vo C., Park C.S., Norbeck J.M. (2007) *Removal of $H_2S$ from steam-hydrogasifier product gas by zinc oxide sorbent*. Industrial & Engineering Chemistry Research 46, 5848-5854.

Kim Y.J., Lee S.H., Kim S.D. (2001) *Coal gasification characteristics in a downer reactor*. Fuel 80, 1915-1922.

Kimura T., Miyazawa T., Nishikawa J., Kado S., Okumura K., Miyao T., Naito S., Kunimori K., Tomishige K. (2006) *Development of Ni catalysts for tar removal by steam gasification of biomass*. Applied Catalysis B: Environmental 68, 160-170.

Kinoshita C.M., Wang Y., Zhou J. (1994) *Tar formation under different biomass gasification conditions*. Journal of Analytical and Applied Pyrolysis 29, 169-181.

Koike M., Ishikawa C., Li D., Wang L., Nakagawa Y., Tomishige K. (2013) *Catalytic performance of manganese-promoted nickel catalysts for the steam reforming of tar from biomass pyrolysis to synthesis gas*. Fuel 103, 122-129.

Li C., Suzuki K. (2009a) *Tar property, analysis, reforming mechanism and model for biomass gasification - An overview*. Renewable & Sustainable Energy Reviews 13, 594-604.

Li C., Hirabayashi D., Suzuki K. (2009b) *Development of new nickel based catalyst for biomass tar steam reforming producing $H_2$-rich syngas*. Fuel Processing Technology 90, 790-796.

Lv P.M., Xiong Z.H., Chang J., Wu C.Z., Chen Y., Zhu J.X. (2004) *An experimental study on biomass air-steam gasification in a fluidized bed*. Bioresource Technology 95, 95-101.

Manara P., Zabaniotou A. (2012) *Towards sewage sludge based biofuels via thermochemical conversion - A review*. Renewable & Sustainable Energy Reviews 16, 2566-2582.

Manganaro J., Chen B., Adeosun J., Lakhapatri S., Favetta D., Lawal A. (2011) *Conversion of residual biomass into liquid transportation fuel: an energy analysis*. Energy & Fuels 25, 2711-2720.

Manyà J.J., Sánchez J.L., Gonzalo A., Arauzo J. (2005) *Air gasification of dried sewage sludge in a fluidized bed: Effect of the operating conditions and in-bed use of alumina*. Energy & Fuels 19, 629-636.

Manyà J.J, Sánchez J.L, Ábrego J., Gonzalo A., Arauzo J. (2006) *Influence of gas residence time and air ratio on the air gasification of dried sewage sludge in a bubbling fluidised bed*. Fuel 85, 2027-2033.

McKendry P. (2002a) *Energy production from biomass (part 1): overview of biomass*. Bioresource Technology 83, 37-46.

McKendry P. (2002b) *Energy production from biomass (part 3): gasification technologies*. Bioresource Technology 83, 55-63.

Meng X., Jong W., Pal R., Verkooijen A.H.M. (2010) *In bed and downstream hot gas desulphurization during solid fuel gasification: a review*. Fuel Processing Technology 91, 964-981.

Midilli A., Dogru M., Howarth C.R., Ling M.J., Ayhan T. (2001) *Combustible gas production from sewage sludge with a downdraft gasifier*. Energy Conversion and Management 42, 157-172.

Miyazawa T., Kimura T., Nishikawa J., Kado S., Kunimori K., Tomishige K. (2006) *Catalytic performance of supported Ni catalysts in partial oxidation and steam reforming of tar derived from the pyrolysis of wood biomass*. Catalysis Today 115, 254-262.

Mondal P., Dang G.S., Garg M.O. (2011) *Syngas production through gasification and cleanup for downstream applications - Recent developments*. Fuel Processing Technology 92, 1395-1410.

Narváez I., Orio A., Aznar M.P., Corella J. (1996) *Biomass gasification with air in an atmospheric bubbling fluidized bed. Effect of six operational variables on the quality of the produced raw gas*. Industrial & Engineering Chemistry Research 35, 2110-2120.

Neeft J.P.A., Knoef H.A.M., Zielke U., Sjöstrom K., Hasler P., Simell P.A., Dorrington M.A., Thomas L., Abatzoglou N., Deutch S., Greil C., Buffinga G.J., Brage C., Suomalinen M. (2002) *Guideline for Sampling and Analysis of Tar and Particles in Biomass Producer Gases (Tar protocol).* Energy project EEN5-1999-00507.

Nilsson S., Gómez-Barea A., Fuentes-Cano D. (2012). *Gasification reactivity of char from dried sewage sludge in a fluidized bed*. Fuel 92, 346-353.

Nilsson S., Gómez-Barea A., Fuentes-Cano D., Campoy M. (2014) *Gasification kinetics of char from olive tree pruning in fluidized bed*. Fuel 125, 192-199.

Nipattummakul N., Ahmed I., Kerdsuwan S., Gupta A.K. (2010) *High temperature steam gasification of wastewater sludge*. Applied Energy 87, 3729-3734.

Nisbet I.C.T, Lagoy P.K. (1992) *Toxic equivalency factors (TEFs) for polycyclic aromatic-hydrocarbons (PAHs)*. Regulatory Toxicology and Pharmacology 16, 290-300.

Nishikawa J., Nakamura K., Asadullah M., Miyazawa T., Kunimori K., Tomishige K. (2008) *Catalytic performance of $Ni/CeO_2/Al_2O_3$ modified with noble metals in steam gasification of biomass*. Catalysis Today 131, 146-155.

Nowicki L., Antecka A., Bedyk T., Stolarek P., Ledakowicz S. (2011) *The kinetics of gasification of char derived from sewage sludge*. Journal of Thermal Analysis and Calorimetry 104, 693-700.

Olivares A., Aznar M.P., Caballero M.A., Gil J., Francés E., Corella J. (1997) *Biomass gasification: produced gas upgrading by in-bed use of dolomite*. Industrial & Engineering Chemistry Research 36, 5220-5226.

Park H.J., Park S.H., Sohn J.M., Park J., Jeon J.K., Kim S.S., Park Y.K. (2010) *Steam reforming of biomass gasification tar using benzene as a model compound over various Ni supported metal oxide catalysts*. Bioresource Technology 101, S101-S103.

Park N.K., Lee D.H., Lee J.D., Chang W.C., Ryu S.O., Lee T.J. (2005) *Effects of reduction of metal oxide sorbents on reactivity and physical properties during hot gas desulphurization in IGCC*. Fuel 84, 2158-2164.

Perry R.H., Green D.W. (1999) *Perry's Chemical Engineer's Handbook. 7th ed*. New York: McGraw-Hill.

Petersen I., Werther J. (2005) *Experimental investigation and modelling of gasification of sewage sludge in the circulating fluidized bed*. Chemical Engineering and Processing: Process Intensification 44, 717-736.

Pinto F., Franco C., André R.N., Tavares C., Dias M., Gulyurtlu I., Cabrita I. (2003) *Effect of experimental conditions on co-gasification of coal, biomass and plastics wastes with air/steam mixtures in a fluidized bed system*. Fuel 82, 1967-1976.

Pokorna E., Postelmans N., Jenicek P., Schreurs S., Carleer R., Yperman J. (2009) *Study of bio-oils and solids from flash pyrolysis of sewage sludges*. Fuel 88, 1344-1350.

Ponzio A., Kalisz S., Blasiak W. (2006) *Effect of operating conditions on tar and gas composition in high temperature air/steam gasification (HTAG) of plastic containing waste*. Fuel Processing Technology 87, 223-233.

Primavera A., Trovarelli A., Andreussi P., Dolcetti G. (1998) *The effect of water in the low-temperature catalytic oxidation of hydrogen sulfide to sulfur over activated carbon*. Applied Catalysis A: General 173, 185-192.

Qin Y.H., Feng J., Li W.Y. (2010) *Formation of tar and its characterization during air-steam gasification of sawdust in a fluidized bed reactor*. Fuel 89, 1344-1347.

Rapagnà S., Jand N., Kiennemann A., Foscolo P.U. (2000) *Steam-gasification of biomass in a fluidized-bed of olivine particles*. Biomass & Bioenergy 19, 187-197.

Richardson S.M., Gray M.R. (1997) *Enhancement of residue hydroprocessing catalysts by doping with alkali metals*. Energy & Fuels 11, 1119-1126.

Ros A., Montes-Morán M., Fuente E., Nevskaia D.M., Martin M.J. (2006) *Dried sludges and sludge-based chars for H2S removal at low temperature: influence of sewage sludge characteristics*. Environmental Science & Technology 40, 302-209.

Rulkens W. (2008) *Sewage sludge as a biomass resource for the production of energy: Overview and assessment of the various options*. Energy & Fuels 22, 9-15.

Salleh M.A.M, Kisiki N.H., Yusuf H.M., Ghani W.A.K. (2010) *Gasification of biochar from empty fruit bunch in a fluidized bed reactor*. Energies 3, 1344-1352.

Sato K., Fujimoto K. (2007) *Development of new nickel based catalyst for tar reforming with superior resistance to sulfur poisoning and coking in biomass gasification*. Catalysis Communications 8, 1697-1701.

Scott S.A., Davidson J.F., Dennis J.S., Fennell P.S., Hayhurst A.N. (2005) *The rate of gasification by $CO_2$ of chars from waste*. Proceedings of the Combustion Institute 30, 2151-2159.

Seok S., Choi S., Park E., Han S., Lee J. (2002) *Mn-promoted $Ni/Al_2O_3$ catalysts for stable carbon dioxide reforming of methane*. Journal of Catalysis 209, 6-15.

Shen L., Zhang D.K. (2003) *An experimental study of oil recovery from sewage sludge by low-temperature pyrolysis in a fluidised-bed*. Fuel 82, 465-472.

Smith K.M., Fowler G.D., Pullket S., Graham N.J.D. (2009) *Sewage sludge-based adsorbents: a review of their production, properties and use in water treatment applications*. Water Research 43, 2569-2594.

Srinakruang J., Sato K., Vitidsant T., Fujimoto K. (2006) *Highly efficient sulfur and coking resistance catalysts for tar gasification with steam*. Fuel 85, 2419-2426.

Ståhl K., Neergaard M. (1998) *IGCC power plant for biomass utilisation, Värnamo, Sweden.* Biomass and Bioenergy 15, 205-211.

Statistical Office of the European Communities (Eurostat). Water statistics: Total sewage sludge production from urban wastewater (2014). Retrieved from *hptt://epp.eurostat.ec.europa.eu.*

Struis R.P.W.J., Schildhauer T.J., Czekaj I., Janousch M., Biollaz S.M.A., Ludwig C. (2009) *Sulphur poisoning of Ni catalysts in the SNG production from biomass: a TPO/XPS/XAS study*. Applied Catalysis A: General 362, 121-128.

Sutton D., Kelleher B., Ross J.R.H. (2001a) *Review of literature on catalysts for biomass gasification*. Fuel Processing Technology 73, 155-173.

Sutton D., Kelleher B., Doyle A., Ross J.R.H. (2001b) *Investigation of nickel supported catalysts for the upgrading of brown peat derived gasification products*. Bioresource Technology 80, 111-116.

Swierczynski D., Libs S., Courson C., Kiennemann A. (2007) *Steam reforming of tar from a biomass gasification process over Ni/olivine catalyst using toluene as a model compound*. Applied Catalysis B: Environmental 74, 211-222.

Tae-Young M., Bo-Sung K., Joo-Sik K. (2009) *Production of a producer gas with high heating values and less tar from dried sewage sludge through air gasification using a two-stage gasifier and activated carbon*. Energy & Fuels 23, 3268-3276.

Tamhankar S.S., Hasatani M., Wen C.Y. (1981) *Kinetic studies on the reactions involved in the hot gas desulfurization using a regenerable iron oxide sorbent - I: Reduction and sulfidation of iron oxide*. Chemical Engineering Science 36, 1181-1191.

Tseng T.K., Chang H.C., Chu H., Chen H.T. (2008) *Hydrogen sulfide removal from coal gas by the metal-ferrite sorbents made from the heavy metal wastewater sludge*. Journal of Hazardous Materials 160, 482-488.

Van der Drift A., van Doorn J., Vermeulen J.W. (2001) *Ten residual biomass fuels for circulating fluidized-bed gasification*. Biomass & Bioenergy 20, 45-56

Wang T., Chang J., Lv P., Zhu J. (2005) *Novel catalyst for cracking of biomass tar*. Energy & Fuels 19, 22-27.

Wender I. (1996) *Reactions of synthesis gas*. Fuel Processing Technology 48, 189-297.

Westmoreland P.R., Harrison D.P. (1976) *Evaluation of candidate solids for high-temperature desulfurization of low-btu gases*. Environmental Science & Technology 10, 659-661.

Xie L., Li T., Gao J., Fei X., Wu X., Jiang Y. (2010) *Effect of moisture content in sewage sludge on air gasification*. Journal of Fuel Chemistry and Technology 38, 615-620.

Yan F., Luo S., Hu Z., Xiao B., Cheng G. (2010) *Hydrogen-rich gas production by steam gasification of char from biomass fast pyrolysis in a fixed bed reactor: Influence of temperature and steam on hydrogen yield and syngas composition*. Bioresource Technology 101, 5633-5637.

Yildirim O., Kiss A.A., Hüser N., Leßmann K., Kenig E.Y. (2012) *Reactive absorption in chemical process industry: a review on current activities*. Chemical Engineering Journal 213, 371-391.

Yoshimura Y., Yasuda H., Sato T., Shimada H. (1995) *Utilization of thermodynamic database in the systems using molybdate and iron based catalysis*. Coal Science and Technology 24, 1275-1278.

Yuan W., Bandosz T.J. (2007) *Removal of hydrogen sulfide from biogas on sludge-derived adsorbents*. Fuel 86, 2736-2746.

Yung M.M., Jablonski W.S., Magrini-Bair K.A. (2009) *Review of catalytic conditioning of biomass-derived syngas*. Energy & Fuels 23, 1874-1887.

Zhang B., Xiong S., Xiao B., Yu D., Jia X. (2011) *Mechanism of a wet sewage sludge pyrolysis in a tubular furnace*. International Journal of Hydrogen Energy 36, 355-363.

Zhang R., Brown R.C., Suby A., Cummer K. (2004) *Catalytic destruction of tar in biomass derived producer gas*. Energy Conversion and Management 45, 995-1014.

Zhang R., Wang Y., Brown R.C. (2007) *Steam reforming of tar compounds over Ni/olivine catalysts doped with $CeO_2$*. Energy Conversion and Management 48, 68-77.